

DEVELOPMENT OF A POWER-SPECTRAL GUST DESIGN PROCEDURE FOR CIVIL AIRCRAFT

TECHNICAL REPORT



JANUARY, 1966

by

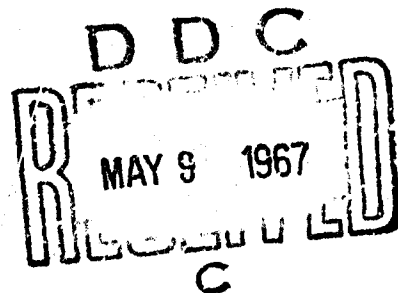
Frederic M. Noblit, Neil Paul, Jerry D. Shelton, and Francis E. Ashford

Lockheed-California Company

Burbank, California

Under Contract FA-WA-4768

for
Federal Aviation Agency
Aircraft Development Service



Best Available Copy

**Best
Available
Copy**

NOTICE AND ERRATA SHEET

1. A limited number of copies of References 21 and 22 are available .

They may be obtained by writing to:

Aircraft Development Service, DS-41
Federal Aviation Agency
Washington, D. C. 20553

2. In the column heading on page C-41 for Columns 17-24, change the word "net" to "incremental".

DEVELOPMENT OF A POWER-SPECTRAL GUST
DESIGN PROCEDURE FOR CIVIL AIRCRAFT

TECHNICAL REPORT

ADS-53

Contract FA-WA-4768

by

Frederic M. Hoblit, Neil Paul, Jerry D. Shelton, and Francis E. Ashford

u

January, 1966

Prepared For
THE FEDERAL AVIATION AGENCY
Under Contract No. FA-WA-4768

by

Lockheed-California Company
Burbank, California

The contents of this report reflect the views of the contractor, who is responsible for the facts and the accuracy of the data presented herein, and do not necessarily reflect the official views or policy of the FAA. This report does not constitute a standard, specification, or regulation.

SUMMARY

Three alternate forms of gust loads criterion based on power-spectral concepts are developed. These include a mission analysis criterion, a design envelope criterion, and a criterion combining advantages of each. The latter is recommended for design use. Design levels are determined based on the strength of three existing satisfactory airplanes, the Lockheed Model 749 (Constellation) and Model 188 (Electra) and the Boeing Model 720B. The determination of a design load level involves dynamic gust analysis of the three airplanes, taking into account the significant rigid body and elastic modes, for both vertical and lateral gust inputs, as well as detailed stress analysis to the resulting loads. The appropriate limit design frequency of exceedance (mission analysis criterion) is found to be 2×10^{-5} exceedances per hour. The appropriate limit design value of $\sigma_v \eta_g$ (rms true gust velocity times ratio of design load to rms load, for use in a design envelope criterion) varies linearly from 56 fps at sea level to 62 fps at 7000 ft., to 55 fps at 27000 ft., to 17 fps at 80000 ft. For a conservative level to be used under the "combined" criterion in the absence of a mission analysis, these values increase to 101 fps at sea level, varying linearly to 110 fps at 7000 ft., to 117 fps at 27000 ft., to 37 fps at 80000 ft. Two techniques have been developed for integrating the statistical determination of loads with the detailed stress analysis. One is the matching condition technique, in which design conditions are generated to closely envelope the statistically defined loads, with phase relations of the various load or stress components properly accounted for. The other is the joint probability technique, in which the joint probability density of axial and shear stresses is determined at all potentially critical locations in the structure and related to the respective strength envelopes. The sensitivity of results to variations in input data is investigated.

This volume covers all parts of the study except the analysis of the Model 720B airplane and the development and illustration of the joint probability technique, which are covered in Report FAA-ADS-54, prepared by The Boeing Company under subcontract.

TABLE OF CONTENTS

Summary	111
Table of Contents	v
References	viii
Introduction	1
1 Nomenclature	8
2 Selection of Airplanes for Analysis	10
3 Airplane Components Treated	13
4 Types of Power-Spectral Gust Loads Criteria Considered	14
4.1 Mission Analysis Criterion	14
4.2 Design Envelope Criterion	17
4.3 Combined Criteria	19
4.4 Other Considerations	20
5 Model of the Atmosphere	21
5.1 Background	21
5.2 Power-Spectral Density Function	23
5.3 Probability Distributions of σ_w	25
5.4 Lateral-Gust σ_w Distributions	36
5.5 Generalized Exceedance Curves for Use with Design Envelope Criterion	36
5.6 VGH and VG Comparisons	39
5.7 Future Improvements	44
6 Mission Profiles for Reference Airplanes	45
6.1 Model 188	45
6.2 Model 749	56
7 Selection of Design Envelope Points for Analysis of Reference Airplanes	72
7.1 Model 188	72
7.2 Model 749	80
8 Mathematical Models of Reference Airplanes	91
8.1 Vertical Gust, Models 188 and 749	91
8.1.1 Equations of Motion	91
8.1.2 One-g Level Flight Loads	93
8.1.3 Input Data for Dynamic Analysis	93
8.2 Lateral Gust, Models 188 and 749	101
8.2.1 Equations of Motion	101
8.2.2 Input Data for Dynamic Analysis	102
9 Results of Analysis	114
10 Design Techniques - Introductory Discussion	147
11 The Matching Condition Technique	153
11.1 Basic Approach	153
11.2 The Fictitious Structural Element Concept	158
11.3 Illustration of the Matching-Condition Technique	174

12	Matching Condition and Joint Probability Techniques - Discussion	175
12.1	Practical Considerations in Selecting a Design Technique	175
12.2	Implications with Respect to Structural Design Philosophy; Rationality	175
12.2.1	Statistical Basis of Design Criteria	179
12.2.2	The Concept of Independent Design Conditions	180
12.2.3	Power Spectral Considerations - Idealized Airplane	181
12.2.4	Power Spectral Considerations - Large, Flexible Airplane	181
12.2.5	Upbending vs Downbending Loads	183
12.2.6	Vertical vs Lateral Gusts	190
12.2.7	Combined Stresses at a Point	190
12.2.8	Summary	200
12.3	Establishment of Equivalent Design Levels	201
12.4	Comparative Application of the Two Techniques to the Model 720B	206
13	Establishment of Limit-Strength and Ultimate-Strength Levels of $N(y)$ and $\sigma_w \eta_d$	212
14	Effect of Parameter Variations	220
14.1	Vertical Gust, Model 188	220
14.1.1	Effect of Airplane Description Parameters	220
14.1.2	Effect of Mission Description Parameters	229
14.2	Lateral Gust, Model 188	232
14.3	Vertical and Lateral Gust, Model 720B	233
14.4	Effect of Mathematical Model, Model 749	233
15	Recommended Gust Design Criteria	247
15.1	Mission Analysis Criterion	247
15.1.1	Design Level of $N(y)$	247
15.1.2	Treatment of Stability Augmentation	251
15.1.3	Fail Safe Design Level	254
15.1.4	Modified Design $N(y)$ for Use in Joint Probability Analysis	254
15.1.5	Combined Vertical and Lateral Gust Loads	255
15.1.6	Suggested Formal Requirement	256
15.2	Design Envelope Criterion	258
15.2.1	Design Levels of $\sigma_w \eta_d$ at Speed V_C	258
15.2.2	Gust Conditions at V_B and V_D	261
15.2.3	Adjustment of Design Levels for Differences in N_0	261
15.2.4	Treatment of Stability Augmentation	263
15.2.5	Fail Safe Design Level	266
15.2.6	Design Levels of σ_w and P	266
15.2.7	Suggested Formal Requirement	267
15.3	Combined Criterion	269
15.3.1	Design $\sigma_w \eta_d$ Levels for Use in Lieu of a Mission Analysis	270
15.3.2	Design $\sigma_w \eta_d$ Levels for Use in Conjunction with a Mission Analysis	271
15.3.3	Suggested Formal Requirement	271

15.4	Evaluation of the Three Forms of Criterion	276
15.5	Formal Requirements for Design Technique	277
16	Summary of Design Procedures	279
16.1	Flight Conditions Required for Analysis	279
16.1.1	Mission Analysis Criterion	279
16.1.2	Design Envelope Criterion	280
16.2	Equations of Motion	280
16.3	Dynamic Analysis and Design-Level Loads	282
16.3.1	Mission Analysis Criterion	282
16.3.2	Design Envelope Criterion	283
16.4	Generation of Matching Conditions; Joint Probability Analysis	284
17	The Place of the Discrete Gust Concept	286
	Conclusions	293
Appendix A - Comparison of ASD TR 61-235 and TN 4332 σ_w Distributions		A-1
Appendix B - Numerical Results		B-1
Appendix C - Application of the Matching Condition Technique to the Model 188 Wing		C-1
C.1	Nomenclature	C-1
C.2	Preliminary Considerations	C-5
C.3	Elementary Distributions	C-10
C.4	Upbending Conditions	C-38
C.5	Downbending Conditions	C-46
C.6	Loads in Other Quadrants	C-46
Appendix D - Application of the Matching Condition Technique to the Model 188 Fuselage (Vertical Gust Loads)		D-1
D.1	Nomenclature	D-1
D.2	Preliminary Considerations	D-3
D.3	Elementary Distributions	D-8
D.4	Fuselage Downbending Conditions	D-9
Appendix E - Establishment of Limit-Strength and Ultimate-Strength Values of $N(y)$ and $\sigma_w \eta_d$, Models 188 and 749		E-1
E.1	Model 188 Wing	E-1
E.1.1	Mission Analysis, Limit Strength	E-1
E.1.2	Mission Analysis, Ultimate Strength	E-2
E.1.3	Design Envelope Criterion	E-3
E.2	Model 749 Wing	E-13
E.2.1	Design Envelope Criterion	E-13
E.2.2	Mission Analysis Criterion	E-27
E.3	Model 188 Fuselage and Tail, Vertical Gust	E-28
E.3.1	Mission Analysis, Limit Strength	E-28
E.3.2	Mission Analysis, Ultimate Strength	E-37
E.3.3	Design Envelope Criterion	E-37
E.4	Model 749 Fuselage and Tail, Vertical Gust	E-38
E.5	Model 188 Fuselage and Tail, Lateral Gust	E-43
E.6	Model 749 Fuselage and Tail, Lateral Gust	E-48

REFERENCES

1. Fuller, J. R.; Richmond, L. D.; Larkins, D. C.; and Russell, S. W.: Contributions to the Development of a Power Spectral Gust Design Procedure for Civil Aircraft. FAA-ADS-54, 1966
2. Press, Harry; and Houbolt, John C.: Some Applications of Generalized Harmonic Analysis to Gust Loads on Airplanes. J. Aero. Sci., Vol. 22, No. 1, Jan. 1955, pp 17-26.
3. Press, Harry; and Tukey, John W.: Power Spectral Methods of Analysis and Their Application to Problems in Airplane Dynamics. AGARD Flight Test Manual. Vol. IV, Part IVc.
4. Press, Harry; and Mazelsky, Bernard: A Study of the Application of Power Spectral Methods of Generalized Harmonic Analysis to Gust Loads on Airplanes. NACA Rep. 1172, 1954. (Supersedes NACA TN 2853.)
5. Press, Harry; Meadows, May T.; and Hadlock, Ivan: A Re-evaluation of Data on Atmospheric Turbulence and Airplane Gust Loads for Application in Spectral Calculations. NACA Rep. 1272, 1956. (Supersedes NACA TN 3362 by Press, Meadows, and Hadlock and TN 3540 by Press and Meadows.)
6. Thorson, Kenneth R.; and Bohne, Quentin R.: Application of Power Spectral Methods in Airplane and Missile Design. J. Aero. Sci., Vol. 27, No. 2, Feb. 1960, pp 107-116.
7. Federal Aviation Agency: Federal Aviation Regulations. Airworthiness Standards: Transport Category Airplanes. FAR Part 25, 1964.
8. Coleman, Thomas L.; and Fitner, Mary W.: An Analysis of Acceleration, Airspeed, and Gust-Velocity Data from a Four-Engine Transport Airplane in Operation on an Eastern United States Route. NACA TN 3483, 1955.
9. VGH Data Samples for L-749, L-188, and B-707-300 Commercial Transport Airplanes enclosed with NASA letter 23365, dated April 9, 1964.
10. L-188 VGH data enclosed with NASA letter to W. A. Stauffer, dated 7-29-60.
11. VGH Data, L-188 and L-749 enclosed with NASA letter, Richard V. Rhode to Warren Stauffer, dated November 17, 1960.

12. Press, Harry; and Steiner, Roy: An Approach to the Problem of Estimating Severe and Repeated Gust Loads for Missile Operations. NACA TN 4332, 1958.
13. Houbolt, John C.; Steiner, Roy; and Pratt, Kermit G.: Dynamic Response of Airplanes to Atmospheric Turbulence Including Flight Data on Input and Response. NASA TR R-199, 1964.
14. Rhyne, Richard H.; and Steiner, Roy: Power Spectral Measurement of Atmospheric Turbulence in Severe Storms and Cumulus Clouds. NASA TN D-2469, 1964.
15. Neuls, G.S.; Maier, H.G.; Leverick, T.R.; Robb, E.A.; and Webster, I.J.: Optimum Fatigue Spectra. Second Phase Report. U.S. Air Force ASD TR 61-235, 1962.
16. Fung, Y. C.: Statistical Aspects of Dynamic Loads. J. Aero. Sci., Vol. 20, No. 5, May 1953, pp 317-330.
17. Walker, Walter G.; and Copp, Martin R.: Summary of VGH and V-G Data Obtained from Piston-Engine Transport Airplanes from 1947 to 1958. NASA TN D-29, September 1959.
18. Walker, Walter G.: Summary of V-G Data Obtained from Turbine Powered Transport Airplanes from 1959 - 1963. NASA TN D-2740, 1965.
19. Ford, J. J.: Basic Cruising Performance of Lockheed Electra Model 188A with Aeroproducts 606 Propellers and Allison D-13 Engines. Lockheed Report 13189, 1958.
20. Storey, R. E.; Shelton, J.; and Paul, N.: Re-Evaluation of Gust Dynamic Loads. Model 188. Lockheed Report 14518, 1960.
21. Shelton, J. D.: A Revised Ten-Degree-of-Freedom Digital Program for Gust Load Determination of Straight Wing Airplanes. Lockheed Report 18267, 1964.
22. Alams, James J.: Theoretical Study of the Lateral Frequency Response to Gusts of a Fighter Airplane Both with Controls Fixed and with Several Types of Autopilots. NACA TN 3603, 1956.
23. Shelton, J. D.: Rigid Airplane Lateral Gust Analysis Program. Lockheed Report 18268, 1964.
24. Burington, Richard E.; and May, Donald C., Jr.: Handbook of Probability and Statistics with Tables. Handbook Publishers, Inc., 1953.

25. Funk, Jack; and Cooney, T. V.: Some Effects of Yaw Damping on Airplane Motions and Vertical-Tail Loads in Turbulent Air. NASA Memo 2-17-59L, 1959.
26. Houbolt, John C.; and Kordes, Eldon E.: Structural Response to Discrete and Continuous Gusts of an Airplane Having Wing-Bending Flexibility and a Correlation of Calculated and Flight Results. NACA TR 1181, 1954.
27. Jackson, Charles C.; and Wherry, John E.: A Comparison of Theoretical and Experimental Loads on the B-47 Resulting from Discrete Gusts. J. Aero/Space Sci., Vol. 26, No. 1, January 1959, pp. 33-45.
28. Strom, A. J.; and Weatherman, T. G.: NB-66B High Altitude Gust Survey. Vol. I, Technical Analysis, and Volume III, Time Series. ASD-TDR-63-145, June 1963.
29. Jones, Jerry W.: High Intensity Gust Investigation (WFT 1217 R3), Model F-106A. Boeing Document No. D-13273-333A, October 1964.
30. Austin, William H., Jr.: Environmental Conditions to be Considered in the Structural Design of Aircraft Required to Operate at Low Levels. SEG-TR-65-4, January 1965.
31. Pratt, Kermit G.; and Walker, Walter G.: A Revised Gust-Load Formula and a Re-Evaluation of V-G Data Taken on Civil Transport Airplanes from 1933 to 1950. NACA Rep. 1206, 1954 (Supersedes NACA TN's 2964 by Kermit G. Pratt and 3041 by Walter G. Walker).

INTRODUCTION

During the past fifteen years, great progress has been made in gust loads theory. The most fundamental advance has been the representation of atmospheric turbulence as a stationary random process, to which power-spectral methods of analysis can be applied. A second important advance has been the widespread development of automatic computer techniques for solving the equations of motion of the airplane in turbulence. It is now practical to represent the dynamics of the airplane in sufficient refinement to cover adequately not only the rigid-body motions but also the airplane elasticity and, if necessary, the effects of artificial stability augmentation devices.

The motivation for these advances, of course, has been to secure a safer and lighter structure from the standpoint of gust loads. Yet these advances in themselves do not result directly in achieving this objective. There are still two steps required. The first, and most important, is to modify or re-develop the structural criteria by which a required strength level is established for any given airplane. The second is to fit the newer methods into the routine by which design loads are obtained, and stress analysis carried out, to assure a consistency in strength throughout all the individual elements of the structure.

The first of these, namely the criteria step, is particularly difficult. Gust severity, as affected by both magnitude and shape of the gust, is inherently a statistical phenomenon. Consequently, it is not possible to define a "worst possible" gust and simply design for this gust. Past gust criteria have consisted of a particular combination of gust intensity, gust shape, airplane flight condition (speed and weight), method of analysis, and factor of safety. This combination has resulted in a satisfactory level of safety. Other combinations, however, such as a higher gust intensity with a lower factor of safety, could equally well have been selected with no significant change in the strength level achieved. Similarly, with a change in the method of analysis, such as an improvement to include flexible-airplane dynamics, or a change in the definition of the gust structure, the remaining factors must be re-evaluated to assure that an adequate yet not excessively high level of strength is defined.

To establish criteria directly, starting with agreement as to an acceptable loss rate, has generally been found not to be practical. Work along this line, however, has usually indicated that past criteria have not been overly severe. Consequently, in modifying existing criteria or devising new criteria, a practical objective is the achievement of a level of safety with respect to gust loads just equal to that of earlier satisfactory airplanes. If this is accomplished, the level of strength is certain to be adequate. It may be greater than actually necessary, but

probably by a rather small margin. More specifically, the new criteria must be of a severity such that when these criteria are applied to the older, satisfactory airplanes, these airplanes are found to be just adequate. A criterion of any greater severity would then indicate these airplanes to be inadequate, in contradiction to their satisfactory service records. A criterion of any lower severity would have permitted less strength; with the reduced strength the safety record might not have been satisfactory. As applied to new design, the new criteria, now incorporating the more realistic definition of the gust structure and the more refined methods of analysis, will more reliably predict the strength required than will the former criteria, established without the benefit of these recent advances.

Unfortunately, to re-write the gust criteria in a simple specific form that is sure to attain the above goal is a complicated task that had not been accomplished prior to the initiation of the present study. Some of the obstacles that had delayed such an undertaking were the following:

1. It had been questionable whether the state of the art of gust loads analysis had advanced sufficiently to permit clear definition of the variables that must be included in the analysis, and in what degree of refinement, in order to achieve results of the required engineering accuracy. As a result, variations in the method of analysis had been found to have a rather sizable effect on the resulting loads.
2. To be realistic, gust criteria should reflect the actual operating usage of the vehicle, which may bear a quite different relation to the design envelope for various vehicles. Furthermore, the operating usage cannot be controlled entirely by placard without undue restriction on operating flexibility. Consideration of actual operating usage inherently complicates the criterion.
3. To confirm that any proposed criterion defines a reasonable level of strength, it should be applied to various existing airplanes. Each such study, if performed with the requisite thoroughness, would be quite costly; such cost was justifiable to individual manufacturers only in connection with the development of a new design, wherein only one or two earlier airplanes built by the same manufacturer were given the required detailed treatment.

Even though no simple, specific gust loads criterion utilizing the new developments was available, practical design techniques were developed that adequately achieved the desired objective in the design of recent aircraft.

The first step in the development of those techniques was taken toward the end of the era of piston engine transports. At that time it became apparent that the earlier airplanes had satisfactory service and safety records, even though no provision had been made in their design loads for dynamic effects that were known to be present. Thus it became evident that the design gust velocities had been set high enough so that for these airplanes no increase in design loads for dynamic effects was needed. On the other hand, it was apparent that, as airplanes become larger, faster, and more flexible, the relative dynamic effects might well increase; and, sooner or later, design to static loads alone could lead to a structure of inadequate strength.

Consequently, to prevent any deficiency in strength that might otherwise have resulted from this trend, the CAA at that time adopted a policy which was summarized as follows:

"During the AIA-CAA Gust Loads Meeting in Washington, it was agreed that if a manufacturer showed that for his new model the percentage increase in load, due to transient effects, was no greater than that of his previous models, it would not be necessary to design for the increased load; however, if the increase was greater than for the previous models, this increase should be designed for."

This policy, reflecting what may be called the concept of "limited dynamic accountability", was applied, for example, in the design of the Lockheed Model 1649 Constellation and the Electra. As was the practice at that time, primary emphasis was placed on a comparison of dynamic magnification factors of wing bending moment. These were obtained utilizing both discrete-gust and power-spectral descriptions of the atmosphere. Even in these analyses, however, it was recognized that comparison of dynamic magnification factors alone would not assure that the new airplane would have as great gust load capability as the previous models. Consequently, consideration was also given to the effect of the following: (a) differences in the margin between design speed and normal operational speed; (b) differences in the static gust loads criteria to which these airplanes had been designed; and (c) positive margins of safety (indicative of strength greater than required) in the reference airplane.

More recently, important potential inadequacies were found in this simple treatment. As a result, more comprehensive and rational methods were developed. In one particular application, the approach was two-fold. First, a full dynamic analysis of the response of the flexible airplane to discrete gusts of various gradient distances was made, for both the new airplane and a reference airplane having a long and satisfactory service record. Complete wing loads were obtained for both

airplanes. A "dynamic accountability factor" was then employed to adjust the loads for the new airplane to the level of gust severity that would just take the reference airplane to limit strength. Second, to confirm the adequacy of the loads thus defined, a power-spectral analysis was performed on a "mission analysis" basis; in this analysis, it was required to show that the new airplane would fly at least as many miles before reaching limit strength as the reference airplane.

The major objection to a continuation of the type of approach described above is that data on the various satisfactory existing airplanes are available, in the necessary detail and scope, only to the manufacturers of those airplanes. Consequently, a manufacturer whose past airplanes may not have been gust-critical, or for other reasons may have had more than the required strength, must design his new aircraft to more severe criteria than the manufacturer whose past aircraft happen to have less margin. Further, no criteria short of "full dynamic accountability" are available to a manufacturer who has no previous aircraft in operation with a long, satisfactory service life.

For this reason, it has long been recognized that eventually it would be necessary to establish a gust criterion that could be employed without reference to any specific reference airplane. With the experience that has now been accumulated, it appears that the time is ripe for the development of such a criterion. The study described herein sets forth the form of such a criterion, provides evidence that the criterion will be practical to apply, and establishes tentative design levels.

As noted earlier, a second problem in the application of the newer advances in gust loads theory is to fit them into the routine by which design loads are obtained and stress analysis is conducted. Normal stress analysis practice utilizes design conditions each of which is defined over the whole of some major structural component at a given instant. Power-spectral methods, however, do not result in this sort of design condition. They lead, instead, to individual design-level values of load of equal probability at various points in the structure, or of various components of load such as wing shear, bending moment, and torsion, with the phasing undetermined. For example, it is not determined whether maximum up shear combines with maximum nose-up or maximum nose-down torsion or with some intermediate value. This difficulty can be circumvented to some extent by determining design-level values of internal loads or stresses, such as front and rear beam shear flows. But this approach is likely to lead to the cumbersome procedure of determining separate power-spectra for loads in every minute element of the structure - literally thousands of elements in a typical modern airplane wing. In addition, there still remains a problem of handling combined stresses or stress redistribution after the material begins to yield or buckle.

Consequently, it is clear that for any criterion involving the power-spectral concept to be useable, there must be some assurance that practical means are available to integrate the gust loads determination into existing design procedures and organizational arrangements. Two rather different techniques that accomplish this purpose have been developed and are described herein.

Finally, it has been noted that variations in the methods of analysis have sometimes been found to have a rather sizable effect on the loads obtained. Consequently, for the envisioned criterion to be relied upon to provide adequate structure, it is necessary to obtain a specific indication of the variations in the resulting design loads that might be produced by variations in the input data used in the loads determination. Therefore, these effects have also been investigated.

In addition to the variations in method or input data that can be studied utilizing a given mathematical model, there are also subtle differences among various mathematical models, even though these models may all be of the same general level of complexity. Since the present study is conducted by two different manufacturers, an excellent opportunity has presented itself to compare the results obtained by two different models using identical input data. Consequently, such a comparison is made as part of the present study.

In summary, the objectives of the program reported herein can be listed as follows:

1. Provide a recommended form for a gust loads criterion based on power-spectral concepts.
2. Establish design levels based on strength of satisfactory existing airplanes, taking into account the significant rigid body and elastic modes.
3. Provide a practical technique for using statistically defined loads in stress analysis, and illustrate by application to an existing airplane.
4. Investigate sensitivity of results to data and methods.

It should perhaps be emphasized that, in carrying out these objectives, the intent has been to utilize the present state of the art of power-spectral gust loads analysis, rather than to advance the state of the art. Accordingly, only a very minor effort has been devoted to improving currently available models of the atmosphere, even though a need for a substantial effort in this direction has been generally recognized. Also, no attempt has been made to account for the effect of

spanwise variations of gust velocity. Various published papers have treated this subject, and eventually it may be necessary to consider the effects of a two-dimensional gust pattern. However, these effects are probably rather small for existing or proposed aircraft; and it is believed to be more important at this stage to proceed to develop criteria that exploit the simpler theory, which is the one that has been employed in most applications to date.

The general plan of this report is fairly evident from the Table of Contents.

Sections 2 and 3 discuss the selection of the three reference airplanes for analysis and the airplane components to be treated. Section 4 indicates the general forms that might be taken by a power-spectral gust loads criterion and that will be used in the present study. Section 5 then discusses the establishment of the particular atmosphere model to be used. A detailed comparison of this with the best-known previous model is given in Appendix A.

The dynamic analysis of two of the three reference airplanes, the Lockheed Model 188 and Model 749, is described in Sections 6 through 9, with detailed numerical results presented in Appendix B. The corresponding material for the Boeing Model 720B is contained in Reference 1.

The two design techniques developed as part of the present study are introduced in Section 10. The "matching condition" technique is developed in Section 11 and the "joint probability" technique in Reference 1. The two techniques are related and compared in Section 12.

Limit-strength and ultimate-strength levels for the three reference airplanes, in terms of the power spectral criteria described in Section 4, are then summarized in Section 13. These are determined from the results of the dynamic analysis, drawing upon the design techniques described in Sections 10 through 12 and performing such stress analysis of the structure as found necessary. Detailed accounts of this determination are included in Appendix E and in Reference 1.

The effect of parameter variations on gust loads is reported in Section 14 and in Reference 1.

Utilizing the limit strength levels presented in Section 13, with the information in Section 14 on the effect of parameter variations as further background, appropriate design levels for new airplanes are considered in Section 15. Suggested formal requirements are provided.

A summary of the over-all procedure for dynamic gust loads determination for new airplanes is then presented in Section 16. Comments on modifications that might be required for application to advanced configurations are included. Finally, in Section 17, consideration is given to the relation of the existing discrete-gust requirement to the power-spectral criteria proposed as a result of this study.

Some prior familiarity of the reader of this report with the concept of a stationary random process and the techniques of power-spectral analysis is assumed. Recommended introductory discussions are contained in References 2 and 3. References 4 through 6 provide additional material that may also be helpful.

1 NOMENCLATURE

\bar{A}	Ratio of root-mean-square value of load to root-mean-square gust velocity
b_1, b_2	Intensity parameters in the expression for probability density of σ_w
\bar{c}	Mean wing chord
C_{L_a}	Slope of curve of C_L vs α , per radian
f	Frequency, cycles per second
\hat{f}	Probability density
h	Altitude
K_g	Gust alleviation factor for one-minus-cosine discrete gust (Reference 31)
K_σ	Dimensionless gust response factor for continuous turbulence (Equation 5-5)
L	Scale of turbulence, a parameter in Equations 5-1 and 5-4
M_x, M_y, M_z	Bending or torsional moment about axis indicated
N_0	Average number of zero crossings with positive slope, per unit time
$N(y)$	Number of exceedances of the indicated value of y per unit time (ordinarily per hour)
P	Probability that stress is in excess of limit load level, or that stress condition is outside the limit-strength envelope
P_1, P_2	Fractions of total flight time in non-storm and storm turbulence respectively - parameters in the expression for probability density of σ_w
q	Dynamic pressure. Shear flow
S	Reference wing area
S_y, S_z	Shear in direction indicated

V	Airspeed
V_B	Design rough-air speed
V_C	Design cruise speed
V_D	Design dive speed
V_e	Equivalent airspeed
V_T	True airspeed
W	Airplane gross weight
y	Any acceleration, load, or stress
ζ	Ratio of actual damping coefficient to critical, or dead-beat, damping coefficient
η_d	Ratio of design load to root-mean-square load
μ_g	Airplane mass parameter as used in Reference 31, $2W/C_{L_a} \rho \bar{c} g S$
$\bar{\mu}$	Same as μ_g but with C_{L_a} taken as airplane instead of wing lift curve slope
ρ	Air density
σ_w	Root-mean-square value of true gust velocity (vertical or lateral component)
σ_y	Root-mean-square value of y
$\phi(\Omega)$	Power-spectral density function
Ω	Reduced frequency, radians per foot

Other quantities, used only in particular sections of the report, are defined where used.

2 SELECTION OF AIRPLANES FOR ANALYSIS

In the selection of a "reference" airplane to use for setting the level of severity of a new gust loads criterion, the most important consideration is a long and successful service life. This is necessary in order to provide a reasonable opportunity for any deficiency in strength to have become evident.

A second important consideration is that, to avoid excessive conservatism, the airplane should be as gust-critical as possible at normal operating speeds. For if the reference airplanes are not gust-critical, the strength put in for other than gust conditions, or perhaps for gust conditions at an unreasonably high design speed, will be interpreted as necessary to provide safety in turbulence. The new criteria would thus require an equivalent, unnecessarily high, strength in the new aircraft.

Another consideration of great practical importance is that complete and detailed data for the reference airplanes be available. These data must include not only the "over-all" aerodynamic, mass, and elastic data needed to solve the equations of motion, but also detailed data as to external and internal load distribution and local structural strength. Adequate data of this type can be obtained only as a result of extensive wind-tunnel tests, flight load measurements, stress analysis of a multitude of structural components, and panel tests to determine structural allowables.

An important additional consideration, although not a vital one, is that VGH data be available for the reference airplane to assist in defining the mission profiles to be used for analysis.

Similarity of the reference airplanes to the new airplanes to which the criterion will be applied, in such configuration characteristics as wing sweep, type of propulsion, number of engines, etc., is not a pertinent consideration in selecting the reference airplanes. The effect of dissimilarity in configuration should be fully accounted for in the dynamic analysis.

For the purpose of the present study, the Lockheed Model 749 Constellation, the Lockheed Electra (Model 188), and the Boeing Model 720B are selected as reference airplanes.

The Model 749 is regarded as particularly suitable as a reference airplane. As of January, 1965, individual ships of this fleet averaged about 43000 hours of service, with several as high as 55000 hours, all with no evidence of structural inadequacy to carry the gust loads that have been encountered.

The Model 749 is gust critical under the current FAR 25 criteria (Reference 7). Furthermore, in comparison with other airplanes of the piston-powered transport era, the 749 appears to be relatively gust critical at normal operational speeds. It has been found to be considerably more gust-critical than later Constellations, for example, primarily as a result of an increase in the wing loading of the later airplanes without any significant change in their typical operating speeds. In addition, VGH data have been published for Model 749 operation (Reference 8).

The particular version of the Model 749 for which the analyses are conducted is the Model 749A including modifications in accordance with Service Bulletin 545. This airplane was designed for a take-off gross weight of 107,000 lb. and a maximum zero-fuel weight of 86,464 lb. The majority of the 145 airplanes in the Model 749 fleet - totaling at least 104 airplanes and probably about 140 - were either delivered in this configuration or later converted to it.

The Electra provides a second suitable reference airplane. Individual airplanes in the Electra fleet as of January 1, 1965, had acquired as much as 18000 hours of service during their eight years of operation. The Electra is gust critical over much of the wing, fuselage, and empennage under FAR 25 criteria. And for it, too, extensive VGH data are available (References 9 through 11).

The particular Electra airplane for which the analyses are conducted has a design take-off weight of 116,000 lb. and maximum zero fuel weight of 86,000 lb. For the purpose of this study, airplane serial numbers 1035 - 1148 and 2001 - 2022, totaling 136 airplanes, can be considered to fall in this category. Actually, a considerable number of these airplanes are certificated for a take-off weight of only 113,000 lb., primarily because the increase in strength of the landing gear support structure required for the 116000 lb. gross weight was serialized somewhat later in the production program. However, the primary wing, fuselage and tail strength is the same for all 136 airplanes, and the flight loads given by the power-spectral analysis are essentially identical at both the 113,000 lb. and 116,000 lb. gross weights. (The last six Electra airplanes also had a small increase in fuselage shell strength to provide additional growth potential; this increase, however, would have no effect on the results of this study, and no further explicit consideration is given to it.)

The Boeing Model 720B provides an additional reference airplane representative of current subsonic jet transports. As of January 1, 1965, the fleet of 720 and 720B airplanes had accumulated a total of nearly 1,300,000 flight hours, with the high-time airplane in excess of 13000 hours. The 720B is selected in preference to other airplanes of the

707 and 720 series because it is the most nearly gust-critical, because its use in medium-range operations probably results in a somewhat more severe gust exposure, and because better and more complete data are available for use in the analysis. Although VGH data are not available for the 720B explicitly, extensive VGH data have been obtained from 707 operations and are available in Reference 9.

The selection of an airplane to use for illustrating the design techniques to be developed can be quite independent of the selection of the reference airplane. The Lockheed Electra and the Boeing 720B are used for this purpose. The basic principles involved can be adequately demonstrated utilizing these airplanes; possible modifications that might be required for other configurations such as arrow wing, variable geometry, or delta-canard are explored without specific numerical illustration.

3 AIRPLANE COMPONENTS TREATED

In developing criteria that will utilize the more recent advances in gust loads theory, major emphasis has usually been placed on determination of design wing loads. However, other airplane components, too, are often designed by gust loads. In fact, one of the more significant applications of power-spectral theory to gust loads has been in the investigation of vertical tail loads for the current subsonic jet transports where low damping in the Dutch roll mode has resulted in loads not adequately accounted for by the discrete-gust approach. In addition, vertical gusts produce loads on the fuselage (primarily due to inertia) and on the horizontal tail, that have been critical for design.

Manifestly it would be desirable for a single design criterion to be applicable to all structural components and to both vertical and lateral components of turbulence. In order to assure, however, that the criterion developed in the present study does have the desired generality, each of these various areas is treated specifically. Primary emphasis is given to the wing. The fuselage and horizontal tail are treated by fairly simple extensions of the mathematical models developed originally to define wing loads. Side gust loads on the vertical tail require a separate treatment, and a significant part of the study is devoted to this aspect.

No explicit consideration has been given to loads on engine nacelles. In any new design, however, especially of a propeller-powered airplane, the determination of nacelle design loads would have to be included in the analysis.

4 TYPES OF POWER-SPECTRAL GUST LOADS CRITERIA CONSIDERED

In developing a gust loads criterion based on power-spectral analysis that can be used without reference to any specific comparison airplane, either of two general types of approach might be followed. The basic features of each of these approaches are discussed in considerable detail in the following paragraphs. A combined criterion, which includes use of both approaches, is then suggested. Finally two subsidiary considerations are discussed - namely, the treatment of stability augmentation systems and specification of structural fail-safe conditions. Throughout the remainder of this report, data applicable to both of the basic types of criteria are developed.

4.1 Mission Analysis Criterion

The first approach utilizes the mission analysis concept. A standard set of gust statistics is established, in the general form employed in NACA TN 4332 (Reference 12). This permits use of the equation

$$N(y) = N_0 \left[P_1 \exp \left(- \frac{y}{b_1 \bar{A}} \right) + P_2 \exp \left(- \frac{y}{b_2 \bar{A}} \right) \right] \quad (4-1)$$

to obtain curves of frequency of exceedance vs load, for each mission segment. In this equation, y can be any load quantity - for example, bending moment at a particular wing station. $N(y)$ is the number of exceedances of y per unit time or distance flown. \bar{A} is the ratio of the rms value of y to the rms gust velocity, and N_0 is a characteristic frequency of y , obtained as the radius of gyration of the power-spectral density of y about zero frequency. Both \bar{A} and N_0 are evaluated by appropriate dynamic analysis, utilizing all pertinent degrees of freedom. P_1 , P_2 , b_1 , and b_2 are parameters defining the gust environment; plots of these are provided as functions of altitude, as described in the next section.

The exceedances determined for each mission segment by means of the above equation are then added to give the exceedances for overall operation of the airplane.

This type of criterion requires, for a new vehicle, establishment of typical mission profiles, which are then broken down into segments. Certain ground rules, or minimum requirements, may properly be specified for accomplishing this step, to assure that sufficient detail is provided to account for the more severe elements of the operational spectrum. The mission analysis results in a curve of frequency of exceedance vs load level for each pertinent load. The frequency of

exceedance corresponding to limit (or ultimate) load is specified; entering the frequency of exceedance curves for the various load quantities with this value then yields a design value of each load. The design frequency of exceedance must be carefully chosen on the basis of providing strength in new vehicles consistent with that found adequate in existing aircraft.

In the present study, the basic task in the development of the mission analysis type of criterion is the determination of the frequency of exceedance of limit (or ultimate) strength, at the most critical point in the structure for each of the three reference airplanes - the Lockheed Model 749 and Model 188 and the Boeing Model 720B. A single value is then to be selected to use in future design. On the basis that each of the three airplanes has demonstrated structural adequacy with respect to gust-induced loads, the rational selection would be the highest of the three frequencies of exceedance - that is, such as to define the lowest loads.

This frequency of exceedance can readily be expressed as a frequency either per flight hour or per flight mile. For application to new design, however, a different load level will result depending upon which way the frequency is stated. To illustrate, consider that a new airplane is being designed, which will fly much faster than the old reference airplane on which the design frequency of exceedance is based. Suppose that this new airplane is designed to reach limit strength, on the average, after the same number of flight miles as the old airplane - i.e., it is designed to the same frequency of exceedance per mile. The new airplane then, as a result of its higher speed, will reach limit load in fewer hours; and by the time it has flown the same number of hours, it will have reached - on the average - some higher load level. Consequently, its design loads would be higher if based on a given frequency of exceedance per hour rather than per mile. Accordingly, it is important to establish as logically as possible whether equivalent safety is properly achieved by design on a per-mile or a per-hour basis.

From the standpoint of a crew member, equivalent safety would appear to require design to reach limit (or ultimate) load after a given number of flight hours, since the crew member will expect to spend about the same number of hours in the air regardless of whether flying in a fast or slow airplane.

From the standpoint of a passenger, on the other hand, it might be argued that equivalent safety would involve design to reach limit (or ultimate) load after a given number of flight miles. A passenger, having decided to take a given trip, would want the same high probability of reaching his destination without mishap regardless of

whether traveling on a fast or a slow airplane. However, there is undoubtedly a tendency to travel more frequently and over greater distances as travel becomes faster and easier. Consequently, even from the passenger standpoint, it appears about as reasonable to design on a per-hour as on a per-mile basis.

It therefore appears that a mission analysis gust loads criterion for civil aircraft should specify a rate of exceedance of limit (or ultimate) load per hour. The results of the analyses conducted in the present program are therefore expressed on this basis.

While it would be a mistake to confuse economics with safety, it might also be noted that the desired fatigue life of a civil transport airplane tends to be roughly a constant number of hours, regardless of the flight speed. As a result, selection of a per-hour limit strength criterion has the added advantage of tending to lead to consistency of fatigue and limit strength and also to consistency in the calculation procedures for repeated loads spectra and design limit loads.

At this point it is pertinent to outline more specifically the steps in the actual computation of a frequency of exceedance curve for a given quantity.

First, it is noted that y in Equation 1 is actually the increment due to the gust - i.e., not including the one-g level flight value. Letting y now denote the net load, including the one-g load, Equation (4-1) becomes

$$N(y) = N_0 \left[P_1 \exp - \left| \frac{y - y_{\text{one-g}}}{b_1 A} \right| + P_2 \exp - \left| \frac{y - y_{\text{one-g}}}{b_2 A} \right| \right] \quad (4-2)$$

For any mission segment, $N(y)$ is obtained as a function of y by selecting a series of values of y and calculating $N(y)$ for each. The value of $N(y)$ thus obtained will be the average number of exceedances per hour of flight (assuming N_0 to have been converted to units of cycles per hour) in the given mission segment. To obtain the number of exceedances within the given segment per hour of over-all flight, $N(y)$ is multiplied by the ratio of time in the given segment to total time. Curves of $N(y)$ vs y are obtained in this way for each mission segment. At each of a series of values of y , the $N(y)$ values for all the segments are then added, to give the over-all $N(y)$ vs y relation.

4.2 Design Envelope Criterion

The second approach disregards all considerations of the specific operational usage of various airplanes to which the criterion might be applied; instead, it leads to a criterion in which design is to a specified design envelope of speed, altitude, gross weight, fuel weight and c.g. position. In this respect, the criterion is similar to the past discrete gust criteria. The criterion resulting from this approach specifies a shape of gust power-spectral density function and a quantity $\sigma_w \eta_d$ (following the notation of reference 13), in which σ_w is an rms gust intensity and η_d is a factor representing the ratio of design load to rms load. The breakdown between the two factors is ordinarily not of consequence, except as an aid in visualizing the physical significance of the criterion; only the product is specified. (In the joint probability treatment of combined stress, however, values of σ_w and η_d must both be specified.) The quantity $\sigma_w \eta_d$ is closely analogous to U_{de} in present criteria; it is specified as a function of altitude, for each of one or more speeds (V_B , V_C and V_D). The design load at any point is then given by multiplying $\sigma_w \eta_d$ by \bar{A} , the ratio of the rms value of load at the given point in the structure to the rms gust velocity. The selection of the values to be specified for $\sigma_w \eta_d$ must be based on providing strength in the new vehicles consistent with that found adequate in existing aircraft. (A refinement that might be made would be to include in the expression for design loads an appropriate multiplying factor, ordinarily close to unity, given as a function of the characteristic frequency of the load response quantity, N_0 ; the effect of such a refinement would be small, however, and the added complexity is therefore believed not to be justified.)

In the development of a design envelope type of criterion, a necessary preliminary step is to establish a variation with altitude of $\sigma_w \eta_d$. For this purpose, it is noted that

$$\begin{aligned} y_{\text{design}} &= \eta_d \sigma_y \\ &= \eta_d \sigma_w \bar{A} \\ &= (\bar{A}) (\sigma_w \eta_d) \end{aligned}$$

whence
$$\frac{y_{\text{design}}}{\bar{A}} = \sigma_w \eta_d$$

or
$$\sigma_w \eta_d = \left(\frac{y}{\bar{A}} \right)_{\text{design}}$$

It is reasonable to require that, as altitude varies, the design value of y/\bar{A} , or of $\sigma_w \eta_d$, should also vary, in such a way that the average

frequency of exceedance of y is the same at all altitudes. Noting that b_1 , b_2 , P_1 , and P_2 are functions of altitude only, it is seen that Equation 4-1 defines $N(y)/N_0$ as a function y/\bar{A} for constant altitude. Also, therefore, it defines y/\bar{A} as a function of altitude for constant $N(y)/N_0$. Curves of the latter type are developed in the next section, "Model of the Atmosphere", and are shown in Figures 5-6 and 5-8. To the extent that N_0 is independent of altitude, a given value of $N(y)/N_0$ reflects a constant frequency of exceedance of load. Consequently, the variation of $\sigma_w \eta_d$ with altitude will be defined by some constant value of $N(y)/N_0$ in Figure 5-6 or 5-8.

The basic task in the development of the design envelope type of criterion is to establish the particular value of $N(y)/N_0$ that will properly define $\sigma_w \eta_d$ as a function of altitude. This is accomplished as follows. For each of the three "reference" airplanes, the limit-strength (or ultimate strength) y/\bar{A} value (at the most critical point in the structure) is determined at as many altitudes as are likely to be critical. The limit strength value of y/\bar{A} is simply the limit-strength value of the load quantity, y , less the one-g value, divided by \bar{A} for this load quantity as obtained by the dynamic analysis. The flight conditions to be investigated at each altitude will consist of the critical combinations of gross weight, c.g. position, fuel load, payload, and airspeed within the structural design envelopes. For each of these limit strength (or ultimate strength) values, $N(y)/N_0$ will be read from Fig. 5-8. The point corresponding to the largest value of $N(y)/N_0$ - i.e., defining a curve farthest to the left in Fig. 5-8 - will determine the $\sigma_w \eta_d$ variation appropriate to that airplane. Three such curves will thus be defined - one for each of the three reference airplanes. A single curve will then be selected for use in future design. On the basis that each of the three airplanes has demonstrated structural adequacy with respect to gust induced loads, the rational selection would be the curve representing the highest value of $N(y)/N_0$ - that is, such as to define the lowest loads.

In establishing design values of $\sigma_w \eta_d$, the investigation first is confined to definition of $\sigma_w \eta_d$ for use at speed V_C . Consideration is then given to establishing values for use at V_B and V_D .

Retention of a V_D gust requirement is undoubtedly appropriate. Although the percent of time at speeds substantially in excess of V_D is probably very small, the highest speeds are likely to result from upsets in very severe turbulence; a reasonable capability to withstand turbulence at dive speed should therefore be assured.

A continued need for increased gust intensities at V_B is less obvious. Operating instructions increasingly emphasize the need for maintaining sufficient speed in rough air to maintain good control, and NASA analysis of their VGH data indicates that the tendency to slow down in

turbulence has been negligible. (Reference 15 does indicate that about 80% of storm turbulence is encountered at reduced speed; but the remaining 20% encountered at cruise speed still represents a substantial exposure.) Consequently, it might be concluded that whatever turbulence intensity is found to be adequate at speed V_C should also be adequate at V_B . However, all three airplanes are found to be good for turbulence intensities at V_B considerably in excess of those at which they reach limit strength at V_C . In the absence of compelling evidence that this capability is not necessary for safety, it is considered prudent to provide a comparable capability in future airplanes. Consequently, a design turbulence intensity at V_B , higher than that at V_C , is also established.

4.3 Combined Criteria

While the type of criterion finally formulated might be simply one or the other of the two described above, it is believed that consideration should also be given to a criterion that would combine both of these approaches.

It appears that only by means of a realistic mission analysis can it be assured that the gust loads defined provide a strength level that is safe yet not overly conservative. Only the mission analysis approach, for example, will provide loads that are adequate for a new aircraft that operates most of its time close to its design envelope, without penalizing aircraft such as the current transports that operate generally rather far within their design envelopes. Yet the mission analysis approach does suffer certain disadvantages. Considerable judgment is required in setting up the design missions, and the design loads obtained are affected to greater or less extent by the decisions made at that stage. Also considerable care may be required to assure that a sufficient variety of off-typical flight conditions are included - e.g., extremes of c.g. position, payload, speed, etc.

Consequently, a combined criterion that would retain the advantages of the mission analysis criterion while minimizing its disadvantages would be attractive.

For example, a combined criterion might establish conservative design values of $\sigma_w \eta_d$ that could be used in lieu of a mission analysis, together with a provision that these need not be met if an acceptable mission analysis is performed. Thus, for an airplane that is rather far from being gust critical, the mission analysis could be eliminated entirely. In addition, even when a mission analysis is performed, a $\sigma_w \eta_d$ analysis might be required, but at some reduced $\sigma_w \eta_d$ level. This would then provide a floor below which the mission analysis loads could not drop. It would thus provide a degree of insurance against omitting pertinent operational elements in setting up the mission profiles and breaking them into segments. Similarly, it would provide insurance against a possible rapid increase in gust response as the boundaries of the design envelope are approached.

4.4 Other Considerations

In any gust criterion, the treatment of automatic stability augmentation devices must be covered. Ordinarily, such devices would be considered operative. However, malfunction must also be provided for. In the mission analysis type of criterion, a certain percentage of flight time can be included with stability augmentation devices inoperative. This percentage can either be stated explicitly or left to the manufacturer to select and then justify by reliability considerations. In the "design envelope", or $\sigma_w \eta_d$, type of criterion, a percentage reduction in $\sigma_w \eta_d$ can be established for use with stability devices inoperative. This percentage can be stated explicitly, or stated as a function of the percent of time that the devices are expected to be inoperative, this percent of time to be selected by the manufacturer and justified by reliability analyses.

Fail safe loads, also, must be covered. In the mission analysis type of criterion, fail safe conditions can be defined in terms of some different frequency of occurrence. In the design envelope type of criterion, fail safe loads can be defined by some different value of $\sigma_w \eta_d$.

5 MODEL OF THE ATMOSPHERE

5.1 Background

The model of the atmosphere adopted for use in the present program follows the general pattern set forth in NACA TN 4332. The atmosphere is first considered to be made up of discrete patches of continuous turbulence of different root-mean-square intensities, σ_w , each of which is "stationary" and "Gaussian." This discrete patch model is then replaced by a model which has a continuously varying distribution of root-mean-square gust velocity, σ_w . This variation is considered to be gradual enough in time, however, so that the various relations of output to input developed for a stationary Gaussian process still apply.

The shape of the power spectral density function of the gust velocity is assumed to be the same for all turbulence encountered, and in TN 4332 it is assumed to be given by the Liepmann equation,

$$\Phi(\Omega) = \sigma_w^2 \frac{L}{\pi} \frac{1 + 3\Omega^2 L^2}{(1 + \Omega^2 L^2)^2} \quad (5-1)$$

with $L = 1000$ ft.

The probability density of σ_w is defined in the mathematical form

$$\hat{f}(\sigma_w) = P_1 \frac{1}{b_1} \sqrt{\frac{2}{\pi}} \exp\left(-\frac{\sigma_w^2}{2b_1^2}\right) + P_2 \frac{1}{b_2} \sqrt{\frac{2}{\pi}} \exp\left(-\frac{\sigma_w^2}{2b_2^2}\right) \quad (5-2)$$

In this expression, the two terms represent the contributions of "non-storm" and "storm" turbulence respectively. P_1 and P_2 are the proportions of total flight time in the two types of turbulence, and b_1 and b_2 are constants indicative of the probable intensities. More precisely, b_1 is the root-mean-square value of σ_w considering only the time spent in non-storm turbulence, and b_2 is the root-mean-square value of σ_w for the time spent in storm turbulence. A sharp distinction between storm and non-storm turbulence is not required, as Equation 5-2 can be regarded as an empirical equation covering all types of turbulence collectively without regard to the motivation leading to its expression as a sum of two terms. The quantities P_1 , P_2 , b_1 , and b_2 depend upon altitude, and values are provided in TN 4332 for various altitude bands.

A particular advantage of the mathematical form utilized in equation 5-2 is that it leads to a simple and convenient equation for load exceedances,

$$\frac{N(y)}{N_0} = P_1 \exp \left(-\frac{y/\bar{A}}{b_1} \right) + P_2 \exp \left(-\frac{y/\bar{A}}{b_2} \right) \quad (5-3)$$

In this equation, y is any load quantity, such as airplane center of gravity acceleration. \bar{A} and N_0 are quantities obtained by solution of the airplane equations of motion; \bar{A} is the ratio σ_y/σ_w , and N_0 is a characteristic frequency given by the radius of gyration of the power-spectral density curve for y with respect to zero frequency. Equation 5-3 is derived by use of Equation 5-2 in conjunction with Rice's equation for exceedances at a given rms level (Equation 2 of Reference 5),

$$N(y) = N_0 \exp \left(-\frac{y^2}{2\sigma_y^2} \right)$$

(As indicated in Reference 5, Rice's equation is an exact expression for the number of positive-slope crossings per second of given values of y ; it is an approximate expression for the number of maximums - or peaks - per second above a given value of y . The approximation is extremely close for a time history characterized by a narrow-band power spectral density. For typical gust load time histories, which are relatively wide-band, the approximation is still very good, especially at y/σ values greater than 2.)

For any given altitude, P_1 , P_2 , b_1 , and b_2 in Equation 5-3 are available as the parameters defining the probability distribution of σ_w . A plot of $N(y)/N_0$ vs y/\bar{A} , as defined by Equation 5-3, then provides a generalized exceedance curve for that altitude. An actual exceedance curve for a particular load quantity on a given airplane then follows by multiplying ordinates by N_0 and abscissas by \bar{A} .

It is seen that the same four parameters, P_1 , P_2 , b_1 , and b_2 , define both the σ_w distributions and the generalized exceedance curves. Thus the generalized exceedance curves provide an alternate to the probability density as a means of describing the statistical distribution of σ_w . This alternate form of presentation is now generally preferred, because of its close relation to the way in which the σ_w distributions are actually used in loads determination.

Inasmuch as TN 4332 represented a rather preliminary effort to define atmospheric turbulence in power-spectral form, it was considered desirable to up-date the information given therein, for use in the present study, to whatever extent this could be done without embarking on a major program.

Accordingly, a meeting was held at the NASA Langley Research Center in March, 1964, for the purpose of determining what improvements in the TN 4332 atmospheric model should be made. This meeting was attended by representatives of NASA, FAA, Lockheed and Boeing.

5.2 Power-Spectral Density Function

As a result of information presented by NASA at this meeting and now available in references 13 and 14, it was the consensus that the gust power-spectral density function should be taken as described by the "isotropic turbulence" equation,

$$\Phi(\Omega) = \frac{\sigma^2 L}{\pi} \frac{1 + \frac{8}{3} (1.339 L \Omega)^2}{[1 + (1.339 L \Omega)^2]^{11/6}} \quad (5-4)$$

with $L = 2500$ ft. This equation is plotted in Fig. 5-1. The quantity Ω is a reduced frequency with units of radians per foot. The constant L is generally called the "scale of turbulence" and defines the frequency at which the bend in the curve occurs (approximately $\Omega L = 1$). It is seen that at the higher frequencies Φ varies as $\Omega^{-5/3}$.

Because of the generally isotropic nature of atmospheric turbulence, the above equation is considered to apply equally to the vertical and lateral components. It should be remarked, however, that the power spectrum of the component parallel to the flight path is inherently somewhat different; it can be derived from the above equation, if needed, by means of relations noted in Reference 14.

For altitudes less than about 2500 ft. above the ground, the scale of turbulence is probably somewhat smaller than the 2500 ft. value selected. For convenience in performing loads analyses, however, the 2500 ft. value will be retained for all altitudes. The effect on design loads is negligible for aircraft having gust response characteristics similar to those of current propeller driven aircraft. Somewhat conservative loads might result for a new vehicle spending large amounts of time in this altitude range if it were to fly very substantially faster than present airplanes or respond at a very much lower frequency.

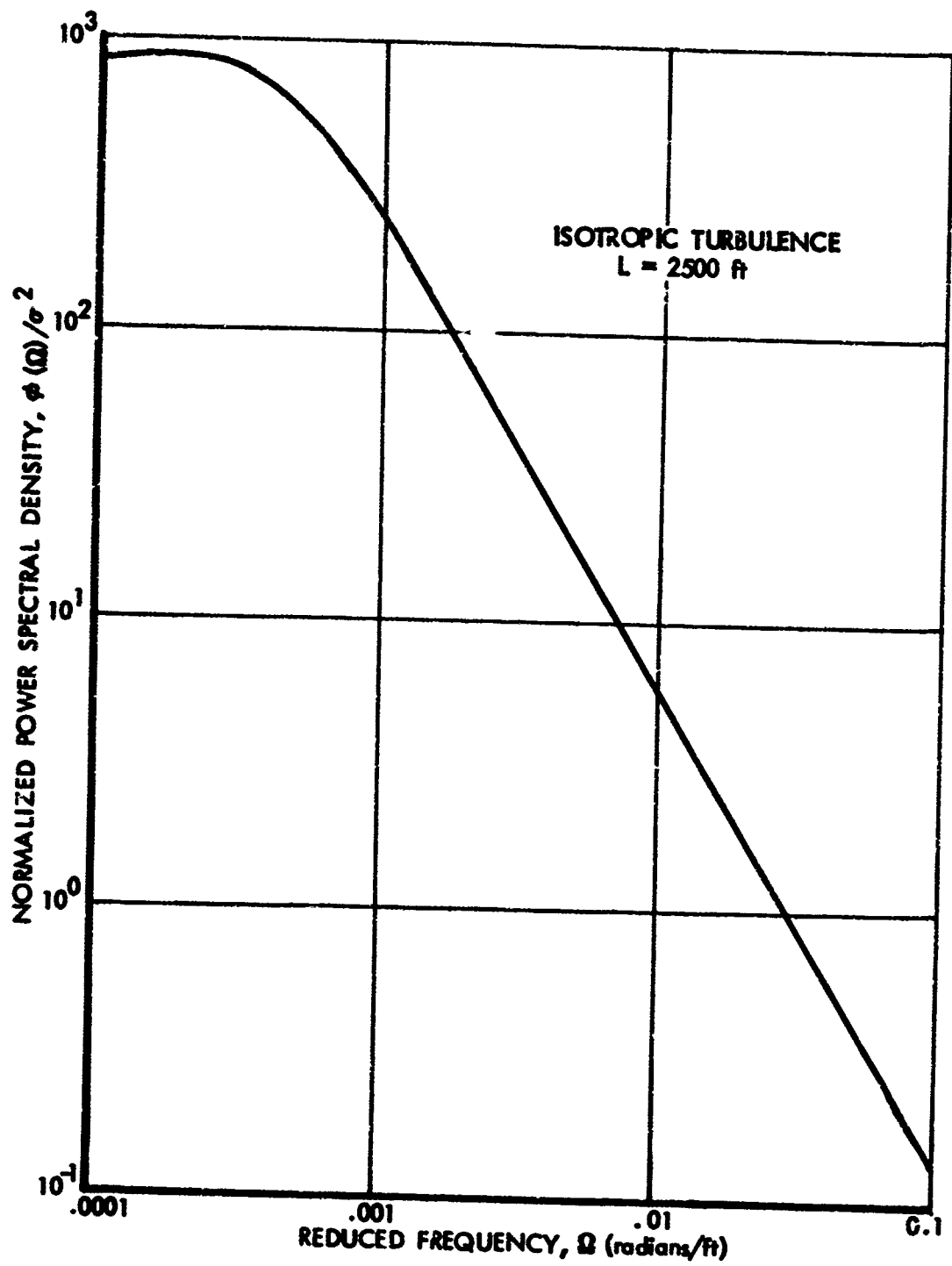


FIGURE 5-1. GUST POWER SPECTRAL DENSITY FUNCTION

5.3 Probability Distributions of σ_w

With respect to the σ_w probability distributions, NASA indicated that they had done no specific work toward refining the b_1 , b_2 , P_1 , and P_2 values given in NASA TN 4332. They felt that such a study should involve a complete redetermination, and it was agreed that this could not be undertaken and completed in time for use in the present program. NASA did emphasize the preliminary nature of the numbers presented in TN 4332 and indicated that if certain simple modifications clearly appeared to represent an improvement in the distributions they could see no objection to such modifications being made for the purpose of the present program.

It might be remarked that, in the present program, any overall conservatism or unconservatism in the σ_w distributions will be automatically offset in the determinations of a design frequency of exceedance. However, it is obviously important that the relative variation of turbulence severity with altitude be accurately represented. Also, it is advantageous for the over-all level of severity to be as realistic as possible - first, in order to avoid giving a misleading impression of actual frequencies of exceedance of limit strength and, second, so that the σ_w distributions can be used directly in fatigue calculations.

Accordingly, further consideration was given to simple means of improving the σ_w distributions presented in TN 4332.

It was found that in ASD TR 61-235, "Optimum Fatigue Spectra" (Reference 15), an extensive re-analysis of available VGH data has already been accomplished. This included not only a substantial sample of the airline data, but also data from military operations at the higher altitudes. The analysis utilized the original Δn measurements from the VGH records; these were immediately converted to y/\bar{A} form and plotted vs $N(y)/N_0$.

Since P_1 , P_2 , b_1 , and b_2 follow directly from the intercept and slope of such curves, the determination of U_{de} 's was bypassed; thus it was unnecessary to assume average airplane characteristics in converting the U_{de} exceedance data to σ_w form, as had been done in TN 4332.

The difference between the ASD TR 61-235 and the TN 4332 σ_w distributions was found not to be great. However, the ASD TR 61-235 distributions do tend to be somewhat less severe. As indicated in Section 5.6, this is in the direction necessary to achieve the best agreement between analytically predicted and measured Δn exceedance for the three airplanes considered in this study.

In view of these advantages, a decision was reached to base the σ_w distributions to be used in the present study on those presented in ASD TR 61-235.

Certain modifications, however, to the b and P values presented therein were considered necessary. As a minimum, the b_1 and b_2 values quoted required modification to account for the difference in spectrum shape. In addition, it was considered desirable to make other simple changes, in order to place the determination on a slightly more rational basis and to eliminate at least a part of the conservatism believed still to be present.

The computation of the modified b_1 and b_2 values from those given in ASD TR 61-235 is shown in Tables 5-1 and 5-2. The computations require certain assumptions as to airplane characteristics, and for this purpose the Table Ia and Table Ib airplanes of TN 4332 are assumed. These two airplanes have quite similar gust response characteristics; for consistency with TN 4332, however, the Table Ia airplane is used for determining modified b_1 values and the Table Ib airplane for the b_2 values.

The modification of the b_1 and b_2 values is based on a consideration of how these quantities are determined from the original Δn data. For a given altitude band, frequency of exceedance of Δn would be plotted, on a log scale, vs Δn . This plot would be made in the generalized form of $N(y)/N_0$ vs y/\bar{A} by dividing exceedances by N_0 and Δn 's by \bar{A} . On the semi-log coordinates, the non-storm and storm contributions will each plot as straight lines. P_1 and P_2 are given by the intercepts of these lines with the vertical axis; and b_1 and b_2 are proportional to the reciprocals of the slopes. Consequently, the numerical values obtained for b_1 and b_2 will be inversely proportional to the \bar{A} value used in obtaining the plot.

In both TN 4332 and ASD-TR-61-235, \bar{A} is obtained by means of the equation,

$$\bar{A} = \frac{\rho C_{L_a} S V_T}{2W} K_\sigma \quad (5-5)$$

The dimensionless coefficient K_σ is evaluated using simple theory, on the assumption that the airplane is rigid and free to plunge (move vertically) but not pitch. The resulting \bar{A} values may, however, be adjusted by estimated factors to account for the effects of elastic mode response and freedom in pitch.

Plots of K_σ as a function of a dimensionless mass parameter and of the ratio of scale of turbulence to mean wing chord are given in Figure 7

TABLE 5-1. RE-EVALUATION OF PARAMETER b_1 BASED
ON ASD TR 61-235 DATA

(1)	(2)	(3)	(4)	(5)	(6)	(7)	(8)	(9)
h Ft.	b_1 ASD TR 61-235	L	Pratt μ_g	$\bar{\mu}$	K_σ Liepmann	K_σ Isotropic, $L = 2500$ FT	$\frac{K_\sigma L}{1.15 K_{\sigma I}}$	b_1
	ASD TR 61-235 Table I		TN4332 Table Ia	(4) 1.15	Function of (3) & (4) TR 1272, Fig. 7	Function of (5) Fig. 3-2	(6) 1.15 (7)	(2) (8)
0-1000	2.72	500	20.6	17.90	.570	.345	1.435	3.903
1000-2500	2.77	750	21.3	18.51	.530	.350	1.316	3.64
2500-5000	2.86	930	22.6	19.64	.495	.360	1.195	3.42
5000-10000	3.02	1000	25.4	22.07	.515	.376	1.190	3.59
10000-20000	2.86	1000	32.3	28.1	.562	.427	1.144	3.27
20000-30000	2.75	1000	45.4	39.5	.635	.482	1.144	3.15
30000-40000	2.62	1000	65.5	57.0	.700	.544	1.119	2.93
40000-50000	3.07	1000	105.0	91.8	.775	.63	1.069	3.28
50000-60000	3.75	1000	170.0	148.0	.830	.708	1.019	3.82
60000-70000	2.95	1000	266.0	231.3	.875	.767	.992	2.93

Data Assumed: $\bar{W} = 77000$ lb; $S = 1463$ ft²; $\bar{c} = 13.7$ ft; $C_{Lg} = 4.95$ per radian (wing alone)
and (1.15) (4.95) = 5.70 per radian (airplane); isotropic turbulence spectrum,
 $L = 2500$ Ft.

TABLE 5-2. RE-EVALUATION OF PARAMETER b_2 BASED
ON ASD TR 61-235 DATA

①	②	③	④	⑤	⑥	⑦	⑧	⑨
h Ft.	b_2 ASD TR 61-235	L	Pratt μ_g	$\bar{\mu}$	K_G Liepmann	K_G Isotropic, $L=2500$ ft	K_{GL} $1.15 K_{GI}$	b_2
	ASD TR 61-235 Table I		TN4332 Table Ib	④ 1.15	Function of ③ & ④ TR 1272, Fig. 7	Function of ⑤ Fig. 5-2	⑤ 1.15 ⑦	② ⑧
0-1000	5.44	500	23.7	20.59	.575	.350	1.427	7.76
1000-2500	6.06	750	24.5	21.29	.510	.355	1.248	7.56
2500-5000	7.17	930	26.0	22.59	.485	.370	1.114	8.17
5000-10000	8.16	1000	29.15	25.33	.495	.380	1.13	9.22
10000-20000	9.20	1000	37.1	32.3	.546	.415	1.143	10.52
20000-30000	10.35	1000	52.0	45.2	.620	.469	1.148	11.88
30000-40000	8.78	1000	75.4	65.6	.688	.533	1.121	9.84
40000-50000	8.13	1000	121.0	105.2	.766	.614	1.084	8.61
50000-60000	6.77	1000	195.4	170.0	.830	.694	1.04	7.04
60000-70000	4.51	1000	306.3	266.2	.843	.762	.961	4.33

Data Assumed: $W = 30000$ lb; $S = 662.4$ ft²; $\bar{c} = 10.5$ ft; $C_{L\alpha} = 4.83$ per radian (wing alone)
and (1.15) (4.83) = 5.55 per radian (airplane);
isotropic turbulence spectrum, $L = 2500$ Ft.

of NACA Report 1272 (Reference 5), based on theory developed by Fung in Reference 16. Similar curves, utilizing more exact expressions for the unsteady lift growth functions, are given in Figure 70 of ASD TR 61-235 and were used therein. Both of these sets of curves assume the Liepmann shape of power-spectral density function. For use with the isotropic turbulence spectral shape, a new set of curves has been obtained. These are shown in Figure 5-2. The assumptions regarding lift growth are the same as for the curves in TR 1272.

The spectral shape affects \bar{A} only through the coefficient K_G , and it is clear that b_1 and b_2 vary inversely as K_G . In Tables 5-1 and 5-2, the K_G curves in NACA TR 1272 and in Figure 5-2 herein are used to determine the K_G ratio. It should be remarked, incidentally, that in TR 1272 the mass parameter is defined in terms of an assumed lift curve slope of 2π ; in the computations in Tables 5-1 and 5-2, however, as well as in the original evaluation of b_1 and b_2 in ASD TR 61-235, the same value of lift curve slope selected for use explicitly in Equation 5-5 was also used in evaluating the mass parameter.

In the ASD TR 61-235 determination of b_1 and b_2 values (as well as in the TN 4332 determination), the lift curve slope, CL_a , was based upon an approximate formula that gives an excellent approximation to the wing lift curve slope but underestimates the airplane lift curve slope by some 15%. The airplane lift curve slope would appear to be the more rational one to use. Also, it leads to lower values of b_1 and b_2 , which, as noted above, are desirable. Consequently, the \bar{A} ratio in Tables 5-1 and 5-2 includes also a 1.15 factor to account for the greater CL_a believed to be realistic. This increased CL_a is, of course, also used in evaluating the mass parameter.

No correction for pitch is included. Response calculations for the Model 749 with and without a pitch freedom indicate roughly a 7% reduction in \bar{A} due to pitch. This percentage is quite small, and the exact value obtained will depend somewhat on the extent to which it is desired to include, at the same time, differences in the unsteady lift growth functions between those assumed in the simple "Fung" analysis and those applied on the various components in the more refined analyses. Furthermore, the pitch effect on the Model 749 undoubtedly differs somewhat from that of other airplanes from which VGH results were obtained for use in ASD TR 61-235. As a result of these considerations, it is believed desirable to ignore the effect of pitch.

(It might be remarked that the correction necessary to account for pitch effects can be minimized by appropriate selection of lift curve slope in the plunge-only analysis. If wing-alone lift curve slope had been used instead of airplane lift curve slope, the indicated correction for pitch would have been comparable in magnitude, although opposite in direction.

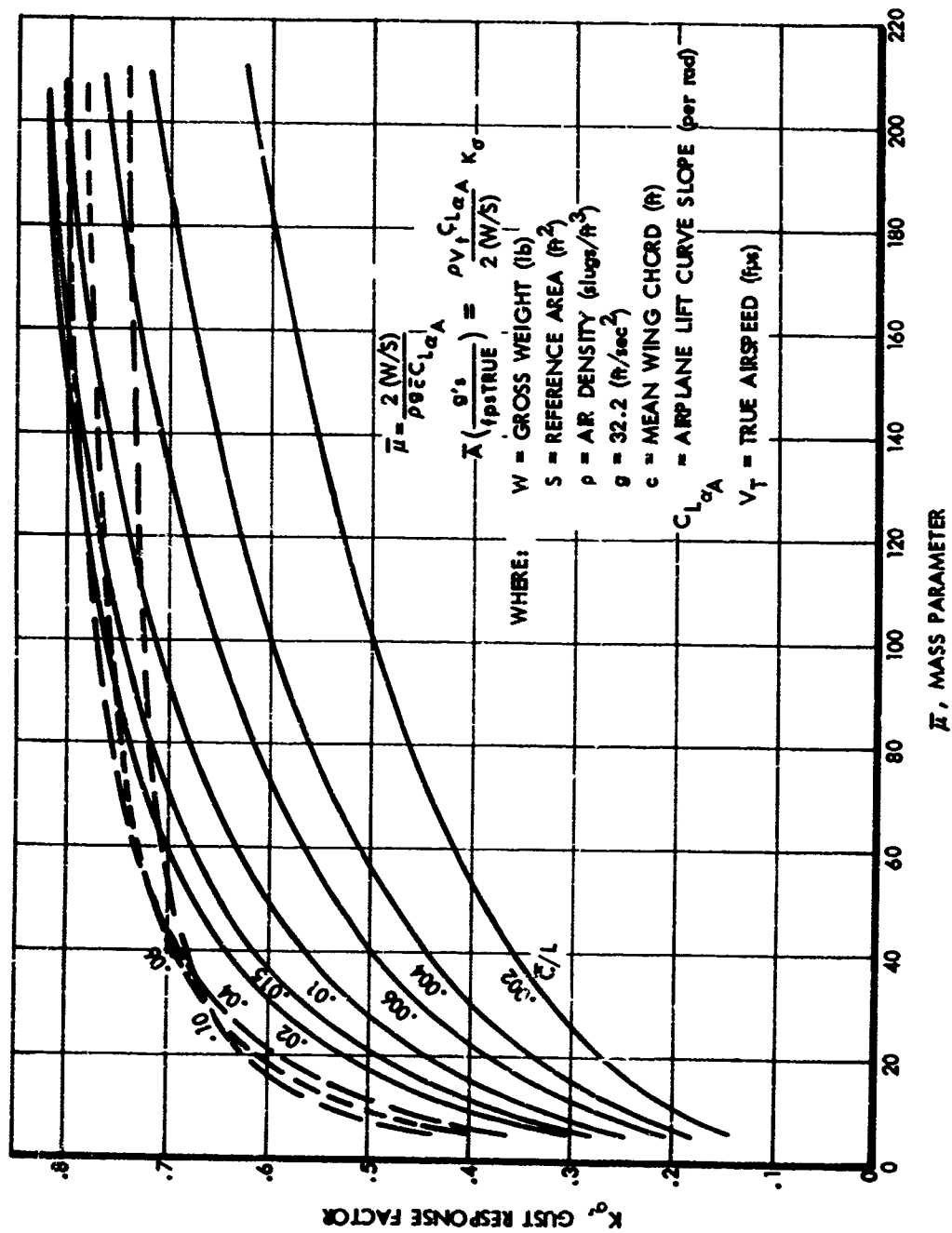
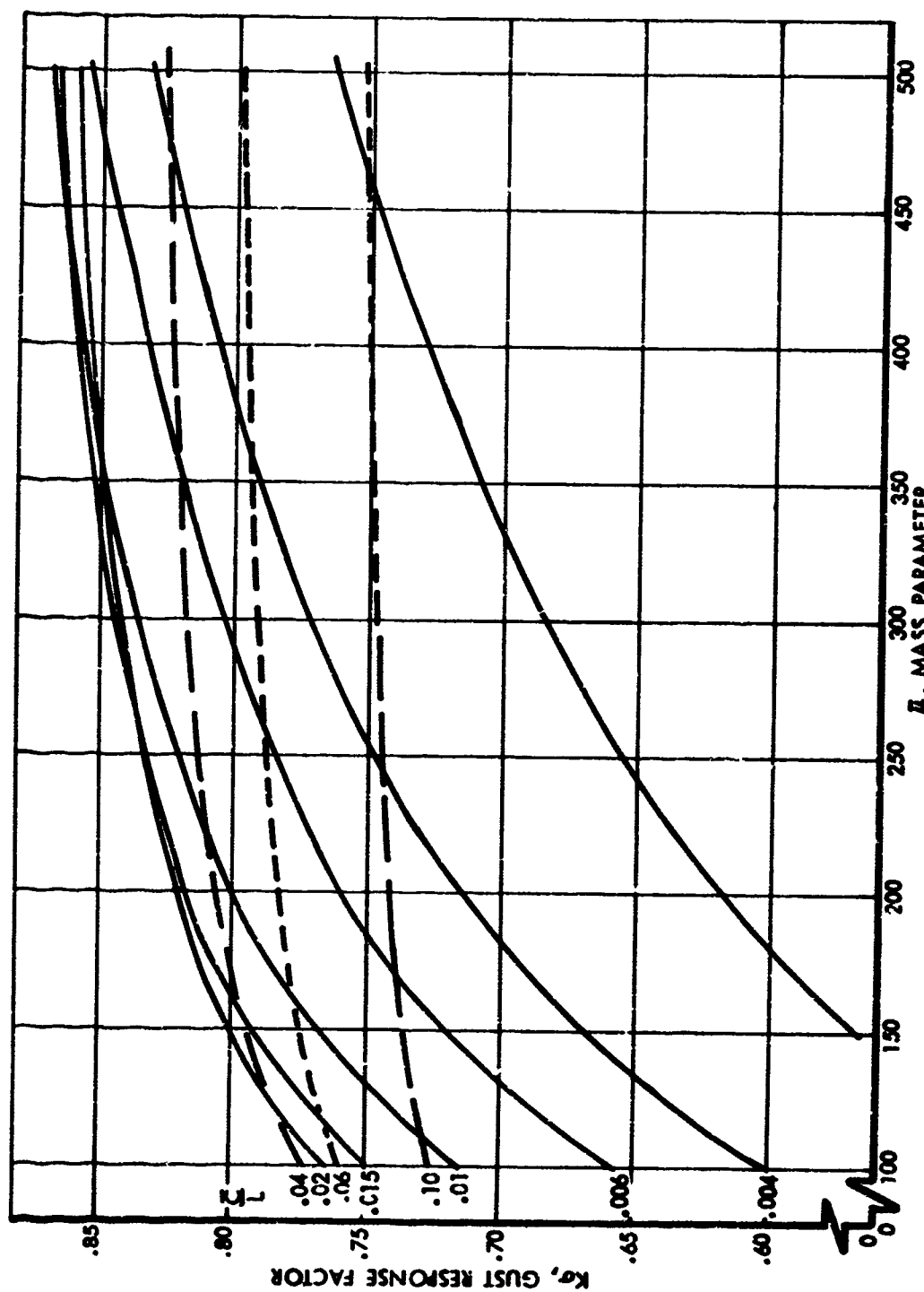


FIGURE 5-2. GUST RESPONSE FACTOR FOR ISOTROPIC TURBULENCE SPECTRUM



(b) $\bar{\mu} = 100$ TO 500
FIGURE 5-2. CONCLUDED

Therefore, in this instance the criterion of a minimum correction for pitch was not helpful in selecting the basis for lift curve slope.)

No correction for elastic mode response is included in Tables 5-1 and 5-2, as this is considered to have been adequately accounted for in the original work. In the calculation of b_1 and b_2 values in ASD TR 61-235, calculated dynamic factors were used for the DC-6 and DC-7 airplanes. For all other airplanes it was reasonably assumed either that the dynamic factor was negligible or that the dynamic factor, static flexibility effect on lift curve slope, and pitch effect were mutually offsetting.

With the foregoing as background, the computations made in Tables 5-1 and 5-2 to obtain modified b values are self-explanatory.

P_1 and P_2 are also modified. The ASD TR 61-235 determination, like that in TN 4332, utilized estimated N_0 values of .7 for non-storm turbulence and .5 for storm turbulence. On the other hand, calculated values for typical airplanes (Lockheed Model 749 and Model 188 and also the Boeing 707/720 series) average about 1.1 cps. Consequently, the TN 4332 P_1 values are multiplied by .7/1.1 and the P_2 values by .5/1.1.

The resulting P_1 , P_2 , b_1 , and b_2 values are plotted as functions of altitude in Figures 5-3 and 5-4. These curves, in conjunction with the given shape of power-spectral density function, constitute the required model of the atmosphere.

Generalized exceedance curves reflecting these P and b values are shown in Figure 5-5. It is suggested that these curves not be used for actual computations, because of the non-linearity of the interpolation between adjacent curves. Instead, P and b values should be read from Figures 5-3 and 5-4.

As a matter of interest, comparisons of the TN 4332 and ASD TR 61-235 σ_w distributions are shown in Appendix A. These are in the form of plot vs altitude of the respective P and b values, and also as comparisons of the respective generalized exceedance curves at various altitudes. The comparisons are shown first for the probability distributions exactly as defined in these two documents. The comparisons are then repeated based on the distributions with appropriate modifications, comparable to those described above for the ASD TR 61-235 distributions. On either basis, it is found that the differences in the b and P values appear rather great, but that the resulting generalized exceedance curves show much closer agreement. At frequencies of exceedance in the vicinity of limit strength ($N(y)/N_0 = 10^{-8}$ to 10^{-6}), and over the altitude range of primary interest, the ASD TR 61-235 distributions are slightly less severe than the TN 4332 distributions, as desired.

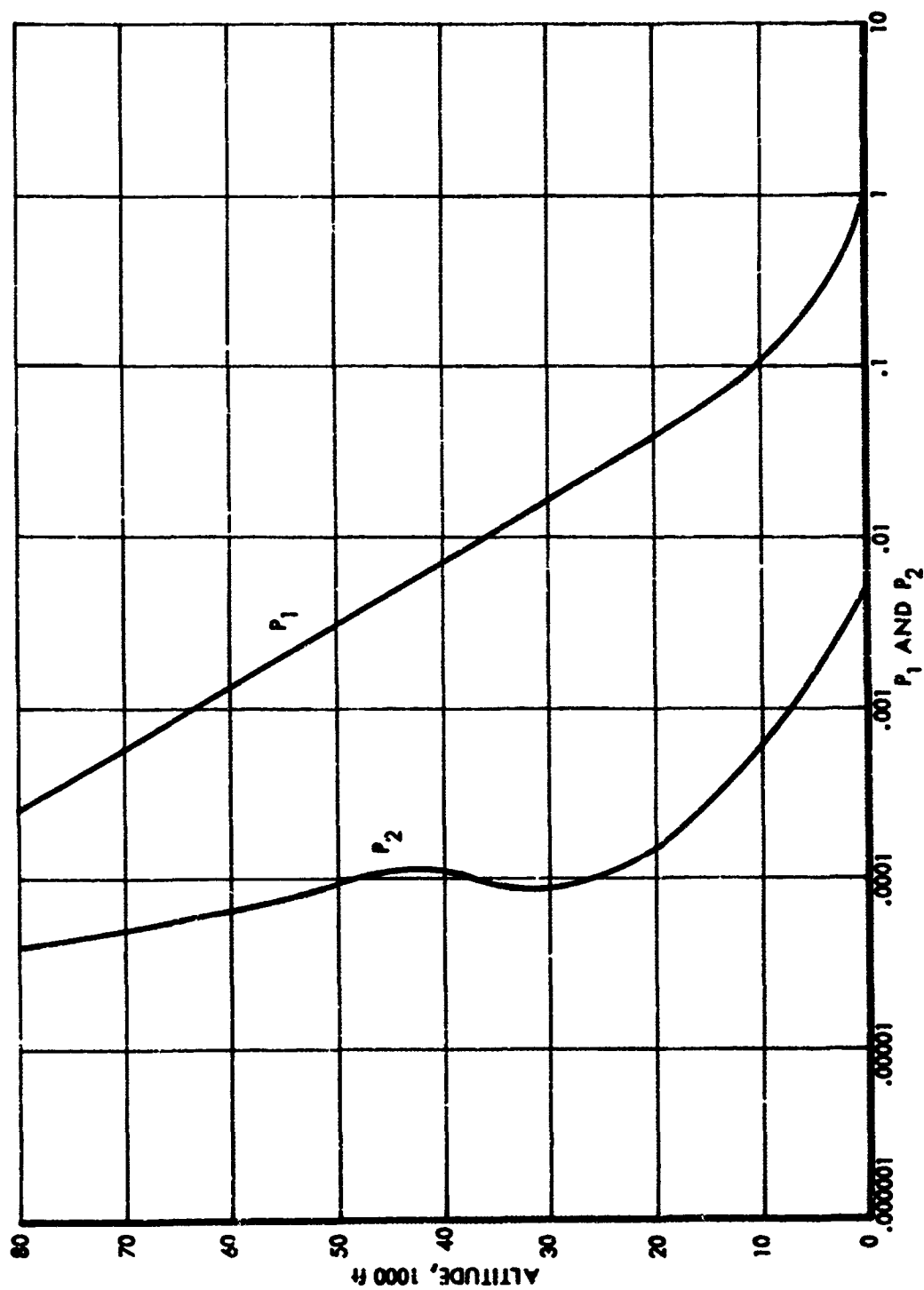


FIGURE 5-3. P_1 AND P_2 VALUES SELECTED FOR USE IN PRESENT STUDY

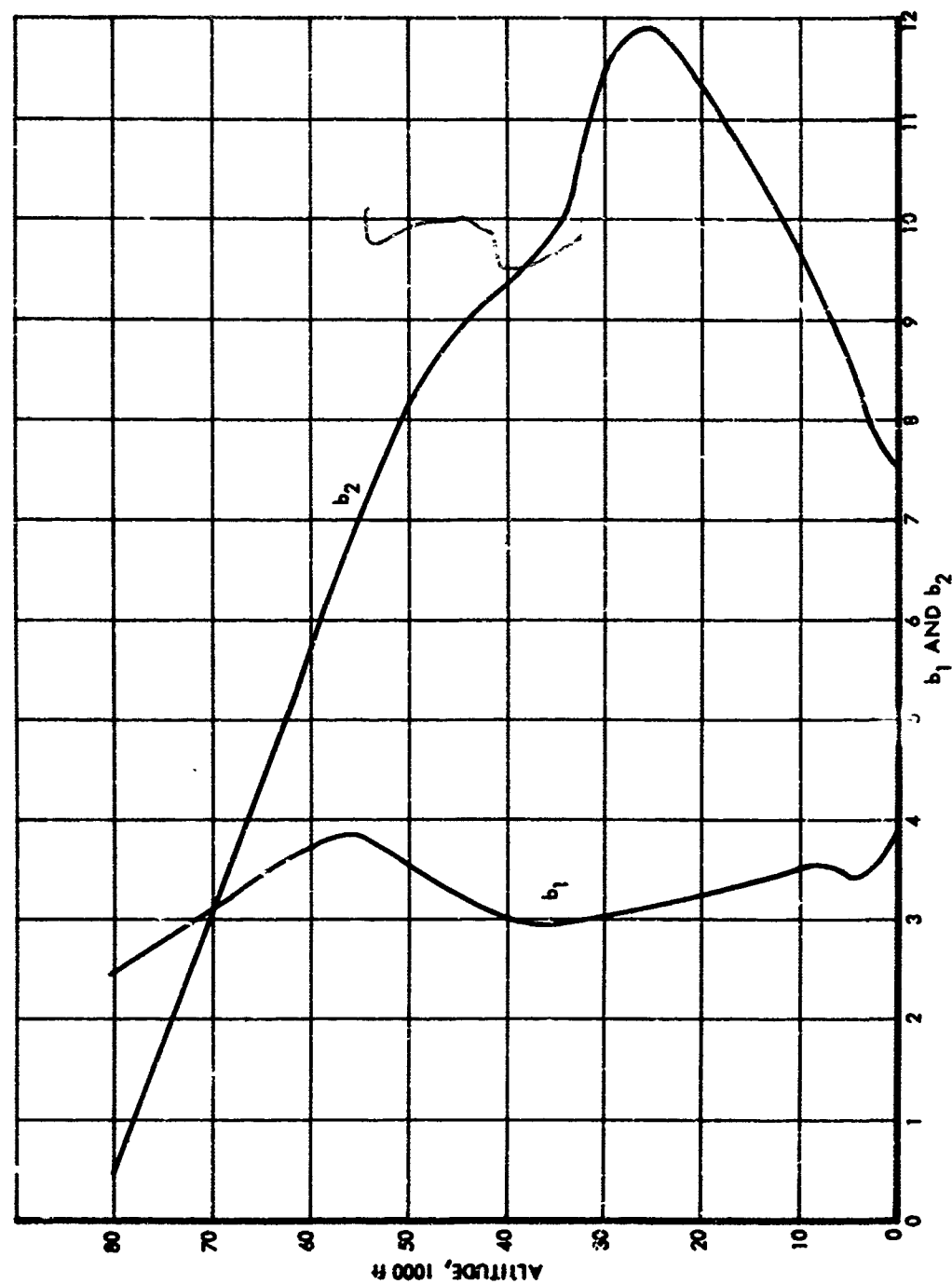


FIGURE 5-4. b_1 AND b_2 VALUES SELECTED FOR USE IN PRESENT STUDY

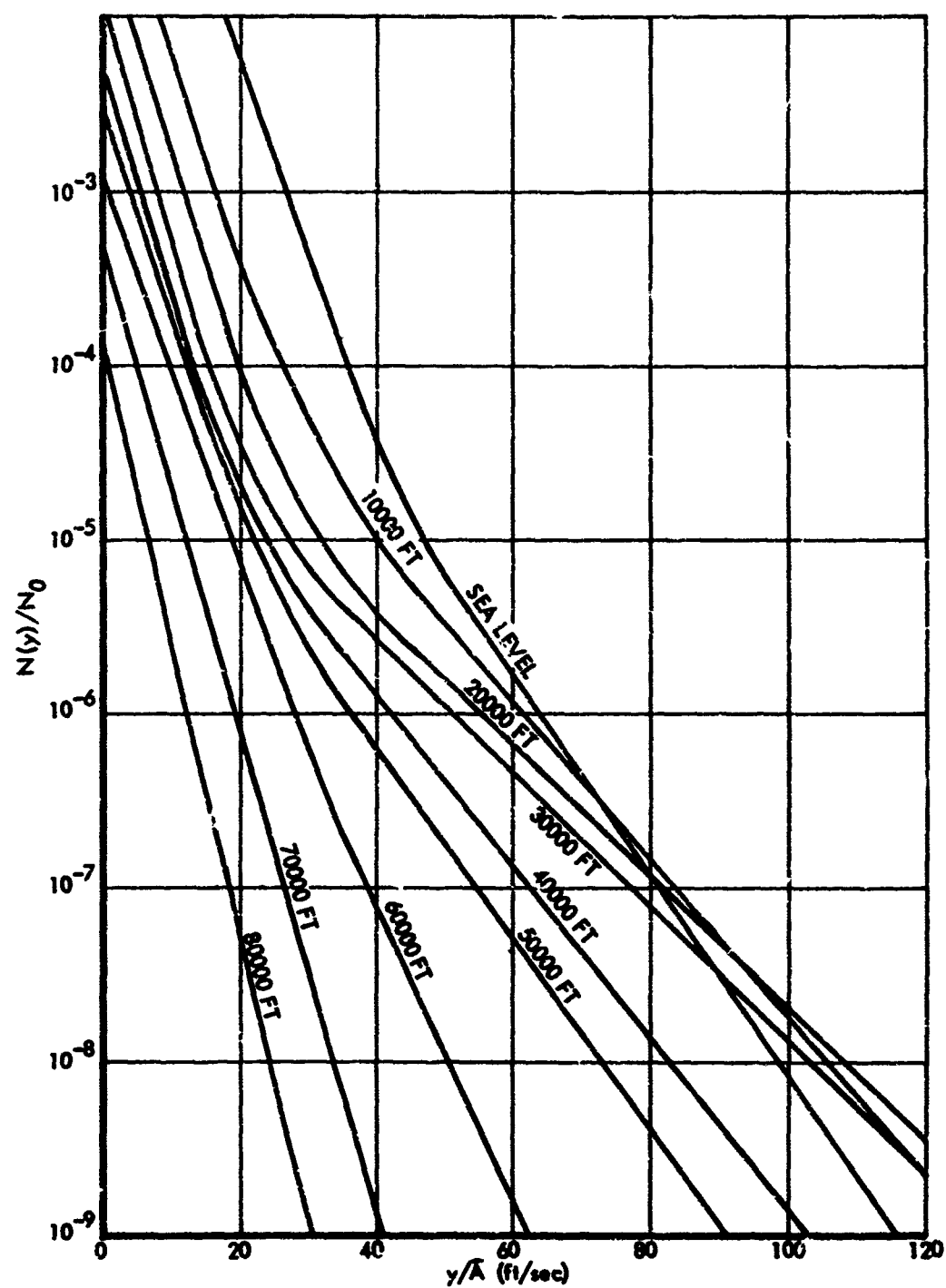


FIGURE 5-5. GENERALIZED EXCEEDANCE CURVES REFLECTING σ_w DISTRIBUTIONS USED IN PRESENT STUDY

5.4 Lateral-Gust σ_w Distributions

Evidence to date is that atmospheric turbulence tends strongly to be isotropic, except within a few hundred feet of the ground. (See, for example, Reference 14.) As a result, σ_w distributions obtained from vertical gust measurements are considered to apply equally to the lateral component of turbulence.

For convenience, the symbol σ_w is applied in this report to the lateral as well as the vertical component of turbulence, despite the origin of the subscript w as a velocity in the z direction.

5.5 Generalized Exceedance Curves for Use With Design Envelope Criterion

To assist in defining design values of $\sigma_w \eta_d$ for use in the design envelope form of criterion, generalized exceedance curves are plotted in a different form in Figure 5-6. Instead of plotting $N(y)/N_0$ vs y/\bar{A} for various altitudes, as in Figure 5-5, y/\bar{A} is now plotted vs altitude for various values of $N(y)/N_0$. The resulting curves are shown by the dash lines in Figure 5-6.

These curves are then simplified for design use as indicated by the solid lines. Because of the complete absence of data above 80000 ft., the curves are conservatively defined for design use by constant y/\bar{A} values above this altitude. As an aid in evaluating the fairing of the curves, the same curves are transformed from a true gust velocity basis to an equivalent gust velocity basis in Fig. 5-7 (i.e., if \bar{A} is defined as σ_y/σ_{wtrue} , in accordance with usual practice, use Fig. 5-6; if \bar{A} is defined as $\sigma_y/\sigma_{wequiv.}$, which would correspond more closely to the usual discrete gust treatment, use Fig. 5-7.) The waviness appearing in the dash lines in Figures 5-6 and 5-7 does not necessarily indicate improper fairing of the P_1 , P_2 , b_1 , and b_2 data in Figures 5-3 and 5-4. It is interesting to note, for example, that the particular bend in the curves at 15000 ft. bears a similarity to the U_{de} data shown in Fig. 8 of NASA TN D-29 (Reference 17). In TN D-29 the U_{de} 's in the 15000 - 20000 ft. band are markedly lower than the trend indicated by the other altitude bands. In the determination of b's and P's in TN 4332, however, the departure from the general trend in the 15000 - 20000 ft. band was faired out. Although the waviness shown by the dash lines is perhaps, therefore, a true reflection of the atmosphere, a rather gross fairing appears appropriate for use in a design envelope criterion. The fact that the airplane must be designed for a range of altitudes tends to compensate for the fact that in some narrow altitude bands less strength might actually be required than indicated by the criterion.

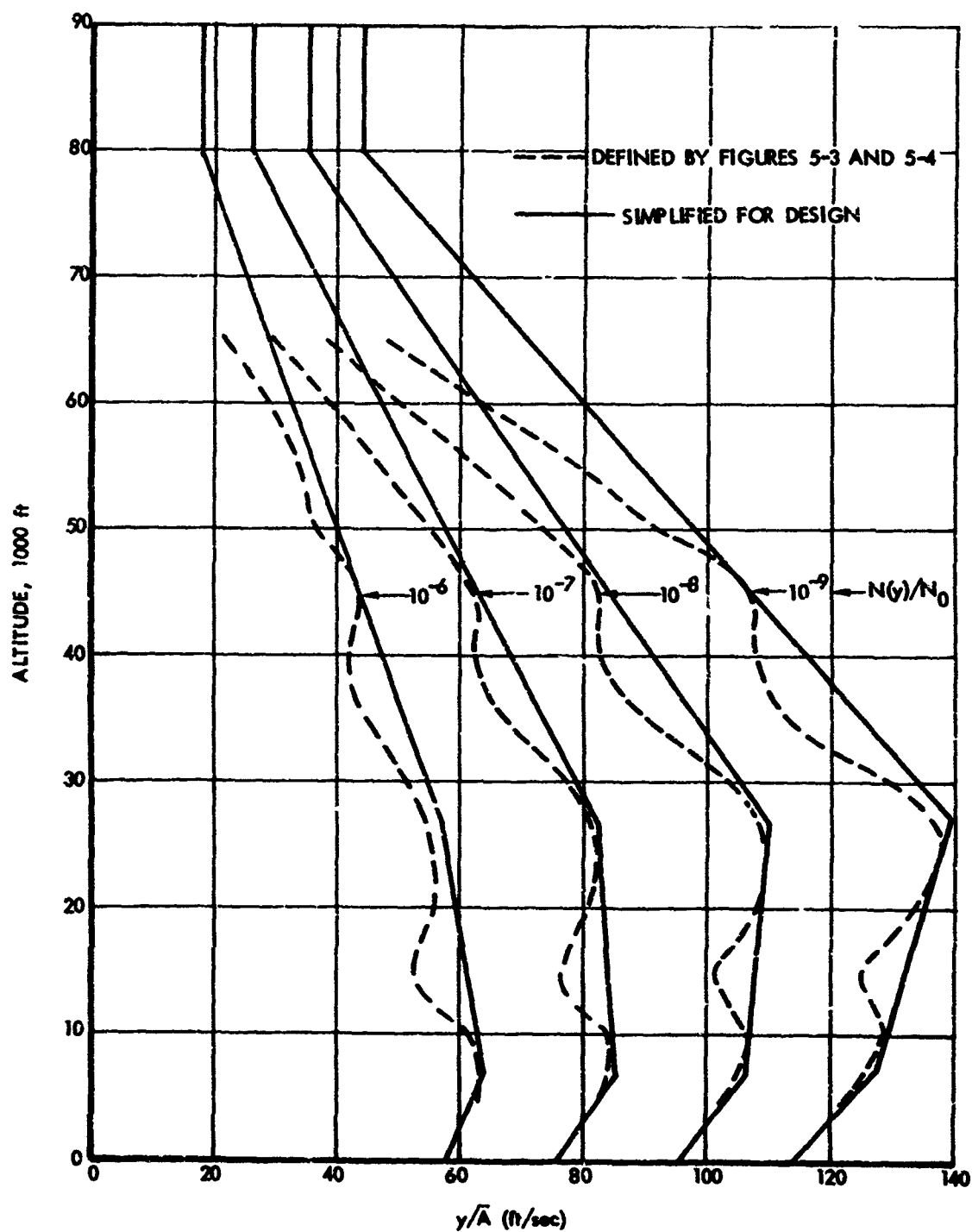


FIGURE 5-6. VARIATION OF y/\bar{A} WITH ALTITUDE FOR CONSTANT $N(y)/N_0$

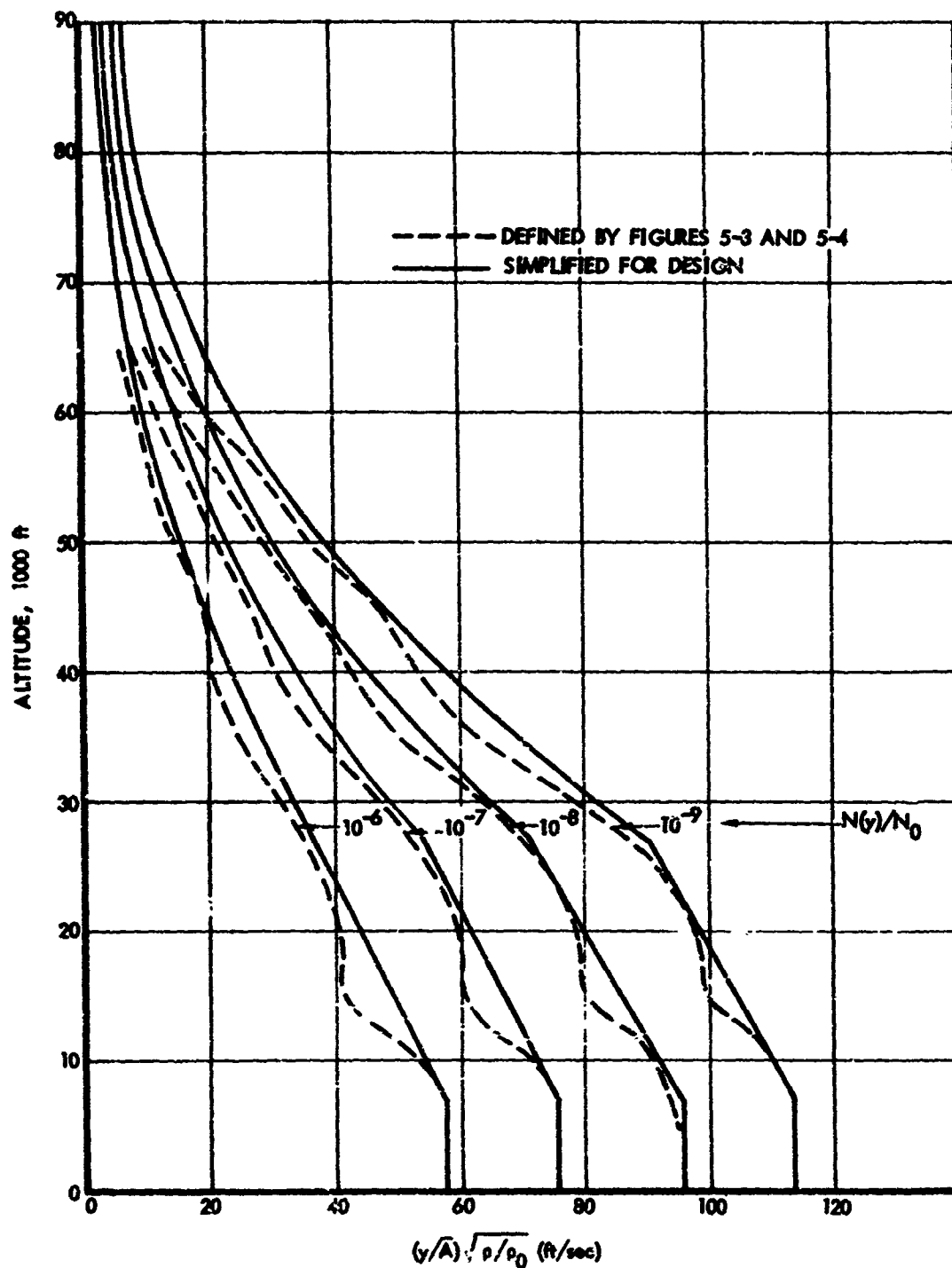


FIGURE 5-7. VARIATION OF $(y/A) \sqrt{\rho/\rho_0}$ WITH ALTITUDE FOR CONSTANT $N(y)/N_0$

The simplified curves in Figures 5-6 and 5-7 are used only in connection with the design envelope criterion; in the mission analysis approach, the data reflected by the dash lines in these figures are retained.

For use in later portions of this report, the solid lines of Figure 5-6 are repeated in Figure 5-8. Intermediate curves are added to facilitate interpolating, and the range is extended to higher load levels. (This extension is by linear extrapolation, which is valid because of the linearity of the $N(y)/N_0$ vs y/\bar{A} curves in this region, as indicated in Figure 5-5). As these curves are intended to be used to establish design levels, the abscissas are relabeled $\sigma_w \eta_d$, the design load equivalent of y/\bar{A} (Section 4-2).

5.6 VGH and VG Comparisons

A qualitative check of the atmospheric model derived above can be obtained by comparing airplane c.g. exceedance curves calculated for the three reference airplanes, using the model, with curves obtained from VG and VGH measurements.

Such comparisons are shown in Figures 5-9, 5-10, and 5-11. The "mission analysis" curves are based upon the results given in Section 9 and Appendix B for the three reference airplanes. VG and VGH data were taken from the sources indicated (References 9, 17, and 18), but were changed to the form of cumulative exceedances of positive load factor per hour for this comparison.

Inasmuch as neither VG nor VGH data are available for the Model 720B, the VGH curve shown is for a Model 707-300. This curve is then adjusted to reflect differences in operating usage between the 707-300 and the 720B. The ratio by which the 707-300 exceedances were increased to compare with the 720B was obtained by recalculating the 720B exceedances using weighting factors for the five flight profiles representative of 707-300 operations. Dividing the exceedances calculated using the actual 720B weighting factors by the exceedances calculated using the 707-300 weighting factors gives a ratio of 1.37; this was then applied to the 707-300 exceedances obtained from the VGH data.

It might be remarked that, for the Model 749, the descent speeds used in the analysis were slightly lower than prevailed at the time the accelerations were measured (see Section 6.2); if consistent descent speeds had been used, the solid line in Figure 5-9 would have moved slightly to the right.

In Figures 5-9 through 5-11, it is seen that the agreement between predicted and measured data, although not perfect, is sufficiently close to indicate that the choice of atmospheric model is reasonable.

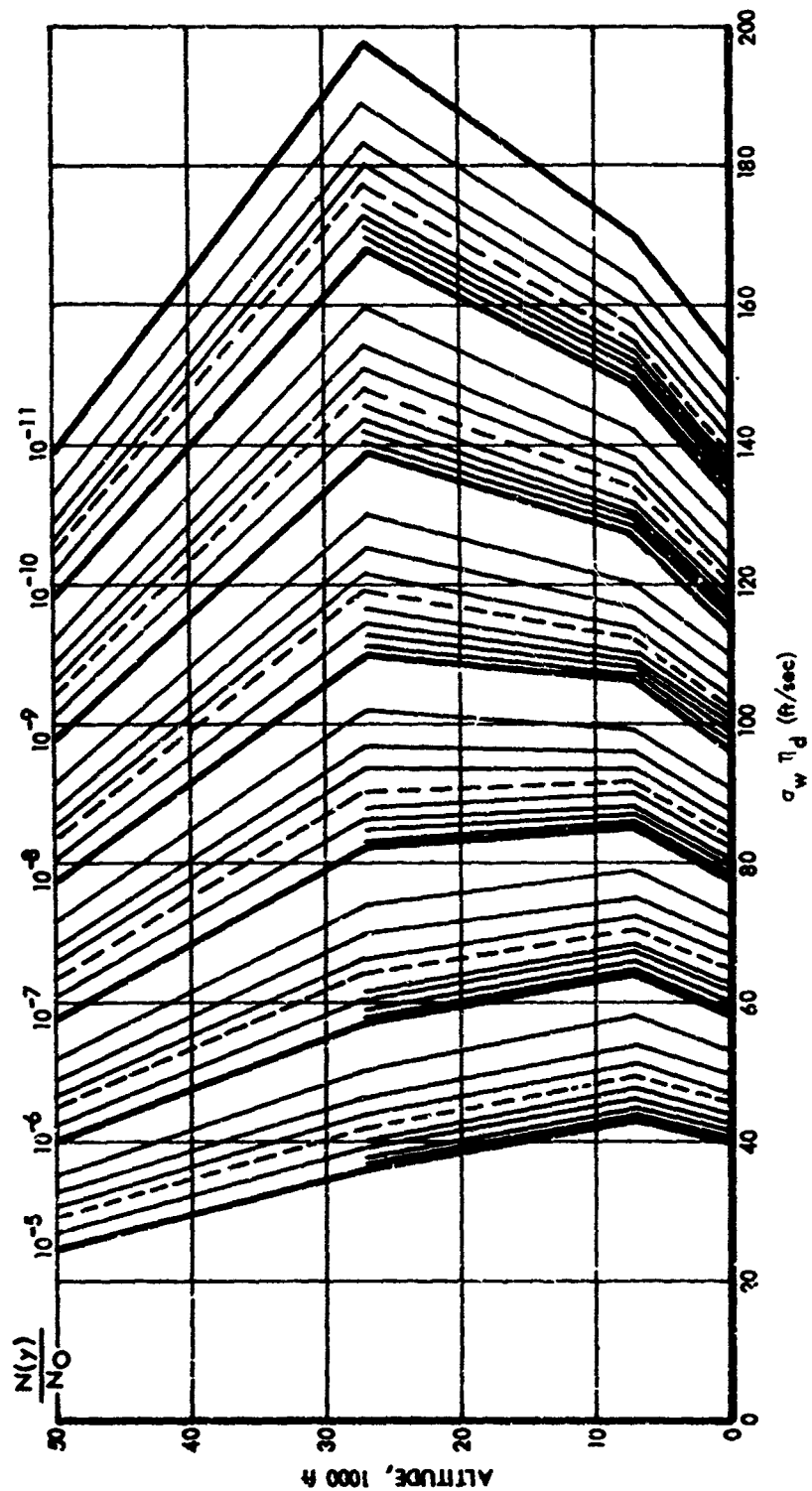


FIGURE 5-8. VARIATION OF $\sigma_w \eta_D$ WITH ALTITUDE

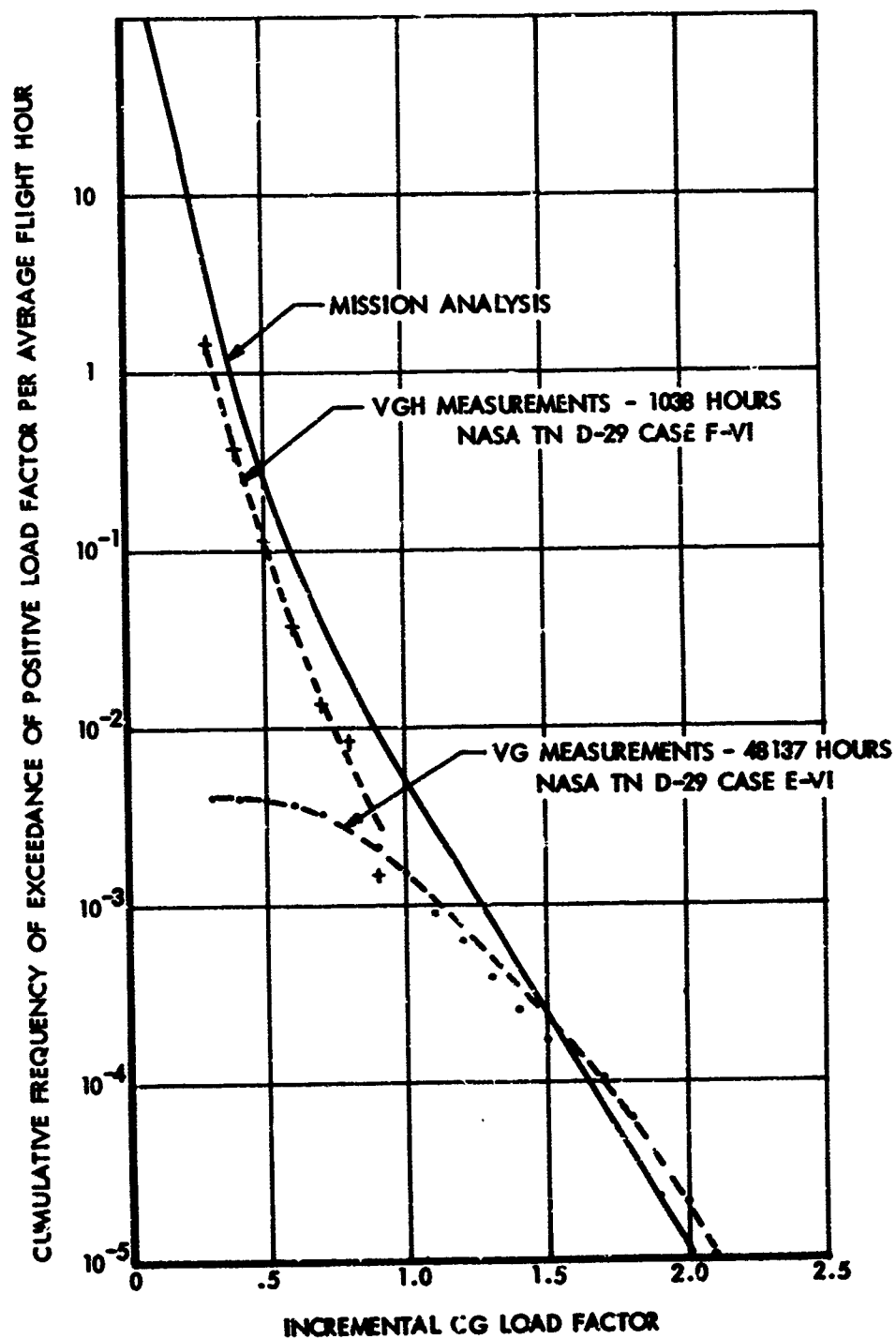


FIGURE 5-9. COMPARISON OF PREDICTED WITH MEASURED LOAD FACTOR EXCEEDANCES, MODEL 749

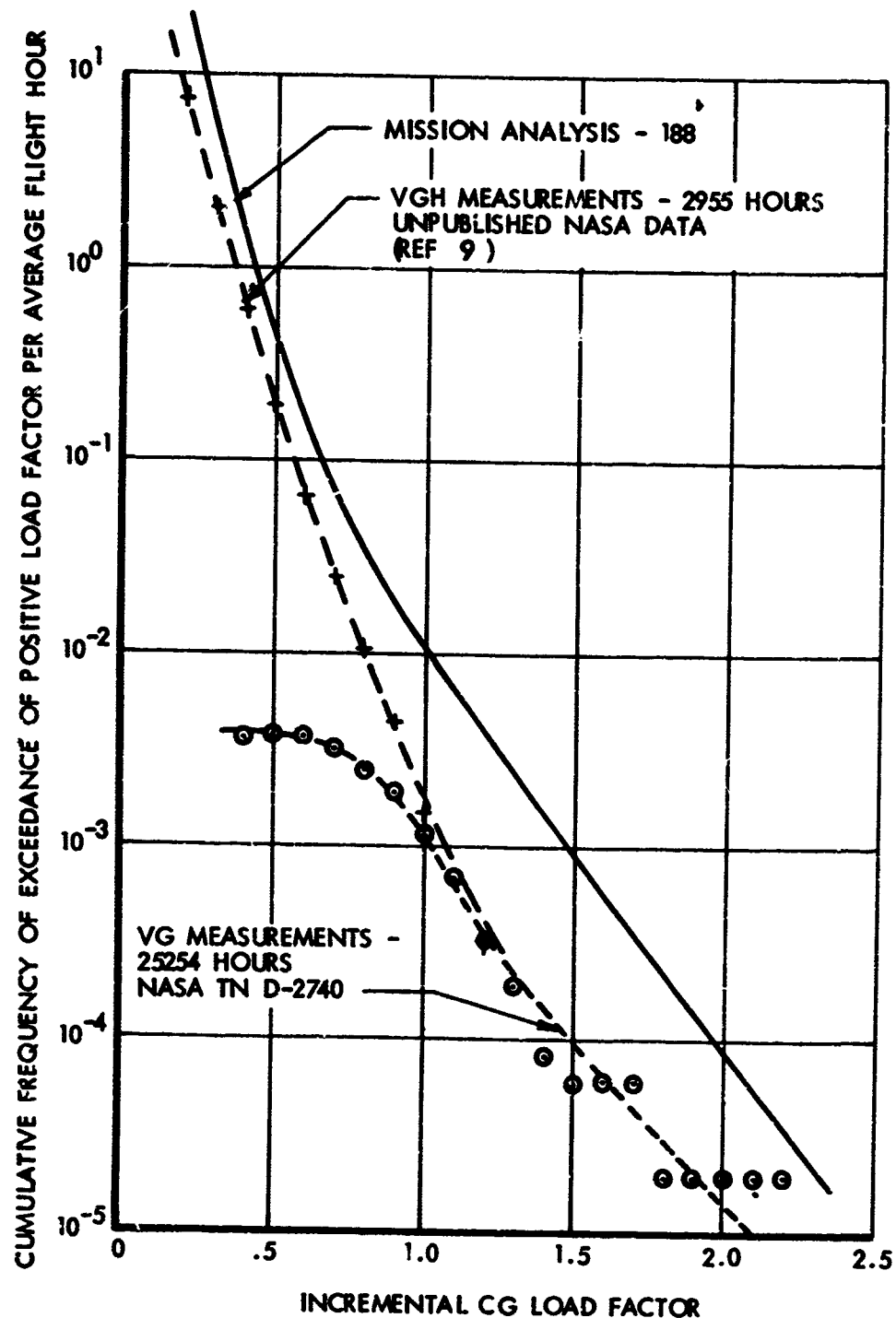


FIGURE 5-10. COMPARISON OF PREDICTED WITH MEASURED LOAD FACTOR EXCEEDANCES, MODEL 188

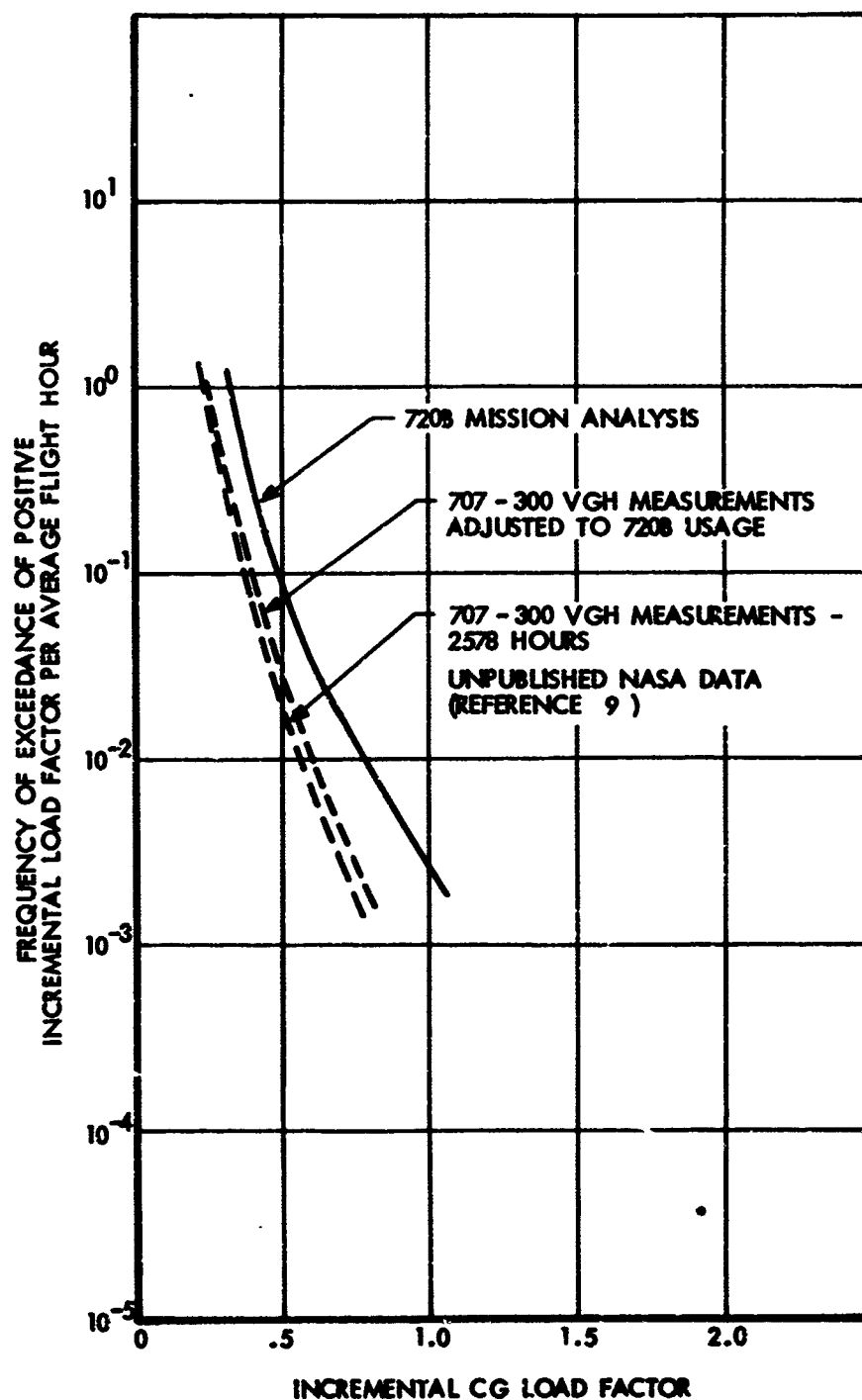


FIGURE 5-11. COMPARISON OF PREDICTED WITH MEASURED LOAD FACTOR EXCEEDANCES, MODEL 720B

Generally, the computed accelerations are somewhat greater than the measured, indicating a somewhat conservative model. The various steps taken to reduce the severity of the model, described earlier, thus appear to be well justified.

5.7 Future Improvements

It is generally recognized that further work to improve the atmospheric models currently available would be highly desirable. The appropriate shape for the power-spectral density function and value of the scale of turbulence are still matters of conjecture; and much greater confidence in the σ_w distributions would result if these were rederived from the vast store of available VG and VGH data utilizing directly \bar{A} and N_0 values obtained from dynamic analyses of the respective airplanes.

However, it must be borne in mind that the design levels ($N(y)$ and $\sigma_w \eta_d$) obtained as a result of the present study are based upon analysis of existing satisfactory airplanes, using the particular model of the atmosphere defined herein. Changes in the atmospheric model would ordinarily require changes in the design levels, and definition of the revised levels would be likely to require extensive reanalysis of the reference airplanes.

Any changes whatever in the shape of the power-spectral density function, including a change in the value of the scale of turbulence, would clearly require such reanalysis.

Changes in the b and P values in the altitude range where the reference airplanes operate would also require such reanalysis. However, the greatest uncertainty in the b and P values is at the higher altitudes, say above 40,000 ft. Improvements in the b and P values in this altitude range could be made freely, as the limit strength values of $N(y)$ and $\sigma_w \eta_d$ for the reference airplanes would not be affected. It is possible, too, that, even at somewhat lower altitudes, changes in the b and P values could be shown not to affect the design levels selected. Consideration would have to be given, in any particular case, to the magnitude of the proposed change, which of the reference airplanes was critical, and at what altitude it was critical.

6 MISSION PROFILES FOR REFERENCE AIRPLANES

6.1 Model 188

The mission profiles for use in the Model 188 mission analysis are based upon the following sources of data:

- (1) NASA VGH statistical data given in References 9, 10, and 11;
- (2) Information gathered from contacts with the various airlines operating Electra airplanes;
- (3) Various published and unpublished Lockheed reports providing weight and operating data on Electra airplanes.

For the purpose of selecting appropriate flight durations, the distribution of flight durations given by Reference 9 is plotted in Figure 6-1. The following three mission durations were selected to represent this distribution:

<u>Duration</u>	<u>% of Flights</u>
40 min.	63
100 min.	28
170 min.	9

The tendency of average cruise altitude to increase with flight duration is depicted in Figure 6-2, which is prepared from data presented in Reference 10. The cruise altitudes appropriate to the three mission durations are read from the faired curve as follows:

<u>Duration</u>	<u>Cruise Altitude</u>
40 min.	11,000 ft.
100 min.	16,000 ft.
170 min.	18,000 ft.

Representative speeds in climb, cruise and descent, based on data in Reference 9, are shown in Figures 6-3 - 6-5 as a function of altitude. (In Reference 9, all speeds quoted are indicated airspeeds; these are assumed equal to equivalent airspeeds.) For the purpose of establishing mission profiles, average speeds are indicated. The average climb speeds are simple averages taken directly from Reference 9. In the cases of cruise and descent, however, the ranges of speed are so great that use of a simple average would be unrealistic. For example, consider the effect on a frequency of exceedance curve for gust loads if a

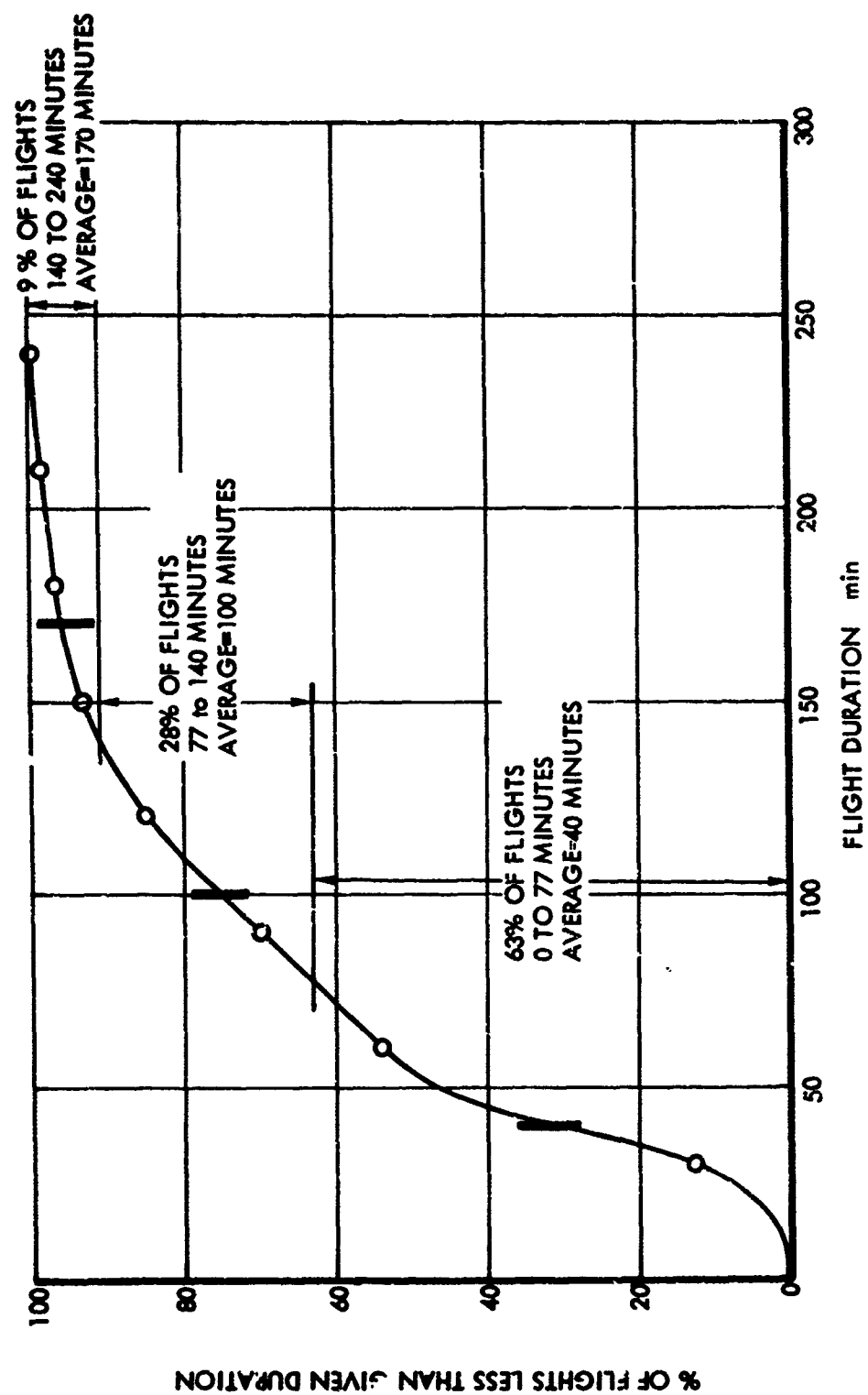


FIGURE 6-1. FLIGHT DURATIONS, MODEL 188

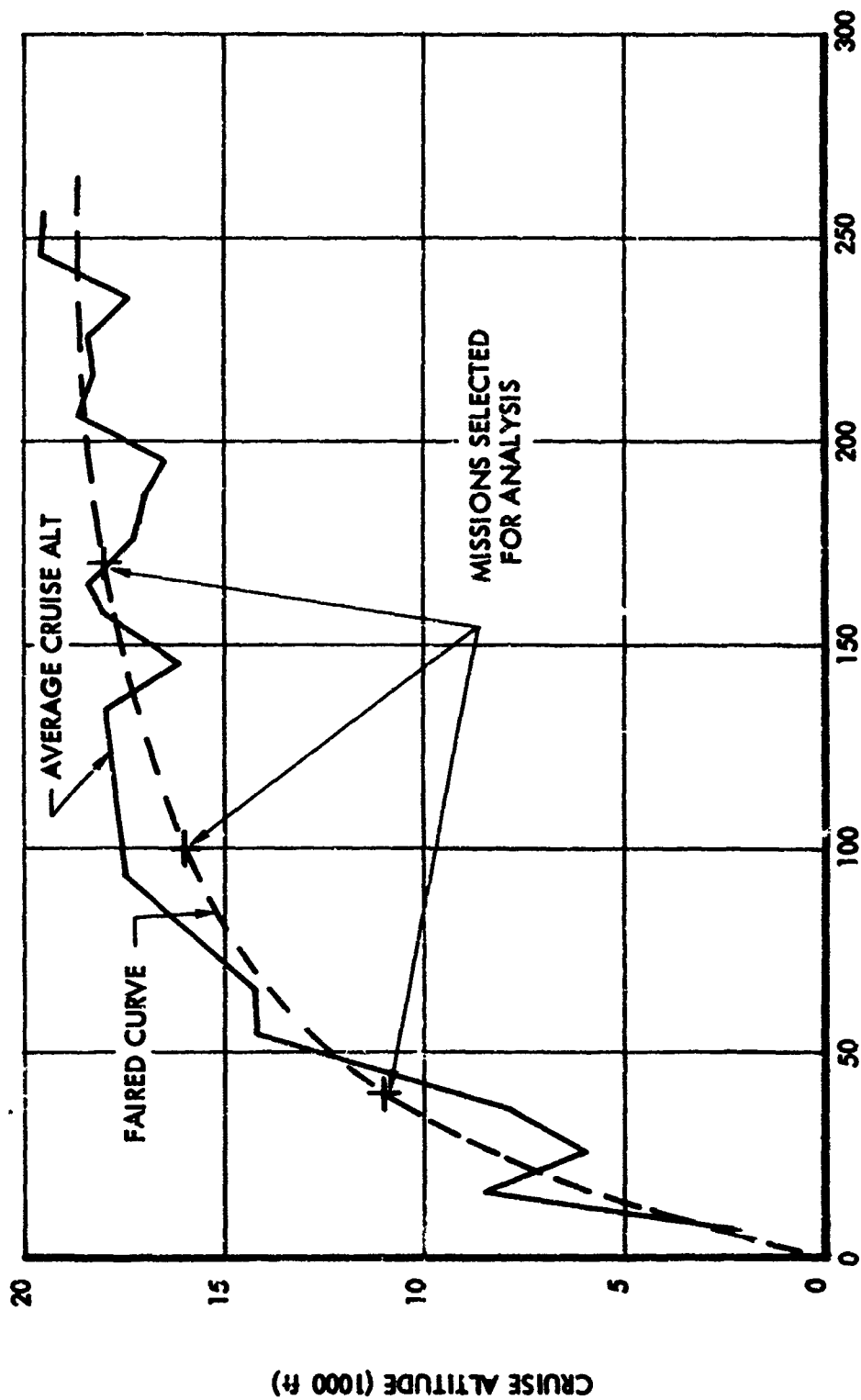


FIGURE 6-2. VARIATION OF AVERAGE CRUISE ALTITUDE WITH FLIGHT DURATION, MODEL 188

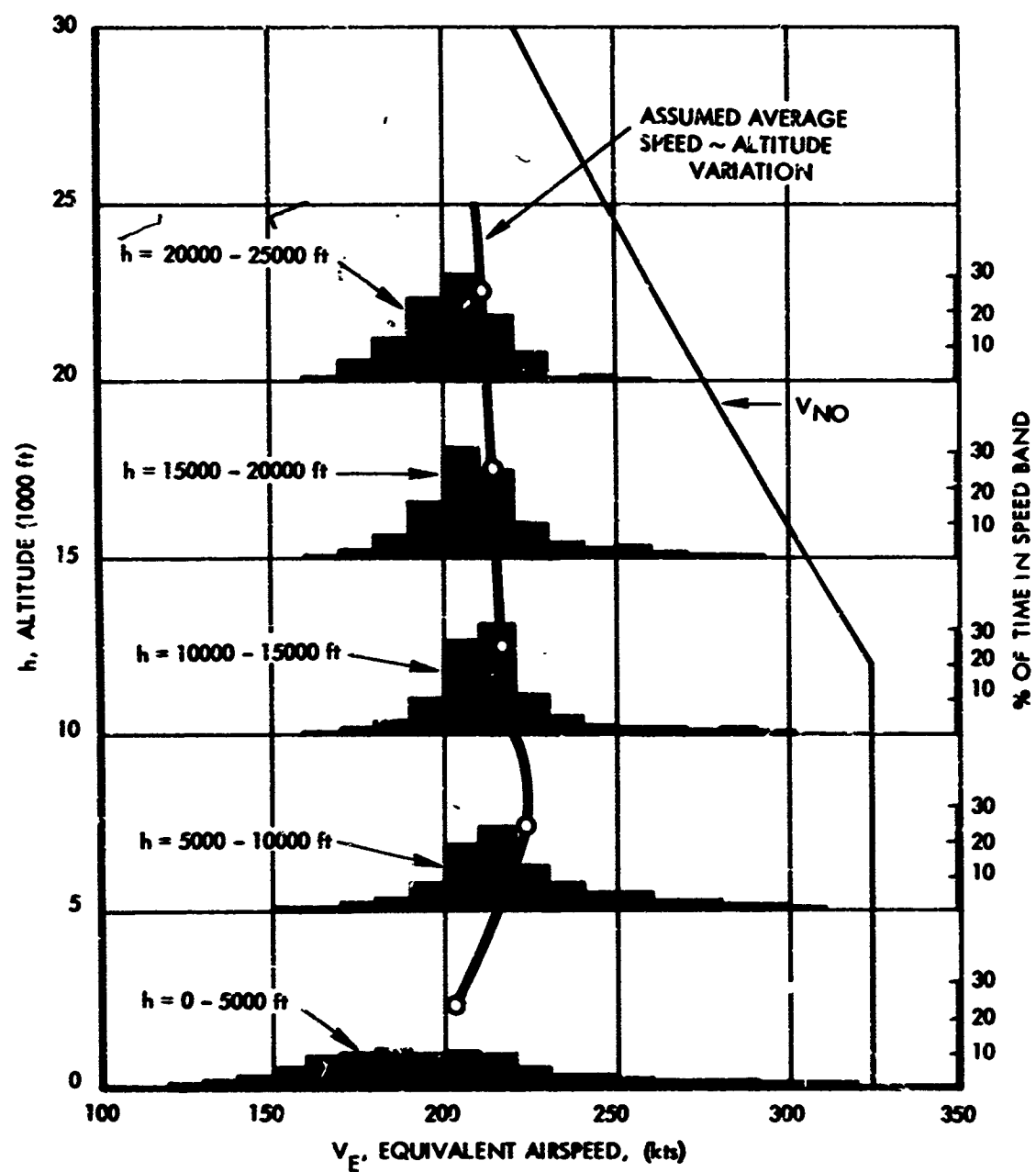


FIGURE 6-3. DISTRIBUTIONS OF AIRSPEED IN CLIMB, MODEL 188

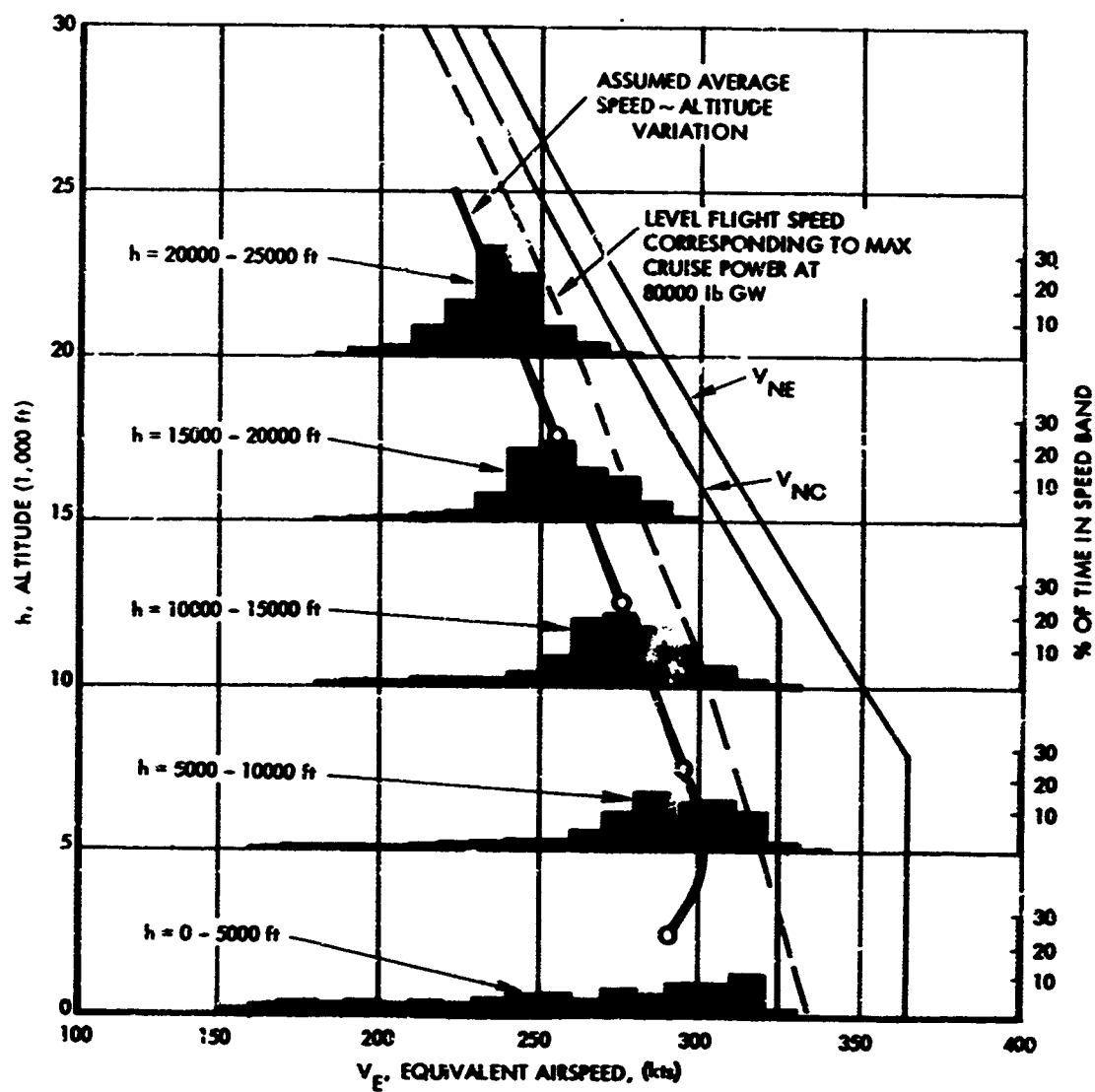


FIGURE 6-4. DISTRIBUTION OF AIRSPEED IN CRUISE, MODEL 188

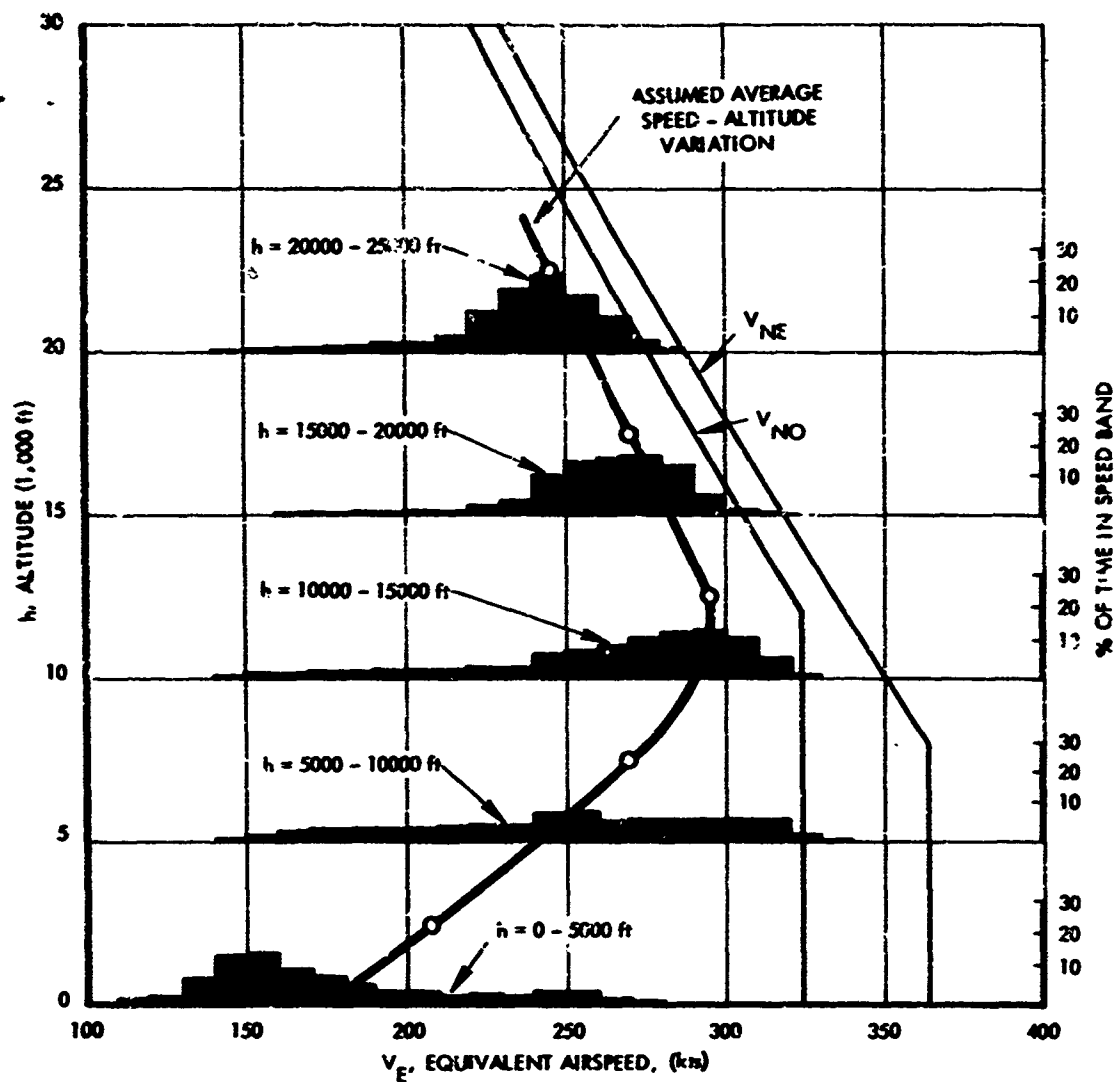


FIGURE 6-5. DISTRIBUTION OF AIRSPEED IN DESCENT, MODEL 188

given speed distribution were to be divided into a high speed and a low speed band, with the average speed in each band used for analysis. The low speed band would contribute negligibly to the exceedance curve. The high speed band would contribute only half as many load cycles as the total distribution, but its average speed would be appreciably higher. The increase in load due to the higher speed would have a far greater effect than the reduction in cycles. In order to approximate this effect, the "average" speeds shown for cruise and descent have been increased somewhat over the simple averages stated in Reference 9.

The mission flight profiles thus established are shown in Figures 6-6a thru 6-6e.

The airplane weights shown in Figure 6-6 were next determined.

Operating weight empty was determined by first examining the weight data available at the time of delivery of the airplanes to the various airlines. The average operating weight empty for the various airlines ranged generally from 59400 lb. to 61800 lb., with one airline as high as 64200 lb. (These weights include an adjustment to account for the increase in weight empty due to the "LEAP" modifications made to all airplanes after delivery.) These values were then increased to account for weight growth after delivery by use of recent Eastern Air Lines information indicating a weight growth of 1100 lb. for their airplanes. Based on the foregoing, a value of operating weight empty of 62,000 lb. was selected as representative of the fleet.

A representative payload was selected based on information obtained from several Electra operators. Average passenger load factors and other pertinent data are shown in the following table:

Airline	Passenger Load Factor	Passenger Capacity	Assumed Weight Per Passenger (Incl. Baggage)	Resulting Average Payload
AA	63%	74	200	9300
EAL	60%	73	200	8800
NAL	60-65%	70	200	9800
PSA	80%(estim.)	96	170	13100
WAL	80%(estim.)	96	200	15400

A representative value of 12000 lb. was selected based upon the above figures. Although the Electra has provision for several thousand pounds of cargo, express, and/or mail in addition to normal passenger baggage, this is seldom utilized; a nominal allowance at 500 lb. is included for this, giving a total average payload to use in analysis of 12500 lb.

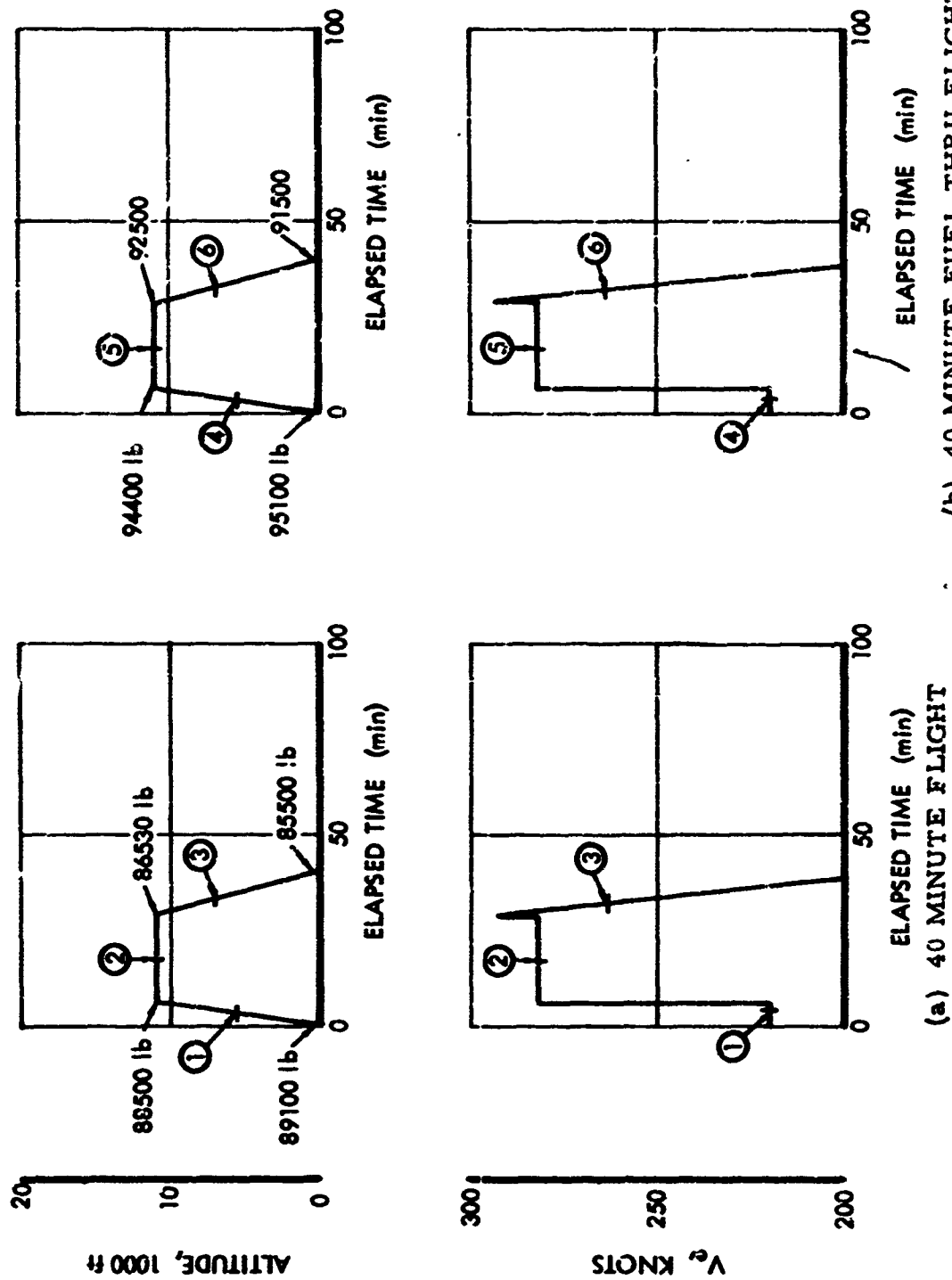
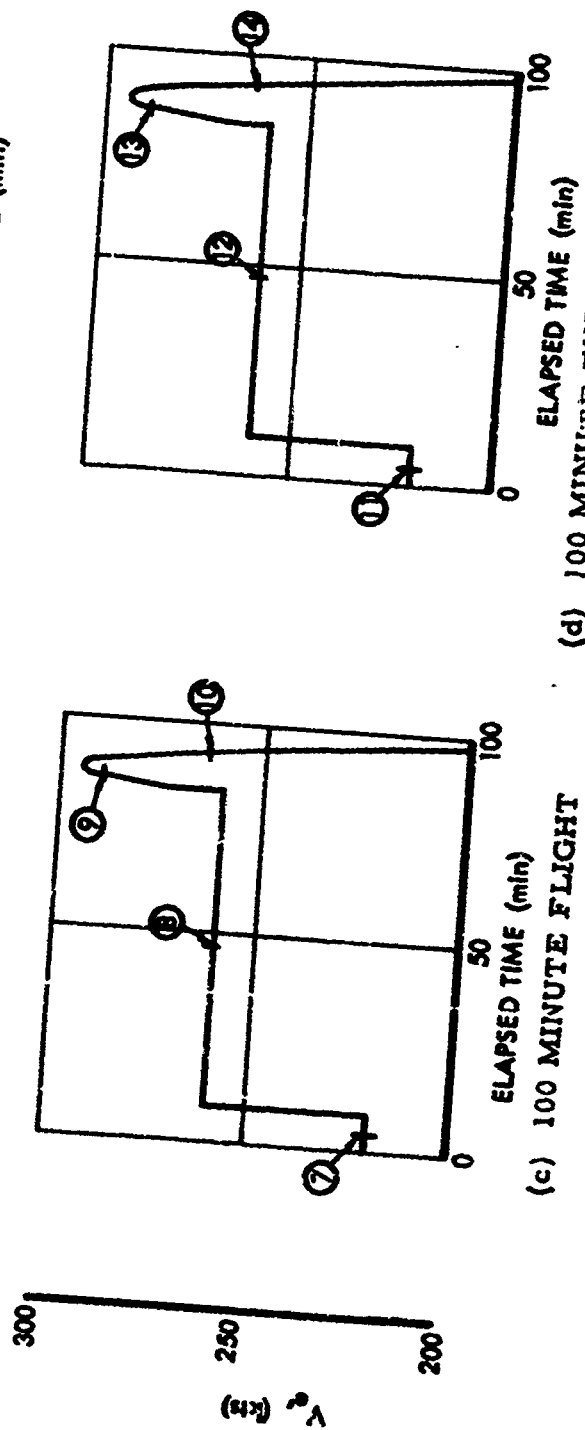
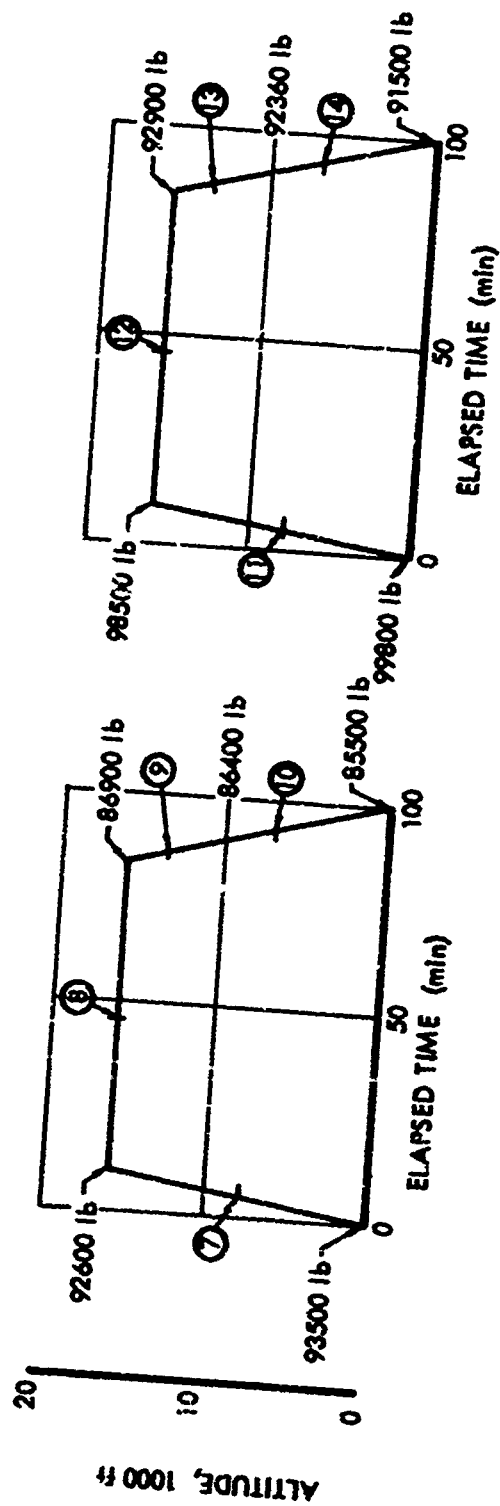
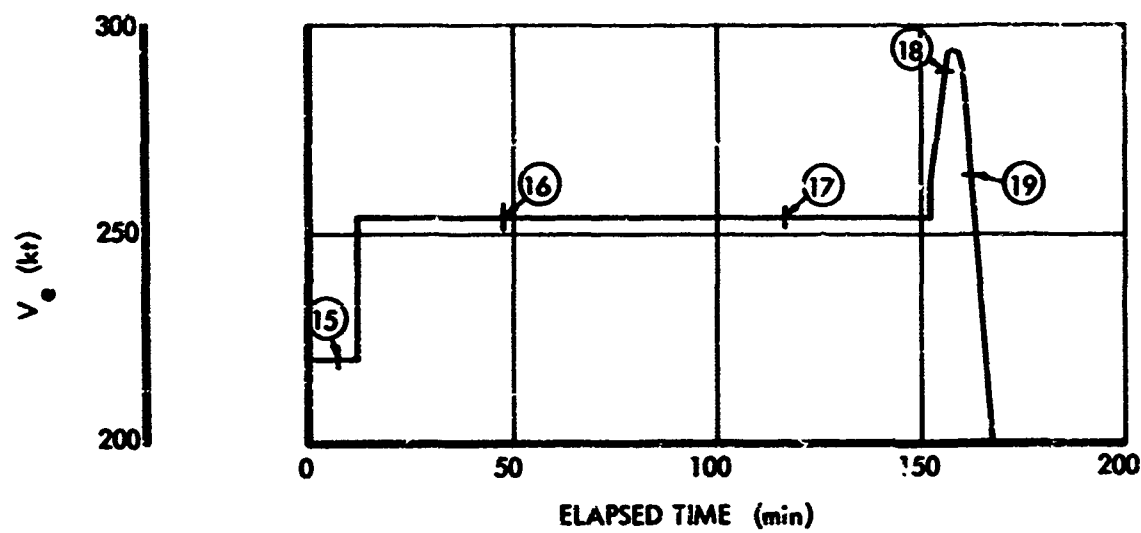
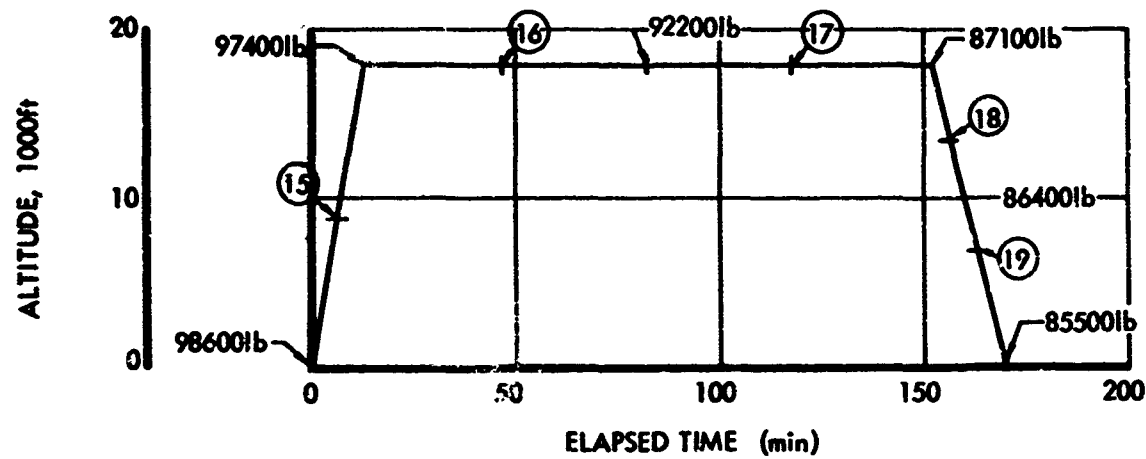


FIGURE 6-6. MISSION PROFILES, MODEL 188



(c) 100 MINUTE FLIGHT (d) 100 MINUTE FUEL THRU FLIGHT
FIGURE 6-6. CONTINUED



(e) 170 MINUTE FLIGHT

FIGURE 6-6. CONCLUDED

The corresponding zero-fuel weight is 74,500 lb. This compares with a design maximum zero-fuel weight of 86,000 lb.

Reserve fuel at landing is the most difficult weight item to estimate reliably. Values used for analysis are based on the following considerations.

1. A nominal value, based primarily upon application of FAA operating regulations, would be about 8000 lb.
2. Based upon a known tendency to load fuel conservatively, average values would be expected to be somewhat greater than this - perhaps on the order of 10,000 - 11,000 lb.
3. The Electra is often "fueled through" - that is, fuel is not taken aboard between flights. Based on the design landing weight of 95,650 lb., an operating weight empty of 62,000 lb., and a first-leg payload of 12,500 lb., the maximum fuel at landing would be about 21,100 lb. This would permit taking off without refueling and making roughly a 170 minute flight while retaining an 8000 lb. reserve. It is clear that for short flights in series there is a likelihood of a wide variation in reserve fuel. It is estimated that roughly 30 to 35% of Electra individual flights are made without refueling before take-off.
4. Previous information provided to NASA and Lockheed by airlines for the purpose of computing gust velocities from airplane normal accelerations has indicated average Electra gross weights at the midpoint of the flight of 92,000 lb. to 101,000 lb. For these weights - especially the latter, which is currently used by NASA - to be consistent with the operating weights empty, payloads, and flight durations indicated herein, considerably more than 8000 lb. reserve fuel is indicated.

As a result of these considerations, it is assumed that 20% of all flights will carry reserve fuel of 17,000 lb., reflecting the more extreme fuel-through situations, and the remaining 80% of flights will carry reserve fuel of 11,000 lb., reflecting non-fuel-through operations together with the remainder of the fuel-through flights. The high-reserve-fuel flights are assumed to be confined to the 40 minute and 100 minute flights, divided 75% to the 40 minute flights and 25% to the 100 minute flights.

The landing weights corresponding to the above assumptions are as follows:

Operating Wt. Empty	62000 lbs.	62000 lbs.
Payload	12500	12500
Reserve Fuel	<u>11000</u>	<u>17000</u>
Landing Wt.	85500 lbs.	91500 lbs.

The airplane weights for various points in the representative missions are found by working backwards from the landing weights using fuel consumption and performance data of reference 19.

The mission profiles thus established and shown in Fig. 6-6 are broken down into segments, or blocks, for analysis as indicated by the circled numbers in Figures 6-6a to 6-6e. These segments are tabulated in detail in Table 6-1.

The mission segments shown in Table 6-1 are then combined for analysis in Table 6-2. Only very nearly identical segments are combined, except in the case of the climb segments, which previous analyses had indicated contribute negligibly to the gust load exposure. Airplane center of gravity positions shown in Table 6-2 are based on a center of gravity midway between forward and aft limits without fuel, in accordance with the best available estimates.

6.2 Model 749

The mission profiles for use in the Model 749 mission analysis are based upon the same general sources of data as the Model 188 mission profiles.

The distribution of flight durations given in Reference 9 is plotted in Figure 6-7. The following three mission durations were selected as representative:

<u>Duration</u>	<u>% of Flights</u>
60 min.	63
120 min.	28
300 min.	9

The flight duration for the intermediate range mission - 120 minutes - was taken slightly lower than the actual average of 140 minutes in order to partially reflect the trend toward shorter stage lengths experienced by the Model 749 since the time the VGR data were obtained (1951 - 1953, in eastern seaboard operations).

TABLE 6-1. MISSION PROFILE DATA, MODEL 188

Mission Description	Percent of Total Flights	Segment No.	Climb, Enroute Or Descent	Time In Segment Per Flight Minutes	V _e Average Speed Knots	h Average Altitude FT	W Average GW LB	Percent Of Total Airplane Time In Segment
40 Min	48	1	C	6	220	5500	88800	4.26
		2	E	23	282	11000	87500	16.32
		3	D	11	264	7000	86000	7.80
40 Min Fuel through	15	4	C	6	220	5500	94700	1.33
		5	E	23	282	11000	93400	5.10
		6	D	11	264	7000	92000	2.44
100 Min	23	7	C	6	220	8000	93100	2.04
		8	E	75	260	16000	89800	25.49
		9	D	6	290	13500	86700	2.04
100 Min Fuel through	5	10	D	10	264	7000	86000	3.40
		11	C	6	220	8000	99000	.44
		12	E	75	260	16000	95700	5.54
170 Min	9	13	D	6	290	13500	92600	.44
		14	D	10	264	7000	92000	.74
		15	C	13	220	9000	98000	1.73
		16	E	70	254	18000	94800	9.31
		17	E	69	254	18000	89600	9.18
		18	D	8	290	13500	86700	1.06
		19	D	10	264	7000	86000	1.33

TABLE 6-2. SUMMARY OF LUMPED FLIGHT SEGMENTS FOR MISSION ANALYSIS, MODEL 188

Note: Zero fuel weight = 74500 pounds for all cases.

Segment Case Number	Segment Number in Table 6-1	Climb, Thrust or Descent	V _e Average Speed Knots	h Average Altitude Feet	W Average Weight Pound	C.G. % MAC	Percent of Total Airplane Time in Segment
201	1,4,7,11,15	C	220	7000	92300	25.2	9.80
202	2	E	282	11000	87500	24.3	16.32
203	8,17	E	258	16500	89750	24.7	34.67
204	5	E	282	11000	92100	25.4	5.10
205	12,16	E	256	17000	55100	25.6	14.85
206	3,10,19	D	264	7000	86500	24.1	12.23
207	9,18	D	290	13500	86500	24.1	3.10
208	6,14	D	264	7000	92300	25.2	3.18
209	13	D	290	13500	92300	25.2	.44

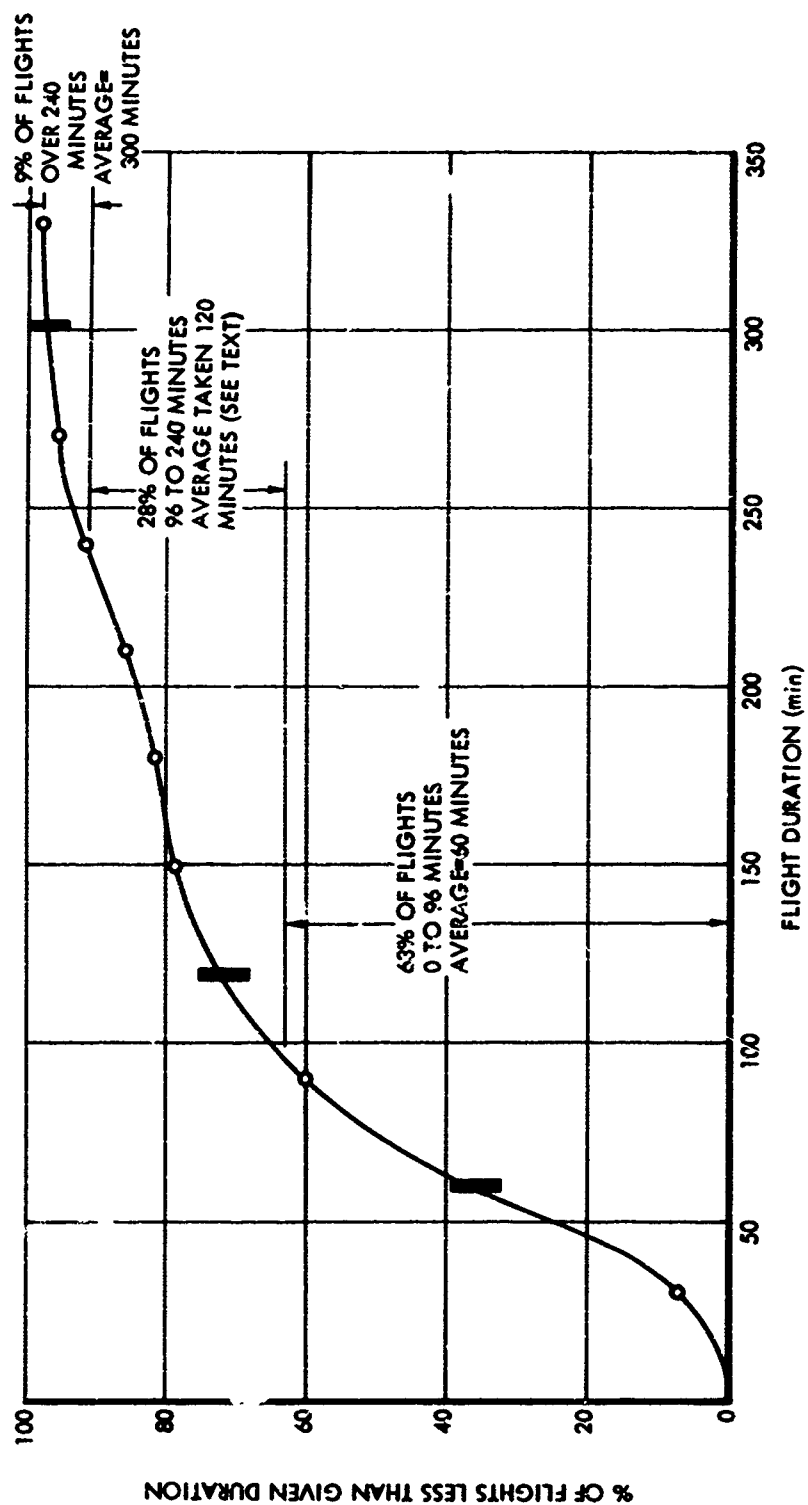


FIGURE 6-7. FLIGHT DURATIONS, MODEL 749

The trend of average cruise altitude with flight duration is estimated in Figure 6-8. Since actual statistical information was not available, this trend was established by plotting the single over-all average cruise altitude and flight duration obtained from Reference 9 and fairing a curve through this point guided by the 188 trend. The cruise altitudes appropriate to the three mission durations are read from the resulting curve as follows:

<u>Duration</u>	<u>Cruise Altitude</u>
60 min.	8,000 ft.
120 min.	13,000 ft.
300 min.	18,000 ft.

Reasonable confirmation of this selection is indicated by Fig. 6-9, which shows the number of cruise hours spent in each altitude band as indicated by the data in Reference 9.

The distributions of speeds for climb, cruise and descent as given in Reference 9 are shown in Figure 6-10. The breakdown of these distributions by altitude band is not available.

The representative climb speed is taken as a constant 157 knots equivalent airspeed for all three missions.

Average cruise speeds as a function of altitude are estimated by means of Figure 6-11. The average cruise speed obtained from Fig. 6-10 and the average cruise altitude shown in Fig. 6-8 are plotted as a single point in Fig. 6-11. The average cruise speeds at the three altitudes required in the mission analysis are then estimated using the curve of speed at maximum cruise power as a guide. The resulting average cruise speeds for the three mission profiles are:

<u>Cruise Altitude</u>	<u>Cruise Speed</u>
8,000 ft.	210 knots EAS
13,000 ft.	205 knots EAS
18,000 ft.	190 knots EAS

The descent speed is taken as a constant 220 knots for each of the three missions, based upon maintaining a reasonable spread - approximately 15 knots - between the actual speed and V_{NO} . The distribution shown in Figure 6-10 indicates typical descent speeds to be somewhat higher. However, this distribution is based on data obtained at a time when normal practice was to descend, in smooth air, at close to V_{NE} . As a result largely of the same data shown in Figure 6-10 (obtained in the period 1951 - 1953), the descent-speed policy was altered to prohibit descent in excess of V_{NO} shortly after the data were obtained.

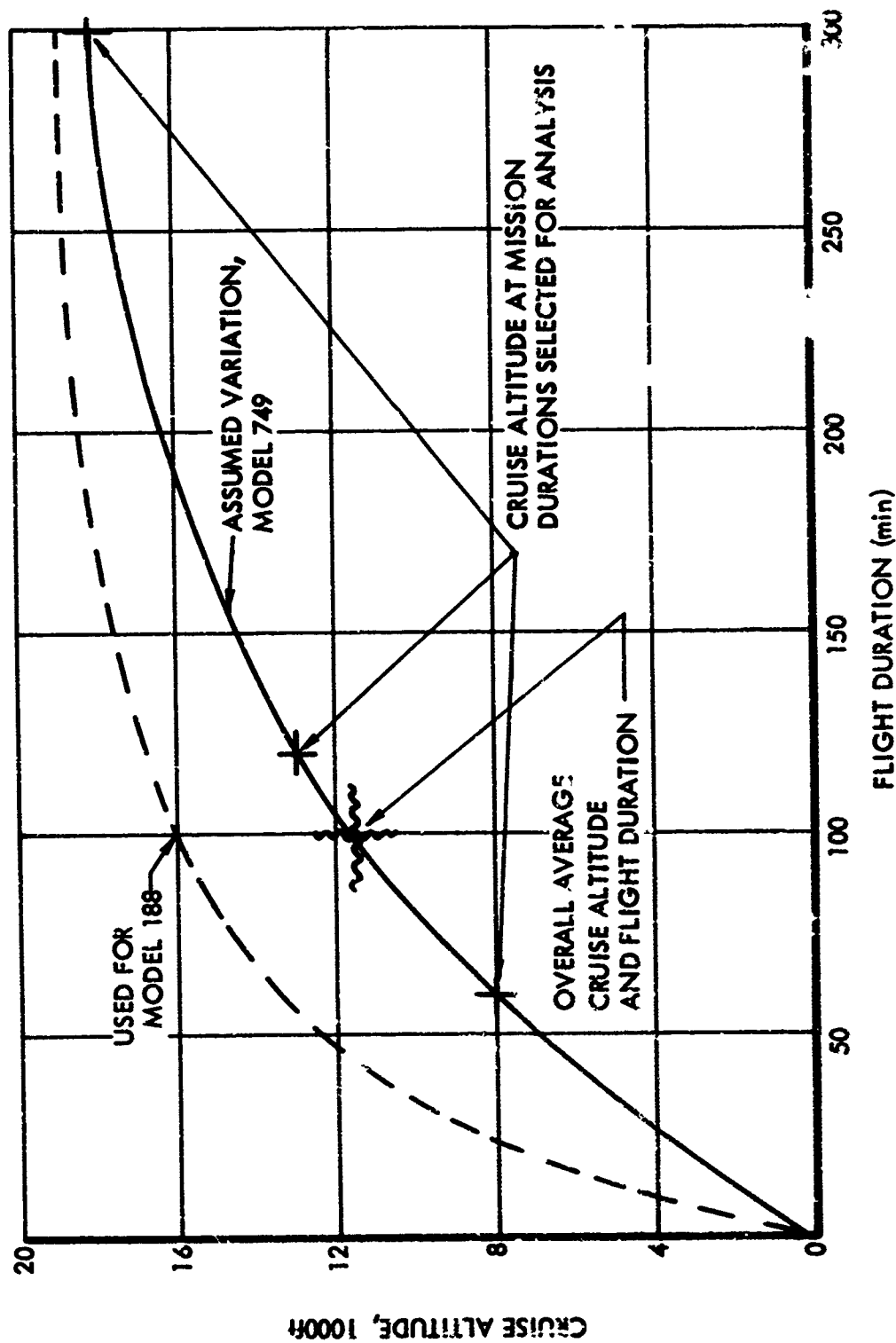


FIGURE 6-8. VARIATION OF AVERAGE CRUISE ALTITUDE WITH FLIGHT DURATION, MODEL 749

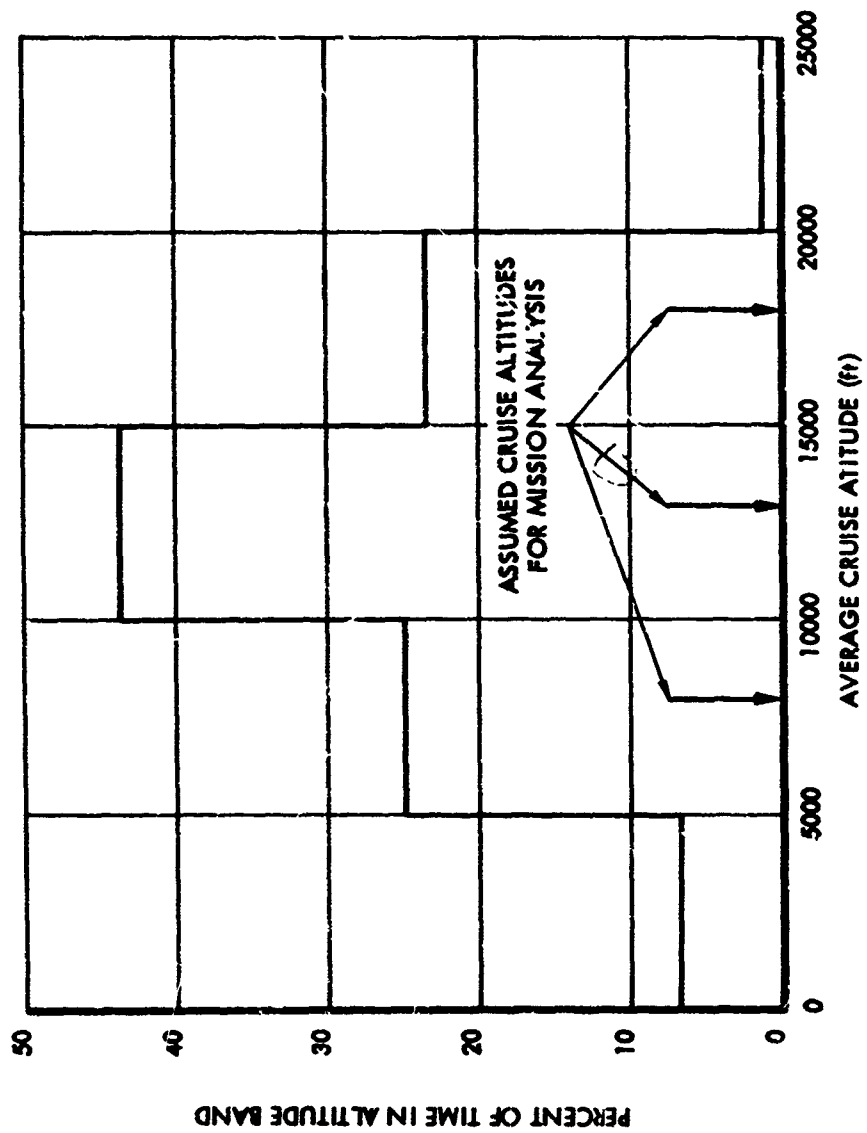


FIGURE 6-9. PERCENT OF CRUISE TIME SPENT IN VARIOUS ALTITUDE BANDS, MODEL 749

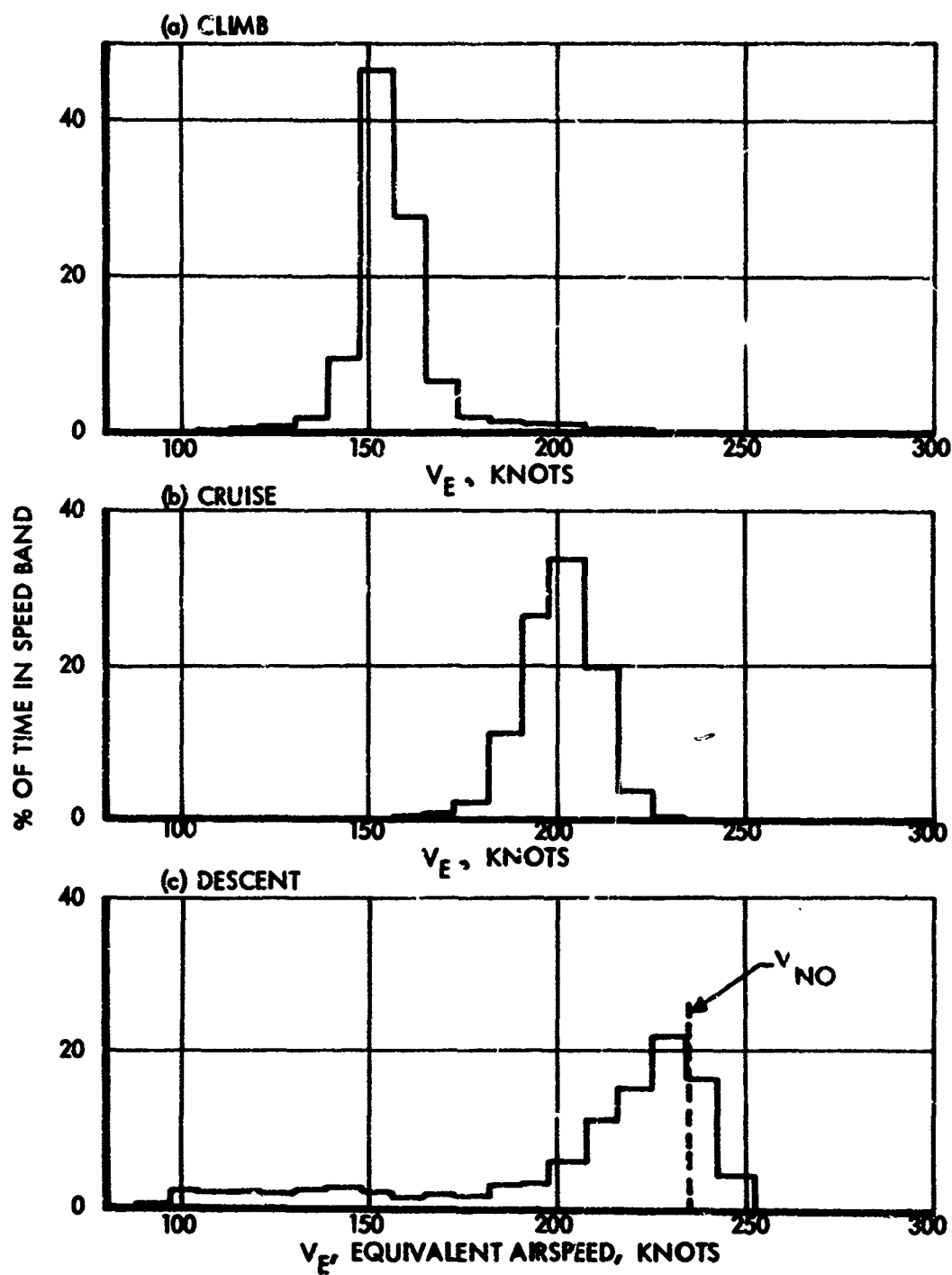


FIGURE 6-10. DISTRIBUTIONS OF AIRSPEED, MODEL 749

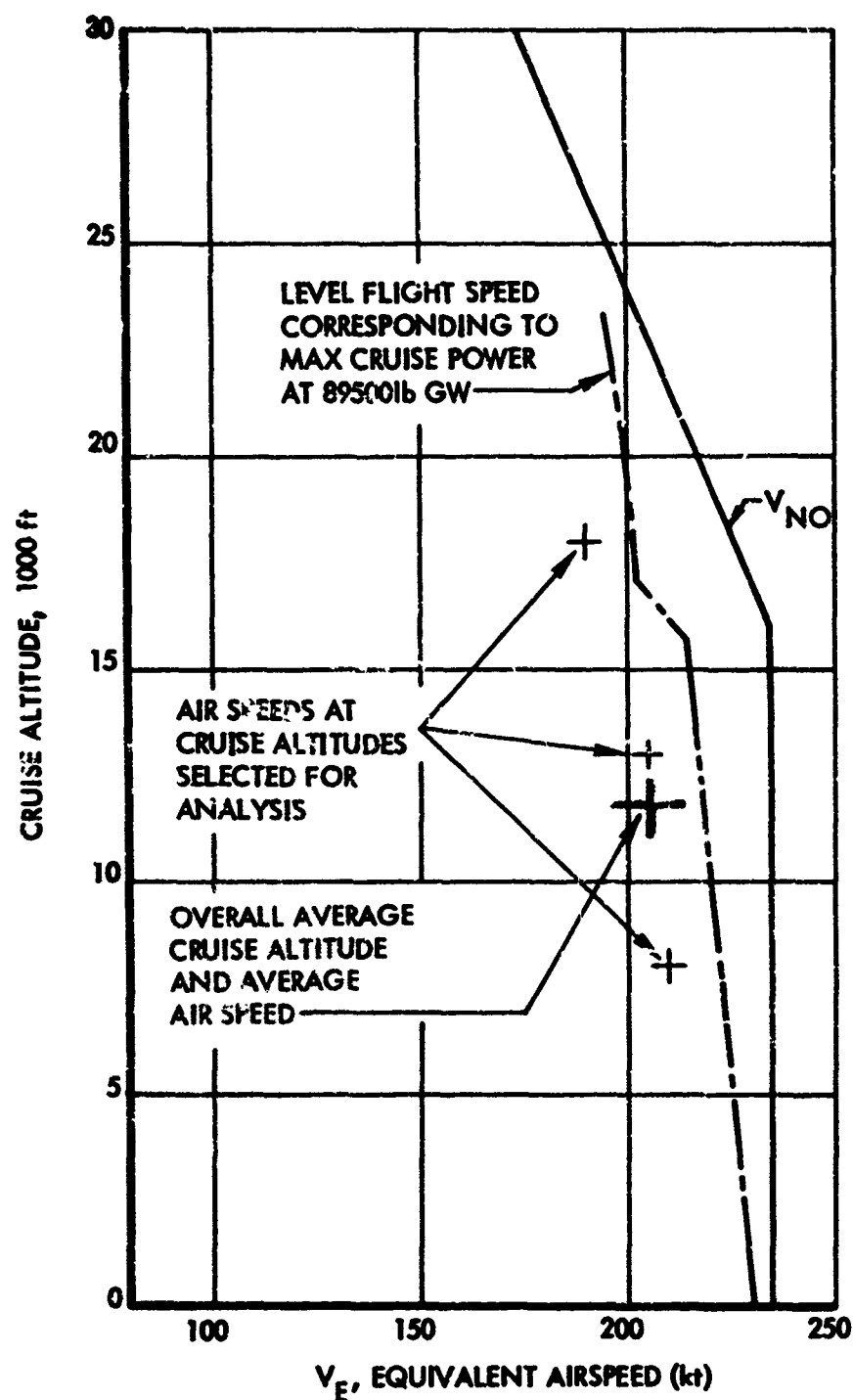


FIGURE 6-11. VARIATIONS OF AVERAGE CRUISE SPEED WITH ALTITUDE, MODEL 749

The three representative mission profiles are shown in Figure 6-12a through 6-12d.

The airplane weights shown in Figure 6-12 were next determined.

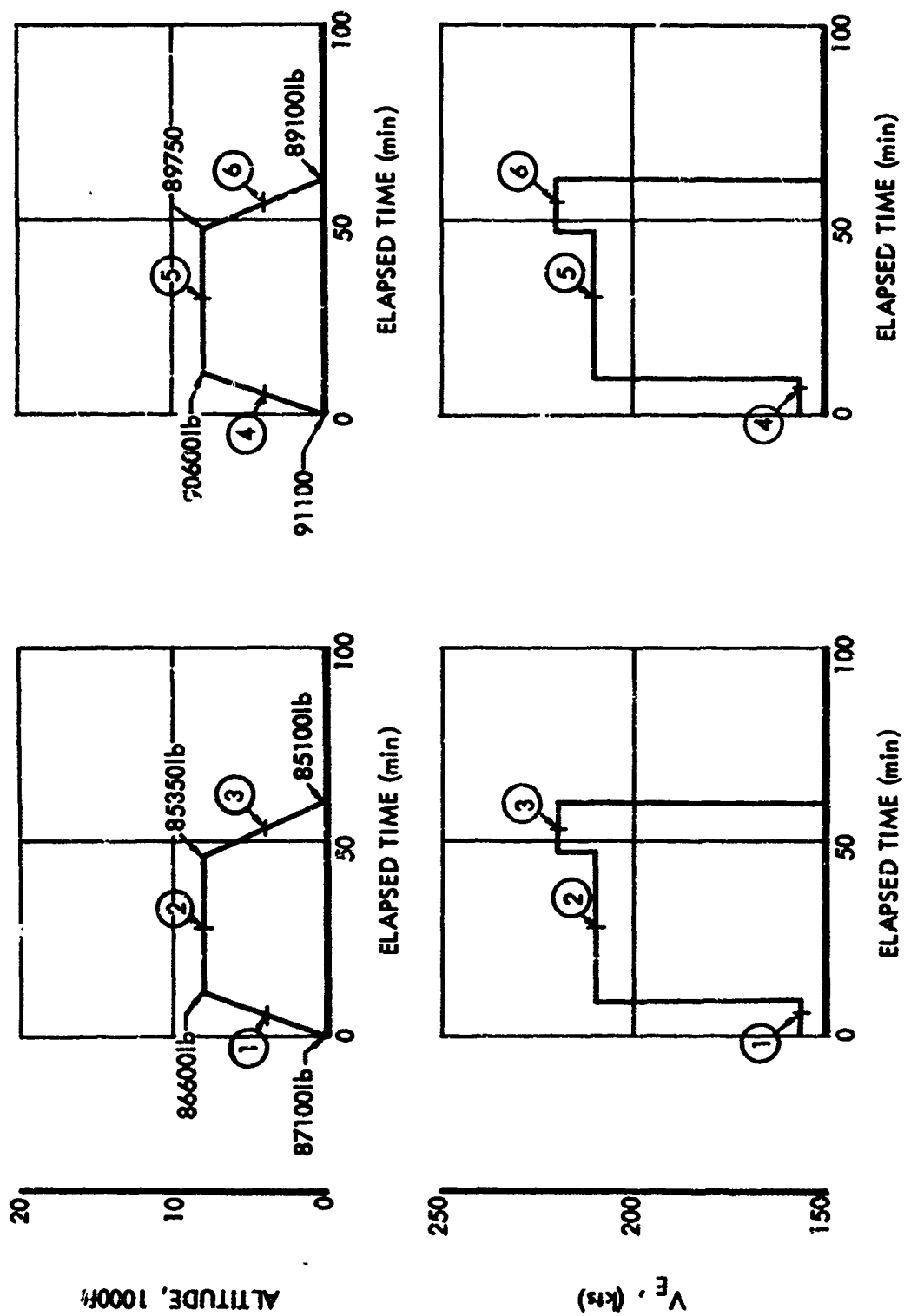
Operating weight empty for the 749 is taken as 68640 lbs. Calculations based upon as-delivered weights indicated an average value of approximately 63,000 lbs. with a variation of several thousand pounds in this weight due to different interior configurations. However, weight growth due to configuration changes, conversions and structural modifications has taken place on the 749 fleet and a detailed weight summary is not readily available. A fleet of 749's presently operating report an average operating weight empty of 68640 lbs. contrasted to an estimated as-delivered operating weight of 63200 lb. This is taken as a representative increase, and, because the original weight of this fleet was close to the overall average, the operating weight of 68640 lbs. is used as representative.

An average 749 payload of 9500 lbs. is selected based upon information obtained from the same major 749 operator. This estimate corresponds to a load factor of 70% applying to a nominal maximum payload of 13590 lbs. It corresponds to a passenger load factor of 77%, based upon a passenger capacity of 62 and a weight per passenger of 200 lb. including baggage, with no cargo carried. It corresponds to 53% of maximum payload as controlled by the placard zero fuel weight of 86464 lb. in combination with the operating weight empty of 68640 lb. The zero-fuel weight corresponding to the 9500 lb. payload is 78140 lb.

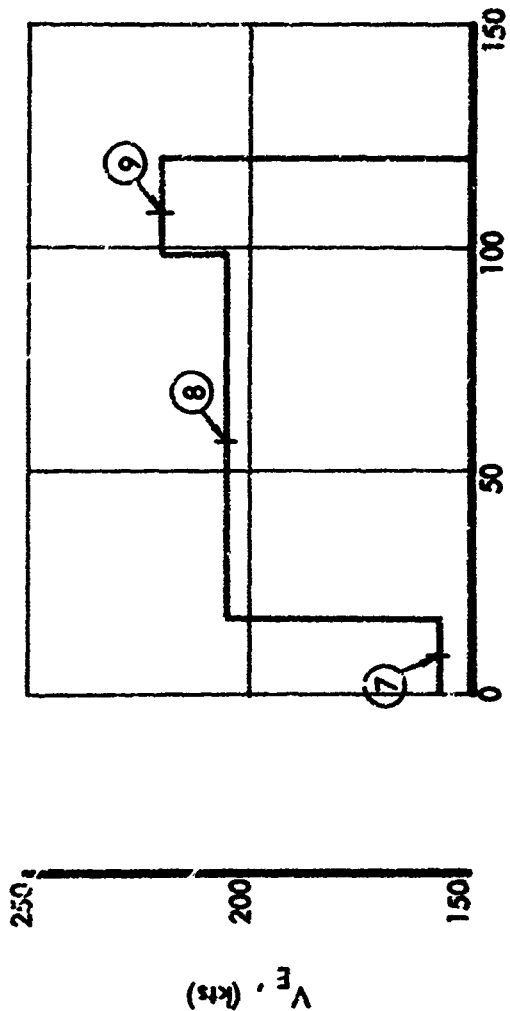
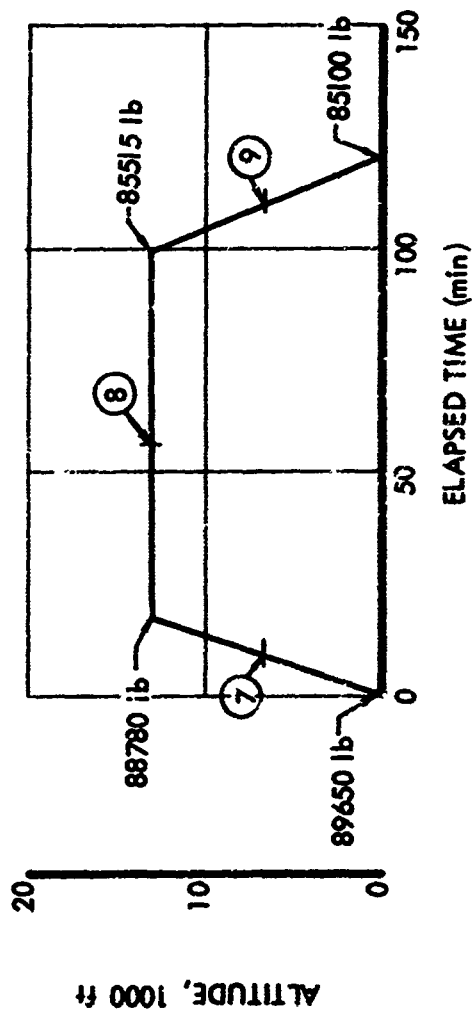
Representative reserve fuel quantities for the assumed operating weight empty and payload range from the FAA required minimum of 4200 lbs. to a maximum of 11360 lbs. The latter figure is the maximum that can be carried at the assumed operating weight empty and payload without exceeding the design landing weight of 89,500 lb. It is estimated that the 749 is operated such that approximately 25% of the missions are fueled through and thus require high landing fuels. As a result, it is assumed that 15% of all flights will carry 11,000 lb. of reserve fuel, reflecting the more extreme fuel-through situations, while the remaining 85% of flights will carry 7000 lb. of reserve fuel, reflecting non-fuel-through operations together with the remainder of the fuel-through flights. The fuel-through operation is limited to the 60 minute flights.

The landing weights corresponding to the above assumptions are as follows:

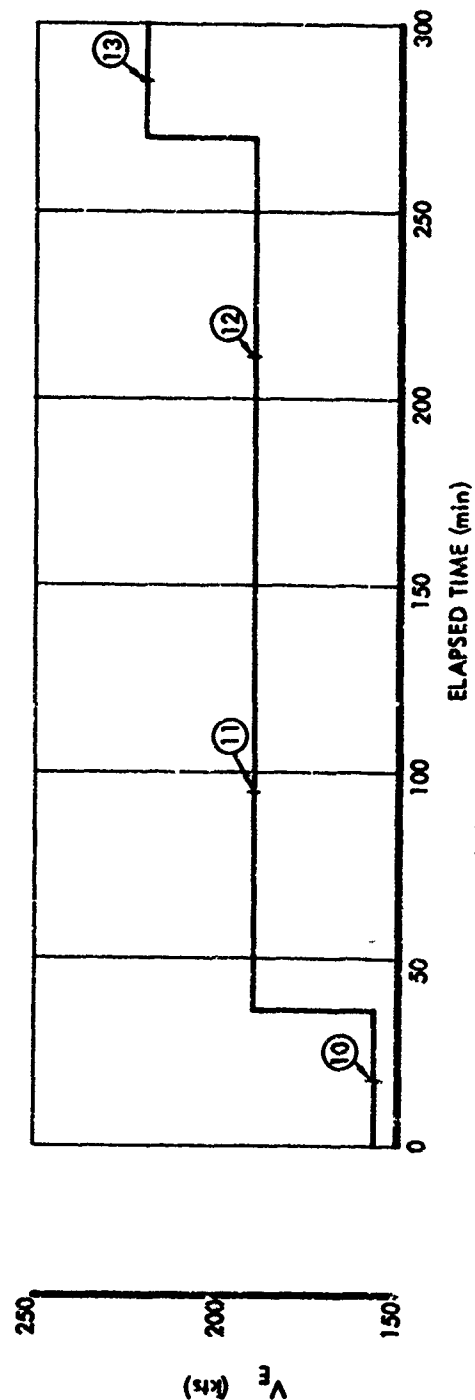
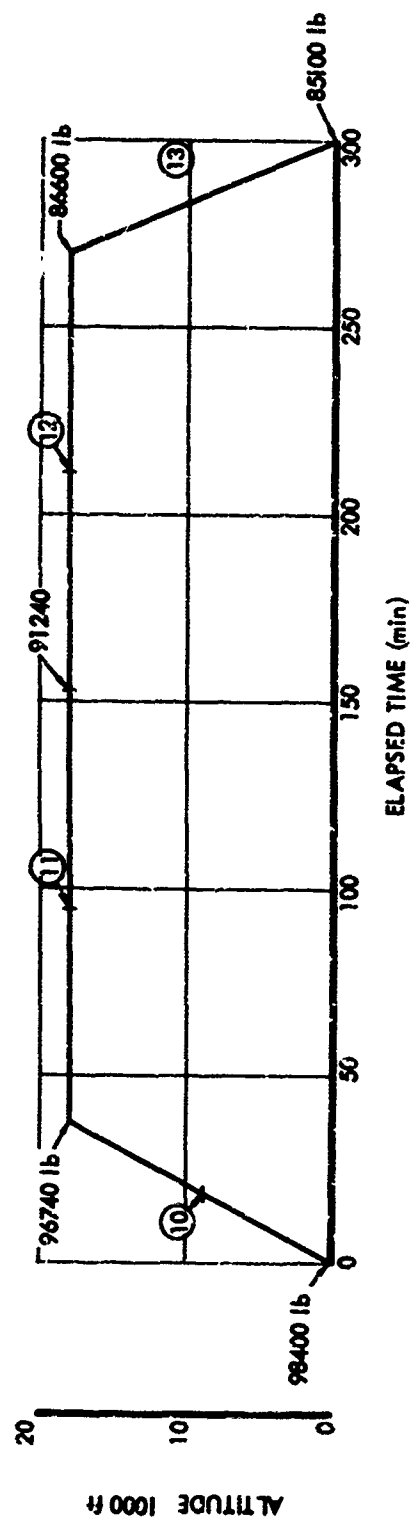
Operating Wt. Empty	68600	68600
Average Payload	9500	9500
Reserve Fuel	<u>7000</u>	<u>11000</u>
Landing Wt.	85100	89100



(a) 60 MINUTE FLIGHT
 (b) 60 MINUTE FUEL THRU FLIGHT
 FIGURE 6-12. MISSION PROFILES, MODEL 749



(c) 120 MINUTE FLIGHT
FIGURE 6-12. CONTINUED



(d) 300 MIN. FLIGHT
FIGURE 6-12. CONCLUDED

The airplane weights for various points in the representative missions are found by working backwards from the landing weights using fuel consumption and performance data available in unpublished form.

The mission profiles thus established and shown in Figure 6-12 are broken down into segments for analysis as indicated by circled numbers in Figures 6-12a to 6-12d. These segments are tabulated in detail in Table 6-3.

The mission segments shown in Table 6-3 are then combined for analysis in Table 6-4. Only very nearly identical segments are combined, except in the case of the climb segments, which previous analyses had indicated contribute negligibly to the gust load exposure. Airplane center of gravity positions shown in Table 6-4 are based on a center of gravity midway between forward and aft limits without fuel, in accordance with the best available estimate.

TABLE 6-3. MISSION PROFILE DATA, MODEL 749

Mission Description	Percent of Total Flights	Segment No.	Climb, Enroute Or Descent	Time In Segment Per Flight Minutes	V _e Average Speed Knots	h Average Altitude Ft	W Average GW Lb	Percent Of Total Airplane Time In Segment
60 Min	38	1	C	10	157	4000	86870	4.83
		2	E	37	210	8000	85994	18.05
		3	D	13	220	4000	85225	6.34
60 Min Fuel through	25	4	C	12	157	4000	90850	1.83
		5	E	35	210	8000	99975	5.33
		6	D	13	220	4000	89225	1.98
120 Min	28	7	C	17.5	157	6500	83215	4.98
		8	E	80.8	205	13000	87150	22.98
		9	D	21.7	220	6500	85308	6.18
300 Min	9	10	C	37.0	157	9000	97570	3.88
		11	E	116.5	190	18000	93990	10.66
		12	E	116.4	190	18000	88470	10.65
		13	D	30.1	220	9000	85402	2.75

TABLE 6-4. SUMMARY OF LUMPED FLIGHT SEGMENTS FOR MISSION
ANALYSIS, MODEL 749

Note: Zero fuel weight = 78100 lb for all cases

Segment Case No.	Segment No. In Table 6-3	Climb, Enroute Or Descent	V _e Average Speed Knots	h Average Altitude Ft	W Average GW Lb	C.G. % MAC	Percent Of Total Airplane Time In Segment
101	1, 4, 7, 10	C	157	6000	90528	25.4	15.07
102	2	E	210	8000	85994	24.9	18.05
103	3	D	220	4000	85290	24.8	6.34
104	5	E	210	8000	89975	25.4	5.33
105	6	D	220	4000	89225	25.3	1.98
106	8	E	205	13000	87150	25.0	22.99
107	9	D	220	6500	85290	24.8	6.18
108	11	E	190	18000	93990	25.7	10.66
109	12	E	190	18000	88470	25.2	10.65
110	13	D	220	9000	85290	24.8	2.75

7 SELECTION OF DESIGN ENVELOPE POINTS FOR ANALYSIS OF REFERENCE AIRPLANES

7.2 Model 188

The design speed-altitude chart for the Model 188 is shown in Figure 7-1, and the weight-c.g. envelope in Figure 7-2.

In Figure 7-1, the V_C and V_D lines reflect the values used for structural design. The V_{NE} speed, while not used directly in structural design, is shown for information. The V_B speed of 180 knots is to a certain extent arbitrary. In existing criteria, V_B is defined as the speed at which a 65 fps gust line on the V-n diagram intersects the stall line. The actual speed depends upon gross weight, and is also subject to some variation depending upon the source of data used in determining the stall speeds. For application in a power spectral criterion, the definition would, of course, have to be recast into power-spectral form, and some difficulty might be encountered in arriving at a simple yet rational definition. The 180 knots V_B speed used in the present analysis is the value indicated by existing criteria at a gross weight of about 95000 lb.

The c.g. limits shown in Figure 7-2 are based upon operating placards and are slightly more restrictive than the limits actually used in the structural design of the airplane.

In addition to the envelopes shown, there are, of course, further restrictions as to location of fuel and payload, which are taken into account in the analyses conducted herein. In particular, it is noted that the minimum fuel for structural design is 3145 lb.

The design envelope cases for which vertical gust dynamic analysis was conducted for the Model 188 are listed in Table 7-1.

In selecting these cases, an effort was made to reduce to a minimum the number of cases for which a full dynamic analysis was required. Manifestly, it was necessary to include enough cases to assure that the critical combinations of airplane speed, altitude, weight, and weight distribution were covered. Moreover, the selection of critical conditions was complicated by the variation of σ_w , η_d , or design y/\bar{A} , with altitude, as shown in Figure 5-8. The number of potentially critical cases is, therefore, very large. In order to reduce the number requiring detailed dynamic analysis, the effect of altitude was

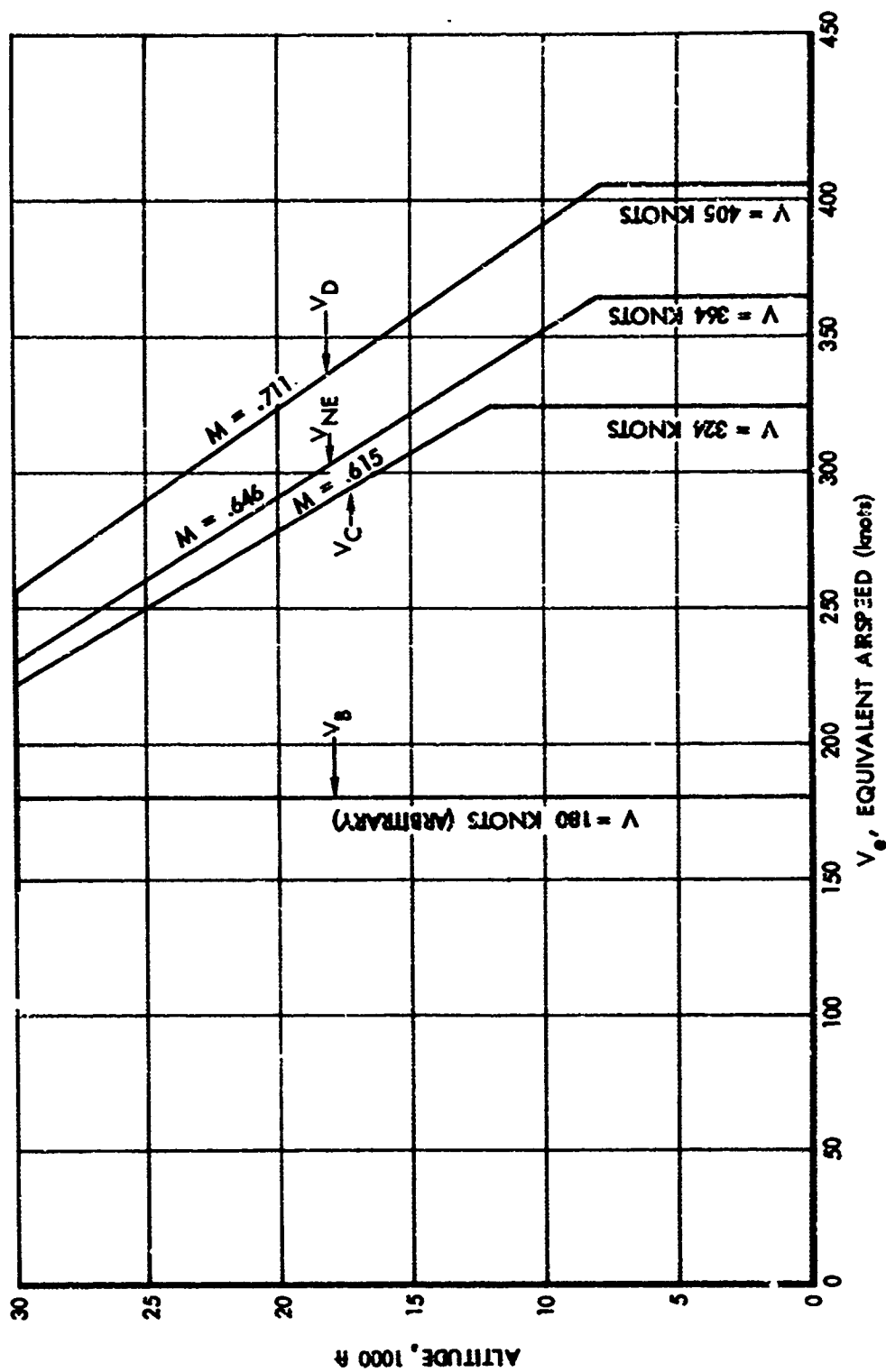


FIGURE 7-1. DESIGN SPEED ALTITUDE CHART, MODEL 188

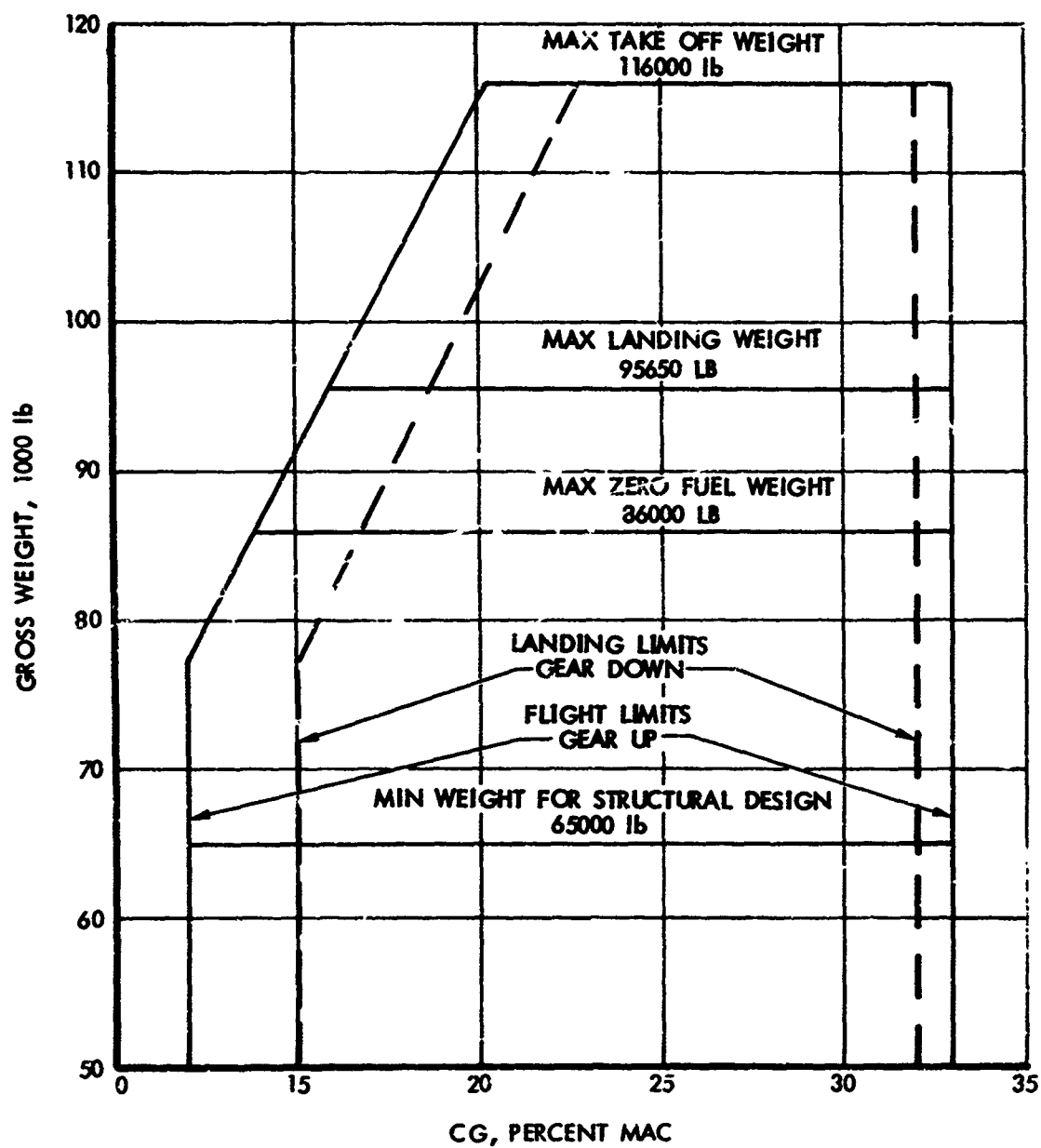


FIGURE 7-2. DESIGN WEIGHT - CG ENVELOPE, MODEL 188

TABLE 7-1. DESIGN ENVELOPE CASES FOR VERTICAL GUST ANALYSIS, MODEL 188

Case	Gross Weight Lb	Zero Fuel Weight Lb	Fuel Weight Lb	C. G. % M/C	Altitude Ft	V_B, V_C Or V_D	V_e Knots
401	65000	61855	3145	12.0	12000	V_C	324
402	65000	61855	3145	33.0	12000	V_C	324
403	97345	61855	35490	16.2	12000	V_C	324
404	97345	61855	35490	33.0	12000	V_C	324
405	116000	80510	35490	20.2	12000	V_C	324
406	116000	80510	35490	33.0	12000	V_C	324
407	89145	86000	3145	14.5	12000	V_C	324
408	89145	86000	3145	33.0	12000	V_C	324
409	95620	86000	9620	15.8	12000	V_C	324
410	95620	86000	9620	33.0	12000	V_C	324
411	101860	86000	15860	17.2	12000	V_C	324
412	101860	86000	15860	33.0	12000	V_C	324
413	107000	86000	21000	18.3	12000	V_C	324
414	107000	86000	21000	33.0	12000	V_C	324
415	113000	86000	27000	19.6	12000	V_C	324
416	113000	86000	27000	33.0	12000	V_C	324
417	116000	86000	30000	20.2	12000	V_C	324
418	116000	86000	30000	33.0	12000	V_C	324
419	39145	86000	3145	14.5	20000	V_C	275
420	89145	86000	3145	14.5	16000	V_C	299
421	89145	86000	3145	14.5	7000	V_C	324
422	89145	86000	3145	14.5	0	V_C	324
423	65000	61855	3145	12.0	7000	V_D	405
424	65000	61855	3145	33.0	7000	V_D	405
425*	89145	86000	3145	14.5	7000	V_D	405
426	89145	86000	3145	33.0	7000	V_D	405
427	89145	86000	3145	14.5	7000	V_B	180
428	89145	86000	3145	14.5	12000	V_B	180
429*	116000	86000	30000	20.2	12000	V_B	180
430	116000	86000	30000	20.2	12000	--	220
431	116000	86000	30000	20.2	27000	--	220

* Cases found to be critical

investigated first by examining center of gravity accelerations obtained on a much simpler basis. For this purpose, the curves of Figure 5-2 were used, which are based on the assumption of a rigid airplane free to plunge only. The c.g. accelerations thus obtained should indicate, to a good first-order approximation, the effect of altitude on wing loads as these would be obtained by the more complex dynamic analysis.

\bar{A} values thus obtained are shown as a function of altitude, for three gross weights, in Figure 7-3. These \bar{A} values are then multiplied by values of y/\bar{A} from the various curves of Figure 5-8, to yield Figures 7-4 and 7-5. These curves represent equal probability values of c.g. load factor, based on the simplified analysis. For any particular gross weight and weight distribution the curves can also be interpreted, to a reasonable approximation, as equal-probability curves for structural loads. Actually, there is a tendency for the load per g to increase with altitude due to reduced aerodynamic damping in the elastic modes; as a result, the true equal-probability curves for most structural loads would tend to shift slightly to the right with increasing altitude.

Inasmuch as the limit design value of $N(y)/N_0$ was expected to fall in the range 10^{-6} to 10^{-8} , it appeared quite certain that the critical altitude would be either 7000 ft. or 12000 ft., with 12,000 ft. perhaps the more likely. The 12,000 ft. altitude, it may be noted, corresponds to the knuckle in the design speed-altitude V_C line, and the 7000 ft. altitude to the knuckle in the curve of y/\bar{A} vs altitude.

Accordingly, the first 18 cases in Table 7-1 were taken at an altitude of 12,000 ft. A wide range of gross weights, payloads (as defined by zero-fuel weight), and fuel weights was covered; and for each of these weight combinations, a case was included at both forward and aft c.g. limits.

Using results obtained for the 18 cases, preliminary limit-strength values of y/\bar{A} were then determined, based upon four load quantities only - namely shear and bending moment at WS 83 and WS 275. Phasings, including the probable effect of torsion, were estimated from the results of earlier analyses (Reference 20) and limit strengths were based upon available design load envelopes. The critical case was indicated to be No. 407. As a result, cases 419 to 422 were then added, to assure that the critical altitude had been selected. (More thorough analysis, discussed in Appendix E, indicated later that Case 417 was actually more critical than 407; however, the pattern of cases actually selected was found to be sufficient to draw the necessary conclusions.)

Four cases were next selected for analysis at design dive speed. These include two weight cases - minimum fuel weight with maximum zero-fuel weight, and minimum flying weight. The former had been found most critical for V_C conditions, but the latter was included to provide for

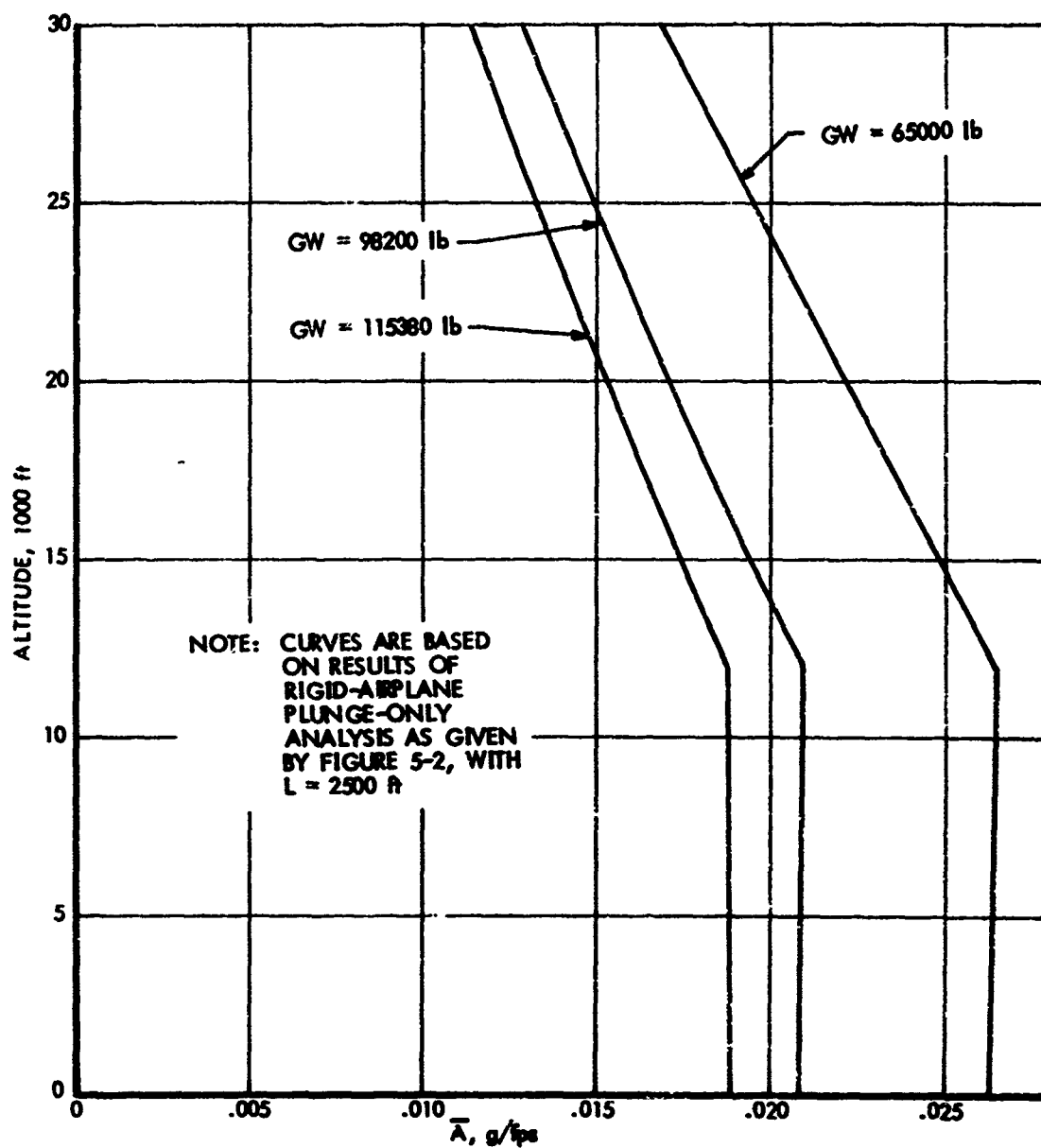


FIGURE 7-3. EFFECT OF ALTITUDE ON \bar{A} FOR CG ACCELERATION, MODEL 188

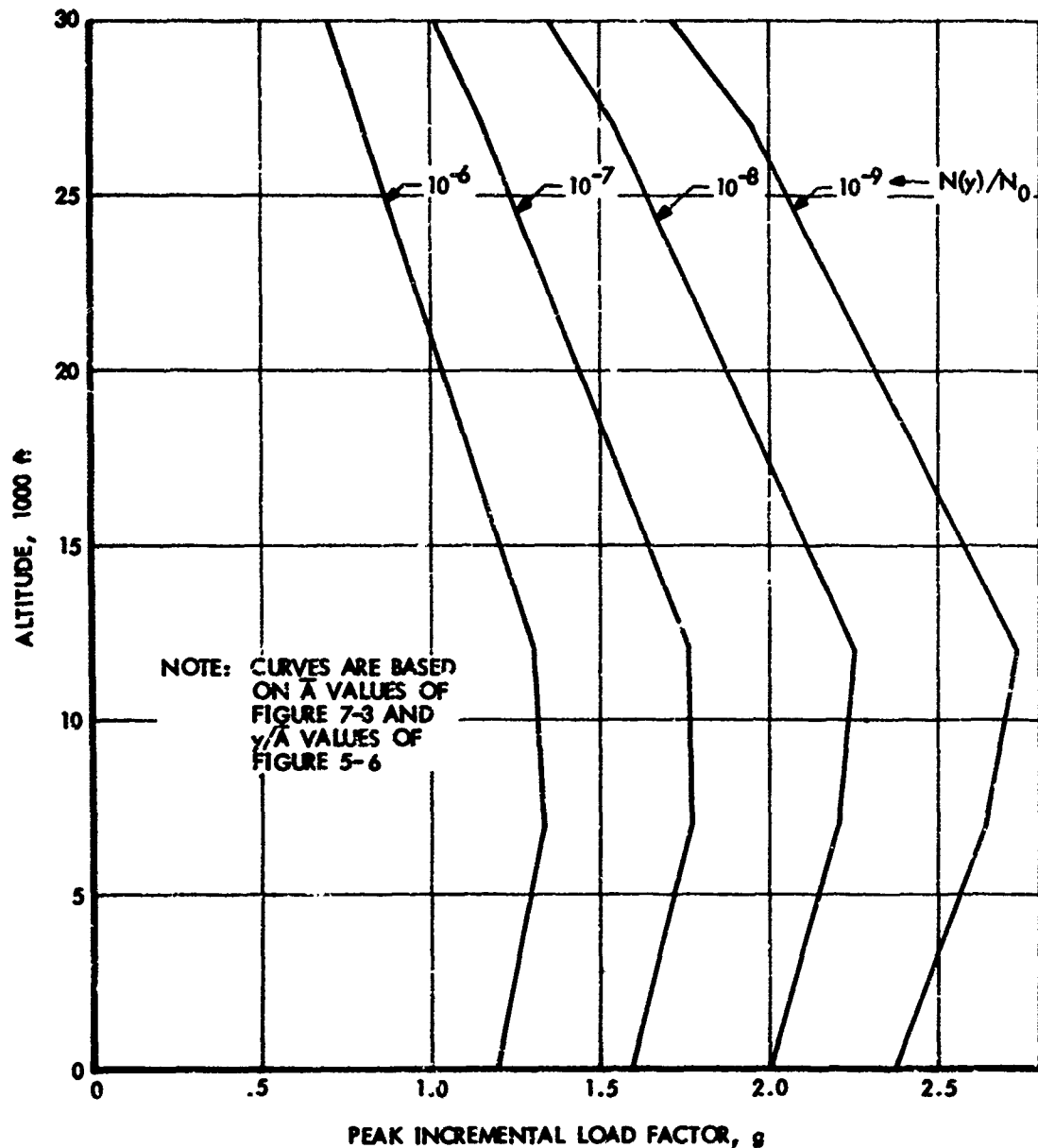


FIGURE 7-4. EFFECT OF ALTITUDE ON DESIGN LEVEL OF C.G. ACCELERATION, MODEL 188 - VARIOUS $N(y)/N_0$ LEVELS, GROSS WEIGHT = 98200 LB

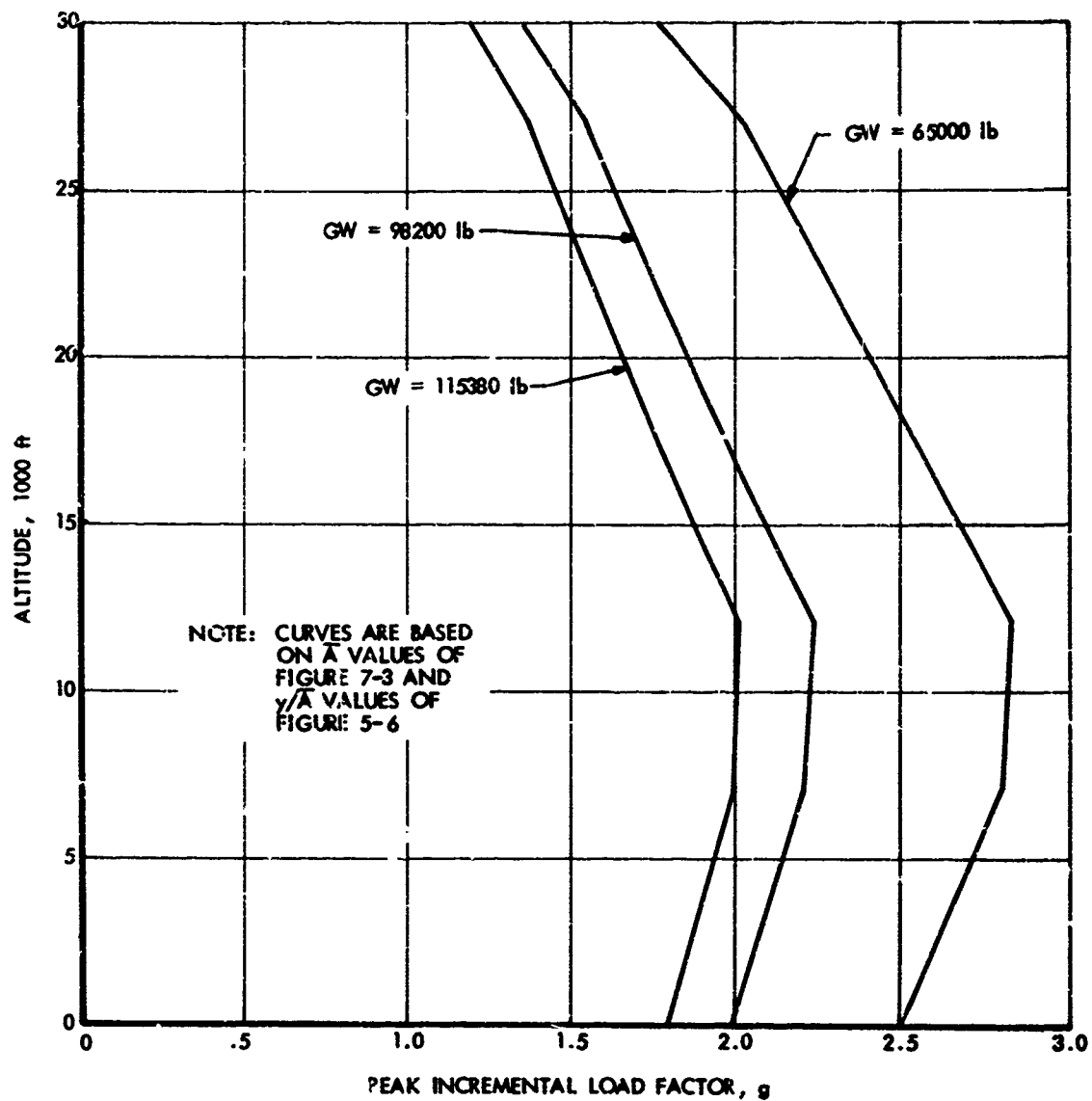


FIGURE 7-5. EFFECT OF ALTITUDE ON DESIGN LEVEL OF C.G. ACCELERATION, MODEL 188 - VARIOUS GROSS WEIGHTS, $N(y)/N_0 = 10^{-8}$

the possibility that a negative gust in combination with level flight loads modified by high speed aeroelastic effects could be more critical in down bending on the wing. The selection was based primarily on results of the earlier design analysis contained in Reference 20. The choice of a critical altitude was not a problem. The knuckle in the speed-altitude envelope shifts down to 8000 ft. at dive speed; this is so close to the 7000 ft. altitude at which the knuckle in the σ_{η_d} vs altitude curve occurs that the loads are sensibly the same at both altitudes.

Inasmuch as reduction of speed from V_C to V_B was expected to have little effect on the critical weight condition, the V_B case was taken for the same weight configuration and c.g. location expected to be critical at V_C . The altitude was reduced from 12000 ft. to 7000 ft., however, as a result of preliminary evaluation of the results obtained in cases 419-422. Following detailed study of loads resulting from cases 401-427 (described in Appendix E), it became evident that the critical V_B condition would occur at a gross weight of 116,000 lbs. rather than 89,145 lbs., and that the critical altitude, too, might be higher than selected. Also, because of the somewhat arbitrary selection of a V_B speed, it appeared desirable to determine the effect of a range of potential V_B speeds. Accordingly, cases 428-431 were added.

The design envelope points for which lateral gust dynamic analysis was made are shown in Table 7-2. The conditions listed cover a range of weights from minimum flying weight to maximum take-off gross weight. The center of gravity travel investigated included both forward and aft design limits, and both V_C and V_D variations with altitude are represented. No V_B cases are included. Preliminary runs, in which fewer load outputs were available, indicated the critical V_B loads to be appreciably lower than 50/66 of the V_C loads and consequently not critical.

The cases in Tables 7-1 and 7-2 later found to be critical (Appendix E) are indicated by asterisks.

7.2 Model 749

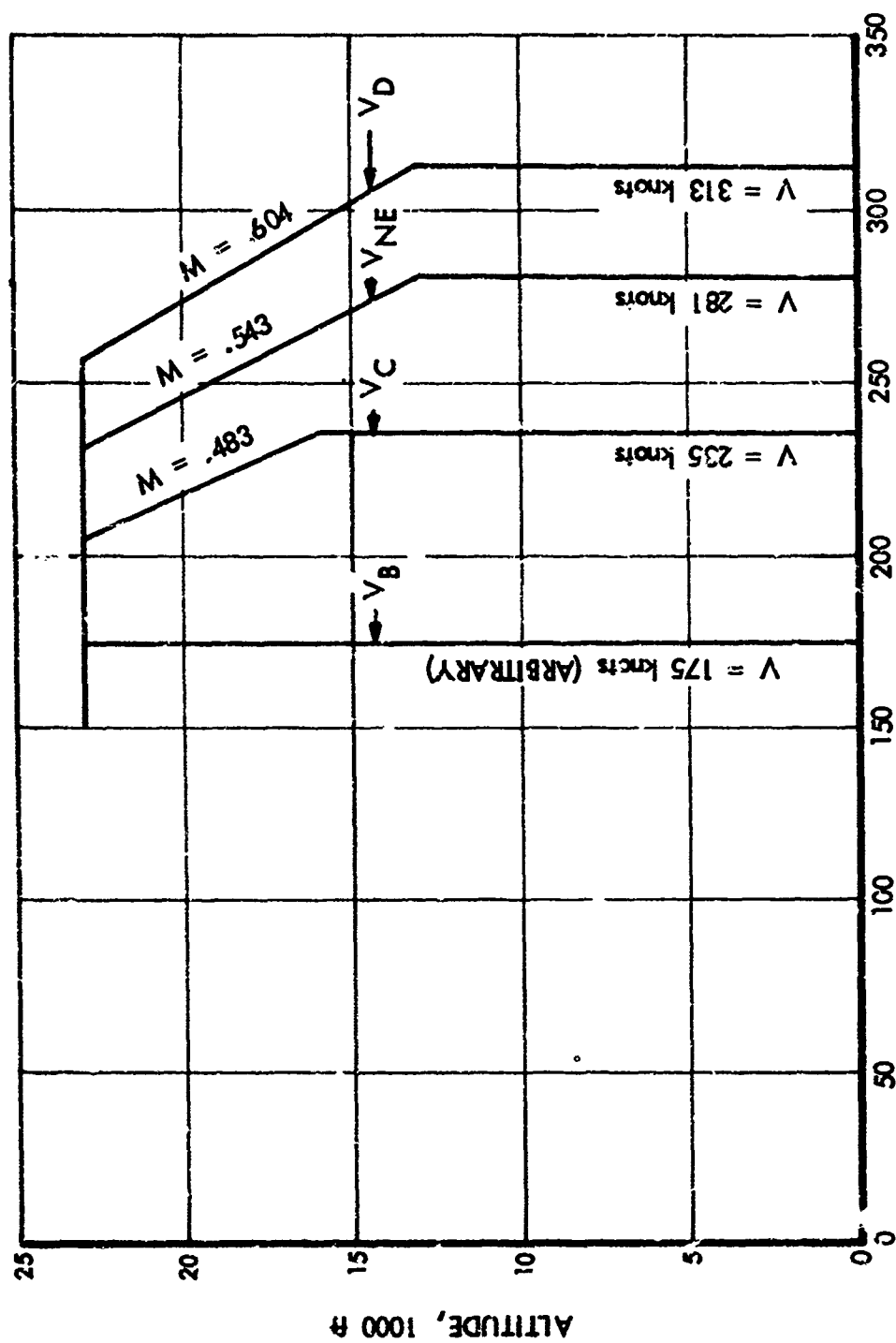
The design speed-altitude chart for the Model 749 is shown in Figure 7-6, and the weight-c.g. envelope in Figure 7-7.

In Figure 7-6, the V_C and V_D constant equivalent airspeed lines at low altitude are the values used for structural design. The knuckle at 16,000 ft. in the V_C line is in accordance with the flight placard. A constant Mach line above this point is assumed for the purpose of the present study, although the actual flight placard is a straight line approximation to this. The knuckle in the V_D line is considered to occur at the same altitude as the knuckle in the V_{NE} line, which is shown at 13,000 ft. in accordance with the flight placard. V_D is assumed to follow a constant Mach line above 13,000 ft. Although a constant Mach line is also shown for V_{NE} , the actual flight placard is a straight line approximation to this line.

TABLE 7-2. DESIGN ENVELOPE CASES FOR LATERAL GUST ANALYSIS, MODEL 188

Case	Gross Weight lb	Zero Fuel Weight lb	Fuel Weight lb	C.G. %MAC	Altitude Ft	V_B , V_C or V_D	V_e Knots
501	116000	86000	30000	35.0	6000	V_C	324
602*	116000	86000	30000	35.0	7000	V_C	324
603	116000	86000	30000	35.0	12000	V_C	324
604	116000	86000	30000	35.0	20000	V_C	276
605	116000	86000	30000	35.0	30000	V_C	221
606	116000	86000	30000	35.0	4000	V_D	405
607	116000	86000	30000	35.0	7000	V_D	405
608*	116000	86000	30000	35.0	8000	V_D	405
609	116000	86000	30000	35.0	20000	V_D	328
610	116000	86000	30000	35.0	30000	V_D	256
611	86500	86000	500	35.0	7000	V_C	324
612	86500	86000	500	35.0	7000	V_D	405
613	65000	61855	3145	35.0	7000	V_C	324
614	65000	61855	3145	35.0	7000	V_D	405
615	86500	86000	500	35.0	12000	V_C	324
616	116000	86000	30000	20.1	20000	V_C	276
617*	116000	86000	30000	20.1	6000	V_C	324
618	116000	86000	30000	20.1	30000	V_C	221
619	116000	86000	30000	20.1	20000	V_C	328
620	116000	86000	30000	20.1	30000	V_D	256
621*	116000	86000	30000	20.1	8000	V_D	405

* Cases found to be critical



V_e , EQUIVALENT AIRSPEED (knots)

FIGURE 7-6. DESIGN SPEED ALTITUDE CHART, MODEL 749

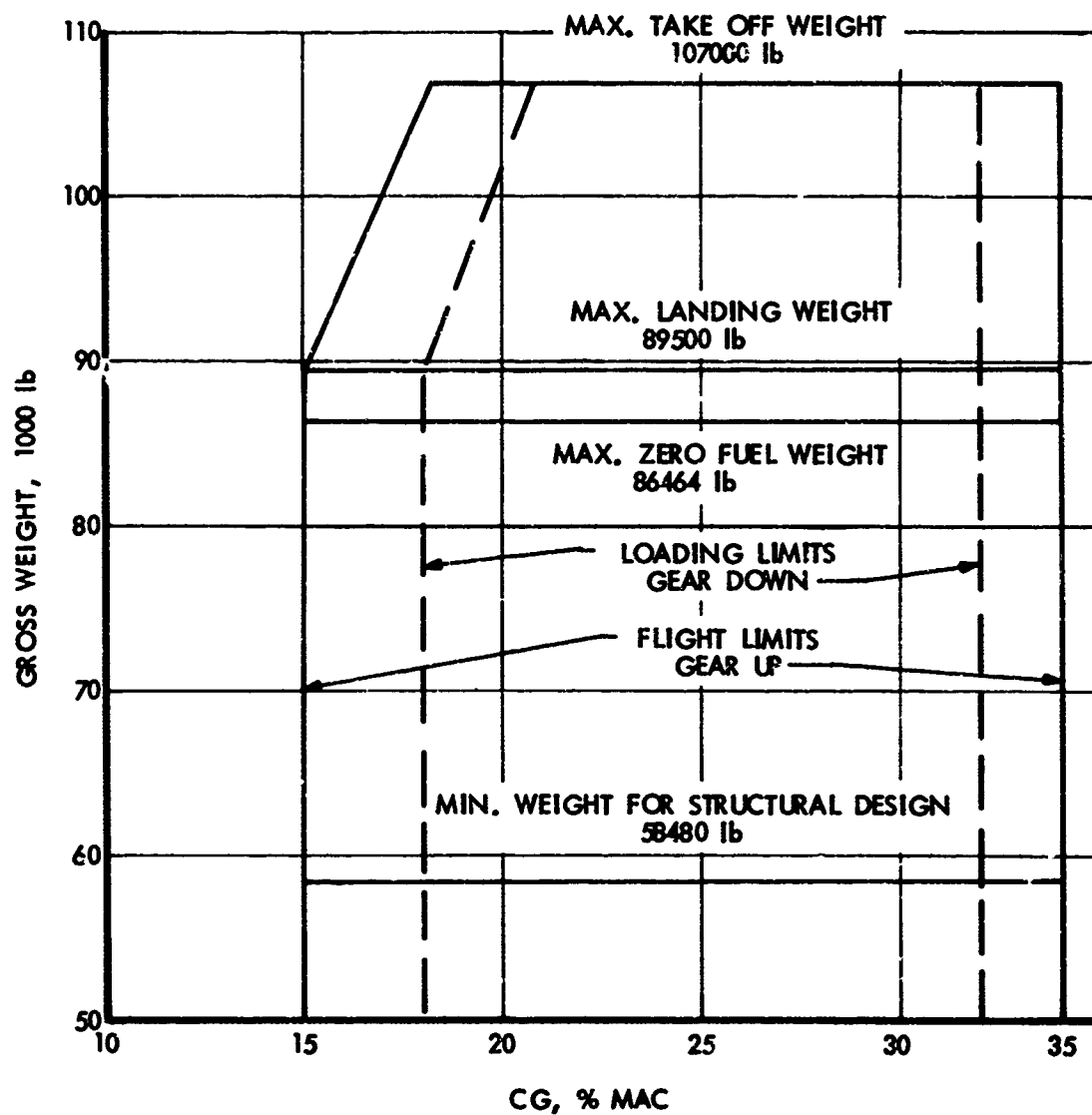


FIGURE 7-7. DESIGN WEIGHT - CG ENVELOPE, MODEL 749

The maximum altitude shown, while not used in the original structural design of the airplane, is a reasonable value based upon performance limitations.

As in the case of the Model 188, the V_B speed is somewhat arbitrary. The 175 knot value used herein is in agreement with present criteria at a gross weight of about 99,000 lb.

The c.g. limits shown in Figure 7-7 are based upon operating placards. Throughout this study, the aft c.g. limit in flight was inadvertently taken equal to the loading limit, at 32% MAC; inasmuch as the results of this study have generally shown the c.g. position to have a very small effect on loads - generally less than 5%, and for the vertical gust loads only 1 or 2%, for the full range between forward and aft limits - no attempt has been made to adjust the results for this discrepancy.

The minimum weight for structural design, shown as 58480 lb., is an early design number and is obviously low for the airplanes as currently operated, with an average operating weight empty of 68640 lb. Cases at minimum weight, however, are found not to be critical.

The design envelope cases for which vertical gust dynamic analysis was conducted for the Model 749 are listed in Table 7-3.

The approximate effect of altitude on loads was determined by means of a simplified analysis, as for the Electra, with the results shown in Figures 7-8, 7-9, and 7-10. It is clear that critical loads will occur at either 7000 ft. or 16000 ft. altitude, with the 16,000 ft. altitude slightly more likely.

Consequently, the first 14 cases in Table 7-3 represent a variety of weight conditions at an altitude of 16,000 ft.

Based on preliminary analysis of the results for these cases, it appeared that Case 308 was critical. Accordingly, a range of altitudes was next investigated for this weight condition; this investigation comprises Cases 315-318.

Selection of four V_D cases and a V_B case was made in the same way as for the Electra.

The design envelope points for which lateral gust dynamic analysis was made for the Model 749 are listed in Table 7-4. Results of the Model 188 analysis were used to eliminate conditions that would clearly not be critical. Critical forebody loads were found to occur in the weight condition having maximum forebody weight combined with minimum fuel and minimum aftbody weight. This result is reasonable; forebody loads are primarily inertial, and maximum values should occur with high forebody weights in combination with the greater accelerations associated with the highest natural frequencies. On the other hand, the aftbody is

TABLE 7-3. DESIGN ENVELOPE CASES FOR VERTICAL GUST ANALYSIS, MODEL 749

Case	Gross Weight Lb	Zero Fuel Weight Lb	Fuel Weight Lb	C. G. % MAC	Altitude Ft	V_B, V_C Or V_D	V_e Knots
301	58480	55980	2500	15.0	16000	V_C	235
302	58480	55980	2500	32.0	16000	V_C	235
303	90900	55980	34920	15.2	16000	V_C	235
304	90900	55980	34920	32.0	16000	V_C	235
305	107000	72080	34920	18.5	16000	V_C	235
306	107000	72080	34920	32.0	16000	V_C	235
307	88964	86464	2500	15.0	16000	V_C	235
308	88964	86464	2500	32.0	16000	V_C	235
309	95000	86464	8536	16.0	16000	V_C	235
310	95000	86464	8536	32.0	16000	V_C	235
311	101000	86464	14536	17.1	16000	V_C	235
312	101000	86464	14536	32.0	16000	V_C	235
313	107000	86464	20536	18.5	16000	V_C	235
314	107000	86464	20536	32.0	16000	V_C	235
315	88964	86464	2500	32.0	20000	V_C	218
316	88964	86464	2500	32.0	12000	V_C	235
317*	88964	86464	2500	32.0	7000	V_C	235
318	88964	86464	2500	32.0	16000	V_C	235
319	58480	55980	2500	15.0	7000	V_D	313
320	58480	55980	2500	32.0	7000	V_D	313
321	88964	86464	2500	15.0	7000	V_D	313
322*	88964	86464	2500	32.0	7000	V_D	313
323*	88964	86464	2500	32.0	7000	V_B	175

* Cases found to be critical

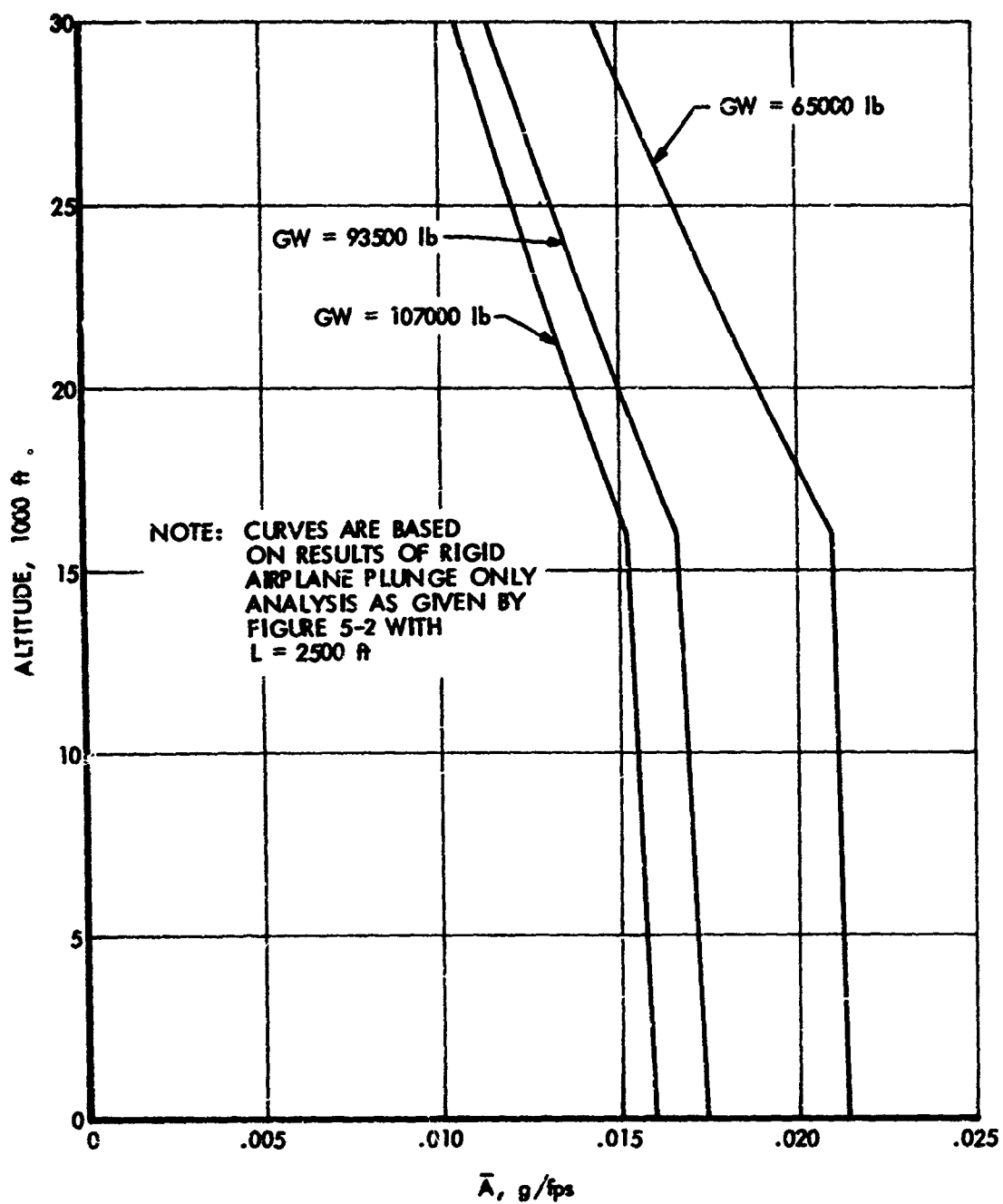


FIGURE 7-8. EFFECT OF ALTITUDE ON \bar{A} FOR C.G. ACCELERATION, MODEL 749

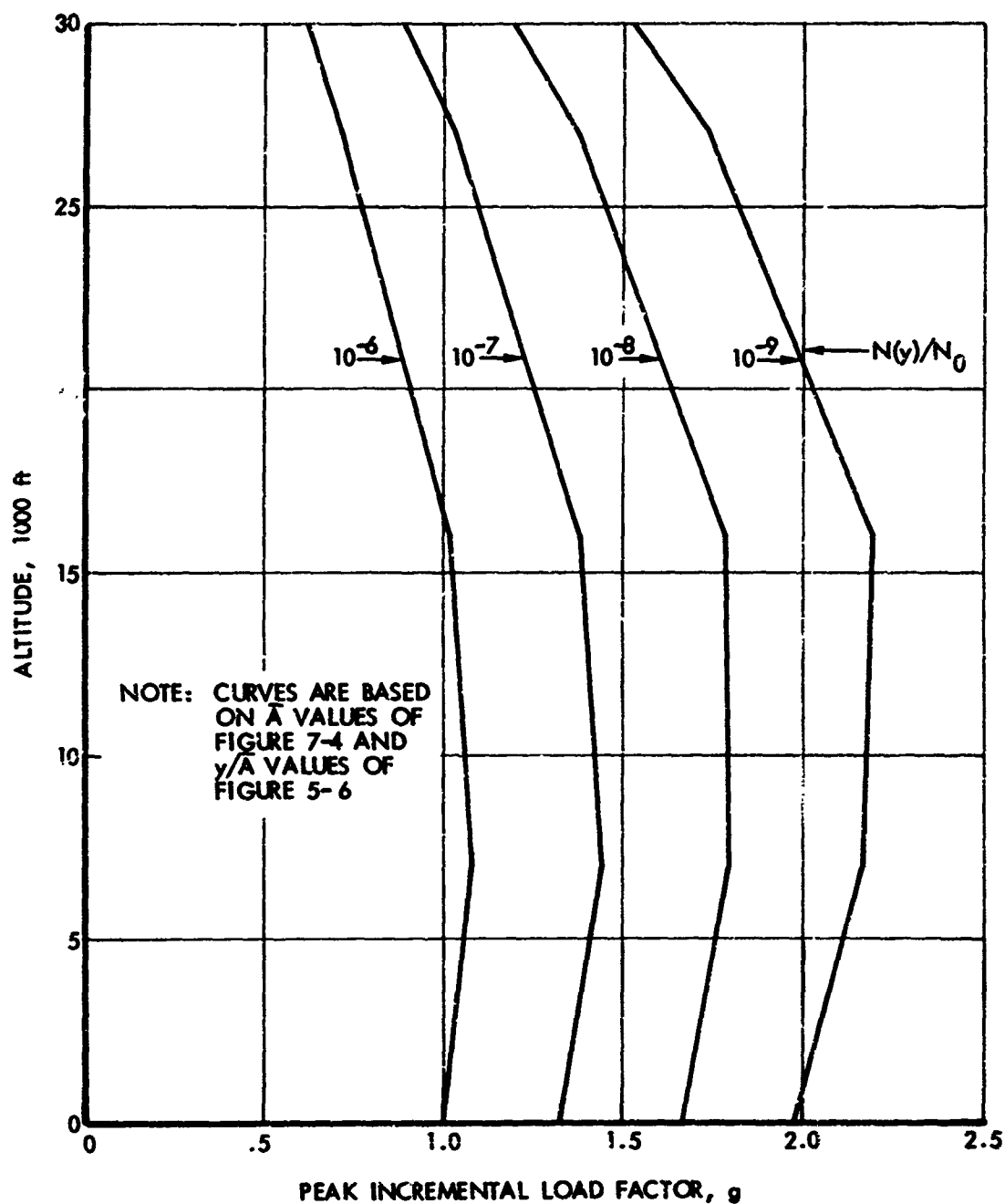


FIGURE 7-9. EFFECT OF ALTITUDE ON DESIGN LEVEL OF CG ACCELERATION, MODEL 749 - VARIOUS $N(y)/N_0$ LEVELS, GROSS WEIGHT = 93500 LB

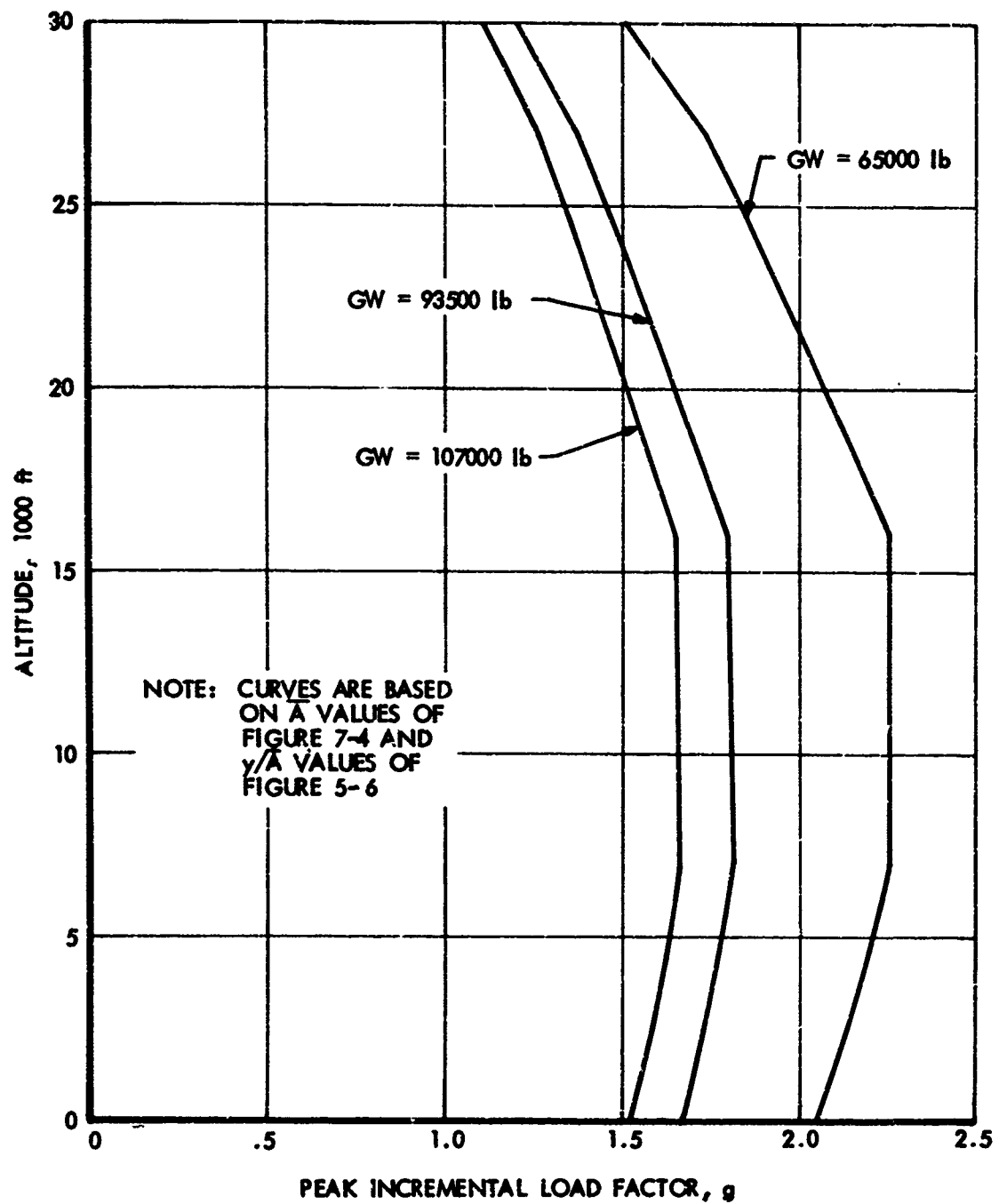


FIGURE 7-10. EFFECT OF ALTITUDE ON DESIGN LEVEL OF CG ACCELERATION, MODEL 749 - VARIOUS GROSS WEIGHTS, $N(y)/N_0 = 10^{-8}$

TABLE 7-4. DESIGN ENVELOPE CASES FOR LATERAL GUST ANALYSIS, MODEL 749

Case	Gross Weight Lb	Zero Fuel Weight Lb	Fuel Weight Lb	C.G. %MAC	Altitude Ft	V _B , V _C or V _D	V _e Knots
501*	107000	86464	20536	32.0	4000	V _C	235
502*	107000	86464	20536	32.0	4000	V _D	313
503*	107000	86464	20536	32.0	10000	V _C	235
504*	107000	86464	20536	32.0	10000	V _D	313
505	107000	86464	20536	32.0	13000	V _D	313
506	107000	86464	20536	32.0	16000	V _C	235
507	107000	86464	20536	32.0	16000	V _D	294
508	107000	86464	20536	32.0	20000	V _C	217
509	107000	86464	20536	32.0	20000	V _D	271
510	107000	86464	20536	32.0	25000	V _C	195
511	107000	86464	20536	32.0	30000	V _C	174
512	107000	86464	20536	32.0	30000	V _D	217

* Cases found to be critical

loaded primarily by the air load on the vertical tail and is, therefore, critical for the high gross weight cases. However, the maximum tail and aftbody loads are much more critical than the maximum forebody loads. Accordingly, in the Model 749 analysis, only the high gross weight, aft c.g. cases were included. Also, inasmuch as V_B conditions were clearly not critical for the Model 188, these also were excluded from the Model 749 analysis.

The combinations of speed and altitude chosen represent both V_C and V_D speeds over a range of altitudes. It should be noted that, for the purposes of this study, several points outside the design operating envelope were obtained - namely, the 25,000 ft. and 30,000 ft. altitude points. These cases are listed in Table 7-4, but are not considered in establishing limit and ultimate strength values of $N(y)$ and of $\sigma_w \eta_d$.

The cases in Tables 7-3 and 7-4 later found to be critical (Appendix E) are indicated by asterisks.

8 MATHEMATICAL MODELS OF REFERENCE AIRPLANES

8.1 Vertical Gust, Models 188 and 749

8.1.1 Equations of Motion. In the mathematical model employed to determine dynamic response of the Model 188 and Model 749 airplanes to the vertical component of turbulence, the airplane is represented by means of a rigid fuselage and horizontal tail, a wing represented elastically by an elastic axis straight and normal to the plane of symmetry, and two nacelles per side having flexibility relative to the wing.

Airplane motions are defined in terms of ten generalized coordinates - fuselage plunge and pitch, two wing bending modes, two wing torsion modes, and plunge and pitch of each nacelle mass relative to the wing. The first wing bending and torsion modes are uncoupled cantilever modes obtained by assuming a reasonable deflection shape and iterating once. The second bending and torsion modes are obtained similarly; however, with only the one iteration, these depart considerably more from the true natural-mode shapes. Provision is also made for specifying both mode shape and frequency for any or all of the four modes, with no further iteration to be made.

Wing masses and aerodynamic forces are lumped at ten spanwise wing stations. Spanwise flow effects are not accounted for, although any desired spanwise variation of $C_{L\alpha}$ can be used; in the present study, panel $C_{L\alpha}$ values were chosen to match static spanwise distributions produced by a constant increment in angle of attack. Definition of the mass of each panel includes the chordwise location of the center of gravity and the pitching moment of inertia.

Each nacelle (in addition to that portion considered rigidly attached to the wing) is represented as a dumbbell mass with translational and rotational inertia. Aerodynamic forces as felt by the propeller as well as the nacelle proper are applied.

The fuselage is assumed to develop aerodynamic lift and moment; lift developed on the forward portion of the forebody is separated out in order to account for the time lag between nose and wing penetration of the gust.

Tail aerodynamic forces include the effect of wing downwash, and the time lags of the gust and downwash proceeding from the wing to the tail are accounted for. Provision is included for aerodynamic force increments on the tail due to elevator float or elevator motions introduced by a stability augmentation system. The elevator float motion is

introduced actually as an eleventh generalized coordinate, with elevator mass (including moment of inertia about the hinge line) as well as aerodynamic forces included. A simple static treatment could have been used, and would have given essentially the same results; this would have eliminated the need to include appropriate external damping in the mode.

Unsteady lift growth functions for gust encounter (Kussner function) and for airplane motions (Wagner function) are represented separately for wing, tail, fuselage, nose, nacelles, and propellers. The customary exponential approximations appropriate to low Mach number and infinite aspect ratio are used for the various wing panels and for the horizontal tail. For the fuselage, nacelles, and propellers, the same exponential expressions are used, but effective values of chord are estimated such as to provide reasonable approximations to the lift growth on these components.

Loads at various points in the airplane are obtained by superimposing the loads produced by the direct effect of the gust and those resulting from the motions in the ten generalized coordinates. Provision is included for computation of the following load quantities as desired: wing shears, bending moments, and torsions at ten spanwise locations; up to 20 wing shear flows (or other internal loads that can be expressed as linear combinations of the shears, bending moments, and torsions); nacelle c.g. shears and pitching moments (two nacelles); and up to ten fuselage loads (shears or bending moments) including load on the horizontal tail. For the wing, the load read-out locations are defined by the initial lumping of mass and aerodynamic data. Loads are determined for the individual panels and summed as appropriate to yield shears, bending moments, and torsions at the panel boundaries. Since the fuselage is considered rigid, its mass and aerodynamic properties need not be broken into numerous panels for solution of the equations of motion. For the purpose of fuselage load determination, however, the aerodynamic forces are distributed to a number of panels. Fuselage shear or bending moment at any given station is then obtained by summing terms consisting of appropriate coefficients multiplying the pitch and plunge accelerations and the airloads on the various panels.

The ten simultaneous differential equations of motion are solved for a forcing function consisting of a steady sinusoidal variation of gust velocity. Frequency-response, or transfer, functions relating both the generalized coordinates and the various airplane load quantities to the input gust velocity are thus evaluated, at up to 100 frequencies. The modulus of each transfer function is then squared and multiplied by the input gust spectrum to obtain an output power spectrum. These in turn are integrated with respect to frequency to give \bar{A} and N_0 values. The upper limit of integration was taken as 10.2 cps.

Provision is also included in the equations of motion for elevator motion instead of gust velocity as an input, in order to obtain transfer functions of maneuver loads for establishing the adequacy of the aerodynamic input data.

All of the calculations indicated above were carried out in a continuous operation on an IBM 7094 automatic digital computer.

A complete presentation of the equations of motion, including their derivation, is contained in Reference 21.

8.1.2 One-g Level Flight Loads. The one-g level flight loads to which the incremental loads due to the turbulence must be added were obtained by appropriate static loads methods.

For the Model 188, the distribution of air loads between the wing, fuselage, and horizontal tail was based upon wind tunnel force data. Wing spanwise lift distributions, for the rigid wing, were obtained by means of theory. Wing and nacelle aerodynamic pitching moments were based on integrated use of published NACA documents, wind tunnel pitch data for the Model 188 wing with and without nacelles, calculated propeller normal forces, and flight-measured wing torsions over a wide range of speed and load factor. Air load increments due to the wing twist resulting from the rigid airplane aerodynamic and inertia forces were calculated and included. Arbitrary adjustments to the theoretical airload distributions were made where necessary to bring the calculated loads into close agreement with flight-measured loads.

For the Model 749, as for the Model 188, the distribution of air loads between wing, fuselage, and horizontal tail was based upon wind tunnel force data. Wing airload distributions, too, were determined in a generally similar manner, although flight-measured torsions were not available. Excellent agreement was found between wing bending moments calculated using these distributions and bending moments obtained by flight measurements on a Model 1049B, which had a wing aerodynamically identical to that of the Model 749.

8.1.3 Input Data for Dynamic Analysis. The scheme for lumping of input data and the locations of load read-out points are shown in Figures 8-1 and 8-2 for the Model 188 and Model 749 respectively.

For the wing, load read-out stations are determined by the panel boundaries defined for lumping of input data. Consequently, a fairly detailed coverage of load outputs was inherently provided. Shear, bending moment, and torsion were obtained at each of the wing load

1. INERTIA AND PITCHING MOMENT OF INERTIA ARE LUMPED AT CHORDWISE CENTER OF GRAVITY OF EACH PANEL.
2. LOCAL AERODYNAMIC CENTER IS ASSUMED TO BE AT LOCAL 24% CHORD.
3. LOCAL CHORD = $C_l = 227 - .229y$:
4. MEAN AERODYNAMIC CHORD = 168.7
LE MAC = FS 545.9
5. NACELLE AERODYNAMICS AND INERTIA CONCENTRATED AT NACELLE CG INBOARD FS 471.7, OUTBOARD FS 480.5

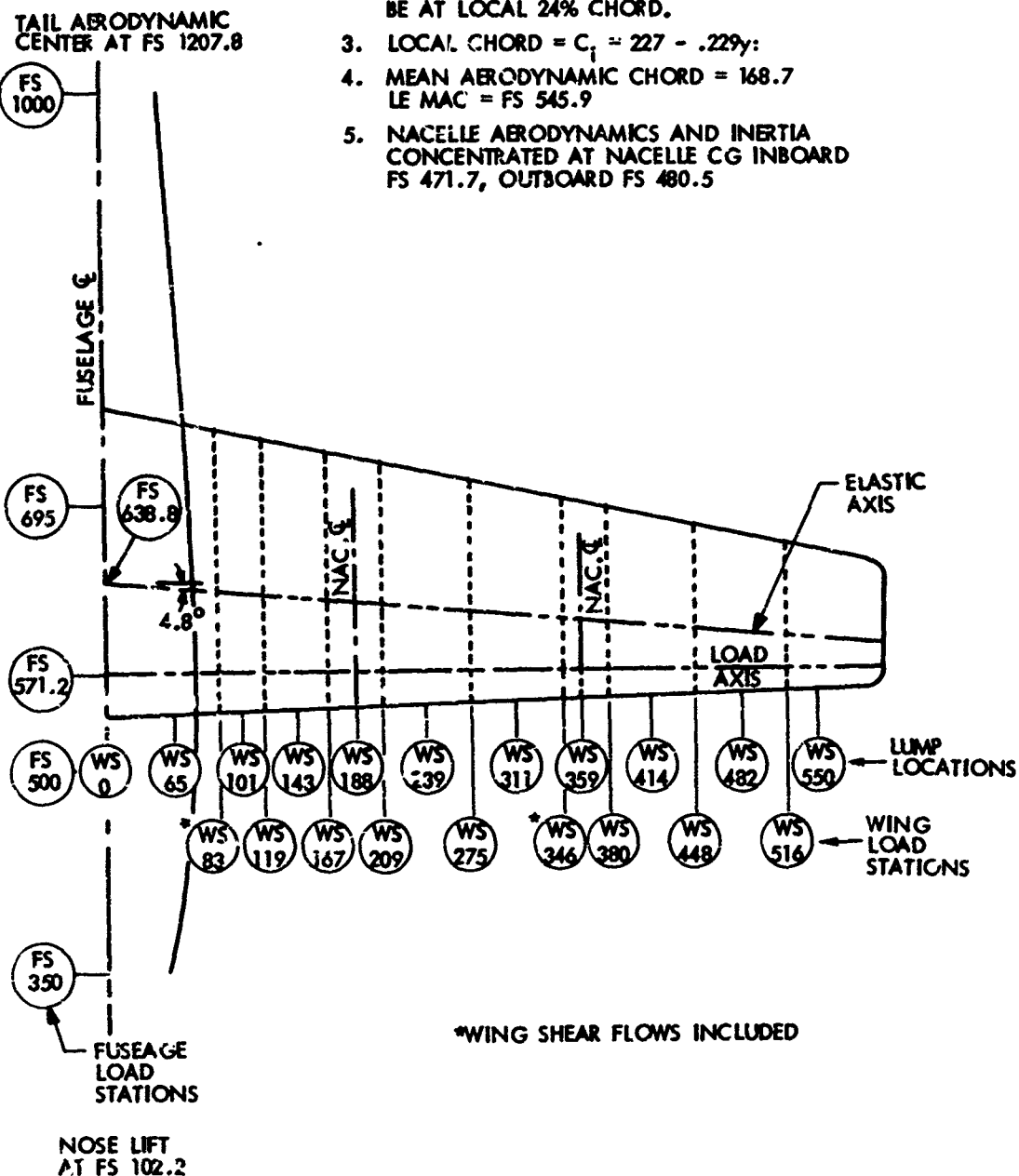


FIGURE 8-1. MODEL 188 GEOMETRY AND LOAD STATIONS

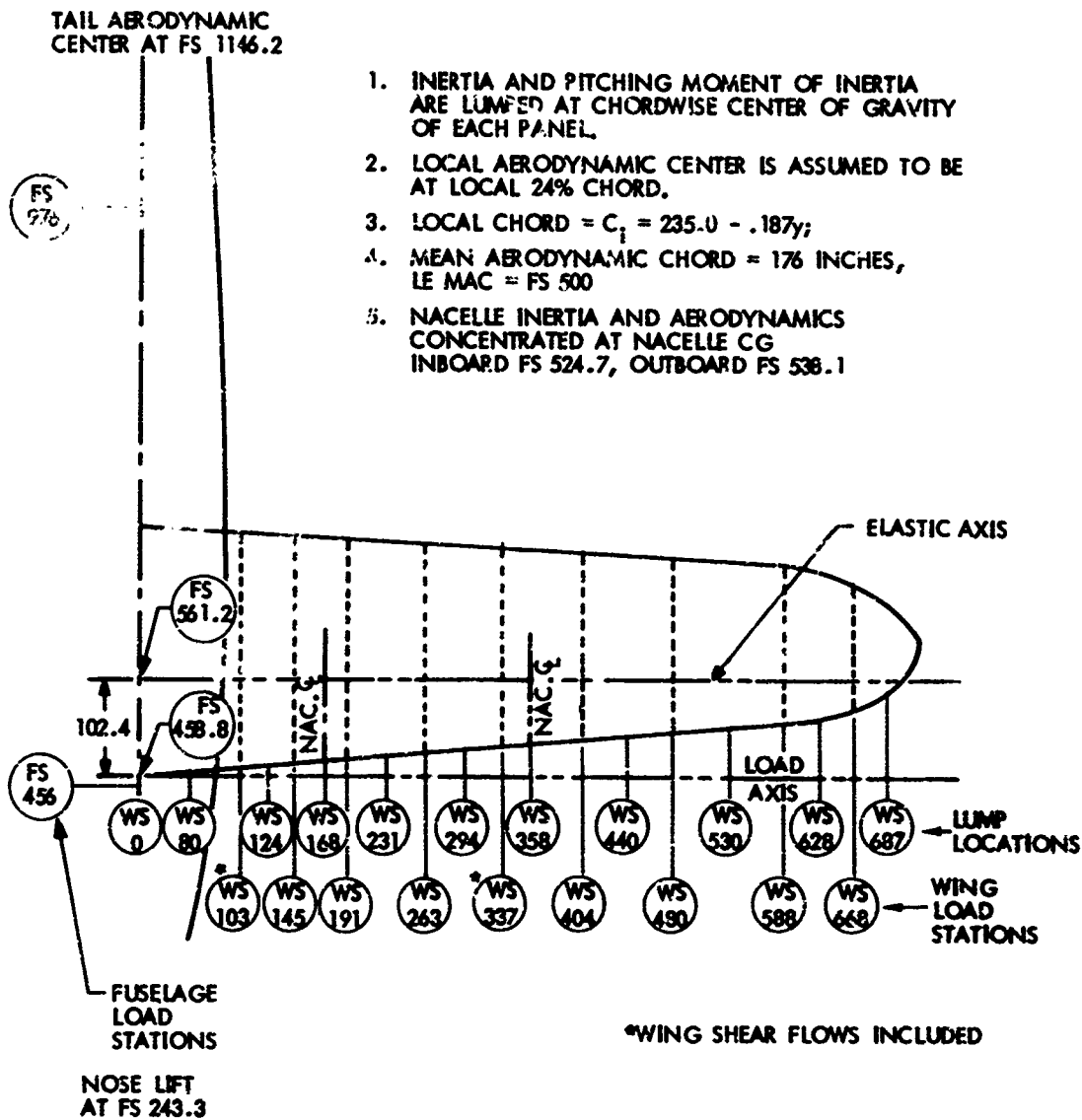


FIGURE 8-2. MODEL 749 GEOMETRY AND LOAD STATIONS

stations indicated in the figures, and front and rear beam shear flows were also obtained at the two wing stations noted.

For the Model 188 fuselage, the selection of load output points was influenced by an examination of margins of safety for the design gust conditions, with the critical locations selected. The Model 749 fuselage was designed to extremely severe criteria and is much less critical than the wing; consequently, only a limited number of load outputs were obtained. In obtaining fuselage load outputs, overlapping assumptions with respect to the distribution of payload were made, in the design envelope cases, in order to simplify the preparation of input data. For a given total payload, the distribution of payload between the forebody and aftbody depends upon whether the airplane c.g. is to be at the forward or the aft limit. However, in determining the increments of fuselage shear and bending moment due to turbulence, the panel weights by which the local accelerations were multiplied in the dynamic analysis were always taken as the higher of the forward limit and aft limit values, regardless of the actual c.g. position for the case being analyzed. Horizontal tail loads were included as outputs for the particular cases found to be potentially critical as a result of examining the fuselage load results.

Mass and aerodynamic data used in the dynamic analysis of the two airplanes are generally consistent with the data used for static loads determination, as described in the previous section.

Wing EI and GJ (flexural and torsional stiffnesses) were obtained by calculation; guidance as to appropriate assumptions regarding extent of effective material was obtained from the results of static load-deflection measurements and ground vibration tests. Nacelle stiffnesses were obtained similarly, with particular reliance on load-deflection data for the individual engine mounts and on nacelle mode natural frequencies obtained in ground vibration tests.

Wing structural damping was assumed to be zero, inasmuch as the substantial aerodynamic damping present overshadows the structural damping.

Inclusion of structural damping in the nacelle modes, however, was considered desirable. Comparison of Model 188 calculated with flight measured power-spectral densities indicated that nacelle response above about 4 cps could not be adequately represented by the ten-degree-of-freedom analysis. Not only is the mechanical representation of the nacelle vertical freedoms too crude, but also: 1) coupling with the yaw motions is not included, 2) there is no way to account for the effect of side gusts and their coupling with vertical motions, and 3) spanwise variations of gust velocity, not considered in the theory, invalidate the couplings assumed between nacelle and wing motions. As a result, power spectral densities of nacelle loads calculated without the inclusion

of structural damping indicated considerably more power above about 4 cps than was actually present. In earlier studies, to assure realistic nacelle load inputs to the wing, the integration of the power-spectral densities had been limited to a maximum frequency of about $4\frac{1}{2}$ cps, thereby eliminating the increased response. This had little effect on wing loads since most of their response is in the short period and first bending-torsion modes. In the present study, as a more rational means of preventing possible over estimation of nacelle response at the higher frequencies, structural damping was introduced into the spring connection of the nacelles to the wing. A structural damping coefficient of .20 was assumed; this is the value of g in the expression $(1 + ig)k$ and corresponds, at the resonant frequency, to a relative viscous damping of .10. This damping value appears reasonable, and it sufficiently reduces the high frequency response to give substantially improved agreement with flight measured power spectral densities.

In order to account adequately for the effect of static aeroelastic deflection on the spanwise load distribution and on the gust load factor of the Model 188, it was found necessary to replace the second dynamic wing torsion mode by a static aeroelastic deflection shape. This was because a significant part of the static aeroelastic deformation occurs outboard of the outboard nacelle, whereas neither of the first two dynamic torsion modes contains significant deformation in this region. While some loss of detail in the dynamic representation results, it appears that, over-all, the static aeroelastic mode is more important than the second dynamic torsion mode. It is therefore included in the present Model 188 analysis.

Considerable effort was put forth to assure that, on a static basis, the ten-degree-of-freedom analysis duplicated loads obtained by the accepted static loads methods. For this purpose, ten-degree-of-freedom loads were obtained for both the Model 188 and Model 749 for a maneuver condition obtained by introducing a low-frequency elevator oscillation. The resulting loads are not sensitive to the exact frequency chosen, as long as it is well below that of the airplane short-period mode. The effect of frequency is shown in Table 8-1. Based on the results shown therein, a frequency of .05 cps was selected for the loads comparison. The comparison of ten-degree-of-freedom loads with static analysis loads, per g of c.g. acceleration, is shown in Tables 8-2 and 8-3. Torsional moments are compared on a difference rather than a ratio basis, since torsional moments can easily be close to zero, depending on the location of the arbitrary moment axis, and ratios have little meaning. For comparison, the approximate limit design torsions are noted in the tables. It is seen that the ten-degree-of-freedom analysis reproduces the loads obtained by the static loads analysis very well. The small differences that do exist are not considered significant, especially since in some respects the ten-degree-of-freedom analysis may be more rational than the static analysis.

TABLE 8-1. EFFECT OF FREQUENCY OF ELEVATOR MOTION ON
MAGNITUDE OF ROOT BENDING MOMENT

Frequency Of Elevator Motion CPS	Model 749			Model 188		
	$10^{-6} M_x / n_z @ W.S. 103$			$10^{-6} M_x / n_z @ W.S. 83$		
	$V_e = 205 \text{ Kt}$	$V_e = 235 \text{ Kt}$	$V_e = 290 \text{ Kt}$	$V_e = 264 \text{ Kt}$	$V_e = 314 \text{ Kt}$	$V_e = 364 \text{ Kt}$
.0125	5.720	5.909	6.383	3.646	3.791	4.085
.025	5.718	5.908	6.387	3.644	3.790	4.085
.050	5.713	5.904	6.384	3.637	3.785	4.082
.100	5.691	5.887	6.373	3.609	3.767	4.070
.200	5.606	5.822	6.330	3.504	3.700	4.027
.400	5.291	5.578	6.165	3.165	3.476	3.884
1.00	3.870	4.406	5.335	1.872	2.640	3.446

TABLE 8-2. COMPARISON OF LOADS COMPUTED BY THE DYNAMIC ANALYSIS PROGRAM AND BY STATIC ANALYSIS METHODS, MODEL 188

Wing Station	Static Analysis			Dynamic Analysis			Comparison			
	$\frac{S_z}{\Delta n_z}$	$\frac{10^{-6} M_x}{\Delta n_z}$	$\frac{10^{-6} M_y}{\Delta n_z}$	$\frac{S_z}{\Delta n_z}$	$\frac{10^{-6} M_x}{\Delta n_z}$	$\frac{10^{-6} M_y}{\Delta n_z}$	$\frac{S_{zDyn.}}{S_{zStat.}}$	$\frac{M_{xDyn.}}{M_{xStat.}}$	$\frac{10^{-6} M_{yDyn.}}{-M_{yStat.}}$	$\frac{10^{-6} M_y}{\text{Limit Design}}$
$V_e = 264 \text{ knots, } h = 13500 \text{ ft}$										
83	11259	3.689	-.127	10948	3.637	-.022	.975	.987	.105	-7.9
119	10497	3.292	-.190	10275	3.264	-.090	.986	.995	.100	-7.8
167	8197	2.813	-.203	8177	2.833	-.109	.995	1.003	.034	-7.7
209	11635	2.378	-.079	11828	2.391	-.045	1.018	1.003	.034	-4.0
275	9512	1.682	-.122	9692	1.700	-.088	1.018	1.007	.034	-3.3
346	6429	1.121	-.123	6599	1.131	-.086	1.023	1.006	.037	-2.6
380	9151	.831	-.091	9384	.842	-.114	1.021	1.011	-.023	-1.25
448	5488	.332	-.053	5593	.340	-.067	1.020	1.021	-.014	-.75
516	2189	.087	-.016	2308	.076	-.025	1.050	.874	-.007	-.35
$V_e = 314 \text{ knots, } h = 13500 \text{ ft}$										
83	11391	3.811	+.056	11225	3.785	.023	.986	.994	-.033	-7.9
119	10702	3.117	-.009	10617	3.401	-.046	.994	1.000	-.037	-7.8
167	8487	2.917	-.024	8595	2.951	-.066	1.010	1.010	-.042	-7.7
209	11977	2.468	+.017	12256	2.494	-.028	1.018	1.010	-.045	-4.0
275	9889	1.749	-.027	10139	1.774	-.071	1.020	1.010	-.044	-3.3
346	6774	1.161	-.027	7003	1.175	-.068	1.033	1.010	-.041	-2.6
380	9455	.861	-.096	9726	.875	-.119	1.028	1.018	-.023	-1.25
448	5687	.345	-.057	5824	.354	-.070	1.023	1.023	-.013	-.75
516	2275	.092	-.019	2412	.079	-.027	1.060	.859	-.008	-.35
$V_e = 364 \text{ knots, } h = 13500 \text{ kts}$										
83	11481	4.016	.247	11860	4.082	.089	1.032	1.016	-.158	-7.9
119	10951	3.605	.179	11394	3.671	.018	1.038	1.017	-.161	-7.8
167	8923	3.100	.159	9452	3.133	-.004	1.055	1.023	-.163	-7.7
209	12535	2.631	.117	13133	2.691	-.003	1.043	1.021	-.120	-4.0
275	10549	1.871	.071	11020	1.913	-.046	1.043	1.021	-.117	-3.3
346	7410	1.238	.071	7773	1.256	-.041	1.043	1.017	-.112	-2.6
380	10027	.917	-.110	10361	.937	-.129	1.036	1.020	-.019	-1.25
448	6055	.371	-.065	6237	.380	-.076	1.030	1.022	-.011	-.75
516	2434	.098	-.023	2594	.085	-.029	1.064	.868	-.006	-.35

NOTE: Torsion Moments, M_y are about load axis AITFS 571.2

TABLE 8-3. COMPARISON OF LOADS COMPUTED BY THE DYNAMIC ANALYSIS PROGRAM AND BY STATIC ANALYSIS METHODS, MODEL 188

Wing Station	Static Analysis			Dynamic Analysis			Comparison			
	$\frac{S_z}{\Delta n_z}$	$\frac{10^{-6} M_x}{\Delta n_z}$	$\frac{10^{-6} M_y}{\Delta n_z}$	$\frac{S_z}{\Delta n_z}$	$\frac{10^{-6} M_x}{\Delta n_z}$	$\frac{10^{-6} M_y}{\Delta n_z}$	$\frac{S_z \text{ Dyn}}{S_z \text{ Static}}$	$\frac{M_x \text{ Dyn}}{M_x \text{ Static}}$	$10^{-6} (M_{y \text{ Dyn}} - M_{y \text{ Stat}})$	$10^{-6} M_y$ Limit Design
$V_e = 205 \text{ knots, } h = 13000 \text{ ft}$										
103	15627	5.838	-1.775	15499	5.713	-1.658	.990	.980	.117	-8.12
145	12499	5.219	-1.648	12469	5.132	-1.532	.995	.983	.116	-7.94
191	18154	4.497	-1.798	16197	4.427	-1.741	1.002	.084	.057	-7.28
263	13730	3.371	-1.528	13813	3.257	-1.470	1.006	.966	.058	-6.53
337	9285	2.496	-1.217	9412	2.424	-1.162	1.014	.971	.055	-5.66
404	12507	1.674	-1.250	12522	1.650	-1.264	1.001	.986	.014	-4.46
480	8453	.883	-.887	8469	.861	-.890	1.002	.975	-.003	-3.26
588	3739	.226	-.417	3761	.219	-.420	1.000	.969	-.003	-1.57
668	1149	.031	-.127	1167	.022	-.135	1.016	.710	-.008	-
$V_e = 235 \text{ knots, } h = 13000 \text{ ft}$										
103	16949	5.993	-1.844	16715	5.904	-1.748	.986	.985	.006	-8.12
145	13015	5.328	-1.664	13017	5.280	-1.577	1.000	.991	.087	-7.94
191	19251	4.569	-1.870	19288	4.537	-1.830	1.002	.993	.040	-7.28
263	14017	3.395	-1.539	14229	3.310	-1.508	1.015	.975	.031	-6.53
337	8950	2.522	-1.176	9280	2.470	-1.155	1.037	.977	.021	-5.66
404	12793	1.687	-1.277	12898	1.681	-1.301	1.008	.996	-.024	-4.46
480	8512	.885	-.893	8610	.873	-.905	1.012	.986	-.014	-3.26
588	3741	.225	-.417	3803	.222	-.424	1.017	.987	-.007	-1.57
668	1146	.031	-.127	1176	.022	-.136	1.026	.710	-.009	-
$V_e = 292 \text{ knots, } h = 13000 \text{ ft}$										
103	18099	6.011	-1.924	19397	6.384	-1.671	1.072	1.082	.253	-8.12
145	13154	5.310	-1.677	14375	5.675	-1.410	1.093	1.069	.267	-7.94
191	20080	4.528	-1.930	21628	4.842	-1.887	1.087	1.069	.043	-7.28
263	13866	3.332	-1.526	15860	3.478	-1.456	1.108	1.044	.070	-6.53
337	8117	2.496	-1.106	9211	2.606	-1.004	1.135	1.044	.102	-5.66
404	12865	1.670	-1.282	13906	1.773	-1.401	1.031	1.062	-.119	-4.46
480	8412	.871	-.882	9040	.910	-.951	1.075	1.045	-.069	-3.26
588	3672	.220	-.409	3946	.229	-.440	1.075	1.036	-.031	-1.57
668	1122	.013	-.124	1213	.023	-.140	1.081	.742	-.016	-

NOTE: Torsion moments, M_y , are about load axis at FS458.8

Inasmuch as results of an analysis including the pitch freedom can be somewhat sensitive to the static stability in pitch, precautions were taken to assure that the pitch stability is correctly reflected in the analysis. Since the pitch stability results from the sum (or difference) of many different contributors - including each wing element, the nacelles, the propellers, the fuselage, the tail, the control system, all of the masses - the many separate contributions do not always add up to the best value for the airplane as a whole, and adjustments were made as needed.

An option with respect to pilot technique is available in that flight can be assumed to be either "stick-fixed" or "stick-free." In order to account realistically for the strongly stabilizing effect of the Model 188 control column bob-weight, it was considered appropriate to assume a stick-free technique. Moreover, recommended techniques for flight through turbulence have generally called for a very light touch on the control column, which would appear to be more closely approximated by a stick-free than a stick-fixed condition. Accordingly, both Model 188 and Model 749 vertical gust analyses were conducted stick-free. A comparison of stick-fixed with stick-free results, however, indicated that the loads produced were not sensitive to the choice between the two assumptions.

8.2 Lateral Gust, Models 188 and 749

8.2.1 Equations of Motion. The equations of motion employed to determine Model 188 and Model 749 loads due to the lateral component of turbulence were derived following closely the derivation presented in NACA TN 3603 (Reference 22).

The equations of motion are written with respect to an Eulerian moving axis system and utilize as generalized coordinates the three rigid-body motions of sideslip, yaw, and roll. Provision is included for inertia coupling between the generalized coordinates through the product of inertia, I_{xz} ; however, for the Model 188 and Model 749 this term is so small as to have negligible effect and is assumed to be zero.

Elastic mode response is not included. For both the Model 188 and the Model 749, the lowest fuselage-tail side bending natural mode is far higher in frequency than the Dutch roll mode - roughly 6 to 8 cps vs .2 to .3 cps. Consequently, for these airplanes, the elastic modes were expected to contribute negligibly to the loads produced by turbulence.

Provision is made to include the effects of rudder and aileron float, if desired, or of artificial stability augmentation systems.

For the purpose of accounting for the penetration of the various aerodynamic elements into the gust, aerodynamic forces are evaluated

separately for the wing, fuselage, and vertical tail. Wing and fuselage aerodynamic forces are lumped at the airplane c.g., and tail forces at the vertical tail aerodynamic center.

Provision is made in the equations of motion for the effect on each aerodynamic element of the sidewash produced by the other elements; but the best indications are that on the Model 188 and Model 749 the side-wash is negligible, and it is assumed zero in the analysis.

Unsteady lift growth functions for gust encounter (Kussner function) and for airplane motions (Wagner function) are represented separately for the vertical tail, the fuselage body, and the wing. Suitable exponential approximations are used; the effective chord for use in these expressions is taken equal to the mean chord for the vertical tail and wing and zero for the fuselage.

Fuselage loads at any desired fuselage station are obtained by superposition of inertia loads due to lateral, rolling, and yawing accelerations (including the lateral component of gravity) and aerodynamic loads due to the net sideslip angle at the airplane c.g.

The three simultaneous differential equations of motion are solved for a forcing function consisting of a steady sinusoidal variation of lateral gust velocity. Frequency-response, or transfer, functions relating both the generalized coordinates and the various airplane load quantities to the input gust velocity are thus evaluated, at up to 40 frequencies. The modulus of each transfer function is squared and multiplied by the input gust spectrum to obtain an output power spectrum. These in turn are integrated with respect to frequency to give \bar{A} and N_0 values. The upper limit of integration was taken as 9 cps. The lower limit of integration was taken as .04 cps instead of 0, in order to exclude a sizeable response associated with an unstable spiral mode which, in practice, would be adequately controlled by the pilot.

All of the calculations indicated above were carried out in a continuous operation on an IBM 7094 automatic digital computer.

A complete presentation of the equations of motion, including their derivation, is contained in Reference 23.

8.2.2 Input Data for Dynamic Analysis. Airplane mass data for use in the Model 188 and Model 749 lateral gust analyses were drawn from calculations made in the course of design loads determination.

The various stability derivatives were obtained from a careful evaluation and integration of such sources as wind tunnel force measurements,

flight-measured stability and control characteristics, theoretical calculations, and published NASA information.

The following quantities were selected for load determination:

Quantity	Location Model 188	Location Model 749
Fin side load	Total for fin	Total for three fins
Fin bending moment	Fin root	(Not obtained)
C.G. lateral acceleration	Actual c.g.	Actual c.g.
Pilot station lateral acceleration	FS 132	FS 200
Vertical tail lateral acceleration	FS 1161	FS 1194
Aftbody side shear	FS 694	FS 1057
Aftbody side bending	FS 694	FS 1057
Aftbody torsion	FS 694	FS 1057
Forebody side shear	FS 571	FS 456
Forebody side bending	FS 571	FS 456

The fin side loads were obtained ignoring the effect of relieving inertia. Results for a representative case - Model 188 mission analysis case 201 - indicated that inclusion of the relieving inertia reduced the load by only about 3%.

In selecting specific values for the Kussner and Wagner unsteady lift growth functions for use in the lateral gust analysis, it appeared at first that any reasonable approximation would be satisfactory. Loads due to lateral gust occur predominantly at frequencies in the vicinity of the Dutch roll natural frequency. As a result of the low frequency of this mode, in combination with a vertical tail chord length considerably less than that of the wing, the unsteady lift growth functions are very close to unity, and it appeared that it would be hard to be very far in error in their determination. Accordingly, for the fin, exponential approximations appropriate to an infinite aspect ratio surface at low Mach number were assumed initially.

Closer examination of the unsteady lift growth functions, however, indicated this assumption to be inadequate. The absolute value and the real part, or in-phase component, of both Kussner and Wagner lift growth functions were indeed close to unity, with values of about .97. The imaginary part, or 90-degree out-of-phase component, of the Kussner function is of no concern, except for the extent to which it might be different for two parts of the same airplane. The imaginary part of the Wagner function, however, is quite significant. Based on the high aspect-ratio, low Mach number assumption, its value is about .07. This, acting upon the aerodynamic spring force - which is several times as great as the damping force - produces a sizeable force in phase with, and in the same direction as, the yaw velocity. Thus a negative damping force increment is introduced. This was found to reduce the damping coefficient, ζ , for the Dutch roll mode to about 2/3 of the value it would have with instantaneous lift growth. Inasmuch as the various \bar{A} values vary approximately inversely as $\sqrt{\zeta}$, the corresponding increase in \bar{A} values due to the unsteady lift growth is about 22%.

Because of this sizeable effect, it became important to use the best available information for the Wagner lift growth function. Accordingly, the assumed exponential approximation was replaced by one which accounts approximately for the actual aspect ratio and Mach number.

The expression used was of the form

$$1 - a e^{-bs}$$

where s is the distance traveled in chord lengths. The values selected for the constants were $a = .40$ and $b = .376$. The original form of the Kussner function was considered satisfactory and was retained.

The effect of the revised lift growth function was evaluated by comparing \bar{A} and N_0 values computed using the two different versions of the Wagner function for both the Model 188 and the Model 749. Generally the \bar{A} values decreased by about 10% and the N_0 values increased by about 8%. Therefore, the improved lift growth representation shown above was used throughout the lateral analysis.

As in the vertical gust analysis, options were available as to assumed pilot technique. The effect of pilot technique on gust loads may be substantial. It is undoubtedly complex, and a completely rational treatment is well beyond the present state of the art. Several idealized techniques, however, are readily amenable to analytical representation.

These include various combinations of the following: (a) Rudder held fixed, or rudder free to float, or rudder controlled so as to eliminate

all yaw motion of the airplane; (b) ailerons held fixed, or ailerons free to float, or ailerons controlled so as to eliminate all roll motion.

In order to determine how much the results of the analysis might be affected by the choice of pilot technique, responses were obtained, for Model 188 mission analysis case 202, for four of the nine available techniques.

- (1) "Rudder fixed" - rudder and ailerons fixed.
- (2) "Rudder free" - rudder free, ailerons fixed.
- (3) "No roll" - rudder fixed, ailerons controlled so as to prevent all roll motion.
- (4) "No roll, no yaw" - rudder and ailerons controlled so as to prevent roll and yaw motion.

Major attention was directed to the first three of these techniques. Although a still more restrictive control action could be assumed, as represented by technique (4), it was considered unlikely that a pilot would attempt much tighter control than represented by techniques (1) through (3).

Consideration was also given to inclusion of autopilot operation. Discussions with persons familiar with operating practices indicated that autopilots are sometimes used in fairly light turbulence, up to peak vertical gust load factors of about .25 to .30. At this point the autopilot is almost certain to be disengaged. Consequently, autopilot action was not further considered in the present study.

The \bar{A} values (ratios of rms response to rms gust velocity) for the four pilot techniques investigated are as follows:

<u>Pilot Technique</u>	<u>C.G. Lateral Load Factor</u>	<u>Pilot Station Lateral Load Factor</u>	<u>Sideload On Vertical Tail</u>
(1) Rudder fixed	.00564	.00233	270
(2) Rudder free	.00715	.00286	304
(3) No roll	.00568	.00236	275
(4) No roll, no yaw	(.00504)	(.00504)	(249)

The corresponding power spectral densities are shown in Figures 8-3 through 8-5.

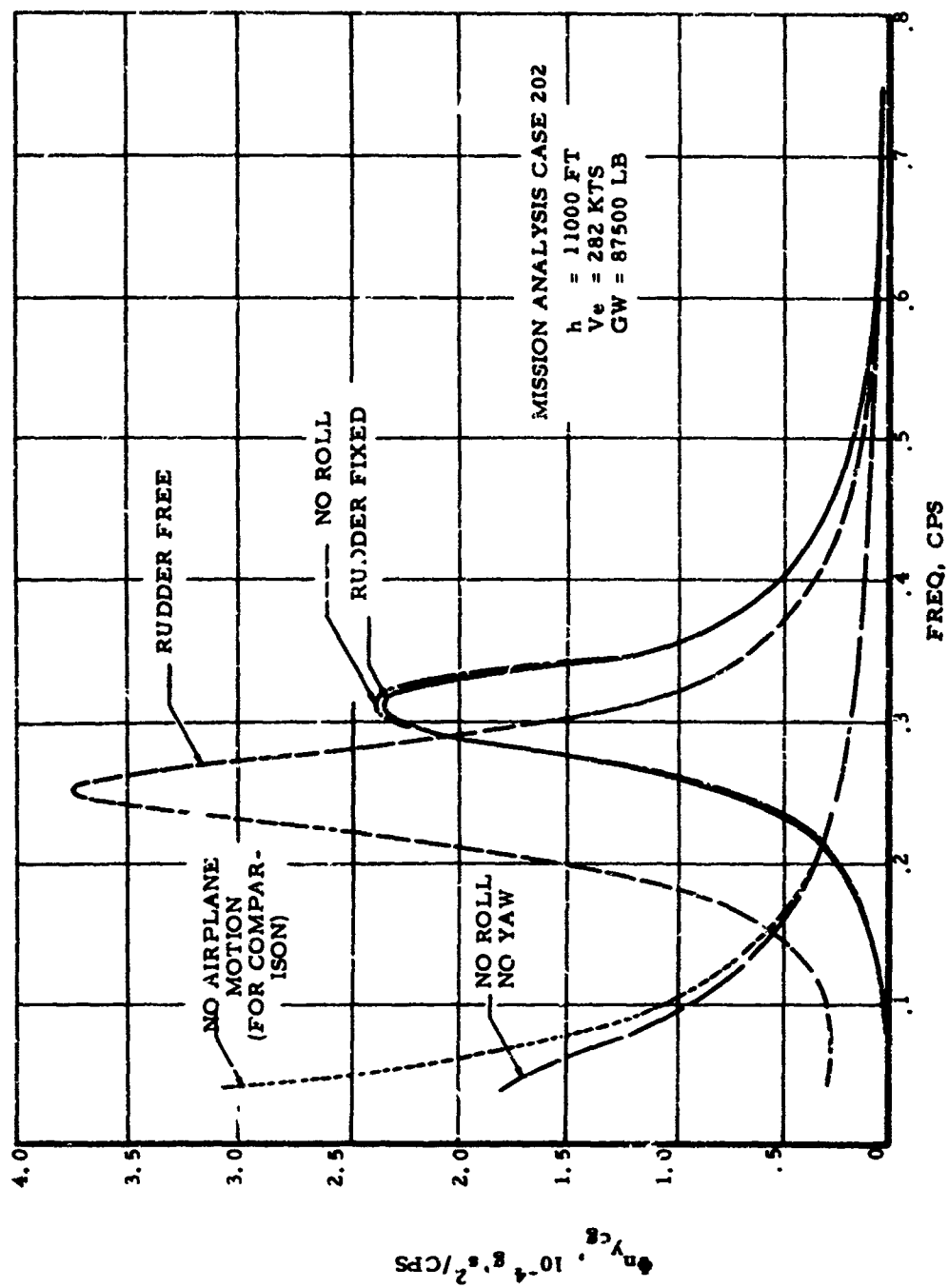


FIGURE 8-3. POWER SPECTRAL DENSITY OF MODEL 188 CG LATERAL LOAD FACTOR FOR VARIOUS PILOT TECHNIQUES

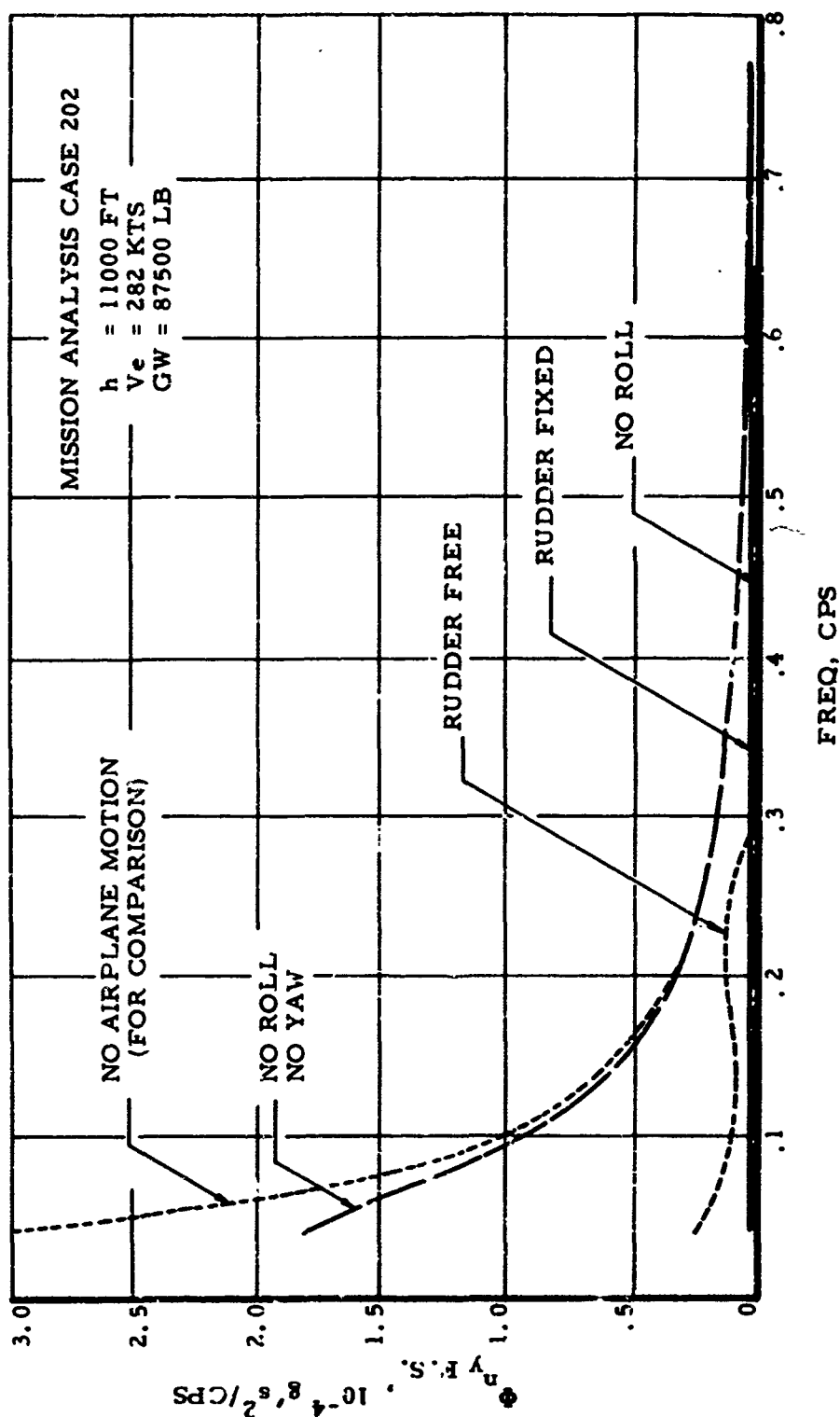


FIGURE 8-4. POWER SPECTRAL DENSITY OF MODEL 188 PILOT
STATION LATERAL LOAD FACTOR FOR
VARIOUS PILOT TECHNIQUES

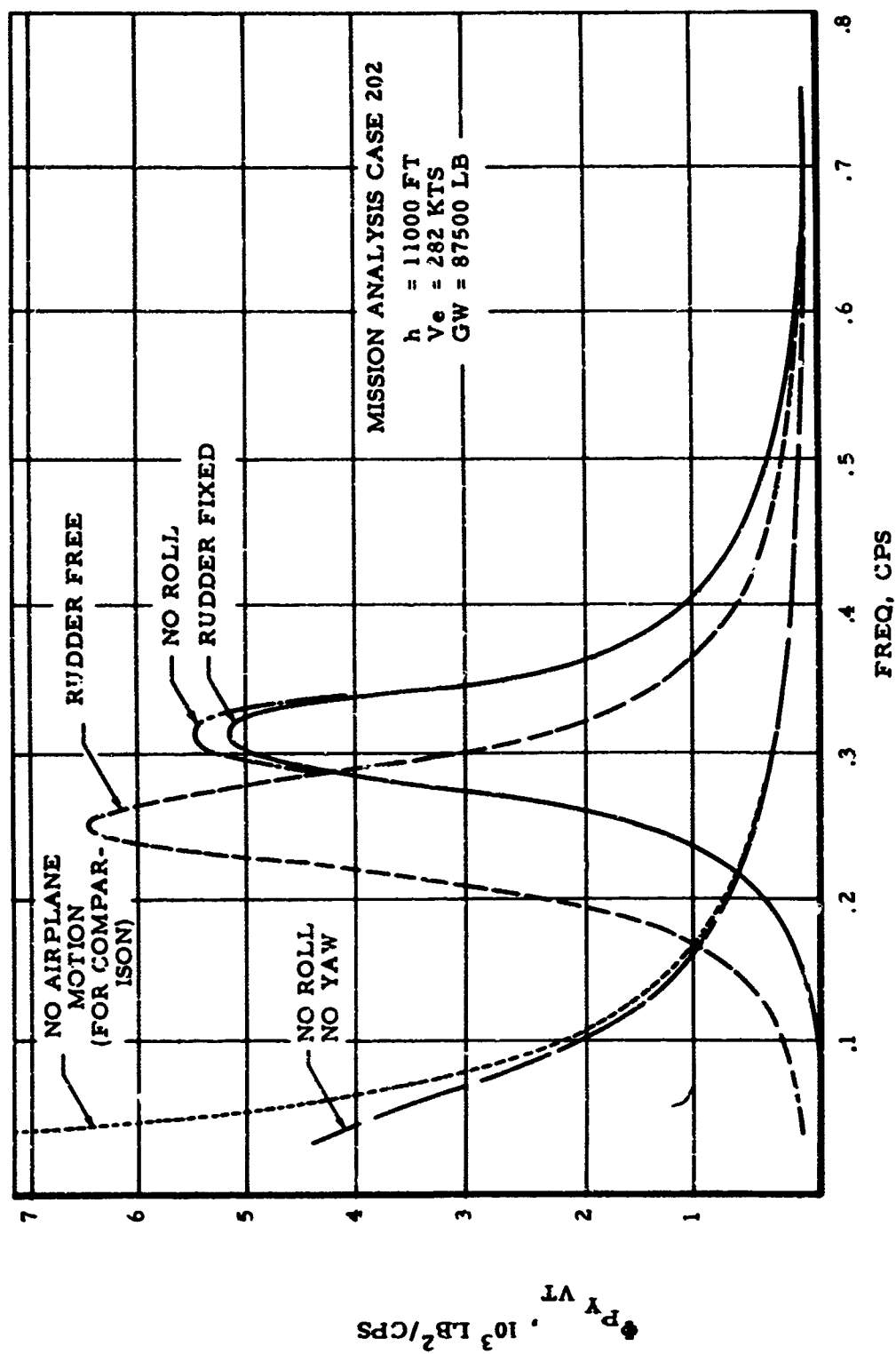


FIGURE 8-5. POWER SPECTRAL DENSITY OF MODEL 188 FIN SIDE
LOAD FOR VARIOUS PILOT TECHNIQUES

The values shown in the above table for the no roll, no yaw case are of limited meaning. As noted earlier, the range of integration had already been set to start at .04 cps in order to exclude the spiral mode at the very low frequencies. For the no roll, no yaw case, however, as can be seen from the power-spectral density plots in Figures 8-3 through 8-5, the frequencies below .04 cps contribute substantially to σ^2 . Including this contribution would increase the \bar{A} values by some 15%. Furthermore, at the very low frequencies where the greatest contribution occurs, it is highly uncertain what the pilot would actually be doing. To eliminate all yaw motion of these frequencies, it would appear necessary for the pilot to devote continuous attention to a heading indicator, or for an autopilot to be used.

For the remaining three cases, which are considered more realistic, the effect of pilot technique on the tail load is seen to be gratifyingly small. The spread from the lowest to the highest \bar{A} value is only about 10%; and Case (4) would even fall within the same range if increased by 15% as would appear appropriate from the discussion above. The lateral accelerations differ somewhat more, but critical stresses due to lateral gust depend far more on tail load than on accelerations.

The power-spectral densities are also quite similar for the three more reasonable techniques. The chief difference is a decrease in the frequency of the peak response for the rudder-free case relative to the rudder-fixed cases, as a result of the decreased static stability. It is interesting to note that locking out the roll motion has a negligible effect on the frequency for peak response as well as on the magnitude of the response. For this airplane, at least, the major characteristics of the "Dutch roll" mode, from the gust load standpoint, seem to be preserved even when roll motion is excluded. The reason may be that for a high aspect ratio airplane the damping in roll is so great as to effectively eliminate the roll motion, without further action by the pilot. For Case (4), the power-spectral density function shapes differ markedly from those shown for Cases (1) - (3), and the close agreement in \bar{A} values must be considered largely coincidental.

The lateral accelerations at the pilot station (second column in the above tabulation, and Figure 8-4) are, for all three cases, somewhat lower than at the c.g., due to the relieving effect of the yaw acceleration. The sharp resonant peak at about .3 cps happens to be almost completely eliminated. The power spectral density remains fairly constant, however, over the entire range from about .05 to 3.0 cps, so that the percentage effect on \bar{A} is not as great as would be inferred from the power spectral density values at the Dutch roll frequency.

In summary, the critical stresses in the airframe due to lateral gusts are essentially unaffected by the pilot technique assumed, within the

range of assumptions investigated herein and considered realistic. Consequently, any of the first three pilot techniques could be selected, without significant effect on the frequency of exceedance of $\sigma_w \eta_d$ values corresponding to limit strength. The rudder-fixed assumption is perhaps as realistic as any. It is probably the one that has been used most generally in the past, and it avoids the need for incorporating rudder float aerodynamic data in the analysis. The rudder-fixed, aileron-fixed pilot technique was therefore assumed in the remainder of the lateral gust investigation.

The characteristics of the Models 188 and 749 are such that lateral gust response had not, in the past, been the subject of extensive analysis. Consequently, it appeared important to gain a better feel for the reasonableness and significance of the results obtained by comparing the results for a particular case, at least qualitatively, with loads and accelerations measured in flight.

Such measurements were available as a result of instrumented flights through turbulence of the Model 188. Although the principal purpose of these flights was to measure the response to vertical gusts, time histories of c.g. lateral acceleration and fin root shear were also included. Rms values, power-spectral densities, and peak counts were available for the c.g. lateral acceleration, but no reduction of the fin shear data had been performed. Although cases corresponding exactly to the flight test conditions were not included in the analysis, mission analysis Case no. 202 did not differ greatly. And by making the comparison on the basis of ratios of side to vertical acceleration, the effects of differences in flight conditions were minimized. The results of the side load factor comparison are shown in the following table.

Test	G.W.	Altitude	V_e (Knots)	RMS Values		
				Δn_y	Δn_z	$\Delta n_y / \Delta n_z$
532	81,600	8,000	260	.0558	.135	.44
544	108,400	1,500	268	.0465	.128	.36
552	85,600	4,700	268	.082	.217	.38
Average						.39
Analysis (Rudder Fixed)	92,300	11,000	282	.00564	.02192	.26

It is seen that the average measured value of the ratio $\Delta n_y / \Delta n_z$ is greater than the analytical value in the ratio $.39 / .26 = 1.50$.

In searching for the reason for this discrepancy, the flight-measured power-spectral density curve was examined. This curve is shown in Figure 8-6. Its most striking feature is a large contribution in the 4.5 - 8.5 cps range, due evidently to elastic mode response. Roughly 60% of the area under the curve occurs beyond 3 cps, indicating a dynamic factor due to elastic mode response of about $\sqrt{1.00/.40} = 1.58$. The analytical model, on the other hand, makes no provision for elastic mode effects. As indicated above, the lowest fuselage-tail side-bending elastic mode, for both airplanes, is far higher in frequency than the Dutch roll mode; consequently, it was expected that the elastic modes would not contribute significantly to the loads produced by turbulence and could be omitted from the mathematical model. If the flight-measured value of $\Delta n_y / \Delta n_z$, .39, is divided by the indicated dynamic factor of 1.58, the result is .25; this is in good agreement with the analytical value of .26.

Although the analytical and flight-measured lateral accelerations were thus reconciled, the presence of a significant elastic mode contribution in the flight-measured load factor did raise the question of the adequacy of the analytical model for the purposes of the present study. In order to obtain a more direct indication of the effect of the elastic mode response on critical structural loads, the flight-measured fin root shear time history from one test only was processed to obtain its power spectral density. The resulting curve is shown in Figure 8-7. Although the frequency resolution is not adequate to define the curve in detail in the vicinity of the Dutch roll frequency, it is clear that the elastic mode effects are relatively small. Also, it is noted that the dynamic response occurs not in the 4.5 - 8.5 cps range, as in Figure 8-6, but in the vicinity of 12 cps.

Consequently, the existing mathematical model should yield quite realistic vertical tail loads. Furthermore, the fuselage is critical for lateral gust loads only in the aftbody. It would appear that airloads from the vertical tail will contribute a good deal more to the critical aftbody loads than will fuselage inertias. In this connection, inspection of Model 188 shake test results indicates a fuselage lateral bending-torsion mode at about 8 cps, which was probably the major contributor to the elastic mode peak in Figure 8-6. This mode has a node line running approximately longitudinally at the fin root. Consequently, there will be some tendency for the inertia forces acting on the fin to offset those acting on the fuselage. In all, it appears that the existing mathematical model should yield fairly realistic values of frequency of exceedance of limit and ultimate strength, and of limit and ultimate strength values of σ_w , η_d .

MODEL 188A SERIAL NO. 1001 TEST 532

GW = 81730 LB

CG = 21.1% MAC

V_e = 266 KTS

h = 8400 FT

SAMPLING INTERVAL
NO. OF DATA POINTS
NO. OF LAGS

.002
7501
100

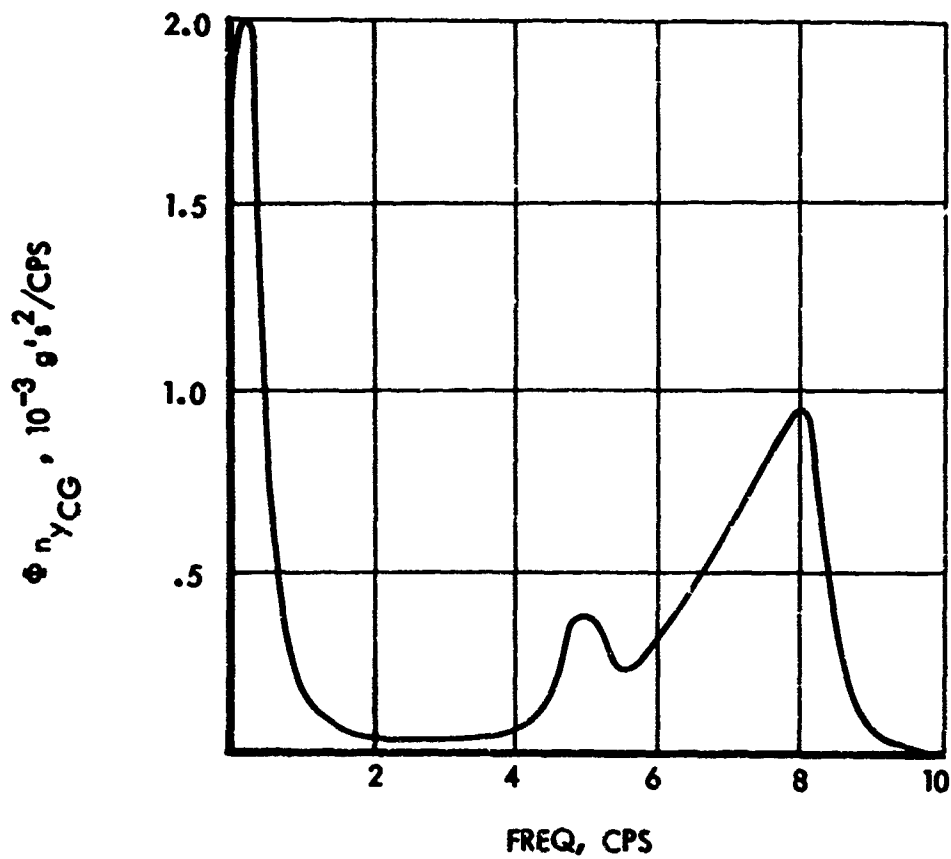


FIGURE 8-6. FLIGHT MEASURED POWER SPECTRAL DENSITY OF
MODEL 188 CG LATERAL LOAD FACTOR

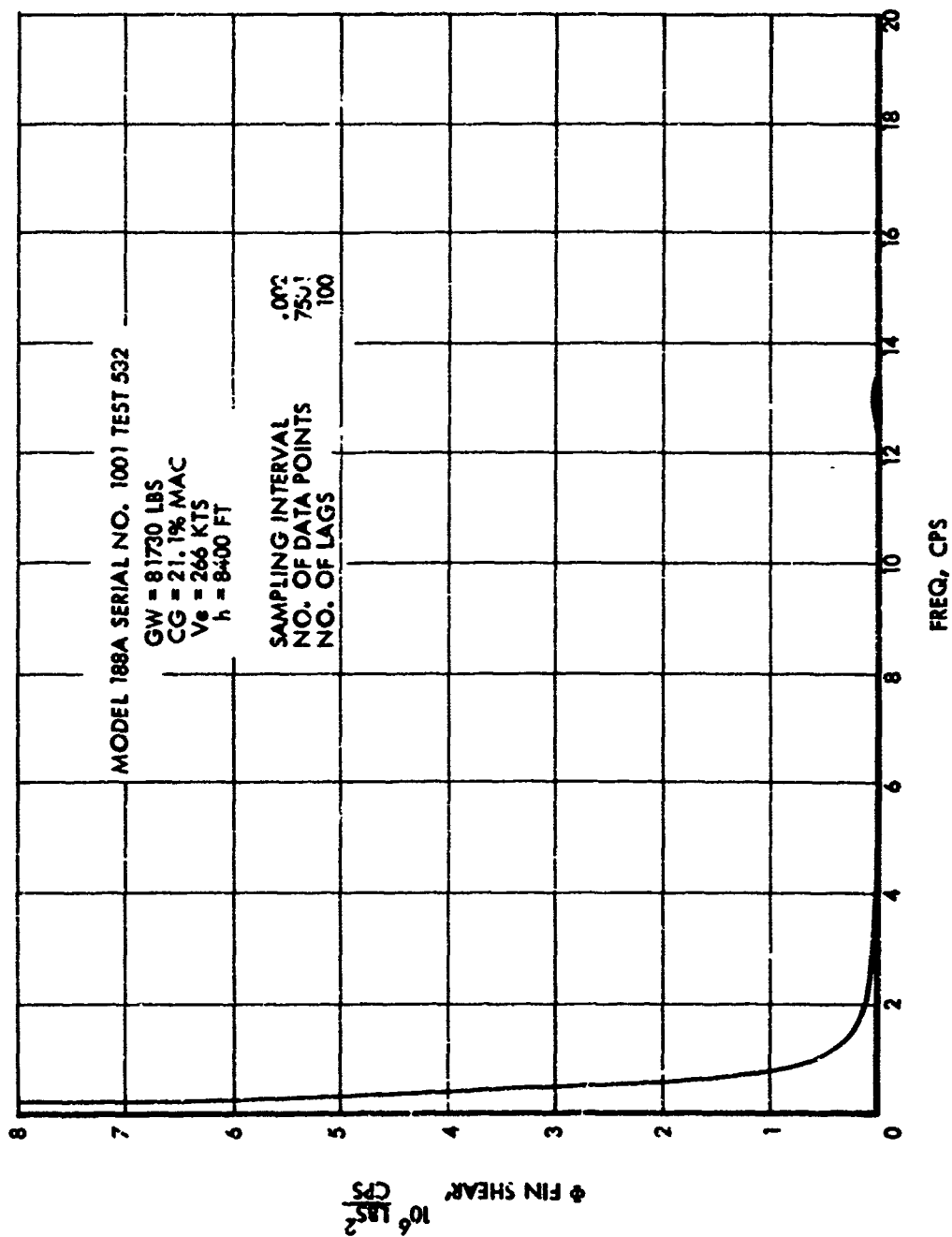


FIGURE 8-7. FLIGHT MEASURED POWER SPECTRAL DENSITY OF
MODEL 188 FIN SIDE LOAD

9 RESULTS OF ANALYSIS

\bar{A} and N_0 values obtained from the vertical gust and lateral gust dynamic analyses of the Model 188 and Model 749, together with the associated one-g level flight loads, are presented for reference in Appendix B.

Sample power-spectral densities of c.g. load factor are shown for the two airplanes in Figures 9-1 and 9-2. These are for a representative mission analysis segment in each case.

Sample power-spectral densities of a number of wing and fuselage load quantities, for the same mission segments, are shown in Figures 9-3 and 9-4 for the Model 188 and in Figure 9-5 for the Model 749.

Sample power-spectral densities for fin root shear and c.g. lateral acceleration, obtained from the lateral gust analyses, are shown in Figures 9-6 and 9-7 for the Model 188 and Model 749 respectively.

For use later in determining $N(y)$ values corresponding to limit and ultimate strength, exceedance curves were prepared for all load quantities. For the various wing load quantities, separate curves were obtained for both positive and negative gust increments. The preparation of these curves followed the procedure outlined at the end of Section 4.1, using b and P values from Figures 5-3 and 5-4 and \bar{A} and N_0 values from Tables B-1, B-3, B-5, and B-7.

Frequency of exceedance curves for Model 188 loads due to vertical gusts, at representative wing and fuselage locations, are shown in Figures 9-8(a) through (d). The curves are plotted in these figures on a compressed scale in order to show the full range from close to zero load increment to loads in the region of ultimate strength. The same quantities are also plotted to expanded scales in Figures 9-9(a) through (d), in order to show in more detail the region of limit strength, including the contributions of the individual mission segments. It is in this latter form that the complete set of exceedance curves referred to above was obtained.

Similar curves are also shown for wing loads in the root region of the Model 749. The compressed-scale curves are shown in Figure 9-10, and the expanded scale curves, showing the contributions of the various mission segments in the region of limit strength, in Figure 9-11.

Frequency of exceedance curves for airplane c.g. load factor, obtained similarly, are shown in Figures 5-9 and 5-10, together with the experimentally determined curves based on airline VGH and VG data for comparison. This comparison was discussed in Section 5.6.

Frequency of exceedance curves for fin root shear are shown in Figures 9-12 through 9-15. Both compressed-scale and expanded-scale plots are shown, as in the corresponding vertical gust presentations.

\bar{A} values of fin root shear for some of the Model 188 design envelope cases are plotted vs altitude in Figure 9-16. To provide a preliminary indication of the critical altitude, \bar{A} values from Fig. 9-16 are then multiplied by y/\bar{A} values given in Figure 5-6, for an $N(y)/N_0$ value of 10^{-6} , and plotted in Figure 9-17. (The 10^{-6} level was selected arbitrarily, but corresponds roughly to the limit strength level.) Similar curves for the Model 749 are shown in Figures 9-18 and 9-19.

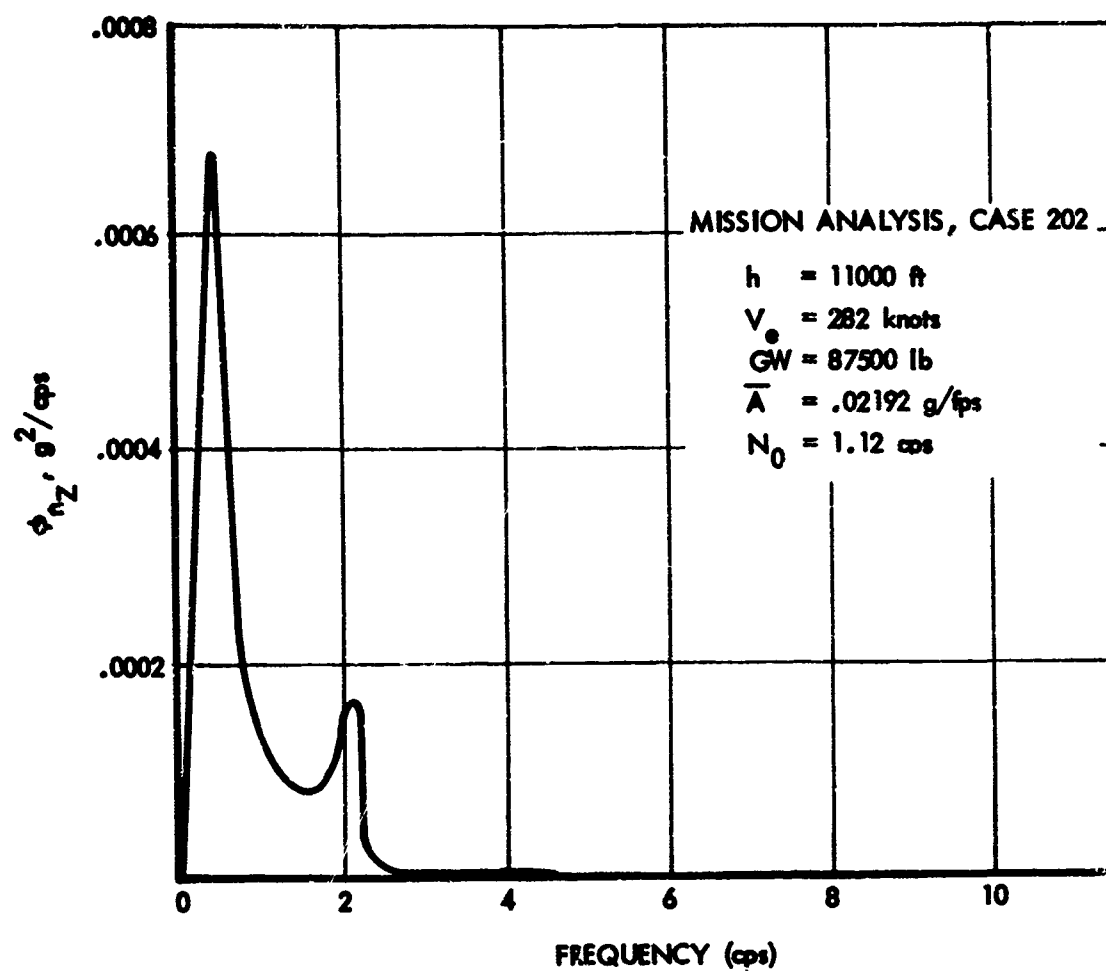


FIGURE 9-1. POWER SPECTRAL DENSITY OF CG LOAD FACTOR
DUE TO VERTICAL GUST, MODEL 188

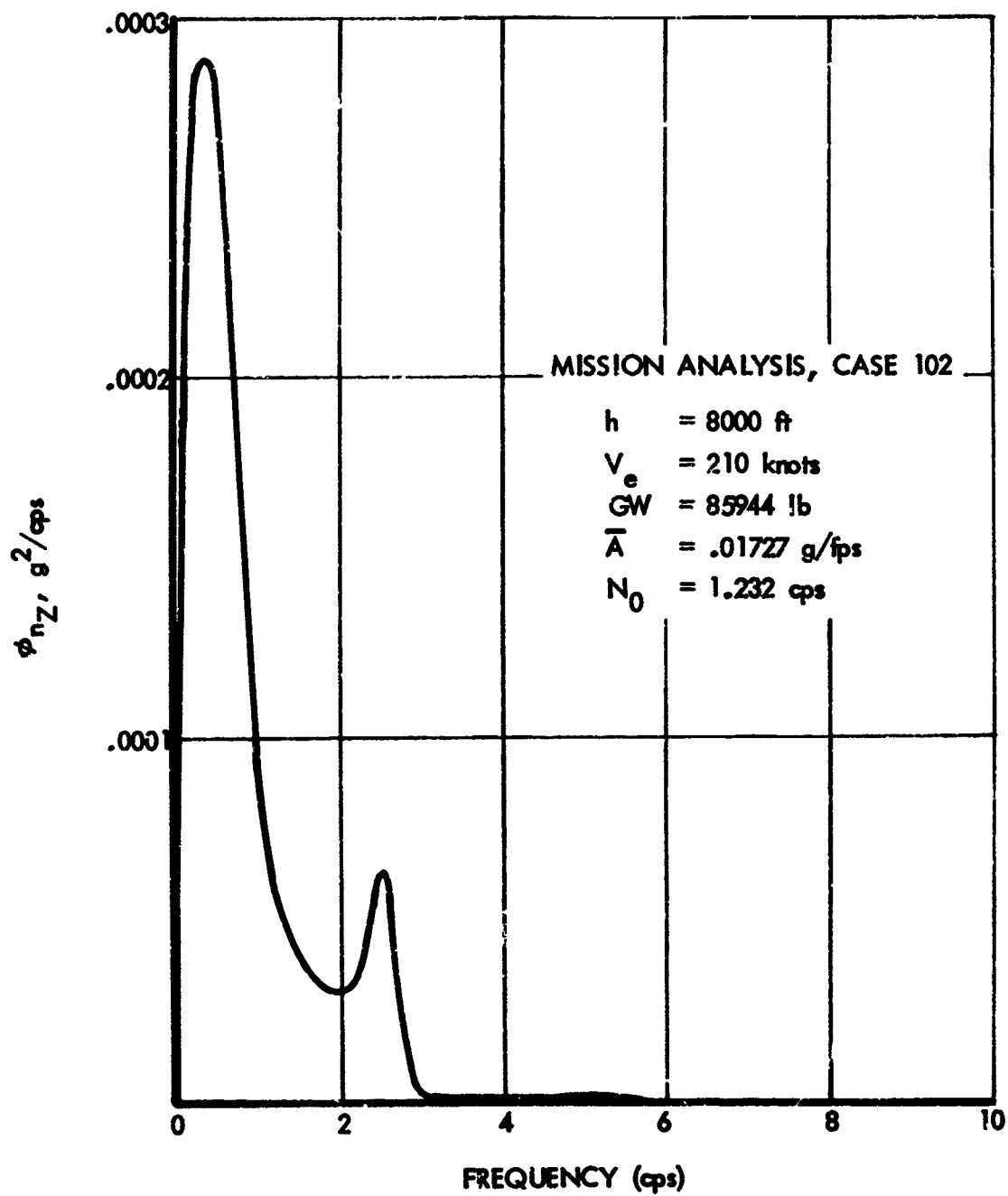
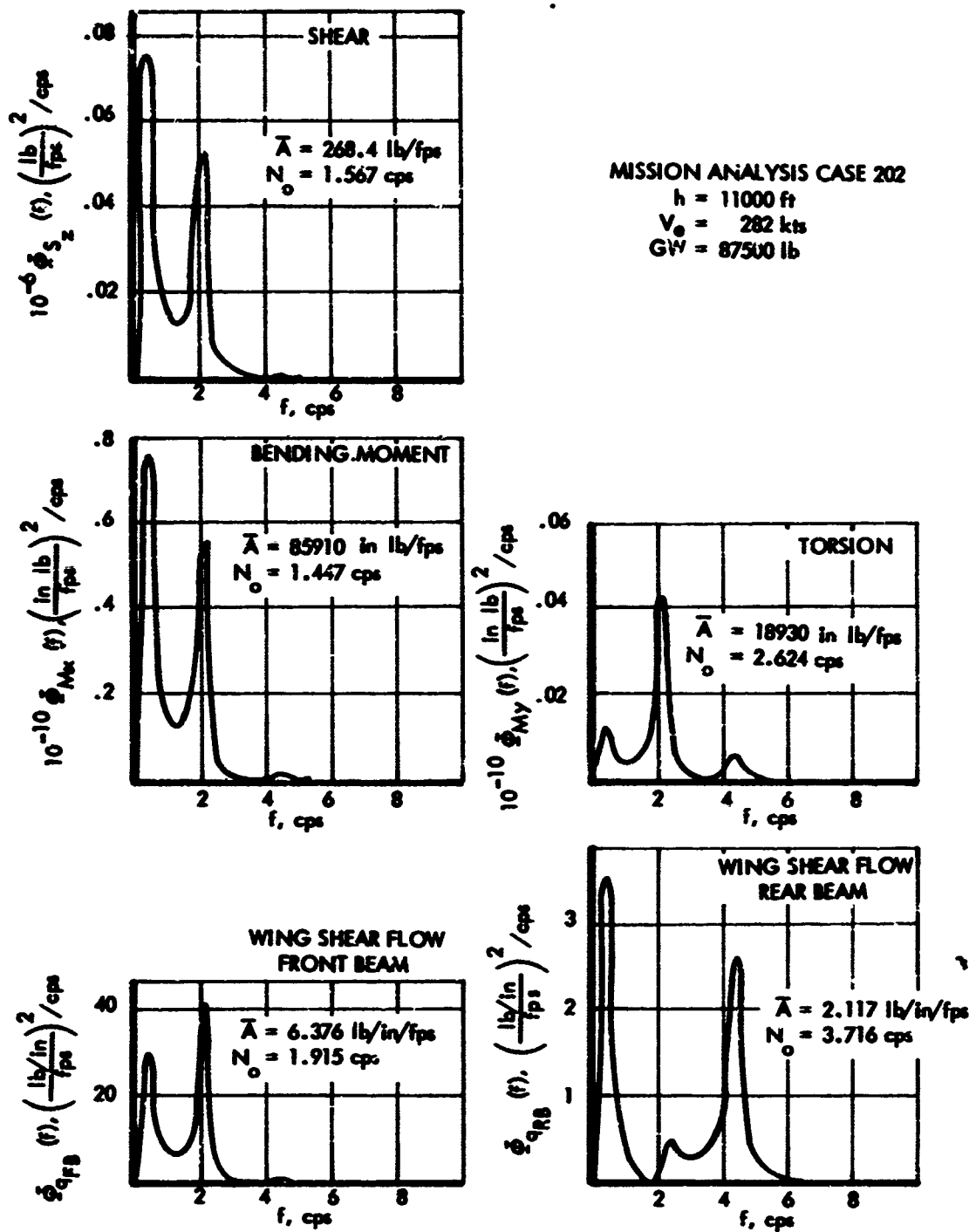


FIGURE 9-2. POWER SPECTRAL DENSITY OF CG LOAD FACTOR
DUE TO VERTICAL GUST, MODEL 749

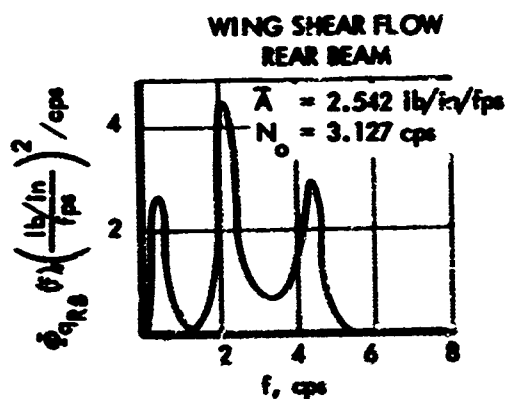
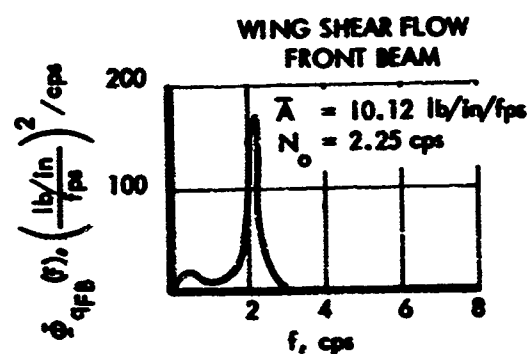
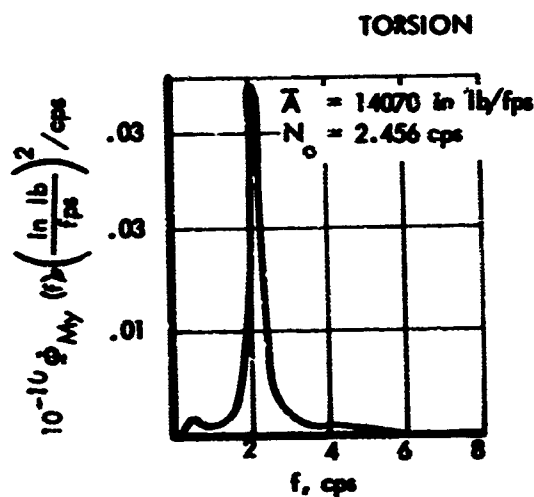
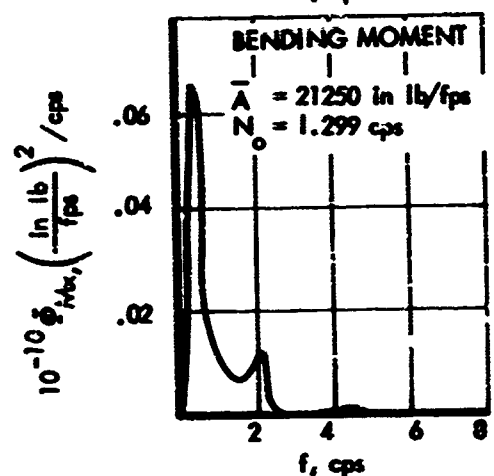
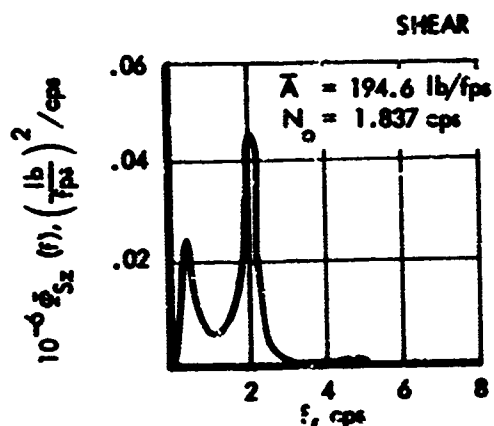


(a) AT WS 83

FIGURE 9-3. POWER SPECTRAL DENSITY OF VARIOUS WING LOADS, MODEL 188

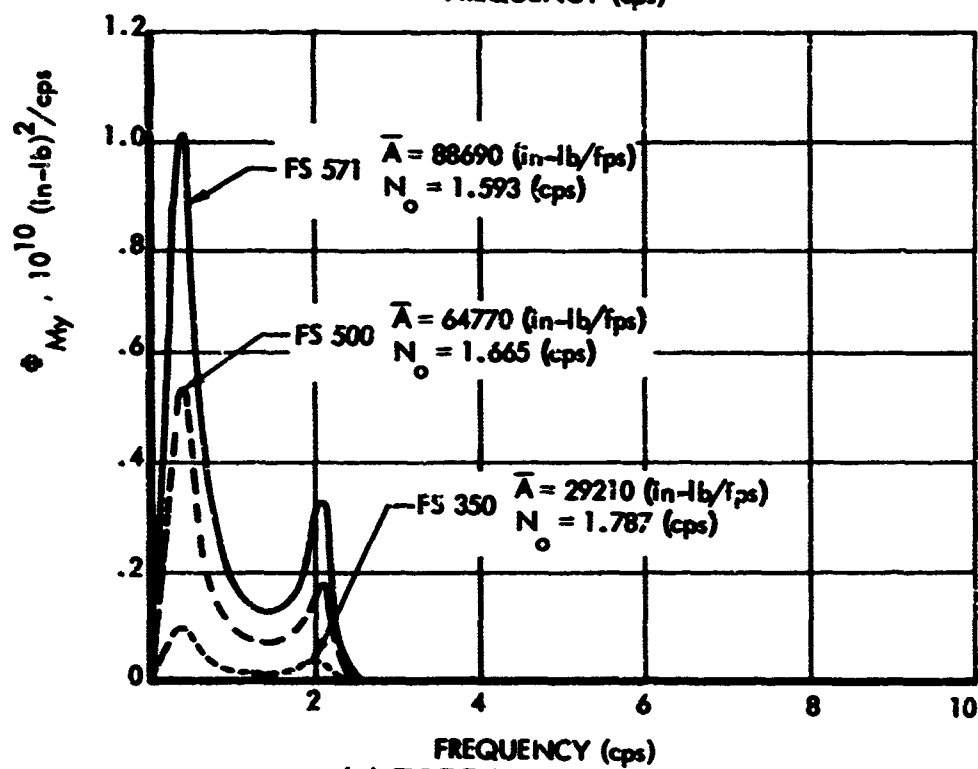
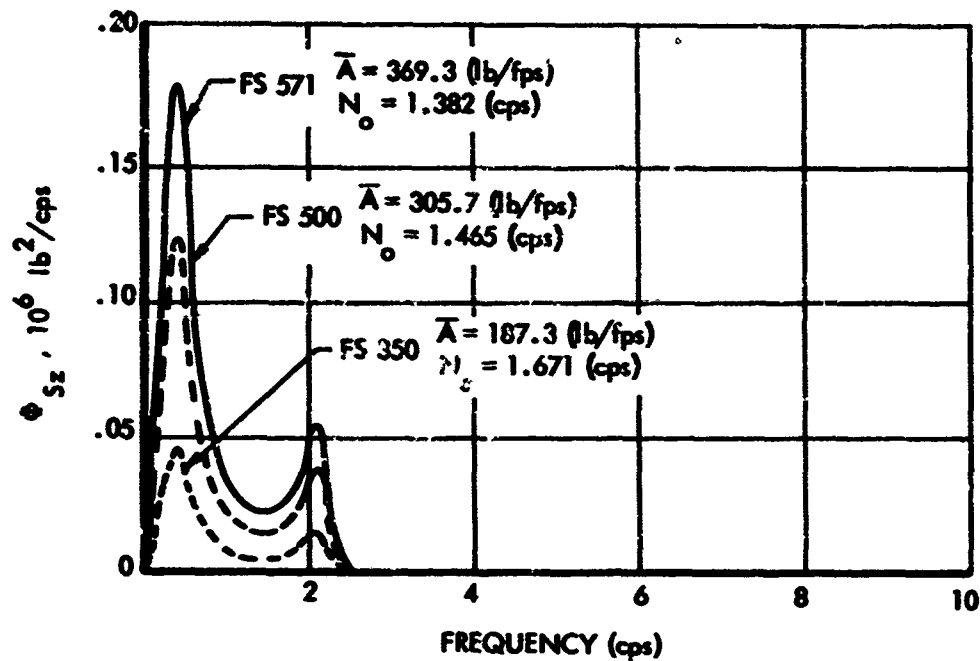
MISSION ANALYSIS, CASE 202

h = 11000 ft
V₀ = 282 kts
GW = 87500 lb



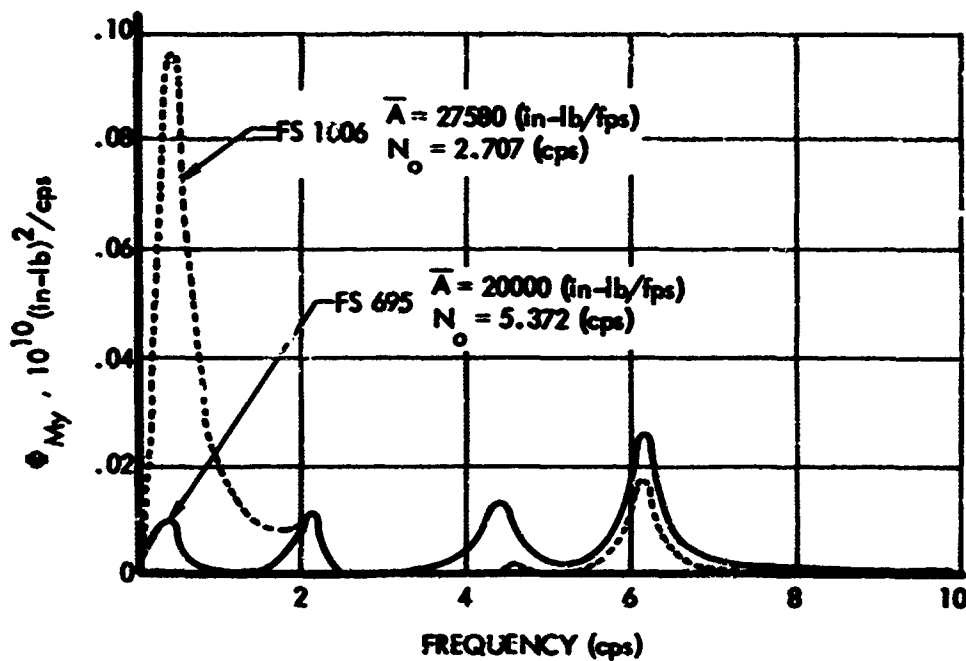
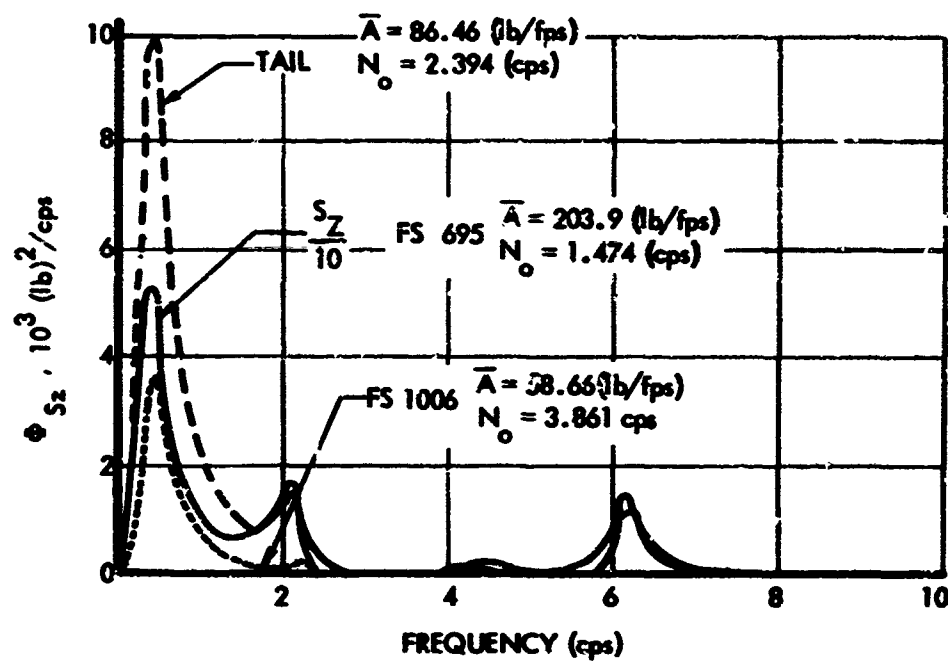
(b) AT WS 346

FIGURE 9-3. CONCLUDED



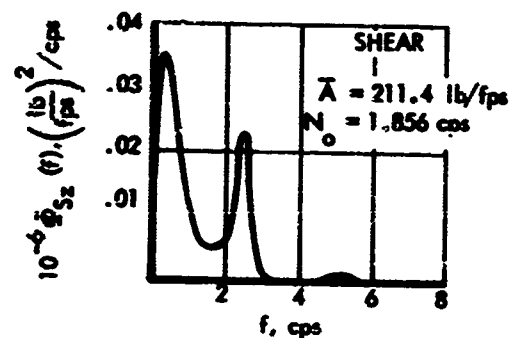
(a) FOREBODY

FIGURE 9-4. POWER SPECTRA OF MODEL 188
FUSELAGE LOADS-CASE 202



(b) AFTBODY

FIGURE 9-4. CONCLUDED



MISSION ANALYSIS, CASE 102

h = 8000 ft
 V₀ = 210 kts
 GW = 85944 lb

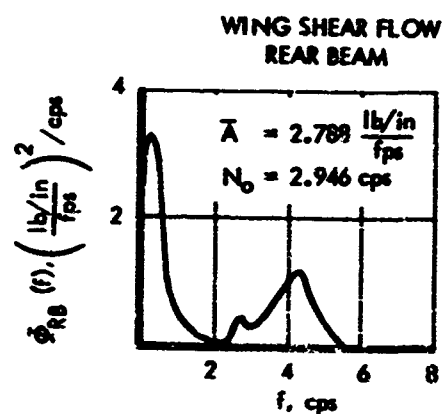
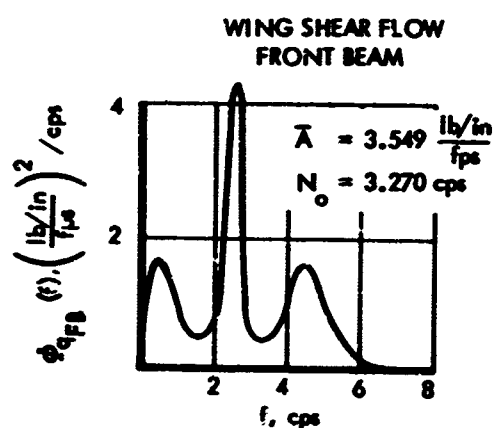
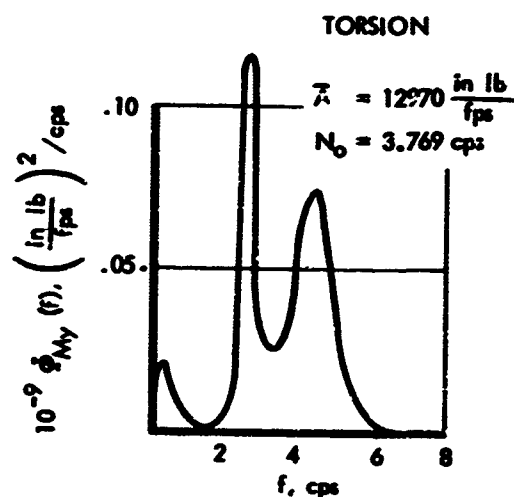
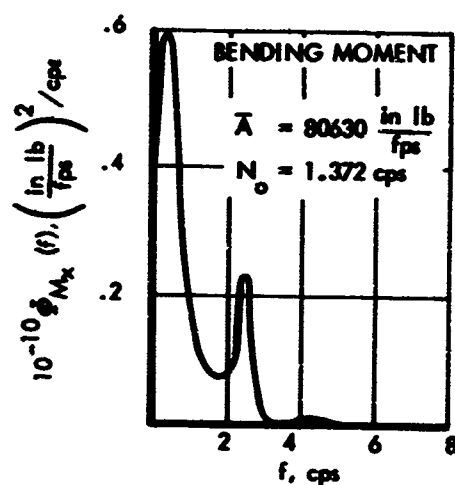


FIGURE 9-5. POWER SPECTRAL DENSITY OF VARIOUS WING LOADS AT WS 145, MODEL 749

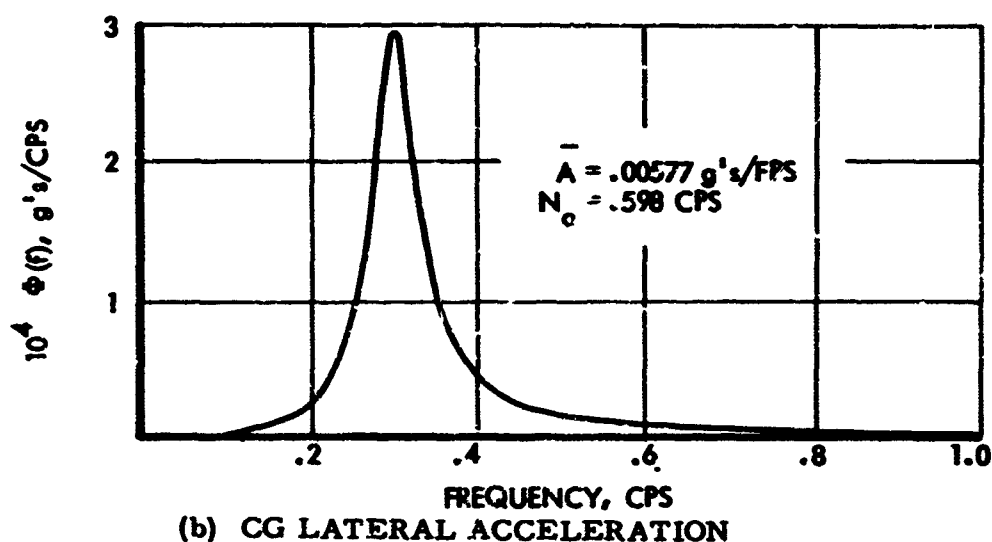
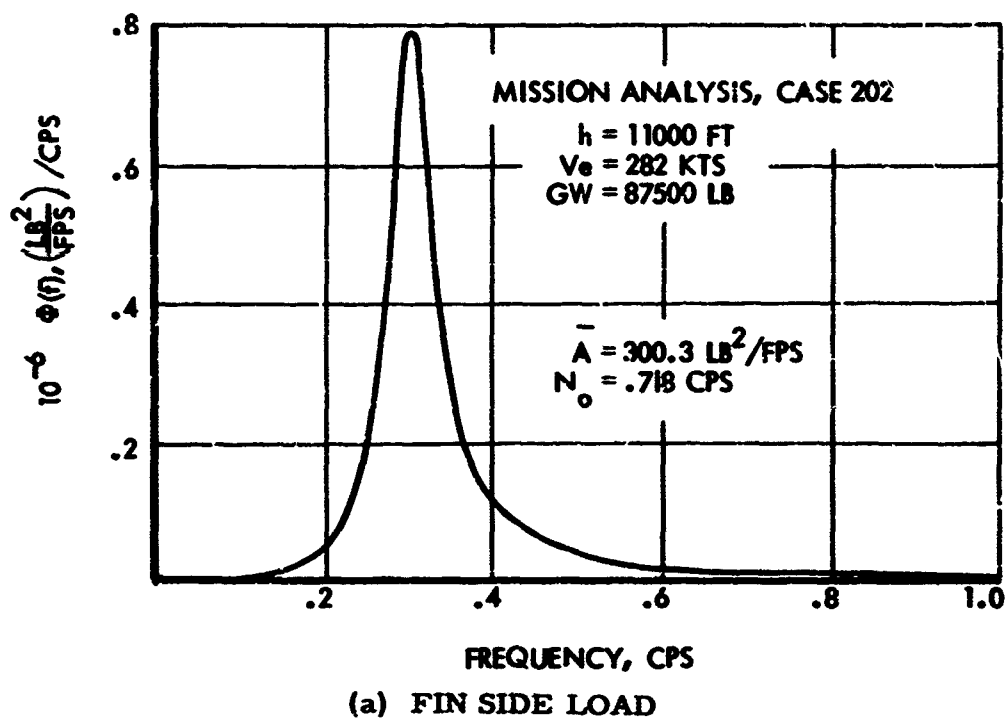


FIGURE 9-6. POWER SPECTRAL DENSITY OF FIN SIDE LOAD AND CG LATERAL ACCELERATION, MODEL 188

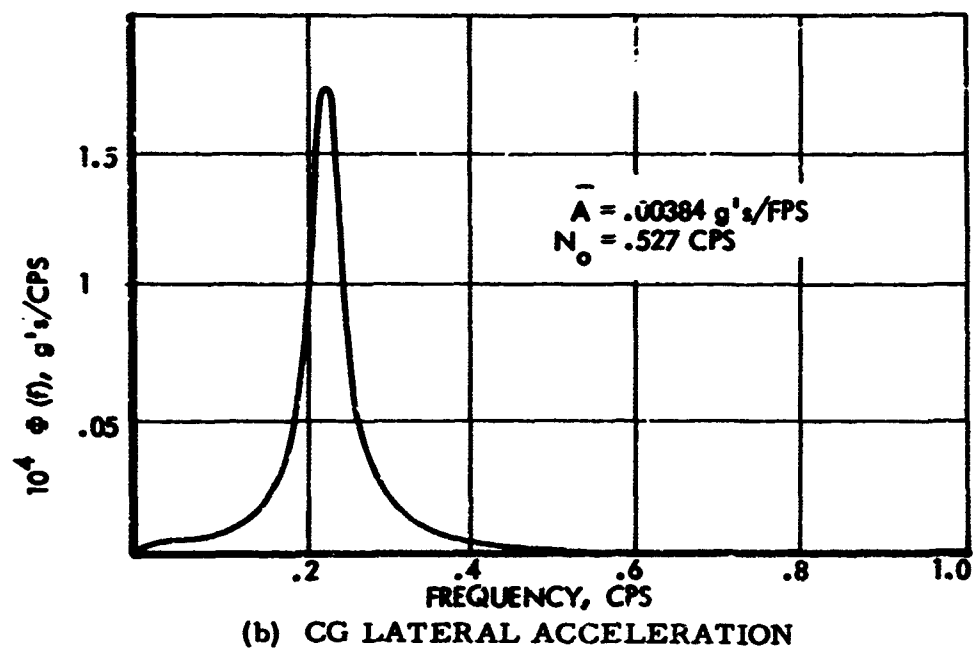
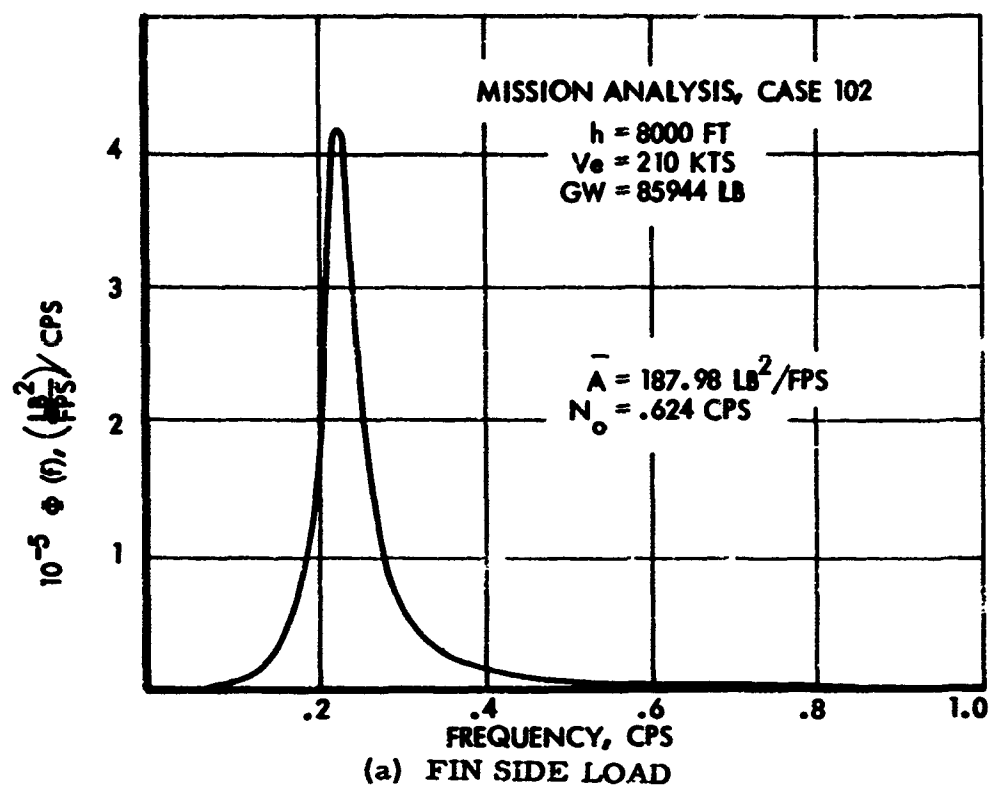
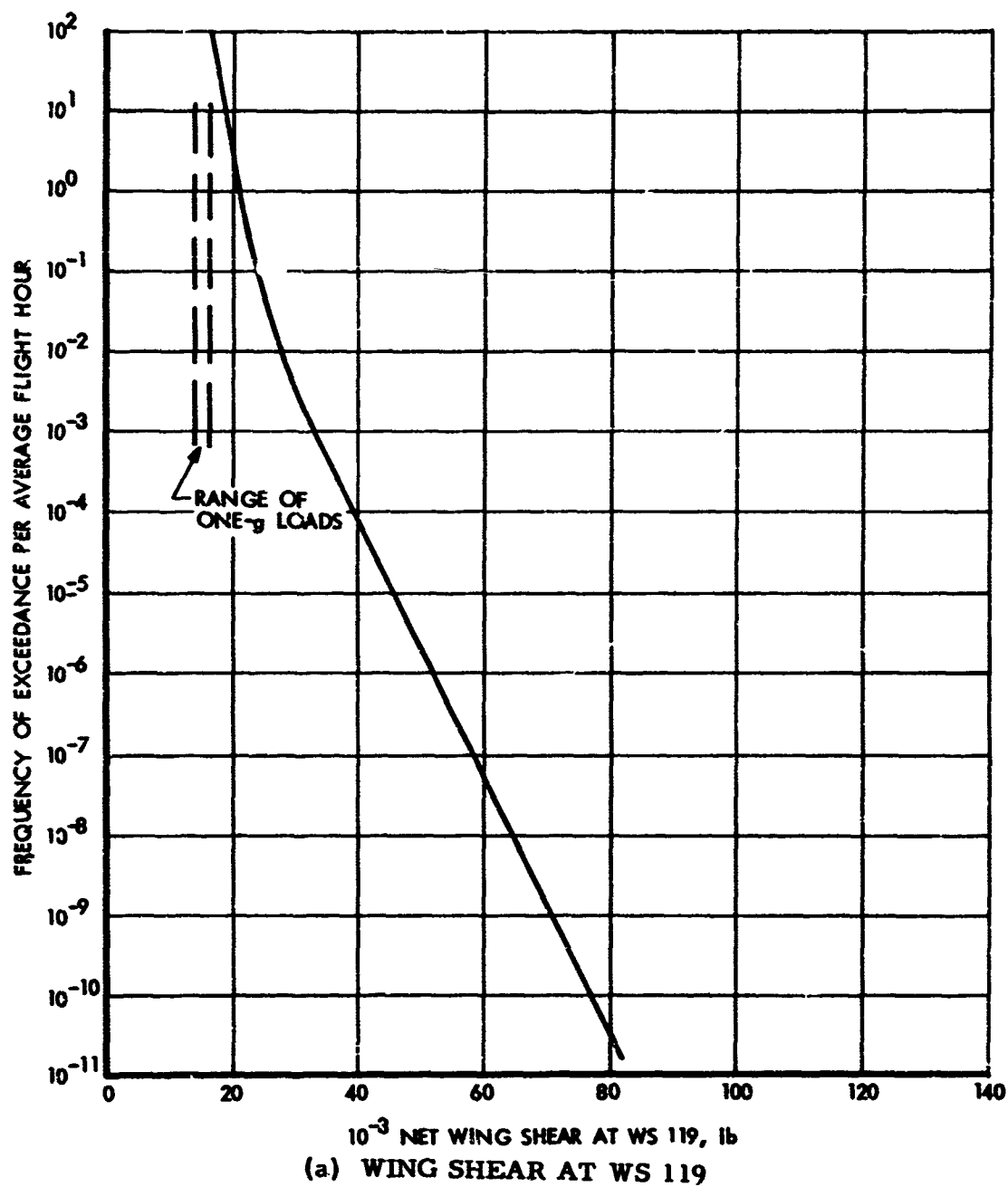
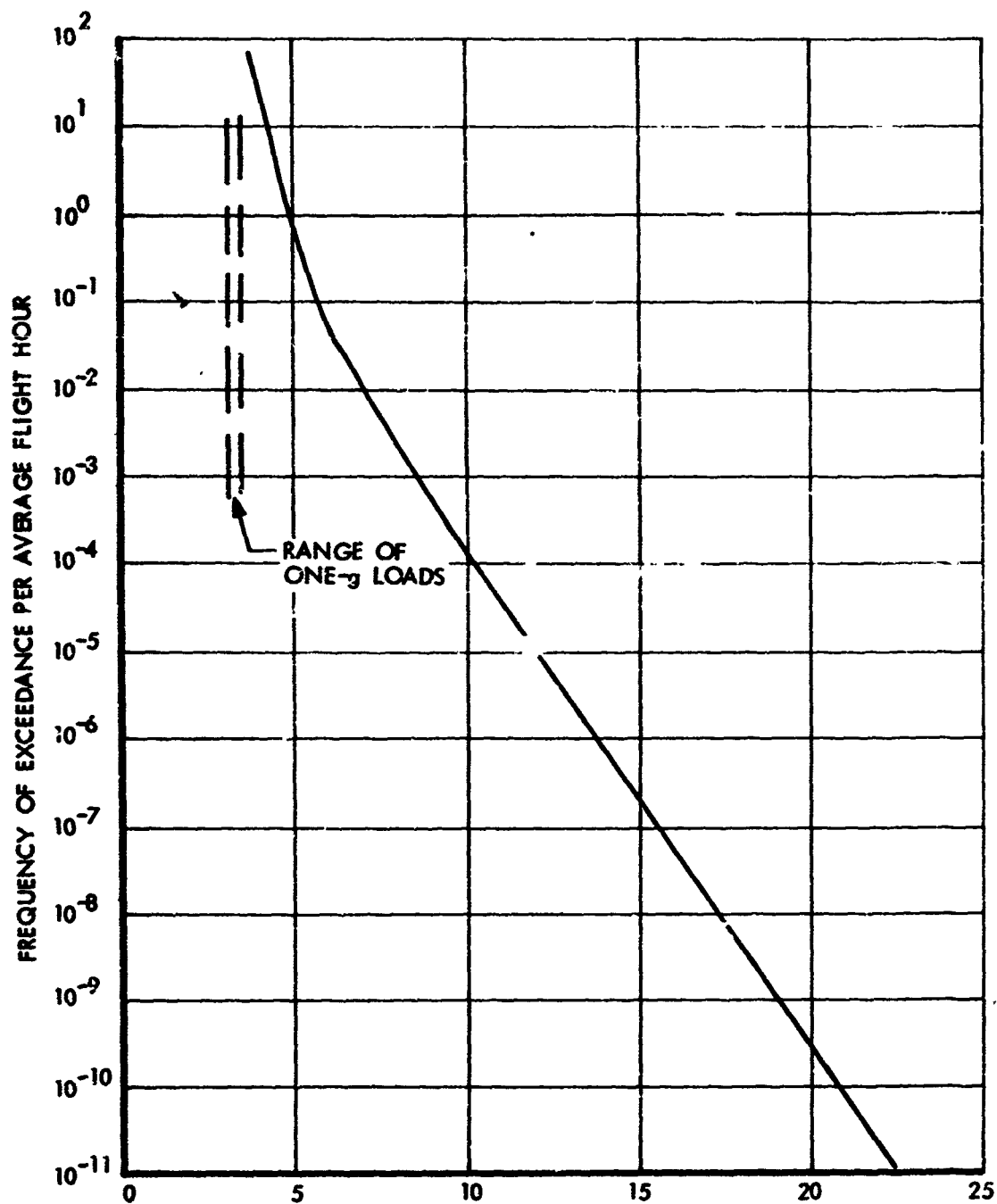


FIGURE 9-7. POWER SPECTRAL DENSITY OF FIN SIDE LOAD AND CG LATERAL ACCELERATION, MODEL 749

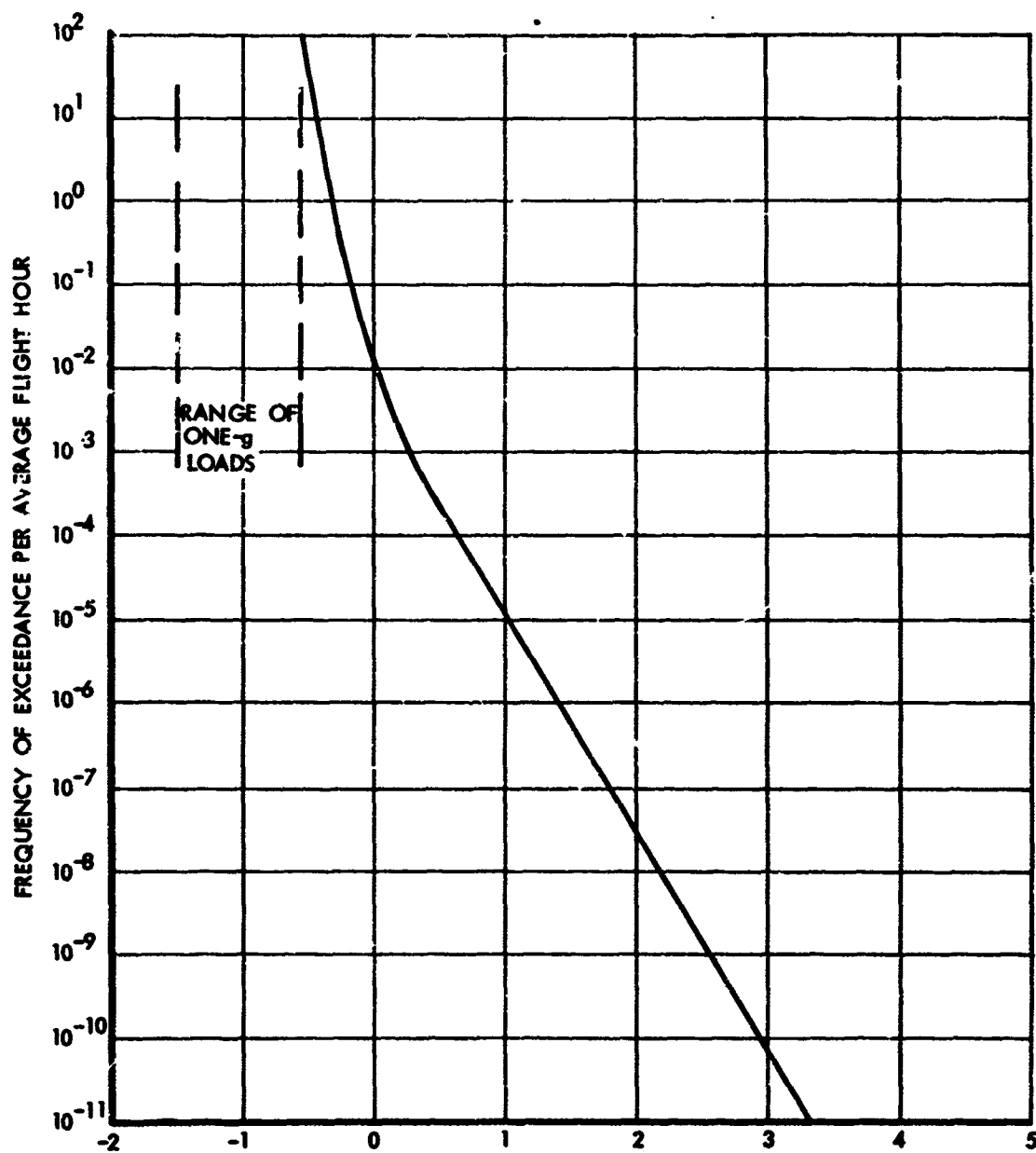




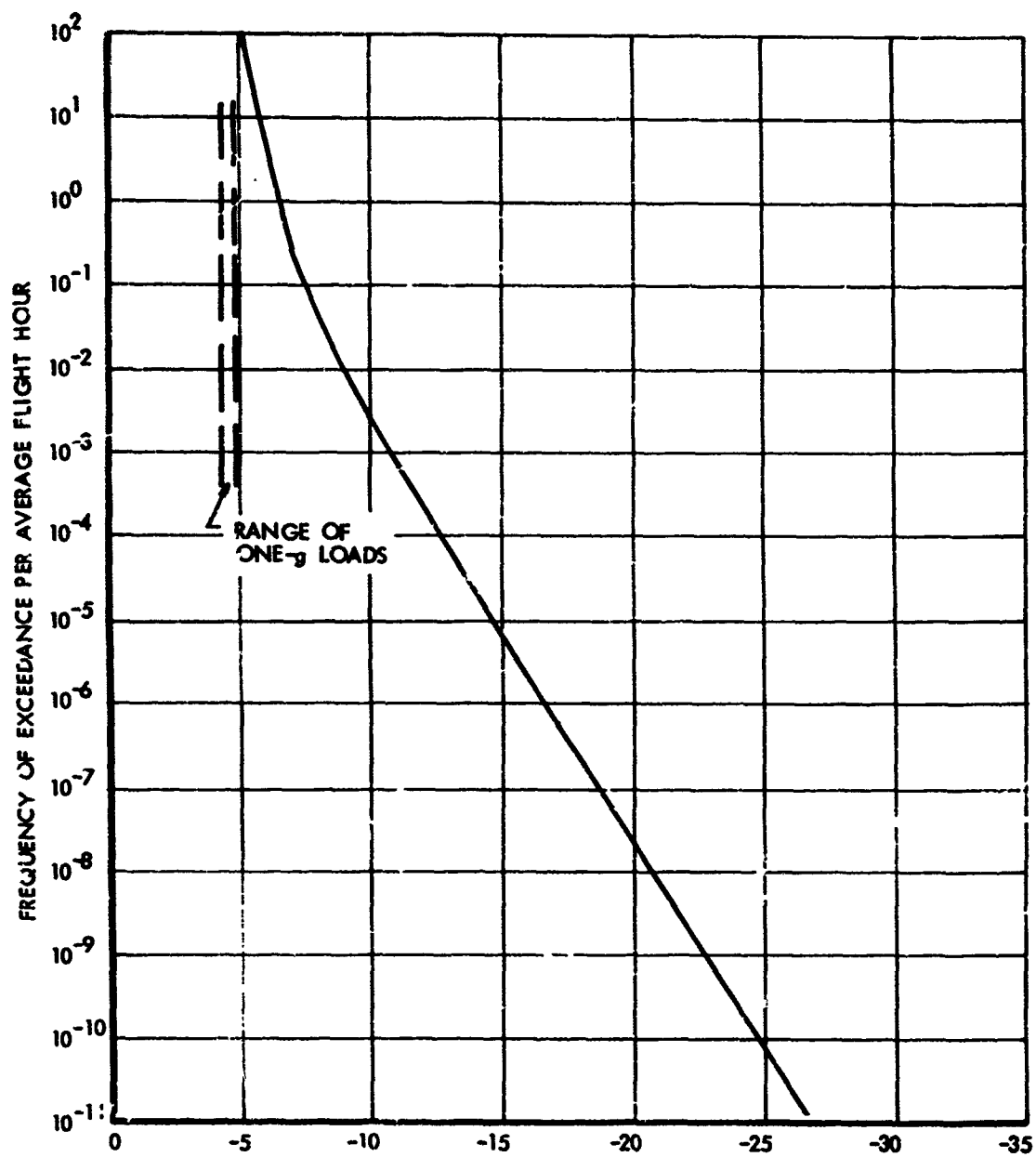
10^{-6} NET WING BENDING MOMENT AT WS 119 (in.-lb)

(b) WING BENDING MOMENT AT WS 119

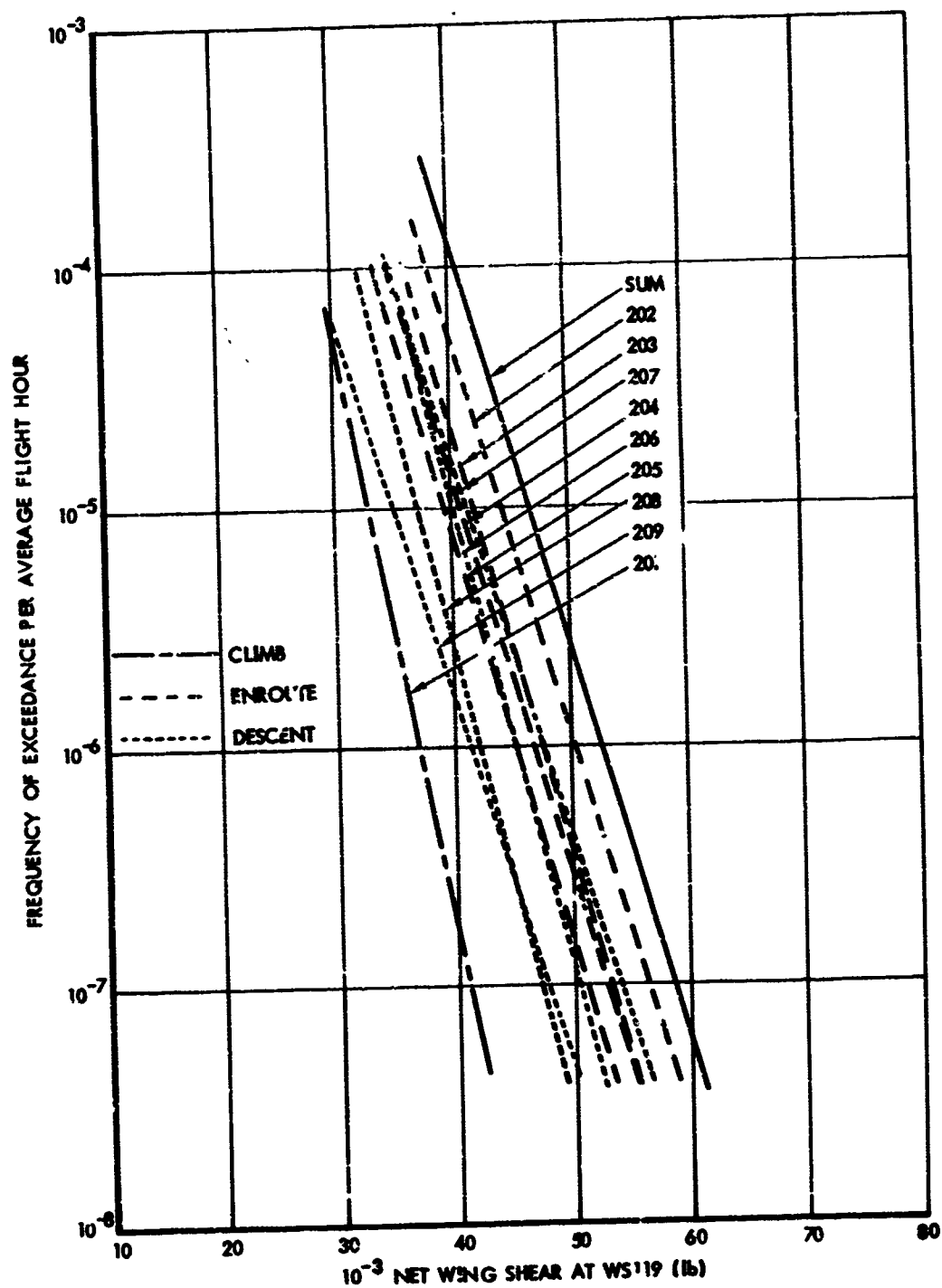
FIGURE 9-8. CONTINUED



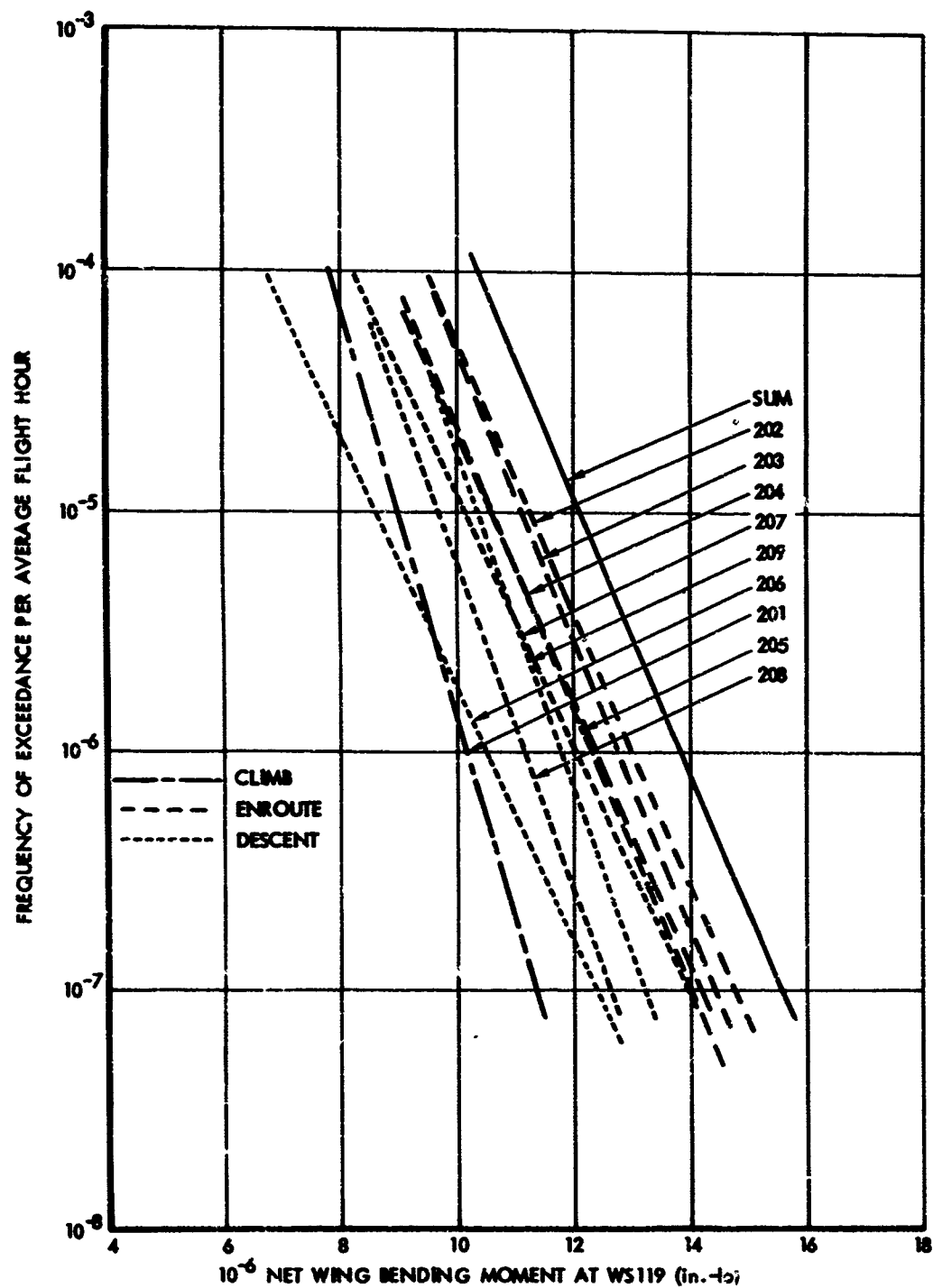
10⁻⁶ WING TORSION AT WS 119 (in.-lb)
 (c) WING TORSION AT WS 119
 FIGURE 9-8. CONTINUED



10⁻⁶ FUSELAGE BENDING MOMENT AT FS 571 (in.-lb)
 (d) FOREBODY BENDING MOMENT AT F.S. 571
 FIGURE 9-8. CONCLUDED.

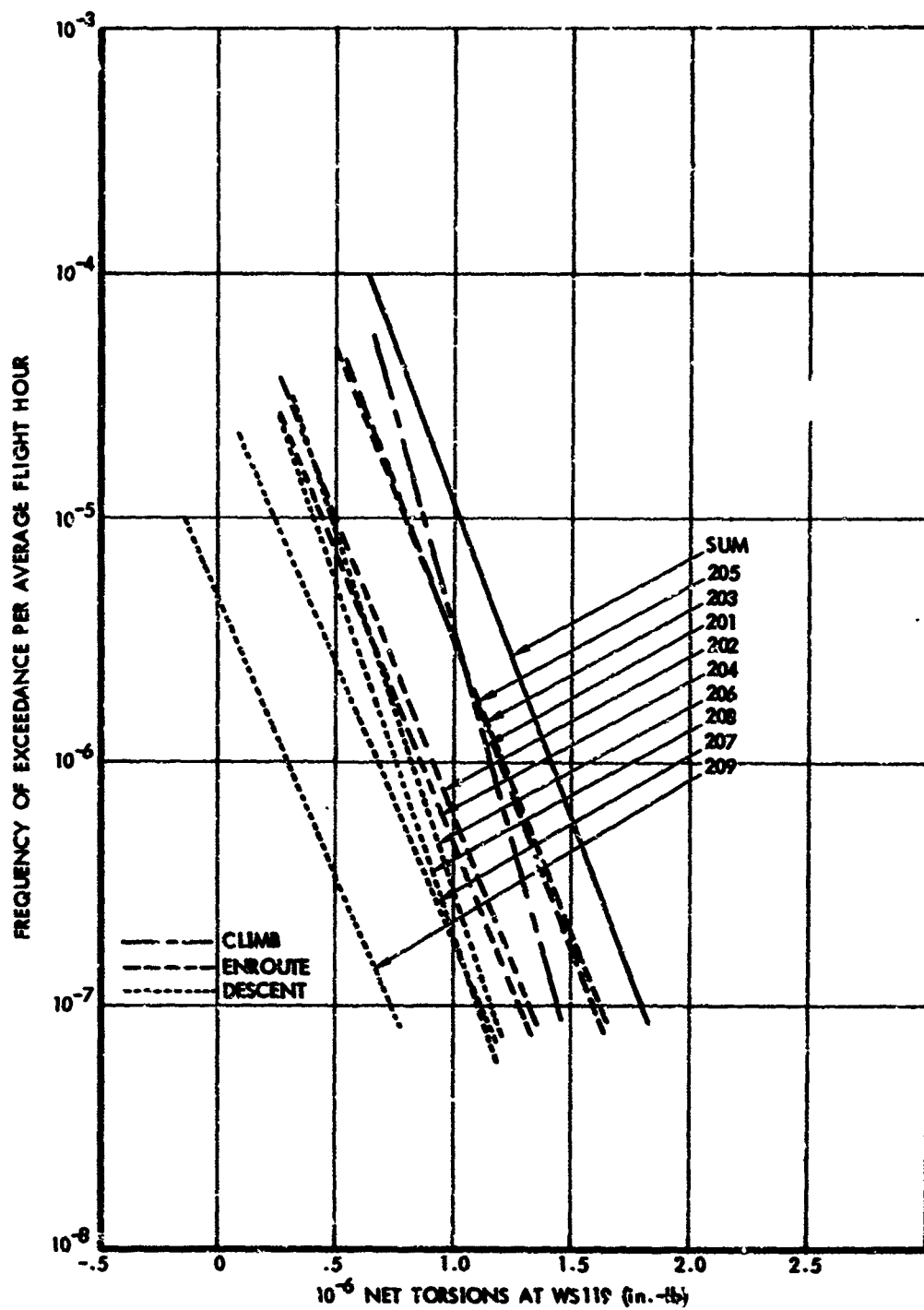


(a) WING SHEAR AT WS 119
 FIGURE 9-9. FREQUENCY OF EXCEEDANCE OF MODEL 188 WING AND FOREBODY LOADS, EXPANDED - SCALE PLOTS



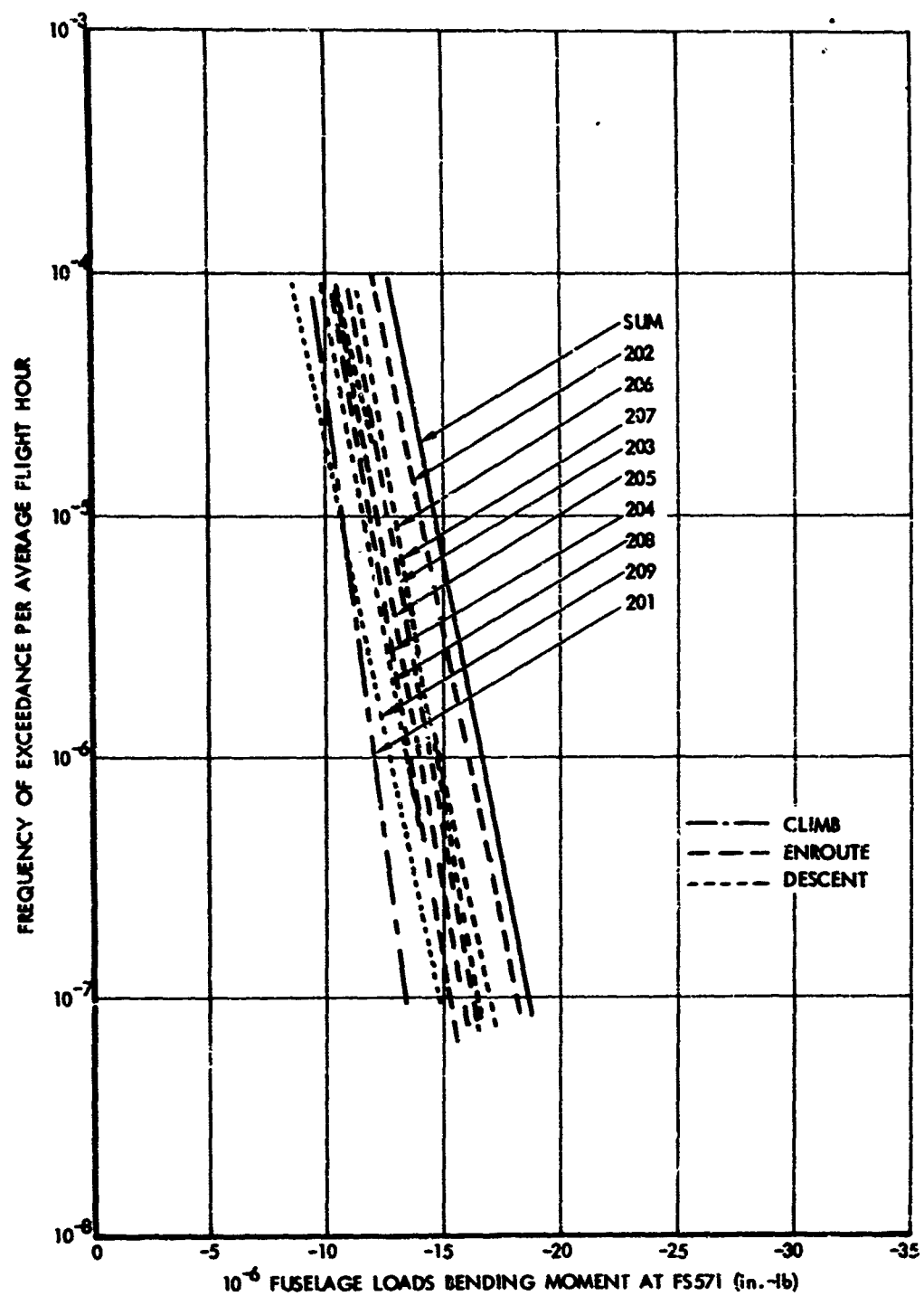
(b) WING BENDING MOMENT AT WS 119

FIGURE 9-9. CONTINUED

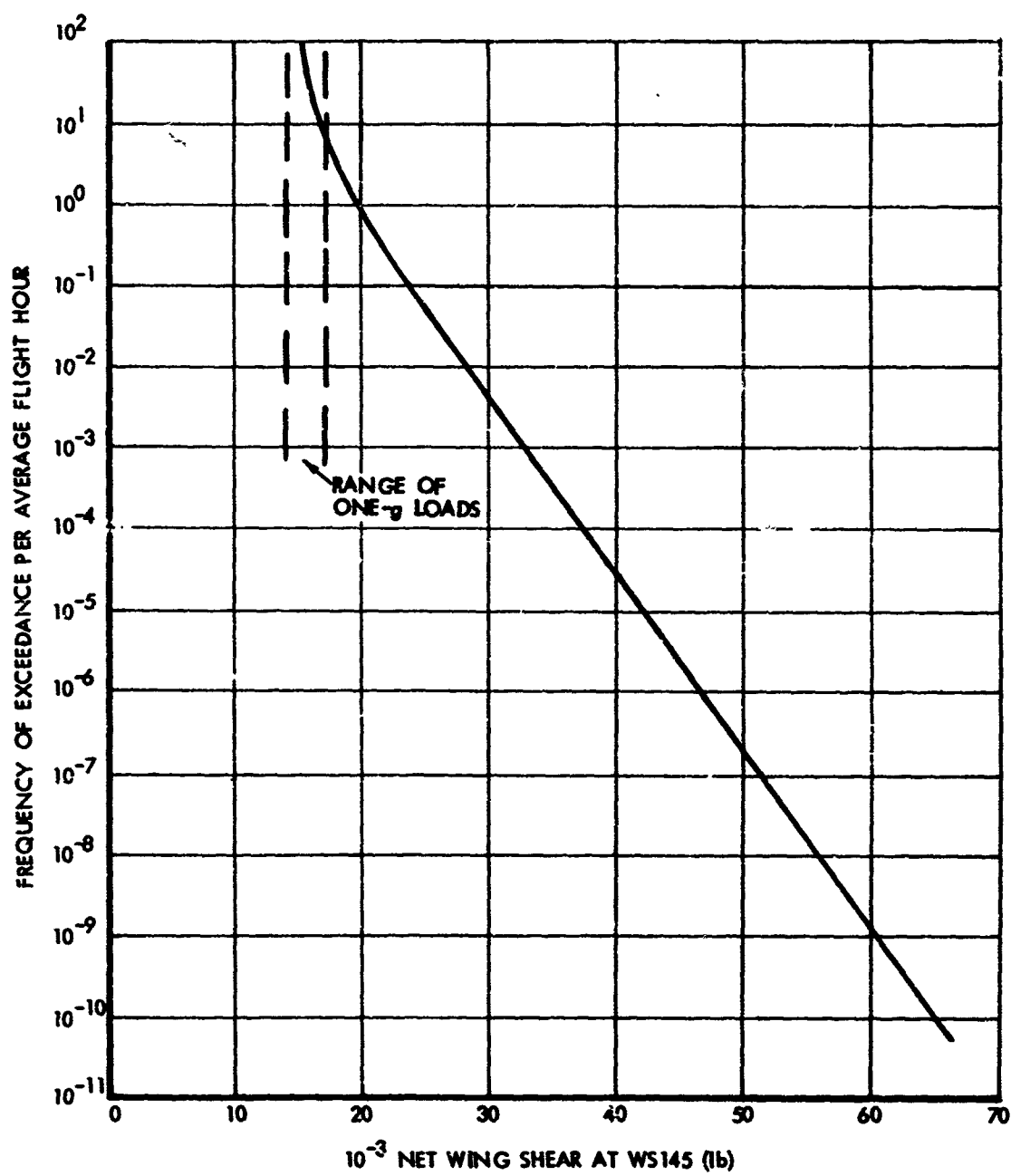


(c) WING TORSIONS AT WS 119

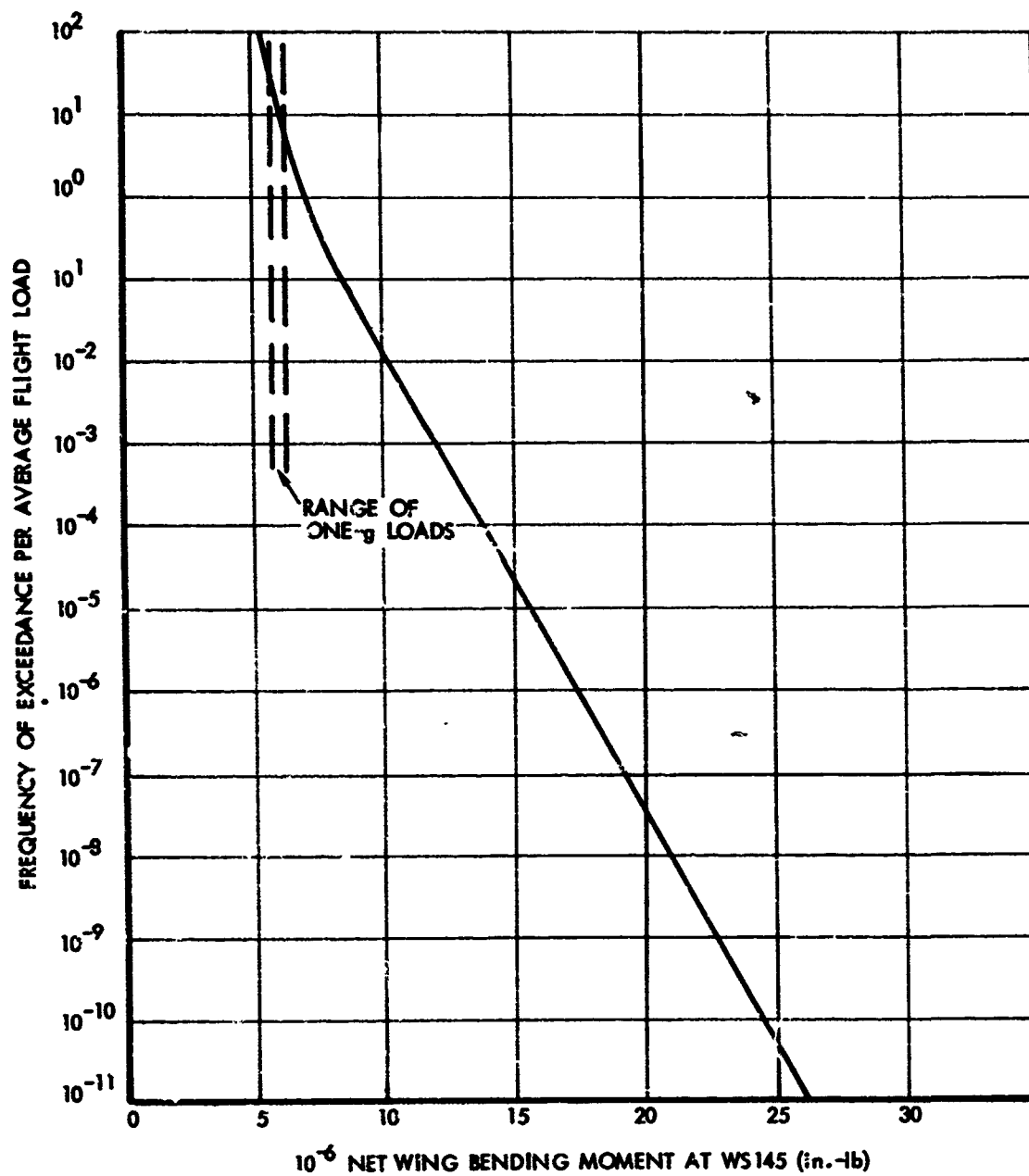
FIGURE 9-9. CONTINUED



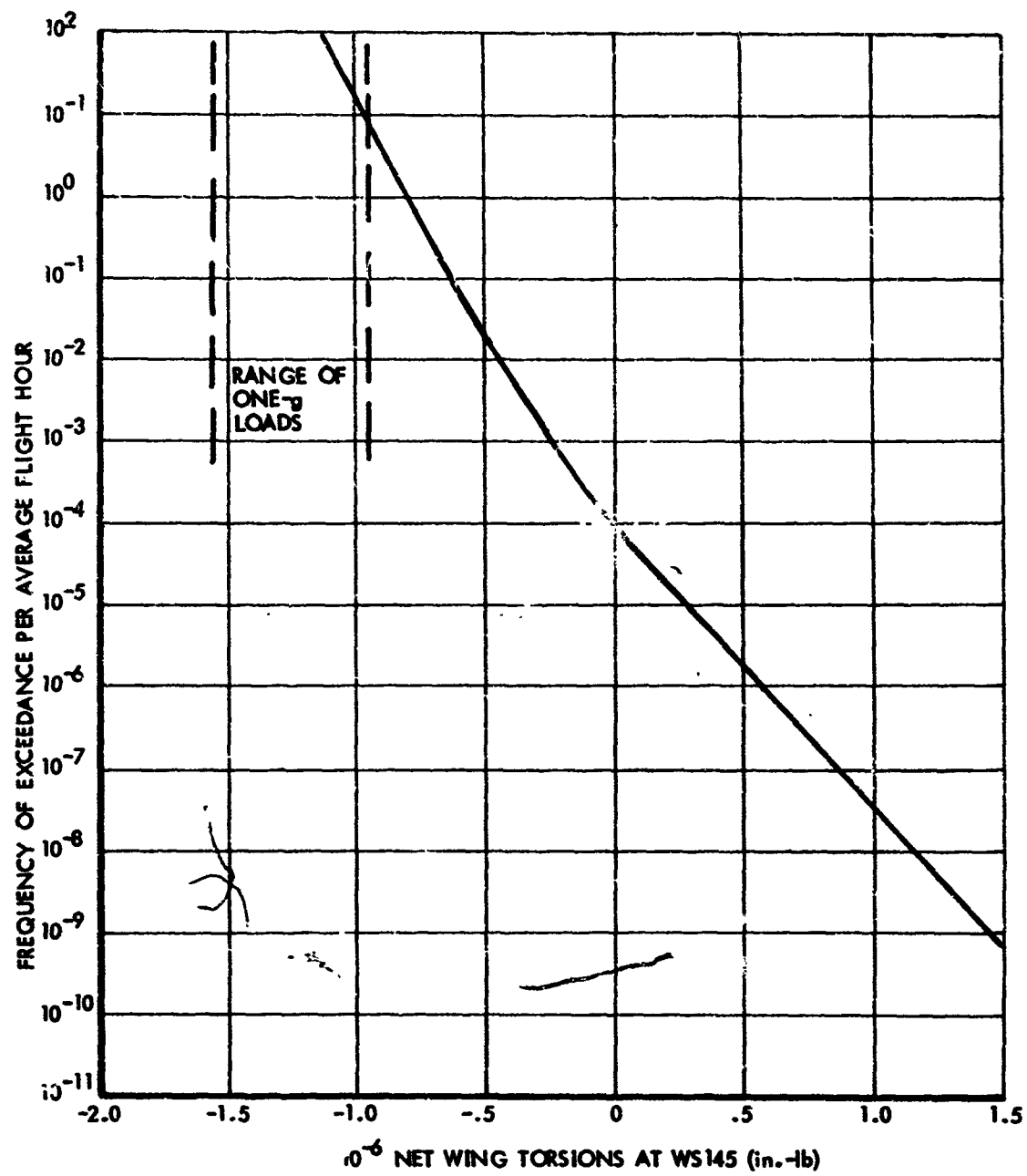
(d) FOREBODY BENDING MOMENT AT FS 571
FIGURE 9-9. CONCLUDED



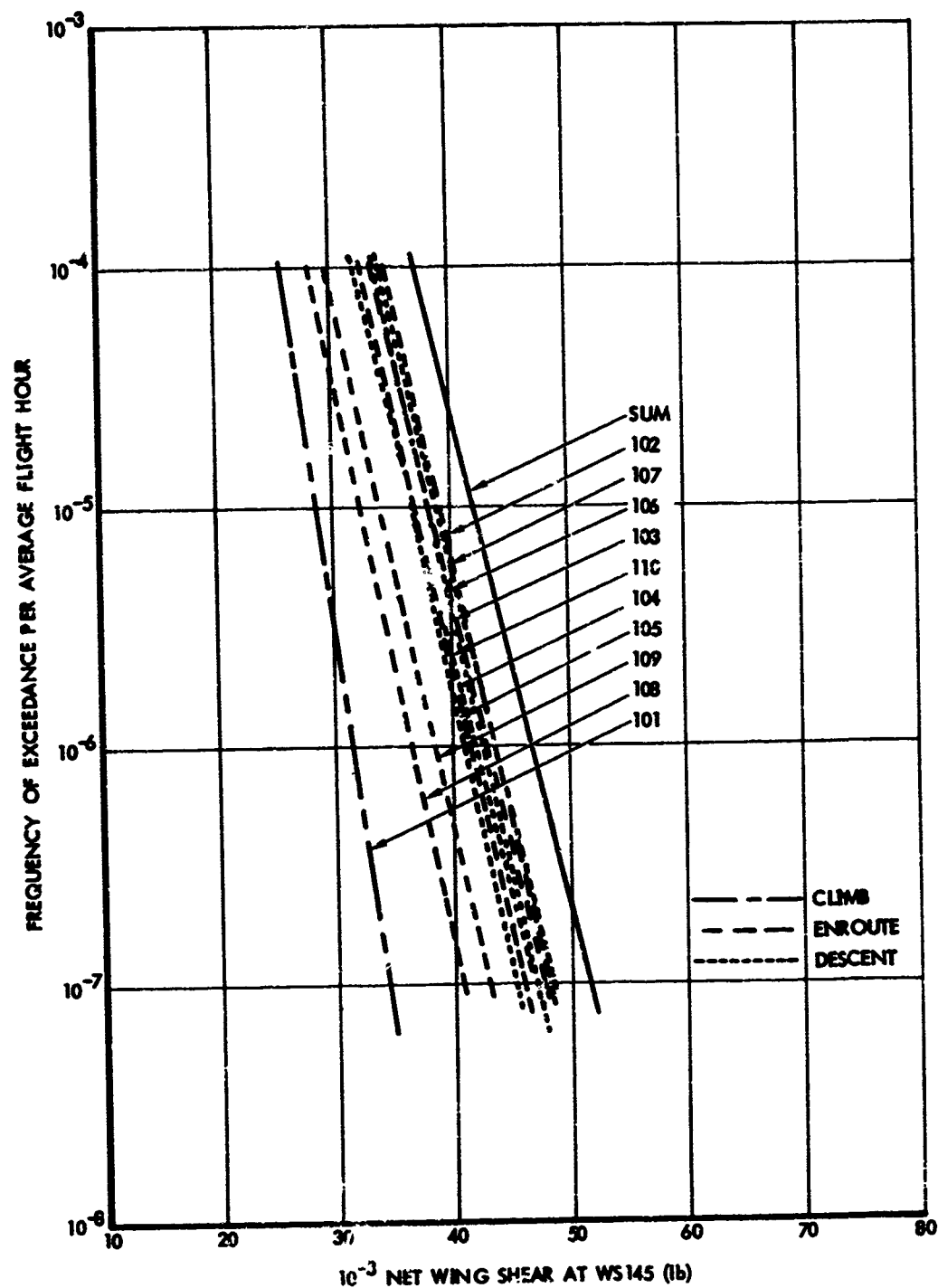
10⁻³ NET WING SHEAR AT WS145 (lb)
 (a) SHEAR AT WS 145
 FIGURE 9-10. FREQUENCY OF EXCEEDANCES OF MODEL 749 WING LOADS



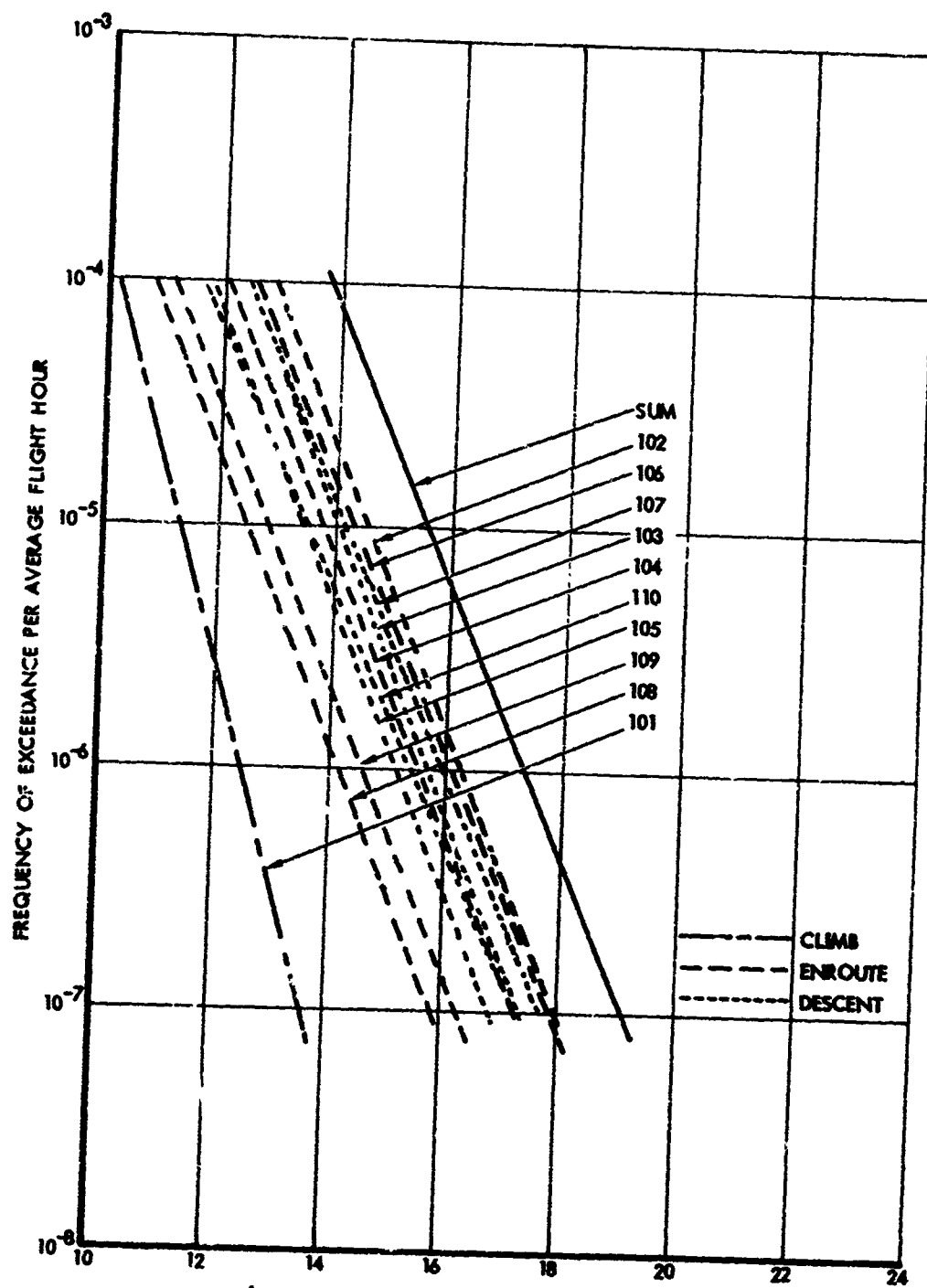
(b) BENDING MOMENT AT WS 145
FIGURE 9-10. CONTINUED



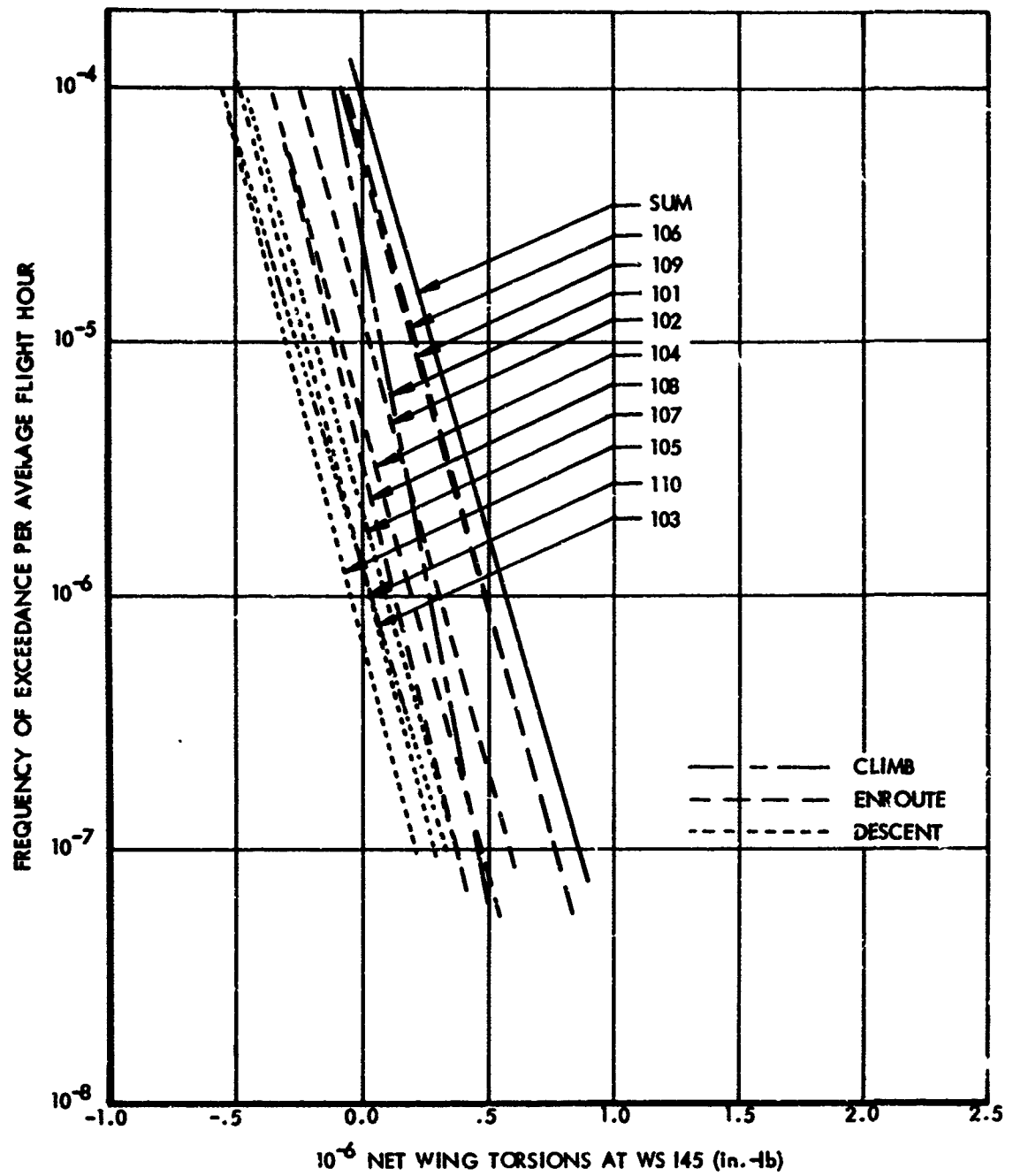
(c) TORSION AT WS 145
FIGURE 9-10. CONCLUDED



(a) SHEAR AT WS 145
 FIGURE 9-11. FREQUENCY OF EXCEEDANCE OF MODEL 749 WING LOADS, EXPANDED SCALE PLOTS



10⁻⁶ NET WING BENDING MOMENT AT WS 145 (in.-lb)
 (b) BENDING MOMENT AS WS 145
 FIGURE 9-11. CONTINUED



(c) TORSION AT WS 145

FIGURE 9-11. CONCLUDED

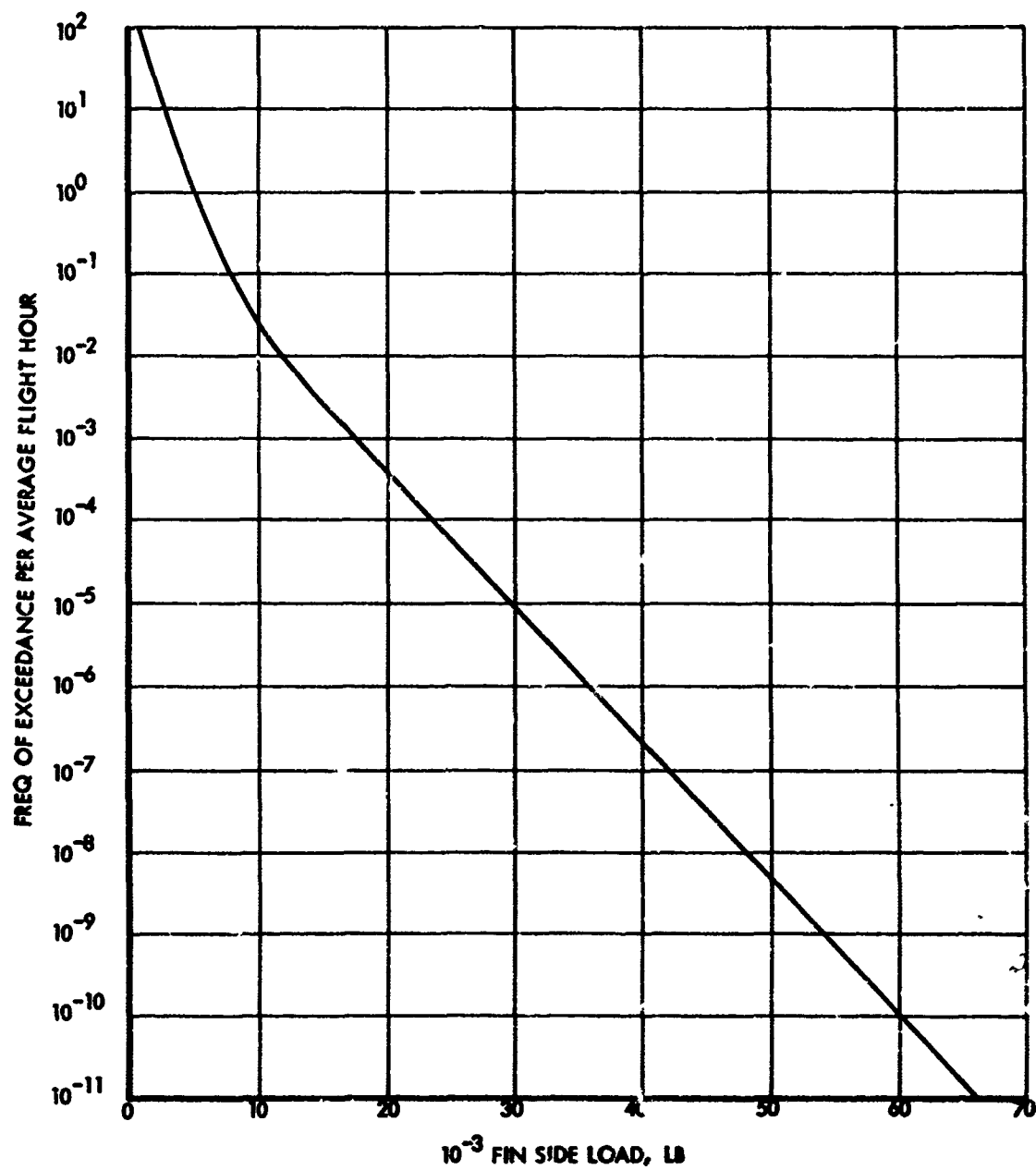


FIGURE 9-12. FREQUENCY OF EXCEEDANCE OF FIN SIDE LOAD, MODEL 188

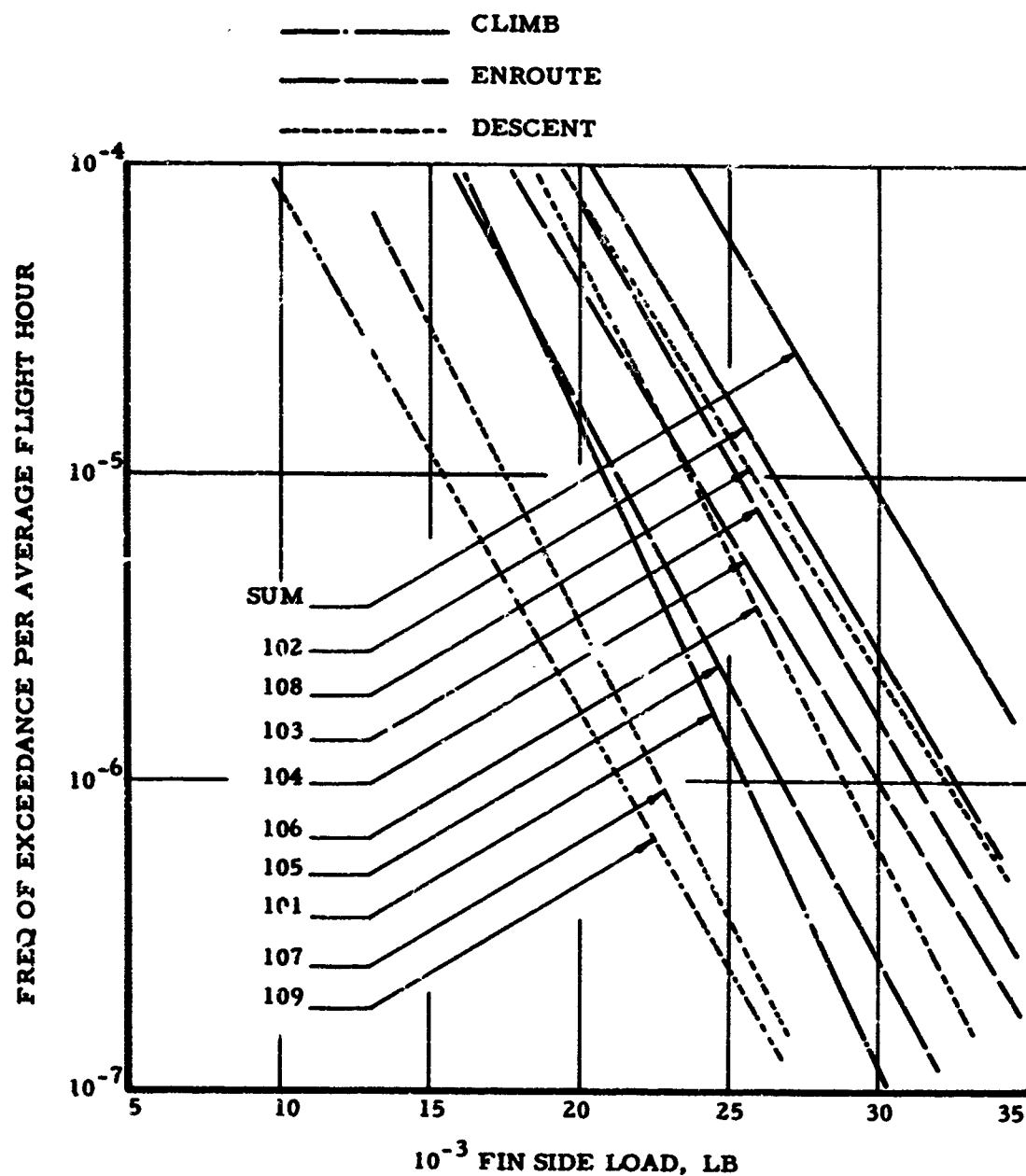


FIGURE 9-13. FREQUENCY OF EXCEEDANCE OF FIN SIDE LOAD,
 MODEL 188 - EXPANDED - SCALE PLOT

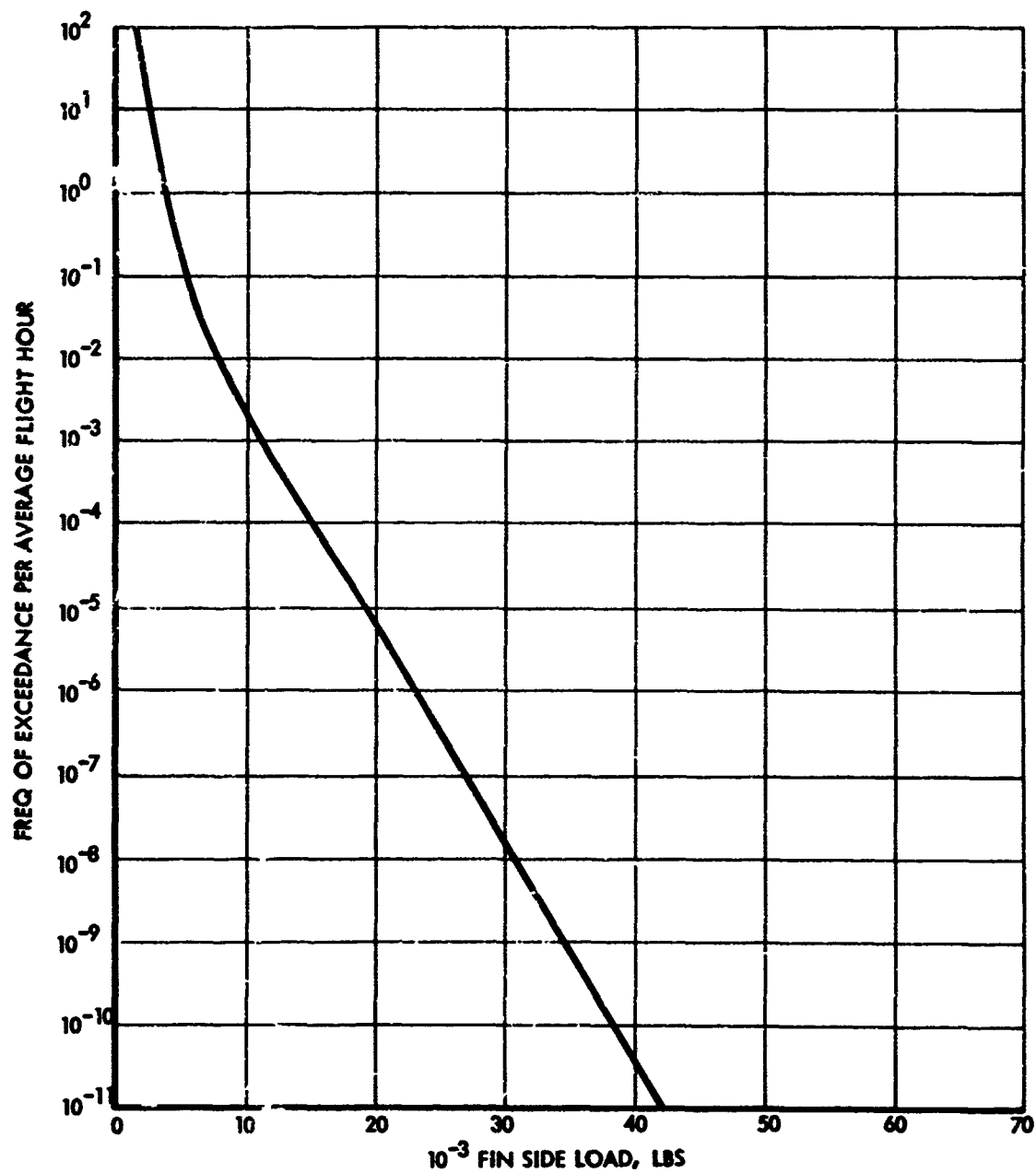


FIGURE 9-14. FREQUENCY OF EXCEEDANCE OF FIN SIDE LOAD, MODEL 749

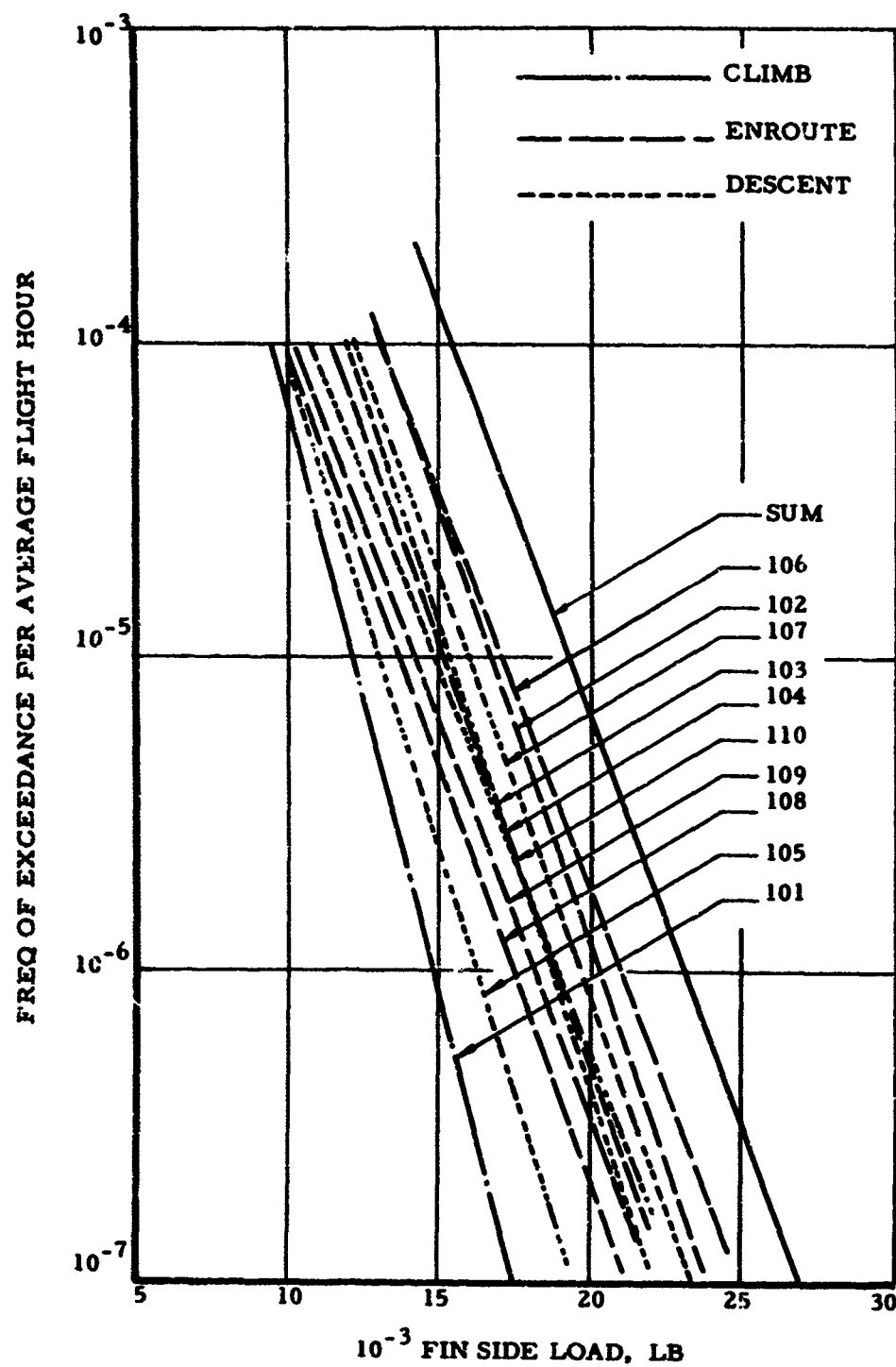


FIGURE 9-15. FREQUENCY OF EXCEEDANCE OF FIN SIDE LOAD, MODEL 749 - EXPANDED SCALE PLOT

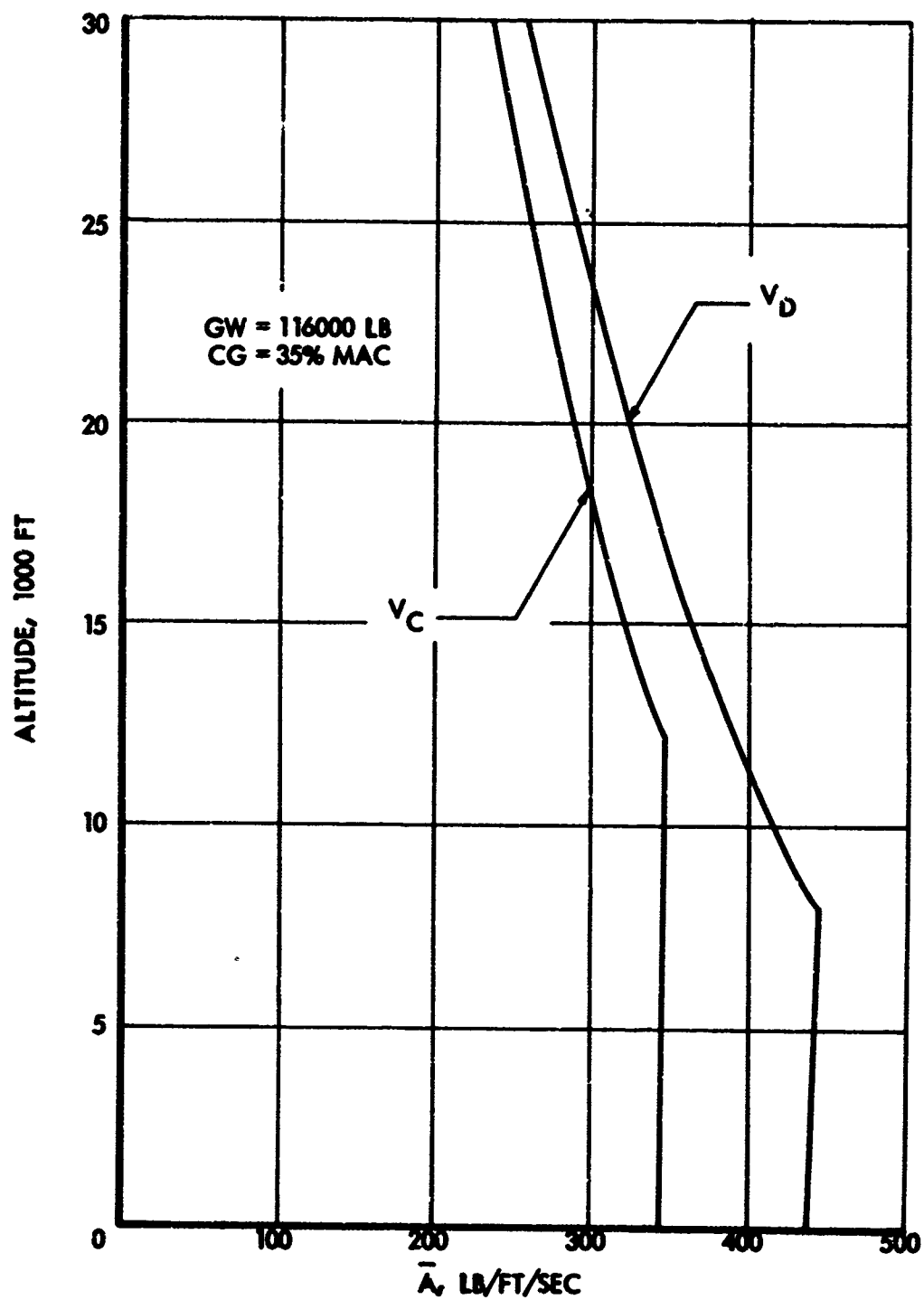


FIGURE 9-16. VARIATION WITH ALTITUDE OF \bar{V} FOR FIN SIDE LOAD, MODEL 188

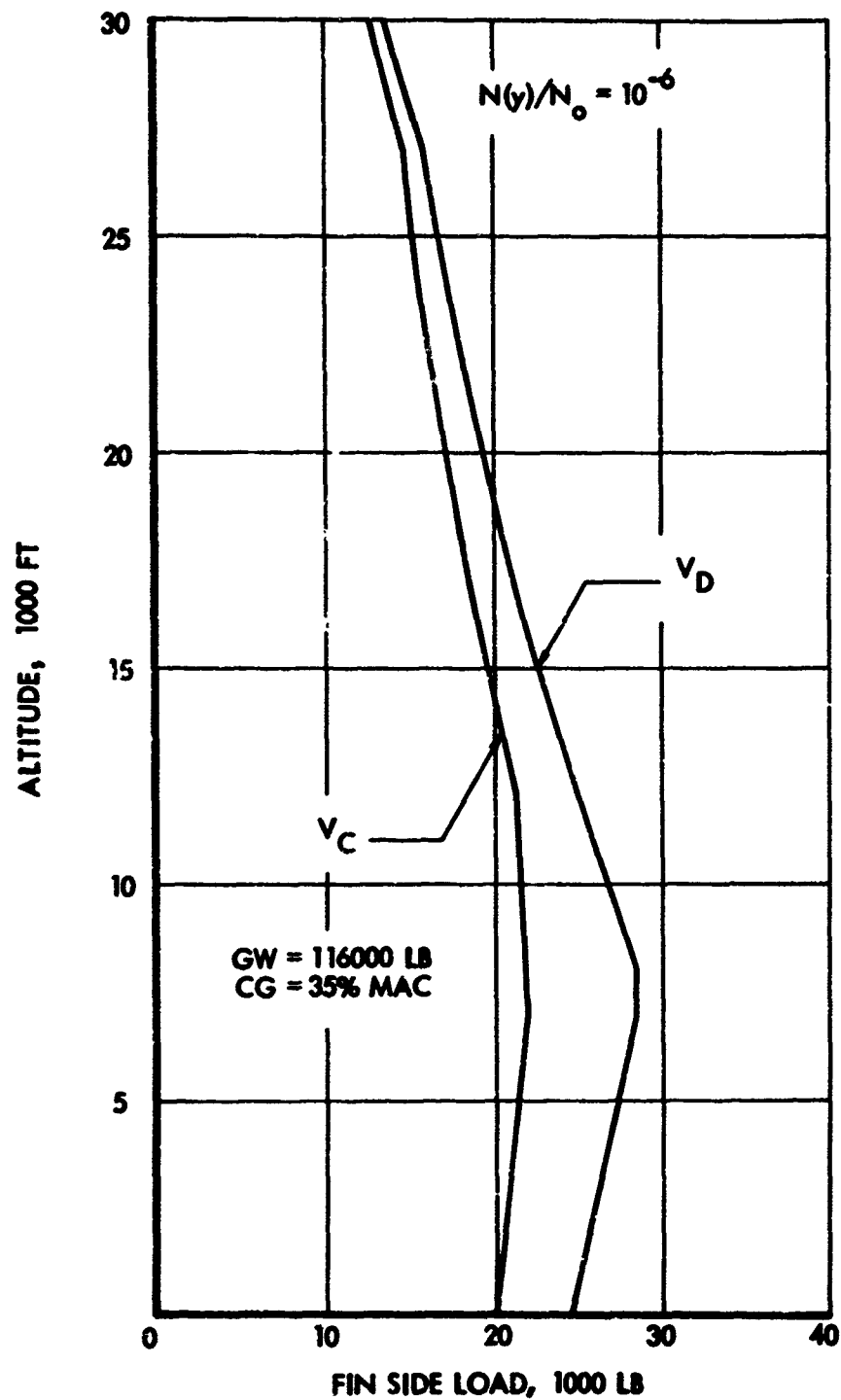


FIGURE 9-17. VARIATION WITH ALTITUDE OF FIN SIDE LOAD AT EXCEEDANCE RATIO $N(y)/N_0 = 10^{-6}$, MODEL 188

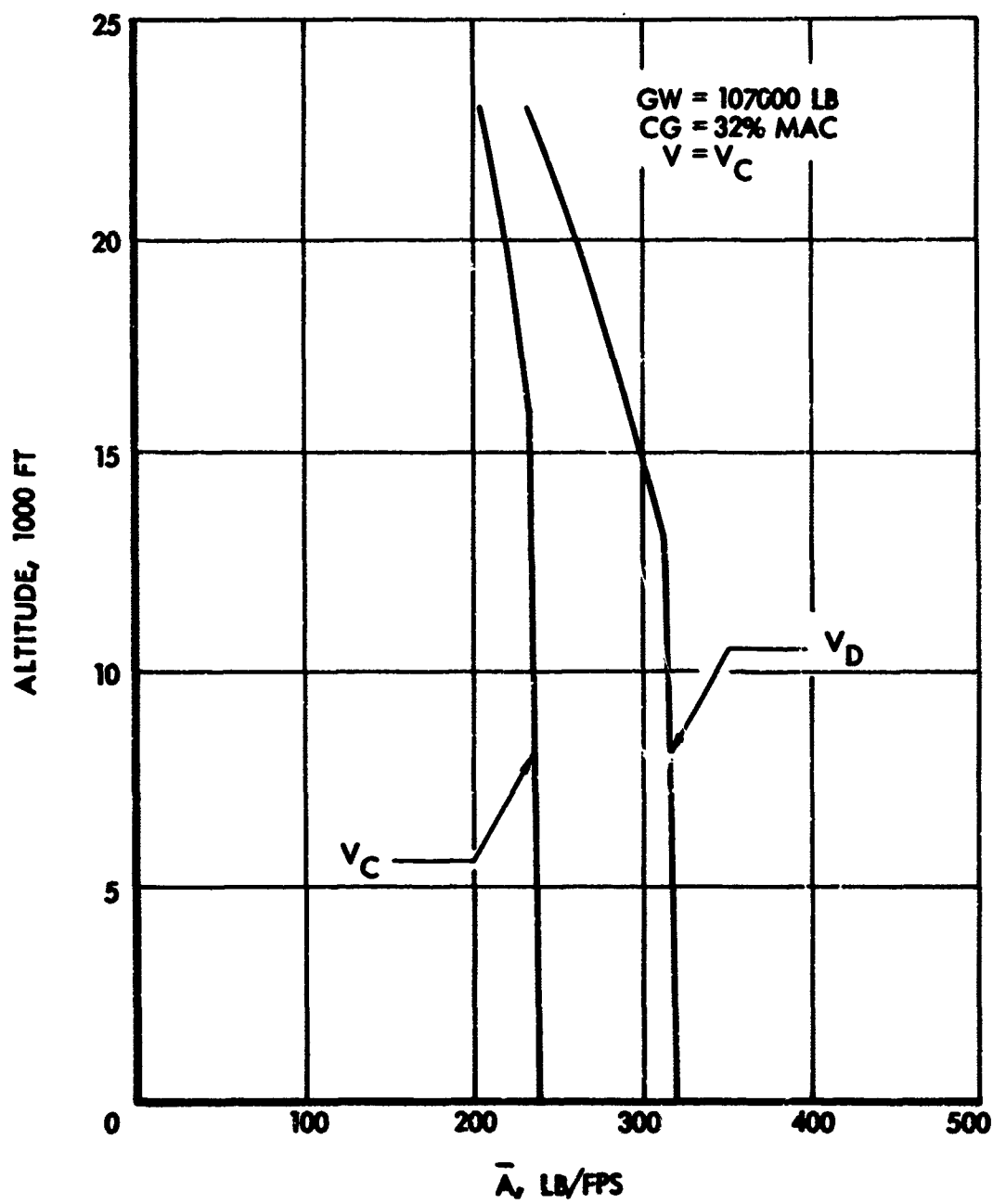


FIGURE 9-18. VARIATION WITH ALTITUDE OF \bar{A} FOR SIDE LOAD ON VERTICAL TAILS. MODEL 749

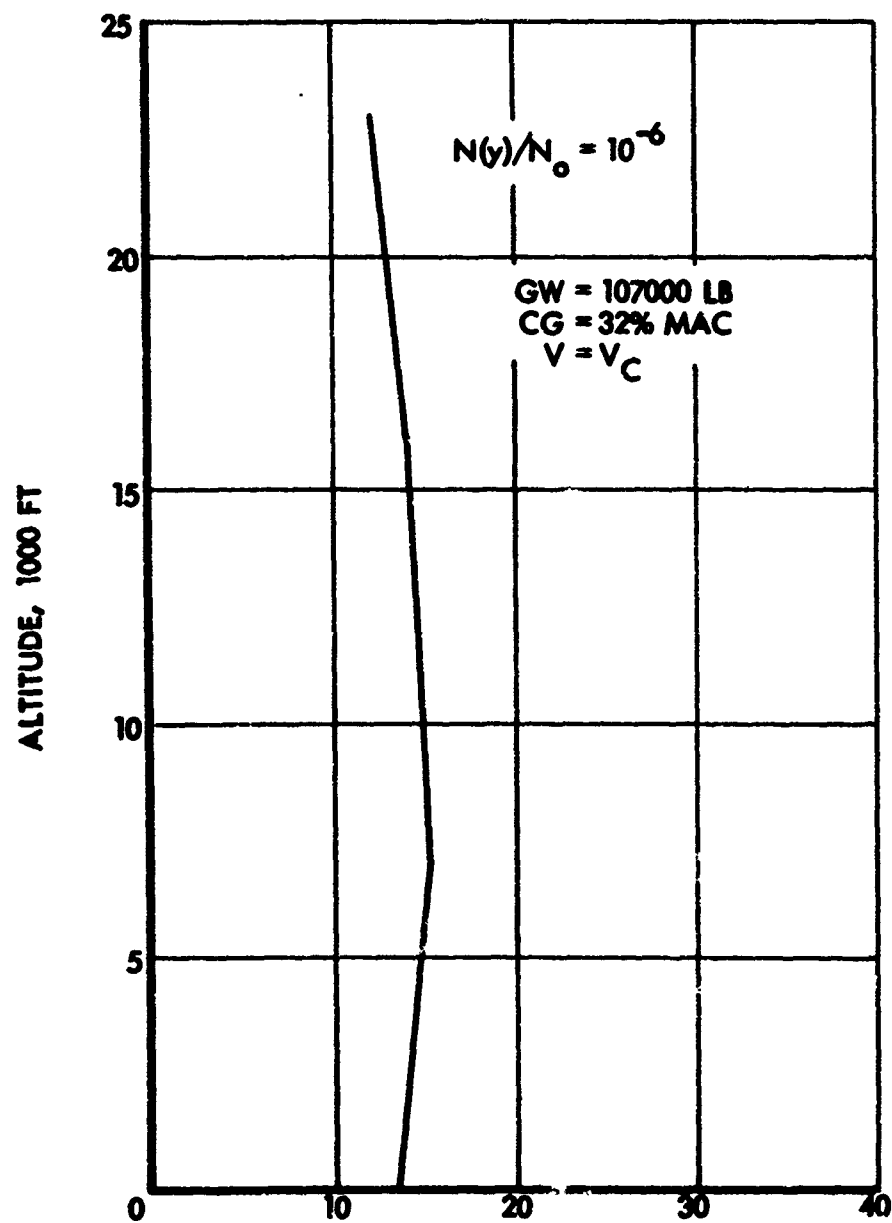


FIGURE 9-19. VARIATION WITH ALTITUDE OF SIDE LOAD ON VERTICAL TAILS AT EXCEEDANCE RATIO $N(y)/N_0 = 10^{-6}$
MODEL 749

10 DESIGN TECHNIQUES - INTRODUCTORY DISCUSSION

In the analysis of the reference airplanes, described in Sections 6 through 9, \bar{A} and N_0 values were obtained for loads at a large number of locations in the airplanes, and frequency of exceedance curves were obtained for these loads. In the design of a new airplane, results would be obtained in similar form. With the specification of a design level - as discussed in Section 15 - design values of these same load quantities would follow at once. These would be obtained - depending upon the form of criterion - either by reading values from the exceedance curves at a design frequency of exceedance, or by multiplying the various \bar{A} values by the design value of $\sigma_w \eta_d$.

At this point, it might be expected that to apply these loads in design and stress analysis would be quite straight forward. The loads defined as described above would be plotted vs wing station, and stress analysis would proceed in the usual way. Unfortunately, however, in actual flight through turbulence, these design-level loads do not all occur simultaneously. As a result, the conditions defined by the simple plots just described can be quite meaningless as a basis for stress analysis. In what proportions the various design-level loads combine - or, as it might be put, how they are phased - remains undetermined.

For example, design-level values of transverse shear and of torsional moment at a given wing station are known. But these are essentially root-mean-square values, without sign. It is not known whether maximum up shear combines with maximum nose-up torsion, or with some intermediate value. If maximum up shear combines with maximum nose up torsion, the shear flows add in the front beam and subtract in the rear beam; if maximum up shear combines with maximum nose down torsion, on the other hand, the shear flows add in the rear beam.

Similarly, it is not known whether design-level shears and bending moments occur simultaneously at all wing stations. Nor is it known whether the shears integrate to give the bending moments. If not, existing stress analysis techniques may well be unusable. In the "unit beam" method, for example, the determination of shear flows does not utilize the familiar " VQ/I " formula. Instead, flange axial loads at various wing stations are first determined, by means of the My/I relation, and differences in axial load at adjacent wing stations are then used to establish the panel shear flows. Clearly, this method cannot be used unless the shears and the bending moments at adjacent stations occur simultaneously. Further, if the shears do not integrate to give the bending moments, no single set of panel loads can be found that could be applied to duplicate the condition in a static test. Here, then, is one of the major problems in applying power-spectral methods to practical detailed stress analysis. Statistically defined loads at a limited number of locations are

available. By what techniques can these loads now be utilized - or what other statistically defined quantities can be used in their place - to establish margins of safety at the many required locations throughout a wing or other major airplane component? The problem might be referred to more briefly as the integration of the power-spectral loads determination with the routines of detailed stress analysis, or, in still more abbreviated form, as the determination of a design technique.

As indicated by the above discussion, the essence of the problem is the establishment of the phasing of two or more load quantities. The term "phasing", incidentally, is used in this context and, in fact, throughout this report, not strictly in accordance with its usual exact definition. The terms "phase" and "phasing" are usually used to denote the angle by which a pure sinusoid leads or lags another pure sinusoid of the same frequency. The phase angle, however, also establishes pairs of simultaneously occurring values of the two variables. For example, if

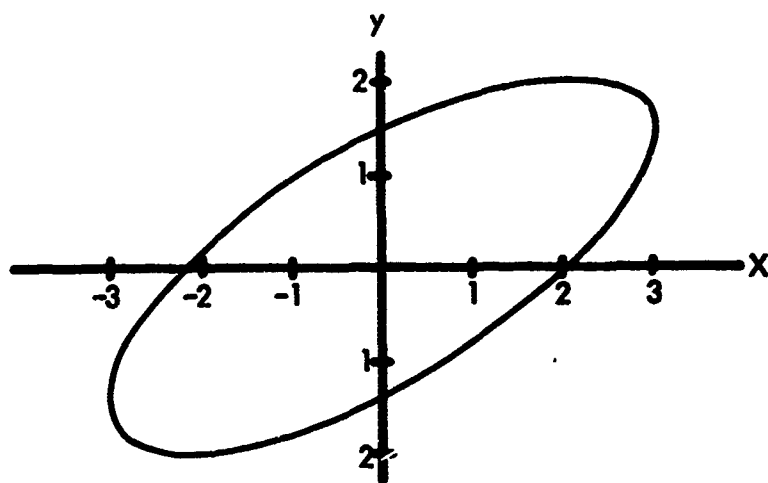
$$x = 3 \sin \omega t$$

$$\text{and } y = 2 \sin (\omega t - 45^\circ),$$

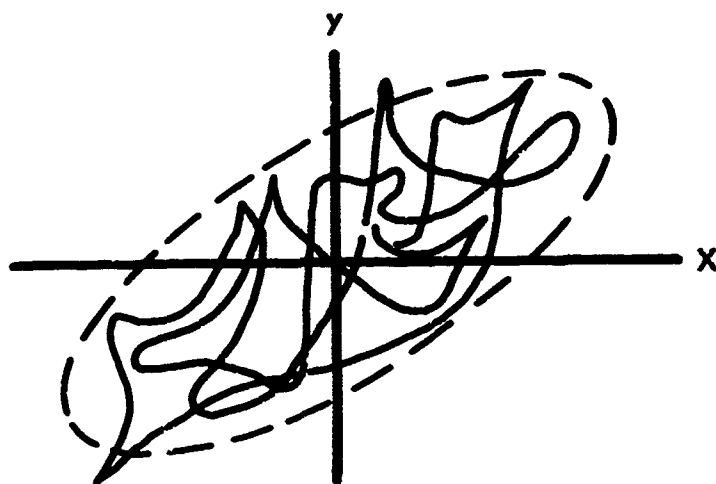
then simultaneously occurring combinations of x and y are given by the ellipse shown on the "phase-plane" plot of Figure 10-1(a). It is seen that, as a result of the 45-degree phase difference between the two variables, the maximum value of y occurs only in combination with a reduced value of x , and the maximum value of x , only with a reduced value of y .

If x and y are now random variables - such as airplane loads in turbulence - the above definition of phase has no meaning, as the two variables are no longer pure sinusoids. There will still be a tendency, however, as illustrated in Figure 10-1(b) for the "maximum," or "equal probability," or "design level" values of the two variables not to occur simultaneously. The term "phasing", as used herein, relates to this tendency. More specifically, it implies a set, or sets, of factors that must be applied to design level values of two or more loads to give statistically appropriate combinations of these loads. Thus the term "unphased loads", would apply to the design level values of shear, moment, and torsion individually. "Phased loads" would be these values as modified by application of appropriate "phasing factors" to provide a statistically appropriate combination.

In attacking the phasing problem, either of two routes might be followed.



(a) EQUAL FREQUENCY SINUSOIDS



(b) RANDOM VARIABLES

FIGURE 10-1. ILLUSTRATIVE PHASE PLANE PLOTS

One involves specific analysis of local areas of the structure. To obtain a correct shear flow, for example, the design-level values of shear and torsion are ignored, and the design-level value of the desired shear flow is determined directly. The shear flow - at each point of interest in the structure - is expressed as a linear combination of the shear, torsion, and bending moment acting at the wing section:

$$q = a S_z + b M_x + c M_y$$

This relation is introduced into the dynamic analysis with phase relations preserved, to give a transfer function for q . This, like the transfer functions for other load quantities, is multiplied by the gust power spectral density, giving a power-spectral density of q , which is then integrated to give the \bar{A} and N_0 values.

By this procedure, design-level values of stresses at all desired locations throughout the structure can be determined.

The phasing problem, however, has only been deferred, rather than solved. Many structural elements are stressed simultaneously by both shear and axial stress, with limit or ultimate strength defined by "interaction curves" or "strength envelopes." The effect of phasing of the shear and axial stresses must, therefore, still be accounted for.

Statistical techniques are available for this purpose. These are developed and applied in Reference 1.

Under the design envelope form of criterion, when using these statistical techniques, it is found necessary to replace a single quantity, $\sigma_w \eta_d$, with values of σ_w and η_d individually. The joint probability density of the axial and shear stresses is determined analytically for the specified σ_w ; a typical result is illustrated in Figure 10-2. The volume under the joint probability density surface outside the strength envelope - the part not shown in Figure 10-2 - is then the probability that the design strength is exceeded. A design value of this probability is then specified, equal to that associated with the design value of η_d .

Under the mission analysis form of criterion, $N(y)$ is redefined as the number of positive slope crossings of the strength envelope, rather than of a given value of a single load quantity.

These two procedures, because of their intimate dependence upon the joint probability functions, are referred to collectively, in this report, as the "joint probability technique."

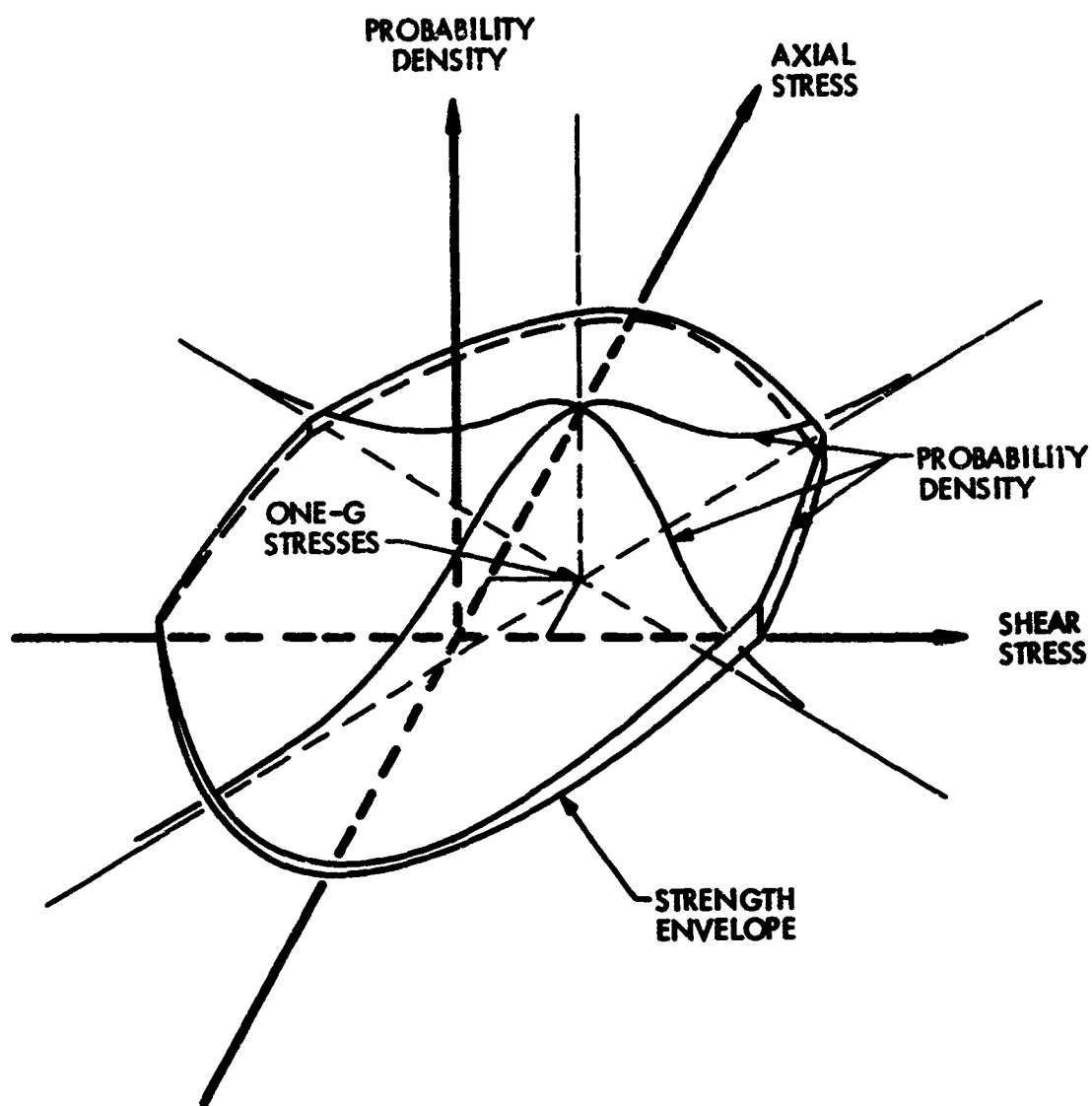


FIGURE 10-2. ILLUSTRATIVE JOINT PROBABILITY DENSITY FUNCTION AND STRENGTH ENVELOPE

An alternate route that might be followed in attacking the phasing problem involves the generation of specific design conditions that closely envelope the statistically defined loads. In order to properly phase the shear, bending moment, and torsion at each wing station, design level values of a limited number of internal stresses are also obtained. To phase the shear and torsion, for example, front and rear beam shear flows are included in the power-spectral analysis. Design combinations of shear and torsion are then established such that the resulting front or rear beam shear flow is just equal to its statistically defined design-level value.

This technique will be designated, in this report, the "matching condition" technique.

Both the matching condition and joint probability techniques are believed to offer entirely acceptable approaches from the standpoint of worthiness requirements. There may be a rather sizeable analysis time and cost advantage of one over the other; but which way this advantage would lie, and by how much, cannot be concluded with assurance at this time. The particular background and capabilities of the engineering organization involved could have a sizeable effect on the result of any such comparison.

Consequently, both approaches are developed at some length in the present study.

The matching condition technique is developed in Section 11. It is applied, for illustration, to the Model 188 wing and fuselage in Appendices C and D.

The joint probability technique is developed in Reference 1 and is applied therein to the Model 720B wing, fuselage, and vertical tail.

Some of the practical considerations that might be involved in making a choice between these two techniques are discussed in Section 12.1.

Each of the two techniques implies certain assumptions as to design philosophy. To assure consistency in application of the two techniques, these assumptions are explored in Section 12.2. How to obtain equivalent design levels under the two techniques is then discussed more explicitly in Section 12.3, and, in Section 12.4, both techniques are applied, for comparison, to a given location in the Model 720B wing.

11 THE MATCHING CONDITION TECHNIQUE

11.1 Basic Approach

A brief preview of the matching condition technique was given in the preceding section. Before actual cases are carried through for illustration, however, the concepts underlying the technique will be discussed more fully and the actual steps will be outlined in general terms.

In outlining the steps to be followed, it will be assumed that wing loads are to be determined for a straight-wing airplane with a single-cell, two-spar wing structure. It would appear, however, that the method could be applied almost without change to a swept wing and to multi-spar construction. It is believed that the same principles can be applied also to a low aspect ratio wing, although the details of the procedure would differ, as discussed in Section 16. The changes involved in extending the technique to fuselage and empennage loads would be primarily in the nature of simplifications, with the general approach remaining quite comparable.

It will also be assumed that the loads determination is for a new airplane. Thus it is presumed that design values of frequency of exceedance or of $\sigma_w \eta_d$ have already been established. For application to the reference airplanes, where the purpose is to establish limit-strength values of frequency of exceedance and $\sigma_w \eta_d$, the same procedure would be followed. However, at least in principle, the analysis would have to be carried out at two different frequency of exceedance or $\sigma_w \eta_d$ values in order to interpolate to the zero margin of safety level. Also, in application to the reference airplanes, short cuts may be possible as a result of knowing which regions of the wing are likely to be critical.

The procedure is then as follows:

1. By means of the power-spectral analysis, obtain design values of shear (S), bending moment (M), and torsion (T), at from 6 to 10 wing stations. Similarly, obtain design values of front and rear beam shear flows (q_{fb} and q_{rb}) at some or all of these wing stations. These "design values", if based on a mission analysis, are values occurring at the design frequency of exceedance. If based on a design envelope analysis, they are values of $\bar{A} \times \sigma_w \eta_d$.
2. Establish several - say three - "unit," or "elementary," spanwise distributions of shear, bending moment, and torsion. These might consist of the following:

- (1) Incremental loads due to a statically applied gust or a maneuver.
- (2) Loads due to inertia forces and displacement-dependent aerodynamic forces in the first elastic mode. If natural modes are used as generalized coordinates, these loads can be obtained directly from the model data. If arbitrary deflection shapes are used as generalized coordinates, the shape of the first elastic mode must be determined from values of the appropriate transfer functions at the first elastic mode frequency.
- (3) Loads due to inertia forces and displacement-dependent aerodynamic forces in the second elastic mode. These can be obtained in the same way as those for the first elastic mode.

These three distributions, or sets of loads, can be at any arbitrary level.

Designate these elementary distributions the E_1 , E_2 , and E_3 distributions, respectively. Designate the shears, moments, and torsions in the E_1 distribution SE_1 , ME_1 , and TE_1 , where, of course, each of these three loads will have different values at the various wing stations. Designate the loads in the other distributions similarly.

Compute for each distribution front and rear beam shear flows - q_{fbE_1} , q_{rbE_1} , q_{fbE_2} , q_{rbE_2} , q_{fbE_3} , and q_{rbE_3} . These will be obtained at the wing stations where statistically defined values of the shear flows are obtained in Step 1.

3. By trial and error, using the E_1 , E_2 , and E_3 distributions as building blocks, generate several design conditions such as to match, or envelope closely, the statistically defined loads, including shear flows, obtained in Step 1.

Any single design condition will be defined by a certain amount, a_1 , of the E_1 distribution, plus a certain amount, a_2 , of the E_2 distribution, plus a certain amount, a_3 of the E_3 distribution. Thus for this one design condition,

$$S = a_1 SE_1 + a_2 SE_2 + a_3 SE_3$$

$$M = a_1 ME_1 + a_2 ME_2 + a_3 ME_3$$

$$T = a_1 T_{E1} + a_2 T_{E2} + a_3 T_{E3}$$

Other conditions are defined by other sets of values of the coefficients a_1 , a_2 , and a_3 .

The superposition of elementary distributions to generate design conditions is exactly analogous to a procedure often used in static wing loads determination, in which the net loads are obtained by a superposition of various distributions such as an "additional" lift distribution, a "basic" lift distribution, an n_z inertia distribution, a pitch inertia distribution, various aeroelastic distributions, etc. Adopting the nomenclature sometimes used in the static loads determination, S_{E1} , for example, would become (S/a_1) , the E_1 distribution would be called simply the a_1 distribution, and the above equations would be written:

$$S = \left(\frac{S}{a_1}\right) a_1 + \left(\frac{S}{a_2}\right) a_2 + \left(\frac{S}{a_3}\right) a_3$$

$$M = \left(\frac{M}{a_1}\right) a_1 + \left(\frac{M}{a_2}\right) a_2 + \left(\frac{M}{a_3}\right) a_3$$

$$T = \left(\frac{T}{a_1}\right) a_1 + \left(\frac{T}{a_2}\right) a_2 + \left(\frac{T}{a_3}\right) a_3$$

Ordinarily, no single condition can be obtained that will match all of the statistically defined loads. Consequently, several conditions will be required. One, for example, may match the shears, bending moments, and shear flows but contain lower torsions than the statistically defined design values; another may match the torsions and shear flows but contain lower shears and bending moments than required. Together, however, the two will envelope - closely - all of the statistically defined values. Or one such pair of conditions may envelope closely the loads in the inboard portion of the wing but be lower than required in the outer wing. This pair of conditions would then be complemented by a second pair that match closely the loads in the outer wing but are lower than required in the inboard region.

To illustrate how such an approach leads to realistic phasings of shear and torsion at a given wing station, reference is made to a typical shear-torsion plot as shown in Figure 11-1. Only combinations of positive (up) shear and positive (nose up) torsion are shown, the same

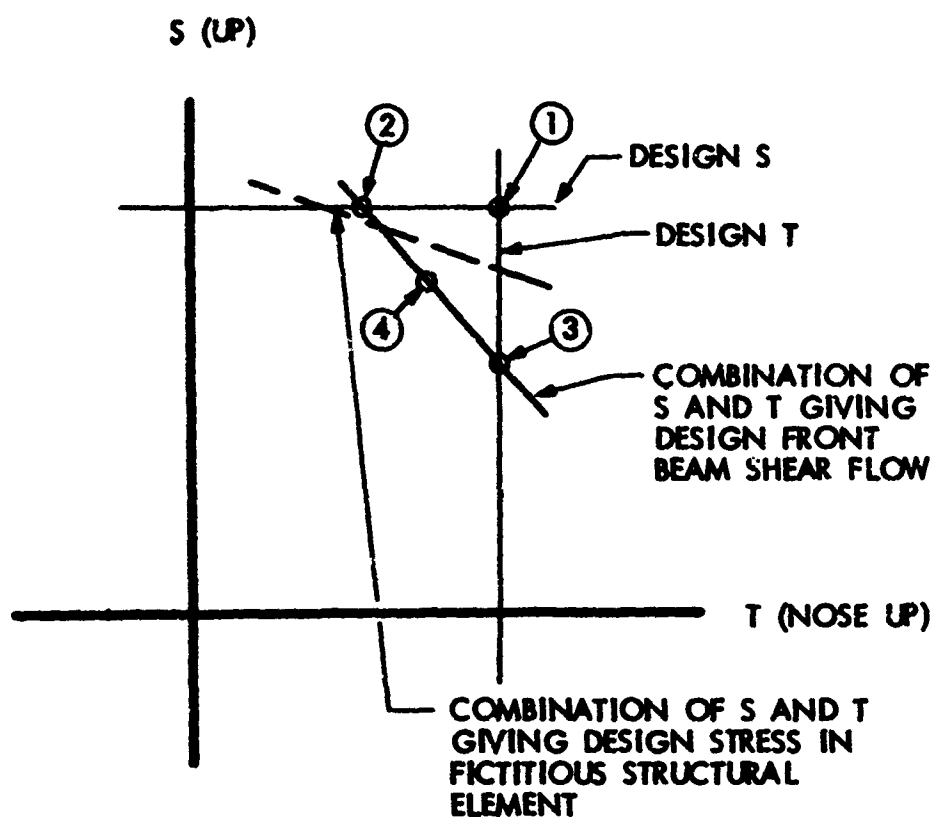


FIGURE 11-1. ILLUSTRATIVE SHEAR-TORSION PLOT

reasoning, however, will also apply to the remaining three quadrants. The design magnitudes of shear and torsion are shown by horizontal and vertical lines in the figure. The diagonal line represents the various combinations of shear and torsion that result in the design magnitude (per Step 1) of front beam shear flow.

Ordinarily, a single design condition containing the design magnitudes of both shear and torsion - that is, treating these as occurring simultaneously - will result in a front beam shear flow considerably in excess of the design value established in Step 1. Such a condition is represented by Point 1 in the figure. To avoid an overly conservative design, it is clearly necessary to reduce either the shear or the torsion or both. Any of Points 2, 3, or 4 will accomplish this purpose, as each results in the correct value of shear flow. However, the front beam shear web is only one element of a complex structure. Other elements may be stressed predominantly as a result of shear or bending moment alone (these tending, probably, to be closely in phase), or possibly by torsion alone, or perhaps by interaction of shear flow and bending moment. Consequently, it appears appropriate that design conditions be selected to include Points 2 and 3. The first condition then matches shear (and, simultaneously bending moment) and shear flow, and the second matches torsion and shear flow. Together, the two conditions envelope closely all three load quantities at the given wing station. Actually, even Point 2 may be slightly conservative. However, it is far less conservative than Point 1, and any remaining conservatism probably has a rather negligible effect.

In establishing values of a_1 , a_2 , and a_3 to define each of the various design conditions, the relative amounts of shear and torsion at various wing stations are controlled by the relative values of a_1 , a_2 , and a_3 . For the Model 749 and Model 188, for example, it has been found that the static distribution contains relatively little torsion, whereas the elastic mode distributions contain sizeable torsions. Point 2, therefore, would result from a condition in which the static distribution predominates. Such a condition would be produced by an attempt to match shear, bending moment, and shear flow simultaneously. Point 3, similarly, would result from a condition in which one or more of the elastic mode distributions predominates. Such a distribution would be produced by an attempt to match torsions and shear flow simultaneously.

In matching design-envelope loads, it seems quite likely that about three elementary distributions, as employed in the above discussion, might suffice. (Each point of the design envelope, however, might require a different set of distributions.) In matching mission analysis loads, on the other hand, more unit distributions are likely to be required. The one-g level flight loads are now included in the statistically defined loads, so that at least one one-g or zero-g condition

will have to be included in the unit distributions to cover the so-called "basic" distributions due to built-in wing twist, C_{m_0} , aero-elastic effects at zero-g etc. Also, the statistically defined loads reflect contributions from various mission segments at a variety of speeds, altitudes, and especially fuel weights; consequently unit distributions based on more than one weight condition may be required.

It should be remarked that the E_1 , E_2 , and E_3 distributions can be quite arbitrary; the only requirement is that the resulting design conditions match the statistically defined loads to the desired degree of accuracy. If the E_1 , E_2 , and E_3 distributions do not provide an adequate match, they can be modified as necessary, or the resulting conditions can be modified arbitrarily. The latter is probably to be preferred, and can be looked upon as adding in a small amount of some additional, highly simplified distribution.

At the same time, there is a distinct advantage in starting with fairly reasonable distributions. In flying through turbulent air, an airplane responds statically to the low frequency components of the turbulence (long gradient gusts) and it responds dynamically in its various elastic modes to the higher frequency components of the turbulence. The two types of response - the static and the dynamic - generally have quite different distributions of load throughout the structure. Moreover, each elastic mode will have its own distinctive load distribution. In flight through typical turbulence there is a random interplay amongst these various distributions. It would appear that use of the actual distributions associated with motions in the various modes would lead most readily to a match with the statistically defined loads. More important, since the statistically defined loads are available at a fairly limited number of locations, the use of rational unit distributions tends to assure a realistic definition of stresses at the intermediate locations.

11.2 The Fictitious Structural Element Concept

In the previous section, proper phasing of torsion with shear or bending was dependent upon matching shear flows in the front and rear beams, and it was necessary to assume that the shear and bending moment would be in phase. Fortunately, an additional tool is available that broadens immeasurably the technique for establishing realistic phasings. This tool is the concept of a fictitious structural element.

It will be recalled from the previous discussion that design combinations of shear and torsion at a given wing station are established so that the resulting front beam shear flow matches its statistically defined value. This was illustrated by Figure 11-1. It was noted that

Point 1 would obviously be conservative as a design point, since the resulting front beam shear flow would be well in excess of the statistically defined value. Point 2 on the other hand would be a realistic design point, probably only very slightly conservative. This point gives the right shear and bending moment (these being assumed in phase) for whatever structural elements are not influenced by torsion, and also the right beam shear flow. Also, however, it gives about the right combination of bending and torsion for design of the upper and lower surfaces midway between front and rear beams. Thus the front beam is seen to serve as an indication of phasing to be applied at another location altogether.

This fact suggests that, for the purpose of establishing phasing, there is no need that a real front beam be present at all. For example, suppose it is desired to see how conservative Point 2 actually is. The shear flow in the real front beam might have been given by

$$q_0 = .014 S + .00020 T \quad (11-1)$$

Now suppose we imagine a fictitious structural element such that its stress is given by

$$q_1 = .014 S + .00010 T \quad (11-2)$$

- i.e., one that is relatively less sensitive to torsion. The statistically defined load for this element is determined in the same way as for the real front beam - that is, by including in the dynamic analysis the determination of its transfer function, power-spectral density, \bar{A} and N_0 . The dash line in Figure 11-1 represents combinations of S and T that give a value of stress equal to the statistically defined value in this fictitious element. (The dash line is defined by substituting the statistically defined value of q_1 in Equation 11-2 and plotting S vs T.) In this case it is seen that Point 2 actually would be slightly conservative; if the fictitious element were actually there, its stress at Point 2 would be higher than defined statistically, precluding Point 2 as a valid design point.

Similarly, by defining a series of fictitious structural elements, employing a series of ratios of the coefficients in the expression of q , a complete design load envelope could be established.

Such an envelope has been computed for shear-torsion of the Model 188 wing at W.S. 83 and is shown in Figure 11-2(a). Only the increments over and above the 1-g load are shown; and the contribution of bending moment to the stress in the fictitious element has been assumed to be zero. The points labelled Condition I, Condition II, etc., on the figure are design conditions generated in Appendix C and can be disregarded for the present.

The solid lines in Figure 11-2(a) clearly circumscribe a figure of roughly elliptical shape which can be regarded - at least intuitively and without precisely defining the term - as a curve of equal probability.

In obtaining this figure, as can be seen, it was necessary to utilize 10 fictitious structural elements, in addition to the two already inherently available - i.e., those that sense shear only and torsion only. The coefficients a_1 and a_2 in the expression

$$q = a_1 S + a_2 T$$

were selected so that

$$\frac{a_2}{a_1} = 0.2 \frac{\bar{A}_S}{\bar{A}_T}, 0.5 \frac{\bar{A}_S}{\bar{A}_T}, 1.0 \frac{\bar{A}_S}{\bar{A}_T}, 2 \frac{\bar{A}_S}{\bar{A}_T}, 5 \frac{\bar{A}_S}{\bar{A}_T}$$

$$-0.2 \frac{\bar{A}_S}{\bar{A}_T}, -0.5 \frac{\bar{A}_S}{\bar{A}_T}, -1.0 \frac{\bar{A}_S}{\bar{A}_T}, -2 \frac{\bar{A}_S}{\bar{A}_T}, -5 \frac{\bar{A}_S}{\bar{A}_T}$$

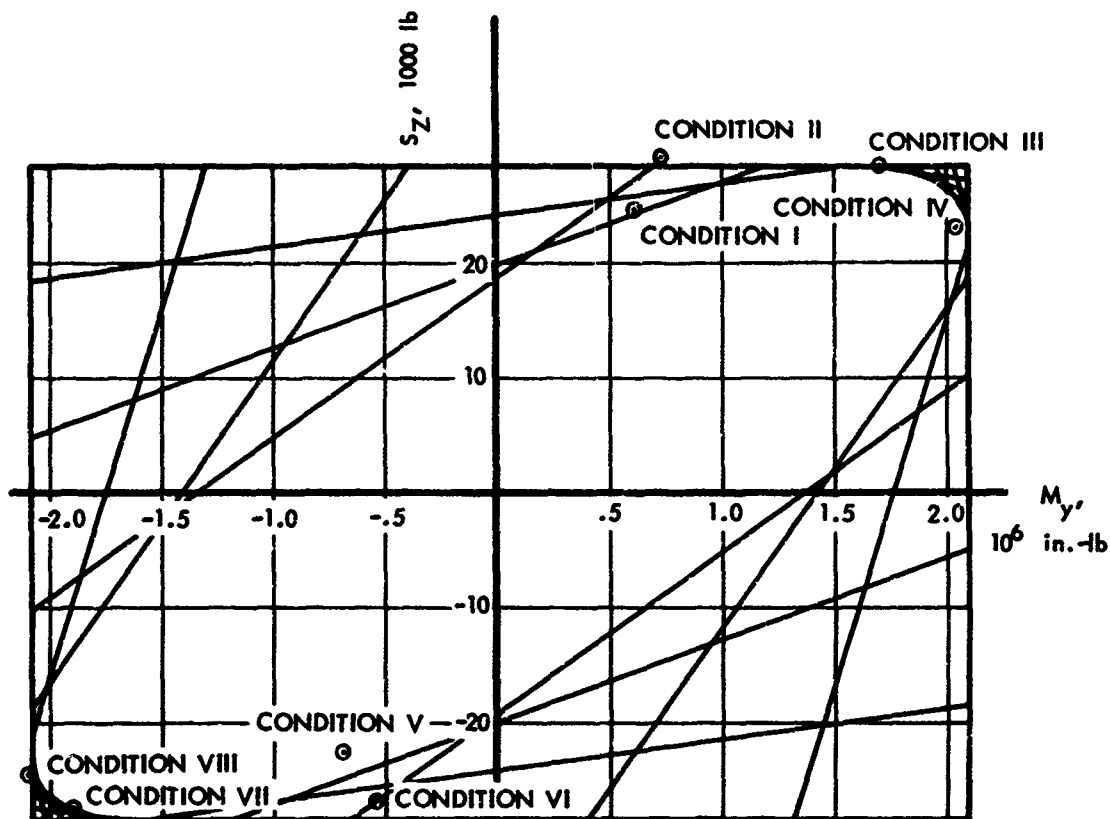
respectively.

The same procedure can now be used to test the assumption that shear and bending moment are in phase. The results for Wing Station 83 of the Model 188 are shown in Figure 11-2(b). It is quite clear that the assumption is an excellent one, as the "equal-probability" ellipse is indeed a very narrow one and its corner occurs virtually at the intersection of the maximum S_z and maximum M_x lines.

The same procedure has also been applied to examine the phasing of the remaining pair of quantities, bending and torsion. The result is shown in Figure 11-2(c). This figure is approximately geometrically similar to the shear torsion envelope, Figure 11-2(a), as expected in view of the shear bending phase relation depicted in Figure 11-2(b).

A similar set of figures applicable to Model 188 Wing Station 346, between the nacelles, is shown in Figures 11-2(d) - (f). Here the shear and bending moment are seen to be less closely in phase, but still closely enough for the in-phase assumption to lead to fairly realistic design loads.

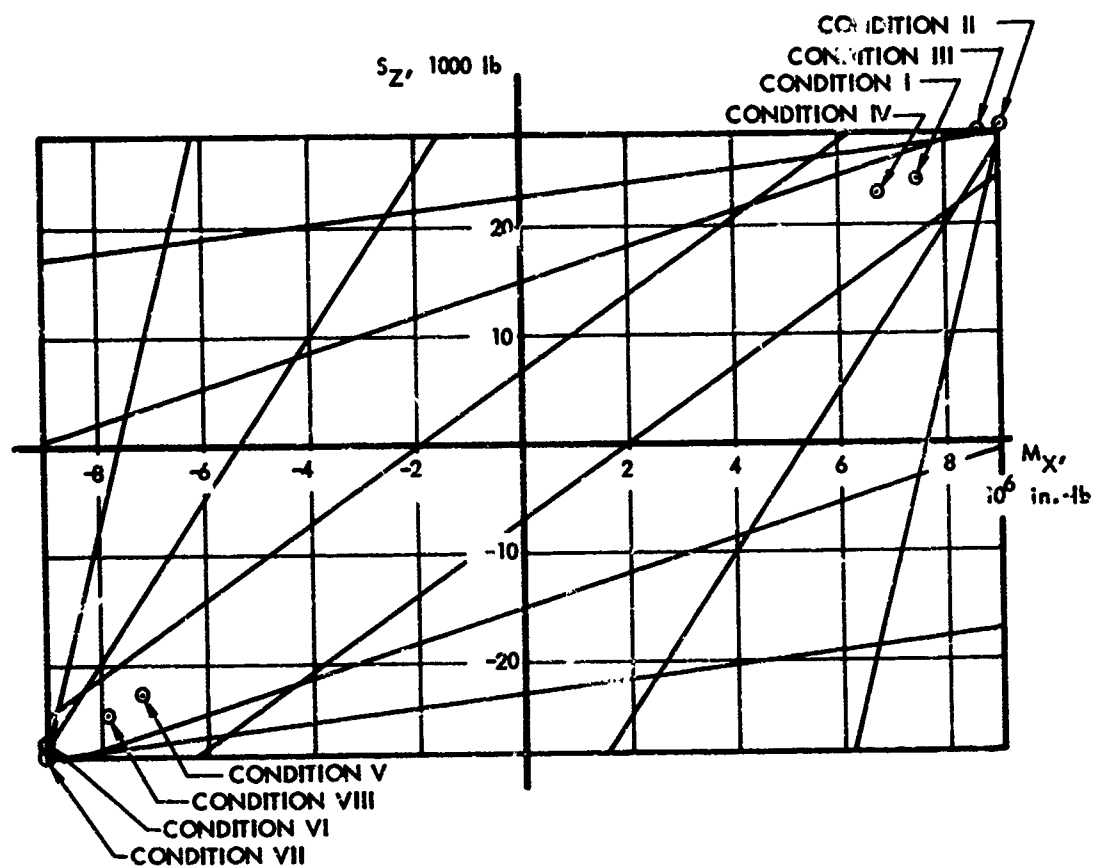
Corresponding figures for the Model 749 are shown in Figures 11-3(a) - (f). These are generally similar to those for the Model 188. The dash lines on the figure are for the actual front and rear beam webs as structural elements, with the contribution of bending moment to the



NOTE: CURVES ARE MISSION ANALYSIS CASE 202 AT $N(y) = 10^{-5}$
EXCEEDANCES PER HOUR

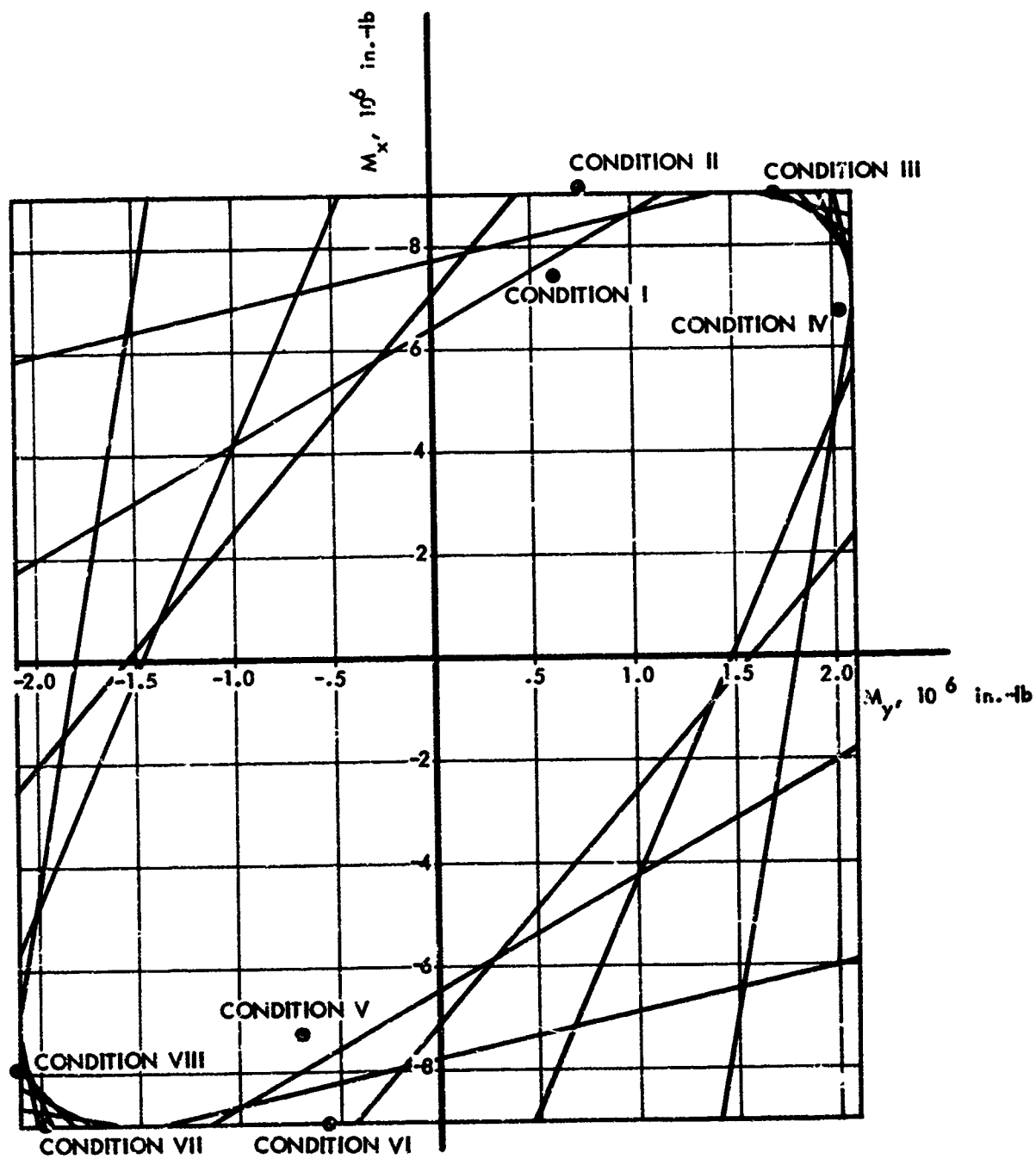
(a) WS 83, SHEAR-TORSION

FIGURE 11-2. "EQUAL PROBABILITY" ENVELOPES, MODEL 188



NOTE: CURVES ARE MISSION ANALYSIS CASE 202 AT $N(y) = 10^{-5}$
EXCEEDANCES PER HOUR

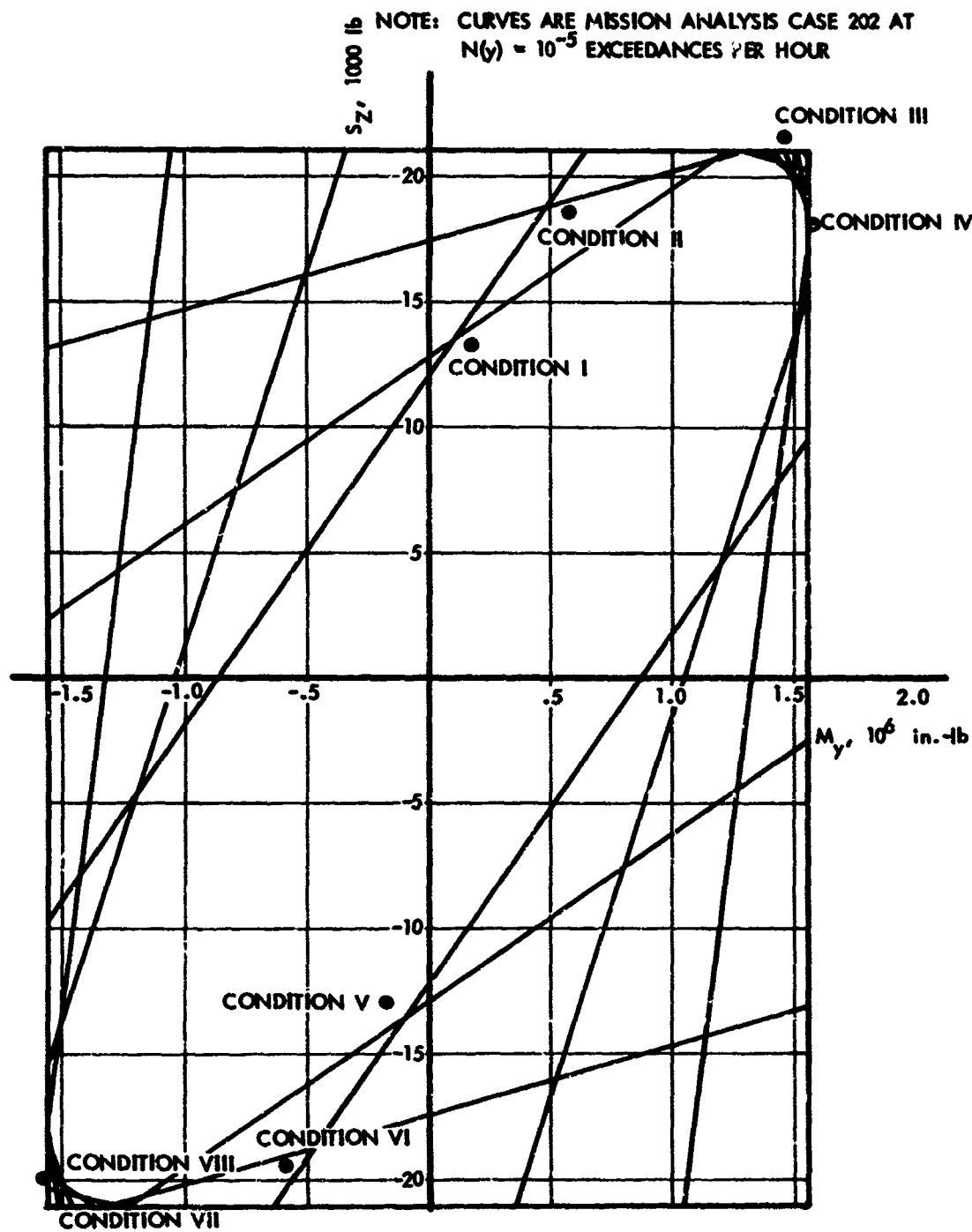
(b) WS 83, SHEAR-BENDING
FIGURE 11-2, CONTINUED



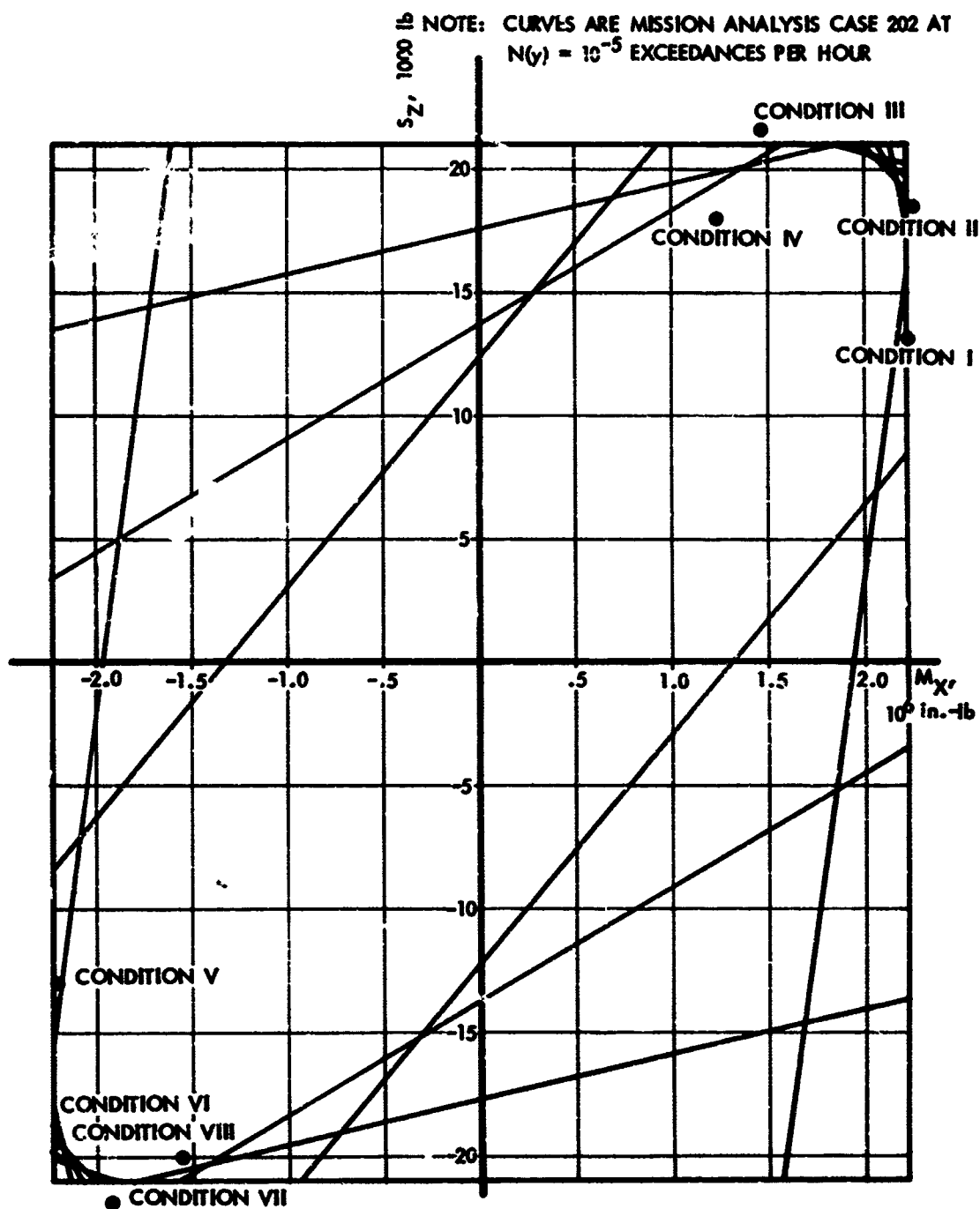
NOTE: CURVES ARE MISSION ANALYSIS CASE 202 AT $N(y) = 10^{-5}$ EXCEEDANCES PER HOUR

(c) WS 83, BENDING-TORSION

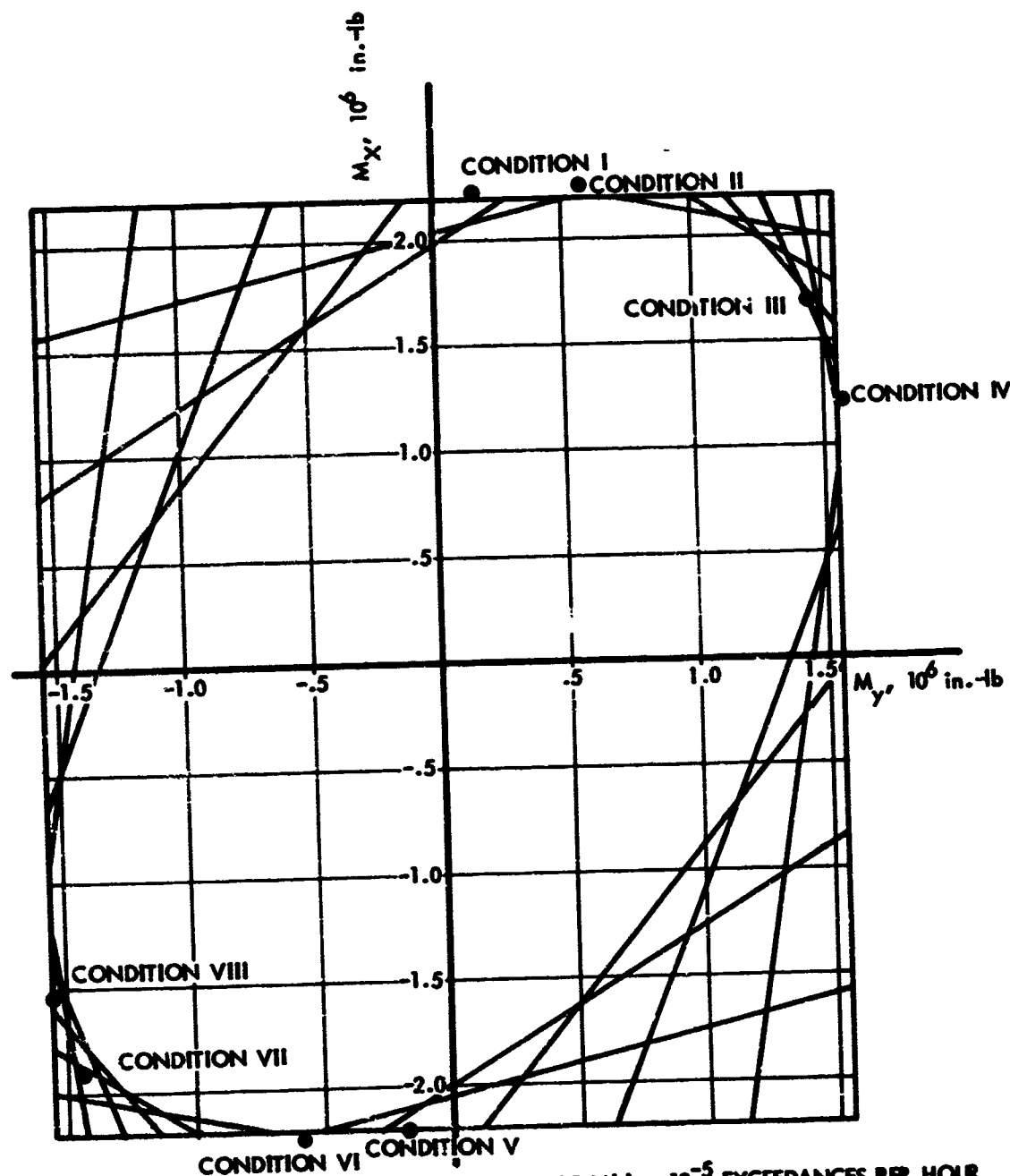
FIGURE 11-2, CONTINUED



(d) WS 346, SHEAR-TORSION
 FIGURE 11-2, CONTINUED

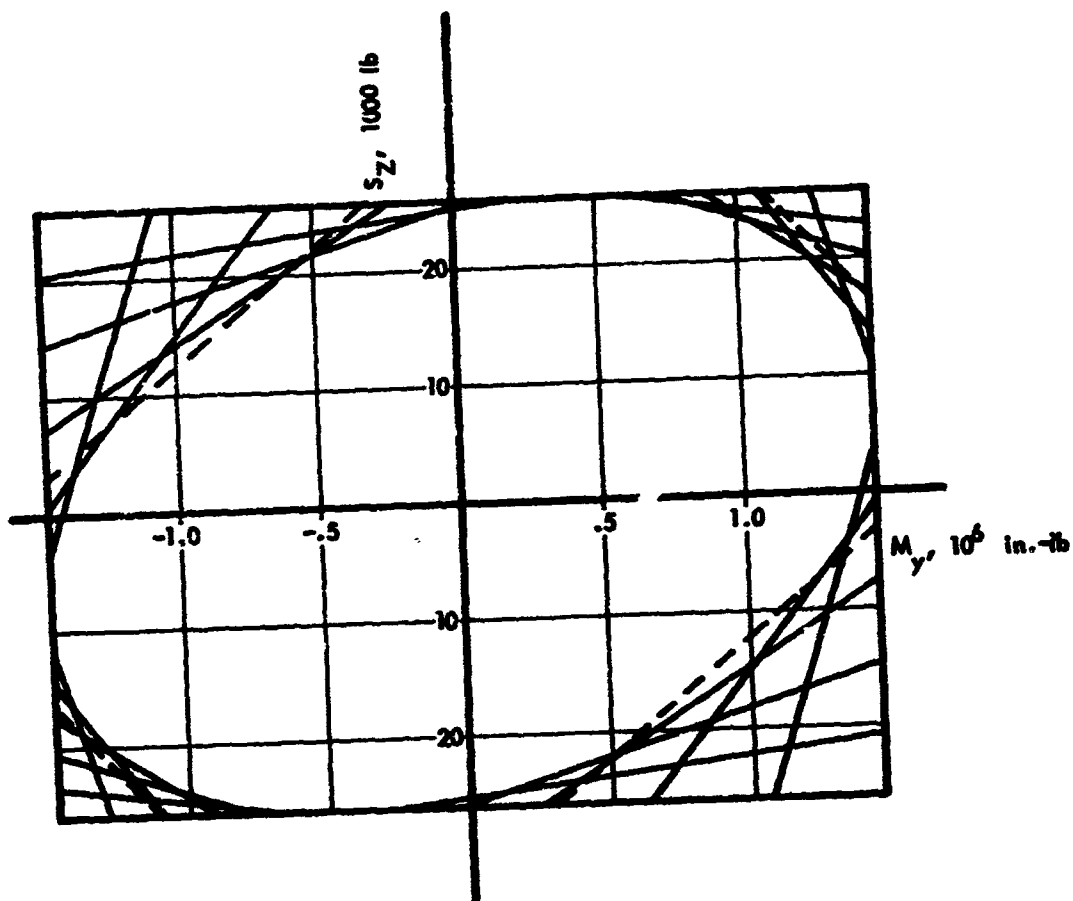


(e) WS 346, SHEAR-BENDING
 FIGURE 11-2, CONTINUED



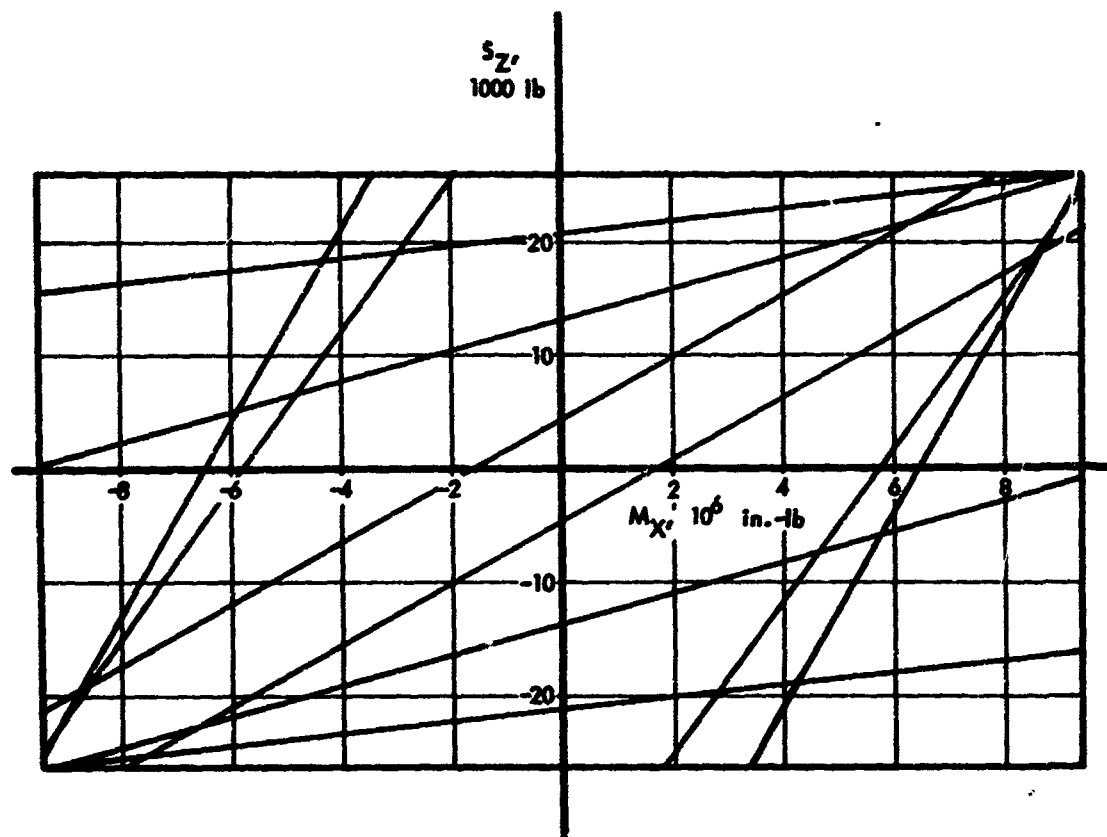
NOTE: CURVES ARE MISSION ANALYSIS CASE 202 AT $N(y) = 10^{-5}$ EXCEEDANCES PER HOUR

(f) WS 346, BENDING-TORSION
FIGURE 11-2, CONCLUDED



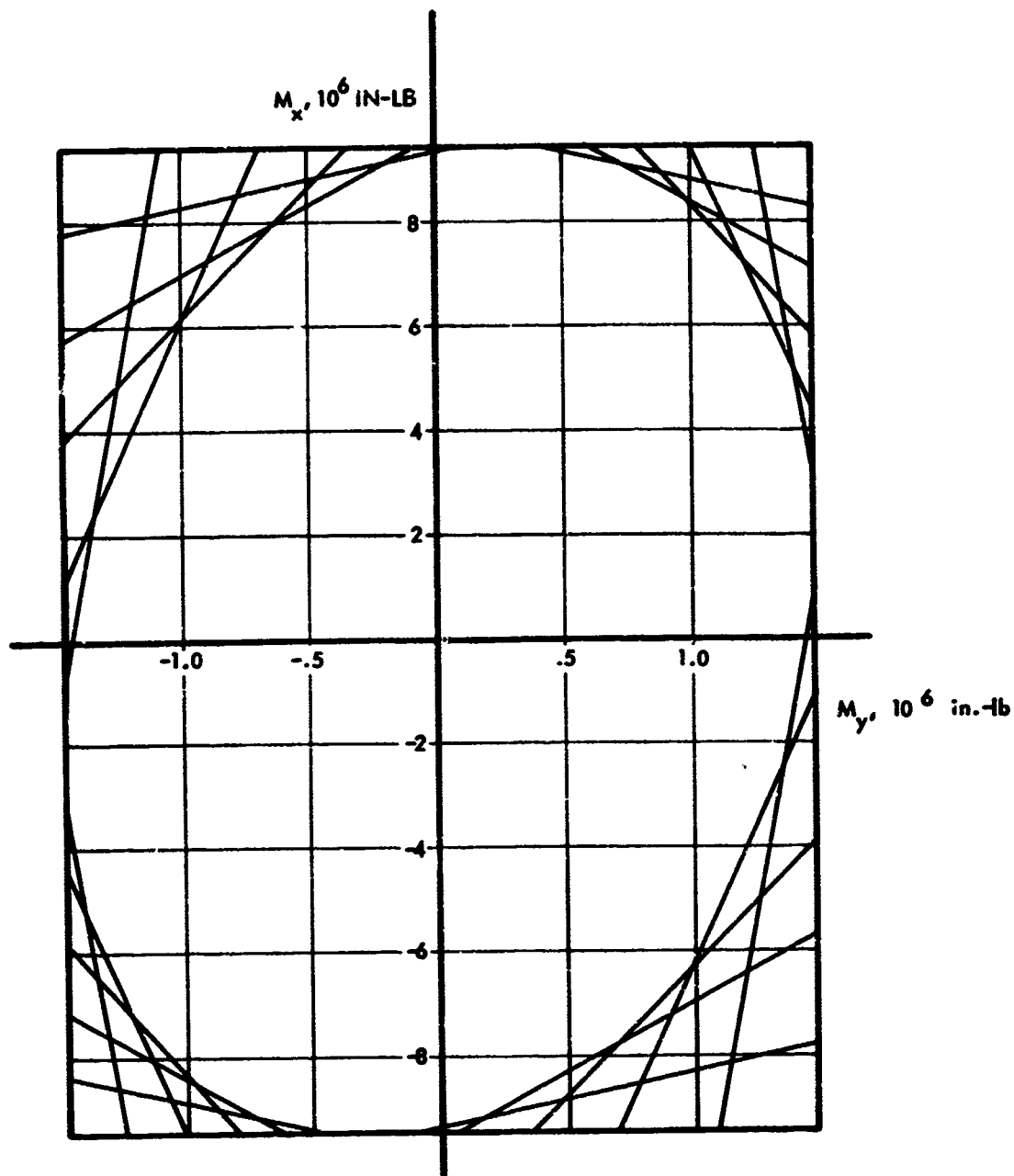
NOTE: CURVES ARE FOR MISSION ANALYSIS CASE 102 AT $N(y) = 10^{-5}$
EXCEEDANCES PER HOUR

(a) WS 103, SHEAR-TORSION
FIGURE 11-3. "EQUAL PROBABILITY" ENVELOPES, MODEL 749



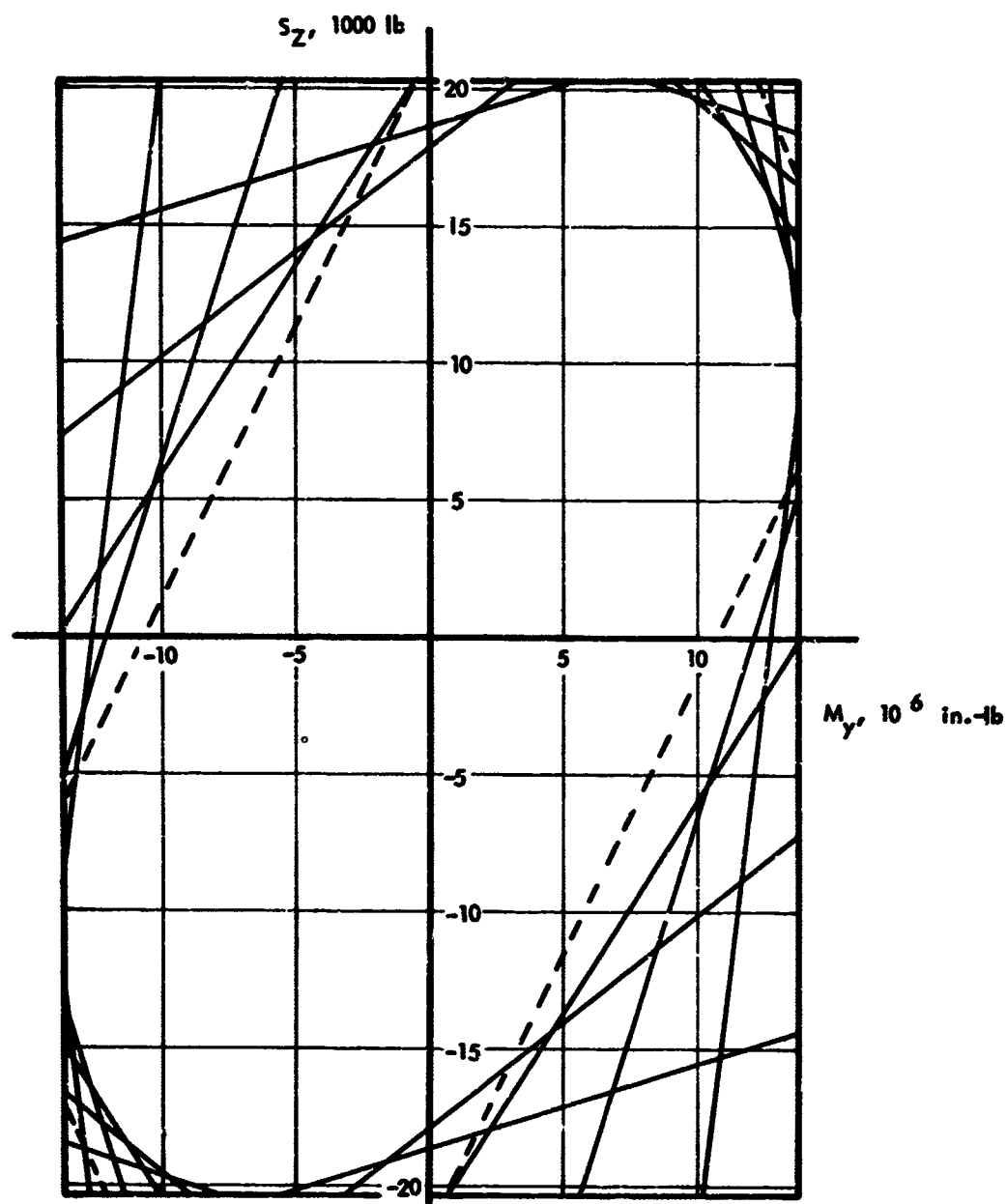
NOTE: CURVES ARE FOR MISSION ANALYSIS CASE 102 AT
 $N(y) = 10^{-5}$ EXCEEDANCES PER HOUR

(b) WS 103, SHEAR-BENDING
 FIGURE 11-3, CONTINUED



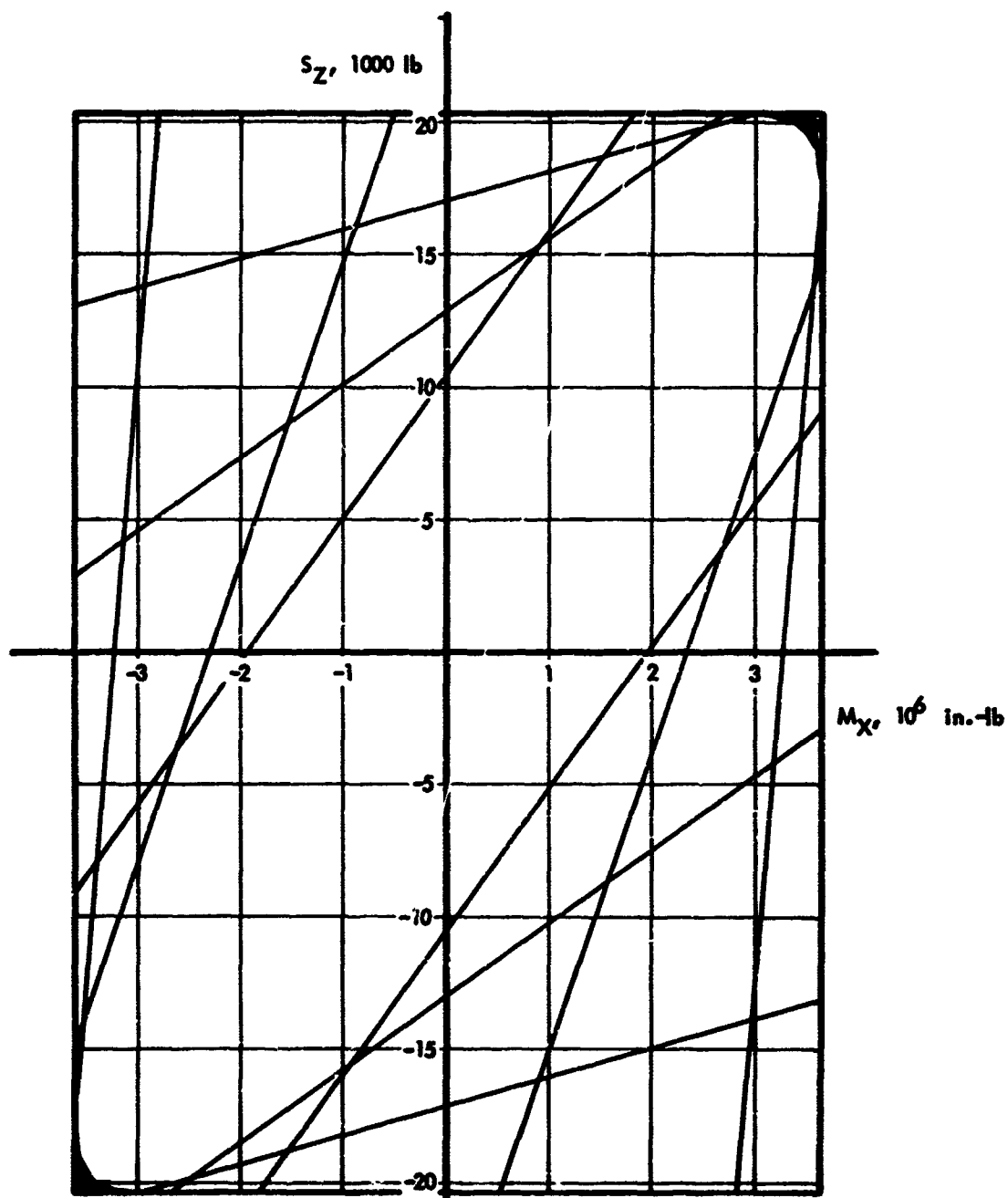
NOTE: CURVES ARE FOR MISSION ANALYSIS CASE 102 AT
 $N(y) = 10^{-5}$ EXCEEDANCES PER HOUR

(c) WS 103, BENDING-TORSION
 FIGURE 11-3, CONTINUED

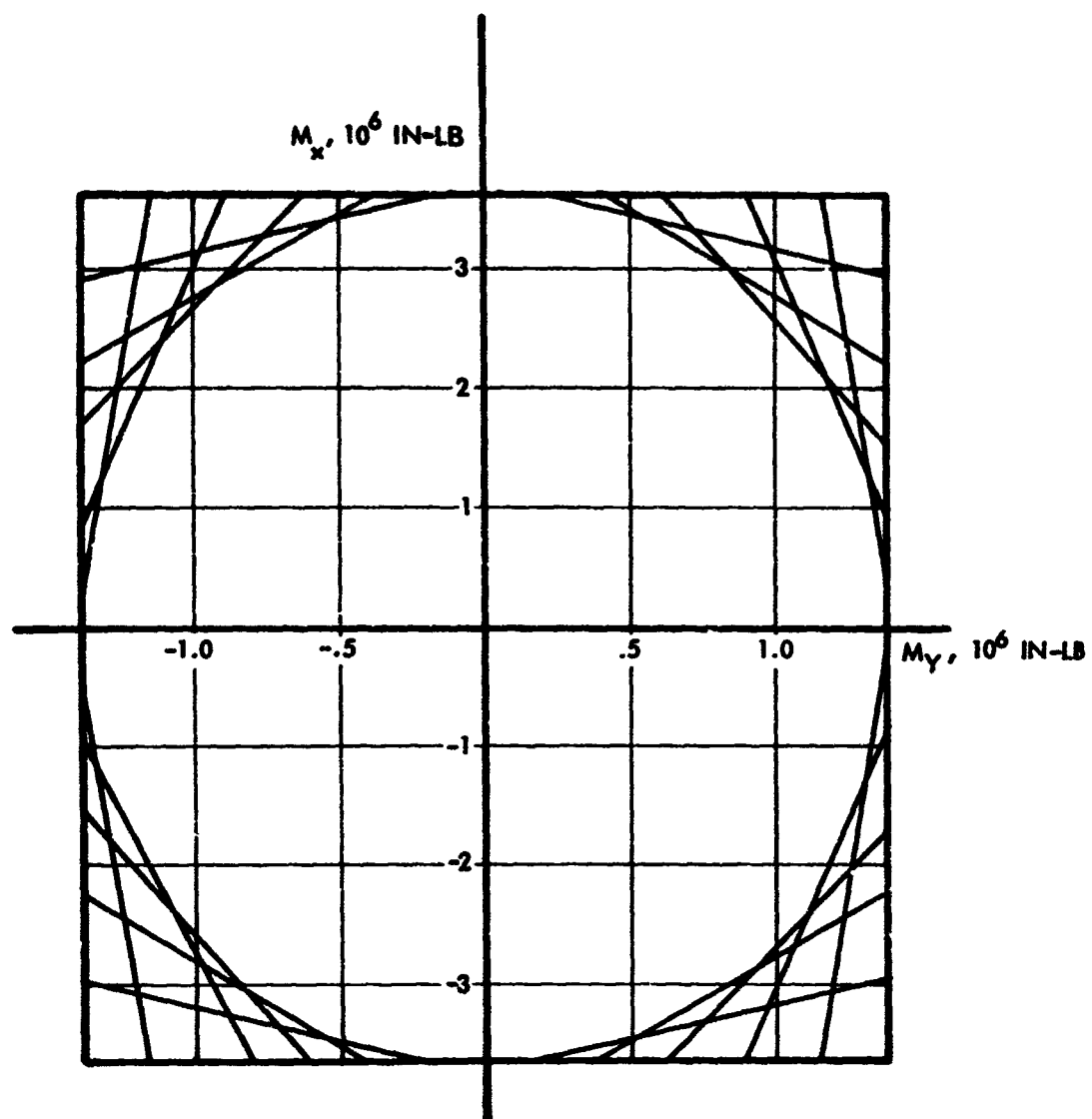


NOTE: CURVES ARE FOR MISSION ANALYSIS CASE 102 AT
 $N(y) = 10^{-5}$ EXCEEDANCES PER HOUR

(d) WS 337, SHEAR-TORSION
 FIGURE 11-3, CONTINUED



NOTE: CURVES ARE FOR MISSION ANALYSIS CASE 102 AT
 $N(y) = 10^{-5}$ EXCEEDANCES PER HOUR
 (e) WS 337, SHEAR-BENDING
 FIGURE 11-3, CONTINUED



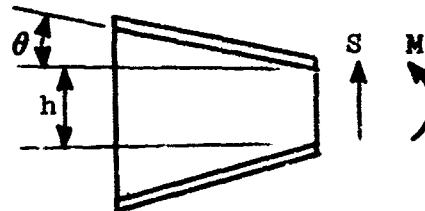
NOTE: CURVES ARE FOR MISSION ANALYSIS CASE 102 AT
 $N(y) = 10^{-5}$ EXCEEDANCES PER HOUR
 (f) WS 337, BENDING-TORSION
 FIGURE 11-3, CONCLUDED

shear flows included. In drawing the dash lines, the combinations of shear and torsion necessary to give the statistically defined shear flow are obtained on the assumption that bending moment is present equal to $(\bar{A}_M/\bar{A}_S)S$.

Reviewing the entire set of figures, the resemblance to ellipses is striking. In fact, to within the accuracy to which a graphical check can be relied upon, the figures are indeed ellipses. However, no analytical substantiation has been attempted. One might speculate that the figures are indeed true ellipses when obtained on a $\sigma_w \eta_d$ basis, but that differences in N_0 for the various elements might create a slight distortion when the figures, as here, are obtained on an $N(y)$ basis.

It should be emphasized that this technique does not depend at all on the presence of any actual structural component that might sense a linear combination of the two load quantities involved. But for the reader who might feel more comfortable if he could visualize such an element, examples can usually be invented. In the case of combined shear and bending, for example, one might consider the shear in the web of a sharply tapered I beam:

$$\begin{aligned} S_{\text{web}} &= S - 2 \frac{M}{h} \tan \theta \\ &= 1.00 S - \frac{2 \tan \theta}{h} M \end{aligned}$$



Nor does the actual shape of the allowable stress interaction curve enter into consideration. We are dealing with applied loads only, and introduce the fictitious structural element only to provide information about the applied loads.

It is of interest to note that the two-dimensional treatment illustrated in Figures 11-2 and 11-3 could be immediately extended to three dimensions. In this case, an ellipsoid would be defined by superscribing planes. The three-dimensional treatment would appear to be too cumbersome, however, for practical use.

It might also be noted, however, that the fictitious structural element approach can be applied to stresses at a point in the structure, as well as to loads. Here the fictitious structural element would be one having

various relative sensitivities to axial and shear stresses at a point, rather than to external shear, moment, and torsion. It would appear that applying the approach in this way could be very useful in those situations where the shear and bending moment are found not to be closely in phase. The technique might be used to test design conditions for proper combination of shear, moment, and torsion. Or, if desired, it could be applied in somewhat the same manner as the joint probability approach, with no attempt made to develop consistent conditions over the entire wing. In this case, the advantage would lie in a possibly closer theoretical relationship to past design philosophy, as will be brought out more fully in Section 12.

In the practical application of the fictitious structural element concept, it may be found advantageous to eliminate the actual definition of fictitious elements and the calculation of \bar{A} and N_0 values for the stresses in these elements. Instead, each "equal probability ellipse" would be generated as an equal probability density contour utilizing the correlation coefficient, ρ , between the two load or stress quantities of interest. Computation of the correlation coefficient can readily be included in the dynamic analysis, using Equation B-13 of Reference 1; the ellipse is then defined by Equations B3a and B3b of Reference 1 at a suitable constant value of the probability density. The value of probability density to be used is that which brings the ellipse tangent to the straight line representing the design value of one of the load quantities of interest.

11.3 Illustration of the Matching-Condition Technique

The use of the matching condition technique is illustrated in Appendices C and D by applying the technique to the generation of wing and fuselage loads for the Model 188.

In these illustrations, it is assumed that a very close match is desired, in order to avoid unnecessary conservatism in the resulting design loads. (In the case of the wing, since the resulting conditions are used in establishing limit and ultimate strength values of $N(y)$ and $\sigma_v \eta_d$ for the Model 188 as reference airplane, a close match is particularly necessary.) As a result, considerable care was taken to obtain a good match. The procedures followed are described and illustrated in some detail, in order to provide a useful guide to the engineer actually making such an application for the first time. The reader interested only in an over-all view of the procedures will find parts of the discussion that need not be followed thoroughly on the first reading. Section C.3, especially, would fall in this category.

12 MATCHING CONDITION AND JOINT PROBABILITY TECHNIQUES - DISCUSSION

12.1 Practical Considerations in Selecting a Design Technique

Both the matching condition and joint probability techniques have been applied in this study. The matching condition technique is illustrated by application to the Model 188 in Appendices C and D, and the joint probability technique by application to the Model 720B in Reference 1. Each has been demonstrated to be practical for design use.

In the course of making these applications, various considerations pertinent to making a choice between the two techniques in any given case have become evident. These are discussed in the following paragraphs. The considerations noted are primarily of a practical nature. From the standpoint of rationality, there is probably little to choose; and numerical results, in the nature of structural sizes required to maintain zero or positive margins of safety, will be very nearly the same for both techniques. Differences in rationality between the two techniques are important more for the purpose of assuring a consistency in application between the two and are discussed more fully in Sections 12.2 through 12.4.

First, some practical consequences of selecting the joint probability techniques will be noted.

First, this technique requires that, potentially, every minute element of structure be carried through the power-spectral analysis. Unless simple and reliable means can be devised to establish which elements are critical prior to making the analysis, the amount of computation can become prohibitive. Consequently, this technique would probably find use only in the final stages of design and analysis, and even then, care would be required to keep the amount of work within reasonable limits. Certainly where the airplane can be shown by simpler means not to be gust critical, the joint probability analysis would not be undertaken. It might be noted, incidentally, that, if the joint probability technique is to be used only in the final stages of design, a switch-over at some point will be required from a one-dimensional, or matching condition, point of view to a joint probability point of view. It would appear that some increased chance for confusion would result.

Second, when the joint probability technique is used, "design conditions", each consisting of an individual, consistent set of loads on an airplane component, are no longer defined. The concept of a design condition has long permeated the entire art of structural analysis. Inasmuch as the various design loading conditions are relatively uninfluenced by changes in the structure, it has been possible to keep the loads

determination function quite distinct from the structural design and stress analysis function. Design and optimization of the structure are thus facilitated. The usual refinements in the stress analysis methods as the design progresses are easily accommodated. And refinements in the load determination can proceed independently of those in the stress analysis. Salvage may be expedited. Thus the abandonment of the design condition philosophy could well introduce complexities into the design procedure; some of these are apparent and there may be others that will appear only as experience is gained with the new approach.

Furthermore, regardless of which technique is used for design and stress analysis, complete, consistent conditions will still be required for static and fatigue testing. Since the static test conditions must be generated eventually, it appears most expeditious to generate them in advance of the stress analysis stage. In addition, complete consistent conditions are needed for fatigue testing. While these would ordinarily be generated independently of the static test loadings, there is believed to be an advantage in developing both the repeated loads and limit design conditions according to the same general philosophy.

An interesting example of the difference in thinking required in using the joint probability technique is illustrated by Figure 12-1. This is essentially the same as Figure 10-2, except that it is redrawn in the form of contours of equal probability density. The heavy solid line shows a possible strength envelope for the particular element under consideration. If it were necessary to define a "critical" condition, one would have no hesitation in selecting, intuitively, point A. But now suppose that the structure were redesigned so as to reduce the compression allowable, resulting in the modified strength envelope shown by the heavy dash line. Neither the loading nor the allowable at the "critical" point are affected, yet the probability of exceeding the limit strength has been increased.

Turning next to the matching condition technique, it is apparent first that the generation of the enveloping conditions - although simple in concept - can easily grow to a rather sizeable task in practice, especially when a very close match to the statistically defined loads is considered necessary. The potential complexity of this approach is evident from the example presented in Appendix C.

Of more significance, application of the matching condition technique requires a considerable degree of judgment and skill - perhaps even ingenuity. And there may also be difficulty in ascertaining, for sure, when an adequate match has been achieved. A method that follows more rigorously and directly from basic principles would be more straightforward to apply and hence more acceptable for use by less-experienced personnel.

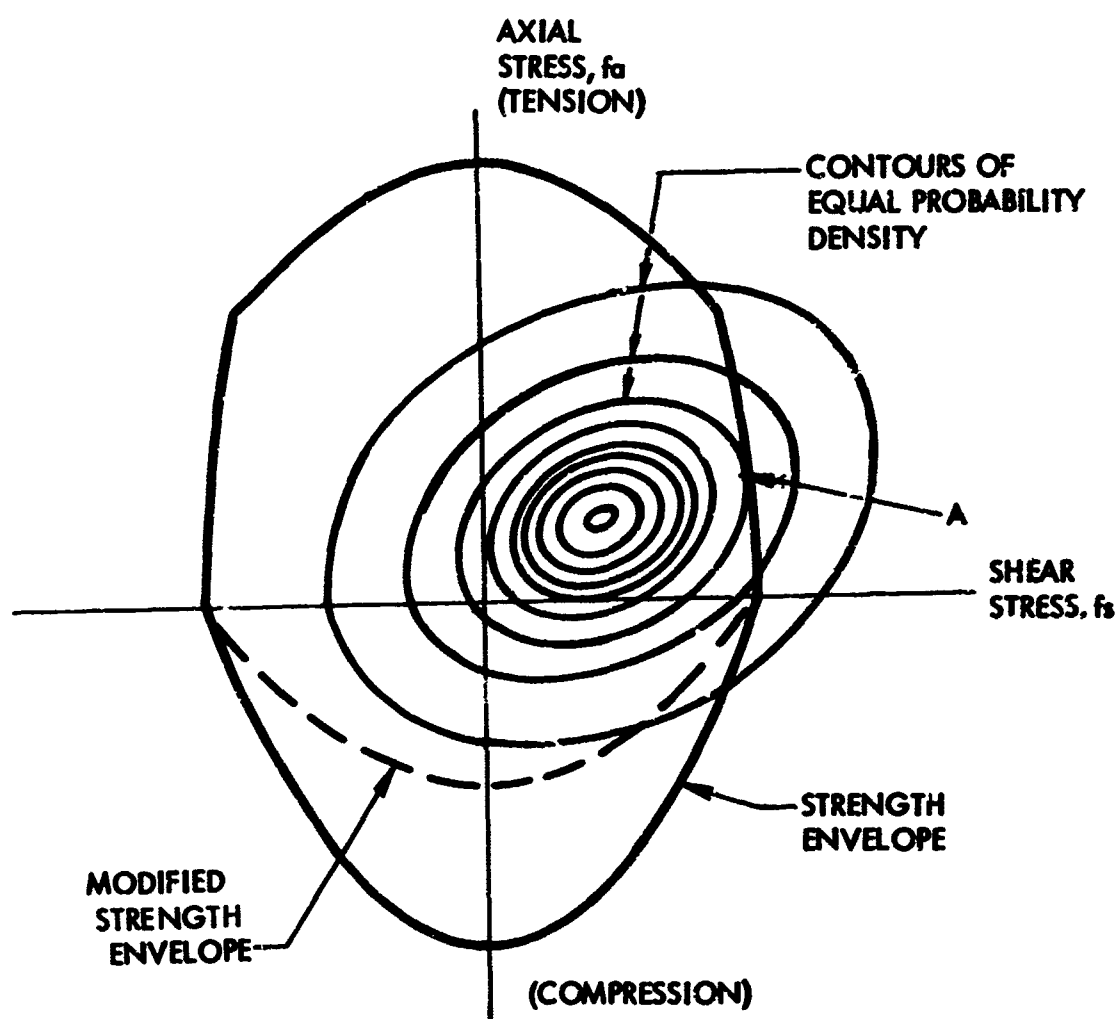


FIGURE 12-1. ILLUSTRATIVE JOINT PROBABILITY DENSITY FOR
COMBINED STRESSES - TYPICAL
STRENGTH ENVELOPE

These difficulties become particularly evident when realistic phase relations must be established considering simultaneously all three load quantities - shear, bending moment, and torsion. When appropriate simplifying assumptions can be made and substantiated - for example, that shear and bending moment are in phase - this problem does not arise. But otherwise, the approach can become extremely cumbersome. In contrast, when attention is focused on stresses at a point in the structure, the three load quantities combine to give just two stresses, axial (in the direction of the flange material) and shear.

At the same time, the generation of consistent design conditions is not believed to be prohibitively difficult. Certainly some leeway can be allowed in the precision to which the statistically defined loads are matched in the design conditions. Even without a perfect match, the loadings will be much more realistic in both level and distribution than provided by a static analysis, or even a discrete gust dynamic analysis. In fact, a vast improvement over a static gust design condition could be achieved quite handily, simply by comparing the static design condition with the statistically defined loads, adjusting the level up or down by a constant factor as indicated, and adding concentrated or distributed forces at a limited number of locations to introduce the major effects of the dynamic response. Or consider the design technique described in the introduction (pages 3 and 4), which was used successfully in a recent design substantiation. Design loads were first established by means of a discrete gust dynamic analysis. But what would have been done had the power-spectral analysis indicated a load increase to be necessary? For example, suppose an increase had been indicated in the wing torsion in the region between nacelles. Clearly, the design condition would have been "doctored up" by introducing an arbitrary pitching couple at the outboard nacelle and, if necessary, an opposite couple at the inboard nacelle. The result would have been a design condition that matched excellently the statistically defined loads. As a result, although there may remain some need for judgment in establishing just how good the match has to be, there seems to be little doubt that a satisfactory match can be obtained.

Furthermore, if there is serious doubt as to whether the enveloping conditions adequately reflect the phasing of the three load components, a limited number of fictitious structural elements can be introduced that sense appropriate combinations of all three load components. Or the fictitious elements can be introduced to define design combinations of axial and shear stress at critical locations in the structure.

12.2 Implications with Respect to Structural Design Philosophy; Rationality

In attempting to compare and evaluate the matching condition and joint probability techniques, it has been found that the two techniques will ordinarily yield numerical results that differ by some small amount. While this difference is not great enough to be significant from an airworthiness standpoint, it does give rise to the question of which technique is the more rational. In attempting to answer this question, it has become evident that the differences between the two techniques are not so much matters of rationality as of the structural design philosophy that each implies. In this section, emphasis is given first to identifying these differences in design philosophy. Some points concerning rationality are then brought out as the discussion proceeds. Background is thus provided for establishing the most consistent basis for use of the two techniques, both in comparing limit-strength levels of the Model 720B with the Model 188 and Model 749, and in new design.

12.2.1 Statistical Basis of Design Criteria. The objective of structural criteria can be regarded as the achievement of a satisfactorily low probability of exceeding design strength, either limit or ultimate, over some given period of time. This time might be an arbitrary period of operation such as one hour or 1000 hours, or one flight, or the life of one or more airplanes. In the present study, the design probability level, however it may be expressed, is to be established equal to that which has led to satisfactory safety records for currently operating transport aircraft.

It is inferred, of course, that the magnitude of structural loads to which an aircraft will be exposed can be described statistically. It is further inferred, moreover, that there is no absolute upper limit on the magnitude of loads that can be encountered. Some loads, to be sure, are inherently limited to a fairly well defined level. Braking loads, for example, are limited by the torque capacity of the brakes and by the tire-to-ground coefficient of friction. Maneuver loads are limited, at some level, by the wing or control surface forces aerodynamically attainable. But gust intensities have no known upper limit; maximum gust velocities continue to increase as more data are accumulated. Likewise, for modern transport aircraft at high speed, any aerodynamic limit on pull-up maneuver loads is at a level so far above the desired design strength as to be of no practical consequence. Similarly, there is no upper limit on the sinking speed that a pilot may inadvertently permit in a landing impact.

The concept of a "probability of exceeding design strength" is, of course, fundamental. Yet this expression is often used rather loosely, and various ambiguities arise when it is desired to interpret it exactly.

These ambiguities become particularly evident in attempting to compare the two design techniques developed herein. In the discussion that follows, some of these ambiguities will be brought to light, and the inference with respect to both design philosophy and validity of the methods will be examined.

12.2.2 The Concept of Independent Design Conditions. First, let us identify one important factor of current structural design philosophy. This is the concept that the many design conditions can be considered independently.

The probability of loss of an airplane in a given period of time - say 1000 hours - is, of course, the sum of the probabilities of its loss due to all causes.* Thus the probability of loss of the airplane is approximately the sum of its probabilities of loss due to gust, maneuver, landing impact, etc. Certainly it is this overall probability of loss to which, ideally and rationally, the airplane should be designed.

But for many years it has been universal practice to accept a rather gross approximation to this ideal; each type of loading is considered individually, and no explicit attempt is made to consider the combined probability of occurrence of several types of load. For example, without assigning actual probability values, let us assume that gust and maneuver loads criteria are based on equal probabilities of exceedance of design load. If one airplane - say Airplane A - just meets the gust requirement but has great excess strength to withstand all other types of loading, then its overall probability of loss is approximately equal to its probability of loss due to gust alone. But now consider Airplane B. It likewise just meets the gust requirement, but in addition is equally critical for maneuver. Remote as the probability of loss may be in either case, there can be no doubt that the probability is twice as great for Airplane B as for Airplane A. To limit the probability of loss of Airplane B to that of Airplane A would require that the gust criteria be increased in severity whenever the maneuver loads are also critical.

Clearly, any attempt to adjust the level of design loads for a given condition according to how critical other conditions may be would be completely unmanageable in practice. To date, therefore, no attempt

* Actually, this statement is true only approximately. More precisely, if the various probabilities are independent and are denoted p_1, p_2, \dots , then the probability that the airplane is not lost is $(1 - p_1)(1 - p_2) \dots$, and that it is lost is $1 - (1 - p_1)(1 - p_2) \dots$. This, for small values of the p 's, is approximately $p_1 + p_2 + \dots$

has been made to incorporate such a concept into structural criteria. Current criteria, however, can be regarded as approximating the objective of a fixed overall probability of exceedance; the degree of approximation depends upon how alike various airplanes are in the degree to which various conditions are equally critical.

12.2.3 Power Spectral Considerations - Idealized Airplane. Now let us consider what ramifications with respect to design philosophy may result from introducing power-spectral concepts into the gust loads determination.

First, consider the idealized case of a rigid airplane, free to plunge only, and short enough in overall length relative to the predominant gust wave length so that all points on the airplane can be assumed to encounter any given gust simultaneously. This idealized airplane does not necessarily represent any actual airplane, although it may be a fairly close approximation to airplanes of the DC-3 generation. Also, this idealization is essentially what has been assumed in determining design gust loads for many years.

For this idealized airplane, all loads are "in phase" and can be measured by a single quantity, the c.g. acceleration. As a result, no new problem of "design technique" enters. Once a design level of c.g. acceleration is established for a given airplane, based on a design probability of exceedance, all loads and stresses follow at once. The c.g. acceleration defines a total airload that is distributed in a particular way, and it also defines the inertia forces at all points in the structure. Consequently, when the c.g. acceleration reaches the value that corresponds to ultimate strength at some point in the structure, failure occurs. Only the "weakest link in the chain" is of interest. No matter how many other links may be equally weak, there will be no reduction in the c.g. acceleration at which failure will occur, nor will there be any increase in the probability that the design strength will be exceeded.

12.2.4 Power Spectral Considerations - Large, Flexible Airplane. For a large, flexible, dynamically responding airplane, however, the situation is more complex. Because of the random input and the partial independence of the responses in the many rigid and elastic modes, the stresses throughout the structure are not all in phase. The bending moment in the outer wing, the bending moment at the wing root, the load on an engine nacelle, and the loads in the fuselage forebody, for example, may all reach their maximum values at quite different times. Likewise, at any given wing station, the shear, bending moment, and torsion may reach their maximum values at different times. And even at a single

point within a given wing section, the shear and axial stresses may reach their maximum values at different times. Thus the many diverse stresses throughout the airframe, rather than following in direct proportion to the c.g. acceleration, tend to go their own individual ways. Now suppose that equal-probability design values are established for each of these many loads or stresses. Then in any given patch of turbulence - because of the random nature of the turbulence - one load, say load "A", might exceed its design value, while all others - B, C, D, etc. - remain below theirs. If at each point in the structure the strength is just equal to the design load, then the design load is certain to have been exceeded - in this case at Point A. But if sizeable positive margins are available at all points but one, there is a good chance that the one load to exceed its design level will be one for which a positive margin is available, and failure will not occur. It appears, therefore, that in the case of the large, flexible airplane the probability of loss is indeed increased as various "links in the chain" are reduced in strength to that of the weakest link. Thus it can be seen that if each point throughout the structure is designed to the same probability of exceedance of design load, the probability that some point will exceed its design load is greater than the probability that any one given point will exceed its design load.

To be sure, the various loads throughout the structure are not all entirely independent. The bending moment at wing station 105, for example, would obviously be very closely correlated with that at wing station 100. But there is enough independence amongst the various loads so that the probability of exceeding design load somewhere in the airplane is clearly greater, by some undefined amount, for the large flexible airplane than for the simple idealized airplane for which all loads are in phase.

To summarize, the safety of the airplane depends not only upon the probabilities of exceeding design load at individual points, but also on the degree of independence of the various loads and the extent of the structure for which positive margins are available as a result of other requirements.

If the pattern of existing criteria were to be followed, design would be to a number of independent conditions - such as an inner wing bending condition, a nacelle condition, perhaps a maximum axial stress condition and a maximum shear stress condition, and so on. Each condition would be established at a level corresponding to a design probability of exceedance. This, essentially, is what is done in the "matching condition" technique for utilizing statistically defined loads in stress analysis.

Such an approach lacks rationality, of course, in that it gives no explicit consideration to the overall probability of exceeding design strength. This lack of rationality, however, corresponds to the lack of rationality in designing to independent gust and maneuver conditions, which has been accepted as a practical necessity for many years.

It seems clear that no manageable way is about to be found to account explicitly for the overall probability of exceeding design load for such completely different conditions as gust and maneuver. But with the introduction of power-spectral methods, the treatment of gust loads has now become quite explicitly statistical; and it might be hoped that at least all the gust conditions could be treated jointly.

The joint probability approach provides a step in this direction. But this approach covers only two stresses at a point. To extend the technique to take account of loads and stresses at many points in the airplane would require a major advance in the state of the art which, even if accomplished, would undoubtedly lead to a much more complicated analysis.

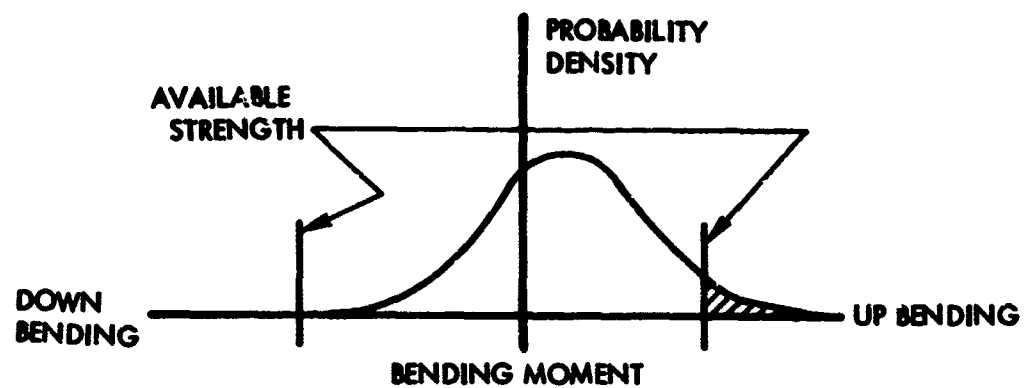
12.2.5 Upbending vs Downbending Loads. Before proceeding further, it will be worthwhile to look at one or two criteria problems that can arise even with respect to the idealized rigid airplane.

The discussion to this point has been implicitly confined to loadings due to vertical gust. Moreover, it has been implicitly assumed that only loads in the positive direction - or, in discrete-gust parlance, loads due to up gusts - are of concern. Now let us consider the problem introduced by considering both up gusts and down gusts.

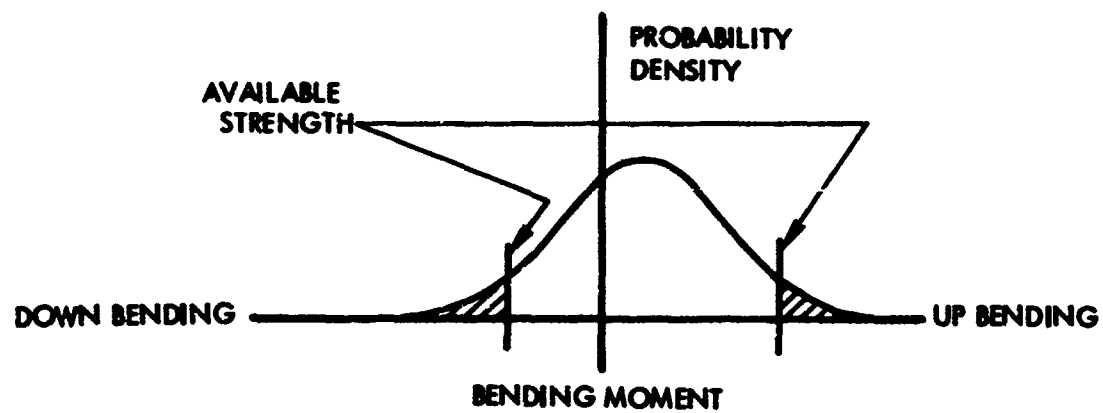
Figure 12-2 shows hypothetical probability densities of wing bending moment due to turbulence. In accordance with the definition of a probability density, the total area under each curve is unity; and the area beyond any particular value of bending moment - such as the shaded area in Figure 12-2(a) - represents the probability that the bending moment is in excess of this value. In both Figures 12-2(a) and 12-2(b) the short vertical lines denote the available strength.

Figure 12-2(a) applies to a structure which is critical in upbending but has substantial excess strength in downbending. The shaded area indicates the probability that the load is in excess of design strength.

Figure 12-2(b) applies to a structure subjected to the same loading but which has been redesigned so that the probability that design strength is exceeded is as great in downbending as in upbending. The overall probability that design strength is exceeded is clearly twice as great for the Figure 12-2(b) structure as for the Figure 12-2(a) structure.



a. UPBENDING CRITICAL



b. UPBENDING AND DOWN BENDING EQUALLY CRITICAL

FIGURE 12-2. ILLUSTRATIVE PROBABILITY DENSITY CURVES - WING BENDING MOMENT

Past structural philosophy has, of course, been to design for up and down gusts independently, disregarding the increased probability of exceeding design strength if the structure is equally critical for both conditions. As will be more apparent later, the matching condition technique inherently treats the upbending and downbending conditions independently. Thus it is consistent with the past philosophy. The joint probability technique, on the other hand, inherently treats the upbending and downbending conditions jointly, taking account of the combined probability of exceeding limit strength due to both.

There is more involved, however, than design philosophy. The question also arises of whether the probability of exceeding the design strength is really twice as great for the Figure 12-2(b) structure as for the Figure 12-2(a) structure. What is actually in question is the statistical independence of the upbending and downbending loadings. For only if these loadings are statistically independent is the overall probability equal to the sum of the two individual probabilities.

There is fairly convincing evidence that the upbending and downbending loadings, are, in fact, not independent. Consider, for example, the extreme case of a random time history of bending moment confined to a very narrow frequency band, as will result when a mode is very lightly damped. An example of such a time history is shown in Figure 12-3. In effect, each positive peak is paired with an adjacent negative peak of very nearly the same value. In the limiting case, the structure of Figure 12-2(b) is no more critical than that of Figure 12-2(a), since no point can occur in the left-hand shaded area of Figure 12-2(b) unless there has already been a point in the right-hand shaded area on the preceding half-cycle.

Furthermore, an airplane actually flies through many patches of turbulence of varying intensity. Even if in any given patch the upbending and downbending loads were independent, there would appear to be a degree of dependence introduced by the variation of intensity between patches. It would appear that the difference in maximum loads resulting from differences in turbulence intensity would be much greater than the expected difference, within any one patch, between the maximum positive and the maximum negative loads. Once the airplane encounters that most severe patch of turbulence that takes any load to its design value, it is quite likely that both positive and negative loads would exceed design somewhere in the patch.

At this point, a word of clarification is pertinent with respect to the exact meaning of a probability density plot such as shown in Figures 12-2(a) and 12-2(b). What is indicated by such a plot - in particular, by the shaded area of such a plot - is the probability that, at a randomly selected instant, the load is in excess of a given value. This is essentially the same as the expected fraction of time, over a long

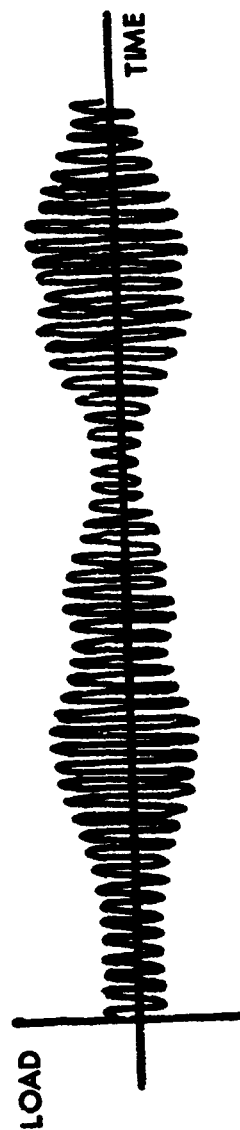


FIGURE 12-3. ILLUSTRATIVE 'NARROW BAND' RESPONSE

period, that the load is in excess of the given value. This probability is not the probability that this load level will be exceeded at some time during a given flight, or over a given number of flight hours, or even while flying through a given constant intensity patch of turbulence. Consequently, it is not the kind of probability that has the most direct significance from a structural criteria standpoint. However, it does have an indirect significance. For a constant σ_w level, two airplanes having the same Figure 12-2 type probability that a load is in excess of design will also have the same design-strength values of $N(y)/N_0$. Since N_0 tends to be fairly constant for various airplanes, as well as for various load quantities for a single airplane, the two airplanes will also have about the same frequency of exceedance of design load. Consequently they will also have the same probability that design load will be exceeded in a given number of flight hours.* Furthermore, very roughly the same percentage change in load level would result from doubling the Figure 12-2 probability and doubling $N(y)/N_0$, as can be seen by study of Table 12-1.

In the above discussion of upbending vs downbending loads, the emphasis was on the type of probability illustrated by Figure 12-2. Similar observations would result, however, if the problem were approached on a frequency of exceedance basis. Figure 12-4 shows hypothetical frequency of exceedance curves for wing bending moment due to turbulence. Clearly, if the downbending strength is exceeded as often as the upbending strength, the overall frequency of exceedance of design strength is twice as great as when a large margin of safety is present for downbending. But if downbending and upbending peaks occur in pairs, as illustrated in Figure 12-3, the probability that design strength will be exceeded is actually no greater, even though the frequency with which it will be exceeded is twice as great.

Thus, from either the probability density or frequency of exceedance point of view, it is observed that:

- (1) The overall probability that design strength will be exceeded is greater when upbending and downbending conditions are equally critical than when only one is critical, assuming that

* The probability that a load will be exceeded in a given number of flight hours, however, is not exactly equal to the average number of exceedances in the same number of hours. For an average number of exceedances, n , in a given time, t , of less than about 0.1, the probability is very nearly equal to n . But, clearly, the average number and the probability cannot be equal when the average number is greater than unity, as the probability cannot exceed unity. The exact expression for the probability is: $P = 1 - e^{-nt}$.

**TABLE 12-1. EFFECT ON LOAD MAGNITUDE OF A FACTOR OF 2
IN CUMULATIVE PROBABILITY OR FREQUENCY OF
EXCEEDANCE FOR A STATIONARY GAUSSIAN PROCESS**

y/σ	Cumulative Probability	Twice the Cumulative Probability	Resulting y/σ	Relative Decrease in y/σ
2	.0228	.0456	1.7	$.3/2.00 = .15$
3	.0013	.0026	2.8	$.2/3.00 = .067$
4	.00003	.00006	3.65	$.15/4.00 = .0375$

y/σ	$\frac{N(y)}{N_0}$	Twice $\frac{N(y)}{N_0}$	Resulting y/σ	Relative Decrease in y/σ
2	.15	.30	1.55	$.45/2.00 = .225$
3	.0111	.0222	2.75	$.25/3.00 = .083$
4	.000332	.00066	3.52	$.18/4.00 = .045$

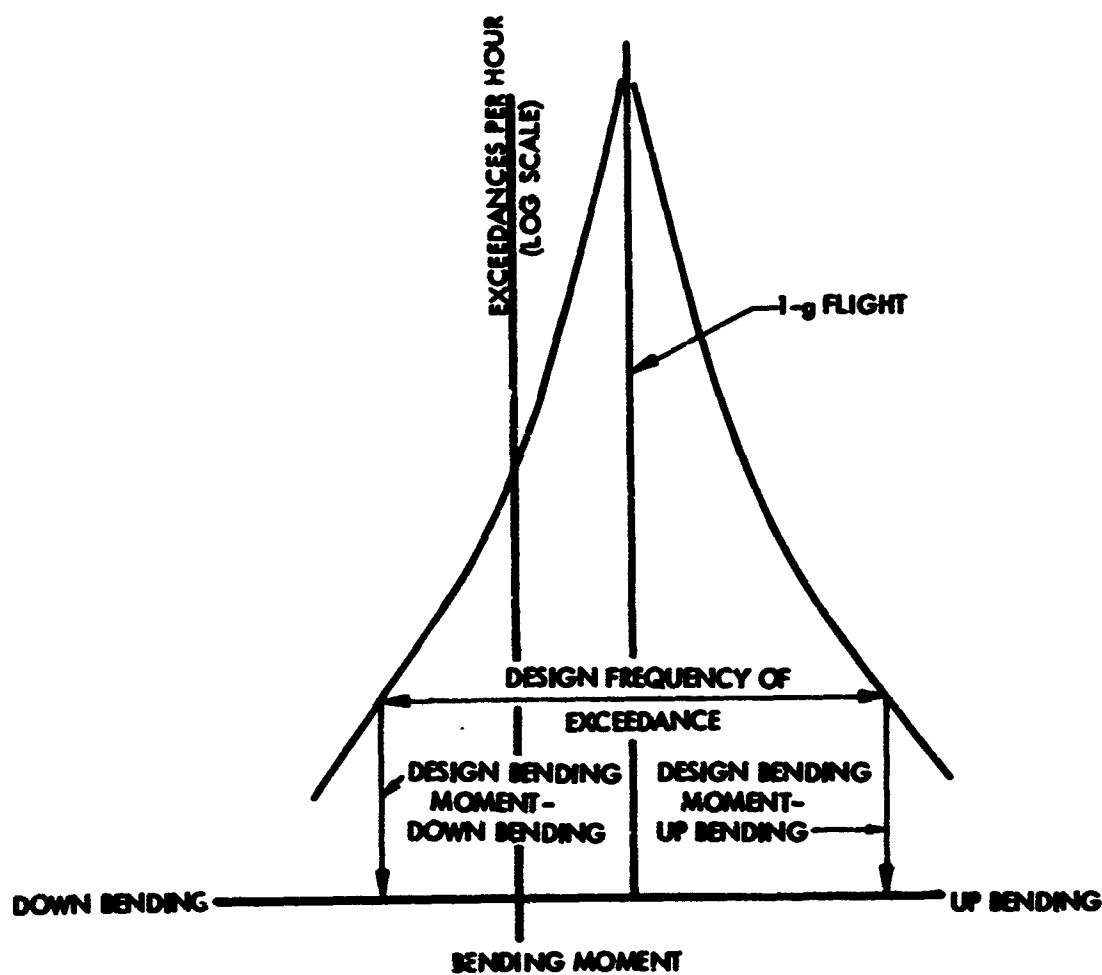


FIGURE 12-4. ILLUSTRATIVE FRZQUENCY OF EXCEEDANCE
CURVES - WIND BENDING MOMENT

each condition is established independently to the same probability level.

- (2) If, as appears probable, upbending and downbending loads are not statistically independent, the increased probability that design strength will be exceeded is less than would be indicated by the probability density or by the frequency of exceedance curve.

It would appear, however, that in most practical cases, the actual probability of exceeding design strength may lie somewhat closer to that given by the total of upbending and downbending probabilities or exceedances than by upbending or downbending alone.

12.2.6 Vertical vs Lateral Gusts. A problem similar to the up vs down gust problem, which likewise arises even with the idealized rigid airplane, involves the joint consideration of vertical and lateral gusts.

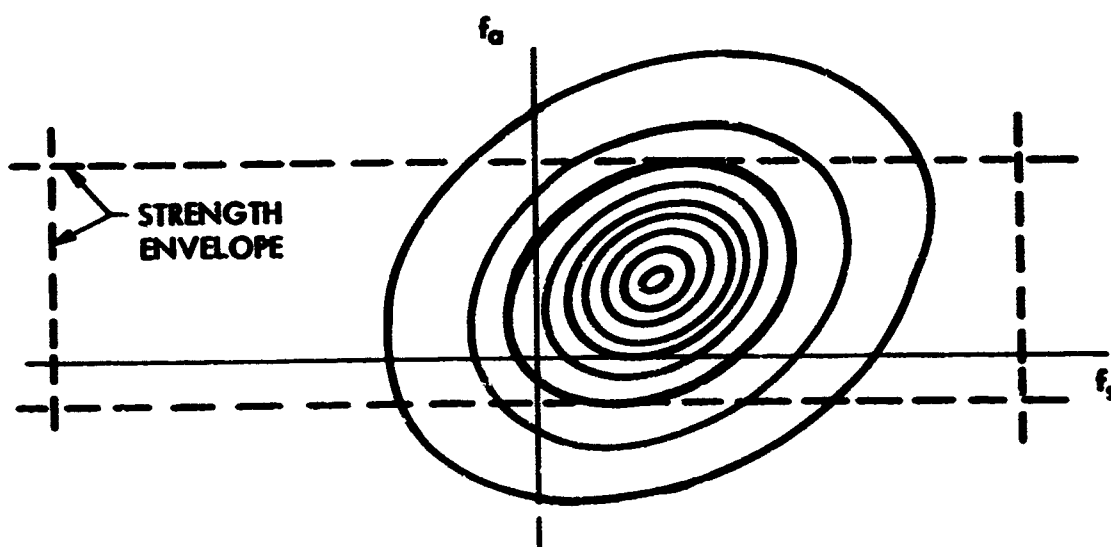
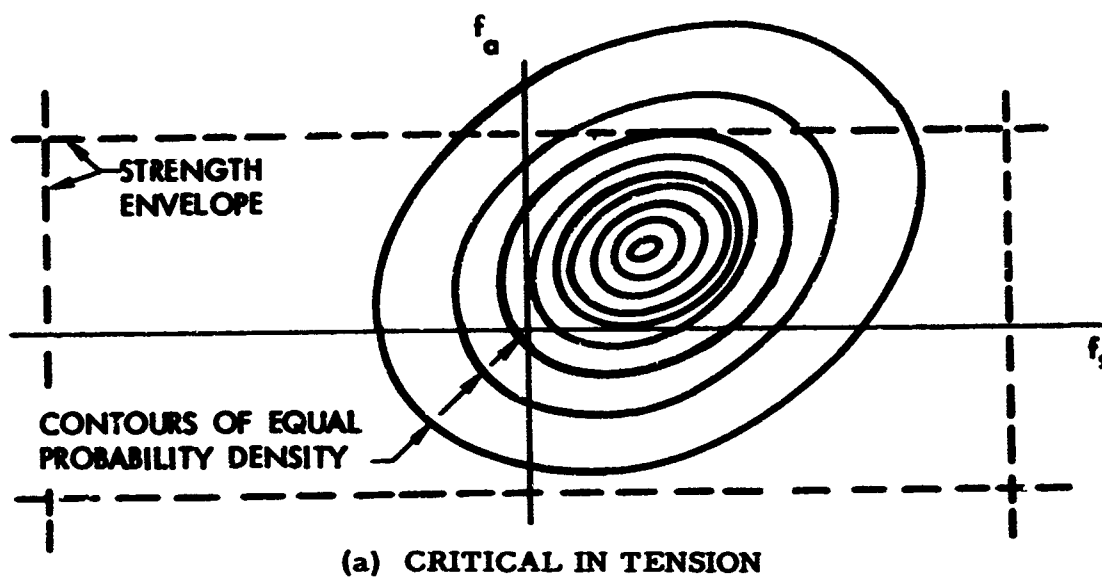
Ordinarily vertical gusts will load primarily the wing, while lateral gusts will load the vertical tail. Under existing criteria, each would be considered independently.

Within any constant-intensity patch of turbulence, the vertical and lateral components of the turbulence can be presumed to be uncorrelated. Consequently, an airplane for which zero margins are present for both lateral and vertical gust would have twice the probability of loss of an airplane critical for only one of the two conditions and having high margins in the other.

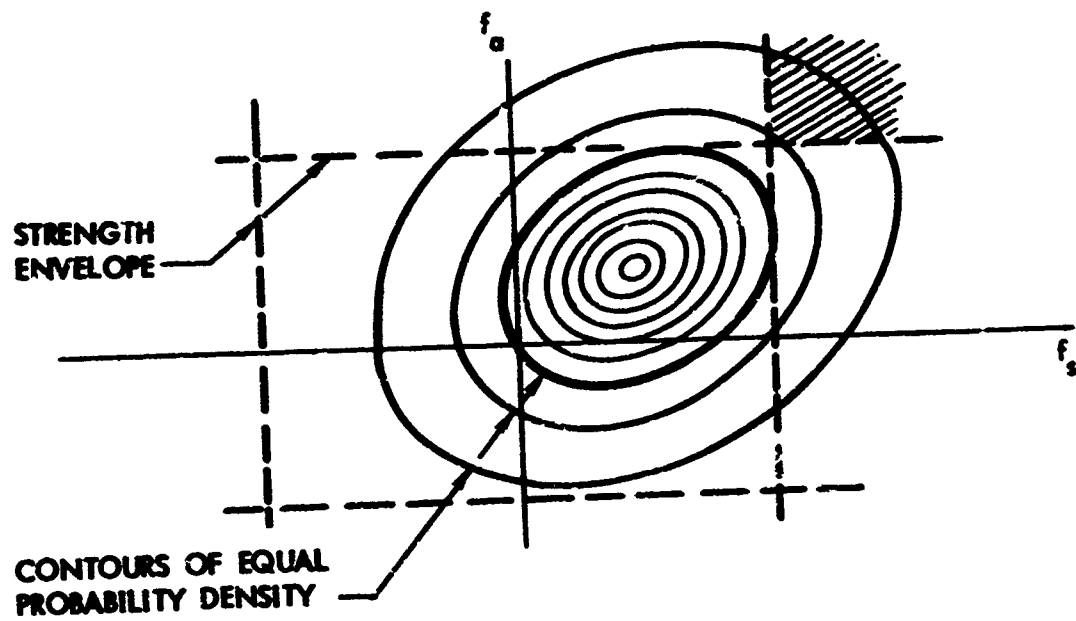
As in the up vs down-gust situation, some degree of dependency may be introduced, however, by the variation in turbulence intensity from one patch of turbulence to another.

12.2.7 Combined Stresses at a Point. In order to explore more explicitly the relation of the two techniques, several special cases involving different relations of strength envelope to joint probability density contours will now be considered.

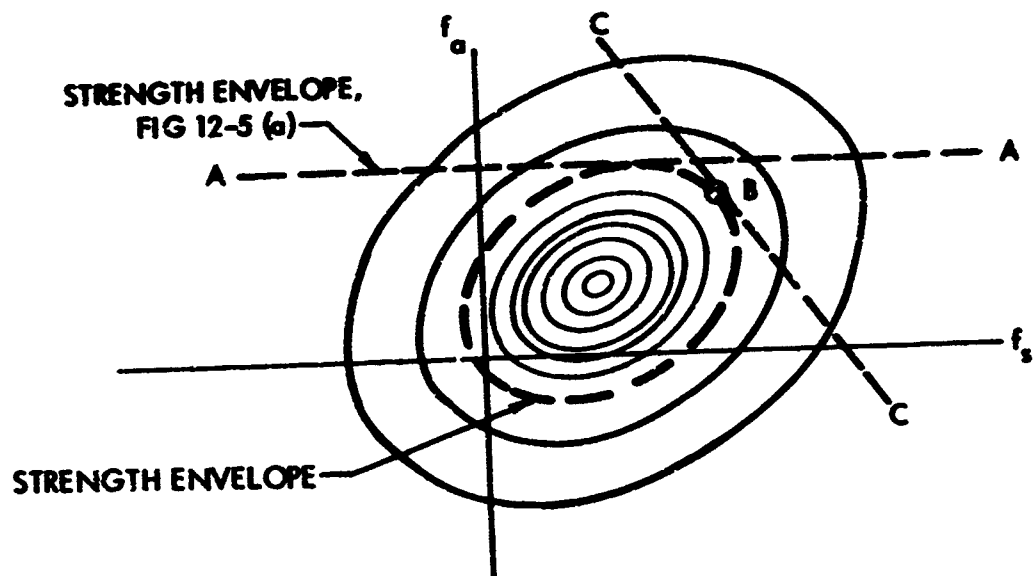
The first is shown in Figure 12-5(a). The rectangular shape of the envelope reflects the limiting case of no interaction, which would actually be approached in a pure tension field structure with closely spaced transverses, or in a truss structure with closely spaced transverses.



(c) EQUALLY CRITICAL IN TENSION AND COMPRESSION
 FIGURE 12-5. ILLUSTRATIVE JOINT PROBABILITY DENSITY
 FOR COMBINED STRESSES WITH VARIOUS
 STRENGTH ENVELOPES



(c) EQUALLY CRITICAL IN TENSION AND SHEAR



(d) EQUALLY CRITICAL IN ALL DIRECTIONS
FIGURE 12-5. CONCLUDED

It is important to note, incidentally, that, once the applied loading is described by probability density contours, and the strength characteristics by a strength envelope, it is entirely immaterial whether the actual load-carrying mechanism involves interaction or not. Thus the strength envelope in Figure 12-5(a) might be regarded as describing combined stress in a tension field panel, or individual stresses in the caps and cross braces of a truss. In the latter case, f_a could be replaced by cap load and f_s by load in a cross brace.

A second feature of the strength envelope of Figure 12-5(a) is that the structure is critical in tension only, with large excess strength available in compression and in both positive and negative shear. Clearly, in this case there was no need to consider combined stress. One could have dealt with axial stress only; and, in fact, the same probability of exceeding the design strength would have been indicated by either treatment.

Now consider Figure 12-5(b). This is the same as Figure 12-5(a), except that the compression allowable has decreased to where compression is as critical as tension. If the joint probability approach is used, the probability of exceeding design strength has doubled. (This is the same situation illustrated by Figure 12-2.) On the other hand, in this particular case, the influence of shear stress might be considered negligible and the usual one-dimensional treatment employed. The calculated probability then does not double - it remains the same as in Figure 12-5(a). Actually, because of the lack of independence of positive and negative loadings, the true probability lies somewhere between. But in any event, there can be a difference by a factor of two depending upon how the problem is treated - whether as a strictly one-dimensional situation or as the limiting case of a two-dimensional situation. Consequently, it would appear highly desirable that, when the joint probability technique is used to handle combined stresses, it also be retained for those parts of the structure subjected to a single stress only. Arbitrary decisions will thus be avoided as to which approach to use at locations in the structure where either might be justified logically but different margins of safety would result.

Next consider Figure 12-5(c). Here instead of a reduced compression allowable there is a reduced shear allowable, so that tension and shear are equally critical. Here again, if the joint probability approach is used, the probability of exceeding design strength has nearly doubled. (It has not quite doubled, because the volume shown shaded is common to both probabilities - that of exceeding design shear and that of exceeding design tension.)

Again, there is a substantial difference in the probability of exceeding design strength depending upon how one chooses to consider the problem - whether as a limiting case of combined stress or as two independent one-dimensional cases.

Here, too, there may well be a question of independence. Since positive and negative stresses appear not to be independent, it seems rather likely that axial and shear stresses may also not be independent. In fact, the example of a lightly damped system illustrated in Figure 12-3 would have a counterpart here in a situation involving a typical bending-torsion flutter mode. If such a mode were only very lightly damped, as would ordinarily occur at speeds just below the flutter speed, large motions in the mode, relative to those that could be produced by the exciting forces acting statically, would develop. These motions would involve bending and torsional motions - and stresses - differing in phase by some constant angle. In Figure 12-5(c), for example, in any one cycle the stresses would follow very closely a single equal probability-density ellipse, traveling once around the ellipse per cycle. Transfer from one ellipse to another would occur only gradually over a period of several cycles. Thus each exceedance of the strength envelope in positive shear would tend to be preceded or followed (depending upon the direction of travel around the ellipse) by an approximately equal exceedance in tension.

Finally, Figure 12-5(d) shows an extreme case for which the probability of exceeding design strength is very much greater under the joint probability than under the one-dimensional approach. The equal probability contours shown are the same as for cases (a) through (c) in the same figure. The strength envelope, however, is now assumed to coincide with one of these contours. The strength envelope assumed in Figure 12-5(a) is also shown; this is a single straight line and is denoted AA.

Even though the strength of the structure to withstand tension, compression or shear alone is no less for this case than for the cases shown in Figures 12-5(a) through (c), the probability of exceeding limit strength is much greater here than for the other cases.

At this point, certain contrasting characteristics of the joint probability and matching condition techniques, that may have been implied in the foregoing paragraphs, should be defined more clearly.

For the purpose of the present discussion, the important characteristic of the matching condition technique is not that statistically defined loads are matched by discrete design conditions - rather, it is that the quantities matched are single loads, in either actual or fictitious structural elements. The matching condition technique might perhaps better be designated - for the purpose of the present discussion - the

"single parameter" technique. The term "single parameter" refers to the fact that in determining the probability of exceeding limit strength, the applied load statistics are defined by a single parameter, σ_x , rather than by three parameters, σ_x , σ_y , and ρ_{xy} . Analogously, the "joint probability" technique might be designated the "multi-parameter" technique. Similarly, the two techniques might be referred to as the "one-dimensional" and "two-dimensional" techniques, respectively. This terminology would reflect the fact that in the matching condition technique the probability density is a function of one load quantity only, whereas in the joint probability technique the probability density is a function of two load quantities jointly.

Neither of these pairs of terms, however, is completely descriptive. In the single parameter, or matching condition technique, it is to be understood that not only is the probability of exceeding limit strength defined for single load quantities only, but also for the positive and negative directions individually. Thus, in Figure 12-5(b), even though only a single load quantity and a single statistical parameter are involved, the joint probability technique can still be used, and still indicates twice the probability of exceeding limit strength as the matching condition technique.

To emphasize further that the single parameter philosophy does not necessarily involve the generation of matching conditions, it might be noted that it can actually be applied directly to stresses at individual locations in the structure. Thus the generation of complete design conditions could be completely bypassed, if desired. In this application, the fictitious structural element concept would, of course, be used, as illustrated in Figure 12-6. Instead of contours of equal probability density, there will now be a single applied stress envelope. Each point on this envelope is considered independently in the stress analysis; clearly, most of the envelope can be disregarded as obviously non-critical.

The quantitative differences resulting from use of the multi-parameter and single parameter techniques can now be emphasized by returning to Figure 12-5.

Consider, for example, the case shown in Figure 12-5(d), and suppose that a design probability of exceedance has been selected, equal to the volume outside the line AA. Under the single parameter approach, fictitious structural elements would be utilized to generate an "equal probability" ellipse as described in Section 11.2. Line AA would be one of the family of lines generating this ellipse. The ellipse thus generated would presumably coincide with one of the contours of equal probability density - in this case, the one indicated by the dash line, which is also the strength envelope. (That the ellipses obtained in these two ways

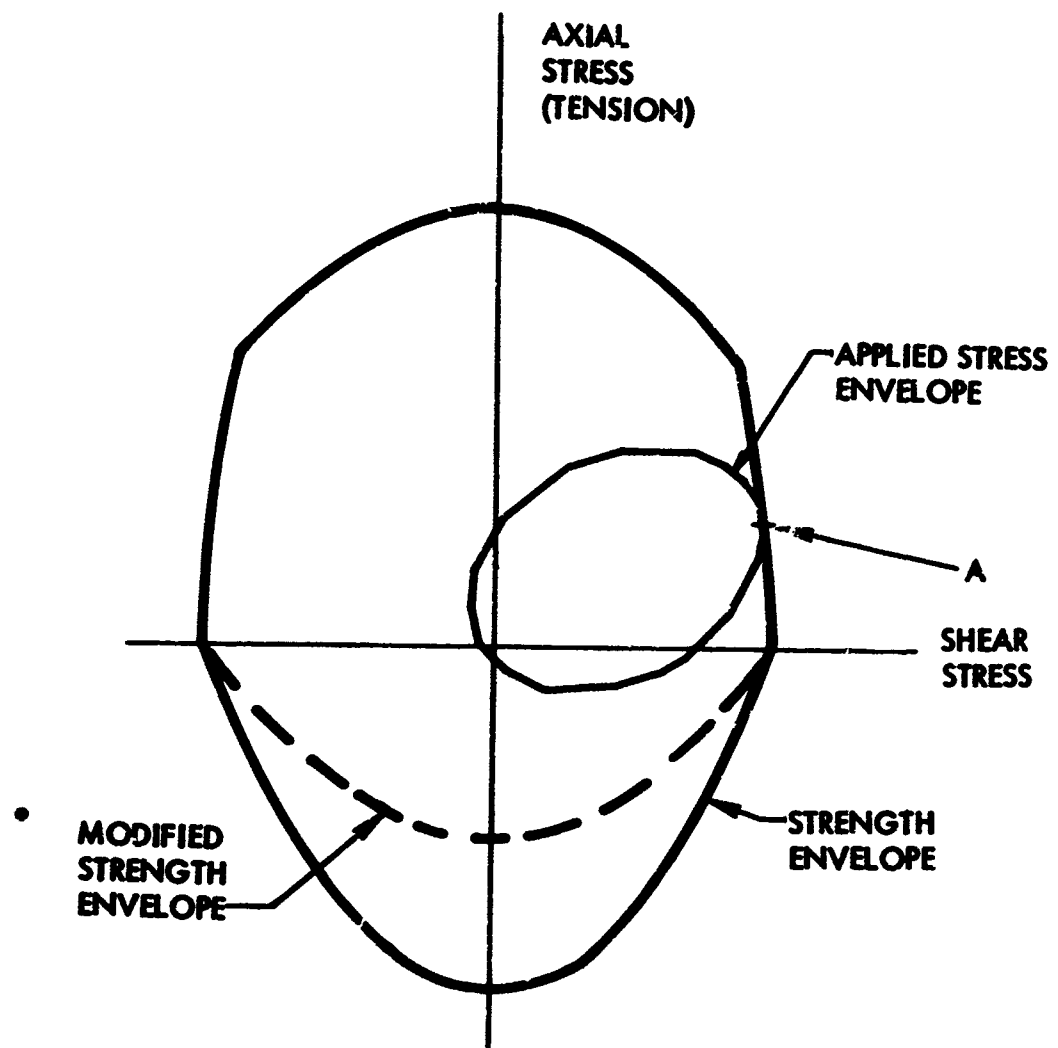


FIGURE 12-6. APPLIED STRESS ENVELOPE FOR COMBINED STRESSES

do coincide appears intuitively quite certain, although no proof has been made.) Design points would be defined at various points around this ellipse. Each point, such as B in the figure, is associated with a straight line tangent at that point (in this case CBC) representing constant stress in a particular fictitious structural element. The volumes outside all of these lines are clearly the same, as can be seen by uniformly stretching or contracting the figure in a direction such as to convert the ellipses into circles. This equality of the volumes, it would appear, would also follow from the fact that the constant-stress lines were each established initially at the same design probability of exceedance.

Each point on the design load ellipse is also, in this example, on the strength envelope. For every point, therefore, the margin of safety is zero.

The probability of exceeding limit strength, as indicated by the single parameter approach, is given by the volume outside any one of the straight lines circumscribing the ellipse.

Under the joint probability approach, on the other hand, the probability of exceeding limit strength is indicated by the volume outside the dash-line ellipse, which is very much greater.

For this limiting case, as well as for the intermediate case defined by Figure 12-5(b), the relative probabilities of exceeding limit strength given by the two approaches are indicated by the cumulative probability curves of Figure 12-7. The probability of exceeding limit strength according to the single parameter technique is given by the "Normal" curve in the figure. This is simply a plot of the expression,

$$P = 1 - \int_{-\infty}^y \hat{f}(y) dy$$

where $f(y)$ is the "normal" or "Gaussian" probability density for any load quantity, y :

$$\hat{f}(y) = \frac{1}{\sqrt{2\pi}\sigma} \exp(-y^2/2\sigma^2)$$

(In these expressions, y is considered to be the gust increment only.)

If positive and negative loading directions are equally critical, the joint probability technique accounts for both the positive and the negative tails of the probability density function. Thus for the situation

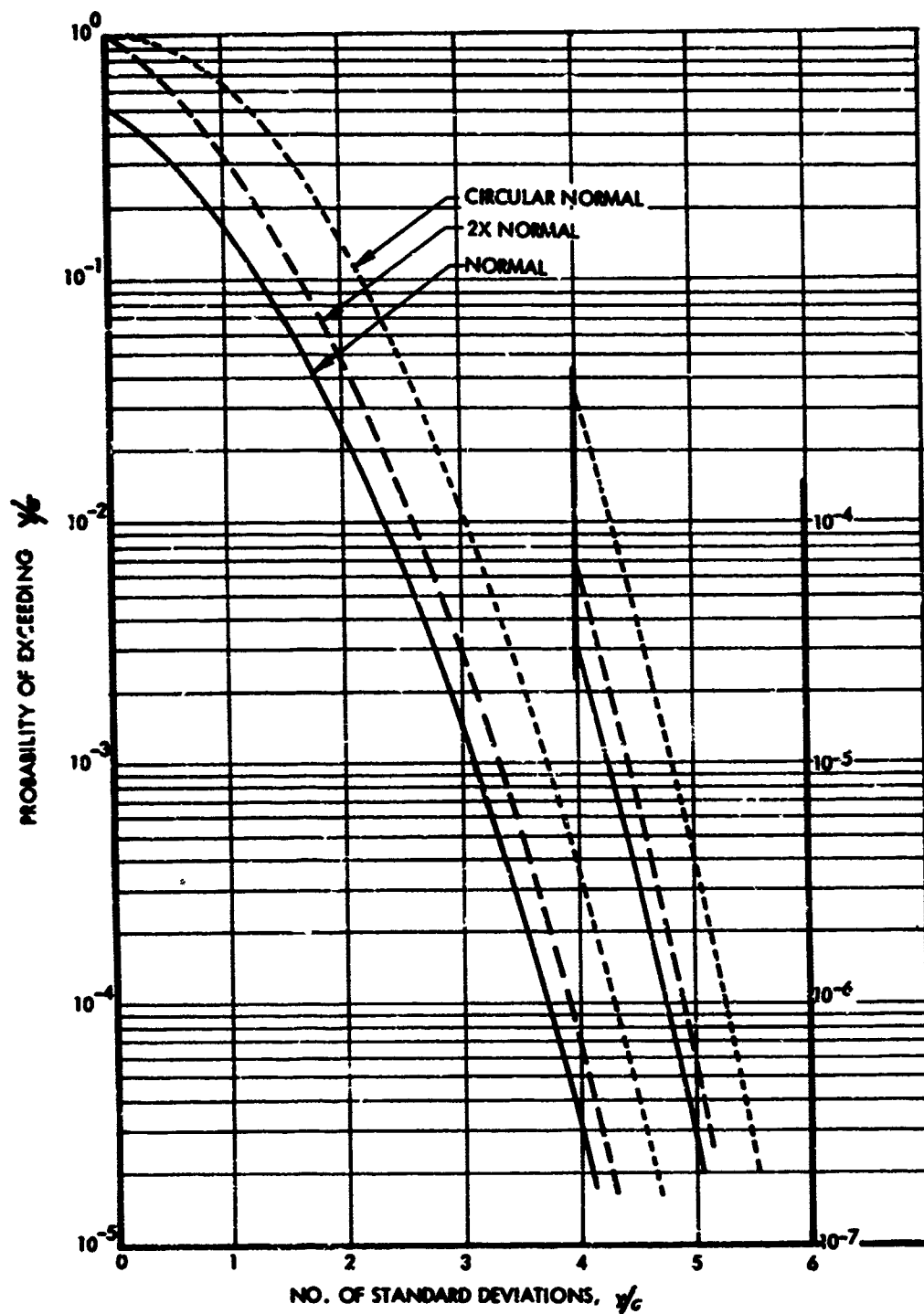


FIGURE 12-7. CUMULATIVE NORMAL PROBABILITY DISTRIBUTIONS

reflected by Figure 12-5(b) it results in a probability twice that given by the "Normal" curve. This is shown by the "2 x Normal" curve in Figure 12-7, which is the "Normal" curve shifted up by a factor of 2. It is given by the expression

$$P = 1 - \int_{-y}^y \hat{f}(y) dy$$

For the limiting case indicated by Figure 12-5(d), the "Circular Normal" curve applies. This is based on a circular two dimensional normal distribution. It denotes the volume under the probability density surface outside an equal probability density circle of radius y , as given by Equation 11.8.5 of Reference 24,

$$P = \exp(-y^2/2\sigma^2)$$

where σ is the rms value of, for example, f_a .

It can be seen from Figure 12-7 that, as the y/σ level increases, the ratio of the probabilities indicated by the "Circular Normal" and "Normal" curves increases gradually. On the other hand, the percentage difference between the two curves at a given probability level decreases. At the 3σ load level, the difference in load between "Normal" and "Circular Normal" curves is seen to be roughly 20%. The percentage difference between the "2 x Normal" and "Normal" curves also decreases as the y/σ level increases. At $y/\sigma = 3$, it is seen to be roughly 7%. Manifestly, the relation of strength envelope to applied stress indicated by Figure 12-5(d) is extreme, and ordinarily it would not be even closely approached. Consequently the difference in load level between a single parameter analysis and a multi-parameter analysis at the same probability level is generally much smaller than it would be for this extreme case.

Either technique can of course be applied to a reference airplane and a probability level corresponding to limit strength established. It is important to note, however, that application of the two techniques to a new airplane, each at its appropriate probability level as derived from the reference airplane, will in general lead to different required strengths. And the required strength may be either higher or lower for the joint probability technique than for the matching condition technique.

Suppose, for example, that the strength envelopes for the reference airplane are generally like Figure 12-5(a) and for the new airplane like Figure 12-5(d). The design probabilities derived from the reference airplane will then be the same for both techniques. But for the new

airplane, the joint probability technique will tend to show a much higher probability of exceeding limit strength, requiring greater strength to achieve the same indicated probability.

On the other hand, suppose the situation to be reversed, so that the strength envelopes for the reference airplanes are generally like Figure 12-5(d) and for the new airplane like Figure 12-5(a). The design probability will now be greater as derived from - and for use with - the joint probability technique. For the new airplane, the two techniques will tend to show equal probabilities of exceeding limit strength. But the joint probability technique will have a higher allowable probability of exceeding limit strength, so that it will actually permit less strength in the new airplane than will the matching condition technique.

It is important to keep these differences in mind when comparing results of joint probability and matching condition analyses. In particular, care must be taken in determining limit strength $\sigma_w \eta_d$ values based upon the joint probability treatment of the Model 720B, inasmuch as $\sigma_w \eta_d$ has meaning, basically, only in terms of a single-parameter analysis.

Fortunately, however, as noted earlier, the numerical differences are not likely to be large. It is believed that in practical cases the strength envelope will seldom be of such a shape, relative to the probability density contours, as to more than double the probability of exceeding limit load, relative to the situation illustrated in Figure 12-5(a). The difference in strength required for the two situations would be indicated by the difference between the "Normal" and "2 x Normal" curves in Figure 12-7. At the 3σ level, this is seen to be only 7%.

12.2.8 Summary. In attempting to evaluate and summarize the relative rationality of the two techniques, it is obvious that the single parameter technique fails to account explicitly for the reduction in safety produced by the presence of more than one "weak link in the chain." In this respect, it may provide a somewhat poorer measure of the relative safety of two airplanes than the joint probability technique. On the other hand, this deficiency is somewhat ameliorated by the following considerations:

- (a) No theory is currently available that does account explicitly for the presence of more than one "weak link in the chain", except at a single point in the structure.
- (b) This situation will continue to exist with respect to gust vs maneuver loads, where the consequences are even greater because of the unquestioned independence of the conditions.

- (c) Because of the lack of complete independence of the various stresses, and of positive and negative values of a single stress, even at a single point in the structure, it is not certain how much more realistic - if any - the joint probability treatment is than a single-load treatment as used in the matching condition technique.
- (d) To whatever extent various airplanes are similar in the degree to which various conditions are equally critical, the effect will be accounted for, at least in part, in establishing the design levels based on past satisfactory airplanes.

The matching condition technique does maintain a very convenient consistency within itself and with current structural design philosophy. It is consistent with the long standing philosophy of independent design conditions. Results are not subject to inconsistencies depending upon structural arrangement or arbitrary choice of treatment. And the common-sense one-dimensional treatment of the idealized rigid airplane falls out naturally as a special case.

The quantitative differences between the results obtained by the two techniques are small, especially when establishment of the respective design levels reflects an adequate understanding of the fundamental differences between the two approaches.

12.3 Establishment of Equivalent Design Levels

With the discussion in the previous section as background, specific consideration can now be given to how the joint probability results for the Model 720B should be used to obtain a limit-strength value of $\sigma_w \eta_0$ for comparison with the values obtained for the Model 188 and Model 749.

It is to be emphasized that no direct relation between the design levels to be used in joint probability and single parameter analyses can be established except in terms of a given location in a given airplane. What particularly characterizes a given location in a given airplane is the relation of the strength envelope to the probability density contours. Various particular relations were noted in the previous section and shown in Figures 12-5(a) through (d).

In the present analysis, the airplanes for which the relation between joint probability and single parameter design levels must be established is clearly the Model 720B, for a combination of the following reasons:

- a. It is the only one for which the joint probability analysis is available.

- b. Based on examination of the relation of the strength envelope to equal-probability-density contours on an f_a vs f_s plot, it should be possible to estimate how the 720B would come out on a single-parameter basis.
- c. There is no readily available way to estimate how the 188 or 749 would come out on a joint probability basis.
- d. To preserve a tie-in with currently used approaches, it is desirable to express the final criterion on a $\sigma_w \eta_d$ basis. This means converting the 720B results to this form, rather than converting the 188 or 749 results to a joint probability form.

One procedure that might be used to establish a limit strength $\sigma_w \eta_d$ value to associate with the results of a joint probability analysis can be outlined as follows:

- a. Pick a σ_w value arbitrarily, guided by the location of the peak of the curve of $P(MS < 0, \sigma_w) \times \hat{f}(\sigma_w)$ vs σ_w as shown, for example, in Figure 19 of Reference 1.
- b. Obtain from the joint probability analysis the probability that $(MS < 0)$ corresponding to this σ_w . For the example shown in Reference 1, this can be read from Figure 16 therein.
- c. Enter the appropriate cumulative probability curve of Figure 12-7 and read y/σ . Inasmuch as η_d is, by definition (Section 4.2), the limit design value of y/σ , the value of y/σ thus obtained is η_d .
- d. The product of σ_w from Step (a) and η_d from Step (c) gives $\sigma_w \eta_d$.

This procedure is not exactly the same as used in Reference 1. It is basically similar, however, and appears to give almost identical results. It may be just as good a procedure, all-in-all, and, for the purpose of understanding the relation of single parameter to multi parameter design levels, it has the advantage of simplicity.

In using this procedure, the one operation that is not clearly defined is the selection of the appropriate curve in Figure 12-7 to use in Step (c).

After an η_d has been determined, its sole use will be in a single-parameter analysis to give a design value of f_a or of some other single stress, perhaps in a fictitious structural element. And positive and negative values of the stress will inherently be treated independently.

Consequently, η_d must be selected so as to give the right limit-strength value of this stress. More specifically, when used in a single-parameter analysis of the airplane from which it is derived, it must yield a value of stress in the critical structural element equal to the actual limit strength of that element.

For example, suppose that a design σ_w has been selected (Step (a) above), and that for the critical location in the structure the joint probability analysis gives $P(MS < 0) = .001$.

Now suppose further that the structure for which the joint probability analysis was conducted has the characteristic indicated by Figure 12-5(a). In this case, the probability of exceeding limit strength is governed by stress in a single member that feels only tensile stress, f_a . The relation of stress to probability for this member is given by the "Normal" curve in Figure 12-7; and this curve duplicates exactly the probability that would be given by a joint probability analysis for various limit-strength values of f_a . Consequently, η_d is the y/σ value read from this particular curve at $P = .001$. With this value of η_d , and a value of σ_w as assumed in the joint probability analysis, the strength is indeed such that the joint probability analysis gives $P = .001$.

If, instead, the structure has the characteristic indicated by Figure 12-5(b), then to give the same $P(MS < 0)$ the strength-envelope value of stress must have been higher, since the total area under the f_a probability density curve beyond the limit strength value must be no greater now for both positive and negative tails than for the positive tail only in the Figure 12-5(a) case. In other words, the horizontal dash lines in Figure 12-5(b) must be slightly farther apart than shown, to keep $P(MS < 0)$ equal to .001. Use of the "2 x Normal" curve in Figure 12-7 results in the higher η_d value required to give this higher stress. It is clearly this higher stress that would have had to be designed to in the single parameter approach in order to provide the strength that was actually present and resulted in $P = .001$ in the joint probability analysis.

If the structure has the characteristic indicated by Figure 12-5(d), then the stress f_a must have been higher still, for the same reason. The "Circular Normal" curve would give the correct single-parameter allowable stress in this case.

Thus it is seen that for the purpose of obtaining limit strength $\sigma_w \eta_d$ values for the Model 70B airplane, the choice of an appropriate curve in Figure 12-7 depends only on the relation of applied stresses (as described by equal probability density contours) to the strength envelope for the critical elements of that airplane.

The same concept and even the same specific conclusions apply if the determination of limit-strength $\sigma_w \eta_d$ is based not on a single σ_w but instead, as in Reference 1, on what might be thought of as a weighted average σ_w , with the weighting in accordance with $\hat{f}(\sigma_w)$.

The procedure used in Reference 1 is an approximation to a more fundamental one that can be outlined as follows:

- (a) Considering the fractions of flight time at various σ_w levels (as defined by the b and P values established in Section 5), obtain an over-all, or weighted-average, probability that the margin of safety is less than zero, based on the joint probability analysis:

$$P(MS < 0) = \int_0^{\infty} P[MS < 0, \sigma_w] \hat{f}(\sigma_w) d\sigma_w$$

where the expression in brackets is to be read "probability that $MS < 0$ for a given σ_w ." That this equation gives the over-all probability is evident if $P(MS < 0)$ is thought of as a fraction of time that $MS < 0$. This fraction of time is the sum of the fractions of total time that $MS < 0$ within the various σ_w bands. For each band, the fraction of the total time spent in the band is $\hat{f}(\sigma_w) d\sigma_w$. The fraction of total time for which $MS < 0$ in the band is then $P(MS < 0, \sigma_w) \times \hat{f}(\sigma_w) d\sigma_w$. The total probability that $MS < 0$, for all bands, is obtained by summing over σ_w .

- (b) Similarly, obtain the over-all probability that a single generalized load quantity, y/\bar{A} , exceeds each of a series of values of $(y/\bar{A})_i$, which might be considered as potential limit-strength values:

$$P[y/\bar{A} > (y/\bar{A})_i] = \int_0^{\infty} P[y/\bar{A} > (y/\bar{A})_i, \sigma_w] \times \hat{f}(\sigma_w) d\sigma_w$$

- (c) Plot $P[y/\bar{A} > (y/\bar{A})_i]$ vs $(y/\bar{A})_i$, as given by Step (b).
 (d) From the curve thus obtained, enter with the probability obtained in Step (a) and read $(y/\bar{A})_i$. This is $\sigma_w \eta_d$.

In Step (b) above, the quantity $P[y/\bar{A} > (y/\bar{A})_i, \sigma_w]$ is evaluated in Reference 1 by means of Equation 12 therein, which can be written in generalized form as:

$$P \left[\frac{y/\bar{A}}{\sigma_w} > \frac{(y/\bar{A})_i}{\sigma_w} \right] = 2 \int_{\frac{(y/\bar{A})_i}{\sigma_w}}^{\infty} \frac{1}{\sqrt{2\pi}} \exp \left[-\frac{1}{2} \left(\frac{y/\bar{A}}{\sigma_w} \right)^2 \right] d \left(\frac{y/\bar{A}}{\sigma_w} \right) \quad (13-1)$$

Once the integration indicated on the right hand side of this equation has been carried out, various values are assigned to σ_w ; $P [y/\bar{A} > y/\bar{A}_i, \sigma_w]$ can then be plotted vs $(y/\bar{A})_i$ for various values of σ_w ; or, as in Figure 17 of Reference 1, vs σ_w for various $(y/\bar{A})_i$ values.

The integrand in Equation 13-1 is simply the normal probability density, and the factor 2 accounts for both positive and negative tails of the probability density in the cumulative probability. Thus it is seen that, in Reference 1, the "2 x Normal" curve in Figure 12-7 was, in effect, assumed. The selection of the appropriate cumulative probability curve in Figure 12-7 is thus required in this step; the same type of choice must be made as in Step (c) of the first procedure, with the three curves of Figure 12-7 providing examples that can be used.

The selection of the "2 x Normal" curve in Reference 1 implicitly assumes a relationship between the strength envelope and the probability density contours equivalent to that of Figure 12-5(b). An "equivalent" relation, in this context, would be any for which the volume outside the strength envelope is the same as that in Figure 12-5(b); Figure 12-5(c), for example, would be very nearly equivalent.

If the "Normal" curve had been used instead, values of η_d , and hence of $\sigma_w \eta_d$, would have been about 5% lower. This percentage follows from a comparison of y/σ values from the "Normal" and "2 x Normal" curves at a y/σ level of 3.5.

It is of interest to note the range of η_d values inferred from the results given in Reference 1. For each case in Table 12 therein, the σ_w value corresponding to the peak of the curve in Figures 75 through 78 was read. This divided into the $\sigma_w \eta_d$ value listed in the Table gave the corresponding η_d . The values ranged generally from 2.8 to 4.2, with the majority falling in the range 3.0 to 3.7.

Limit strength values of $\sigma_w \eta_d$ listed in Reference 1, for the critical locations in the Model 720B, are as follows:

Wing	$\sigma_w \eta_d = 111$ at 22000 ft.
Body and Tail, Vertical Gust (aftbody critical)	$\sigma_w \eta_d = 175$ at 22000 ft.

Body and Tail, Lateral Gust
(tail critical)

Yaw damper off $\sigma_w \eta_d = 99$ at 23000 ft.

Yaw damper on $\sigma_w \eta_d = 137$ at 23000 ft.

Care must also be taken in relating limit strength $N(y)$ values as given by joint probability and single-parameter analyses. Clearly there will be more crossings per hour of a two dimensional strength envelope than of limit strength in any single member. Consequently, for any given airplane, the limit strength $N(y)$ on a joint probability basis will be higher than on a single-parameter basis. It would appear that if the "2 x Normal" curve in Figure 12-7 is considered appropriate in establishing $\sigma_w \eta_d$ values to associate with the joint probability analysis, then the equivalent single-parameter $N(y)$ values should be approximately 1/2 the joint probability values. Consequently $N(y)$ values obtained for the Model 720B by means of the joint probability analysis should be multiplied by 1/2 for comparison with Model 188 and Model 749. Critical limit strength values for the Model 720B, on a single parameter basis, are therefore as follows:

Wing	$N(v) = 1/2 (2.3 \times 10^{-5})$ $= 1.1 \times 10^{-5}$ cycles per hour
Body and tail, vertical gust (aftbody critical)	$N(y) = 1/2 (2.0 \times 10^{-9})$ $= 1.0 \times 10^{-9}$ cycles per hour
Body and tail, lateral gust	
Yaw damper off (tail critical)	$N(y) = 1/2 (8 \times 10^{-6})$ $= 4 \times 10^{-6}$ cycles per hour
Yaw damper on (aftbody critical)	$N(y) = 1/2 (2.4 \times 10^{-8})$ $= 1.2 \times 10^{-8}$ cycles per hour

12.4 Comparative Application of the Two Techniques to the Model 720B

To provide a further numerical check of the effect of the choice of design technique on numerical results, the matching condition technique was applied to the Model 720B at one location, namely wing eta station .33. This analysis was for design envelope Case 27; this case was selected and the work performed before it was found that Case 24c was somewhat more critical.

"Equal probability" ellipses relating torsion and shear, shear and bending moment, and torsion and bending moment were obtained using the fictitious structural element concept as described in Section 11.2. These are shown in Figure 12-8. Inasmuch as the analysis was for a design envelope case, all of the constant stress lines were for a given value of $\sigma_w \eta_d$. This value was taken as 108.3, the limit-strength value obtained for this case based upon consideration of bending moments alone.

The joint probability analysis indicated that Element No. 9 (See Figure 68 of Reference 1) was critical for this case. The torsion-bending interaction (Figure 12-8(c)) was considered most indicative of the wing strength. As a result, a torsion-bending limit-strength envelope was determined; this was based upon stresses in Element No. 9, assuming shear to be in phase with bending moment.

It is seen from Figure 12-8(c) that the limit-strength value of $\sigma_w \eta_d$ is somewhat greater than the assumed value of 108.3. The value that brings the ellipse tangent to the strength envelope is found to be 114.

Limit strength values of $\sigma_w \eta_d$ based on Case 27 at wing eta station .33 can be summarized as follows:

<u>Basis</u>	<u>$\sigma_w \eta_d$</u>
Bending moment alone (typical shear and torsion included)	108.3
Single-parameter treatment using fictitious structural elements, Figure 12-8(c)	114
Joint probability treatment, Table 12 of Reference 1, "2 x Normal" curve of Figure 12-7 assumed	118.4
Joint probability treatment, adjusted to basis of "Normal" curve of Figure 12-7	112

The last value is obtained by ratioing according to the y/σ values given by the "Normal" and "2 x Normal" curves of Figure 12-7 at $P = .0005$.

It is seen that the joint probability value of 118.4 differs from the single-parameter (i.e., matching condition) value of 114 by less than 4%. If the joint probability value had been based upon the "Normal curve" in Figure 12-7, it is seen that the difference would have been less than 2%.

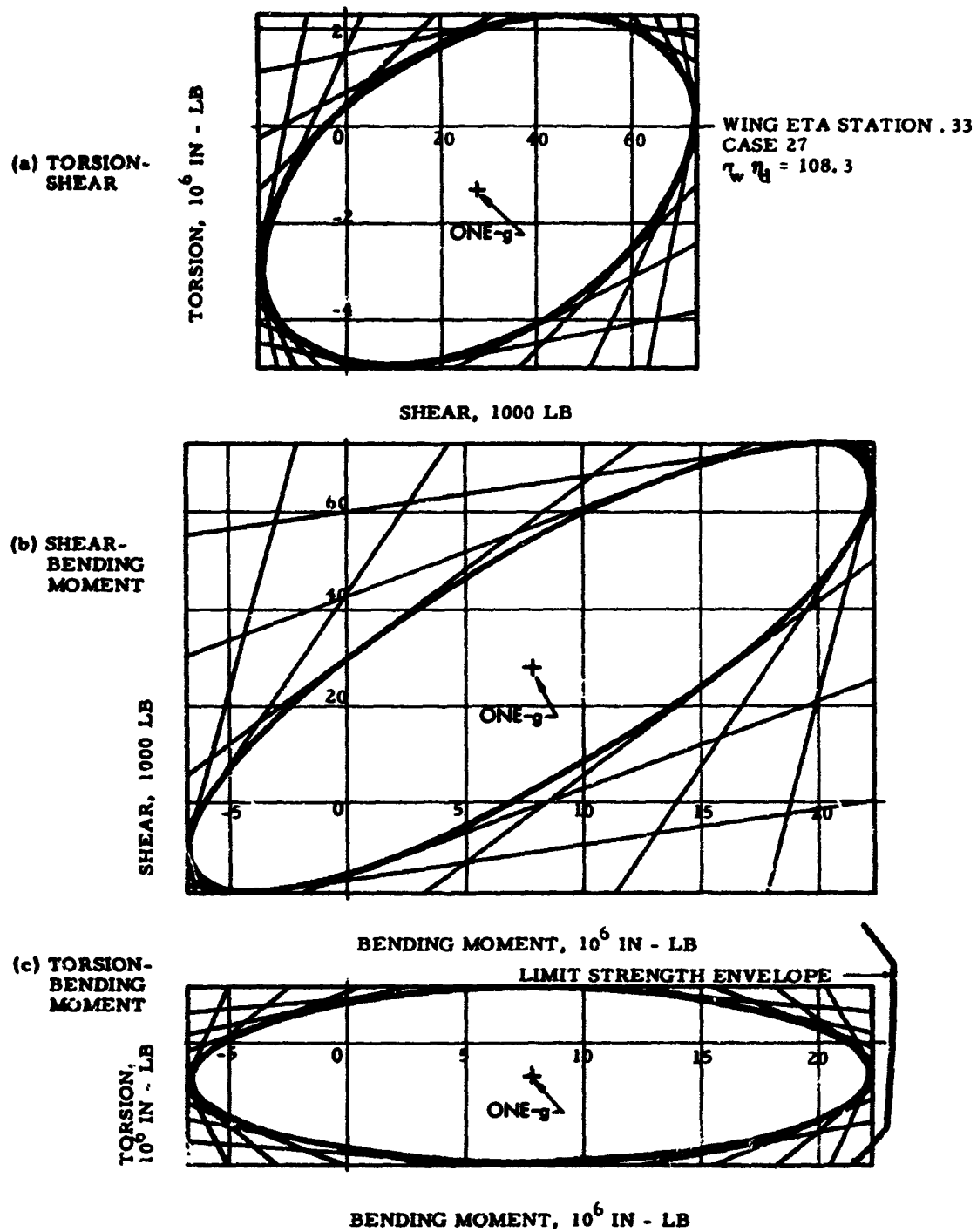
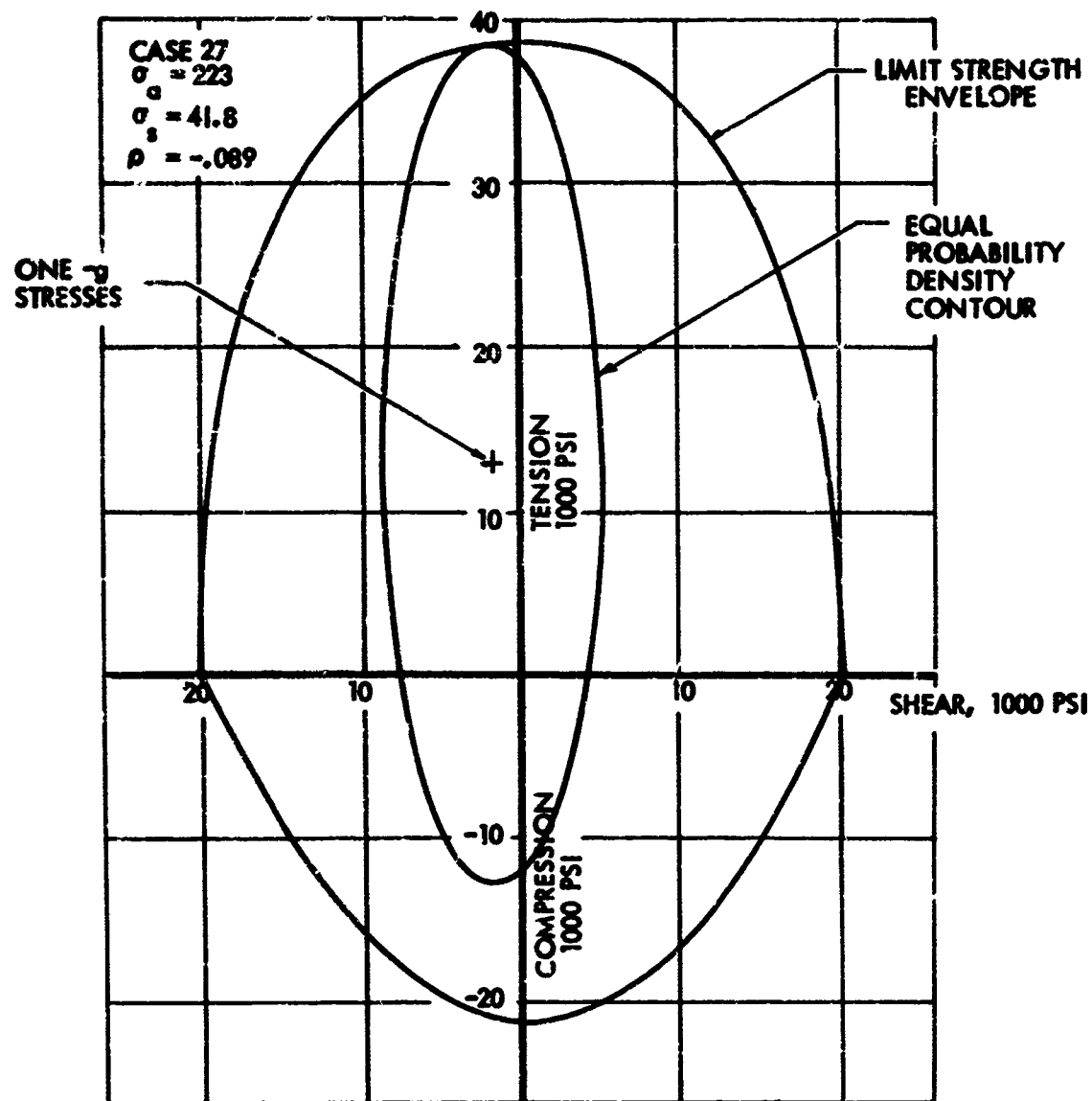


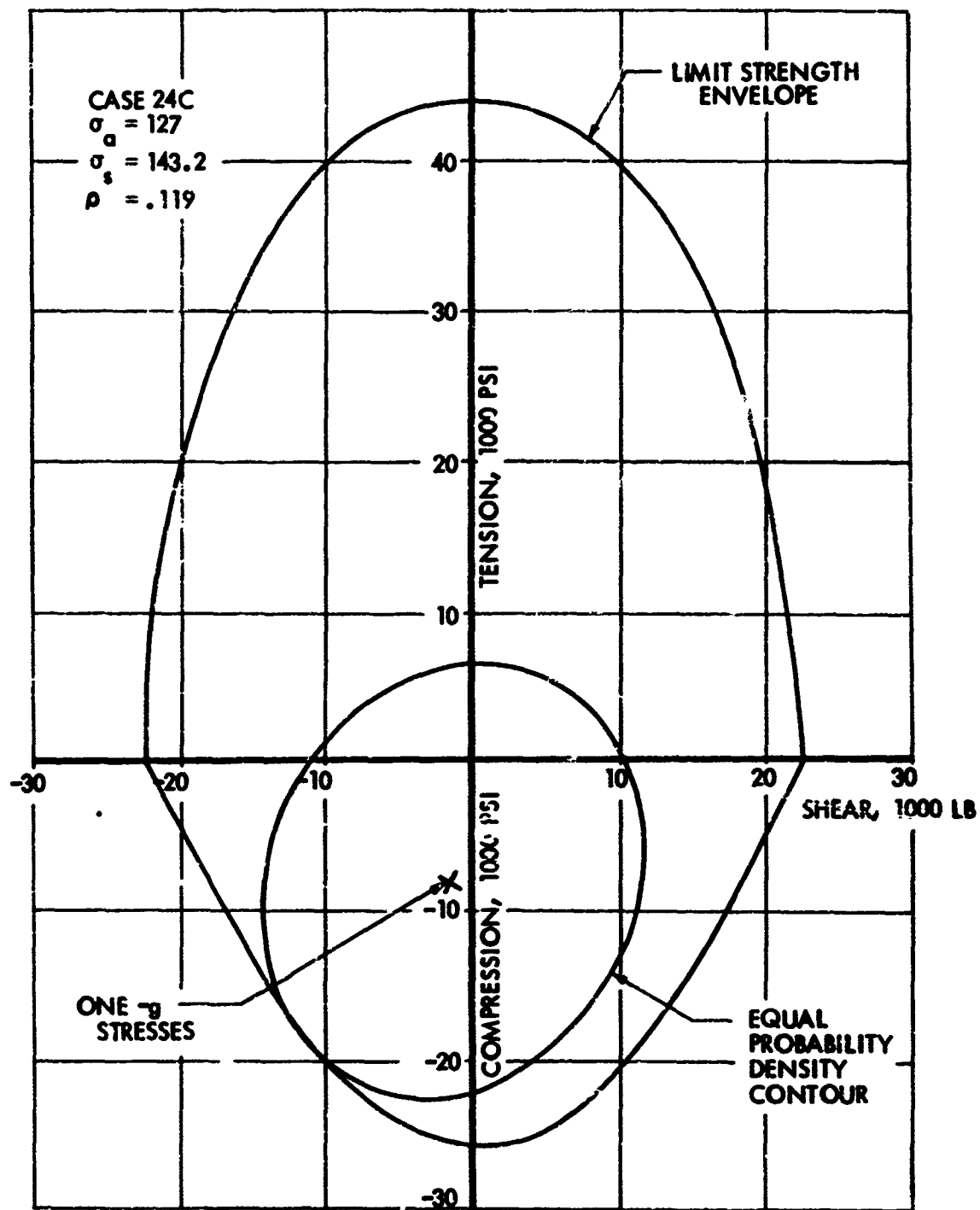
FIGURE 12-8. "EQUAL PROBABILITY" ENVELOPE, MODEL 720B

To determine whether these relative values are what might be expected based upon the discussion in Section 12.3, the stress picture at Element No. 9 is examined in Figure 12-9(a). It is seen that the relation of the equal probability density contour to the strength envelope is quite close to that of Figure 12-5(a). The additional probability of exceeding limit strength due to the finite - as contrasted to infinite - strength in the compression and positive and negative shear regions of the strength envelope can be evaluated roughly by adding probabilities from the "Normal" curve in Figure 12-7 at the higher y/σ levels appropriate to these regions. The increment is found to be negligible. Consequently, in this case, the $\sigma_w \eta_d$ corresponding to the joint probability results should more properly have been obtained using a curve much closer to the "Normal" curve than to the "2 x Normal" curve in Figure 12-7. Thus the single-parameter value of $\sigma_w \eta_d$ of 114 is seen to bear a quite reasonable relation to the values of 112 and 118.4 obtained from the joint probability results.

It is also of interest to examine in the same way the stresses for the critical case, No. 24c, at its critical element, No. 122. The equal probability density contours and the strength envelope for this case are shown in Figure 12-9(b). Here, too, it would appear that a curve somewhere between the "Normal" and "2 x Normal" curves in Figure 12-7 should be used, but probably not quite as close to the "Normal" curve as for Case 27 and Element 9.



(a) WING ETA STATION .33, ELEMENT 9, CASE 27
 FIGURE 12-9. RELATION OF JOINT PROBABILITY DENSITY TO
 STRENGTH ENVELOPE, MODEL 720B



(b) WING ETA STATION .33, ELEMENT 122, CASE 24C
 FIGURE 12-9. CONCLUDED

13 ESTABLISHMENT OF LIMIT-STRENGTH AND ULTIMATE-STRENGTH LEVELS OF $N(y)$ AND $\sigma_w \eta_d$

Limit strength and ultimate-strength values of $N(y)$ and $\sigma_w \eta_d$ are obtained for the Model 188 and Model 749 in Appendix E. For the wing, this determination generally involved estimating a design level ($N(y)$ or $\sigma_w \eta_d$), determining properly phased loads at this level at the potentially critical regions of the wing, performing stress analysis to obtain margins of safety, and adjusting the level as required to give a zero margin. Inasmuch as only the critical region of the structure is of interest, complete matching conditions generally did not have to be generated, and the matching condition concepts were applied on a more local basis. Fuselage loads were found to be less critical than wing loads so that a less exact analysis was permissible and phasing could generally be disregarded.

For the Model 720B, limit strength levels were obtained in Reference 1. These follow directly from the joint probability analysis. The limit strength values of $\sigma_w \eta_d$ were obtained based upon assumptions discussed more fully in Section 12.3 herein, where the critical values are summarized. The limit-strength values of $N(y)$ given in Reference 1 were divided by 2 to provide a reasonable estimate, consistent with the $\sigma_w \eta_d$ determination, of the exceedances that would occur on a single parameter basis. This adjustment is shown in Section 12.3 for the critical locations in the structure.

Limit strength values of $N(y)$ for all three airplanes, and ultimate strength values for the Model 188 and Model 749, are summarized in Table 13-1 and plotted in Figure 13-1.

Lateral gust values for the Model 720B are shown both for yaw damper off and for yaw damper on. Although use of the yaw damper is not required by the flight manual, its use is recommended; and apparently it has been the practice to utilize the yaw damper virtually 100% of the time. If it were assumed, for example, that the damper were in use 99% of the time, the limit-strength value of $N(y)$ would be about $(1/100)(4 \times 10^{-6}) + (99/100)(1.2 \times 10^{-8}) = 5.2 \times 10^{-8}$ exceedances per hour.

In order to give a quantitative indication of the effect of frequency of exceedance on load level, several typical exceedance curves are shown in Figure 13-2. Each of these is multiplied by a factor, in the horizontal direction, such to give a load value of unity at 10^{-5} exceedances per hour. The vertical scale is selected to line up with that of Figure 13-1. Differences amongst the various curves are due largely to different ratios of one-g to incremental load.

TABLE 13-1. SUMMARY OF MISSION ANALYSIS RESULTS

Component and Airplane	Frequency of Exceedance, N(y), Per Average Flight Hour	
	Limit Strength	Ultimate Strength
Wing		
188	2.1×10^{-5}	1.4×10^{-8}
749	1.8×10^{-5}	4.2×10^{-9}
720B	1.1×10^{-5}	-
Body and Tail-Vertical Gust		
188 (Forebody)	6.0×10^{-6}	1.0×10^{-9}
749 (Tail)	4.5×10^{-9}	1.7×10^{-14}
720B (Aftbody)	1.0×10^{-9}	-
Body and Tail-Lateral Gust		
188 (Aftbody)	6.0×10^{-5}	5.0×10^{-7}
749 (Tail)	2.5×10^{-4}	5.0×10^{-6}
720B, Yaw Damper Off (Tail)	4.0×10^{-6}	-
720B, Yaw Damper On (Body)	1.2×10^{-8}	-

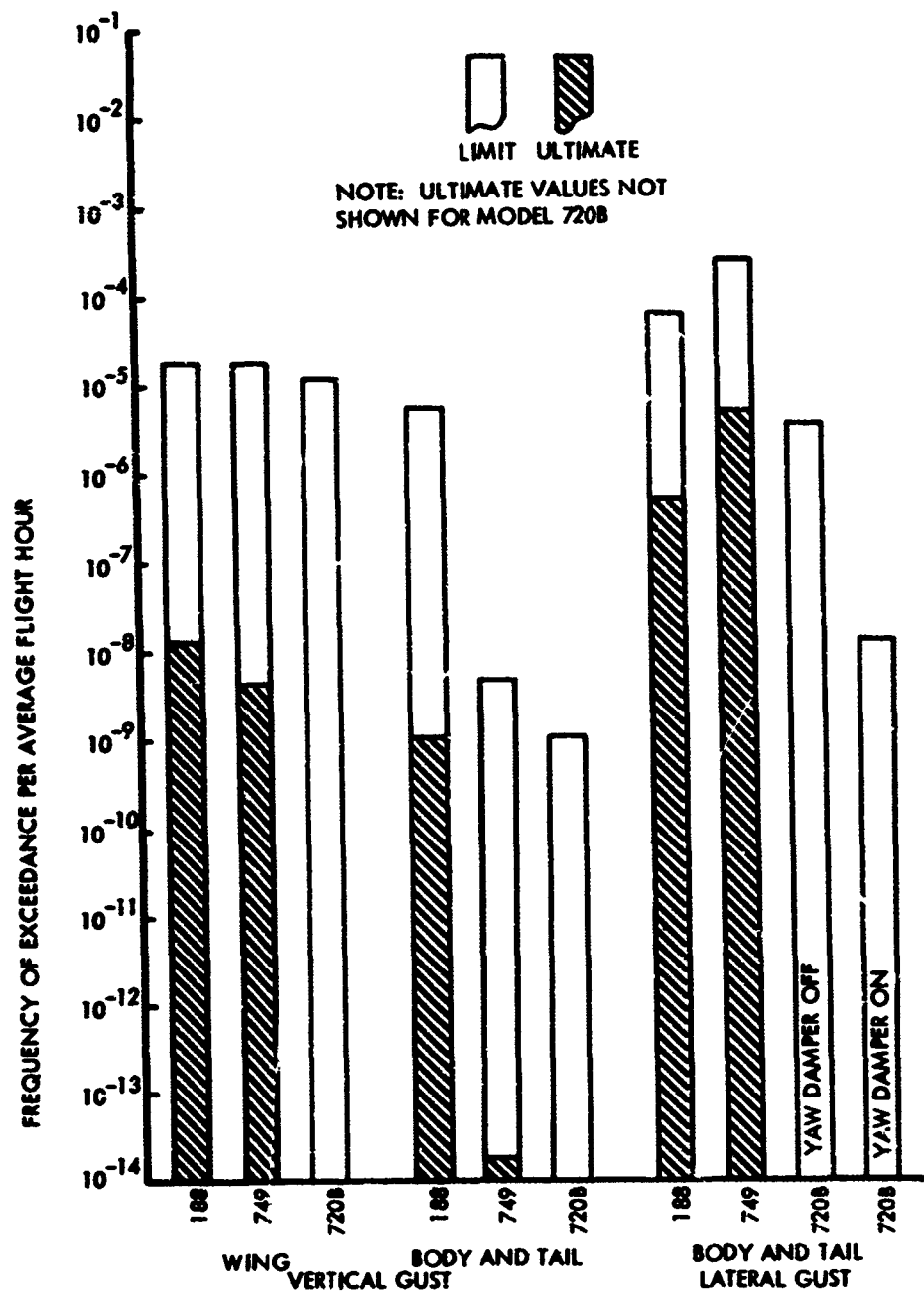


FIGURE 13-1. SUMMARY OF MISSION ANALYSIS RESULTS

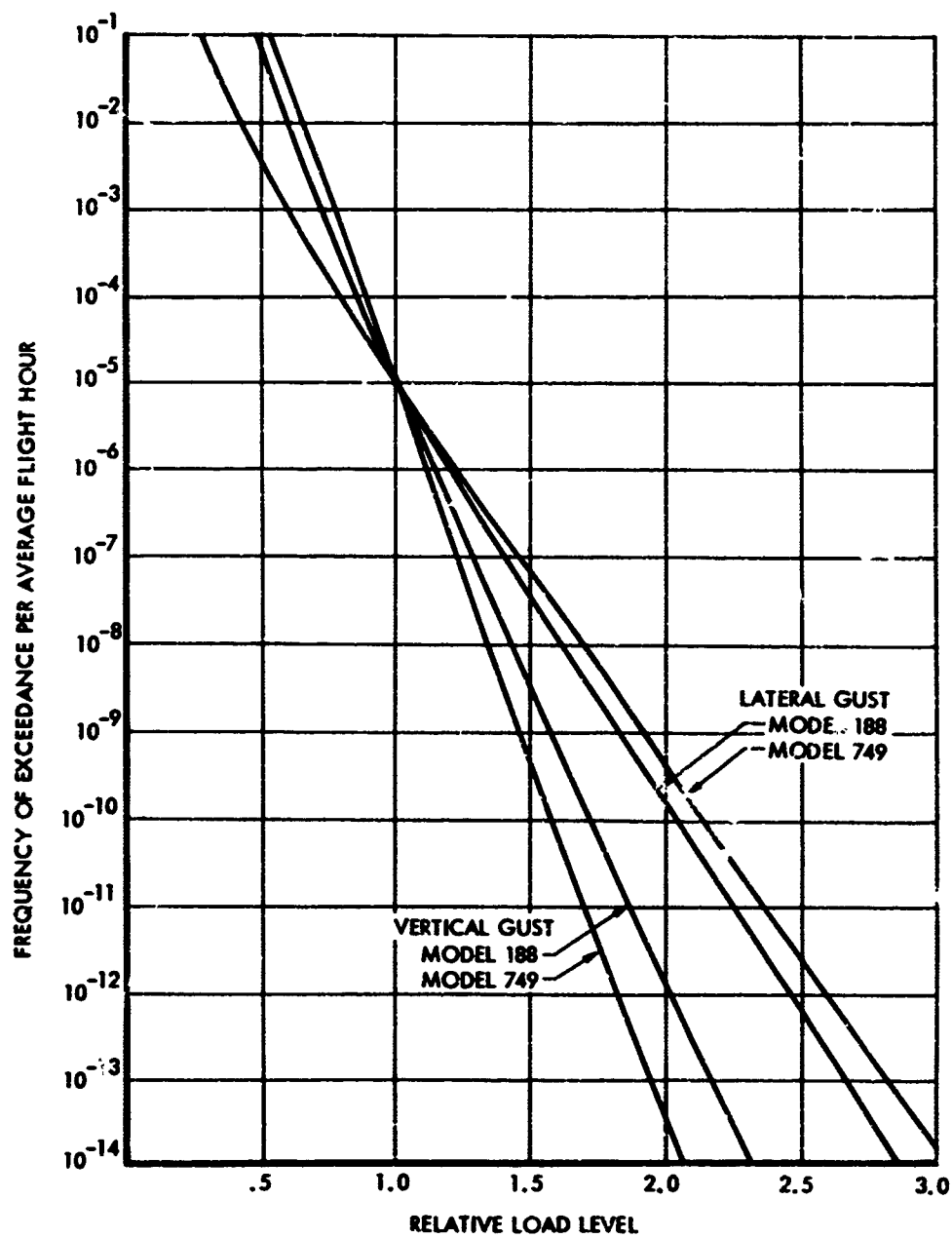


FIGURE 13-2. TYPICAL VARIATION OF LOAD LEVEL WITH FREQUENCY OF EXCEEDANCE

Limit and ultimate strength values of $\sigma_w \eta_d$ are summarized in Table 13-2 and plotted in Figures 13-3 and 13-4. Only the critical condition for each major component is shown. Values of $\sigma_w \eta_d$ shown in the last two columns of Table 13-2 and in Figure 13-4 are adjusted to a common altitude of 7000 ft. by moving along lines of constant $N(y)/N_0$ in Figure 5-8.

Lateral gust values for the Model 720B are again shown both for yaw damper off and for yaw damper on. It should be noted that the 720B lateral gust cases were generally confined to the V_C boundary of the speed-altitude envelope. It appears that the yaw-damper-off loads would be higher at somewhat-reduced speeds because of the lower Dutch roll damping. However, it is believed that the pilot would be aware of the reduced damping, would not like it, and would either put the damper on, if possible, or improve the damping himself by suitable control action.

Limit strength values of $\sigma_w \eta_d$ are shown for the V_C condition only. From the discussions in Appendix E and the data shown in Reference 1, it appears that all three airplanes can withstand a $\sigma_w \eta_d$ at V_D of at least 25/50 the V_C value. (The factor 25/50 will be recognized as the ratio of currently specified U_{de} gust velocities at the respective speeds.) For the Model 188 wing, the V_D value is just 25/50 of the V_C value. For the Model 749 wing the V_D value is slightly greater than 25/50 of the V_C value. For the Model 720B, based on wing bending moment alone, it appears that the limit strength $\sigma_w \eta_d$ is even greater at V_D than for the critical speed within the V_C boundary. It also appears that all three airplanes can withstand a somewhat higher $\sigma_w \eta_d$ at V_B than at V_C , but not, in all cases, in the full 66/50 = 1.32 ratio of current U_{de} values. The ratio for the Model 188 wing is well in excess of 66/50. For the Model 749 wing, the ratio is only about 1.25. However, a more pertinent ratio, in this case, is that of limit-strength $\sigma_w \eta_d$ at V_B for the Model 749 to limit-strength $\sigma_w \eta_d$ at V_C for the critical airplane (the Model 188); this ratio is $(1.25 \times 88)/(62) = 1.77$. (The number 62 is the limit-strength $\sigma_w \eta_d$ for the Model 188 at V_C , adjusted to an altitude of 7000 ft.) This ratio, too, is well in excess of 66/50. For the Model 720B, the ratio of V_B to V_C limit strength $\sigma_w \eta_d$'s is roughly 1.15, as indicated by Figure 42 of Reference 1. For this airplane, too, the more pertinent ratio of limit-strength, $\sigma_w \eta_d$ at V_B to limit strength $\sigma_w \eta_d$ at V_C for the Model 188, is well in excess of 66/50.

Generally, it is believed that the stress analysis methods used in establishing these results were realistic and reasonably consistent with the methods that would be used on new designs today.

A minor exception might be the Model 749 wing, where possibly some load redistribution from the critical element to less critical elements, not accounted for in the stress analysis, might occur. The critical elements are indicated in Appendix E to be the beam web and beam web splice; however, the critical stress was produced predominantly by wing bending moment rather than shear and torsion, and some slip in the web splice

TABLE 13-2. SUMMARY OF DESIGN ENVELOPE RESULTS

Component and Airplane	$\sigma_w \eta_d$, Fps At Altitude Indicated		$\sigma_w \eta_d$, Fps At 7000 Ft	
	Limit Strength	Ultimate Strength	Limit Strength	Ultimate Strength
Wing				
188	60 @ 12000 Ft	101 @ 12000 Ft	62	100
749	88 @ 7000 Ft	155 @ 16000 Ft	88	147
720B	111 @ 22000 Ft	-	107	-
Body and Tail-Vertical Gust				
188 (Forebody)	67 @ 12000 Ft	120 @ 12000 Ft	69	118
749 (Forebody)	110 @ 16000 Ft	186 @ 16000 Ft	108	174
720B (Aftbody)	175 @ 22000 Ft	-	158	-
Body and Tail-Lateral Gust				
188 (Aftbody)	61 @ 7000 Ft	120 @ 7000 Ft	61	120
749 (Tail)	65 @ 7000 Ft	97 @ 7000 Ft	65	97
720B, Yaw Damper Off (Tail)	99 @ 23000 Ft	-	97	-
720B, Yaw Damper On (Tail)	137 @ 23000 Ft	-	128	-

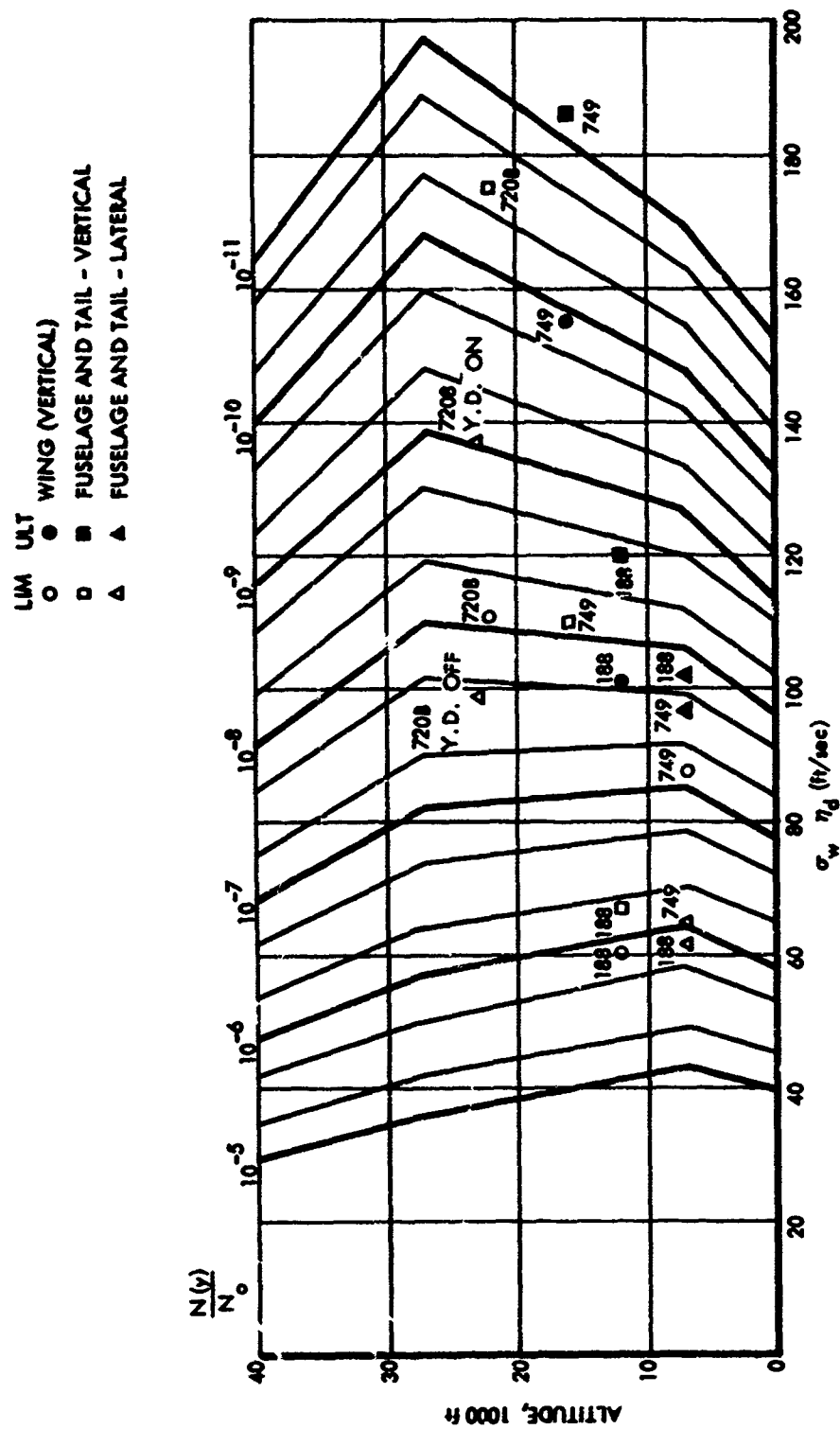


FIGURE 13-3. SUMMARY OF DESIGN ENVELOPE RESULTS

would permit the beam caps and surface material to carry additional load. The increase in limit-strength load due to this mechanism is probably no more than about 5%, however. Previous dynamic gust analysis of the Model 749 indicated an allowable bending moment nearer the wing root, governed by combined tension and shear in the lower surface, that would be reached at less than a 5% increase in the loads found to give a zero margin of safety in the present study.

It should also be borne in mind that, as noted earlier, fuselage loads and fuselage strength were both treated conservatively in the vertical gust analysis of the Model 188 and Model 749. Consequently, for these cases, the actual limit and ultimate strength $\sigma_w \eta_d$'s are somewhat higher than indicated, and the actual frequencies of exceedance of limit and ultimate strength are somewhat lower.

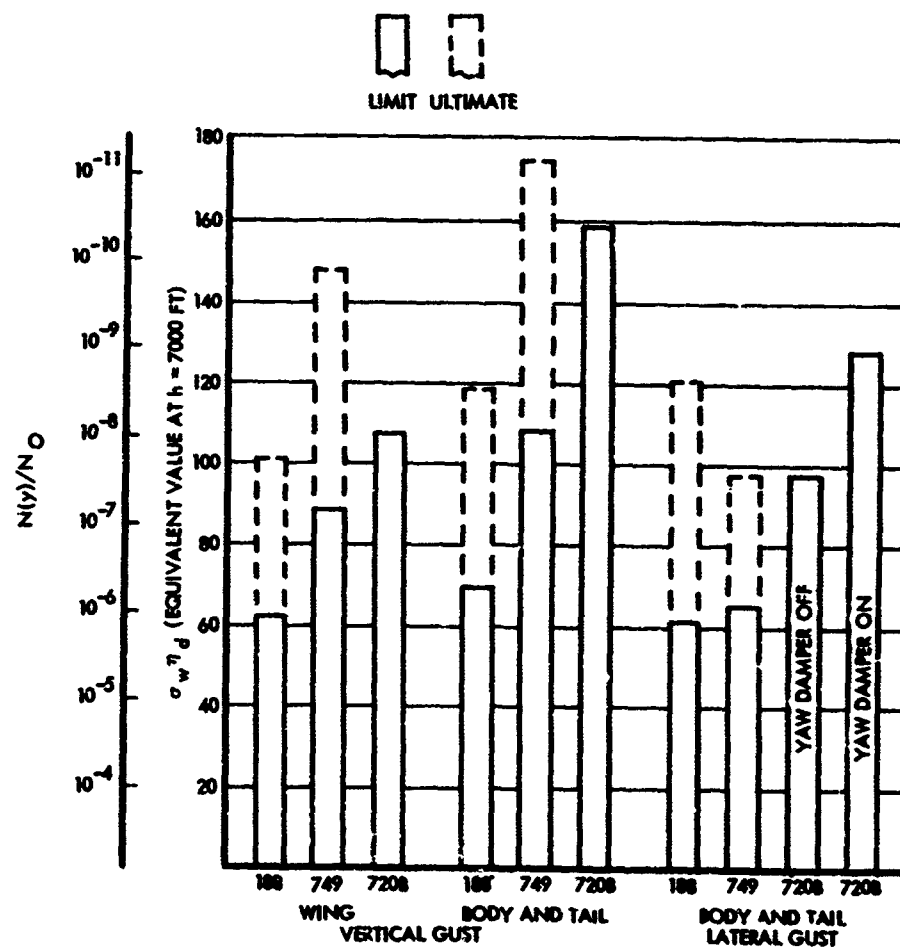


FIGURE 13-4. CONSOLIDATED SUMMARY OF DESIGN ENVELOPE RESULTS

14 EFFECT OF PARAMETER VARIATIONS

14.1 Vertical Gust, Model 188

The effect on loads of changes in airplane and mission profile descriptions has been investigated by variation of a number of the analysis parameters. The parameters selected for variation were those for which precise values might be difficult to obtain during the design stage and which might be expected to have a significant effect on loads. These parameters fall naturally into two categories - first, those descriptive of the airplane itself, and second, those descriptive of the airplane usage in the mission analysis.

\bar{A} and N_0 values and one-g loads for the various parameter variation cases investigated are listed in detail in Appendix B, Table B-9. Select values are taken from this table for further analysis, comparison, and discussion in Sections 14.1.1 and 14.1.2 following.

14.1.1 Effect of Airplane Description Parameters. In determining the effect on loads of variation in the airplane description parameters, a single airplane condition is used as a reference. Mission analysis case 202, as defined in Table 6-2, was selected for this purpose. As indicated by Figures 9-9 (a) through (d), this leg generally contributed the major part of the total load exceedances. Results based upon this mission segment alone will therefore be applicable, to a close approximation, to the mission analysis as a whole. They should also approximate fairly closely the effect of parameter variations relative to the critical V_C design envelope condition.

Airplane loads for which the effect of parameter changes are studied are wing loads at wing stations 119 and 346, fuselage loads at fuselage stations 571 and 1000, and accelerations at the center of gravity. The wing torsions are taken about the elastic axis. The bending moment at fuselage station 1000 is also a fairly good measure of tail load, inasmuch as the relieving inertia is only about 30% of the contribution from the tail airload. Where the direction of loading is pertinent, only wing upbending and fuselage downbending loads are considered. The wing and forebody loads are therefore "up gust" loads, and the aftbody loads are "down gust" loads. Except at design dive speed, these are the critical loading directions.

The results of the variations in the airplane description parameters are listed in Tables 14-1, 14-2, and 14-3.

Table 14-1 indicates the proportionate changes in \bar{A} ; these are simply percentage changes divided by 100. For wing torsions, a percentage expressed in the usual way is relatively meaningless because of the

TABLE 14-1. EFFECT OF PARAMETER VARIATIONS ON \bar{A} VALUES,
MODEL 188 VERTICAL GUST ANALYSIS

Case	Description of Variation From Reference Case	\bar{A} Reference - 1								
		C.G. Accel	WS 119			WS 246			FS 571	
			δ_z	M_x	M_y^*	δ_z	M_x	M_y^*	δ_z	M_y
202-1	Wing EI Decreased 20%	.004	.011	.007	-.012	.009	.004	-.008	.003	.002
202-2	Wing GI Decreased 20%	.007	.016	.019	.010	.014	.025	0	.009	.007
202-3	Wing EI and GI Decreased 20%	.011	.028	.028	.002	.028	.030	-.003	.012	.011
202-4	Wing EA Shifted Forward 5% C	-.008	-.017	-.017	-.017	-.021	-.014	-.015	-.011	-.009
202-5	Mode Damping Added $\xi = .03$	-.006	-.020	-.017	-.040	-.029	-.006	-.042	-.008	-.008
202-6	Airplane CG Shifted .09% Aft	.024	-.018	-.006	-.032	-.020	.018	-.026	.069	.085
202-6 Rigid	Rigid - Airplane CG Shifted .09% Aft	.040	.002	.025	-.032	.019	.039	-.022	.087	.103
202-7	Fuselage Aero Penetration Equal To Wing	-.008	-.008	-.006	-.007	-.008	-.006	-.013	-.005	-.004
202-7 Rigid	Rigid - Fuselage Aero Penetration Equal to Wing	-.009	-.005	-.008	.004	-.007	-.009	.004	-.005	-.003
202-8	Approximate Lift-Lag Function	.012	-.004	.005	-.084	-.018	.030	-.089	.014	.014
202-9 Rigid	Rigid - Approximate Lift-Lag Function	.017	.017	.023	-.011	.018	.029	-.006	.018	.021
202-10	Nacelle Aero Increased 30%	.061	.140	.116	.166	.151	.055	.170	.074	.076
202-10 Rigid	Rigid - Nacelle Aero Increased 30%	.027	.082	.041	.254	.096	-.005	.234	.030	.030
202-11	Increase Speed From 282 to 324 Knots	.219	.272	.274	.167	.279	.260	.183	.218	.215
202-13	Increase ZFW From 74500 to 86000 Lb	-.066	.265	.175	.138	.199	.102	.110	.145	.185
202SF	Stick Fixed - No Elevator Motion	.099	.085	.080	.003	.038	.114	-.012	.153	.187

*For special treatment of wing M_y , see text.

TABLE 14-2. EFFECT OF PARAMETER VARIATIONS ON N_0 VALUES,
MODEL 188 VERTICAL GUST ANALYSIS

Case	Description of Variation From Reference Case	N ₀ /N ₀ Reference									
		C.G. Accel	WS 119			WS 346			FS 571		FS 1000
			S _z	N _x	N _y	S _z	N _x	N _y	S _z	N _y	N _y
202-1	Wing XI Decreased 20%	1.03	1.02	.93	.99	.94	1.07	.96	1.03	1.02	.94
202-2	Wing GJ Decreased 20%	1.00	1.01	.96	.96	.95	.98	.96	1.00	.99	.83
202-3	Wing XI and GJ Decreased 20%	1.04	1.03	.90	.94	.90	1.05	.91	1.03	1.02	.80
202-4	Wing EA Shifted Forward 5% C	1.01	1.04	1.03	1.00	1.03	1.05	1.02	1.05	1.08	1.13
202-5	Mode Damping Added $\xi = .03$.97	.98	.97	.98	.98	.98	.99	.98	.99	.97
202-6	Airplane CG Shifted .09% Aft	.97	1.00	.98	1.04	1.00	.97	1.03	.98	.99	.95
202-6 Rigid	Rigid - Airplane CG Shifted .09% Aft	.96	.94	.94	1.07	.95	.95	1.07	.98	.97	.92
202-7	Fuselage Aero Penetration Equal to Wing	1.01	.99	1.00	1.00	1.00	1.01	.99	1.00	1.01	1.07
202-7 Rigid	Rigid - Fuselage Aero Penetration Equal to Wing	1.04	.97	.98	.96	.98	1.00	.96	1.01	1.02	1.07
202-9	Approximate Lift-Lag Function	.97	.92	.95	1.00	.96	.89	.98	1.00	1.02	1.00
202-9 Rigid	Rigid - Approximate Lift-Lag Function	.97	.91	.88	1.11	.88	.87	1.14	.97	1.01	1.20
202-10	Nacelle Aero Increased 30%	.99	.99	.99	.83	.98	1.03	.91	1.03	1.02	1.04
202-10 Rigid	Rigid - Nacelle Aero Increased 30%	1.02	1.02	1.02	.84	1.04	1.01	.77	1.02	1.02	1.04
202-11	Increase Speed From 282 to 324 Knots	1.06	1.01	.98	.97	.97	1.00	.96	1.06	1.05	.88
202-13	Increase ZFW From 74500 to 86000 lb	.95	.90	.94	.89	.93	.93	.94	.95	.92	.95
202B	Stick Fixed-to Elevator Motion	.86	.96	.92	1.08	.97	.88	1.04	.97	.98	.53

TABLE 14-3. EFFECT OF PARAMETER VARIATIONS ON EFFECTIVE \bar{A} VALUES, MODEL 188 VERTICAL GUST ANALYSIS

Case	Description of Variation From Reference Case	\bar{A} Effective Effective Reference - 1									
		C.G. Accel	WS 119			WS 346			FS 571		FS 1000
			S_z	M_x	M_y^*	S_z	M_x	M_y	S_z	M_y^*	M_y
202-1	Wing EI Decreased 20%	.011	.016	-.009	-.014	-.004	.021	-.017	.009	.006	-.025
202-2	Wing GJ Decreased 20%	-.008	.016	.009	.001	.002	.021	-.009	.009	.004	-.075
202-3	Wing EI and GJ Decreased 20%	.019	.035	.002	-.010	.005	.042	-.023	.020	.015	-.086
202-4	Wing EA Shifted Forward 5% C	-.006	-.009	-.011	-.017	-.015	-.003	-.011	0	.008	.058
202-5	Mode Damping Added $\xi = .03$	-.013	-.026	-.023	-.044	-.033	-.010	-.044	-.012	-.008	-.016
202-6	Airplane C.G. Shifted .09% Art	.018	-.017	-.011	-.024	-.021	.010	-.020	.065	.085	.194
202-6 Rigid	Rigid - Airplane CG Shifted .09% Art	.030	-.003	.014	-.019	.008	.028	-.008	.053	.099	.162
202-7	Fuselage Aero Penetration Equal To Wing	-.005	-.010	-.006	-.007	-.009	-.003	-.015	-.005	-.001	.016
202-7 Rigid	Rigid - Fuselage Aero Penetration Equal to Wing	0	-.012	-.009	-.004	-.012	-.008	-.005	-.004	0	.031
202-9	Approximate Lift-Lag Function	.004	-.023	.003	-.084	-.028	.002	-.093	.014	.018	-.024
202-9 Rigid	Rigid - Approximate Lift-Lag Function	.010	-.002	-.003	.009	-.009	.002	.020	.013	.022	.080
202-10	Macelle Aero Increased 30%	.057	.138	.114	.123	.154	.062	.147	.082	.081	.011
202-10 Rigid	Rigid - Macelle Aero Increased 30%	.033	.085	.045	.210	.103	-.003	.166	.033	.032	.010
202-11	Increase Speed From 282 to 324 Knots	.248	.276	.269	.160	.270	.261	.178	.235	.230	.080
202-13	Increase ZFW From 74500 to 86000 lb	-.068	.235	.157	.134	.140	.083	.096	.131	.161	-.044
202SF	Stick Fixed-No Elevator Motion	.020	.074	.066	.019	.030	.080	-.004	.145	.122	-.449

*For special treatment of wing M_y , see text.

possibility of a value close to zero for the reference case. Instead, the proportionate change in the torsion \bar{A} is obtained by dividing the actual change by an appropriate measure of the allowable strength in torsion. This measure is obtained by multiplying the reference case shear \bar{A} at the given wing station by the ratio of maximum design torsion to maximum design shear at that station. The ratios of maximum design torsion to maximum design shear used for this purpose are 100 inches at wing station 119 and 91 inches at wing station 346.

Table 14-1 is primarily of interest with respect to the design envelope criterion, as \bar{A} is a direct measure of the gust increment of load in this application.

In Table 14-2, the effect of the parameter variations on N_0 is indicated by ratios of N_0 to reference case N_0 . It should be emphasized that large percentage changes in N_0 have a far smaller percentage effect on loads. For example, Figure 13-2 indicates that a change in N_0 by a factor of 2 results in only about a 5% change in load at a given frequency of exceedance.

To indicate the combined effect of changes in \bar{A} and N_0 on mission analysis gust incremental loads, "effective" \bar{A} changes are shown in Table 14-3. These "effective" \bar{A} changes include not only the effect of the \bar{A} change itself but also the effect of the N_0 change on the incremental load at a given frequency of exceedance. The N_0 contribution was obtained by calculating the increase or decrease in \bar{A} required to exactly offset the increase or decrease in N_0 at a load exceedance level of 10^{-5} exceedances per hour. The effective \bar{A} change thus calculated was then divided by the reference case \bar{A} to indicate the proportionate change. Reference case wing torsion \bar{A} 's were defined in the same special way in preparing Table 14-3 as in preparing Table 14-1. Generally the effective \bar{A} changes indicated by Table 14-3 are very nearly the same as the actual \bar{A} changes indicated by Table 14-1. It should be remarked that the effect of parameter changes on the one-g loads is not included in the information provided in any of the three tables. It was felt that the relative effects of a parameter change on the gust increment and on the one-g loads could well be peculiar to a given configuration and that in the present study emphasis should be placed on the effect on the gust increment.

The magnitudes of the parameter variations for which load changes are indicated in Tables 14-1 through 14-3 are rather arbitrary. They do not necessarily bear any particular relation to the expected uncertainty in establishing values for use in the analysis, and in all cases a sufficient variation was selected to assure that the differences indicated would not be clouded by possible inaccuracies in the solutions.

In cases 201-1, 202-2, and 202-3, the wing stiffness was decreased by 20 percent, first in bending, then in torsion, and finally in both

bending and torsion. These stiffness changes are fairly sizeable, and design-stage calculations would probably give stiffnesses closer to actual values, in most instances, than reflected by the differences considered here. As can be seen from Table 14-1, the \bar{A} 's are affected very little by these changes. The average change is approximately 2-1/2 percent, with a decrease in stiffness giving an increase in load. Table 14-3 shows comparable small changes in the effective \bar{A} values.

In case 202-4, the position of the wing elastic axis was shifted forward 5 percent of the local chord. This amounts to 11 inches at the root and 5 inches at the tip. Design-stage calculations would be expected to locate the elastic axis to within 2 or 3 percent chord. Torsions are compared using the reference case elastic axis as the load axis in both cases. The effects of this variation are also seen to be small, averaging 2 percent on either an \bar{A} or effective \bar{A} basis.

Case 202-5 indicates the effect of adding structural damping in the wing bending and torsion modes. A structural damping coefficient of .03 was used; this is the value of g in the expression $(1 + ig)k$ and corresponds, at the resonant frequency, to a relative viscous damping of .015. This value is probably close to what is actually present. It also probably represents about the expected degree of uncertainty in establishing a value for design use. The effect is seen to be about a 2 percent reduction in incremental loads.

In case 202-6, the airplane center of gravity is moved aft 9 percent of the mean aerodynamic chord. This is 15 inches and is roughly half the available range of travel between forward and aft limits. This case serves two purposes. Besides giving an indication of the effect of a change in airplane center of gravity, it also indicates the effect of a change in the static stability of the airplane. In interpreting the results of this change, it should be noted that fuselage panel weights were not changed. Thus the fuselage load changes reflect the effect of the stability change, or of a change in wing center of gravity, but do not realistically reflect the effect of varying the c.g. position by moving payload.

In a design envelope analysis, the c.g. position can be regarded as known precisely. In a mission analysis, it can probably be estimated to within at most 5 percent of the mean aerodynamic chord and perhaps usually somewhat closer. The static stability would probably be known to within about 3 to 5 percent of mean aerodynamic chord.

The rather large change investigated results in only about a 2 percent change in the incremental wing loads. This change is an increase and results from the lower natural frequency of the short-period mode due to the decreased static stability. If this change results from an actual center of gravity shift, it will tend to be offset by a decrease in the one-g flight loads due to a shift of load from the wing to the tail.

The change in loads on the forebody is somewhat greater, amounting to about 8 percent. This may be due primarily to a first order effect noted in determining design discrete-gust loads. If the wing and tail are assumed to encounter the gust simultaneously, a sizeable pitch acceleration is produced by the offset between the airplane aerodynamic center and the center of gravity. As the center of gravity moves aft (or the aerodynamic center forward), there is an increase in nose-up pitching acceleration on the forebody (or a decrease in nose-down pitching acceleration), resulting in an increase in the down inertia forces. It is quite interesting to note that the fuselage bending moment at station 1000, which is also a measure of the tail load, increases much more markedly still, by about 19 percent. This may be due to the lower short-period frequency, which delays and/or reduces the development of pitch velocity which would alleviate the tail angle of attack produced by the gust. This parameter change was investigated on both a flexible-airplane and a rigid-airplane basis; the effects are seen to be comparable. As in all cases where a rigid airplane as well as a flexible airplane comparison is shown, the reference loads for the rigid-airplane comparison are obtained for the rigid-airplane.

Case 202-7 indicates the changes in wing and aftbody loads that might result from inability to properly distribute the fuselage airloads and account for the earlier penetration of the nose into the gust. In the reference analysis, what is believed to be a realistic representation was used. Case 202-7 indicates the effect of shifting the forebody lift back to the region of the wing, while retaining the same static stability. It is seen that the effect on the loads is very small, averaging less than 1 percent.

Case 202-9 shows the effect of changes in the unsteady lift growth functions used in the analysis. A comparison of the lift growth functions used in the reference case and in case 202-9 is shown, on an indicial basis, in Figure 14-1. The functions used in the reference case are two and three term exponential approximations to the Wagner and Kussner functions respectively, matching the theoretical functions for the low Mach number, high aspect ratio case. The functions used in case 202-9 are one-term approximations selected to better reflect the actual Mach number and aspect ratio of the Model 188 ($M = .53$ at case 202 speed and altitude, $AR = 7.5$). The results shown in Tables 14-1 and 14-3 indicate that this particular set of changes has a quite negligible effect on loads. It might be remarked, however, that at substantially higher Mach numbers and lower aspect ratios, the lift growth functions may depart substantially from those shown in Figure 14-1, and considerably more variation in load could result from use of unrealistic data.

Case 202-10 indicates the effect of a 30 percent increase in the aerodynamic forces on the propellers and the forward portions of the nacelles. The airplane static stability was unchanged. This variation was

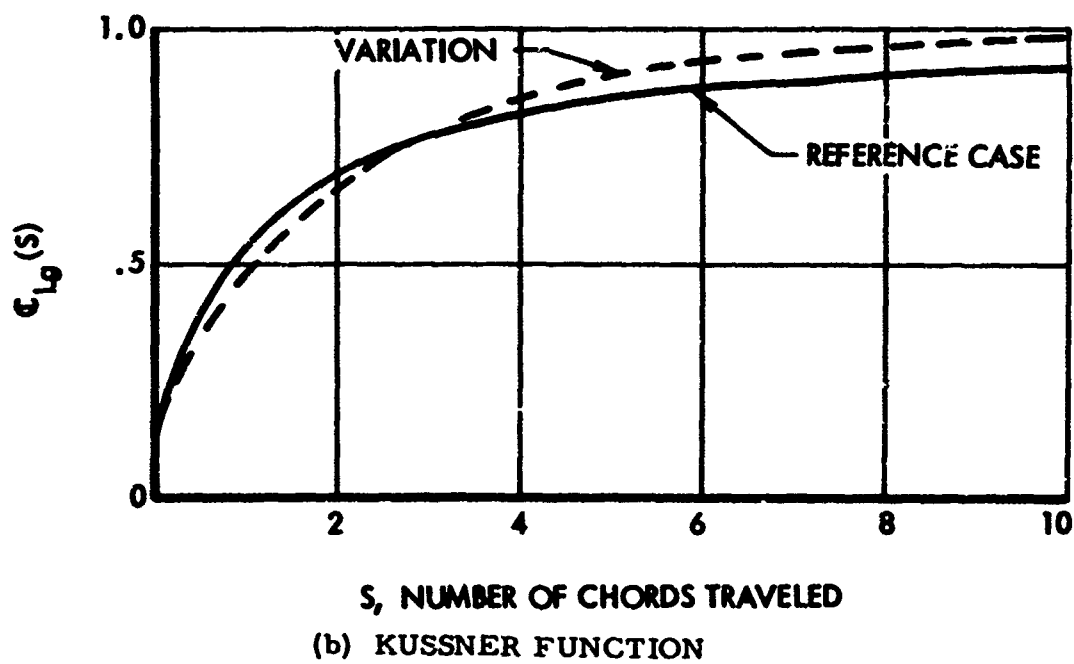
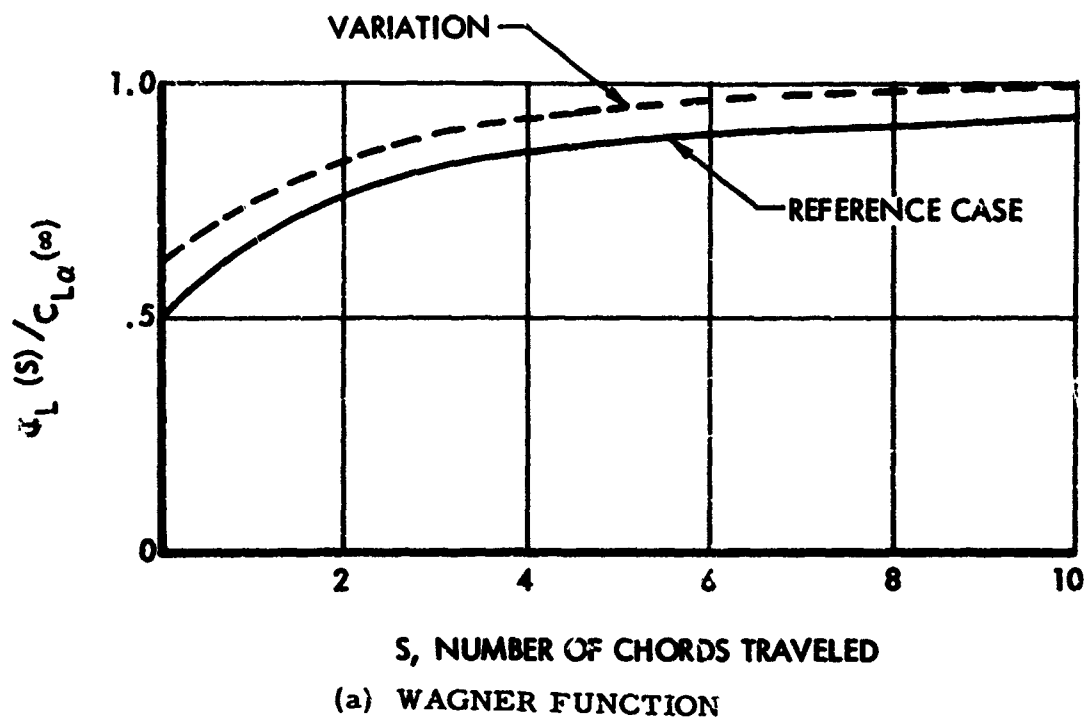


FIGURE 14-1. LIFT-LAG FUNCTIONS USED IN PARAMETER VARIATION STUDY

introduced as a result of difficulty encountered in the design of the Model 188 in securing sufficiently reliable data on pitching moment inputs to the wing due to the nacelles and propellers. With proper recognition of the problem, it would appear that nacelle and propeller aerodynamic forces should be predictable in the design stage to within 15 or 20 percent. It might be noted, too, that in the design of the Model 188, it was the pitching moments, rather than the forces, that were difficult to evaluate, whereas in case 202-10 both were increased in the same proportion.

Fairly substantial load increases are seen to result from this change. On a rigid airplane basis, the torsions and shears both increased significantly, due to the direct effect of the additional airload input at the nacelles. It might be noted, incidentally, that the percentage increases in forebody load and in c.g. acceleration are roughly the same as the 3.1% increase in airplane $C_{L\alpha}$ due to the additional nacelle airload. For the flexible airplane, although the increase in the torsions is somewhat less, the other loads generally increase by about twice as much as for the rigid airplane. Examination of the power-spectral density curves for c.g. acceleration and wing station 119 bending moment indicates that about half this increase is due to static aeroelastic effects and half due to first elastic mode response. To place these rather large increases in perspective, it should be noted that the Model 188, as a very highly powered propjet airplane, develops nacelle aerodynamic forces that are unusually large in comparison with other airplanes, especially the pure jets.

Cases 202-11 and 202-13 were calculated primarily for the investigation of the effects of speed and payload assumptions on the mission analysis results, as described in the next section. They are included in Tables 14-1 through 14-3 as a matter of interest and convenience.

The 15% speed increase reflected by Case 202-11 is seen to produce sizeable load increases. The c.g. acceleration increase of 22% is closely in accordance with the 15% increase in speed and the 6% increase in $C_{L\alpha}$ due to the higher Mach number. The various wing loads generally increase by somewhat larger percentages. It is interesting to note, and will become evident in the next section, that the increase in gust incremental wing loads is substantially offset by a reduction in the one-g flight loads due to a greater aeroelastic nose-down wing twist at the higher speed.

The increase in payload to the placard amount, reflected by case 202-13, is also seen to result in fairly sizeable wing load increases; the effect on one-g loads is actually by a somewhat larger percent.

Case 202-SF indicates the effect of a "stick-fixed," relative to a "stick-free," pilot technique. It is seen that, with the stick fixed,

the effective A's for wing loads increase by from roughly 3 to 8%. This results primarily from the reduction in static stability due to the loss of the effect of the control column bob weight. An even greater increase is indicated for the forebody loads, which is consistent with the effect of a static stability change as shown by Case 202-6.

14.1.2 Effect of Mission Description Parameters. The effect on loads of changes to the mission profile description is investigated by changing a number of the pertinent mission profile characteristics in turn. Several of the changes considered could be investigated without analysis of additional flight conditions. Three additional flight conditions, however, required analysis. Two of these cases, 202-11 and 202-13, are listed in Tables 14-1 through 14-3. The third, case 202-12, consists of case 202 with altitude increased to 16,500 ft. and equivalent air speed decreased to 258 knots.

The effect of these changes on loads is measured by comparing net loads calculated with and without the mission change, at a frequency at exceedence of 10^{-5} exceedences per hour. Loads are compared at the same locations as in the preceding section. The results of the changes in mission description are given in Table 14-4 as ratios of load after the change to load before the change. For wing torsions, because of the possibility of a reference value close to zero, increments instead of ratios are given. To place these increments in perspective, it is noted that the limit design wing torsions are approximately -5.0×10^6 in. lb. at wing station 119 and -2.9×10^6 in. lb. at wing station 346.

As in Section 14.1.1, the magnitudes of the parameter changes selected for investigation are rather arbitrary and the significance of each must be considered individually.

The first modification made was to consider the airplane to be used 100% of the time in the short-range, non-fuel-through mission defined in Table 6-1. Although this mission accounts for only 28% of the total flight hours, it was found to be the major contributor to the load exceedences. A surprisingly small increase in load resulted, averaging only about 3%. It should be pointed out, however, that a converse change, namely operation 100% of the time in a long-range-mission, might be expected to have a slightly greater effect, as indicated by the next case considered.

In case 2, using the case 1 mission as a reference, the cruise altitude was increased from 11000 to 16500 ft. The cruise speed was also modified, in accordance with Figure 6-4. The climb and descent times were increased realistically. Load calculations were carried out assuming all flight time to be in this short mission. It is seen that the increase in cruise altitude results in a load reduction of about 9%.

TABLE 14-4. EFFECT OF MISSION PROFILE VARIATIONS ON NET
LOADS AT $N(y) = 10^{-5}$ CYCLES PER HOUR, MODEL 188
VERTICAL GUST ANALYSIS

Case	Profile Variation	Net Wing Load (U_y Bending)						Net Fuselage (Down Bending)			
		$\frac{S_z}{S_{zRef}}$		$\frac{M_x}{M_{xRef}}$		ΔM_y Change Inlet Load (106 In. lb)		$\frac{S_z}{S_{zRef}}$	$\frac{M_y}{M_{yRef}}$	$\frac{M_y}{M_{yRef}}$	$\frac{M_y}{M_{yRef}}$
		WS 119	WS 346	WS 119	WS 346	WS 119	WS 346	FS 571	FS 571	FS 571	FS 1000
1	Change to Short Range Flights	1.030	1.007	1.038	1.000	-.09	-.02	1.047	1.048	1.038	
2	Change in Cruise Altitude From 11000 to 16500 Ft	.913	.913	.898	.937	.070	.060	1.022	1.046	.893	
3	Change in Cruise Speed From 282 to 324 Knots (Short Range)	1.129	1.066	1.056	1.057	.025	-.082	1.318	1.327	1.170	
4	Change Payload to Give Max. Zero Fuel Weight	1.250	1.184	1.180	1.148	.510	.292	1.225	1.262	.980	
5	Increase Reserve Fuel From 11000 to 17000 lb	.990	1.042	1.000	1.042	.050	.030	.927	.997	.944	
6	Effect of 10 Min Additional Hold Time Each Flight	.996	.993	.992	.994	-.010	-.020	.992	.990	.996	
7	Increase Descent Legs From Two to Four	1.020	.990	1.010	1.005	.160	0	-	-	-	

In case 3, the cruise speed was increased to the VC placard. Again, the case 1 mission was used as a reference: No change was made in descent speed, as the descent segment contributed rather negligibly to the load exposure. It is believed that average cruise speeds can probably be estimated to within about 5% in the design stage, which is only one-third of the variation reflected by the case 3 figures. Table 14-4 indicates that wing loads increased only 6 to 12% due to the 15% speed increase in comparison with the 16 to 28% increase shown for case 202-11 in Table 14-3. The smaller increase here is due to the offsetting changes in the one-g flight loads. The forebody loads, on the other hand, do not benefit from a reduction in the one-g flight contribution, and still show sizeable increases.

Case 4 considers the effect of increasing the payload to a value as limited by the placard zero fuel weight. The zero fuel weight thus increases from 74500 lbs. to 86000 lb., or by 16%. The payload increases from 12500 lb. to 24000 lb. or by 92%. The gross weight at the midpoint of cruise increases from 87500 lb. to 99000 lb., or by 13%. The comparison is again based on the short-range-mission alone. Payload is probably the most difficult of all mission description parameters to predict accurately. However, it is believed that predictions of average payload should be reliable to within about 15% of total payload, or about one-third the variation made here. The figures in Table 14-4 show increases in wing net load of 15 to 25% and comparable increases in fuselage net load. Comparing the results of Table 14-4 with those of 14-3, it is seen that the net loads increase by somewhat greater percentages than the gust increments because of the relatively greater effect of zero fuel weight on one-g loads than on the gust increment.

In case 5, the assumed reserve fuel is increased from 11000 lb. to 17000 lb. The average reserve fuel quantity can probably be predicted to within about half this increment. The comparison is again based on the short range mission alone. It is seen that outer wing loads, where the increased inertia relief due to the added fuel is less effective, increase about 4%, while the inner wing loads remain approximately constant. Fuselage forebody loads actually decrease due to the lower acceleration at the higher gross weight.

In case 6, a low speed holding time of 10 minutes is added to each of the 5 missions included in the overall operation of the airplane as defined in Table 6-1. The comparison, of course, is based on the overall mission. The decrease in loads is generally less than 1%. This result is to be expected, and in fact, illustrates the relation between loads and exceedances indicated by Figure 13-1. The increase in flight time per 100 flights is from 6850 minutes to 7850 minutes, or in the ratio 1.15; therefore, the overall $N(y)$ will decrease in the ratio $1/1.15$, and, as indicated by Figure 13-2, the loads decrease by less than 1%.

Case 7 was included to determine whether a finer breakdown into mission segments might be required. A relatively extreme case is considered. The descent from 16000 ft. in the fuel-through 100-minute flight described in Table 6-1, was originally broken into only two segments for analysis. Over this altitude range, however, both the speed and the turbulence parameters vary markedly. Consequently, it appeared that a finer breakdown might be necessary to adequately determine the load exceedance relationship. This descent leg was therefore broken into four segments, lumped at altitudes of 13500, 10000, 7000, and 2000 ft. (For this analysis, only one additional case was required, No. 207-1; this case was the same as No. 207 except that the altitude was changed to 2000 ft. and the speed to 202 knots.) The resulting load comparisons, based upon the descent leg of this one mission, are shown in Table 14-4. Going to the finer breakdown is seen to have only about a 1% effect on the loads. Moreover, for the Model 188 the descent leg actually accounts for only a minor fraction of the load exceedances, and the resulting effect on the total mission loads would be much smaller still.

14.2 Lateral Gust, Model 188

Because of the expected greater susceptibility of swept wing airplanes to lateral gust parameter changes, the major coverage of the lateral gust part of the parameter variation program was conducted based on the Model 720B.

The effects of certain parameter changes for the Model 188, however, were also considered to be of interest.

In Section 8.2.2, the effects of various pilot techniques were investigated, in order to assure that the dynamic analysis of the reference airplanes would be on a sound basis. Also, for the same purpose, the sensitivity of the lateral gust loads to the rate of growth of the lift produced by change in angle of attack was investigated; the sensitivity was found to be much greater than would have been expected, and accordingly a more realistic lift growth function was incorporated into the analysis.

An additional parameter of which the effect of variations is of interest is the Dutch roll damping. Variations in damping were introduced by introducing into the analysis a fictitious yaw damper giving a yaw couple proportional to yaw velocity. Values of damper coefficient, expressed in the form $(b/2V)(C_{n\dot{\psi}_{\text{damper}}}/C_{n\dot{\psi}_{\text{tail}}})$, of -.1, +.2, and +.5 were investigated. Mission analysis case 201 was used as a reference, and the lift growth functions used were the original functions before the above-described modification was incorporated. The results are shown in Figure 14-2. To obtain the damping values at which the fin \bar{A} 's were plotted, a stability solution of the equations of motion was first obtained, with instantaneous lift growth assumed. A constant $\Delta\zeta$ was then

subtracted to account for the effect of the lag in the lift growth. This decrement in ζ was selected such that the relation of \bar{A} values for fin side load for the two lowest- ζ cases in Figure 14-2 was in accordance with the simple theoretical relationship, $\bar{A} \propto \zeta^{-.5}$. The decrement in ζ was also very close to the value inferred by applying this relationship to fin side load \bar{A} 's given by analyses with and without the lift lag functions included.

At low ζ values, the theoretical proportionality is seen to apply quite closely. But as ζ increases beyond about .2, the tail load begins to decrease much more slowly. This result is qualitatively in agreement with Figure 1 of Reference 25, although there the leveling off occurs at a slightly lower ζ . (To convert the scale used in Figure 1 of Reference 25 to a ζ scale, it can be noted that the quantity $1/c_{l/2}$ used therein is equal to approximately 9.0 ζ).

14.3 Vertical and Lateral Gust, Model 720B

The effects of variations of various parameters on the vertical and lateral gust loads of the Model 720B are discussed in Reference 1.

14.4 Effect of Mathematical Model, Model 749

In addition to variations in method or input data that can be investigated utilizing a given mathematical model, there are also subtle differences amongst various mathematical models, even when the models may all be of the same general level of complexity. In order to gain an impression as to the differences in loads that might result from this source, \bar{A} and N_0 values for wing loads and airplane c.g. accelerations were obtained for the Model 749 by means of both the Lockheed and Boeing mathematical models. Mission analysis case 106, as defined in Section 6, was used for this comparison.

Inasmuch as the Boeing model did not include provision for nacelle structural damping or elevator float, it was decided that the comparison should be based upon analyses in which the nacelle structural damping was assumed zero and the elevator was considered fixed. Accordingly, the Lockheed analysis was repeated on this basis. This analysis is designated Case 106x.

In addition, in conducting the Boeing analysis, it was found impractical to represent the nacelle and propeller aerodynamics and to include aerodynamic pitching moments on a rigid fuselage. As a result, in the Boeing analysis, the nacelle and propeller aerodynamic forces were

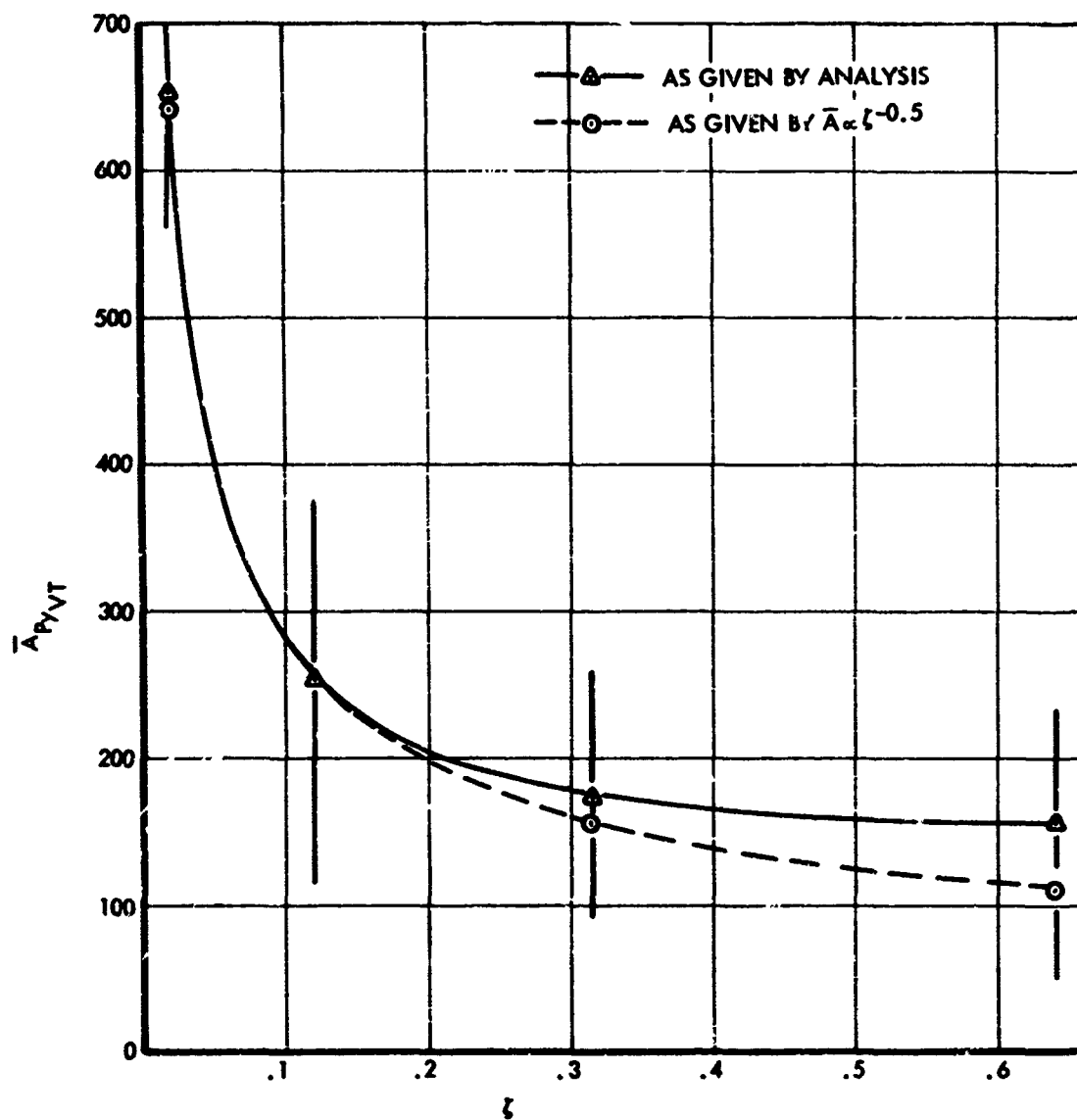


FIGURE 14-2. EFFECT OF DUTCH ROLL DAMPING ON TAIL LOAD

applied to the fuselage. Fuselage lift was then lumped with the innermost wing segment and the tail was relocated in order to maintain the proper total-airplane pitching moment derivative, $dC_m/d\alpha$. Moreover, since the Boeing analysis treated wing and tail induction effects on a unified theoretical basis, it inferred a value of wing downwash at the tail that happened not to agree with that given by the Lockheed sources. In the Boeing analysis, therefore, the tail was modified in area to correct the difference in downwash given by the two analyses and thus maintain the same tail lift due to a change in airplane angle of attack. The Lockheed analysis was also performed with these additional changes, in order to provide the most meaningful comparison. The resulting case is designated 106y. The actual differences in input data between Cases 106x and 106y are indicated by the following summary, in which all $C_{L\alpha}$ values are referenced to the wing area and l/\bar{c} designates the distance in wing chords from the wing elastic axis to the tail aerodynamic center:

	Case 106x	Case 106y
$C_{L\alpha}$, wing	5.17	5.28
$C_{L\alpha}$, nacelles (total for four)	.21	0
$C_{L\alpha}$, nose	.10	0
$C_{L\alpha}$, fuselage center section	-.49	-.18
$C_{L\alpha}$, tail	1.09	1.65
$1 - d\epsilon/d\alpha$, tail	.60	.33
$(C_{L\alpha})(1 - d\epsilon/d\alpha)$, tail	.65	.54
$C_{L\alpha}$, total for airplane	5.64	5.64
l/\bar{c}	3.32	2.31
Short period undamped natural frequency, cps	.46	.44
Short period damping ratio, ζ	.73	.70

The short period frequency and damping values given are computed on the basis of instantaneous lift growth.

A and N_0 values obtained by the Lockheed analysis for cases 106x and 106y are listed in Table B-3 (Appendix B).

\bar{A} values given by the Boeing analysis and by the corresponding Lockheed analysis (Case 106y) are compared in Figure 14-3. The N_0 values are compared in Figure 14-4. The N_0 values are seen to agree excellently. The \bar{A} values agree in the general shape of the spanwise variations, but the Boeing values are significantly higher. At W.S. 191, indicated in Section E.2.2 (Appendix E) to be the critical location in the wing, the Boeing \bar{A} 's are about 1.36 times the Lockheed values.

To provide a rough indication of the source of this difference - that is, whether it is in the rigid airplane or elastic mode response characteristics - the comparison of \bar{A} values is repeated on a rigid airplane basis in Figure 14-5. ("Static-elastic" values as given by the Boeing analysis are also shown, as a matter of interest; these are obtained by setting equal to zero, in the analysis, all forces, aerodynamic and inertia, produced by velocities and accelerations in the elastic modes.) It is seen that the percentage differences between the Boeing and Lockheed analyses are substantial on a rigid airplane as well as a flexible airplane basis. Although the exact percentages vary somewhat with the spanwise location and with the load quantity, it appears that, on the average, differences in elastic mode response would account for about a 5 percent difference between Boeing and Lockheed \bar{A} values; the balance of the difference in the flexible-airplane values is then due to the differences in rigid-airplane response characteristics.

The differences in elastic mode response may be due largely to the reduced aerodynamic damping in the Boeing analysis due to the inclusion of aerodynamic induction effects in the elastic mode response. In the Lockheed analysis, strip theory is used, with panel $C_{L\alpha}$ values taken so as to give the correct lifts when the entire wing is given an increment in angle of attack. These values are too high, however, to define correctly the forces due to motions in the elastic modes. For motion in the first bending mode, for example, the two nodal points are comparable to additional wing tips, in separating positive pressure and negative pressure regions; as a result, an effective aspect ratio, for roughly estimating the reduction in $C_{L\alpha}$ due to spanwise flow, for motion in this mode, would be only 1/3 of the actual aspect ratio of the complete wing. Consequently, the actual aerodynamic damping is somewhat less than obtained by the strip theory analysis.

Good qualitative agreement of the elastic mode responses between the two analyses is indicated by plots of the various power-spectral density functions (not shown). The frequencies of the various elastic mode response peaks were found to agree very closely, and the general shapes of the curves were quite similar.

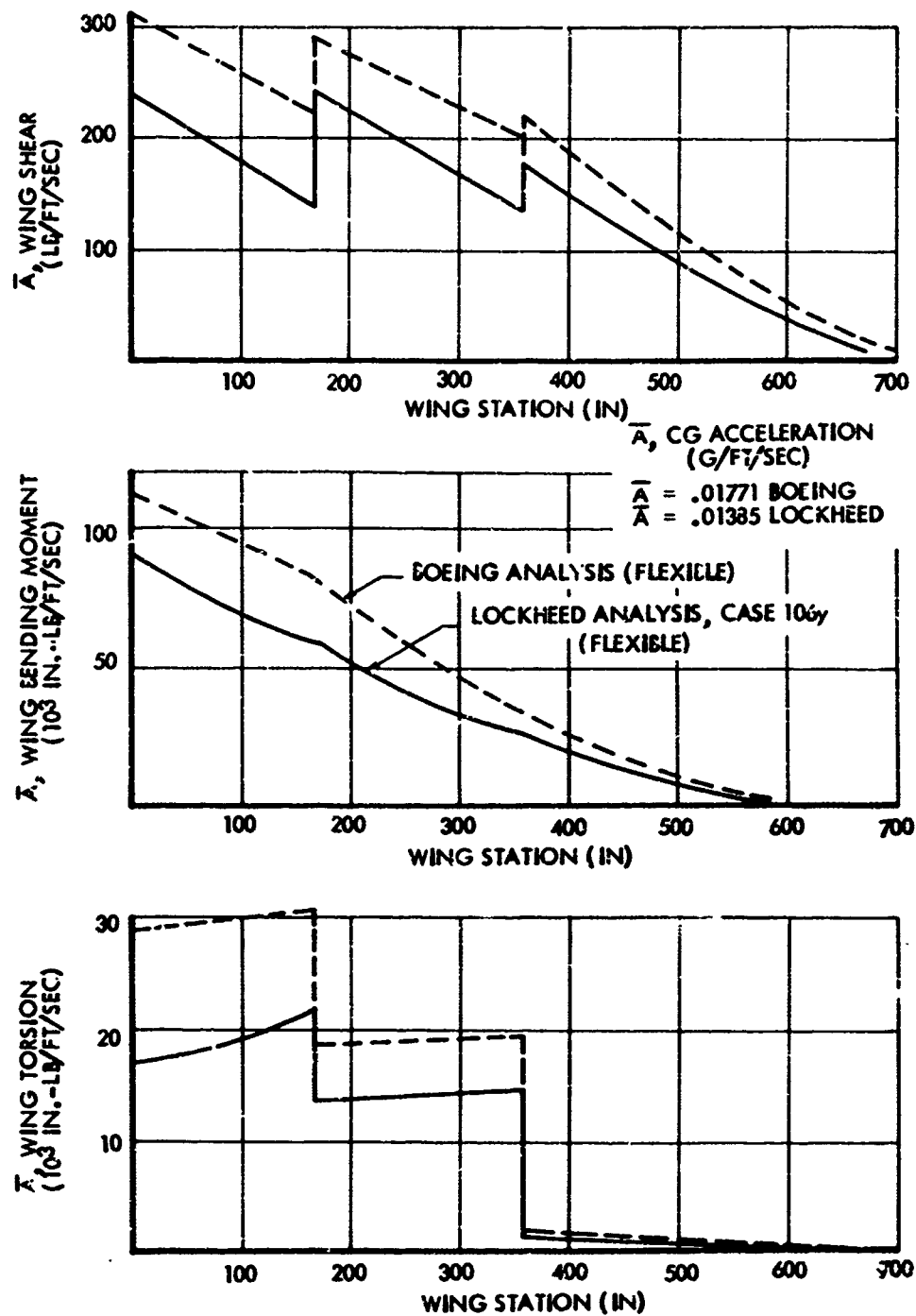
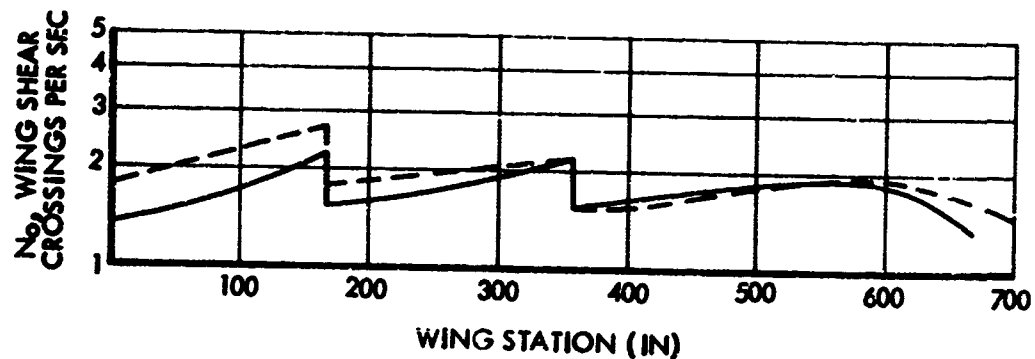


FIGURE 14-3 COMPARISON OF \bar{A} VALUES GIVEN BY BOEING AND LOCKHEED ANALYSIS OF THE MODEL 749



N_0 , CG ACCELERATION, PER SEC

$N_0 = 1.173$ BOEING

$N_0 = 1.354$ LOCKHEED

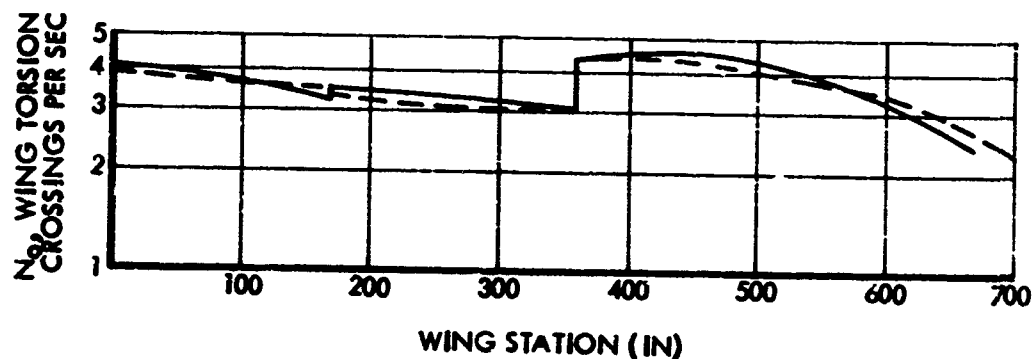
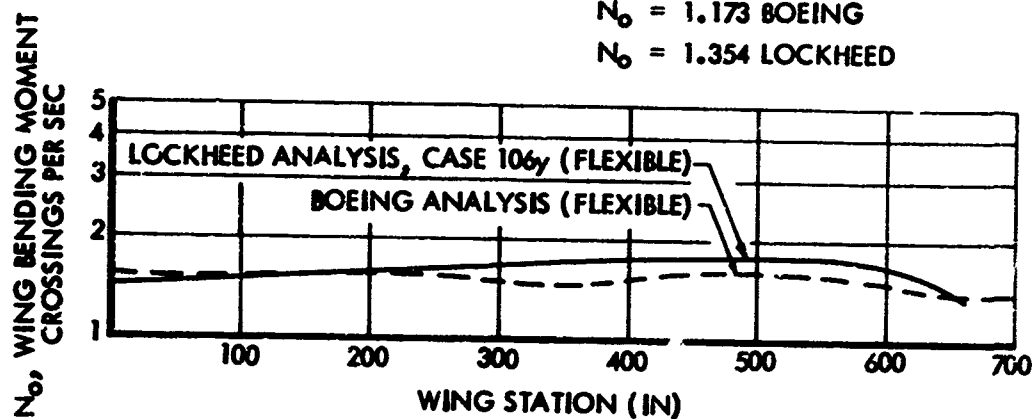


FIGURE 14-4. COMPARISON OF N_0 VALUES GIVEN BY BOEING AND LOCKHEED ANALYSIS OF THE MODEL 749

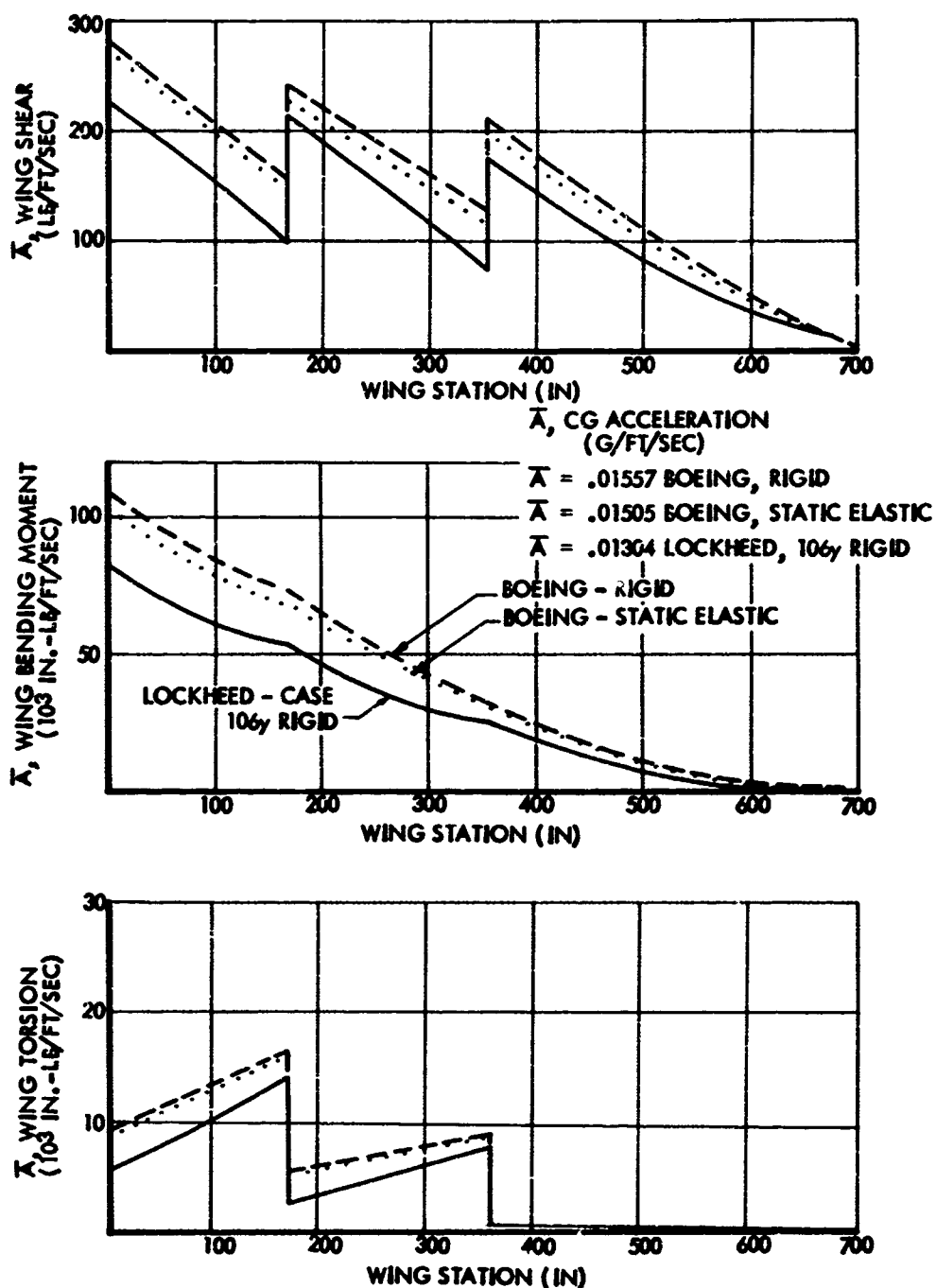


FIGURE 14-5. COMPARISON OF \bar{A} VALUES GIVEN BY BOEING AND LOCKHEED ANALYSES OF THE MODEL 749 - RIGID AND STATIC ELASTIC ANALYSES

The reasons for the sizeable differences in the rigid-airplane results are not clear. In an effort to gain an understanding of these differences, the rigid airplane analysis was repeated making various changes in the treatment of the aerodynamics. For this purpose, use was made of a separate two-degree-of-freedom mathematical model. In this model, the airplane is free to plunge and pitch. The airplane is broken down into several aerodynamic elements, such as wing, tail, nose, and remainder of the fuselage. Gust penetration, transient lift growth, and downwash are handled separately for each element. Analyses were conducted for both the "Lockheed Configuration," Case 106x, and the "Boeing Configuration", Case 106y.

Results are shown by means of plots of power-spectral density of c.g. acceleration in Figures 14-6, 14-7, and 14-8, and tabulations of \bar{A} for c.g. acceleration in Table 14-5.

A comparison of power spectral densities for the Boeing analysis and the directly comparable Lockheed analysis is shown first, in Figure 14-6.

In Figure 14-7, comparisons of ten-degree-of-freedom (rigid) with two-degree-of-freedom power spectral densities are made, in order to provide a check of the ten-degree-of-freedom results. For Case 106y, the \bar{A} values agree to within 1 percent and the power spectral densities are also in reasonably close agreement. For Case 106x, the two analyses are in less exact agreement, with the \bar{A} values differing by about 7 percent. The possibility of the differences being due to the use of local wing chord as a basis for the transient lift growth in the ten-degree-of-freedom analysis was investigated by repeating the ten-degree-of-freedom analysis basing all wing lift growths on the mean aerodynamic chord as in the two-degree-of-freedom analysis; the effect of this change, however, was found to be slight.

It is also interesting to note from Figure 14-7 that Cases 106x and 106y differ considerably from each other in c.g. acceleration \bar{A} values and power spectral densities - even through the mass parameter, mean chord, and short period frequency and damping are virtually identical for both cases.

Figure 14-8 shows the effect on Case 106y results of various changes in the lift growth and downwash assumptions. The effects of the transient lift growth assumptions are seen by comparing curves A, B, C, D, and E. The peculiar two-hump shape displayed by Curve A (the basic case, also shown in Figures 14-6 and 14-7) is seen to result from introduction of the Wagner lift growth function. A plot of the Wagner function vs frequency, however, does not show any obvious reason why such humps should appear.

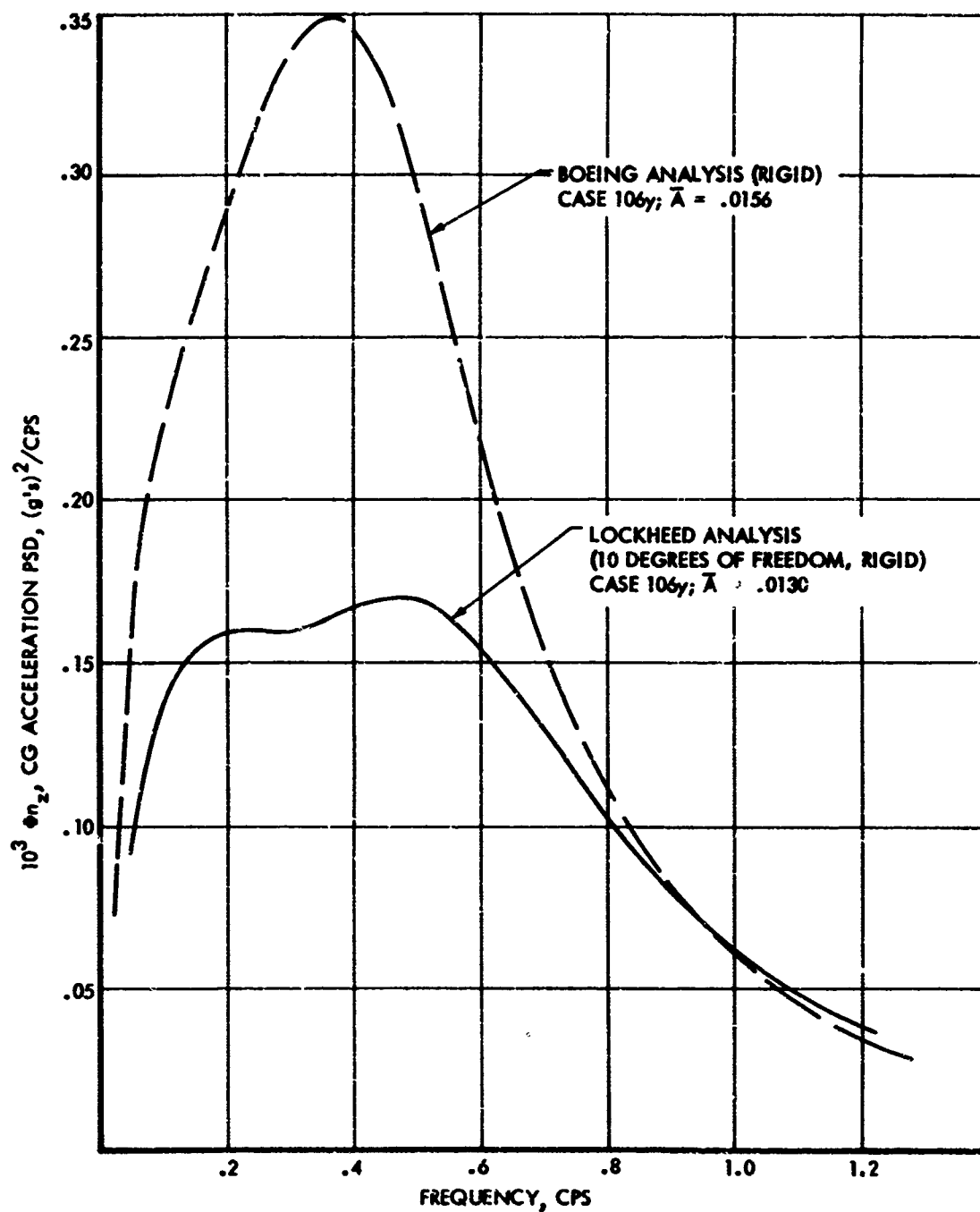


FIGURE 14-6. COMPARISON OF POWER SPECTRAL DENSITY OF CG ACCELERATION AS GIVEN BY BOEING AND LOCKHEED ANALYSES, MODEL 749

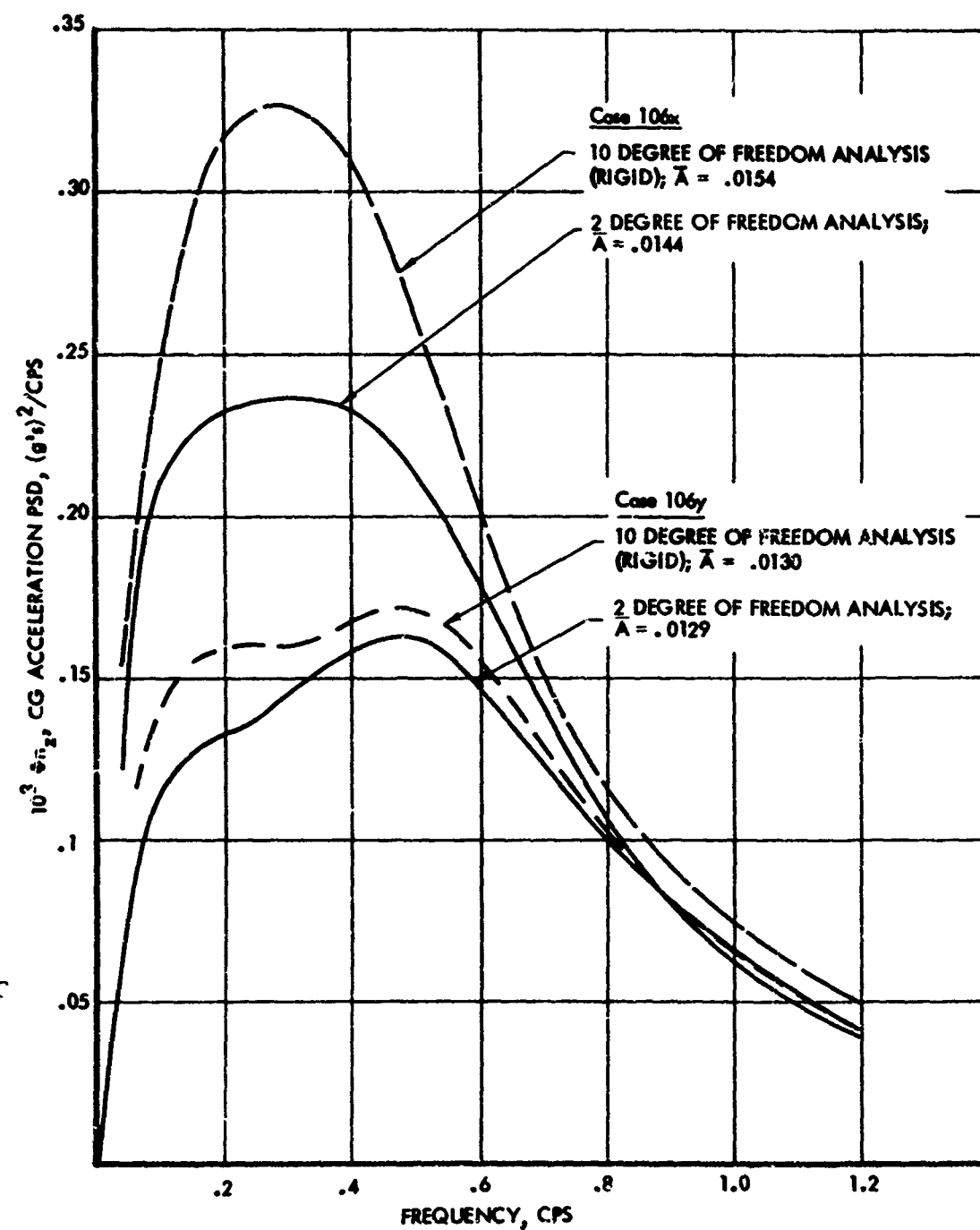


FIGURE 14-7. COMPARISON OF POWER SPECTRAL DENSITY OF CG ACCELERATION AS GIVEN BY TWO AND TEN DEGREE OF FREEDOM ANALYSES, MODEL 749

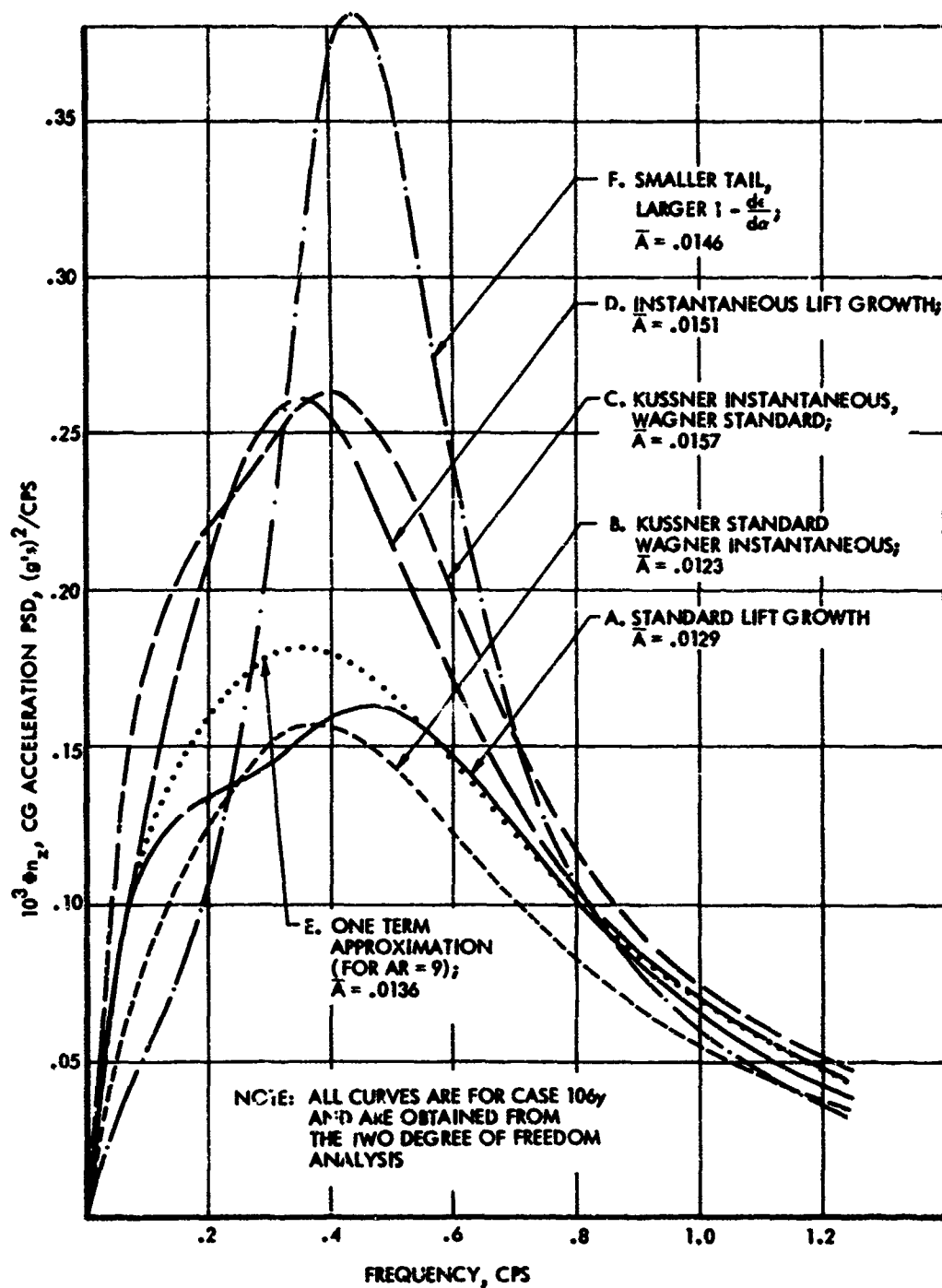


FIGURE 14-8. EFFECT OF LIFT GROWTH AND DOWNWASH ASSUMPTIONS ON POWER SPECTRAL DENSITY OF CG ACCELERATION, MODEL 749

TABLE 14-5. EFFECT OF ANALYSIS ASSUMPTIONS ON RELATIVE \bar{K} VALUES
FOR CG ACCELERATION, MODEL 749, CASE 106

Case	Analysis	Lift Growth Assumptions			Relative \bar{K} *		
		Kussner Function	Wagner Function	Wing Chord	Case 106x (Lockheed Configuration)		Case 106y (Boeing Configuration)
					Free to Plunge Only	Free to Plunge and Pitch	
A	2 DOF	3-Term	2-Term	MAC	.99	.89	1.00
B	2 DOF	3-Term	Instantaneous	MAC	.95	.86	.96
C	2 DOF	Instantaneous	2-Term	MAC	1.08	1.07	1.09
D	2 DOF	Instantaneous	Instantaneous	MAC	1.04	1.04	1.04
E	2 DOF	1-Term	1-Term	MAC	-	-	1.02
F**	2 DOF	3-Term	2-Term	MAC	-	-	1.00
G	10 DOF Rigid	3-Term	2-Term	MAC	-	.96	-
H	10 DOF Rigid	3-Term	2-Term	Local C	-	.96	-
I	Boeing Rigid	As described in Appendix A of Reference 1			-	-	-

*Relative \bar{K} of 1.00 corresponds to \bar{A} of .0161 g's/ft/s.

**In case F, tail area is divided by 1.83 and $(1 - d\bar{e}/d\bar{e})$ is multiplied by 1.83.

Inasmuch as the two-hump shape was much less pronounced for Case 106x than for Case 106y, it appeared that the difference in wing downwash assumptions between the two cases might be a significant factor in determining whether the Wagner lift growth would produce such a shape. Consequently, a case was run in which the tail area and the wing downwash at the tail were changed to the values associated with Case 106x, while the tail location was retained as in Case 106y. The result is shown by Curve F. For this case, the short period frequency decreased slightly, to .42 cps. The damping ratio, ζ , however decreased markedly, to .46.

While these results do not point to concrete conclusions, they do suggest that the differences between Boeing and Lockheed \bar{A} values might be due to an inter-related effect of differences in treatment of transient lift growth and aerodynamic induction. If the \bar{A} differences are indeed due to such a cause, rigid-airplane gust load factors are very much more sensitive to the assumptions made in these areas than had been realized heretofore.

The difference in rigid-airplane \bar{A} values between the Boeing and Lockheed analyses tends to be somewhat greater for wing load quantities, especially for bending moment in the critical region, than it does for c.g. acceleration (ratio of 1.36 vs 1.28). As a result, it appears that part of the difference in wing load \bar{A} 's may be due to a difference in the way in which the wing was divided into panels for analysis and masses and aerodynamic forces assigned to these panels.

The lack of closer agreement between the Boeing and Lockheed analyses does, of course, raise the question of the adequacy of the analyses upon which the calculated limit-strength values of $N(y)$ and $\sigma_w \eta_d$ for the three reference airplanes were calculated. It might appear that the Boeing analysis, with its more sophisticated treatment of aerodynamic induction effects, should give the more reliable results. However, it is believed that the Model 749 and Model 188 results obtained in this report may be very much closer to the correct values than would be implied by the comparisons shown in Figure 14-3, for the following reasons:

1. The two-hump shape of power-spectral density function given by the Lockheed analysis for Case 106y, and not appearing in the Boeing results, does not appear in the Lockheed analysis of Case 106x. If the Boeing analysis had actually been made for the configuration described by Case 106x, instead of the fictitious Case 106y, the difference might have been much less.
2. Airplane $C_{L\alpha}$ in the Boeing analysis is actually about 2 percent greater than in the Lockheed analysis, because the effect

on wing $C_{L\alpha}$ of upwash from the tail was not included in the Lockheed analysis (or in the tabulation given earlier of Case 106x and Case 106y $C_{L\alpha}$ values).

3. The lumping of masses and aerodynamic forces is very likely less realistic in the Boeing analysis of the Model 749 than in the Lockheed analysis of this airplane and the Model 188 and the Boeing analysis of the Model 720B.
4. The overestimation of the aerodynamic damping by the Lockheed analysis is at least partially offset, in determining limit-strength levels, by the fact that the structural damping is not included.

15 RECOMMENDED GUST DESIGN CRITERIA

In this section, three alternate forms of gust loads criteria are developed in detail. Finally, the selection of a recommended form is discussed.

15.1 Mission Analysis Criterion

15.1.1 Design Level of $N(y)$. In establishing a design value of $N(y)$, it is necessary to decide first whether the proposed gust loads criterion should be on a limit or an ultimate basis.

It is quite apparent, from a brief study of exceedance curves such as shown in Figures 9-8, 9-10, 9-12, and 9-14 (keeping in mind the limit strength $N(y)$ values obtained in Section 13) that airplanes occasionally experience gust loads substantially in excess of limit strength. The satisfactory safety record of current transport aircraft with respect to gust loads would undoubtedly not have prevailed were it not for the additional strength beyond limit provided by the 1.5 ultimate factor of safety.

As a result, there would be some logic in defining gust loads criteria on an ultimate rather than a limit basis.

On the other hand, the considerations favoring an ultimate basis for gust loads apply also, to greater or less degree, to various other loading conditions. At some future time, a thorough reconsideration of the limit load concept, as it applies to structural criteria generally, may be in order. For the present, it is believed desirable to restrict the scope of criteria changes to those directly related to the incorporation of the continuous turbulence description of the atmosphere.

Accordingly, design load levels will be defined herein on a limit basis. Should it be desired to convert at any future time to an ultimate basis, the results obtained in the present study will provide a ready means of establishing appropriate design levels.

It might be added that a further reason for hesitating to go to an ultimate basis for a gust loads criterion at this time is the progressively decreasing reliability of the model of the atmosphere as the load level increases.

Although it is proposed that an ultimate level not be considered explicitly in a gust criterion, it must be borne in mind that the safety of the aircraft still depends primarily upon its capacity to withstand

ultimate loads. As a result, there should be at least qualitative assurance that for the new airplane, as for current designs, the structural deformation and damage as the ultimate load level is approached are not so great as to prevent safe return of the airplane. Similarly, under conditions of turbulence corresponding to loads in excess of limit, functioning of all systems should remain such as not to jeopardize safe return of the airplane.

In setting a limit design value of $N(y)$, consideration is given first to a value for vertical gust analysis. For all three airplanes, the wing is more critical than the fuselage or tail. Limit strength values of $N(y)$ for the three airplanes, summarized in Figure 13-1, are as follows:

Model 188	2.1×10^{-5} cycles per hour
Model 749	1.8×10^{-5} cycles per hour
Model 720B	1.1×10^{-5} cycles per hour

These three values are remarkably close to each other. The full range from the lowest to the highest value corresponds to a variation in net load of only about 5%. In view of the satisfactory operational experience of all three airplanes, the least severe value - that is, the highest - is the rational choice for future design. Accordingly, a value of 2×10^{-5} is considered appropriate.

All evidence to date is that the atmospheric turbulence producing limit or ultimate loads on transport aircraft is essentially isotropic, and it has been so assumed in the present analyses. Consequently, the same value of $N(y)$ should logically be used for lateral gust loads as for vertical gust loads.

For both the Model 188 and Model 749, however, as indicated in Figure 13-1, loads in excess of limit strength occur more frequently for lateral gusts than for vertical gusts. $N(y)$ values for the three airplanes for lateral gust loads are:

Model 188	6×10^{-5} cycles per hour
Model 749	2.5×10^{-4} cycles per hour
Model 720B (yaw damper off;	9×10^{-6} cycles per hour

It is seen that, even with yaw damper off, the Model 720B is considerably less critical than the Model 188 and Model 749. Considering the latter two airplanes, an appropriate limit design value of $N(y)$ would lie in the

range 6×10^{-5} to 2.5×10^{-4} exceedances per hour. Again, the least severe value - that is, the highest - is the rational choice for design. Thus a value of 2.5×10^{-4} would be selected.

This is higher by a factor of 12.5 than the value of 2×10^{-5} considered appropriate based on vertical gust. Based on Figure 13-2, it represents a load level of roughly 76% of that associated with the 2×10^{-5} exceedance rate.

Three alternatives are available at this point:

- (1) Design for both vertical and lateral gusts at the less severe $N(y)$, of 2.5×10^{-4} exceedances per hour, at which limit strength of the reference airplanes is reached due to lateral gusts.
- (2) Design for vertical gust loads at the vertical gust frequency of exceedance of limit strength, $N(y) = 2 \times 10^{-5}$ exceedances per hour; and design for lateral gust loads at the lateral gust frequency of exceedance of limit strength, 2.5×10^{-4} exceedances per hour.
- (3) Design for both vertical and lateral gust at the more severe $N(y)$, of 2×10^{-5} exceedances per hour, at which limit strength is reached due to vertical gusts.

The first of these - use of the less severe frequency of exceedance - is, on the surface, the logical course. If 2.5×10^{-4} exceedances per hour is really the exceedance rate for limit strength due to lateral gust loads, there is no apparent reason why this same exceedance rate should not be equally acceptable for vertical gust loads. (In fact, it might even be argued that an even less severe limit frequency of exceedance of vertical gust loads might be justified, in order to maintain a more nearly comparable frequency of exceedance of ultimate load.) This course, however, is considered unacceptable. Experience in conducting vertical gust analyses and comparing the results with measurements on airplanes in flight has been accumulating for many years. The state of the art of lateral gust analysis, however, is much less advanced. Furthermore, it appears that the results of a lateral gust analysis may be considerably more subject to variation depending upon the aerodynamic input data used and, even more, upon the assumptions made regarding pilot action. Consequently, a reduction in the design levels to be used for wing design, based on the results of the lateral gust analysis cannot be justified at this time.

The second alternative, to have different values of $N(y)$ for vertical and lateral gust analysis, would appear to have some merit, especially as an interim measure. However, this alternative, too, is considered unacceptable, for two reasons.

First, the conclusion has already been reached that the higher (less severe) $N(y)$ derived from the lateral analysis cannot be justified for use in the vertical analysis, because of concern that the lateral analysis may overestimate the loads. But if the lateral gust analysis does overestimate the loads, advances to be expected in the state of the art of lateral gust analysis will undoubtedly lead soon to analyses that do not overestimate the loads. At that time, if an artificially high value of $N(y)$ has been adopted - in effect to compensate for conservatism in the analysis - unsafe loads will result. If the higher $N(y)$ value cannot be justified for vertical gust loads, a comparable hazard exists with respect to its use for lateral gust loads.

Second, the lack of theoretical consistency would be liable to lead to confusion in application. Complexities would arise, for example in application to stresses produced by the combined action of lateral and vertical gusts. Fortunately, the greater part of the structure of current aircraft can be considered to be stressed either by vertical gusts alone or by lateral gusts alone. Yet even in present aircraft, some regions, such as the aftbody and the engine nacelles, can be stressed by lateral and vertical gusts simultaneously. For proposed delta and arrow wing configurations with vertical fins on the wind tips, rational superposition of vertical and lateral gust loads would be imperative.

Thus the second alternative, like the first, is seen to be unacceptable.

This leaves, as a final alternative, adoption of the lower (more severe) value of $N(y)$ for both lateral and vertical gust analysis.

As indicated by Figure 9-12 in combination with the discussion in Appendix E, Section E.5, design of the Model 188 to this more severe criterion would have resulted in an 11% increase of strength of the vertical tail. Similarly, as indicated by Figure 9-14, an increase in tail strength of 30% would have been required for the Model 749.

To adopt a criterion that present satisfactory aircraft do not meet is not an attractive course of action. On the other hand, the percentage increase in strength that would be indicated for the Model 188 is probably no greater than the range of uncertainty that characterizes many theoretical loads determinations. Further, as noted above, it is quite possible that future improvements in our capability of predicting lateral gust loads may lead to lower predicted loads at the same frequency of exceedance.

It is believed that reasonable means could be found, even now, to reduce calculated lateral gust loads to levels comparable to limit strength of the Model 188 and Model 749, if a new airplane similar to those were to be designed today. The high tail loads shown by the analysis are associated with low damping in the Dutch roll mode. But with this low damping, the yaw response will tend to be a fairly pure sinusoid of only gradually varying amplitude. The relatively narrow band width of the yaw response relative to the vertical gust response is illustrated in Figures 15-1 and 15-2. It would appear that such a motion, at typical Dutch roll frequencies, could be controlled fairly effectively by the pilot. Flight tests reported in Reference 25, in fact, confirm this possibility. For a large swept wing airplane flying at $M = 0.6$ at 21,000 ft., use of a yaw damper effected roughly a 50% reduction in loads, relative to a damper off, "hands-off" case. But action by the pilot, without the damper, also reduced the loads, by about half this amount, or 25%. An arbitrary increase in the relative damping constant, ζ , by .05, through inclusion of a rudder angle proportional to yaw velocity, would appear to be a simple yet realistic way to account for pilot action, as long as the Dutch roll frequency does not exceed about .3 or .4 cps. This would increase the Dutch roll damping for the Model 188 (for Mission Analysis Case 202) from very roughly $\zeta = .14$ to $\zeta = .19$. The tail load would then decrease roughly in the ratio $\sqrt{.14/.19} = 1/1.17$. For airplanes having greater damping, pilot action would be less effective because of the broader frequency band of the yaw motion. But in such cases, the addition of the constant $\zeta = .05$ would have a much smaller - or even negligible - effect on the loads.

15.1.2 Treatment of Stability Augmentation. When stability augmentation systems are relied upon to reduce the gust loads, provision must be made for malfunction of the system. This can be done easily in a mission analysis by including an appropriate amount of flight time with the system inoperative. Selection of the percent of time that the system is inoperative must, of course, be based upon substantiable estimates of the reliability of the system.

In the incorporation of a stability augmentation system in the dynamic analysis, care must be taken to account for the effect of "saturation" of the system on loads at the limit design level. Such saturation may result from a specifically limited system authority, other nonlinearities within the system, or aerodynamic nonlinearities in the control surface force-displacement relationship. Time history studies in which these nonlinearities are specifically included may be helpful in establishing adequate linearizations for use in the power spectral analysis. Some earlier experience (unpublished) indicates that, as the gust intensity is increased beyond the level where the control system "stops" are first reached, the effectiveness of the stability augmentation system decreases quite slowly. Consequently, no sudden decrease in effectiveness as the ultimate load level is approached is to be expected.

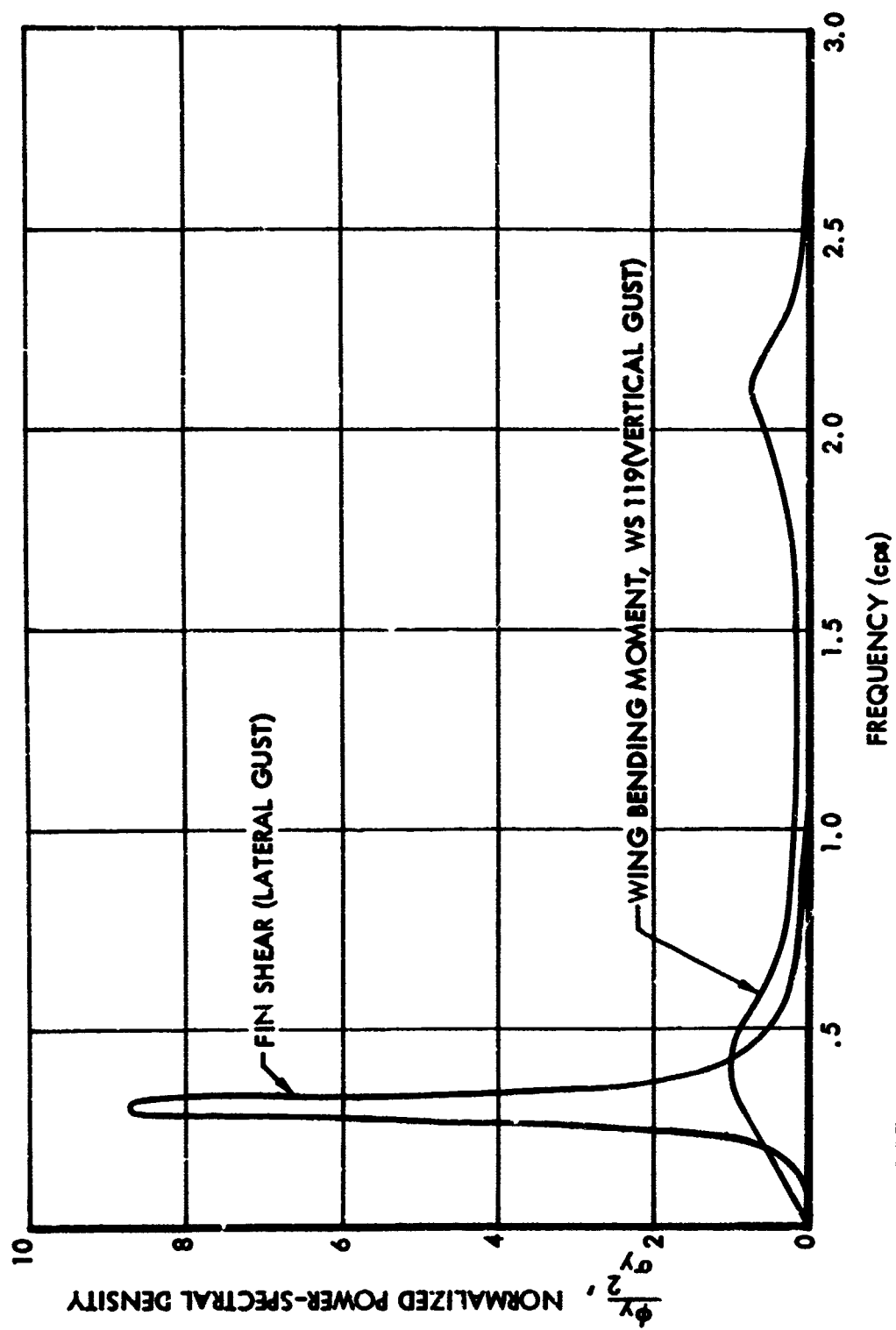


FIGURE 15-1. COMPARISON OF POWER SPECTRAL DENSITIES OF VERTICAL AND LATERAL GUST LOADS, MODEL 188

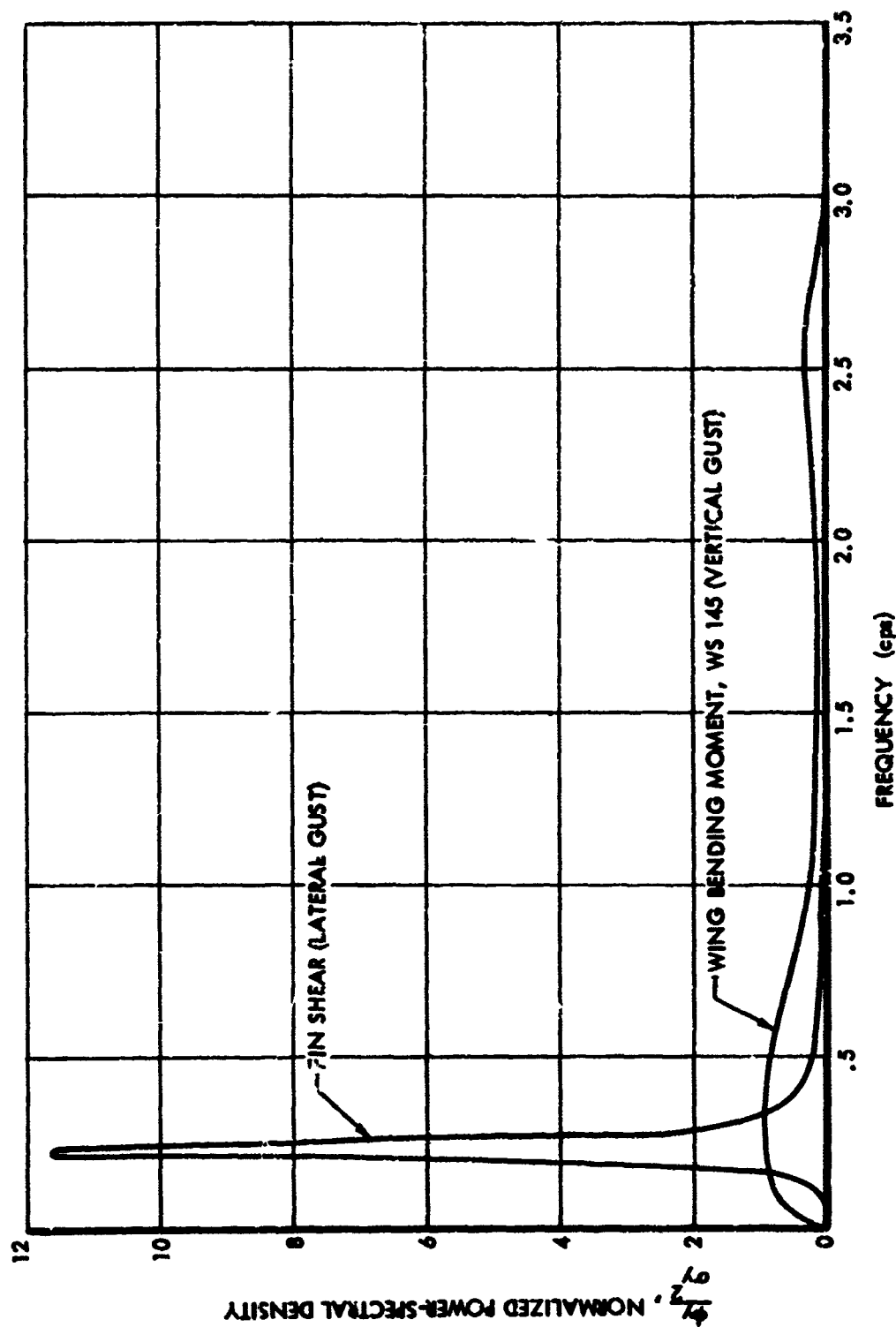


FIGURE 15-2. COMPARISON OF POWER SPECTRAL DENSITIES OF VERTICAL AND LATERAL GUST LOADS, MODEL 749

15.1.3 Fail Safe Design Level. The use of a mission analysis form of gust criterion can be expected to facilitate a rational determination of fail safe design levels. Such a determination would relate the fail safe frequency of exceedance to the inspection period and to the expected frequency of occurrence of potentially dangerous cracks. The procedure to be used is not self-evident, however, and its development is beyond the scope of the present study.

For the present, therefore, it is suggested that the fail safe level be set to be roughly consistent with existing fail safe requirements. Currently specified U_{de} values (for the altitude range 0 - 20,000 ft.) are as follows:

<u>Speed</u>	<u>U_{de}, Fail Safe</u>	<u>U_{de}, Limit</u>	<u>Ratio</u>
V_B	49 fps	66	.74
V_C	33 fps	50	.66
V_D	15 fps	25	.60

From Figures 9-8(b), 9-10(b), 9-12, and 9-14, a factor of .66 applied to the gust increment, at a limit-strength frequency of exceedance of 2×10^{-5} cycles per hour, is found to give approximately 1×10^{-3} cycles per hour. This value is therefore suggested for use as a design ultimate fail safe frequency of exceedance.

15.1.4 Modified Design $N(y)$ For Use in Joint Probability Analysis. In Section 12.3, it was pointed out that the joint probability technique will indicate a greater number of crossings of the limit load level per hour than will the matching condition technique. With the joint probability technique, all crossings of the strength envelope are counted, whereas with the matching condition technique, crossings are counted for only one straight line at a time.

In establishing limit strength values of $N(y)$ for the reference airplanes, it was necessary to bring all three airplanes onto a common basis for comparison. For this purpose, the Model 720B $N(y)$ values were converted to a matching condition, or single parameter, basis, by dividing by an estimated ratio of joint probability exceedances to single-parameter exceedances. This ratio was taken as 2.0.

Use of some such factor would also be appropriate for new design in order to avoid a conservative result when the joint probability technique is used. If, for example, the factor of 2.0 were retained, the design frequency of exceedance for use with the joint probability technique would be $2.0 \times (2 \times 10^{-5} \text{ cycles per hour}) = 4 \times 10^{-5} \text{ cycles per hour}$.

As a result of the discussion in Section 12.4, however, it appears that a factor of 2.0 is too great and that a value of 1.3 to 1.5 would be more

appropriate. The resulting difference in incremental load, however, then becomes so small (only 2 or 3%) that use of separate values of frequency of exceedance is not warranted. Consequently, the same value - 2×10^{-7} cycles per hour - will be used with both the matching condition and the joint probability techniques.

15.1.5 Combined Vertical and Lateral Gust Loads. In the past, it has not been customary to superimpose loads due to vertical and lateral gusts. Various important parts of an airplane, such as the wing and the vertical tail, obviously are loaded almost exclusively by vertical gusts or lateral gusts alone. But various parts of the fuselage, as well as engine nacelles on propeller driven airplanes, clearly are stressed by both vertical and lateral gusts. Power spectral theory now provides excellent guidance as to the manner in which gusts in the two directions combine; and it has become clear that failure to account for such combination can lead to structure that is under-strength relative to that required, for example, for the wing and vertical tail. It is generally accepted that, within any patch of turbulence, vertical and lateral gust velocities can properly be assumed to be uncorrelated. Under this condition, it can be shown that the appropriate design stress in any structural element is

$$\sqrt{f_v^2 + f_L^2} ,$$

where f_v and f_L are the design-level stresses due to the vertical and lateral components of turbulence individually.

Combinations of vertical with lateral gust loads were not considered explicitly in the analysis of the reference airplanes. It is believed that for these airplanes, such consideration would lead to only slight modifications in the limit strength values of $N(y)$ and $\sigma_w \eta_d$. And as brought out in Section 15.1.1, an increase in $N(y)$ (or a decrease in $\sigma_w \eta_d$) as given by the lateral gust analysis would probably not affect the value selected for future design.

In the design of a new airplane, however, it is believed that combination of vertical and lateral gust loads must be realistically or conservatively accounted for in those portions of the vehicle for which such combination is potentially critical. It is seen from the expression given above for the total incremental stress that this stress can be as much as 1.414 times f_v or f_L alone, for the limiting case in which f_v and f_L are equal.

The above discussion applies to a design envelope type of criterion (Section 15.2) as well as to a mission analysis type of criterion.

15.1.6 Suggested Formal Requirement. The following is suggested as a formal statement of a gust loads requirement based upon the mission analysis concept.

- (a) The limit gust loads shall be determined utilizing the continuous turbulence concept in accordance with the provisions of Paragraphs (b) through (h) following.
- (b) The expected utilization of the airplane shall be represented by one or more flight profiles in which the payload and the variation with time of speed, altitude, gross weight, and center of gravity position are defined. These profiles shall be divided into mission segments, or blocks, for analysis, and average or effective values of the pertinent parameters defined for each segment.
- (c) For each of the mission segments defined under Paragraph (b) and each of the load and stress quantities selected in accordance with Paragraph (e) below, values of \bar{A} and N_0 shall be determined by dynamic analysis. \bar{A} is defined as the ratio of root-mean-square load to root-mean-square gust velocity and N_0 as the radius of gyration of the load power-spectral density function about zero frequency. The effects of all pertinent rigid and elastic degrees of freedom shall be included. The power-spectral density of the atmospheric turbulence shall be as given by the equation,

$$\phi(\Omega) = \frac{\sigma^2 L}{\pi} \frac{1 + \frac{8}{3} (1.339 L \Omega)^2}{[1 + (1.339 L \Omega)^2]^{11/6}}$$

where

ϕ = power-spectral density

σ = root-mean-square gust velocity

Ω = reduced frequency, radians per foot

L = 2500 ft.

- (d) For each of the load and stress quantities selected in accordance with Paragraph (e) below, the frequency of exceedance shall be determined as a function of load level by means of the equation,

$$N(y) = \sum t N_o \left[P_1 \exp \left(-\frac{y - y_{one-g}}{b_1 \bar{A}} \right) + P_2 \exp \left(-\frac{y - y_{one-g}}{b_2 \bar{A}} \right) \right]$$

where

y = net value of the load or stress

y_{one-g} = value of the load or stress in one-g level flight

$N(y)$ = average number of exceedances of the indicated value of the load or stress in unit time

\sum = Symbol denoting summation over all mission segments

t = fraction of total flight time in the given segment

N_o, \bar{A} = parameters determined by dynamic analysis as defined in Paragraph (c)

P_1, P_2, b_1, b_2 = parameters defining the probability distribution of root-mean-square gust velocity, to be read from Figures 5-3 and 5-4 herein.

The limit gust loads shall be read from the frequency of exceedance curves at a frequency of exceedance of 2×10^{-5} exceedances per hour. Both positive and negative load directions shall be considered in determination of the limit loads.

- (e) A sufficient number of load and stress quantities shall be included in the dynamic analysis to assure that stress distributions throughout the structure are realistically or conservatively defined.
- (f) If the joint probability technique, as described in Sections 10 and 12 herein and more particularly in Reference 1, is employed, the frequency of exceedance of limit strength shall not be greater than 2×10^{-5} exceedance per hour.
- (g) For structural components that are stressed significantly by both the vertical and lateral components of turbulence, the resultant stress shall be determined assuming that, within any patch of turbulence, the vertical and lateral components are uncorrelated. For example, in a structural element subjected to a single stress, the resultant stress shall be taken as given by

$$\sqrt{f_v^2 + f_L^2} \quad ,$$

where f_v and f_L are the stresses due to the vertical and lateral components of turbulence respectively.

- (h) If a stability augmentation system is utilized to reduce the gust loads, a conservative estimate shall be made of the fraction of flight time that the system may be inoperative. The flight profiles of Paragraph (b) shall include flight with the system inoperative for this fraction of the flight time. When a stability augmentation system is included in the analysis, the effect of system nonlinearities on loads at the limit load level shall be realistically or conservatively accounted for.
- (i) The fail safe gust loads defined in FAR 25.571(c)(2) shall be replaced by loads defined as in Paragraphs (a) through (h) above at a frequency of exceedance of 1×10^{-3} exceedances per hour.

15.2 Design Envelope Criterion

15.2.1 Design Levels of $\sigma_w \eta_d$ at Speed V_C . For the design envelope criterion, as for the mission analysis criterion, design levels will be defined herein on a limit load basis. The reasons for preferring a limit to an ultimate basis are the same for the design envelope criterion as for the mission analysis criterion and are discussed in Section 15.1.1. Precautions necessary in designing to a limit criterion are also noted in Section 15.1.1.

Design values of $\sigma_w \eta_d$ for use at the design cruise speed, V_C , are considered of basic importance and will be developed first. In the next section, the treatment of V_B and V_D gust conditions will be discussed.

Limit strength values of $\sigma_w \eta_d$ at speed V_C for the major components of the three reference airplanes are summarized in Figures 13-3 and 13-4. The limit design value to be established for $\sigma_w \eta_d$ will, of course, vary with altitude in accordance with the lines of constant $N(y)/N_0$ shown in Figure 13-3 and in Figure 5-8. In discussing possible selections of limit design $\sigma_w \eta_d$, the various constant $N(y)/N_0$ lines in Figure 13-3 (or Figure 5-8) will be identified, for convenience, by the $\sigma_w \eta_d$ value at 7000 ft. Thus reference to a $\sigma_w \eta_d$ value of 70, for example, will

actually denote a $\sigma_w \eta_d$ variation with altitude as given by the line $N(y)/N_0 = 5 \times 10^{-7}$.

As in the discussion of a limit design value of $N(y)$, attention will be directed first toward limit-strength results for vertical gust.

For all three airplanes, the wing is seen to be more critical than the fuselage or tail. Limit strength values of $\sigma_w \eta_d$ for the three airplanes (adjusted to an altitude of 7000 ft.) are as follows:

Model 188	62 fps
Model 749	88 fps
Model 720B	108 fps

Again, the logical selection is the lowest value, or 62 fps.

Whatever value of $\sigma_w \eta_d$ might be picked based upon the analysis of the reference airplanes, there is a possibility that a new airplane might normally operate closer to its design envelope than do the reference airplanes. There can be no assurance, of course, that an adequate strength level will be defined for such an airplane. But the only means of providing for this contingency would be to establish a $\sigma_w \eta_d$ level higher than can be met by the existing airplanes. A new airplane similar to the reference airplanes could then meet the criterion only by an increase in strength (and weight) or by a reduction in speed and payload placards, with the attendant loss in operating flexibility and economy.

This dilemma is inherent in the design envelope approach, and possibly it should not be taken too seriously. It may well be that economic pressures will continue to demand operating placards - and hence design envelopes - considerably in excess of normal operational speeds and payloads. Nevertheless, it is pertinent to inquire whether perhaps the lowest figure in the above list of limit strength $\sigma_w \eta_d$'s may not represent an operation where placard speeds and payloads are more than ordinarily in excess of the normal operational values.

For this purpose, the Model 188 is compared with the Model 749. For the five Model 188 mission analysis cases contributing most to the total load exposure in Figure 9-9 (b), the average ratio of V_C placard speed to mission speed is 1.14. For the seven Model 749 mission analysis cases contributing most to the total in Figure 9-11(b), the average ratio is 1.10. Thus the amount by which the Model 188 placard speed exceeds the normal operational speed is only 14%, which is judged to be rather typical. Further, the ratio of placard to typical speed for the Model

188 is only 4% greater than for the Model 749, and it is known, because of the source of the data, that the Model 749 mission speeds were taken on the high side if anything. It is concluded that the ratio of placard to normal operational speeds for the Model 188 is not out of line.

With respect to payloads, it appears that neither the Model 188 nor the 749 ordinarily carry significant amounts of cargo. A bare-minimum zero fuel weight placard that might more closely reflect actual operations of the two airplanes could be derived as follows. It would make provision for capacity passengers (96 in the Model 188, 62 in the Model 749) at 200 lb. plus a nominal 500 lb. of cargo:

	Model 188	Model 749
Operating weight empty	62000 lb.	68640 lb.
Passengers	19200	12400
Cargo	<u>500</u>	<u>500</u>
Zero fuel weight	81700	81500

The actual placard zero fuel weights, used in the analysis, are 86000 lb. and 86464 lb. respectively. It is seen that the difference between the placard zero fuel weight and the bare-minimum design zero fuel weight as derived above is almost identical for the two airplanes. Again, there is no evidence that the Model 188 is out of line, even though the normal operational zero fuel weight is somewhat lower for the Model 188 (74500 lb.) than for the Model 749 (78100 lb.).

Consequently, the value of $\sigma_w \eta_d$ of 62 fps at 7000 ft. appears to be a legitimate value for limit design.

For lateral gust loading, the limit strength values of $\sigma_w \eta_d$ (adjusted to an altitude of 7000 ft.) are:

Model 188	61 fps
Model 749	65 fps
Model 720B (yaw damper off)	99 fps

As these values are approximately equal to or greater than the appropriate vertical gust design value of 62 fps, the vertical gust value is simply retained for use in lateral gust analysis. The evidence of possible conservatism in current methods of lateral gust analysis, discussed in Section 15.1.1, is still pertinent, however.

It is concluded that the appropriate limit design value of $\sigma_v \eta_d$ for both vertical and lateral gust analysis is defined by a constant $N(y)/N_0$ line in Figure 5-8 such as to give a $\sigma_v \eta_d$ of approximately 62 at an altitude of 7000 ft.

15.2.2 Gust Conditions at V_B and V_D . As indicated in Section 4.2, it is considered appropriate that a design envelope criterion include design gust intensities at V_B and V_D as well as at V_C , paralleling in this respect the current discrete gust requirements.

With respect to a design intensity at V_D , the limit strength $\sigma_v \eta_d$ at V_D for the critical airplane (the Model 188) is just 25/50 of the V_C value. Consequently, it is recommended that the current ratio of V_D to V_C design U_{de} 's be retained in the power-spectral criterion.

This ratio can be applied throughout the altitude range; or it can be applied at a single altitude considered representative of current aircraft and a constant $N(y)/N_0$ line in Figure 5-8 followed. In the latter case, the ratio of V_D to $V_C \sigma_v \eta_d$'s would vary slightly with altitude.

This approach is perhaps slightly more reasonable; but the difference is fairly small, the logic is not compelling, and the decision is perhaps best based on convenience.

With respect to a design intensity at V_B , it was noted in Section 13 that the lowest limit-strength $\sigma_v \eta_d$ at V_B for any of the three reference airplanes is well in excess of 66/50 of the V_B limit strength value for Model 188 (62 fps at 7000 ft), selected in Section 15.2.1 above as the V_C design value. As a result, it is considered appropriate to retain, in the power spectral criterion, the 66/50 ratio of V_B to V_C gust intensities that was selected when the present discrete-gust criteria were established. This ratio, like that for the V_D intensity, can be applied as a constant ratio at all altitudes, or it can be applied at a single representative altitude and a constant $N(y)/N_0$ line in Figure 5-8 followed.

For consistency with present discrete gust criteria, it is proposed that the V_B speed be defined as the lowest speed at which stall would not occur at a load level given by the $\sigma_v \eta_d$ value defined for design at V_B .

An example of how this speed might be determined is given in Appendix E, Section E.1.3.

15.2.3 Adjustment of Design Loads for Differences in N_0 . The maximum load to be expected in traversing either a given patch of turbulence, or a series of patches of various intensities, depends not only upon \bar{A} but also upon N_0 . The higher the N_0 value, the higher will be the expected maximum load. In Section 4.2, the design value of a load quantity y was given as

$$y_{\text{design}} = \bar{A} (\sigma_w \eta_d) \quad (15-1)$$

To account for the effect of N_0 , the appropriately modified expression is

$$y_{\text{design}} = \bar{A} (\sigma_w \eta_d) \left[1 + \frac{2.306 b_2}{\sigma_w \eta_d} \log_{10} \frac{N_c}{N_{0_{\text{ref}}}} \right] \quad (15-2)$$

In this expression, $\sigma_w \eta_d$ is the design value established as in Section 15.2.1 or 15.2.2, independently of N_0 . $N_{0_{\text{ref}}}$ is the N_0 value for the load quantities that established the limit-strength $\sigma_w \eta_d$ for the critical reference airplane. The appropriate value of $N_{0_{\text{ref}}}$ is approximately 1.4 cps. This was determined by examining the N_0 values for bending moments, shears, torsions, and front beam shear flows in the critical region of the Model 182 wing (WS 83-167).

The above expression (Equation 15-2) is derived by considering the generalized exceedance curve at the appropriate altitude, as given, for example, in Figure 5-5. With the design $N(y)$ considered fixed, it is clear that the design $N(y)/N_0$ will vary depending on N_0 ; hence the design y/\bar{A} and the design y will also vary with N_0 . This variation takes the simple form indicated by Equation 15-2 because in the region of limit load the generalized exceedance curve is a straight line governed by the storm turbulence contribution alone.

For an average b_2 value of 10 and an average design $\sigma_w \eta_d$ of 60 (appropriate average values over the altitude range 0 to 30,000 ft.), the factor in the brackets in Equation 15-2 becomes

$$\left[1 + .39 \log_{10} \frac{N_0}{N_{0_{\text{ref}}}} \right]$$

Based on this expression, a factor of 2 increase in N_0 is found to result in an 11% increase in design incremental load or stress.

It is of interest to note that, under a mission analysis criterion, a factor of 2 increase in N_0 results in only about a 7% increase in incremental load, in contrast to the 11% increase under the design envelope criterion. This difference results from the fact that, in Equation 15-2, $\sigma_w \eta_d$ is equal to $y_{\text{design}}/\bar{A}$, where \bar{A} is inherently smaller for typical mission segments than for critical design envelope points.

The "exact" expression for y_{design} given by Equation 15-2 is available for use if desired. However, it is believed preferable, if the design envelope criterion is used, to retain the simpler form given by Equation 15-1. Any increase in accuracy due to consideration of N_0 is in part illusory. It has already been noted that, under a mission analysis criterion, the effect of a difference in N_0 is less than under a design envelope criterion. Since the mission analysis criterion probably gives the truer picture of the strength actually required, use of Equation 15-2 would appear, therefore, to over-correct for differences in N_0 . Further, numerical values of N_0 are subject to considerable uncertainty. They are often sensitive to the upper limit of integration used in their numerical evaluation, and in fact, there is a very good possibility that the theoretical value will be infinite in some practical cases. As a result, it is believed that, in choosing between Equation 15-1 and 15-2 for design use, the practical advantages offered by use of Equation 15-1 outweigh the greater theoretical accuracy of Equation 15-2.

15.2.4 Treatment of Stability Augmentation. When stability augmentation systems are relied upon to reduce gust loads, provision must be made for malfunction of the system. As in the mission analysis form of criterion a percent of flight time that the system will be inoperative must be assumed. This must be substantiable, based upon either analysis or actual service records of the reliability of the system.

The objective now should be to establish $\sigma_w \eta_d$ levels such that the over-all frequency of exceedance of design limit load, at each design envelope point, is no greater for an airplane with stability augmentation than for an airplane without. This frequency of exceedance is, of course, measured by $N(y)/N_0$ in Figure 5-8.

As a first approximation, at least, it would appear plausible simply to establish a reduced value of $\sigma_w \eta_d$ for use with the system inoperative.

With the system operating, the "basic" $\sigma_w \eta_d$ value as established in Section 15.2.1 would be retained. An appropriate system-off value of $\sigma_w \eta_d$ would be determined by means of Figure 5-8. Letting p denote the fraction of time the system is inoperative, the system-off $\sigma_w \eta_d$ would simply be defined by an $N(y)/N_0$ value equal to $1/p$ times the "basic" $N(y)/N_0$. For example, suppose the basic $N(y)/N_0$ to be 1.0×10^{-6} and p to be .01. $N(y)/N_0$ for system-off design would then be $(1/.01)(1.0 \times 10^{-6}) = 1.0 \times 10^{-4}$. The resulting system-off $\sigma_w \eta_d$ (at 7000 ft.) would be 28 fps, as compared to the 64 fps value system on. Based upon system-off operation alone, the overall $N(y)/N_0$ is then $(1.0 \times 10^{-4})(.01) = 1.0 \times 10^{-6}$, which is the same as the design value system-on.

If the system-on loads are well below the system-off loads (each obtained using its appropriate $\sigma_w \eta_d$), the contribution of the system-on loads to the overall $N(y)/N_0$ will be negligible and can be disregarded. The airplane with a stability augmentation system will then have an overall $N(y)/N_0$ (at the given design envelope point) no greater than the airplane without, and the objective will have been met.

This simple approach can be seen to be unconservative, however, if the system-off and system-on operation are equally critical. For the given example, the overall $N(y)/N_0$ is now 1.99×10^{-6} , obtained as follows:

$$\text{System on: } N(y)/N_0 = (.99)(1.0 \times 10^{-6}) = .99 \times 10^{-6}$$

$$\text{System off: } N(y)/N_0 = (.01)(1.0 \times 10^{-4}) = \underline{1.00 \times 10^{-6}}$$

$$\text{Net: } N(y)/N_0 = 1.99 \times 10^{-6}$$

This value of $N(y)/N_0$ is nearly twice as great as the assumed "basic" value of 1.00×10^{-6} that would apply to an airplane that did not depend upon a stability augmentation system. In fact, it is rather clear that under the above simple approach, whenever the system-on loads are critical, the airplane having a stability augmentation system is bound to be less safe than the airplane that does not require such a system. This conclusion is valid no matter what the system-off design level may be - except, of course, if the system-off design level were no lower at all than the system-on level or if the system were absolutely reliable. One might, of course, consider system-on and system-off operation to be two different flight conditions to be treated independently, just like two different gross weights. But in treating two gross weights, the same $\sigma_w \eta_d$ value is used for both, whereas here consideration is being given to a reduced severity for one of the two conditions. It is hard to see how a criterion could be justified that would clearly permit a higher frequency of exceedance of limit strength for an airplane that depends upon a stability augmentation system than one that does not.

If, in the above example, the design $N(y)/N_0$ values for both system-on and system-off cases were decreased by a factor of 2 (resulting in increased $\sigma_w \eta_d$'s), the net $N(y)/N_0$ would then be approximately 1.0×10^{-6} , as desired. To accomplish this decrease would require an increase of strength. Based upon the system-on loads, it can be seen that the required increase in strength would be in the ratio $70.5/64 = 1.10$. Based on the system-off loads (actually off scale in Figure 5-8) it would be somewhat higher. The actual required ratio would be between the two values, probably about 1.12. No reasonable decrease in $N(y)/N_0$ (i.e., increase in $\sigma_w \eta$) for the system-off case alone will give a net $N(y)/N_0$ equal to the desired value. $N(y)/N_0$ values or $\sigma_w \eta_d$'s for both system-off and system-on cases must be modified.

If it were desired as a matter of convenience to alter only the system-off $N(y)/N_0$, the 12% unconservatism could be reduced. For example, if the system-off $N(y)/N_0$ were to be specified as $1/2p$, instead of $1/p$, times the basic value, then the overall $N(y)/N_0$ would be (still assuming the airplane to be equally critical system-off and system-on):

$$\begin{aligned} \text{System on: } N(y)/N_0 &= (.99)(1.0 \times 10^{-6}) = .99 \times 10^{-6} \\ \text{System off: } N(y)/N_0 &= (.01)(5 \times 10^{-5}) = .50 \times 10^{-6} \\ \text{Net: } N(y)/N_0 &= 1.49 \times 10^{-6} \end{aligned}$$

An increase of strength of about 7% would be required in this case to achieve the desired net $N(y)/N_0$ of 1.0×10^{-6} . Conversely, the use of the simplified criterion could still lead to an airplane that would be understrength by 7% (of the gust increment) relative to the airplane without a stability augmentation system.

If the system-off $N(y)/N_0$ were to be specified as $1/3p$, instead of $1/p$ or $1/2p$, times the basic value, the 7% unconservatism would decrease to about 5%.

The above percentages have been found not to be sensitive to the value of p assumed.

To eliminate the unconservatism associated with modification of only the system-off $\sigma_w \eta_d$, both system-off and system-on $\sigma_w \eta_d$'s must be altered. A fully rational approach would be to select arbitrarily values of $N(y)/N_0$ system-off and system-on such as to satisfy the equation,

$$p \left(\frac{N(y)}{N_0} \right)_{\text{system-off}} + (1 - p) \left(\frac{N(y)}{N_0} \right)_{\text{system-on}} = \left(\frac{N(y)}{N_0} \right)_{\text{basic}}$$

This equation is satisfied, for example, by taking

$$\left(\frac{N(y)}{N_0}\right)_{\text{system-off}} = \frac{1}{2p} \left(\frac{N(y)}{N_0}\right)_{\text{basic}}$$

and

$$\left(\frac{N(y)}{N_0}\right)_{\text{system-on}} = \frac{1}{2(1-p)} \left(\frac{N(y)}{N_0}\right)_{\text{basic}} \approx \frac{1}{2} \left(\frac{N(y)}{N_0}\right)_{\text{basic}}$$

leading to a system-on $\sigma_w \eta_d$ 10 to 12% greater than the basic value, depending upon altitude. This special case will provide a useful rule-of-thumb, but it is believed desirable to provide the flexibility offered by use of the above equation without individually specified values of $N(y)/N_0$ system-off and system-on.

The comments made in Section 15.1.2 with respect to system nonlinearities are equally applicable in connection with a design envelope type of criterion.

15.2.5 Fail Safe Design Level. As in connection with the mission analysis form of criterion, it is considered appropriate to retain the ratios of fail safe gust intensity to limit design gust intensity currently in use on a U_{de} basis. Thus to determine fail safe values of $\sigma_w \eta_d$, the V_C limit design value at any given altitude should be multiplied by the following factors, based upon the tabulation in Section 15.1.3:

$$V_C: \quad = .66$$

$$V_D: (.50)(.60) = .30$$

If preferred, these ratios can be applied instead at a single representative altitude and a constant $N(y)/N_0$ line in Figure 5-8 followed.

15.2.6 Design Levels of σ_w and P. For analyses in which the joint probability technique is employed, design values of σ_w and of P, the allowable probability that limit strength is exceeded, rather than of $\sigma_w \eta_d$, are necessary.

Based upon the results given in Reference 1 and in Section 12.3 herein, a value of η_d of 3.5 is considered appropriate.

The design value of σ_w is then given by the design value of $\sigma_w \eta_d$ divided by η_d .

The design value of P, the probability that limit strength is exceeded, is read from an appropriate curve in Figure 12-7, entering with $\eta_d = y/\sigma = 3.5$.

In establishing limit-strength values of $\sigma_w \eta_d$ for the reference airplanes, it was necessary to bring the Model 720B to a common basis with the Model 188 and Model 749, inasmuch as the analysis of the Model 720B had been on a joint probability basis and that of the Model 188 and Model 749, on a single parameter basis. For this purpose, the "2 x Normal" curve in Figure 12-7 was used. For use in new design, it is believed that a slightly more conservative value of P should be used, intermediate between the "Normal" and "2 x Normal" curves. At $\eta_d = 3.5$, the P values given by the three curves are:

"Normal"	$P = 2.3 \times 10^{-4}$
"2 x Normal"	$P = 4.7 \times 10^{-4}$
"Circular Normal"	$P = 2.1 \times 10^{-3}$

A value of 3×10^{-4} is suggested for design.

15.2.7 Suggested Formal Requirement. The following is suggested as a formal statement of a gust loads requirement based upon the design envelope concept:

- (a) The limit gust loads shall be determined utilizing the continuous turbulence concept, in accordance with the provisions of paragraphs (b) through (h) following.
- (b) The limit loads shall be determined for all critical altitudes, weights, and weight distributions, in accordance with FAR 25.321(b), and for all critical speeds within the ranges indicated in Paragraph (d) below.
- (c) In determining the limit loads, values of \bar{A} (ratio of root-mean-square load to root-mean-square gust velocity) for various load and stress quantities selected in accordance with Paragraph (e) below shall be determined by dynamic analysis. The effects of all pertinent rigid and elastic degrees of freedom shall be included. The power-spectral density of the atmospheric turbulence shall be as given by the equation,

$$\Phi(\Omega) = \frac{\sigma^2 L}{\pi} \frac{1 + \frac{8}{3} (1.339 L \Omega)^2}{[1 + (1.339 L \Omega)^2]^{11/6}}$$

where

Φ = power-spectral density

σ = root-mean-square gust velocity

Ω = reduced frequency, radians per foot

L = 2500 ft.

- (d) The limit loads shall be obtained by multiplying the \bar{A} values given by the dynamic analysis by the following values of $\sigma_w \eta_d$:
- (1) At speed V_C : as given by the line $N(y)/N_0 = 1.2 \times 10^{-6}$ in Figure 5-8 herein.
 - (2) At a speed V_B , to be selected by the manufacturer but in no event to be below the lowest speed at which stall would not occur at the limit load levels resulting from the criteria: as given by 1.32 times the values obtained under subparagraph (1) above.
 - (3) At speed V_D : as given by 1/2 the values obtained under subparagraph (1) above.
 - (4) At speeds between V_B and V_C , and between V_C and V_D : as given by linear interpolation.
- (e) A sufficient number of load and stress quantities shall be included in the dynamic analysis to assure that stress distributions throughout the structure are realistically or conservatively defined.
- (f) If the joint probability technique, as described in Sections 10 and 12 herein and more particularly in Reference 1, is employed, σ_w shall be obtained by dividing the $\sigma_w \eta_d$ values defined in paragraph (d) by 3.5. The allowable probability of exceedance of limit strength shall be taken as 0.0003.

- (g) For structural components that are stressed significantly by both the vertical and lateral components of turbulence, the resultant stress shall be determined assuming the vertical and lateral components of turbulence to be uncorrelated. For example, in a structural element subjected to a single stress, the resultant stress shall be taken as given by

$$\sqrt{f_v^2 + f_L^2},$$

where f_v and f_L are the stresses due to the vertical and lateral components of turbulence respectively.

- (h) If a stability augmentation system is utilized to reduce the gust loads, a conservative estimate shall be made of the fraction of flight time, p , that the system may be inoperative. Limit loads shall be determined separately for the system operative and system inoperative, using $\sigma_w \eta_d$ values defined by a pair of $N(y)/N_0$ values meeting the condition that:

$$p \left(\frac{N(y)}{N_0} \right)_{\text{system off}} + (1 - p) \left(\frac{N(y)}{N_0} \right)_{\text{system on}} = \left(\frac{N(y)}{N_0} \right)_{\text{Par. (d)}} \quad (d)$$

When a stability augmentation system is included in the analysis, the effect of system nonlinearities on loads at the limit load level shall be realistically or conservatively accounted for.

- (i) The fail safe gust loads defined in FAR 25.571(c)(2) shall be replaced by loads defined as in Paragraphs (a) through (h) above at the following $\sigma_w \eta_d$ values:

At V_C : .66 of the value given by Paragraph (d)(1) above.

At V_B : .74 of the value given by Paragraph (d)(2) above.

At V_D : .60 of the value given by Paragraph (d)(3) above.

At speeds between V_B and V_C , and between V_C and V_D : as given by linear interpolation.

15.3 Combined Criterion

As indicated in Section 4, a combined mission analysis and design envelope criterion gives promise of providing the advantages of each basic form while minimizing the associated disadvantages.

The proposed combined criterion provides for a choice between the following in any given application:

- (1) A design envelope analysis in accordance with Section 15.2 but at a level considerably in excess of that defined therein. This level would be set such that no matter how severe the actual operation might be, as restricted only by the design envelope, a realistic mission analysis would be extremely unlikely to indicate higher loads.
- (2) A mission analysis in accordance with Section 15.1, in combination with a design envelope analysis at a level equal to or slightly below that defined in Section 15.2, the highest loads from either analysis to be used for design.

For an airplane that is not gust critical, the simple, conservative approach offered by Option (1) above would be selected. If for a given design the conservatism of Option (1) were unacceptable, Option (2) could be selected. A mission analysis would then be performed. But a floor below which the loads could not drop would be established by a design envelope analysis at a reduced severity. This floor would provide insurance against either a rapid increase in loads as the design envelope is approached or an unconservative definition of the design missions.

The purpose of this section is primarily to establish the two $\sigma_w \eta_d$ levels required.

15.3.1 Design $\sigma_w \eta_d$ Levels for Use in Lieu of a Mission Analysis. To establish the desired conservative value of $\sigma_w \eta_d$, two somewhat independent approaches will be followed to indicate an upper limit.

First, using the Model 188 as an example, it will be assumed that the airplane operates 100% of the time at its critical design envelope point. The $\sigma_w \eta_d$ value corresponding to the mission analysis limit strength $N(y)$ of 2×10^{-5} cycles per hour will then be determined.

The critical case is No. 417, at 116000 lb. G.W. and altitude 12,000 ft. Considering wing bending moment at WS 83 to be a critical load quantity, N_0 is 1.3 cps (Table B-2). $N(y)/N_0$ corresponding to the limit design frequency of exceedance of 2×10^{-5} cycles per hour is then

$$\frac{N(y)}{N_0} = \frac{2 \times 10^{-5}}{(3600)(1.3)} = 4.3 \times 10^{-9}$$

From Figure 5-5, the corresponding y/\bar{A} at $h = 12000$ ft. is seen to be 114 fps. This is the required $\sigma_w \eta_d$.

It is noted that Model 188 characteristics entered only to the extent of establishing N_0 and h . The Model 188 N_0 is considered quite typical, and the result would be about the same for all altitudes in the range 10000 - 30000 ft. As the altitude increases further, the required $\sigma_w \eta_d$ would decrease.

Second, again using the Model 188 as an example, it will be assumed that the airplane is operated so as to duplicate the overall exceedance curves such as shown in Figure 9-9, but that the placards are reduced so as to just envelope Case 202, which is the predominant contributor to the load exceedances.

The limit strength value of $\sigma_w \eta_d$ is determined for this case by the same method described in Appendix E, Section E.1.3, in connection with the preparation of Table E-1. The value is found to be 111 fps. As the Model 188 just meets the suggested mission analysis limit strength criterion of $N(y) = 2 \times 10^{-5}$ cycles per hour, this is the required value of $\sigma_w \eta_d$. Inasmuch as the airplane is not operated, in this example, 100% of the time at its critical design envelope point, the 111 value obtained here is slightly less than the 114 fps value obtained above.

By either approach, the "upper limit" $\sigma_w \eta_d$ lies in the very narrow range of 111 to 114 fps (at 12000 ft.). In comparison, the actual limit strength value is 60 fps.

It seems highly unlikely that any actual operation could be as severe, relative to the operating placards, as assumed in the above two calculations. Consequently, some reduction from the 111 - 114 fps range of $\sigma_w \eta_d$ is in order, and a value of 110 fps (at 7000 ft.) would appear to be ample.

15.3.2 Design $\sigma_w \eta_d$ Levels for Use in Conjunction with a Mission Analysis.

To establish a $\sigma_w \eta_d$ level to use as a floor in conjunction with a mission analysis, specific quantitative guides are difficult to come by. However, the Model 188 appears to represent a fairly extreme degree of difference between normal operating conditions and design placards. As a result, it would appear that any $\sigma_w \eta_d$ selection appreciably below the Model 188 limit strength value would be unlikely to satisfy the need for a $\sigma_w \eta_d$ floor. A value equal to the Model 188 limit strength value, of 62 fps at 7000 ft., is suggested.

Under Option (2), the design envelope floor should include V_B and V_D as well as V_C conditions; it should also include the appropriate treatment of stability augmentation devices as discussed in Section 15.2.4 and the determination of fail safe conditions in accordance with Section 15.2.5.

15.3.3 Suggested Formal Requirement. The following is suggested as a formal statement of a gust loads requirement that would combine the mission analysis and design envelope concepts:

- (a) The limit gust loads shall be determined utilizing the continuous turbulence concept, in accordance with the provisions of either Paragraph (b) or Paragraphs (c) and (d) below.
- (b) Design envelope analysis. The limit loads shall be determined in accordance with the following:
- (1) All critical altitudes, weights, and weight distributions, as specified in FAR 25.321(b), and all critical speeds within the ranges indicated in Paragraph (b)(3) below, shall be considered.
 - (2) Values of \bar{A} (ratio of root-mean-square load to root-mean-square gust velocity) for various load and stress quantities selected in accordance with Paragraph (b)(4) below shall be determined by dynamic analysis. The effects of all pertinent rigid and elastic degrees of freedom shall be included. The power spectral density of the atmospheric turbulence shall be as given by the equation,

$$\phi(\Omega) = \frac{\sigma^2 L}{\pi} \frac{1 + \frac{8}{3} (1.339 L \Omega)^2}{[1 + (1.339 L \Omega)^2]^{11/6}}$$

where

ϕ = power-spectral density

σ = root-mean-square gust velocity

Ω = reduced frequency, radians per foot

$L = 2500$ ft.

- (3) The limit loads shall be obtained by multiplying the \bar{A} values given by the dynamic analysis by the following values of $\sigma_w \eta_d$:
 - (i) At speed V_Q : as given by the line $N(y)/N_0 = 6 \times 10^{-9}$ in Figure 5-8 herein.
 - (ii) At a speed V_B , to be selected by the manufacturer but in no event to be below the lowest speed at which stall would not occur at the limit load levels resulting from these criteria: as given by 1.32 times the values obtained under subparagraph (i) above.

- (iii) At speed V_D : as given by 1/2 the values obtained under subparagraph (i) above.
- (iv) At speeds between V_B and V_C , and between V_C and V_D : as given by linear interpolation.
- (4) A sufficient number of load and stress quantities shall be included in the dynamic analysis to assure that stress distributions throughout the structure are realistically or conservatively defined.
- (5) If the joint probability technique, as described in Sections 10 and 12 herein and more particularly in Reference 1, is employed, σ_w shall be obtained by dividing the $\sigma_w \eta_d$ values defined in paragraph (b)(3) by 3.5. The allowable probability of exceedance of limit strength shall be taken as 0.0003.
- (6) For structural components that are stressed significantly by both the vertical and lateral components of turbulence, the resultant stress shall be determined assuming the vertical and lateral components of turbulence to be uncorrelated. For example, in a structural element subjected to a single stress, the resultant stress shall be taken as given by

$$\sqrt{f_v^2 + f_L^2} ,$$

where f_v and f_L are the stresses due to the vertical and lateral components of turbulence respectively.

- (7) If a stability augmentation system is utilized to reduce the gust loads, a conservative estimate shall be made of the fraction of flight time, p , that the system may be inoperative. Limit loads shall be determined separately for the system operative and system inoperative, using $\sigma_w \eta_d$ values defined by a pair of $N(y)/N_0$ values meeting the condition that:

$$p \left(\frac{N(y)}{N_0} \right)_{\text{system-off}} + (1 - p) \left(\frac{N(y)}{N_0} \right)_{\text{system on}} = \left(\frac{N(y)}{N_0} \right)_{\text{Par. (b)(3)}}$$

When a stability augmentation system is included in the analysis, the effect of system nonlinearities on loads at the limit load level shall be realistically or conservatively accounted for.

- (8) The fail safe gust loads defined in FAR 25.571(c)(2) shall be replaced by loads defined as in Paragraphs (b)(1) through (7) above at the following $\sigma_w n_d$ values:

At V_G : .66 of the value given by Paragraph (b)(3)(i) above.

At V_B : .74 of the value given by Paragraph (b)(3)(ii) above.

At V_D : .60 of the value given by Paragraph (b)(3)(iii) above.

At speeds between V_B and V_G and between V_G and V_D : as given by linear interpolation.

- (c) Flight profile analysis. Limit loads shall be determined in accordance with the following:

- (1) The expected utilization of the aircraft shall be represented by one or more flight profiles in which the payload and the variation with time of speed, altitude, gross weight, and center of gravity position are defined. These profiles shall be divided into mission segments, or blocks, for analysis, and average or effective values of the pertinent parameters defined for each segment.
- (2) For each of the mission segments defined under Paragraph (c)(1) and each of the load and stress quantities selected in accordance with Paragraph (4) below, values of \bar{A} and N_0 shall be determined by dynamic analysis. \bar{A} is defined as the ratio of root-mean-square load to root-mean-square gust velocity and N_0 as the radius of gyration of the load power-spectral density function about zero frequency. The effects of all pertinent rigid and elastic degrees of freedom shall be included. The power-spectral density of the atmospheric turbulence shall be as given by the equation,

$$\Phi(\Omega) = \frac{\sigma_L^2}{\pi} \frac{1 + \frac{8}{3} (1.339 \Omega)^2}{[1 + (1.339 \Omega)^2]^{11/6}}$$

where

Φ = power spectral density

σ = root-mean-square velocity

Ω = reduced frequency, radians per foot

L = 2500 ft.

- (3) For each of the load and stress quantities selected in accordance with Paragraph (4) below, the frequency of

exceedance shall be determined as a function of load level by means of the equation,

$$N(y) = \sum t N_0 \left[P_1 \exp \left(- \frac{y - y_{one-g}}{b_1 \bar{A}} \right) + P_2 \exp \left(- \frac{y - y_{one-g}}{b_2 \bar{A}} \right) \right]$$

where

- y = net value of the load or stress
- y_{one-g} = value of the load or stress in one-g level flight
- $N(y)$ = average number of exceedances of the indicated value of the load or stress in unit time
- \sum = Symbol denoting summation over all mission segments
- t = fraction of total flight time in the given segment
- N_0, \bar{A} = parameters determined by dynamic analysis as defined in Paragraph (c)(2)
- P_1, P_2, b_1, b_2 = parameters defining the probability distributions of root-mean-square gust velocity, to be read from Figures 5-3 and 5-4 herein.

The limit gust loads shall be read from the frequency of exceedance curves at a frequency of exceedance of 2×10^{-5} exceedances per hour. Both positive and negative load directions shall be considered in determination of the limit loads.

- (4) A sufficient number of load and stress quantities shall be included in the dynamic analysis to assure that stress distributions throughout the structure are realistically or conservatively defined.
- (5) If the joint probability technique, as described in Sections 10 and 12 herein and more particularly in Reference 1, is employed, the frequency of exceedance of limit strength shall not be greater than 2×10^{-5} exceedances per hour.

- (6) For structural components that are stressed significantly by both the vertical and lateral components of turbulence, the resultant stress shall be determined assuming that, within any patch of turbulence, the vertical and lateral components are uncorrelated. For example, in a structural element subjected to a single stress, the resultant stress shall be taken as given by

$$\sqrt{f_v^2 + f_L^2} ,$$

where f_v and f_L are the stresses due to the vertical and lateral components of turbulence respectively.

- (7) If a stability augmentation system is utilized to reduce the gust loads, a conservative estimate shall be made of the fraction of flight time that the system may be inoperative. The flight profiles of Paragraph (c) (1) shall include flight with the system inoperative for this fraction of the flight time. When a stability augmentation system is included in the analysis, the effect of system nonlinearities on loads at the limit load level shall be realistically or conservatively accounted for.
- (d) Supplementary design envelope analysis. In addition to the limit and fail safe loads defined by Paragraph (c) above, limit and fail safe loads shall also be determined in accordance with Paragraph (b) above modified as follows:
- (1) In Paragraph (b)(3)(1), the value $N(y)/N_0 = 6 \times 10^{-9}$ is replaced by $N(y)/N_0 = 1.2 \times 10^{-6}$.
- (2) In Paragraph (b)(7), the reference to Paragraph (b)(3) is to be understood as referring to the paragraph as modified by Paragraph (d)(1) above.
- (3) In Paragraph (b)(8), the reference to Paragraph (b)(3)(i) through (b)(3)(iii) is to be understood as referring to the paragraph as modified by Paragraph (d)(1) above.

15.4 Evaluation of the Three Forms of Criterion

Structural design criteria to date have almost universally been of the design envelope type. However, in recent years, whenever there has been any real question of the adequacy of a given airplane to withstand the

gust loads to which it may be exposed, or of the adequacy of existing criteria for application to new vehicles operating on vastly different flight profiles, mission analyses have been performed. Only in this way can it be assured that the new airplanes do not become less safe than the old as a result of possibly more severe operational usage relative to the design envelope. For this reason, the mission analysis format for a gust loads criterion appears to be almost a necessity.

Furthermore, only if the original design is substantiated on a mission analysis basis can the effects of changes in operating practices during the life of a fleet be conveniently evaluated.

On the other hand, as discussed in Section 4.3, the mission analysis form of criterion suffers certain disadvantages. Judgement is required in setting up the design missions, and as a result, differences of opinion may arise and be difficult to reconcile in administration of the criterion. Also, considerable care may be required to assure that a sufficient variety of off-typical flight conditions are included; in fact this is an area that has been barely touched upon in the present study. Another possible disadvantage is the increased difficulty in matching statistically defined loads with conditions for stress analysis. This may be of rather small consequence, however, and may even be overshadowed by the possibility that under a design envelope criterion many more sets of statistically defined loads would have to be matched in order to establish the critical design point.

Should it be decided to retain the design envelope form of criterion, it is believed that a major gain over the existing discrete gust criteria would still be achieved, as a result of the more realistic evaluation of the airplane response to turbulence provided by the power-spectral approach.

The combined criterion developed in Section 15.3 is believed to largely overcome the disadvantages of using either of the two basic forms of criterion alone. While it will involve somewhat more analysis in some instances, this is offset by the simpler treatment possible for those airplanes that are not gust critical and by the more straight-forward treatment of non-typical operating conditions. The combined criterion is therefore believed to be most appropriate for use at this time.

15.5 Formal Requirements for Design Technique

It will be noted that the suggested formal requirements provided in Sections 15.1.5, 15.2.6, and 15.3.3 do not specify a particular technique for integration of the power spectral loads determination with the routines of detailed stress analysis. Both the matching condition and joint

probability techniques developed in the present program are considered adequate, and sufficient information is provided in the suggested formal requirements so that either can be used. Furthermore, it is to be expected that improvements in these techniques, or new techniques altogether, will be developed in the future. It is believed that the design technique must, necessarily, be left to the selection of the individual manufacturer in order that he may adequately integrate power spectral results with his overall philosophy of structural design and testing.

16 SUMMARY OF DESIGN PROCEDURES

The purpose of this section is to discuss how the criteria suggested in Section 15 would ordinarily be implemented in application to a new design. Other portions of this report, dealing specifically with the analyses of the three reference airplanes, will be drawn upon or referenced as appropriate. The procedure will, of course, differ to some extent depending upon whether the analysis is to a mission analysis or design envelope form of criterion. The choice between the two forms of criterion will presumably depend in part on policy action to be taken by the Federal Aviation Agency based on the results of this study. As noted in Section 15.4, the "combined" form of criterion, which makes provision for both mission analysis and design envelope approaches (Section 15.3), is recommended by the present authors.

16.1 Flight Conditions Required for Analysis

The first step in a gust design procedure is to establish the various flight conditions for which analysis will be required.

16.1.1 Mission Analysis Criterion. Where loads are to be determined according to a mission analysis type of criterion, it is first necessary to establish the design missions and lump into segments for analysis.

The missions developed for the three reference airplanes in Section 6 herein and in Reference 1 are considered appropriate guides to the type of mission profile suitable for a new design. Usually, however, no actual operational data will be available; and, as a result, realistic estimates of typical operating conditions will be required. Ratios of typical to placard values of speed, payload, etc., based upon the operation of existing aircraft can be used as a guide, but careful thought will have to be given as well to how the new airplane will probably be operated.

As in the analysis of the reference airplanes, values of the various parameters required in the analysis can usually be taken at the midpoint of each segment, or as average values over the segment. It should be noted, however, that where one or more parameters vary over a wide range within any one segment, use of average values tends to be unconservative. (For example, see the discussion of speed selection in Section 6.1.) Consequently, such segments should be lumped nearer to the critical end of the segment, or the profile should be broken into more segments.

As noted in Section 15.1, for airplanes which depend upon a stability augmentation system to limit the gust loads, the design missions must

include an appropriate fraction of flight time with the system inoperative. In addition, if a specific emergency procedure - for example, an emergency descent procedure - involves a substantial increase in gust exposure, this too should be included in the design missions.

For advanced designs the chief difference in the generation of the design missions is likely to be a need for a finer breakdown into mission segments. For a typical supersonic transport, for example, ranges of equivalent airspeed, Mach number, and altitude throughout the flight are all much greater than for current airplanes; and both the turbulence exposure and the response characteristics vary markedly as the flight proceeds. Variable configuration geometry, such as introduced by a variable sweep wing, would also lead to a need for a finer mission breakdown.

16.1.2 Design Envelope Criterion. Where loads are determined according to a design envelope criterion, the first step is to select a variety of potentially critical combinations of speed, altitude, payload, fuel weight, and c-g. location. V_B , V_C , and V_D conditions should all be included. Some elimination of non-critical conditions can perhaps be accomplished at this stage by use of a simplified analysis as illustrated in Section 7. Probably the best approach to determination of critical conditions is to run a somewhat limited number of cases at first, then examine the results and add other cases as indicated.

16.2 Equations of Motion

The next step - which actually can be carried out simultaneously with the definition of flight conditions for analysis - is to write the necessary equations of motion and program these for automatic digital solution. This is ordinarily a major undertaking, which requires a high order of capability in the field of aeroelastic dynamic analysis. All pertinent elastic as well as rigid-airplanes modes must, of course, be included, as well as the effects of automatic control and stability augmentation systems if present. Examples of equations of motion appropriate for various specific applications, together with their derivations, are given in References 1, 21, 22, 26 and 27. Solution of these equations is such as to provide the steady-state response to a sinusoidal variation of gust velocity of unit amplitude at each of various frequencies. Response outputs are obtained for a variety of accelerations, loads, and stresses. Multiplication by the gust power-spectral density and integration with respect to frequency leads to values of \bar{A} and K_0 for each output quantity.

Because of the complexity of a modern dynamic gust analysis and the need for judgment in establishing values of the various input parameters,

various checks should be made in order to keep the studies in perspective and to provide confidence in the results. Of particular importance is a maneuver loads check such as illustrated for two of the reference airplanes in Section 8.1.3. A flutter check also is desirable, as this will tend to bring to light any inconsistencies between the dynamic gust analysis and the formal flutter analysis with respect to representation of the elastic mode dynamics and aerodynamics. Over-all reasonableness checks of \bar{A} values should also be made by comparing with \bar{A} values obtained from a simple static analysis using curves such as those in Figure 5-2.

For some airplanes, a much simpler dynamic analysis than implied by the above discussion may suffice. For example, published NACA data (Reference 26) indicate that, for an airplane comparable to the DC-3, the dynamic factor for wing bending is on the order of only 1.05; and there is no reason to expect that dynamic increments to the shears and torsions would be significantly greater. For other airplanes that are generally comparable in size, mass distribution, first wing elastic mode natural frequency (above 4 cps), etc., the dynamic effects could be expected to be no greater and therefore could be adequately accounted for by means of a simple factor of 1.05 to 1.10 applied to the static loads.

For such an airplane, the equations of motion would, of course, be much simpler, as the elastic-mode degrees of freedom would not be included. Further, it appears that, for past airplanes, the effects of pitch have generally been small and tend to reduce the loads slightly. (For example, for the Model 749 Constellation the inclusion of pitch reduces the load factor by about 7%.) Thus it appears that - for an airplane having conventional stability characteristics - the pitch freedom can also be eliminated. With the representation thus simplified, the airplane remains free only to plunge. For this representation, solutions of the equations of motion are already available in the form of curves such as provided in Figure 5-2. These provide the \bar{A} value for airplane load factor; air loads are then assumed to be distributed on a static basis and are placed in equilibrium with inertia loads in the usual way. The estimated dynamic factor must, of course, be applied to the gust incremental loads thus obtained.

It may be remarked that the particular curves shown in Figure 5-2 are known to be slightly unconservative because of approximations made to the left growth functions in their derivation. It would be desirable, therefore, to recompute these curves, following the procedure used in Reference 15. Pending such revision, an approximate correction factor, on the order of 1.08, can be applied to K_G values read from Figure 5-2.

Values of N_0 , which are needed if the mission analysis form of criterion is used, can be estimated. A value of 1.0 cps is generally realistic.

For advanced configurations, the equations of motion will be derived following the same general principles as for current aircraft. Differences in treatment may be required, however, and the analysis may become more complex. For a low aspect ratio delta wing, for example, the concept of an elastic axis loses its meaning, and a lifting-line treatment of the aerodynamics will no longer suffice.

As analysis methods are modified to suit new configurations, or as advances are made in analysis techniques, the intent should be to secure as realistic a representation as is practical. In particular, no attempt should be made to purposely retain the specific conservatism that might be present in the reference-airplane analyses. The factors affecting gust response are complex, and various airplanes differ greatly in the detailed characteristics of their dynamic response. As a result, it is believed that the only practical approach is to judge the adequacy of the representation of each airplane on an individual, absolute basis.

On the other hand, one must not completely lose sight of the fact that the design levels are set based upon the strength of the reference airplanes. Whenever a significantly different method of analysis is introduced, therefore, the probable effect on the reference airplanes should be reviewed. Examples of changes that would clearly require review of the reference airplane analyses would include the introduction of the spanwise variation of the vertical gust velocity, and the inclusion of the transfer function of the human pilot.

16.3 Dynamic Analysis and Design-Level Loads

Under either the mission analysis or design envelope form of criterion, the next step is to determine the necessary input data for the various flight conditions and perform the dynamic analysis. This will result in A and N_0 values for as many load quantities - loads, stresses, and fictitious stresses - as may be needed to define loads, stresses, or margins of safety throughout the structure. If the joint probability technique is to be used, this step will include also the computation of the pertinent correlation coefficients, ρ . (The quantities σ_a and σ_b , used when the joint probability technique is applied on a mission analysis basis, are given by $2\pi N_0 \bar{A}_x$ and $2\pi N_0 \bar{A}_y$ respectively.)

16.3.1 Mission Analysis Criterion. Under the mission analysis form of criterion, the A and N_0 values obtained from the dynamic analysis are next used to obtain exceedance curves for each load quantity, as described in the last paragraph of Section 4.1 and illustrated, for example, by Figure 9-9. The design level value for each load quantity is then read at the design frequency of exceedance of 2×10^{-5} cycles per hour defined in Section 15.

Advanced configurations where aerodynamic heating must be considered will require some modification to this procedure. One major effect of aerodynamic heating is the reduction of material allowables in the supersonic portion of the flight, in general resulting in different allowables for each flight segment. For representative supersonic transport designs, the highest gust loads have been found to occur during subsonic climb, where the structure is cold. Supersonic speeds, resulting in hot structure and reduced allowables, are reached only at high altitudes, where the gust loads are very much reduced. An obvious simple, but conservative approach would be to define design-level loads in the usual way and to apply these loads in conjunction with the lowest (high temperature) allowables. This conservatism is likely to be unacceptable, however. It can be eliminated by arbitrarily allocating the design frequency of exceedance amongst several portions of the flight. For example, the permissible 2×10^{-5} exceedances per hour might be divided equally, 1×10^{-5} to a low-temperature portion of the flight and 1×10^{-5} to a high-temperature portion. If, under this arbitrary allocation, the low-temperature portion is found to be critical, the allocation could be changed, say, to 1.8×10^{-5} exceedances per hour for the low-temperature portion and 0.2×10^{-5} for the high-temperature portion. Under any arbitrary allocation, as long as each set of loads is within the limit strength corresponding to its allowables, the total exceedances of limit strength will not exceed the design value of 2×10^{-5} per hour defined in Section 15. (It will be noted that the allocation principle used here is quite similar to that described in Section 15.2.3 for treatment of stability augmentation system malfunction under a design envelope form of criterion.)

The same objective might also be achieved by obtaining exceedance curves for y/y_{limit} instead of for y . The value of y_{limit} would, in general, be different for each mission segment. This approach would make unnecessary the arbitrary allocation of exceedances amongst mission segments. It would, however, appear to lead to a variety of difficulties in practical application, especially where the "matching condition" technique is to be used.

Transient stresses due to non-uniform thermal expansion will also require special treatment. In principle, these stresses can simply be added to the one-g level flight stresses for each mission segment.

16.3.2 Design Envelope Criterion. Under the design envelope form of criterion, the A value for each load quantity for each flight condition is multiplied by the appropriate $\sigma_w \eta_d$ value as specified in Section 15 to obtain a design load value.

The problems mentioned above as likely to occur in application of the mission analyses form of criterion to advanced configurations do not appear with the design envelope form of criterion.

16.4 Generation of Matching Conditions; Joint Probability Analysis

At this stage, the procedures become quite different, depending upon whether the matching condition or joint probability technique is to be used.

If the matching condition technique is to be used, some consideration should be given to the degree of conservatism that will be acceptable in matching the statistically defined loads. If gust loads are critical, a refined technique comparable to that described and illustrated in detail in Appendices C and D would ordinarily be appropriate. On the other hand, if considerable conservatism can be allowed, conservative assumptions should be made as appropriate to minimize the work. For example, maximum bending moments and maximum torsions (about the elastic axis) can be assumed to occur simultaneously, with each of the four combinations of sign.

The technique to be followed in matching the statistically defined loads will be essentially the same for a mission analysis as for a design envelope form of criterion. Some minor differences are pointed out in Section 11.1 and others will be evident from a study of Appendix C. In addition, it might be noted that, in utilizing the design envelope form of criterion, a major effort should be made to eliminate non-critical conditions based on values of $(\bar{A}) (\sigma_w \eta_d)$ prior to generation of the matching conditions, so that the number of design envelope points for which matching conditions are generated can be held to a minimum.

If the joint probability technique is to be used, it will be generally in accordance with the procedures described in Reference 1. The amount of computation indicated therein in conjunction with the design envelope form of criterion, however, will be greatly reduced, inasmuch as the calculations need be carried out for only a single σ_w value for each flight condition.

For advanced configurations, particularly those characterized by low-aspect-ratio wings, some increased difficulty in applying either the matching condition or joint probability technique is likely to be encountered.

In the matching condition technique, more matching conditions may be required, and it will probably be necessary to examine a greater number of internal stresses, both actual and fictitious. As a result, however, of limited experience in matching statistically defined taxi loads for a delta wing airplane, it appears that the matching condition concept will still be quite practical to apply.

Considerably increased difficulty would be expected, in either the matching condition or joint probability technique, if it became necessary

to include wing rib bending stresses. The stress condition at a point on the surface would then be defined by tension-compression stresses in two directions and a shear stress, rather than only one tension-compression stress and a shear stress. A three dimensional instead of a two dimensional treatment would then be required. Hopefully, simple conservative assumptions regarding rib bending stresses will usually be acceptable, so that the complexities of treating rationally the additional stress component can be avoided.

17 THE PLACE OF THE DISCRETE GUST CONCEPT

The present study has been directed explicitly toward the development of a power-spectral gust design procedure, with the future role of the present discrete gust requirement not intended to be a part of the study. At the same time, the selection and development of a power spectral gust criterion is bound to be influenced at least indirectly by the role which the discrete gust concept will continue to play. In addition, in the course of developing the power-spectral criteria, various thoughts have crystallized regarding the relation between the power-spectral and discrete-gust approaches. As a result, some discussion of the future role of the discrete gust criterion is considered appropriate.

Historically, as the continuous turbulence concept gradually gained acceptance, good engineering judgment dictated the use of both the old and the new concepts in combination until sufficient experience could be gained to assure that the newer approach would be adequate by itself. Now, however, it appears that the need for a discrete gust criterion is diminishing. Some of the factors leading to such a conclusion are indicated by the following comments.

1. First, while reasonably discrete gusts undoubtedly occur in the atmosphere, there is accumulating evidence that the preponderance of gusts are better described in terms of continuous turbulence. It has long been accepted that clear air turbulence at moderate intensity levels is generally continuous in nature. Thunderstorm gust velocity profiles are now available in considerable quantity, for example in References 14 and 28; these almost invariably display the characteristics of continuous turbulence. Also, the extremely severe low level turbulence of which measurements are reported in references 29 and 30 is also understood to have consisted largely of continuous turbulence, although a number of severe discrete gusts were also encountered.
2. Second, it has become more and more evident that elastic mode dynamic efforts must be treated on a power-spectral basis. The elastic mode effects, in a discrete gust analysis, are highly sensitive to the gust gradient distance. Yet the problems of selecting a gust gradient distance and of relating the gust velocity to this gradient distance appear as insurmountable now as when the continuous turbulence concept was first introduced, offering for the first time a practical way of bypassing this knotty problem. In order for a discrete-gust dynamic analysis to be realistic for design loads determination, data on the joint probability of gradient distance and gust velocity for discrete gusts would be required. Such data simply are not available, nor are they likely to become available. One cannot help feeling, however, that the relation of gust intensity to

gust wavelength inherent in the power-spectral description of atmospheric turbulence is probably quite representative of discrete gusts as well as continuous turbulence. Consequently, as long as the various elastic modes are all fairly well damped, the power spectral analysis should duplicate reasonably well the results that a discrete gust analysis would yield if the necessary statistical data were available and incorporated. For a system with poorly damped modes, of course, the continuous turbulence analysis would be required regardless of whether a discrete gust analysis were performed, in order to account for resonant build-up of load at the natural frequencies.

3. From a static loads standpoint, the impression has prevailed that gust loads are not sensitive to the gradient distance and that the discrete-gust and power-spectral approaches should lead to nearly identical results. Instances have been found, however, where discrete-gust and power-spectral approaches give results differing by rather sizable amounts.

In order to study these differences, values of $\sigma_w \eta_d$ necessary to give the same airplane load factor as a 50 fps discrete gust (U_{de}) have been obtained for a number of representative airplanes. The discrete gust is defined as in FAR 25, and the gust velocity is considered to decrease with altitude above 20000 ft. as indicated therein. For the purpose of this comparison, the airplanes are considered to be rigid and restrained to plunge only. Under these assumptions, the desired $\sigma_w \eta_d$ values are given by

$$\sigma_w \eta_d = U_{de} \frac{K_g}{K_\sigma} \frac{1}{\sqrt{\sigma}}$$

where K_g is the discrete gust alleviation factor, evaluated in accordance with FAR 25, and σ is the atmospheric density ratio. Values of K_σ are read from Figure 5-2. (These K_σ values are slightly low due to the approximations to the lift growth functions used in obtaining the curves; use of "precise" values would have decreased the $\sigma_w \eta_d$ values obtained by about 8%).

If, at each altitude, the value of $\sigma_w \eta_d$ necessary to give the same load factor as a 50 fps discrete gust were found to be the same for all airplanes, it would make no difference whether a discrete gust or power-spectral criterion were used. But suppose that different values are found. If the various airplanes had all been designed to the same U_{de} , their capabilities to withstand continuous turbulence, as measured by the $\sigma_w \eta_d$ value made good, would then differ. If the airplane making good the highest $\sigma_w \eta_d$ were considered just adequate from

a gust loads standpoint, its $\sigma_w \eta_d$ would define the appropriate design level of $\sigma_w \eta_d$, and the other airplanes would be deficient.

Results for the various airplanes are shown by the dash lines in Figure 17-1. The background grid of lines of constant $N(y)/N_0$ is the same as in Figure 5-8. Curve A shows the $\sigma_w \eta_d$ values corresponding to the prescribed U_{de} for the Table 1a airplane of NACA TN 4332. This is a typical 4-engine piston-powered transport. Curve B reflects a 50% increase in wing loading and is roughly representative of the Model 188. Curve C reflects a further increase of 33% in wing loading. Curve D represents a large delta wing airplane representative of proposed supersonic transport configurations; $W/C_{L\alpha} S$ is the same as for curve C, but the wing chord is increased by a factor of five. Curve E reflects the result of a 50% decrease in wing loading relative to curve A and is representative of the DC-3 generation of transports.

The knuckle in each curve at 20000 ft. reflects the variation of U_{de} with altitude. The slight unfairness that may be noted in some of the curves apparently is the result of difficulty in reading the curves of Figure 5-2 accurately at the low values of μ .

The fairly substantial differences between these curves indicate that the discrete gust and power-spectral approaches can give significantly different results, even where resonant build-up in poorly damped modes cannot be a contributing factor. For example, suppose that airplanes A and D were each designed to a 50 fps discrete gust. For flight through continuous turbulence at sea level, airplane A would be good for a turbulence intensity of $\sigma_w \eta_d = 93$ fps. Airplane D, on the other hand, would be good for a turbulence intensity of only $\sigma_w \eta_d = 65$ fps. Its actual loads in a given patch of turbulence, relative to those of airplane A, would be greater than predicted by discrete gust theory, therefore, in the ratio $93/65 = 1.43$.

The reasons for this difference are not hard to understand.

First, in the discrete gust methods now in use, the length of gust is assumed to be proportional to the wing mean chord. This assumption simplifies the calculations, and for past airplanes it may have been fairly realistic. However, the extremely long chord of airplane D results in a gust so long that the airplane tends to rise with the gust and develop relatively little load. Further, this alleviating effect of gust length is not offset by any increase in gust velocity.

CURVE A: TABLE 1a AIRPLANE OF TN 4332
 CURVE B: SAME AS A EXCEPT W/CL_{α} INCREASED IN RATIO 1.5
 CURVE C: SAME AS A EXCEPT W/CL_{α} INCREASED IN RATIO 2.0
 CURVE D: SAME AS A EXCEPT W/CL_{α} INCREASED IN RATIO 2.0 AND τ IN RATIO 5.0
 CURVE E: SAME AS A EXCEPT W/CL_{α} DECREASED IN RATIO .5
 CURVE F: DESIGN LEVEL^o SECTIONS 15.2.7 AND 15.3.3(a)
 CURVE G: DESIGN LEVEL^o SECTION 15.3.3(b)

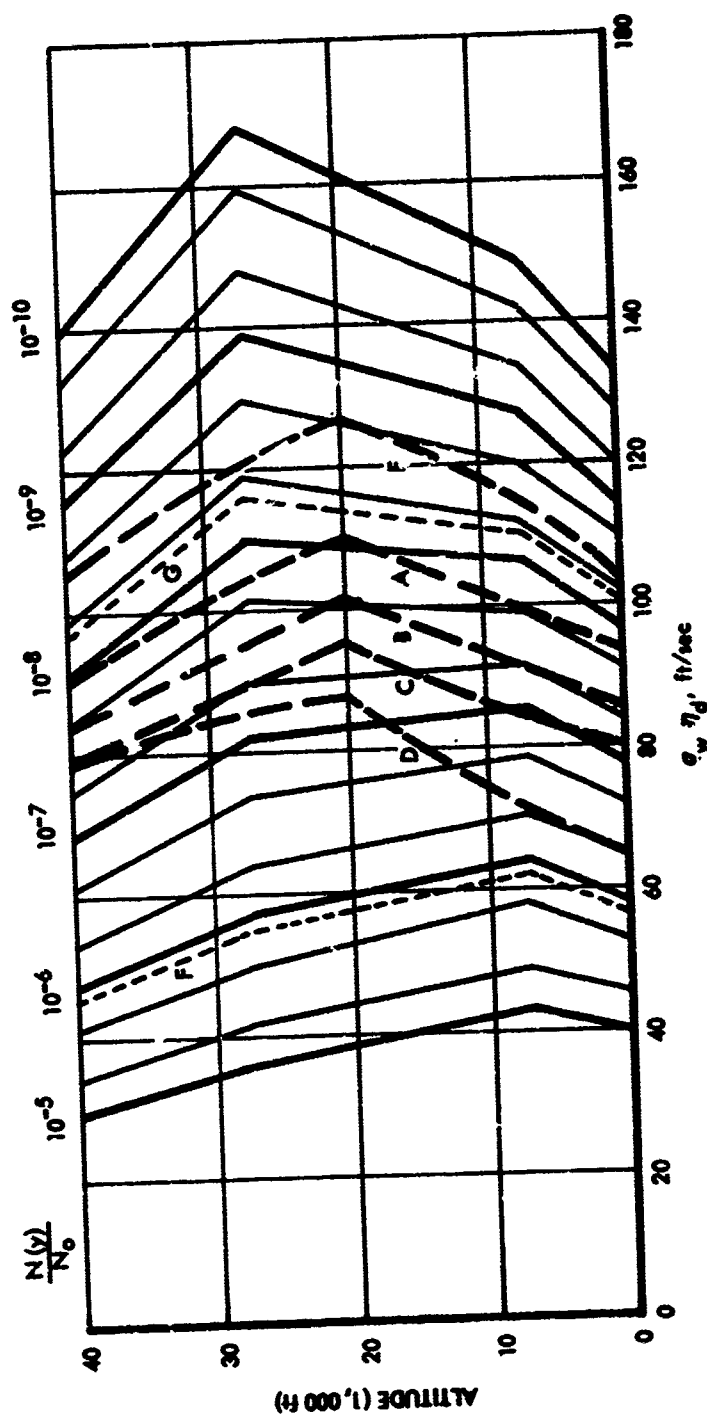


FIGURE 17-1. q_w VALUES GIVING SAME LOAD FACTOR AS FAR 25
 V_c DISCRETE GUST ($U_{de} = 50$ FPS BELOW 20000 FT)

On the other hand, the power-spectral treatment of atmospheric turbulence reflects the fact that the longer-gradient gusts tend to have significantly higher gust velocities. This effect of wing chord explains the difference between curves C and D in Figure 17-1.

Second, because of its higher value of $W/C_L \alpha S$, airplane D acquires vertical velocity less rapidly as it enters any given gust. This phenomenon is reflected in higher alleviation factors on both discrete gust and power spectral bases. On encountering gusts of various wavelengths, however, airplane D - and likewise airplane C - will tend to feel the longer wavelength gusts that airplane A rides over. In contrast to the discrete gust formula, the power spectral treatment reflects the mixture of gusts of all wavelengths and the higher gust velocities associated with the longer wavelengths. This effect of a higher value of $W/C_L \alpha S$ explains the difference between curves A and C in Figure 17-1.

Thus it is evident that the relation of gust intensity to gradient distance is important from the standpoint of static as well as dynamic loads determination.

4. As indicated by the above discussion, it appears that the power spectral approach accounts much more realistically for the actual mix of gust gradient distances in the atmosphere and for the variation of gust intensity with gradient distance than does the present discrete gust formula, on a static as well as on a dynamic loads basis. As a result, the power spectral approach probably does a better job of accounting for loads due to actual discrete gusts than does the present discrete gust requirement. With a comprehensive power spectral gust loads criterion in use - which will be necessary in any event to provide for the situation of a possible resonant build-up of response in poorly damped modes - it would appear that the discrete gust situation is inherently provided for and that a specific dynamic or static discrete gust criterion is not necessary in addition.
5. A power-spectral method of analysis is not necessarily more difficult to apply than a discrete gust method. The present static-load plunge-only discrete-gust method can, in fact, be converted to a power-spectral basis by making just two changes:
 - (a) Replace the discrete-gust alleviation factor by an alleviation factor read from curves such as those of Figure 5-2 herein.

- (b) Replace the specified value of U_{de} with a specified value of $\sigma_w \eta_d$ (varying appropriately with altitude).

The discrete gust and power spectral procedures in this case are essentially identical. In using the power spectral rather than the discrete gust data, one needn't even be aware that it is no longer discrete gusts that are described.

To be sure, this simple rigid-airplane analysis does not exploit the full potentiality of the power-spectral approach. But it does account more realistically for the actual mix of gust gradient distances in the atmosphere and the variation of gust intensity with gradient distance. Furthermore, as additional rigid and elastic degrees of freedom are introduced, the added complexity is due to the additional degrees of freedom rather than to the power-spectral treatment. And if the added degrees of freedom are important to the result, they are likely to be important on a discrete-gust as well as a power-spectral basis.

6. To further emphasize the parallelism of the discrete gust and power-spectral forms of criterion, it is of interest to compare the dash-line curves in Figure 17-1, representing the levels produced by the 50 fps discrete gust criterion, with the design levels selected in Section 15. The latter are $N(y)/N_0 = 1.2 \times 10^{-6}$ for the design envelope criterion and $N(y)/N_0 = 1.2 \times 10^{-6}$ as a lower bound and 6×10^{-9} as an upper bound for the combined criterion (Curves F and G respectively in Figure 17-1). In making this comparison, it should be borne in mind that the 50 fps discrete gust velocity has generally been employed on a static basis and has provided sufficient strength to cover whatever dynamic effects are present - on the order of 40% of the static loads in the case of the Model 188, for example, as indicated by the \bar{A} values for cases 202 and 202 Rigid in Tables B-9(b) and (c). Consequently, when the elastic-mode dynamic effects are to be included explicitly in the analysis, the $\sigma_w \eta_d$ values indicated by the dash lines would be divided by the dynamic factor of 1.40 as well as by the factor of about 1.08 which accounts for the unconservatism in Figure 5-2. Dividing the Curve B (Model 188) value at 12,000 ft. by (1.08) (1.40) gives $\sigma_w \eta_d = 63$, which is very close to the value of 60 actually obtained in Section 13.

As a result of the above considerations, it appears that the discrete gust concept has largely served its purpose and that airworthiness requirements based thereon can be dropped at such time as suitable power-spectral criteria are adopted.

CONCLUSIONS

1. Three forms of power-spectral gust loads criteria have been developed. All of these properly account for the continuous nature of atmospheric turbulence. They differ, however, in the degree to which they take account of how closely normal operational flight conditions approach the design envelope.
2. A combined form of criterion, embodying both the mission analysis and design envelope concepts, is considered to be the most desirable. In this criterion, two alternatives are offered. Under the first, appropriate for an airplane that is not gust critical, loads are obtained on a design envelope basis at a sufficiently severe $\sigma_w \eta_d$ level to assure an adequate structure no matter how severe the actual airplane operation may be relative to the design envelope, subject only to the design envelope not being exceeded. In the second, loads are obtained on a mission analysis basis, reflecting the actual operation expected; in addition, loads are obtained on a design envelope basis, at a considerably lower $\sigma_w \eta_d$ level, in order to provide a "floor" below which the loads will not be allowed to fall.
3. The "combined" form of dynamic gust loads criterion is sufficient to assure adequacy of a new design from a gust loads standpoint. A static or dynamic discrete gust criterion would not be necessary in addition to the power-spectral criterion.
4. Limit-strength frequency of exceedance values for the reference airplanes, based upon mission analysis calculations, are:

Vertical gust

Model 188	$N(y)$	=	2.1×10^{-5}	exceedances per hour
Model 749	$N(y)$	=	1.8×10^{-5}	exceedances per hour
Model 720B	$N(y)$	=	1.1×10^{-5}	exceedances per hour

Lateral gust

Model 188	$N(y)$	=	6.0×10^{-5}	exceedances per hour
Model 749	$N(y)$	=	2.5×10^{-4}	exceedances per hour
Model 720B	$N(y)$	=	4.0×10^{-6}	exceedances per hour

For these airplanes, vertical gust values are governed by wing strength and lateral gust values by tail strength. The Model 720B lateral gust value is for yaw damper off.

5. Limit strength values of $\sigma_w \eta_d$ for the reference airplanes at speed V_C , based upon critical design envelope points are:

Vertical gust

Model 188	$\sigma_w \eta_d$	=	60 fps at 12,000 ft. ($N(y)/N_0 = 1.2 \times 10^{-6}$)
Model 749	$\sigma_w \eta_d$	=	88 fps at 7,000 ft. ($N(y)/N_0 = 7 \times 10^{-8}$)
Model 720B	$\sigma_w \eta_d$	=	111 fps at 22,000 ft. ($N(y)/N_0 = 8 \times 10^{-9}$)

Lateral gust

Model 188	$\sigma_w \eta_d$	=	61 fps at 7,000 ft. ($N(y)/N_0 = 1.4 \times 10^{-6}$)
Model 749	$\sigma_w \eta_d$	=	65 fps at 7,000 ft. ($N(y)/N_0 = 8 \times 10^{-7}$)
Model 720B	$\sigma_w \eta_d$	=	99 fps at 23,000 ft. ($N(y)/N_0 = 2.4 \times 10^{-8}$)

Again, the vertical gust values are governed by wing strength. The lateral gust values are governed by tail and aftbody strength. The Model 720B lateral gust value is for yaw damper off.

6. Although both the Model 188 and Model 749 limit-strength frequency of exceedance due to lateral gust is higher than due to vertical gust - that is, the vertical tail is critical - the design frequency of exceedance should be taken at the more conservative level based on wing strength. It is believed that actual lateral gust loads may be somewhat lower than indicated by the analysis because of the ability of the pilot to provide additional Dutch roll damping by use of the controls.
7. Appropriate design levels for use on new airplanes are concluded to be:

For a mission analysis: $N(y) = 2 \times 10^{-5}$ exceedances per hour.

For a design envelope criterion if used alone or for the design envelope "floor" in the combined criterion: $\sigma_w \eta_d$ to be as defined by $N(y)/N_0 = 1.2 \times 10^{-6}$ in Figure 5-8 (corresponding to $\sigma_w \eta_d = 62$ fps at 7000 ft.)

For the conservative design envelope loads obtained in lieu of a mission analysis under the combined criterion: $\sigma_w \eta_d$ to be as defined by $N(y)/N_0 = 6 \times 10^{-9}$ in Figure 5-8 (corresponding to $\sigma_w \eta_d = 110$ fps at 7000 ft.)

The above $\sigma_w \eta_d$ values are for speed V_C . At speed V_B , design should be to 66/50 of the V_C values, and at speed V_D , to 25/50 of the V_C values.

8. The description of the atmosphere to be used in conjunction with the stated design levels of $N(y)$ and $\sigma_w \eta_d$ utilizes a shape of power spectral density function given by the isotropic turbulence equation,

$$\phi(\Omega) = \frac{\sigma_L^2}{\pi} \frac{1 + \frac{8}{3} (1.339 L \Omega)^2}{[1 + (1.339 L \Omega)^2]^{11/6}}$$

with $L = 2500$ ft. The σ_w distributions for use in the mission analysis are defined by b and P values in equation 5-2 herein as given by Figures 5-3 and 5-4. This description, were it to be used on an absolute basis (that is, independently of the limit design levels established herein) would be slightly conservative.

9. Either a "matching condition" or a "joint probability" technique can be used to integrate the statistical loads determination with the stress analysis operation. The application of each is illustrated. Use of the joint probability technique is likely to be limited to the final stage of design. The matching condition, or single parameter, technique can be applied in various degrees of refinement and is appropriate for use at all stages of design.
10. Exact consistency of the joint probability and the matching condition or single parameter techniques is not to be expected, because of the subtle difference in the design philosophy reflected. However, the numerical differences are very small.
11. There is some indication that aerodynamic induction effects and transient lift growth may have a much greater influence on the gust response of a rigid airplane free to pitch than has previously been realized. Inasmuch as rather crude assumptions in this area have generally been regarded as entirely acceptable, further research is considered urgent.

APPENDIX A

COMPARISON OF ASD TR 61-235 AND TN 4332 σ_v DISTRIBUTIONS

Comparisons of the ASD TR 61-235 and TN 4332 P and b values are shown in Figures A-1 through A-4. The over-all effect on the σ_v distributions, as reflected in plots of $N(y)/N_0$ vs y/\bar{A} , is then shown in Figures A-5 and A-6.

In these comparisons, the "As Published" P and b values are taken directly from the respective sources. They are for use with a Liepmann spectral shape with $L = 1000$ ft., except that the ASD TR 61-235 values below an altitude of 5000 ft. are associated with reduced values of L. Although not applicable in the present work, TN 4332 "Missile" P₂'s (no storm avoidance) are included as a matter of interest.

The ASD TR 61-235 "Modified" P and b values are as defined by Figures 5-3 and 5-4.

The TN 4332 "Modified" values are obtained so as to be generally consistent with the ASD TR 61-235 "Modified" values. The same factors are applied to P₁ and P₂ as in obtaining the ASD TR 61-235 "Modified" values. The computation of b₁ and b₂ values is shown in Tables A-1 and A-2. These tables follow the format of Tables Ia and Ib of TN 4332, but the computations differ as follows:

- (1) The quantity labeled $\sqrt{I(K,S)/w}$ in TN 4332 and designated K_0 herein is read from curves based upon the "isotropic turbulence" spectrum (Figure 5-2), at a value of $L = 2500$ ft., instead of from Fig. 7 of NASA TR 1272 (based upon the Liepmann spectrum) at $L = 1000$ ft.
- (2) The lift curve slope is taken as

$$1.15 \frac{6A}{A + 2}$$

where A is the aspect ratio, the quantity $6A/(A + 2)$ is an excellent approximation of the lift curve slope for wing alone, and the factor 1.15 accounts for the average ratio of airplane to wing lift curve slope. The value thus obtained is used both where the lift curve slope appears explicitly in Equation (17) of TN 4332 (Equation 5-5 herein) and in evaluation of the mass parameter. The inclusion of the 1.15 factor in the equation itself results in its appearance in the heading of Column 9 of Tables A-1 and A-2.

Its inclusion in the mass parameter accounts for its appearance in the heading of Column 4.

Column 4, designated $\bar{\mu}$, corresponds to "K" in Tables Ia and Ib of TN 4332. However, a factor of 4 has been omitted for consistency with the Pratt mass parameter (NASA TR 1206, Reference 31); and, as noted above, the theoretical lift curve slope of 2π is replaced by an estimated actual lift curve slope.

- (3) A revised estimate of dynamic factor is included in the final evaluation of b_1 and b_2 in Column 10. The dynamic factor calculated for the Lockheed Model 749A Constellation (ratio of rms values, flexible to rigid, based on the Liepmann spectrum with $L = 1000$ ft.) is 1.07. Values quoted for the DC-6 and DC-7 in ASD TR 61-235 range from 1.02 to 1.07. A value of 1.06 is considered representative, and the ratio of the value 1.20 used in TN 4332 to this value is 1.13. This factor provides what is in effect an adjustment to the U_{de} levels and could properly have been applied as a factor to either the 2.2 coefficient in Column 2 or to \bar{C} in Column 9.

No correction for pitch is included. As indicated in connection with the modification of the ASD TR 61-235 b_1 and b_2 values, analysis based on the Model 749 has shown the effect of pitch to be small. Further, whereas inclusion of pitch would reduce \bar{A} by about 7%, use of more exact lift growth functions in the plunge-only analysis would increase \bar{A} by almost exactly the same amount.

It will be noted that the "ASD TR 61-235 Modified" and the "TN 4332 Modified" b 's are inconsistent to the extent of about 7%, because of the differences in the lift growth functions assumed in the original determinations. To remove this inconsistency it would be necessary to increase the ASD TR 61-235 b values.

It may be remarked that no inconsistency results from not modifying the lift curve slope in evaluating the Pratt mass parameters (Column 3) or in the equation for \bar{C} (Column 9). A modification to \bar{C} will result in an equal and opposite modification to the coefficient 2.2 in Column 2 and hence will have no effect on the results.

It is interesting to note that although the differences between TN 4332 and ASD TR 61-235 b and P values appear rather great (Figures A-1 through A-4), the resulting generalized exceedance curves (Figures A-5 and A-6) show much closer agreement.

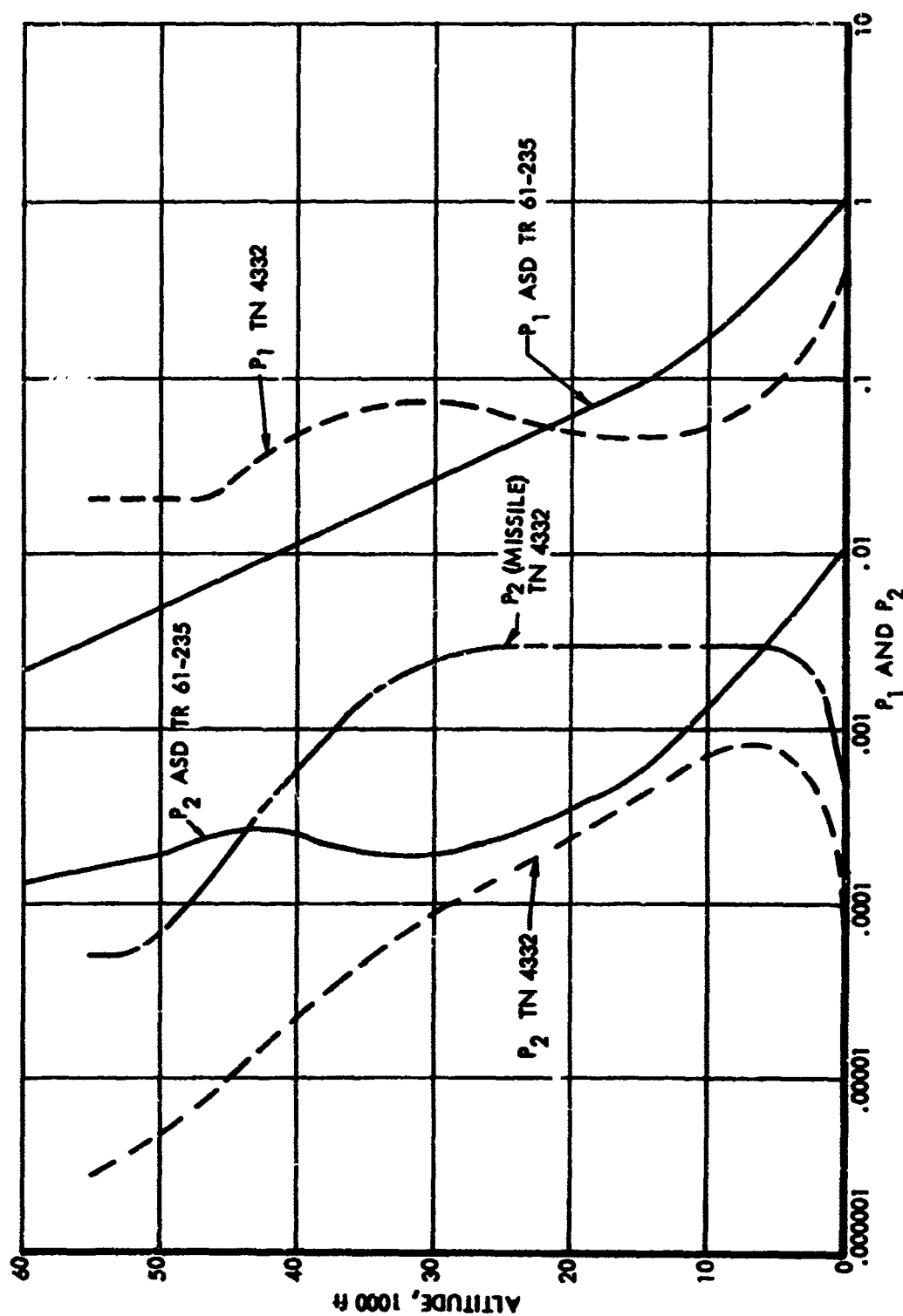


FIGURE A-1. COMPARISON OF P₁ AND P₂ VALUES - TN4332 VS ASD TR 61-235, AS PUBLISHED

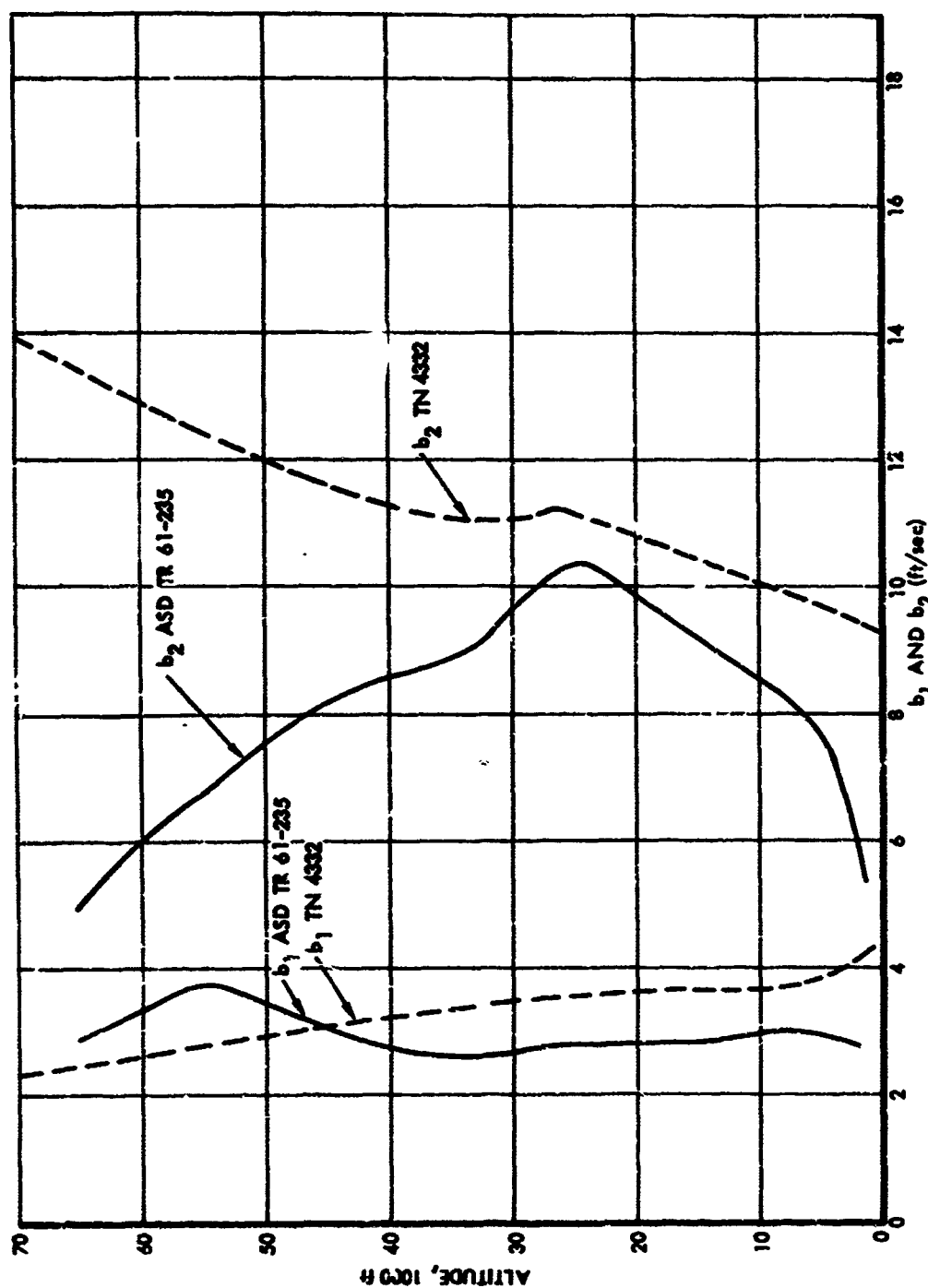


FIGURE A-2. COMPARISON OF b_1 AND b_2 VALUES -
TN 4332 VS ASD TR 61-235, AS PUBLISHED

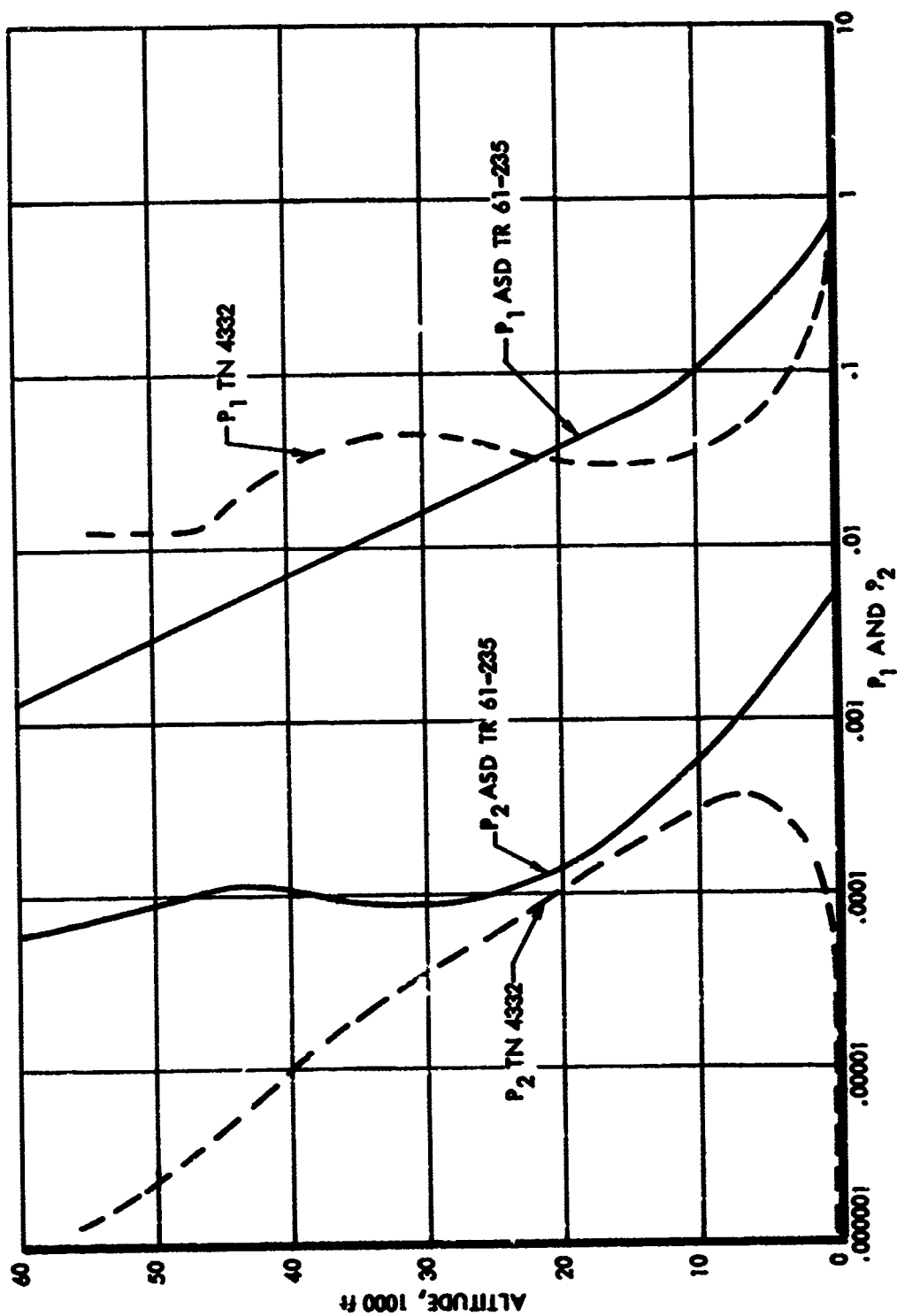


FIGURE A-3. COMPARISON OF P_1 AND P_2 VALUES -
TN 4332 VS ASD-TR-61-235, MODIFIED

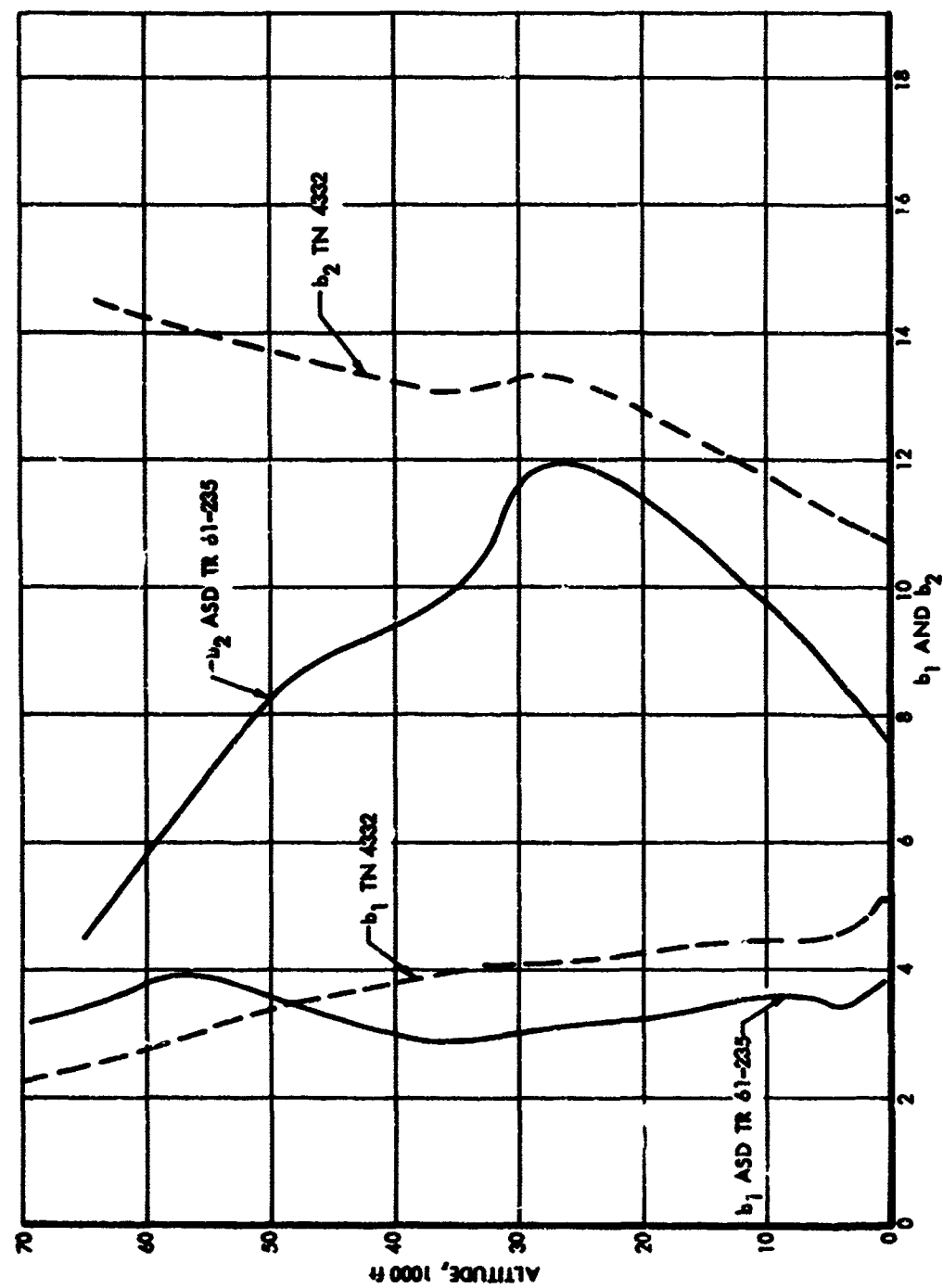
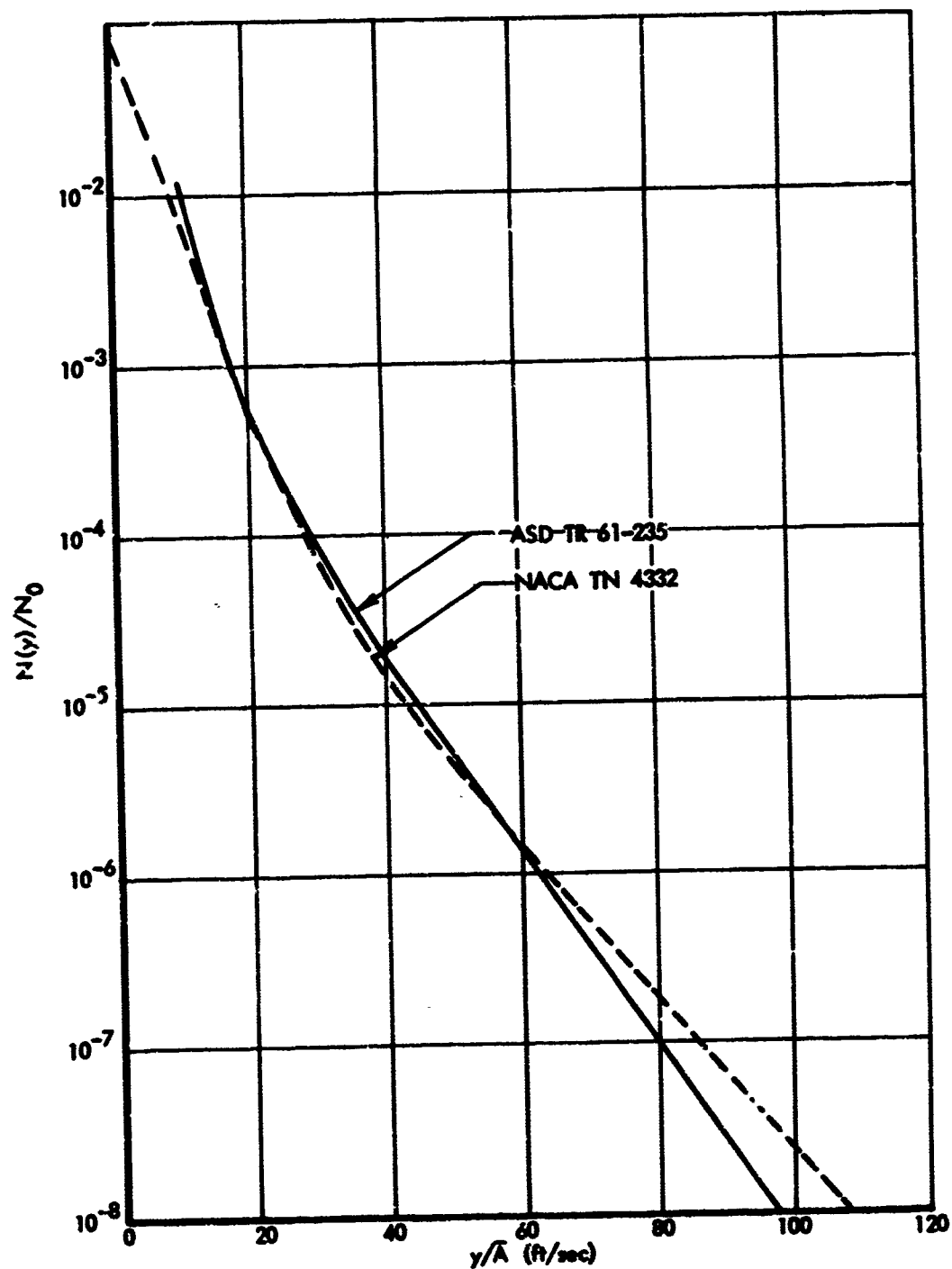
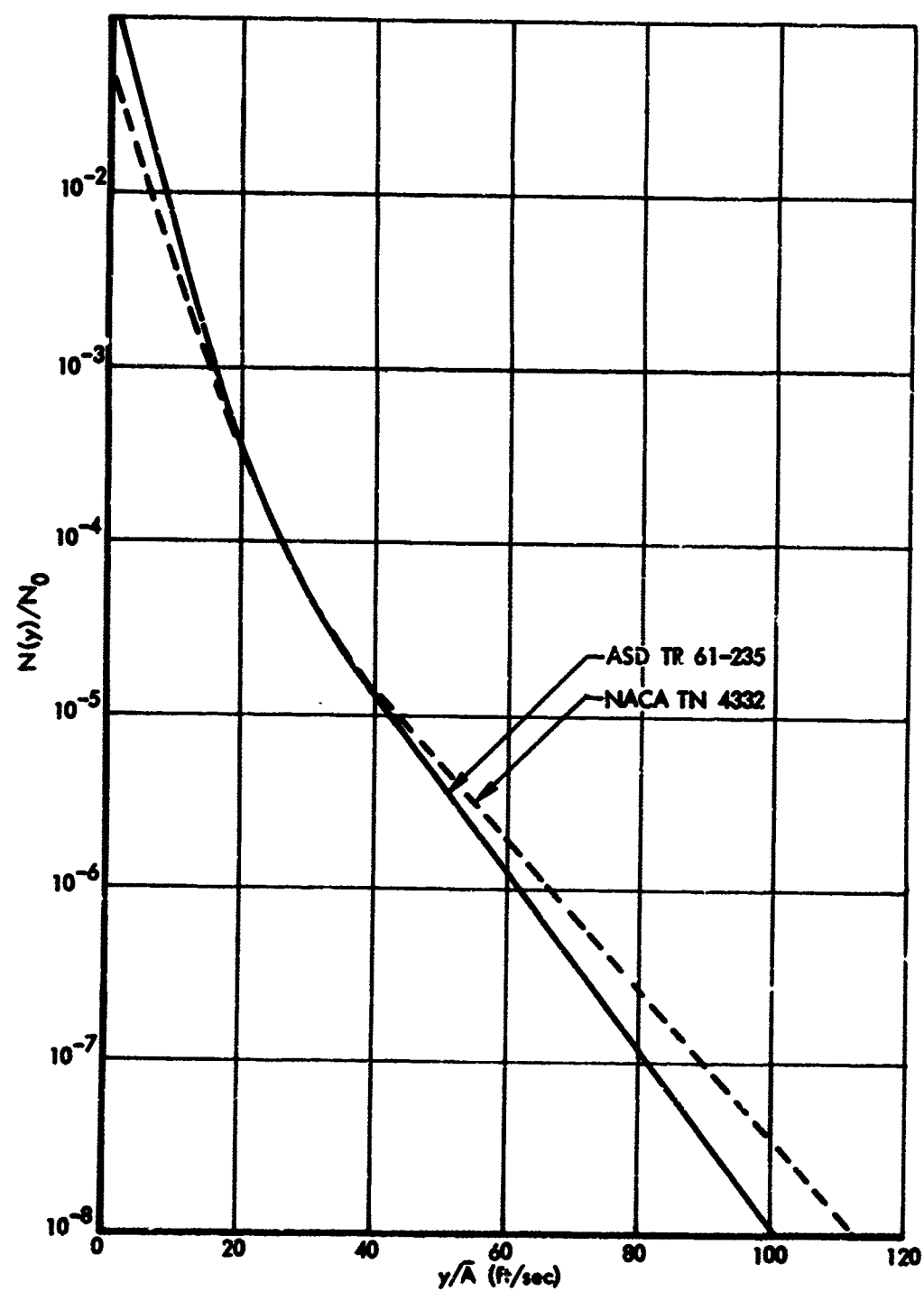


FIGURE A-4. COMPARISON OF b_1 AND b_2 VALUES -
TN 4332 VS ASD TR 61-235, MODIFIED

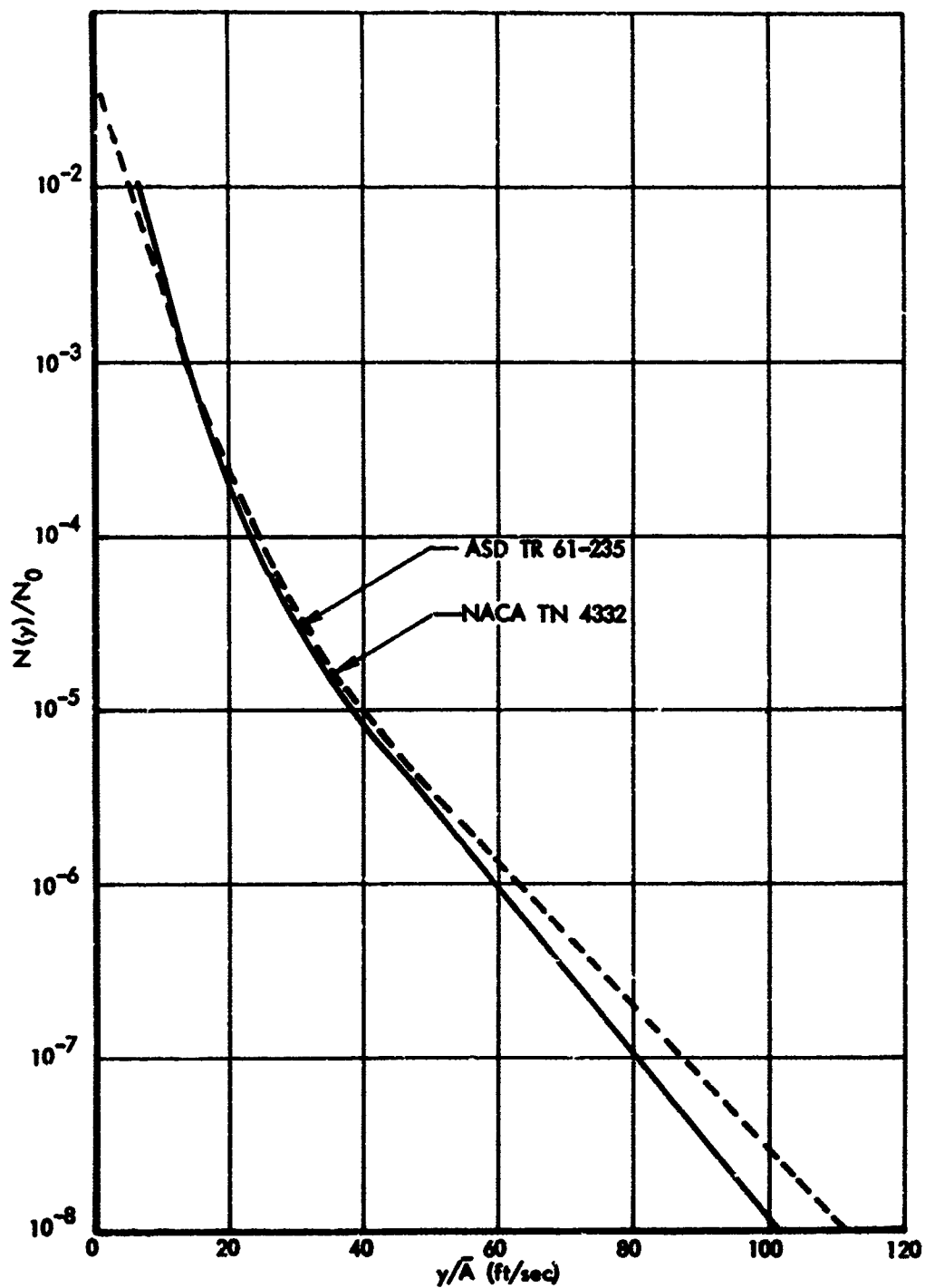


(a) $h = 5000$ FT

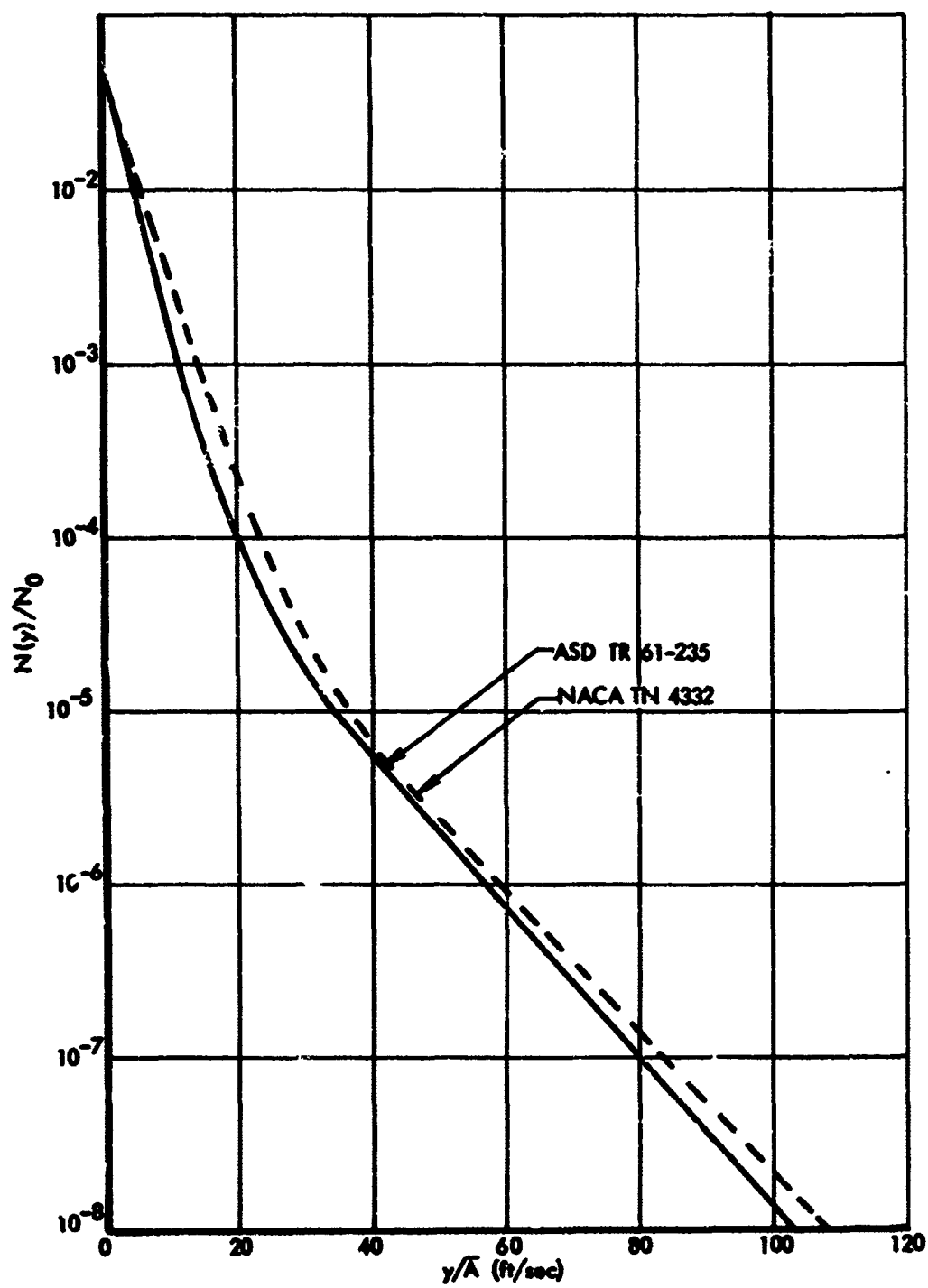
FIGURE A-5. COMPARISON OF GENERALIZED EXCEEDANCE CURVES - TN 4332 VS ASD TR 61-235, BASED ON b and P VALUES AS PUBLISHED



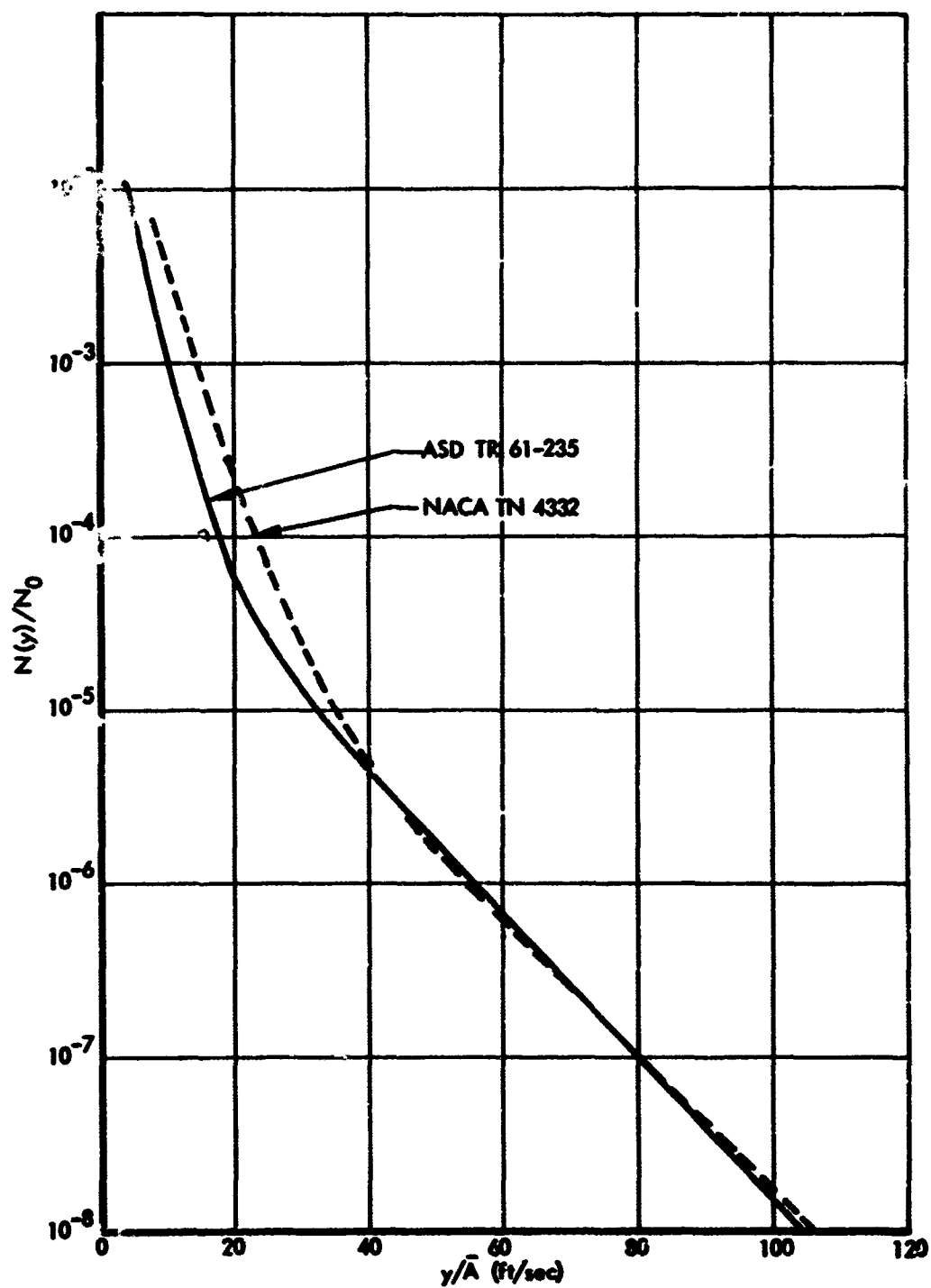
(b) $h = 10000$ FT
FIGURE A-5. CONTINUED



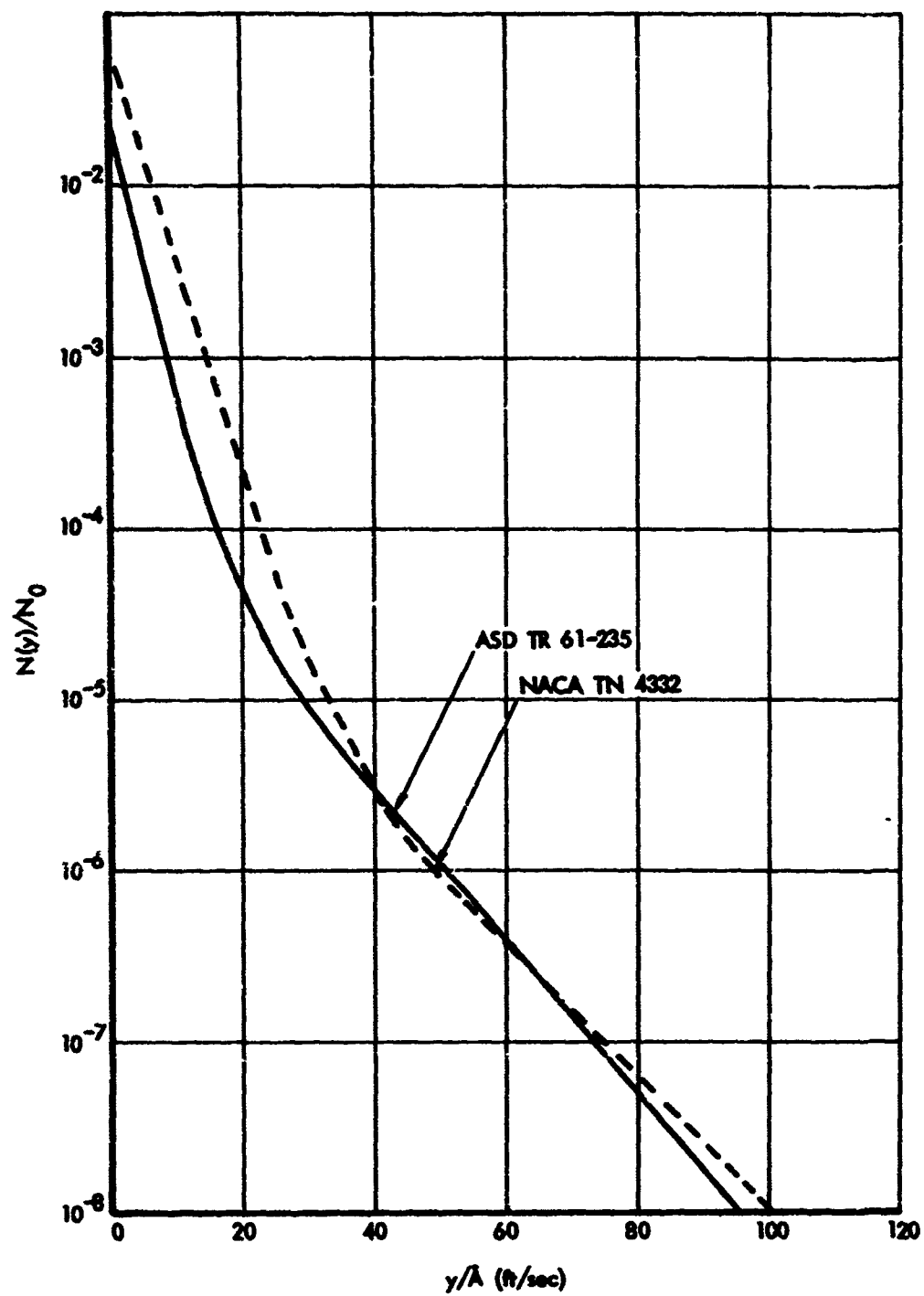
(c) $h = 15000$ FT
FIGURE A-5. CONTINUED



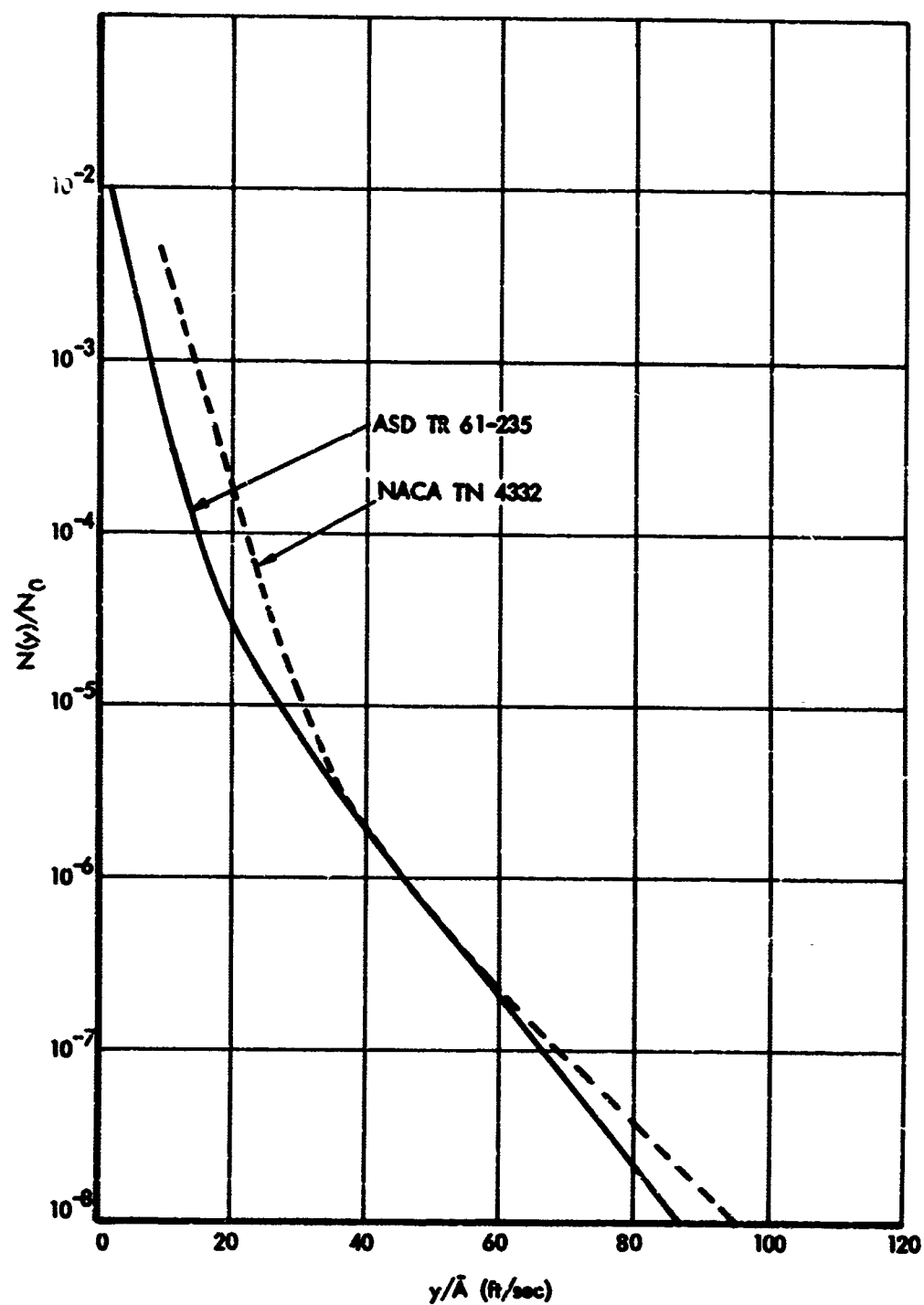
(d) $h = 20000$ FT
FIGURE A-5. CONTINUED



(e) $h = 25000$ FT
FIGURE A-5. CONTINUED



(f) $h = 30000$ FT
 FIGURE A-5. CONTINUED



(g) $h = 35000$ FT
 FIGURE A-5. CONTINUED

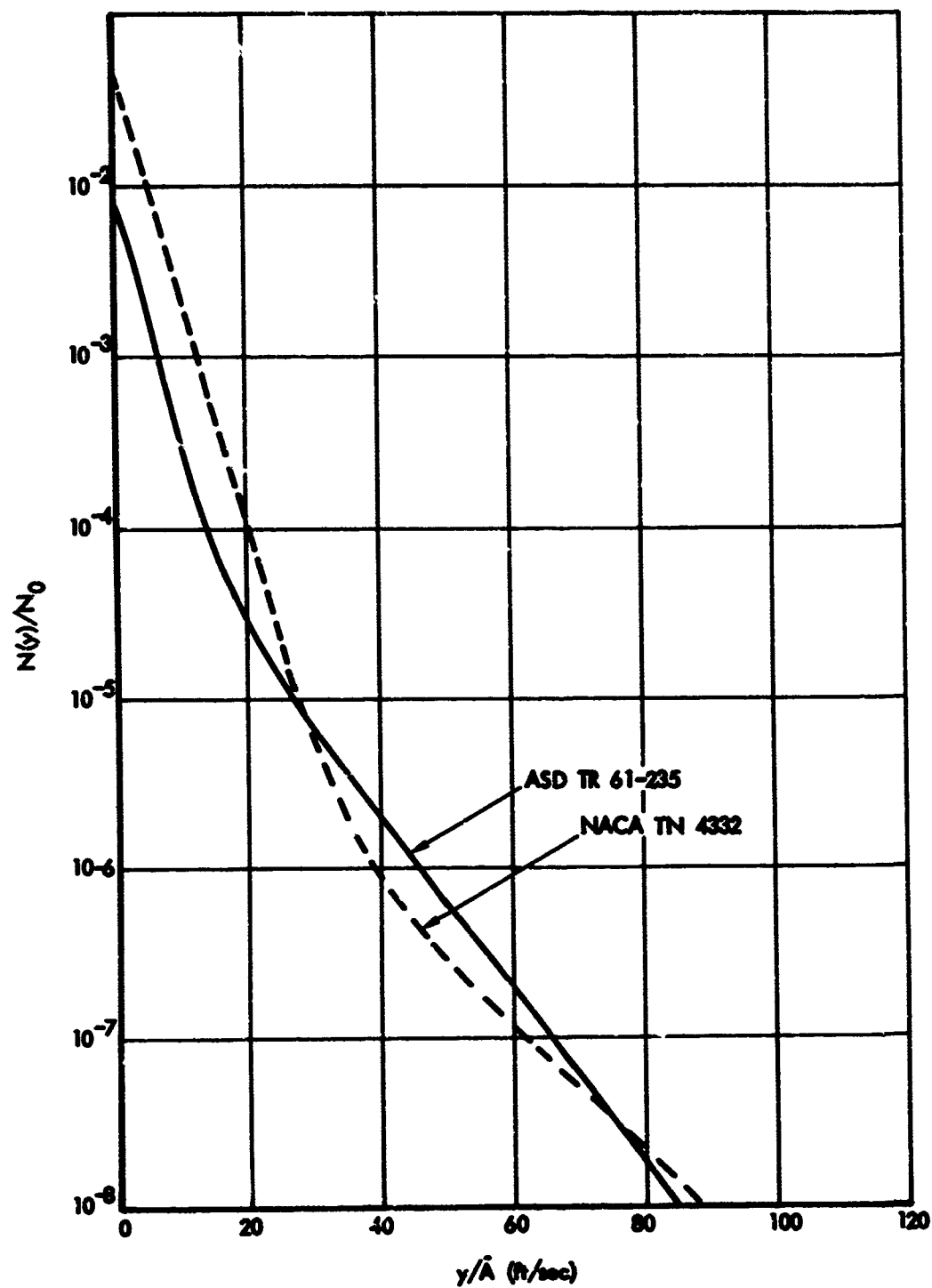
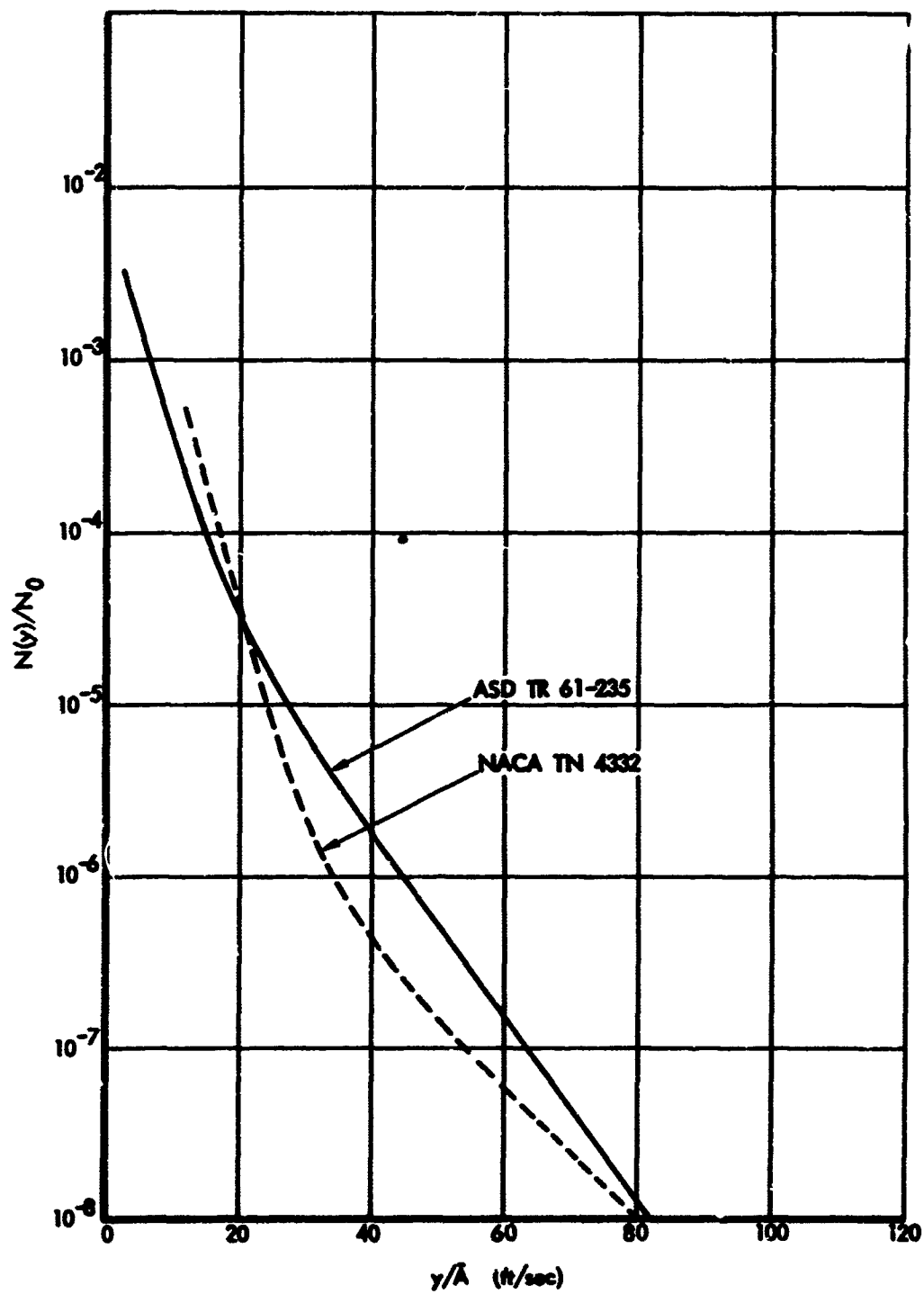
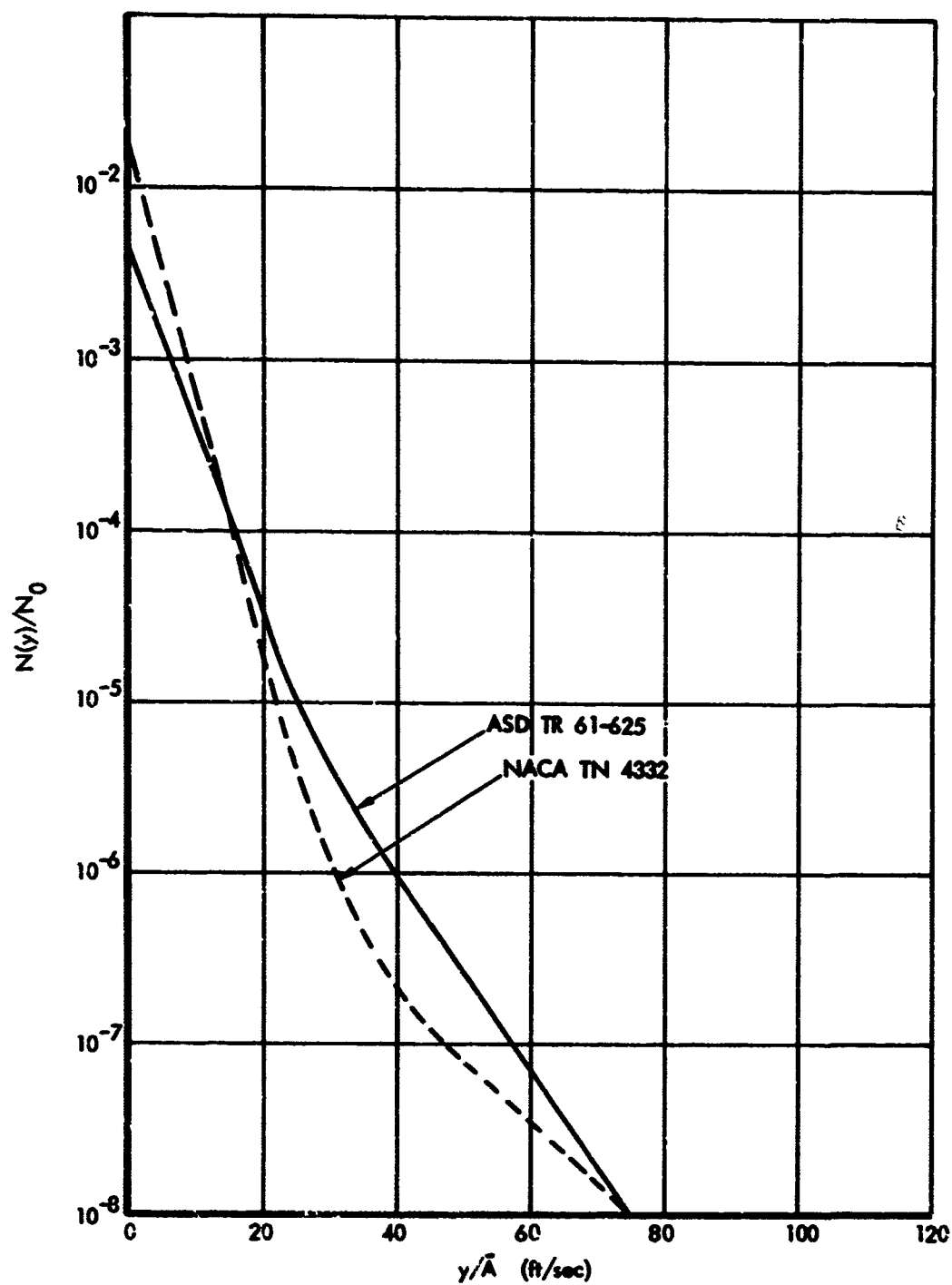


FIGURE A-5. CONTINUED

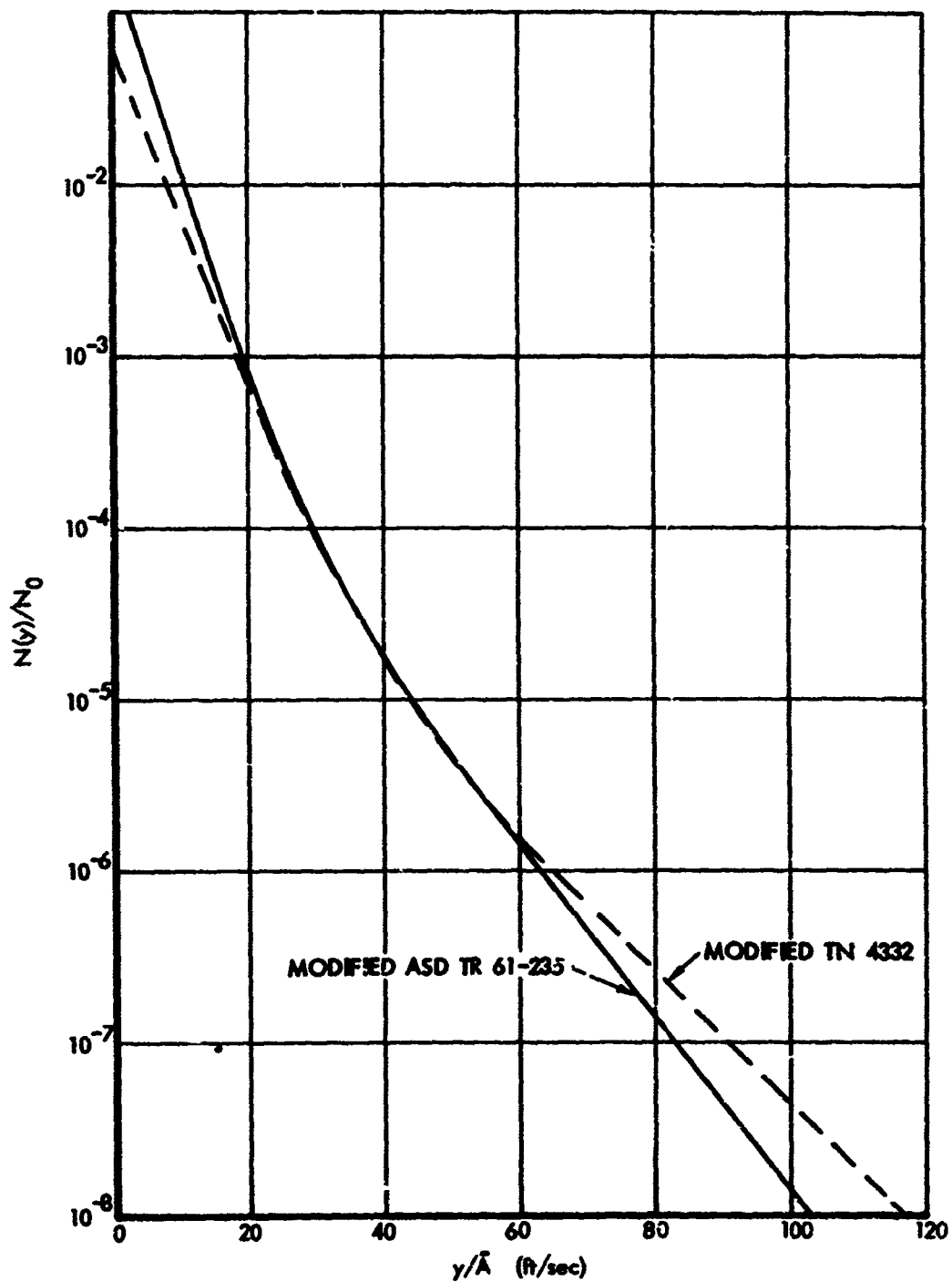


(i) $h = 45000$ FT
FIGURE A-5. CONTINUED



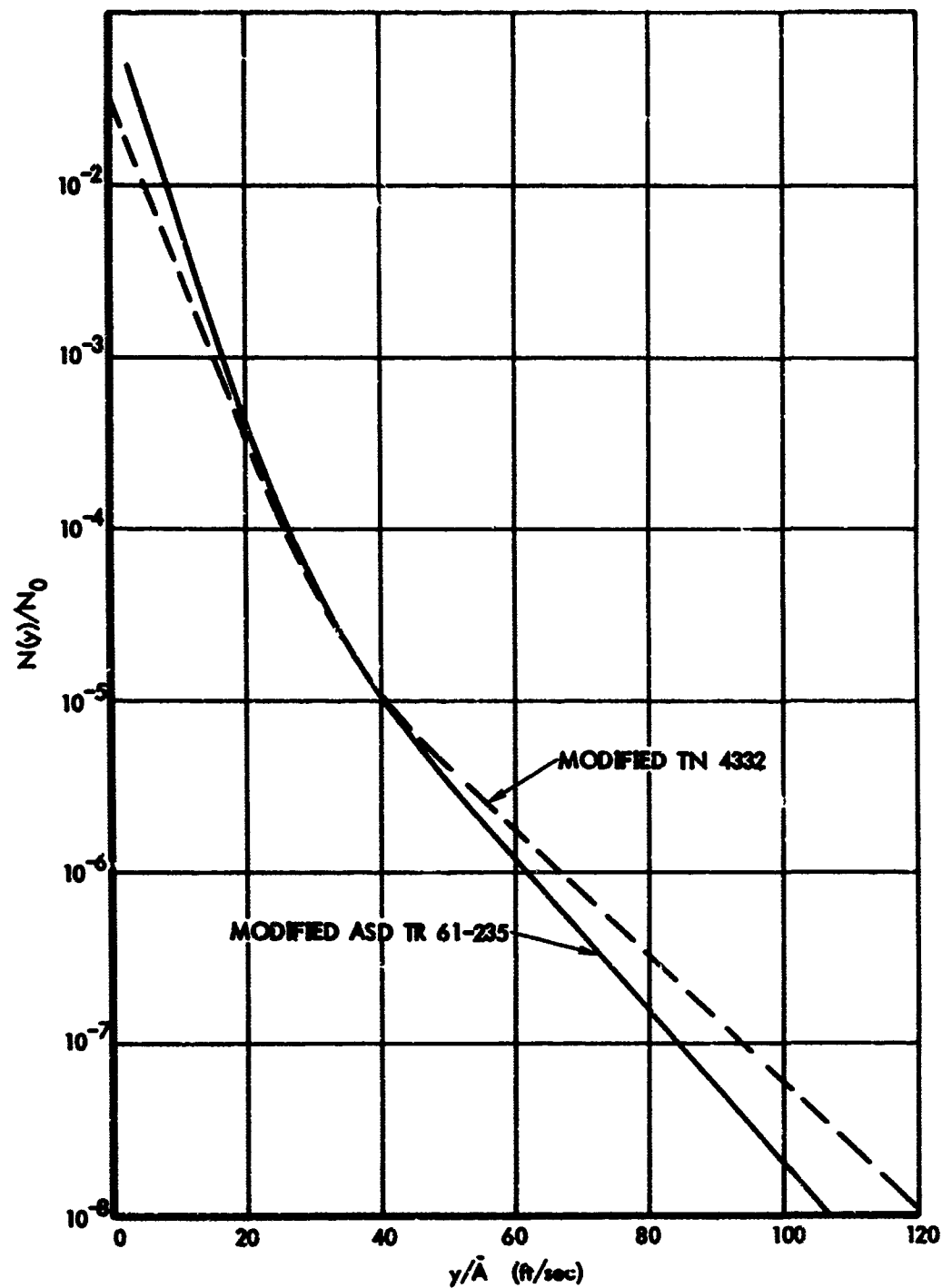
(j) $h = 50000$ FT

FIGURE A-5. CONCLUDED

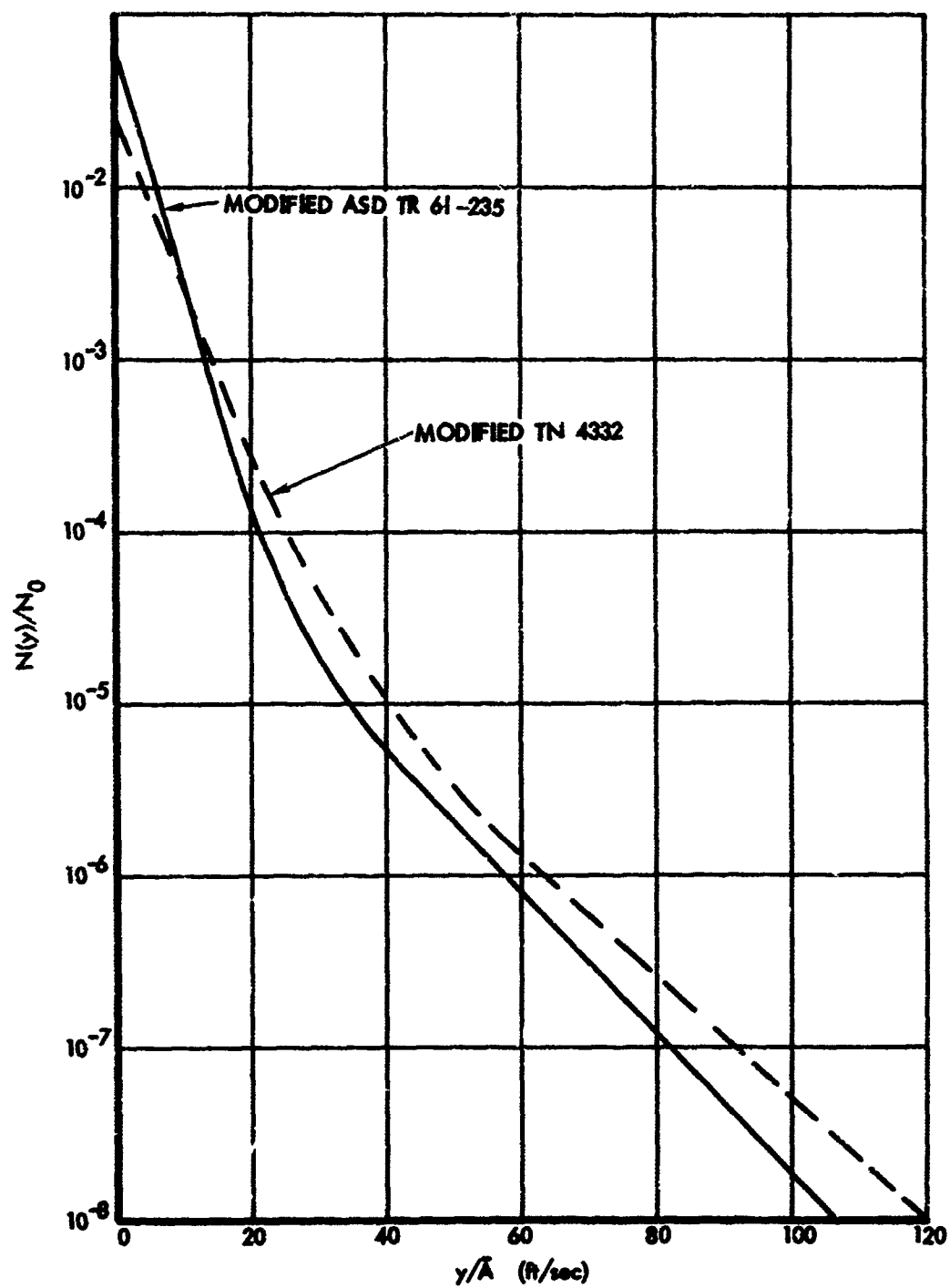


(a) $h = 5000$ FT

FIGURE A-6. COMPARISON OF GENERALIZED EXCEEDANCE CURVES - TN 4332 VS ASD TR 61-235, BASED ON MODIFIED b AND P VALUES

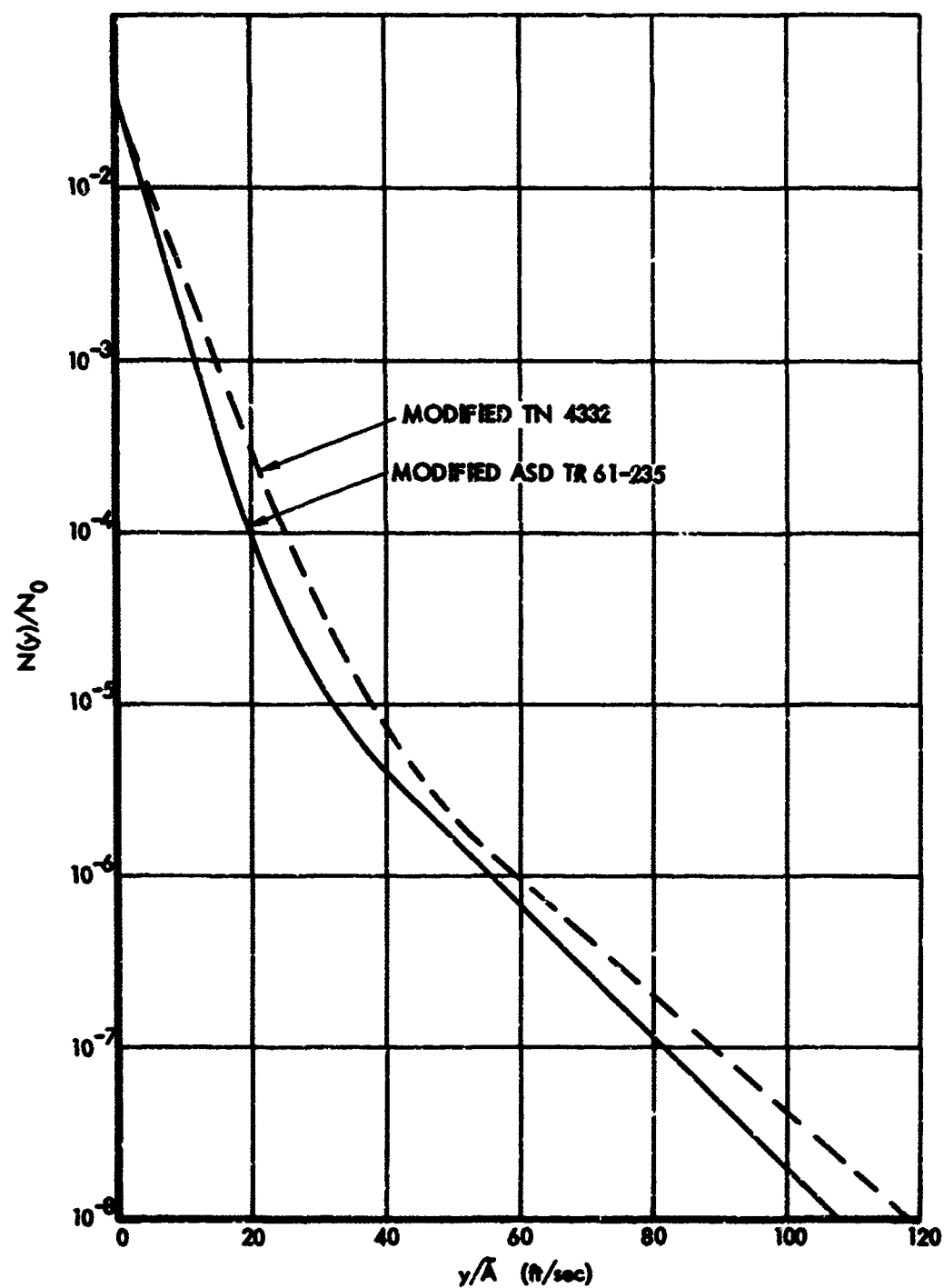


(b) $h = 10000$ FT
FIGURE A-6. CONTINUED

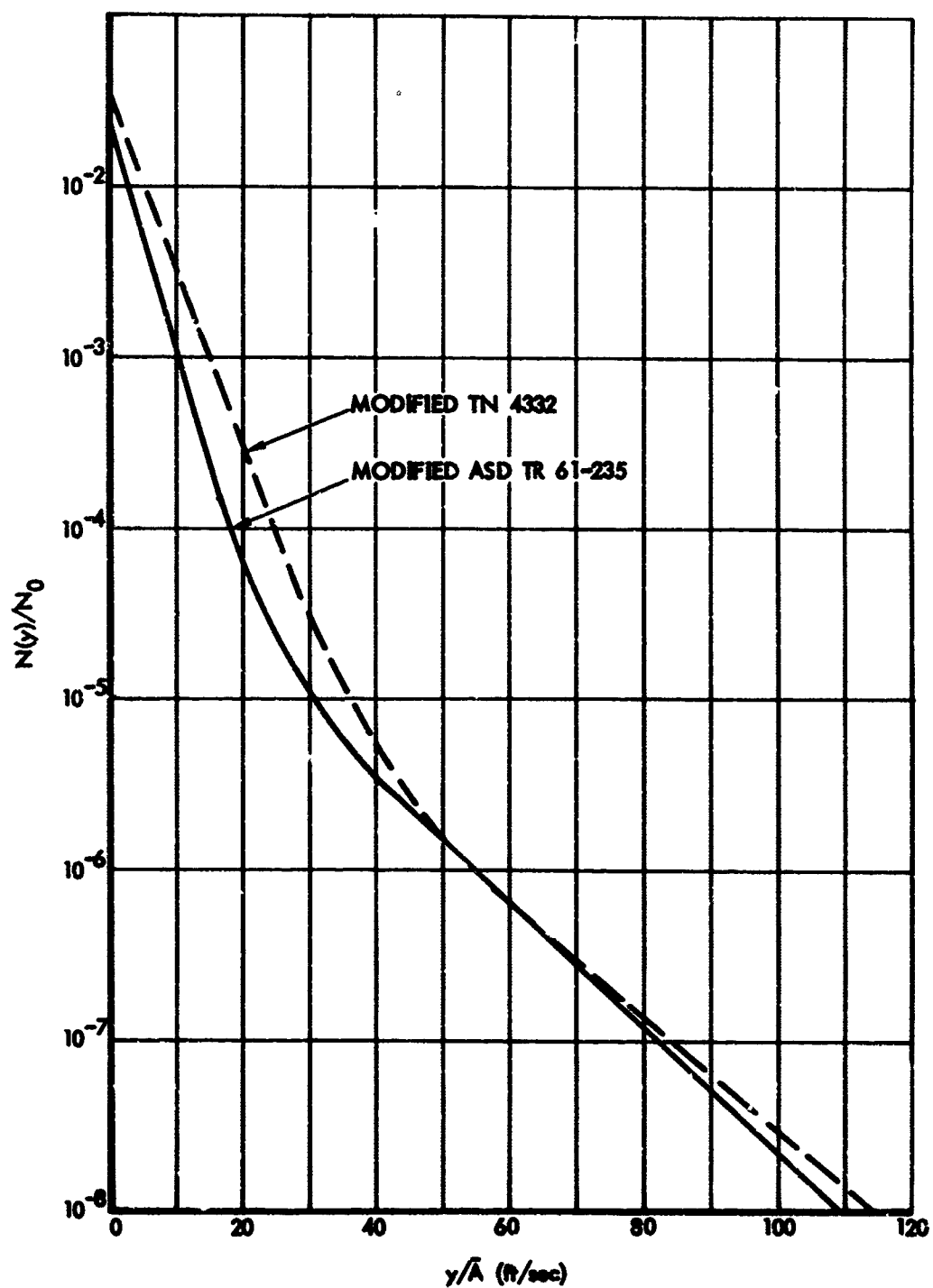


(c) $h = 15000$ FT

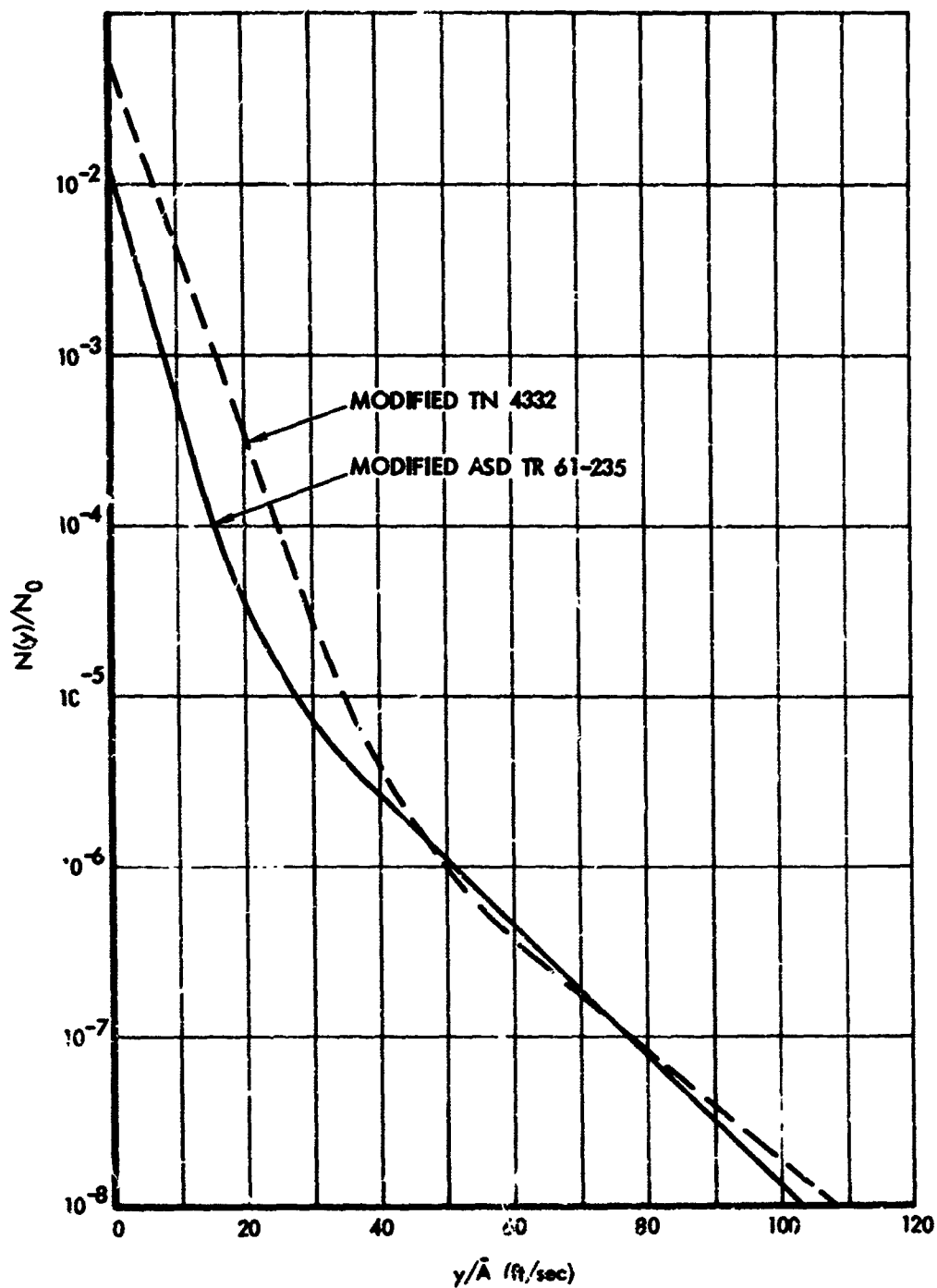
FIGURE A-6. CONTINUED



(d) $h = 20000$ FT
FIGURE A-6. CONTINUED

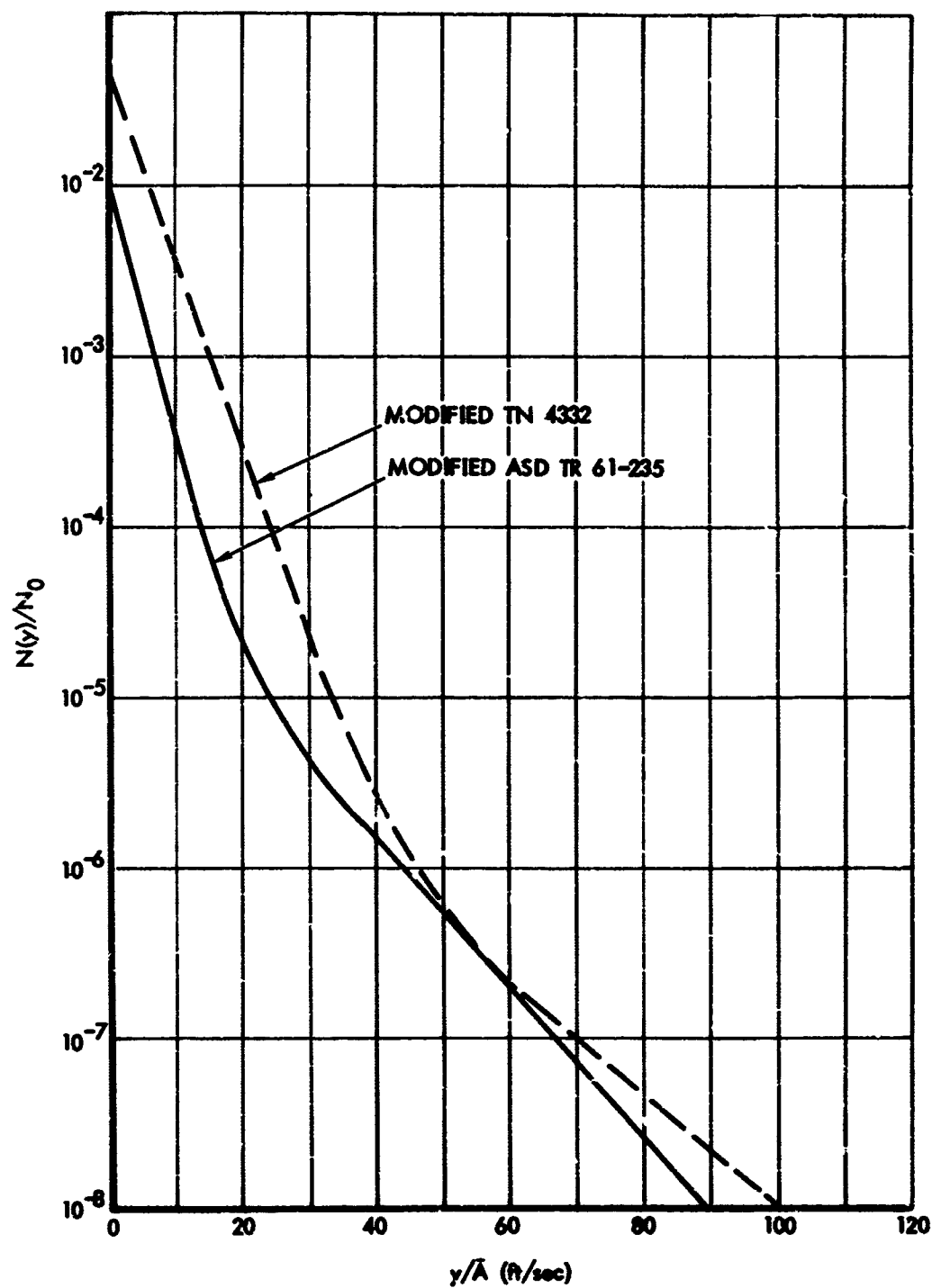


(e) $h = 25000 \text{ FT}$
 FIGURE A-6. CONTINUED

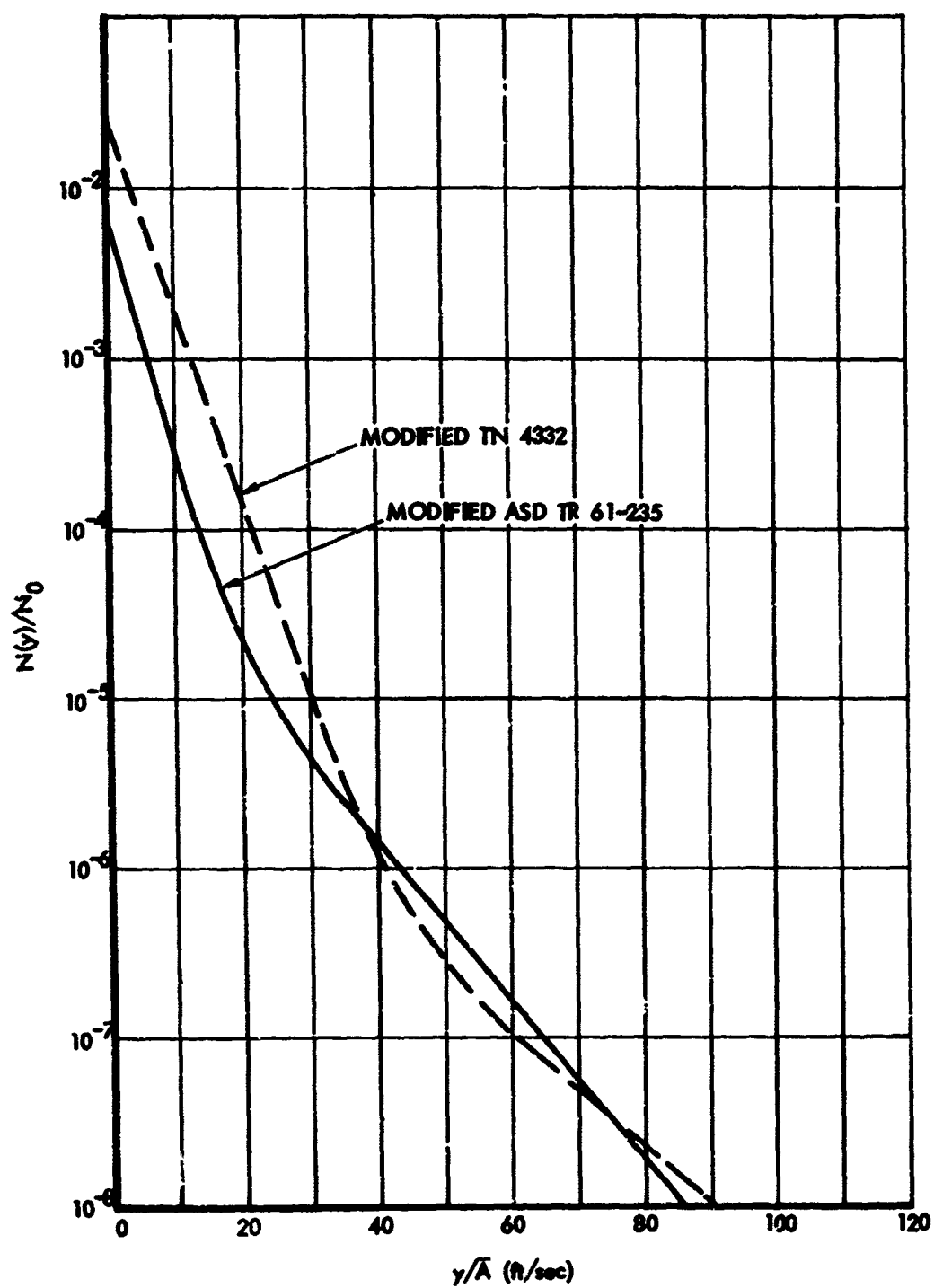


(f) $h = 10000$ FT

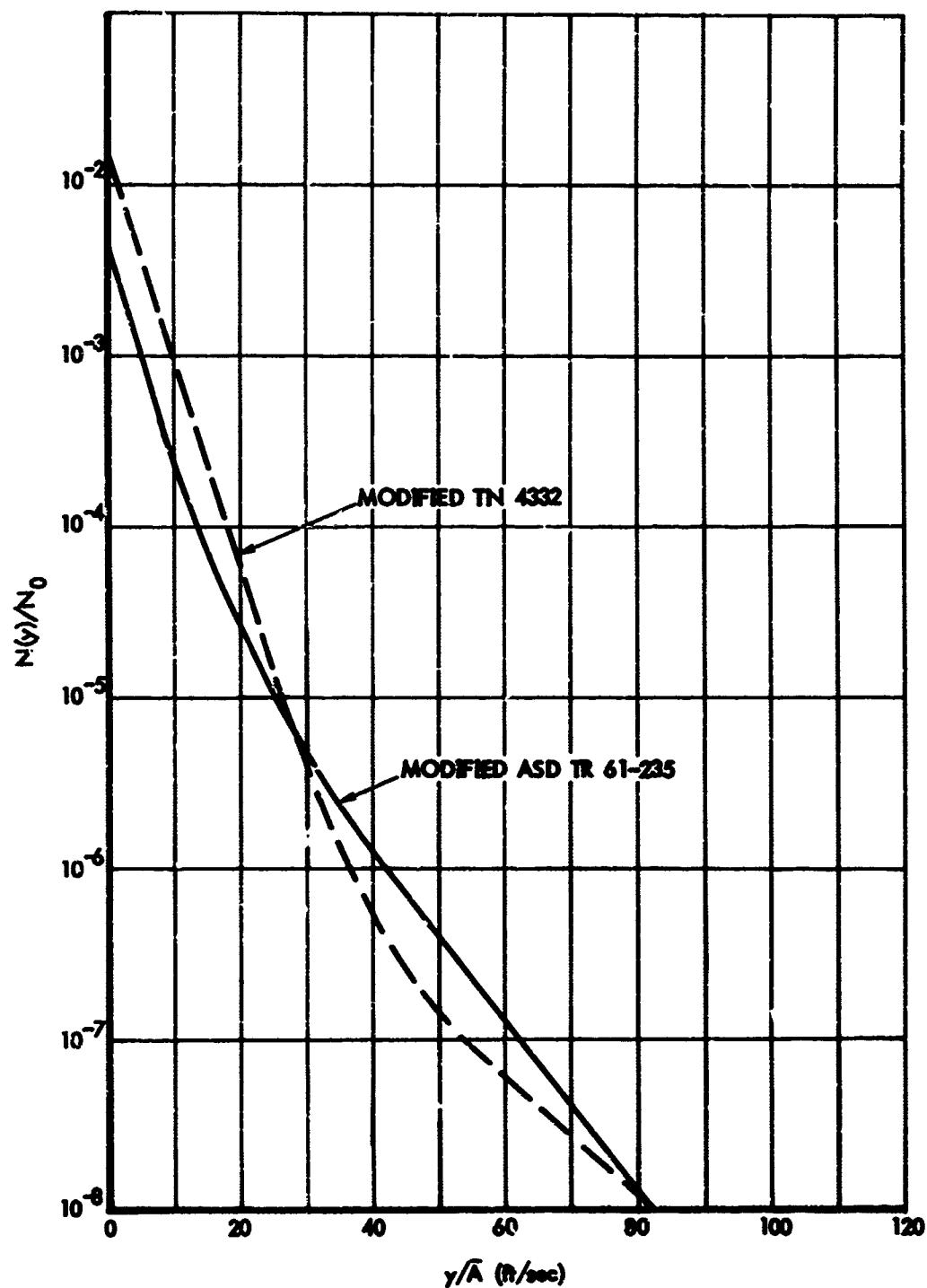
FIGURE A-6. CONTINUED



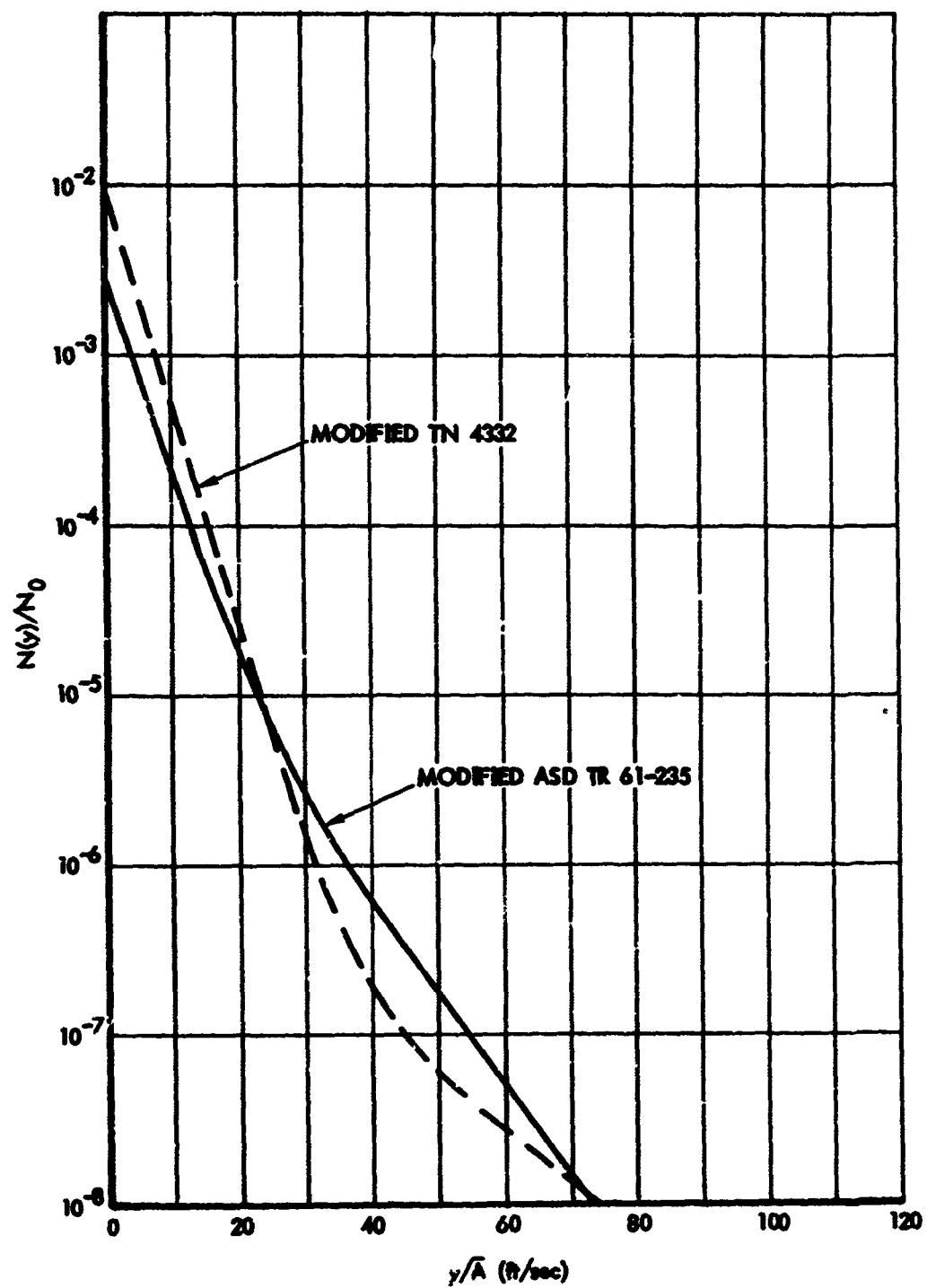
(g) $h = 35000$ FT
FIGURE A-o. CONTINUED



(h) $h = 40000$ FT
 FIGURE A-6. CONTINUED



(i) $h = 45000$ FT
 FIGURE A-6. CONTINUED



(j) $h = 50000$ FT

FIGURE A-6. CONCLUDED

TABLE A-1. RE-EVALUATION OF PARAMETER b_1 BASED ON TN 4332 DATA

①	②	③	④	⑤	⑥	⑦	⑧	⑨	⑩
h Ft.	$2.2 K_1$	Pratt μ_g	$\bar{\mu}$	K_g	K_σ	$\frac{K_g}{K_\sigma}$	$\sqrt{\frac{A_0}{\rho}}$	$\frac{\bar{r}}{A}$	b_1
	TN4332 Table Ia	TN4332 Table Ia	③ 1.15	Function Of ③ TN4332 Table Ia	Function Of ④ Figure 5-2	⑤ ⑥		⑦ ⑧ 1.15	② ⑨ 1.13
0-2000	2.6	21.0	18.3	.703	.363	1.94	1.015	1.71	5.03
2000-10000	2.2	24.3	21.1	.722	.385	1.88	1.094	1.79	4.45
10000-20000	2.0	32.3	28.1	.758	.427	1.78	1.261	1.95	4.40
20000-30000	1.7	45.4	39.5	.798	.482	1.65	1.464	2.14	4.12
30000-40000	1.5	65.5	57.0	.823	.544	1.51	1.797	2.36	4.00
40000-50000	1.2	105.5	91.8	.840	.63	1.33	2.278	2.64	3.58
50000-60000	.9	170.0	148.0	.850	.708	1.20	2.893	3.02	3.06

Data Assumed: $\bar{W} = 77000$ lb; $S = 1463$ ft²; $\bar{c} = 13.7$ ft; $C_{L\sigma} = 4.95$ per radian (wing alone)
and (1.15) (4.95) = 5.70 per radian (airplane); isotropic turbulence
spectrum, $L = 2500$ ft.

TABLE A-2. RE-EVALUATION OF PARAMETER b_2 BASED ON
TN 4332 DATA

①	②	③	④	⑤	⑥	⑦	⑧	⑨	⑩
h ft.	$5.3 K_E$	Prett μ_g	$\bar{\mu}$	K_g	K_v	$K \frac{K_g}{K_v}$	$\sqrt{\frac{P_0}{\rho}}$	$\frac{\bar{c}}{\lambda}$	b_2
	TN4332 Table Ib	TN4332 Table Ib	③ 1.15	Function Of ③ TN4332 Table Ib	Function Of ④ Fig. 5-2	⑤ ⑥		⑦ ⑧ 1.15	⑨ ⑩ 1.13
0-2000	5.3	24.0	20.8	.718	.352	2.04	1.015	1.80	10.79
2000-10000	5.3	27.9	24.3	.736	.373	1.97	1.094	1.88	11.27
10000-20000	5.3	37.1	32.3	.768	.415	1.85	1.261	2.03	12.17
20000-30000	5.3	52.0	45.2	.798	.469	1.70	1.494	2.21	13.22
30000-40000	4.8	75.4	65.6	.824	.533	1.55	1.797	2.42	13.13
40000-50000	4.4	121.0	105.2	.840	.614	1.37	2.278	2.72	13.50
50000-60000	4.0	195.4	170.0	.856	.694	1.23	2.893	3.10	14.02

Data Assumed: $W = 30000 \text{ lb.}; s = 662.4 \text{ ft.}^2; \bar{c} = 10.5 \text{ ft.}; C_{lq} = 4.83 \text{ per radian (wing alone)}$
 and $(1.15) (4.83) = 5.55 \text{ per radian (airplane)}; \text{isotropic turbulence spectrum,}$
 $I = 2500 \text{ ft.}$

APPENDIX B

NUMERICAL RESULTS

\bar{A} and N_0 values obtained from the vertical gust dynamic analysis of the Model 188 and Model 749, together with the associated one-g level flight loads, are listed in Table B-1 through B-4. Results for both the mission analysis and design envelope cases are shown.

Units in the tables are as follows:

Acceleration	g's
Shears, tail loads	pounds
Bending and torsion moments	inch pounds
Shear flows	pounds per inch
N_0	cycles per second

All \bar{A} values are in the units indicated above, per fps true gust velocity.

Sign conventions are as follows:

- Wing shear and bending moment, positive up
- Wing torsion, positive leading edge up
- Wing shear flows, positive clockwise
- Fuselage shear, positive up (relative to a fixed midbody)
- Fuselage bending moment, forebody positive up and aftbody positive down (relative to a fixed midbody)
- Tail load, positive up

Torsions and bending moments are with respect to the elastic axis in all cases.

It should be remarked that the \bar{A} and especially the N_0 values listed in Tables B-1 through B-4 for tail and aftbody loads are somewhat higher than would actually be realistic, as a result of the way in which the elevator float was treated. This motion was introduced, as noted in Section 8.1.1, in such a way as to permit an elevator flapping dynamic

mode. Inasmuch as the damping that would actually be provided by the control system was not included in the analysis, large elevator motions at about 6 cps resulted. By examination of the various load power-spectral densities for the Model 188 tail and aftbody, it was seen that, for example, a more realistic value of N_0 would be about 1.5 cps in all cases and that \bar{A} should be reduced from the value shown by about 4% for tail load, by 7% for shear and bending moment at F.S. 1000, and, for bending moment at F.S. 695 where the A value is already relatively very small because of the offsetting effect of inertia and air loads, by 25%.

\bar{A} and N_0 values obtained from the lateral gust dynamic analysis are summarized in Tables B-5 through B-8.

Units are identical to those of Figures B-1 through B-4.

As only \bar{A} and N_0 values are listed, all signs are inherently positive.

\bar{A} and N_0 values obtained in connection with the Model 188 vertical gust parameter variation study (Section 14) are presented in Table B-9. Units, sign conventions, and other particulars are the same as in Tables B-1 through B-4.

TABLE B-1. RESULTS OF VERTICAL GUST DYNAMIC ANALYSIS,
MODEL 188 MISSION ANALYSIS SEGMENTS
(a) C.G. ACCELERATIONS AND WING SHEARS, CASES 201-209

Case	1	2	3	4	5	6	7	8	9	10
	C.G. Accel	WS 83	WS 119	WS 157	WS 209	WS 275	WS 346	WS 380	WS 448	WS 516
201	\bar{A} No 1g Load	.01599 1.044 1.0	188.1 1.673 14241	172.4 1.877 10979	207.7 1.661 13663	182.5 1.675 10598	142.1 1.812 6787	126.7 1.131 9257	74.79 1.282 5385	31.15 1.649 2087
202	\bar{A} No 1g Load	.02192 1.124 1.0	263.4 1.681 16386	236.3 1.902 11862	289.8 1.606 13979	252.9 1.644 9889	194.6 1.837 5300	171.3 1.214 7679	100.8 1.365 4161	42.24 1.688 1531
203	\bar{A} No 1g Load	.01913 1.100 1.0	228.9 1.711 15597	208.3 1.920 11623	252.7 1.658 13973	222.2 1.672 10334	172.4 1.829 6057	151.2 1.204 8461	89.14 1.361 4756	37.35 1.711 1798
204	\bar{A} No 1g Load	.01897 1.113 1.0	228.8 1.648 18607	233.6 1.746 16336	218.0 1.918 12156	259.1 1.715 14050	180.3 1.794 5826	156.1 1.254 8222	92.60 1.420 4577	38.22 1.809 1700
205	\bar{A} No 1g Load	.01836 1.100 1.0	224.2 1.753 15498	211.0 1.912 11853	250.4 1.730 14020	222.1 1.696 10493	174.7 1.776 6518	152.9 1.260 8966	91.14 1.417 5157	38.17 1.815 1963
206	\bar{A} No 1g Load	.02047 1.102 1.0	241.2 1.649 15819	213.9 1.884 11586	264.2 1.581 13997	229.1 1.639 10160	175.5 1.852 5672	155.6 1.175 8064	91.23 1.324 4466	38.15 1.643 1675
207	\bar{A} No 1g Load	.02299 1.145 1.0	276.2 1.684 16653	247.2 1.906 11906	303.8 1.596 13927	265.0 1.642 9647	203.8 1.848 4907	178.0 1.228 7275	104.7 1.367 3880	43.97 1.668 1406
208	\bar{A} No 1g Load	.01980 1.092 1.0	238.3 1.700 15784	219.3 1.886 11873	264.2 1.669 14060	232.7 1.657 10411	181.2 1.778 6226	160.6 1.230 8615	95.04 1.396 4870	39.74 1.776 4263
209	\bar{A} No 1g Load	.02205 1.138 1.0	265.1 1.655 18961	248.8 1.926 12079	297.3 1.638 13897	264.4 1.663 9830	206.0 1.769 5416	181.6 1.271 7795	107.8 1.430 1839	45.22 1.786 1562

TABLE B-1. CONTINUED
(b) WING BENDING MOMENTS, CASES 201-209

Case		Wing Bending Moments, M_x									
		11	12	13	14	15	16	17	18	19	
		WB 83	WB 119	WB 167	WB 219	WB 275	WB 346	WB 380	WB 448	WB 516	
201	\bar{X}	61890	55170	46680	38860	26290	19560	11900	4657	1099	
	P_0	1.455	1.447	1.408	1.384	1.299	1.233	1.285	1.444	1.649	
	1g Load	4.144x10 ⁶	3.604x10 ⁶	2.976x10 ⁶	2.498x10 ⁶	1.671x10 ⁶	1.074x10 ⁶	.791x10 ⁶	.303x10 ⁶	.076x10 ⁶	
202	\bar{X}	89910	76390	64590	53720	36140	21250	15330	6293	2436	
	P_0	1.447	1.414	1.417	1.398	1.339	1.299	1.358	1.506	1.698	
	1g Load	3.923x10 ⁶	3.298x10 ⁶	2.609x10 ⁶	2.080x10 ⁶	1.318x10 ⁶	.811x10 ⁶	.999x10 ⁶	.211x10 ⁶	.053x10 ⁶	
203	\bar{X}	75170	66970	56650	47150	31800	18760	13730	5566	1270	
	P_0	1.469	1.464	1.431	1.396	1.342	1.299	1.353	1.515	1.711	
	1g Load	4.129x10 ⁶	3.537x10 ⁶	2.800x10 ⁶	2.271x10 ⁶	1.691x10 ⁶	.937x10 ⁶	.690x10 ⁶	.254x10 ⁶	.064x10 ⁶	
204	\bar{X}	77440	69160	59510	48695	32940	19450	14330	5781	1320	
	P_0	1.473	1.465	1.408	1.380	1.344	1.347	1.421	1.591	1.809	
	1g Load	4.031x10 ⁶	3.435x10 ⁶	2.735x10 ⁶	2.195x10 ⁶	1.424x10 ⁶	.833x10 ⁶	.658x10 ⁶	.236x10 ⁶	.079x10 ⁶	
205	\bar{X}	74940	67040	56780	47270	32100	19070	13980	5690	1298	
	P_0	1.468	1.456	1.417	1.377	1.332	1.349	1.423	1.592	1.815	
	1g Load	4.173x10 ⁶	3.589x10 ⁶	2.912x10 ⁶	2.374x10 ⁶	1.588x10 ⁶	1.013x10 ⁶	.716x10 ⁶	.278x10 ⁶	.070x10 ⁶	
206	\bar{X}	78010	69250	59500	48630	32640	19220	14070	5691	1297	
	P_0	1.443	1.442	1.415	1.386	1.334	1.267	1.417	1.463	1.643	
	1g Load	3.984x10 ⁶	3.581x10 ⁶	2.711x10 ⁶	2.154x10 ⁶	1.409x10 ⁶	.877x10 ⁶	.646x10 ⁶	.240x10 ⁶	.079x10 ⁶	
207	\bar{X}	89960	79960	67600	56200	37760	22110	16150	6545	1495	
	P_0	1.452	1.450	1.426	1.400	1.352	1.302	1.423	1.498	1.668	
	1g Load	3.845x10 ⁶	3.208x10 ⁶	2.512x10 ⁶	1.986x10 ⁶	1.234x10 ⁶	.753x10 ⁶	.596x10 ⁶	.192x10 ⁶	.048x10 ⁶	
208	\bar{X}	78850	70390	59600	49640	33610	19950	14610	5929	1331	
	P_0	1.440	1.432	1.393	1.358	1.315	1.321	1.395	1.564	1.776	
	1g Load	4.116x10 ⁶	3.519x10 ⁶	2.838x10 ⁶	2.301x10 ⁶	1.517x10 ⁶	.957x10 ⁶	.704x10 ⁶	.299x10 ⁶	.066x10 ⁶	
209	\bar{X}	89900	79920	67750	56450	38260	22640	16570	6734	1533	
	P_0	1.449	1.439	1.406	1.373	1.333	1.352	1.427	1.546	1.786	
	1g Load	3.828x10 ⁶	3.211x10 ⁶	2.621x10 ⁶	2.089x10 ⁶	1.334x10 ⁶	.888x10 ⁶	.611x10 ⁶	.215x10 ⁶	.054x10 ⁶	

TABLE B-1. CONTINUED
(c) WING TORSIONS AND WING SHEAR FLOWS, CASES 201-209

Case	Wing Torsions, M_{T2A}												Wing Shear Flows			
	20	21	22	23	24	25	26	27	28	29	30	31	32			
	WS 83	WS 119	WS 167	WS 209	WS 275	WS 346	WS 380	WS 446	WS 516	WS 583	WS 633	WS 686	WS 746			
201	\bar{A} No 1g Load	14360 2.515 -1.498x10 ⁶	13590 2.595 -1.537x10 ⁶	12790 2.690 -1.587x10 ⁶	12500 2.710 -1.600x10 ⁶	11340 2.718 -1.671x10 ⁶	10950 2.467 -1.593x10 ⁶	2393 1.075 -1.052x10 ⁶	2933 1.075 -1.052x10 ⁶	1171 1.092 -1.033x10 ⁶	449.8 1.276 -1.037x10 ⁶	4.590 1.480 152.39	1.438 4.063 -305.1	7.508 2.252 20.08	WS 346 Front Beam	WS 346 Rear Beam
202	\bar{A} No 1g Load	10930 2.624 -1.519x10 ⁶	17910 2.703 -1.480x10 ⁶	16850 2.797 -1.429x10 ⁶	16730 2.092 -1.908x10 ⁶	15180 2.291 -1.866x10 ⁶	14070 2.456 -1.732x10 ⁶	217.1 1.154 -1.701x10 ⁶	2937 1.230 -1.260x10 ⁶	1560 1.390 -1.144x10 ⁶	546.5 1.591 -1.011x10 ⁶	6.376 1.915 61.79	2.117 3.716 -537.51	10.10 2.205 -177.1		
203	\bar{A} No 1g Load	17110 2.617 -1.177x10 ⁶	16240 2.692 -1.159x10 ⁶	15320 2.780 -1.125x10 ⁶	14980 2.127 -1.669x10 ⁶	13620 2.311 -1.624x10 ⁶	12660 2.463 -1.567x10 ⁶	21.8 1.280 -1.201x10 ⁶	2937 1.230 -1.260x10 ⁶	1384 1.308 -1.144x10 ⁶	489.2 1.510 -1.031x10 ⁶	5.551 1.913 85.52	1.836 3.952 -492.93	9.033 2.246 -97.98		
204	\bar{A} No 1g Load	18010 2.445 -1.101x10 ⁶	17440 2.743 -1.156x10 ⁶	15950 2.657 -1.118x10 ⁶	15630 2.067 -1.845x10 ⁶	14160 2.257 -1.769x10 ⁶	13380 2.422 -1.633x10 ⁶	2937 1.230 -1.260x10 ⁶	2937 1.230 -1.260x10 ⁶	1126 1.247 -1.180x10 ⁶	449.8 1.443 -1.096x10 ⁶	5.667 1.843 68.06	1.681 4.559 -507.44	9.430 2.204 -147.33		
205	\bar{A} No 1g Load	17240 2.497 -1.041x10 ⁶	16290 2.584 -1.088x10 ⁶	15230 2.660 -1.011x10 ⁶	15010 2.060 -1.600x10 ⁶	13560 2.257 -1.564x10 ⁶	12500 2.429 -1.517x10 ⁶	2865 1.201 -1.186x10 ⁶	2937 1.230 -1.260x10 ⁶	1404 1.208 -1.136x10 ⁶	449.8 1.400 -1.078x10 ⁶	5.367 1.828 95.23	1.599 4.122 -421.44	9.058 2.197 -64.43		
206	\bar{A} No 1g Load	17290 2.626 -1.394x10 ⁶	16370 2.708 -1.263x10 ⁶	15460 2.599 -1.239x10 ⁶	15270 2.131 -1.748x10 ⁶	14890 2.273 -1.640x10 ⁶	13950 2.477 -1.608x10 ⁶	2902 1.288 -1.204x10 ⁶	2937 1.230 -1.260x10 ⁶	1424 1.324 -1.092x10 ⁶	449.8 1.521 -1.015x10 ⁶	5.880 1.902 80.25	2.023 3.453 -455.0	9.209 2.281 -121.75		
207	\bar{A} No 1g Load	15710 2.548 -1.517x10 ⁶	18650 2.727 -1.499x10 ⁶	17540 2.822 -1.473x10 ⁶	17460 2.097 -1.938x10 ⁶	15930 2.269 -1.884x10 ⁶	14690 2.455 -1.794x10 ⁶	3293 1.417 -1.286x10 ⁶	2937 1.230 -1.260x10 ⁶	1620 1.456 -1.206x10 ⁶	567.7 1.660 -1.114x10 ⁶	6.691 1.945 76.43	2.272 3.046 -546.15	10.56 2.249 -209.46		
208	\bar{A} No 1g Load	17810 2.488 -1.189x10 ⁶	16780 2.563 -1.159x10 ⁶	15730 2.711 -1.117x10 ⁶	15480 2.053 -1.691x10 ⁶	14060 2.255 -1.639x10 ⁶	12910 2.432 -1.578x10 ⁶	2998 1.205 -1.214x10 ⁶	2937 1.230 -1.260x10 ⁶	1460 1.221 -1.132x10 ⁶	513.3 1.408 -1.076x10 ⁶	5.745 1.802 86.33	1.733 4.387 -456.03	9.374 2.115 -98.41		
209	\bar{A} No 1g Load	19630 2.627 -1.596x10 ⁶	18520 2.660 -1.497x10 ⁶	17410 2.787 -1.441x10 ⁶	17010 2.094 -1.933x10 ⁶	15380 2.266 -1.763x10 ⁶	14180 2.485 -1.644x10 ⁶	3368 1.352 -1.284x10 ⁶	2937 1.230 -1.260x10 ⁶	1655 1.469 -1.195x10 ⁶	5787 1.561 -1.105x10 ⁶	6.349 1.914 71	2.015 4.426 -538.72	10.38 2.230 -218.36		

**TABLE B-1. CONCLUDED
(d) FUSELAGE LOADS AND HORIZONTAL TAIL LOAD, CASES 201-209**

Case	Fuselage Loads												Horiz. Tail Load
	33	34	35	36	37	38	39	40	41	42	43		
	\bar{a}_x	\bar{M}_y	\bar{a}_x	\bar{M}_y	\bar{a}_x	\bar{M}_y	\bar{a}_x	\bar{M}_y	\bar{a}_x	\bar{M}_y	\bar{M}_y		
	P.S. 350	P.S. 350	P.S. 350	P.S. 350	P.S. 372	P.S. 372	P.S. 393	P.S. 393	P.S. 4106	P.S. 4106	P.S. 4106		
201	\bar{a}_x	\bar{M}_y	\bar{a}_x	\bar{M}_y	\bar{a}_x	\bar{M}_y	\bar{a}_x	\bar{M}_y	\bar{a}_x	\bar{M}_y	\bar{M}_y		
202	\bar{a}_x	\bar{M}_y	\bar{a}_x	\bar{M}_y	\bar{a}_x	\bar{M}_y	\bar{a}_x	\bar{M}_y	\bar{a}_x	\bar{M}_y	\bar{M}_y		
203	\bar{a}_x	\bar{M}_y	\bar{a}_x	\bar{M}_y	\bar{a}_x	\bar{M}_y	\bar{a}_x	\bar{M}_y	\bar{a}_x	\bar{M}_y	\bar{M}_y		
204	\bar{a}_x	\bar{M}_y	\bar{a}_x	\bar{M}_y	\bar{a}_x	\bar{M}_y	\bar{a}_x	\bar{M}_y	\bar{a}_x	\bar{M}_y	\bar{M}_y		
205	\bar{a}_x	\bar{M}_y	\bar{a}_x	\bar{M}_y	\bar{a}_x	\bar{M}_y	\bar{a}_x	\bar{M}_y	\bar{a}_x	\bar{M}_y	\bar{M}_y		
206	\bar{a}_x	\bar{M}_y	\bar{a}_x	\bar{M}_y	\bar{a}_x	\bar{M}_y	\bar{a}_x	\bar{M}_y	\bar{a}_x	\bar{M}_y	\bar{M}_y		
207	\bar{a}_x	\bar{M}_y	\bar{a}_x	\bar{M}_y	\bar{a}_x	\bar{M}_y	\bar{a}_x	\bar{M}_y	\bar{a}_x	\bar{M}_y	\bar{M}_y		
208	\bar{a}_x	\bar{M}_y	\bar{a}_x	\bar{M}_y	\bar{a}_x	\bar{M}_y	\bar{a}_x	\bar{M}_y	\bar{a}_x	\bar{M}_y	\bar{M}_y		
209	\bar{a}_x	\bar{M}_y	\bar{a}_x	\bar{M}_y	\bar{a}_x	\bar{M}_y	\bar{a}_x	\bar{M}_y	\bar{a}_x	\bar{M}_y	\bar{M}_y		
	136.4	21300	228.3	47190	868.7	64990	135.8	23140	31.11	22510	137.30		
	1.404	1.483	1.249	1.399	1.211	1.350	1.319	1.407	2.169	2.077	1.672		
	-9.962	-1.473x10 ⁶	-1.0936	-3.237x10 ⁶	-1.781	-4.400x10 ⁶	-1.7946	5.108x10 ⁶	-5.07	1.078x10 ⁶	-3.944		
	187.3	89810	309.7	64770	369.3	88690	201.9	20000	58.66	27380	172.98		
	1.671	1.787	1.268	1.665	1.328	1.593	1.474	5.378	1.861	2.127	2.394		
	-1.0189	-1.601x10 ⁶	-1.6168	-3.319x10 ⁶	-1.9848	-6.778x10 ⁶	-2.1436	7.308x10 ⁶	-1.8896	1.987x10 ⁶	-6.778		
	160.8	25040	263.4	59630	318.8	76210	171.6	17860	37.61	25690	179.88		
	1.683	1.733	1.488	1.617	1.348	1.549	1.338	5.118	1.377	2.337	2.101		
	-9.641	-1.549x10 ⁶	-1.5673	-3.407x10 ⁶	-1.8648	-6.617x10 ⁶	-2.0849	6.198x10 ⁶	-1.0946	1.613x10 ⁶	-6.608		
	199.4	24880	261.1	55130	316.0	75970	157.2	17500	39.33	25980	160.94		
	1.594	1.698	1.410	1.548	1.337	1.523	1.643	5.963	2.984	2.889	2.084		
	-9.993	-1.571x10 ⁶	-1.5881	-3.434x10 ⁶	-1.8911	-6.688x10 ⁶	-2.1093	7.069x10 ⁶	-1.2300	1.883x10 ⁶	-9.188		
	154.4	24090	249.7	57700	309.7	73180	156.0	17400	68.13	26060	160.04		
	1.577	1.688	1.393	1.570	1.350	1.507	1.688	5.817	2.803	2.158	1.978		
	-9.997	-1.493x10 ⁶	-1.5139	-3.403x10 ⁶	-1.8699	-6.482x10 ⁶	-1.8834	6.134x10 ⁶	-1.0311	1.494x10 ⁶	-9.970		
	174.4	27200	284.9	60330	344.4	86800	188.9	18800	56.44	26340	163.54		
	1.599	1.706	1.411	1.593	1.333	1.527	1.483	5.828	3.729	2.507	2.110		
	-1.0041	-1.580x10 ⁶	-1.5990	-3.469x10 ⁶	-1.8991	-6.710x10 ⁶	-2.0510	6.693x10 ⁶	-1.1452	1.680x10 ⁶	-7.272		
	193.0	30040	316.8	66700	381.6	92600	228.7	23090	53.41	27310	160.0		
	1.714	1.872	1.517	1.717	1.404	1.637	1.407	5.904	5.373	2.948	2.1		
	-9.704	-1.577x10 ⁶	-1.59490	-3.394x10 ⁶	-1.8413	-6.557x10 ⁶	-1.9845	6.396x10 ⁶	-1.0870	1.635x10 ⁶	-9.724		
	169.1	26380	273.8	58470	333.3	80950	171.7	18040	68.00	27060	169.66		
	1.536	1.633	1.363	1.531	1.294	1.470	1.386	5.856	3.834	2.582	2.147		
	-1.0411	-1.637x10 ⁶	-1.6504	-3.506x10 ⁶	-1.9589	-6.879x10 ⁶	-2.2339	7.866x10 ⁶	-1.3845	2.171x10 ⁶	-9.723		
	185.2	28950	303.5	64080	367.4	87840	208.1	20890	58.60	27930	174.06		
	1.728	1.866	1.500	1.783	1.407	1.641	1.343	5.479	6.053	2.806	2.189		
	-1.0080	-1.599x10 ⁶	-1.6211	-3.443x10 ⁶	-1.9061	-6.728x10 ⁶	-2.1877	7.509x10 ⁶	-1.3821	2.064x10 ⁶	-9.804		

TABLE B-2. RESULTS OF VERTICAL GUST DYNAMIC ANALYSIS,
MODEL 198 DESIGN ENVELOPE CASES
(a) C.G. ACCELERATIONS AND WING SHEARS, CASES 401-412

Case		Wing Shears, %										
		1	2	3	4	5	6	7	8	9	10	
		C.G. Accel										
		W883	W8115	W8167	W8209	W8275	W8346	W8380	W8448	W8516		
401	T	.03257	238.1	216.7	177.3	276.7	230.8	169.1	167.8	99.17	41.68	
	N	1.349	1.972	2.140	1.632	1.836	2.405	2.405	1.409	1.500	1.758	
	1g Load	1.0	1.0664	1.1143	1.0732	1.0976	1.147	1.28	1.351	1.380	1.46	
402	T	.03121	221.9	198.3	157.6	264.2	216.5	154.9	167.6	99.00	41.46	
	N	1.346	1.870	2.072	1.603	1.829	2.490	2.490	1.342	1.434	1.709	
	1g Load	1.0	1.0595	1.1075	1.0559	1.089	1.137	1.253	1.327	1.351	1.434	
403	T	.02162	156.1	185.0	194.1	254.5	221.6	191.6	181.2	127.8	54.18	
	N	1.111	2.017	1.942	1.806	1.806	1.806	1.806	1.576	1.558	1.775	
	1g Load	1.0	1.1477	1.2238	1.117	1.128	1.171	1.283	1.351	1.372	1.46	
404	T	.02546	163.8	172.0	176.9	242.1	216.9	177.1	178.9	118.6	52.89	
	N	1.056	2.088	2.148	1.746	1.801	1.801	1.801	1.801	1.801	1.801	
	1g Load	1.0	1.2720	1.0543	1.000	1.085	1.133	1.257	1.333	1.333	1.405	
405	T	.02796	175.9	196.5	191.4	266.1	244.6	208.1	206.3	150.8	68.25	
	N	1.109	1.450	1.502	1.404	1.404	1.404	1.404	1.404	1.404	1.404	
	1g Load	1.0	1.2130	1.1533	1.0624	1.0954	1.134	1.257	1.333	1.333	1.405	
406	T	.02362	111.0	131.9	123.4	174.7	130.4	266.5	235.4	149.5	67.41	
	N	1.030	1.455	1.486	1.408	1.408	1.408	1.408	1.408	1.408	1.408	
	1g Load	1.0	1.0706	1.0558	1.037	1.0816	1.133	1.257	1.333	1.333	1.405	
407	T	.02663	177.4	195.4	189.3	267.5	247.0	208.0	226.4	133.7	56.53	
	N	1.212	1.425	1.500	1.404	1.404	1.404	1.404	1.404	1.404	1.404	
	1g Load	1.0	1.2632	1.1740	1.0779	1.0994	1.131	1.257	1.333	1.333	1.405	
408	T	.02711	159.6	184.3	164.8	233.8	190.7	270.4	228.6	134.9	56.84	
	N	1.140	1.346	1.434	1.386	1.386	1.386	1.386	1.386	1.386	1.386	
	1g Load	1.0	1.2444	1.107	1.046	1.086	1.133	1.257	1.333	1.333	1.405	
409	T	.02572	174.6	196.6	181.5	267.5	247.0	208.0	226.4	133.7	56.53	
	N	1.179	1.416	1.486	1.404	1.404	1.404	1.404	1.404	1.404	1.404	
	1g Load	1.0	1.2590	1.1798	1.0834	1.0994	1.131	1.257	1.333	1.333	1.405	
410	T	.02681	157.9	186.7	169.0	237.8	190.7	270.4	228.6	134.9	56.84	
	N	1.099	1.315	1.414	1.386	1.386	1.386	1.386	1.386	1.386	1.386	
	1g Load	1.0	1.2415	1.107	1.046	1.086	1.133	1.257	1.333	1.333	1.405	
411	T	.02492	139.4	156.2	140.8	213.9	173.9	240.9	240.9	142.1	59.79	
	N	1.164	1.360	1.434	1.386	1.386	1.386	1.386	1.386	1.386	1.386	
	1g Load	1.0	1.2398	1.107	1.046	1.086	1.133	1.257	1.333	1.333	1.405	
412	T	.02547	144.3	163.0	146.5	216.5	173.9	240.9	240.9	142.1	59.79	
	N	1.078	1.307	1.414	1.386	1.386	1.386	1.386	1.386	1.386	1.386	
	1g Load	1.0	1.2452	1.107	1.046	1.086	1.133	1.257	1.333	1.333	1.405	

TABLE B-2. CONTINUED
(c) C.G. ACCELERATIONS AND WING SHEARS, CASES 413-424

Case		1	2	3	4	5	6	7	8	9	10
		Wing Shears, S_z									
		C.O. Accel	W883	W1119	W16167	W18209	W18273	W18346	W18350	W18418	W18516
413	\bar{x} No 1g Load	1.05431 1.1453 1.0	425.9 1.473 24941	433.7 1.518 21649	409.7 1.643 16333	449.9 1.518 16793	377.3 1.580 11399	312.5 1.580 6116	249.8 1.580 3006	146.7 1.438 3398	68.69 1.743 1569
414	\bar{x} No 1g Load	1.08489 1.1067 1.0	418.0 1.407 23051	416.7 1.485 20102	389.3 1.614 14761	435.2 1.519 15986	384.4 1.501 10440	299.1 1.564 5486	256.0 1.506 7643	152.8 1.336 8096	64.41 1.650 1434
415	\bar{x} No 1g Load	1.02961 1.1141 1.0	410.0 1.485 24449	428.6 1.511 21573	415.3 1.600 16420	451.8 1.575 16887	399.9 1.535 11359	317.0 1.504 6831	253.3 1.395 8465	152.4 1.491 4726	64.87 1.711 1743
416	\bar{x} No 1g Load	1.08424 1.1075 1.0	397.4 1.463 22212	413.2 1.563 20072	396.7 1.566 15114	442.2 1.548 15706	388.1 1.513 10422	324.7 1.549 5581	259.8 1.565 7937	157.1 1.391 4416	66.24 1.634 1616
417	\bar{x} No 1g Load	1.08377 1.1189 1.0	407.2 1.478 24073	426.4 1.517 21296	420.8 1.566 16387	453.8 1.575 16717	403.4 1.531 11028	320.3 1.555 6016	255.0 1.374 8036	154.1 1.509 4765	65.06 1.684 1868
418	\bar{x} No 1g Load	1.08392 1.1044 1.0	397.2 1.414 22469	413.7 1.563 19481	403.1 1.587 15090	446.7 1.546 15579	391.9 1.510 10127	308.6 1.540 5367	261.4 1.383 7771	159.0 1.404 4454	67.84 1.570 1701
419	\bar{x} No 1g Load	1.08061 1.1134 1.0	354.8 1.404 24460	337.4 1.499 20735	398.2 1.688 15288	376.8 1.604 17354	271.6 1.561 11960	215.1 1.912 6157	170.9 1.158 8852	100.5 1.840 4524	42.50 1.475 1605
420	\bar{x} No 1g Load	1.08325 1.1167 1.0	415.5 1.409 23353	385.8 1.497 21259	335.2 1.678 15330	396.1 1.588 17050	323.2 1.556 11274	246.7 1.877 5482	195.8 1.172 7380	113.5 1.846 3895	48.83 1.460 1599
421	\bar{x} No 1g Load	1.08379 1.1224 1.0	414.4 1.423 26368	410.8 1.511 21788	354.5 1.697 15333	405.3 1.585 16648	336.0 1.536 10426	253.6 1.845 4216	212.4 1.208 6381	125.4 1.878 3133	32.90 1.448 1655
422	\bar{x} No 1g Load	1.08350 1.1224 1.0	440.8 1.409 26041	406.5 1.488 21788	349.3 1.688 15460	400.9 1.546 16797	331.3 1.530 10985	247.1 1.830 4363	210.5 1.196 6453	124.1 1.866 3821	32.23 1.442 1093
423	\bar{x} No 1g Load	1.08389 1.1464 1.0	349.4 1.482 18686	323.9 1.711 12140	274.7 1.827 3555	440.7 1.584 16797	373.5 1.589 10985	253.6 1.845 4216	212.4 1.208 6381	125.4 1.878 3133	32.90 1.448 1655
424	\bar{x} No 1g Load	1.08245 1.1408 1.0	314.3 1.531 17070	285.0 1.741 10648	233.8 1.890 3225	408.7 1.500 16886	334.1 1.613 10985	241.1 1.878 4363	210.5 1.196 6453	124.1 1.866 3821	32.23 1.442 1093

TABLE B-2. CONTINUED
(c) C.G. ACCELERATIONS AND WING SHEARS, CASES 425-427

Case	C.G. Accel	Wing Shears, S_z									
		1	2	3	4	5	6	7	8	9	10
		WB83	WB119	WB167	WB209	WB275	WB346	WB380	WB443	WB516	
425	\bar{X} 1.03949 1.257 1.0 1g Load	754.0 1.265 28041	715.2 1.312 20012	640.3 1.426 11261	761.3 1.208 20302	659.2 1.357 1733	506.7 1.560 -5244	390.0 1.219 -2711	230.7 1.252 -3075	97.36 1.453 -1694	
426	\bar{X} 1.04007 1.280 1.0 1g Load	736.5 1.303 26312	695.5 1.367 19213	617.6 1.510 7445	720.7 1.285 9051	613.7 1.393 732	466.8 1.688 -5970	381.2 1.173 -3306	226.0 1.227 -3426	95.48 1.357 -1798	
427	\bar{X} 1.01284 1.052 1.0 1g Load	213.6 1.351 21120	195.8 1.480 18292	167.3 1.712 1344	293.6 1.415 16903	160.3 1.607 12217	122.9 1.982 7344	97.27 1.037 9555	56.82 1.146 5547	23.79 1.428 2163	
428	\bar{X} 1.01272 1.028 1.0 1g Load	215.9 1.311 21047	197.3 1.436 18270	168.7 1.663 17017	297.0 1.397 16899	161.1 1.587 12519	123.0 1.962 10075	98.31 1.033 9555	57.47 1.142 5549	24.09 1.425 2174	
429	\bar{X} 1.01094 1.099 1.0 1g Load	176.9 1.447 18618	183.8 1.559 17560	177.9 1.662 17818	292.4 1.668 16619	168.1 1.682 12744	132.9 1.726 11334	106.5 1.265 11234	64.29 1.287 6995	27.05 1.447 2862	
430	\bar{X} 1.01339 1.085 1.0 1g Load	220.9 1.490 19892	229.7 1.552 18037	222.3 1.633 18059	240.7 1.645 16677	210.4 1.627 12588	166.6 1.681 11242	134.7 1.295 10917	81.65 1.398 6745	34.40 1.593 2747	
431	\bar{X} 1.01317 1.043 1.0 1g Load	215.6 1.500 19905	225.4 1.582 18596	219.4 1.660 18945	236.8 1.699 17100	208.1 1.642 12917	165.4 1.691 11472	131.6 1.301 11100	79.87 1.406 6851	33.71 1.597 2790	

TABLE B-2. CONTINUED
(d) WING BENDING MOMENTS, CASES 401-412

Case		Wing bending Moments, M_x									
		11	12	13	14	15	16	17	18	19	
Wing											
		W803	W8119	W8167	W8209	W8275	W8346	W8380	W8418	W8516	
401	\bar{X}	76370	68540	59470	50210	33720	20130	13260	6198	1417	
	H_0	1.616	1.623	1.621	1.624	1.594	1.477	1.501	1.508	1.758	
	1g Load	2.179e106	1.659e106	1.161e106	8.19e106	3.9e106	.907e106	.170e106	.086e106	5700	
402	\bar{X}	72160	64740	56370	48000	34400	20490	12934	6177	1410	
	H_0	1.590	1.599	1.588	1.431	1.545	1.414	1.439	1.472	1.709	
	1g Load	2.24e106	1.34e106	.943e106	.61e106	.24e106	.136e106	.126e106	.097e106	.032e106	
403	\bar{X}	77720	71690	62310	53610	37920	23790	17810	7680	1842	
	H_0	1.504	1.500	1.492	1.490	1.521	1.479	1.491	1.513	2.375	
	1g Load	2.15e106	1.69e106	1.15e106	.83e106	.48e106	.28e106	.19e106	.08e106	.03e106	
404	\bar{X}	73570	67720	58330	51070	35300	23220	17500	7519	1798	
	H_0	1.487	1.476	1.461	1.453	1.480	1.450	1.480	1.489	2.243	
	1g Load	1.75e106	1.42e106	.91e106	.65e106	.29e106	.14e106	.18e106	.04e106	.01e106	
405	\bar{X}	119800	107900	91600	76500	52770	32820	22880	9757	2320	
	H_0	1.328	1.334	1.335	1.348	1.381	1.342	1.348	1.390	2.105	
	1g Load	3.70e106	3.00e106	2.37e106	1.83e106	.94e106	.57e106	.45e106	.15e106	.04e106	
406	\bar{X}	113700	104200	88770	74210	51390	30830	22710	9689	2292	
	H_0	1.294	1.300	1.304	1.312	1.342	1.349	1.377	1.397	1.997	
	1g Load	3.13e106	2.90e106	1.96e106	1.44e106	.81e106	.50e106	.39e106	.12e106	.03e106	
407	\bar{X}	132000	113100	94700	78960	51380	32610	22610	8383	1982	
	H_0	1.361	1.371	1.378	1.384	1.362	1.352	1.359	1.335	1.448	
	1g Load	4.24e106	3.45e106	2.56e106	1.91e106	1.06e106	.59e106	.44e106	.13e106	.03e106	
408	\bar{X}	127100	111400	92600	75960	50080	30840	20800	8447	1933	
	H_0	1.306	1.319	1.323	1.325	1.297	1.270	1.276	1.255	1.365	
	1g Load	3.89e106	3.03e106	2.30e106	1.70e106	.93e106	.52e106	.39e106	.11e106	.08e106	
409	\bar{X}	137000	120300	99660	81450	53700	30070	21590	8776	2011	
	H_0	1.345	1.350	1.345	1.340	1.312	1.240	1.270	1.237	1.472	
	1g Load	4.50e106	3.66e106	2.76e106	2.10e106	1.22e106	.69e106	.51e106	.16e106	.04e106	
410	\bar{X}	132500	116500	96880	79430	52640	30820	21900	8392	2033	
	H_0	1.289	1.295	1.291	1.283	1.241	1.153	1.173	1.272	1.391	
	1g Load	4.10e106	3.37e106	2.49e106	1.91e106	1.08e106	.63e106	.46e106	.14e106	.03e106	
411	\bar{X}	119600	119720	99880	82170	54820	30990	22300	9068	2076	
	H_0	1.350	1.343	1.330	1.311	1.283	1.210	1.230	1.210	1.668	
	1g Load	4.65e106	3.83e106	2.91e106	2.24e106	1.35e106	.79e106	.57e106	.19e106	.04e106	
412	\bar{X}	131800	116700	97620	80610	54130	31370	22770	9254	2115	
	H_0	1.298	1.294	1.272	1.246	1.208	1.223	1.293	1.422	1.583	
	1g Load	4.26e106	3.49e106	2.63e106	2.03e106	1.21e106	.71e106	.50e106	.15e106	.03e106	

TABLE B-2. CONTINUED

Case	Wing Bending Moments, M_x										19
	11	12	13	14	15	16	17	18	19		
	W119	W119	W127	W1209	W1275	W1346	W1380	W1448	W1516		
413	λ	19700	10100	93160	95780	31700	78500	9314	2130		
	μ	1.341	1.314	1.894	1.873	1.344	1.430	1.568	1.763		
1g Load		1.753	3.003	2.364	1.502	0.961	0.671	0.216	0.037		
414	λ	13200	11800	81800	51500	32840	23430	9596	2183		
	μ	1.890	1.883	1.870	1.197	1.817	1.339	1.474	1.650		
1g Load		1.568	3.594	2.744	1.081	0.762	0.571	0.198	0.048		
415	λ	137100	108000	89660	56440	38990	23130	9549	2185		
	μ	1.368	1.896	1.877	1.873	1.368	1.461	1.608	1.741		
1g Load		1.078	3.860	2.513	1.009	0.691	0.481	0.167	0.037		
416	λ	134100	119600	88930	56330	38930	23010	9644	2253		
	μ	1.879	1.871	1.816	1.800	1.398	1.398	1.499	1.634		
1g Load		1.689	3.610	2.531	1.078	0.731	0.571	0.201	0.070		
417	λ	138000	109000	87400	56980	38990	23560	9663	2212		
	μ	1.319	1.890	1.870	1.869	1.395	1.461	1.587	1.684		
1g Load		1.792	3.961	2.509	1.009	0.691	0.481	0.167	0.037		
418	λ	133400	109000	87800	56740	31960	23660	9978	2286		
	μ	1.871	1.883	1.810	1.199	1.301	1.395	1.479	1.570		
1g Load		1.591	3.632	2.781	1.011	0.731	0.581	0.201	0.096		
419	λ	98600	86430	58370	38930	21460	15510	6301	1445		
	μ	1.308	1.406	1.417	1.394	1.409	1.844	1.341	1.475		
1g Load		1.702	3.989	2.481	1.009	0.691	0.481	0.167	0.037		
420	λ	113600	99340	67180	41060	24740	17610	7841	1660		
	μ	1.178	1.395	1.396	1.374	1.247	1.849	1.337	1.460		
1g Load		1.568	3.754	2.871	1.093	0.796	0.581	0.201	0.080		
421	λ	118000	104600	70440	46480	26570	19390	7893	1798		
	μ	1.490	1.442	1.437	1.399	1.277	1.872	1.343	1.442		
1g Load		1.502	3.658	2.576	1.069	0.691	0.481	0.167	0.037		
422	λ	118300	109000	69600	45790	26670	19130	7763	1776		
	μ	1.488	1.434	1.436	1.397	1.248	1.865	1.304	1.442		
1g Load		1.502	3.582	2.601	1.093	0.796	0.581	0.201	0.080		
423	λ	121600	109600	80730	54210	30900	23530	9573	2194		
	μ	1.317	1.519	1.496	1.484	1.477	1.530	1.604	1.710		
1g Load		1.468	3.116	2.592	1.011	0.691	0.481	0.167	0.037		
424	λ	109700	96940	73780	49000	30430	22580	9180	2096		
	μ	1.508	1.523	1.487	1.441	1.481	1.480	1.564	1.689		
1g Load		1.502	3.461	2.846	1.009	0.691	0.481	0.167	0.037		

TABLE B-2. CONTINUED
(f) WING BENDING MOMENTS, CASES 425-427

Case	Wing Bending Moments, M									
	11	12	13	14	15	16	17	18	19	
	WB3	WB19	WB67	WB85	WB 275	WB 346	WB 380	WB 448	WB 516	
425										
\bar{X}	225300	199100	146700	137800	90600	49060	35370	11490	3387	
M_0	1.285	1.890	1.889	1.879	1.867	1.832	1.832	1.828	1.833	
1g Load	1.179e106	.613e106	-.122e106	-.336e106	-.386e106	-.678e106	-.174e106	-.382e106	-.0679e106	
426										
\bar{X}	213900	188400	157100	149800	89630	48340	34790	11110	3246	
M_0	1.848	1.849	1.875	1.858	1.877	1.804	1.823	1.860	1.851	
1g Load	1.077e106	.301e106	-.36e106	-.746e106	-.1.017e106	-.756e106	-.388e106	-.300e106	-.0738e106	
427										
\bar{X}	16380	49090	40430	38930	21480	18080	8778	3546	808.7	
M_0	1.484	1.439	1.435	1.477	1.373	1.176	1.133	1.272	1.428	
1g Load	4.892e106	4.192e106	3.403e106	2.753e106	1.794e106	1.116e106	.818e106	.326e106	.081e106	
428										
\bar{X}	56090	49430	40740	33370	21600	18810	8978	3548	818.9	
M_0	1.430	1.421	1.480	1.414	1.383	1.173	1.147	1.287	1.485	
1g Load	5.013e106	4.351e106	3.497e106	2.891e106	1.896e106	1.157e106	.846e106	.392e106	.088e106	
429										
\bar{X}	37630	51160	44970	34890	23300	19470	9804	4.9	919.7	
M_0	1.443	1.442	1.418	1.347	1.333	1.273	1.300	1.358	1.447	
1g Load	5.894e106	4.632e106	3.811e106	3.141e106	2.173e106	1.421e106	1.076e106	.430e106	.116e106	
430										
\bar{X}	78490	64350	55620	44000	28490	17090	12460	5125	1170	
M_0	1.388	1.376	1.349	1.314	1.293	1.330	1.390	1.485	1.573	
1g Load	5.823e106	4.797e106	3.783e106	3.074e106	2.112e106	1.373e106	1.019e106	.419e106	.111e106	
431										
\bar{X}	71480	63370	58800	43540	29030	16740	12190	5007	1146	
M_0	1.408	1.396	1.368	1.338	1.309	1.338	1.397	1.490	1.591	
1g Load	5.407e106	4.702e106	3.846e106	3.142e106	2.157e106	1.398e106	1.032e106	.419e106	.113e106	

TABLE B-2. CONTINUED
(g) WING TORSIONS AND WING SHEAR FLOWS, CASES 401-412

Case	Wing Torsions, M_{WT}														Wing Shear Flows			
	20	21	22	23	24	25	26	27	28	29	30	31	32					
	WS83	WS119	WS167	WS209	WS275	WS316	WS380	WS448	WS516	WS583	WS653	WS716	WS786	WS846				
401	\bar{X} 15240 No -2.53x10 ⁶	14720 3.917 -2.47x10 ⁶	14600 3.868 -2.13x10 ⁶	14370 2.564 -1.58x10 ⁶	13840 2.823 -1.46x10 ⁶	12520 3.003 -1.21x10 ⁶	3316 1.881 -1.01x10 ⁶	1631 1.960 -1.28x10 ⁶	579.0 2.238 -1.15x10 ⁶	5.124 3.096 -104.7	2.640 3.014 -695	2.715 2.796 -474.2	2.723 3.795 -475.8	2.723 3.795 -475.8	WS346 Rear Beam			
402	\bar{X} 13940 No -2.60x10 ⁶	13830 3.025 -2.50x10 ⁶	14270 3.821 -2.37x10 ⁶	13070 2.056 -1.62x10 ⁶	11980 2.918 -1.47x10 ⁶	11570 3.059 -1.29x10 ⁶	5339 1.836 -1.53x10 ⁶	1647 1.912 -1.29x10 ⁶	586.7 2.185 -1.16x10 ⁶	4.470 3.211 -136.1	2.857 2.851 -684.2	7.903 2.900 -497.1	2.862 3.584 -472.9	2.862 3.584 -472.9	WS346 Front Beam			
403	\bar{X} 2.3140 No -1.96x10 ⁶	21282 2.664 -1.88x10 ⁶	19970 2.844 -1.78x10 ⁶	18370 2.074 -1.25x10 ⁶	15560 2.420 -1.11x10 ⁶	13190 2.797 -1.96x10 ⁶	4523 1.574 -1.37x10 ⁶	2318 1.632 -1.25x10 ⁶	847.0 1.678 -1.33x10 ⁶	4.908 2.585 -64	2.973 3.004 -556.7	6.866 2.900 -370.3	3.965 3.003 -379.1	3.965 3.003 -379.1	WS346 Rear Beam			
404	\bar{X} 20830 No -2.65x10 ⁶	19000 2.779 -1.96x10 ⁶	16770 2.057 -1.65x10 ⁶	16960 2.116 -1.30x10 ⁶	14140 2.075 -1.16x10 ⁶	11930 2.931 -1.00x10 ⁶	4638 1.477 -1.38x10 ⁶	7386 1.540 -1.54x10 ⁶	874.5 1.590 -1.53x10 ⁶	4.355 2.715 -106.5	2.769 3.055 -543.4	7.319 2.667 -409.5	3.718 3.033 -577.3	3.718 3.033 -577.3	WS346 Front Beam			
405	\bar{X} 29190 No -1.61x10 ⁶	27080 2.197 -1.57x10 ⁶	24360 2.428 -1.48x10 ⁶	22470 1.845 -1.06x10 ⁶	19350 2.097 -1.96x10 ⁶	16630 2.384 -1.83x10 ⁶	4907 1.451 -1.36x10 ⁶	2502 1.516 -1.23x10 ⁶	909.0 1.588 -1.50x10 ⁶	8.402 1.758 100.7	2.611 3.554 -599.8	12.55 1.999 -261.9	4.047 3.050 -386.2	4.047 3.050 -386.2	WS346 Rear Beam			
406	\bar{X} 27230 No -1.70x10 ⁶	25080 2.250 -1.63x10 ⁶	22320 2.412 -1.56x10 ⁶	21300 1.852 -1.31x10 ⁶	18100 2.143 -1.01x10 ⁶	15370 2.575 -1.87x10 ⁶	5100 1.356 -1.39x10 ⁶	2612 1.421 -1.23x10 ⁶	982.1 1.494 -1.28x10 ⁶	8.011 1.763 61.3	2.532 3.533 -596.1	11.64 2.673 -292	3.928 3.070 -386.1	3.928 3.070 -386.1	WS346 Front Beam			
407	\bar{X} 28490 No -2.05x10 ⁶	26940 2.446 -1.99x10 ⁶	25230 2.658 -1.90x10 ⁶	24320 2.016 -1.33x10 ⁶	22180 2.194 -1.18x10 ⁶	20510 2.357 -1.07x10 ⁶	4054 1.588 -1.39x10 ⁶	1977 1.655 -1.26x10 ⁶	698.2 1.909 -1.37x10 ⁶	11.24 1.840 121.8	3.561 2.367 -755.7	14.76 2.151 -312	3.235 3.504 -484.6	3.235 3.504 -484.6	WS346 Rear Beam			
408	\bar{X} 25560 No -2.16x10 ⁶	24120 2.728 -2.07x10 ⁶	22630 2.844 -1.98x10 ⁶	22340 2.074 -1.37x10 ⁶	20320 2.277 -1.22x10 ⁶	18840 2.453 -1.06x10 ⁶	4141 1.515 -1.40x10 ⁶	1307 1.579 -1.29x10 ⁶	719.2 1.865 -1.38x10 ⁶	10.14 1.832 78.8	3.864 2.208 -714.1	13.75 2.130 -343.2	3.308 3.372 -485.2	3.308 3.372 -485.2	WS346 Front Beam			
409	\bar{X} 30260 No -1.95x10 ⁶	28480 2.139 -1.89x10 ⁶	26680 2.439 -1.81x10 ⁶	25380 1.929 -1.28x10 ⁶	23070 2.078 -1.13x10 ⁶	21180 2.239 -1.98x10 ⁶	4209 1.498 -1.38x10 ⁶	2073 1.547 -1.25x10 ⁶	722.1 1.763 -1.13x10 ⁶	11.40 1.733 123	3.129 2.849 -727.1	15.58 2.044 -272.7	3.163 3.298 -48.6	3.163 3.298 -48.6	WS346 Rear Beam			
410	\bar{X} 27300 No -2.04x10 ⁶	25700 2.493 -1.97x10 ⁶	23960 2.604 -1.88x10 ⁶	23450 1.758 -1.31x10 ⁶	21220 2.154 -1.17x10 ⁶	19490 2.333 -1.01x10 ⁶	4319 1.419 -1.39x10 ⁶	2135 1.464 -1.26x10 ⁶	717.40 1.671 -1.36x10 ⁶	10.99 1.707 81.3	3.477 2.657 -715	14.38 2.113 -303.2	3.277 3.322 -483.6	3.277 3.322 -483.6	WS346 Front Beam			
411	\bar{X} 27730 No -2.17x10 ⁶	26050 2.168 -1.79x10 ⁶	24980 2.255 -1.72x10 ⁶	25920 1.866 -1.20x10 ⁶	23120 1.972 -1.07x10 ⁶	21030 2.142 -1.93x10 ⁶	4321 1.371 -1.37x10 ⁶	2131 1.415 -1.25x10 ⁶	710.0 1.596 -1.23x10 ⁶	10.80 1.616 125.4	2.521 4.080 -698.7	15.66 2.044 -240.6	2.925 3.183 -480.9	2.925 3.183 -480.9	WS346 Rear Beam			
412	\bar{X} 27930 No -2.28x10 ⁶	26230 2.302 -1.87x10 ⁶	24310 2.464 -1.77x10 ⁶	23790 1.819 -1.23x10 ⁶	21380 2.045 -1.11x10 ⁶	19430 2.239 -1.97x10 ⁶	4461 1.296 -1.37x10 ⁶	2207 1.346 -1.25x10 ⁶	769.9 1.497 -1.35x10 ⁶	10.06 1.571 84.7	2.746 3.819 -686.1	14.54 2.018 -270.2	3.005 3.117 -473.4	3.005 3.117 -473.4	WS346 Front Beam			

TABLE B-2. CONTINUED
(h) WING TORSIONS AND WING SHEAR FLOWS, CASES 413-424

Case		Wing Torsions, K_{in}										Wing Shear Flows				
		20	21	22	23	24	25	26	27	28	29	30	31	32	33	34
		Wing Torsions, K_{in}										Wing Shear Flows				
		W83	W819	W8167	W8209	W8275	W8346	W8380	W8418	W8516	W8583	W863	W863	W863	W863	W863
413	λ	31210	29470	27250	25800	23210	20980	18441	1581	755.8	10.61	2.198	15.81	2.656		
	λ_0	2.013	2.021	2.129	1.743	1.919	2.096	1.319	1.321	1.481	1.540	1.856	1.910	3.323		
	1g Load	-1.711x10 ⁶	-1.712x10 ⁶	-1.636x10 ⁶	-1.194x10 ⁶	-1.036x10 ⁶	-899x10 ⁶	-361x10 ⁶	-246x10 ⁶	-1.32x10 ⁶	136.6	-665.4	-220.1	-473.5		
414	λ	28460	26800	24580	21330	21370	19440	1630	2268	789.7	9.914	2.375	14.7	2.761		
	λ_0	2.120	2.159	2.235	1.782	1.986	2.196	1.234	1.230	1.380	1.490	1.856	1.910	3.292		
	1g Load	-1.867x10 ⁶	-1.858x10 ⁶	-1.782x10 ⁶	-1.189x10 ⁶	-1.085x10 ⁶	-947x10 ⁶	-370x10 ⁶	-270x10 ⁶	-1.13x10 ⁶	84.3	-665.8	-253.0	-475.2		
415	λ	31180	29360	27010	25370	22900	20520	1469	2244	713.7	10.29	1.890	15.78	2.259		
	λ_0	1.944	1.966	2.035	1.680	1.862	2.068	1.257	1.248	1.365	1.475	1.856	1.910	3.321		
	1g Load	-1.670x10 ⁶	-1.612x10 ⁶	-1.537x10 ⁶	-1.103x10 ⁶	-992x10 ⁶	-863x10 ⁶	-351x10 ⁶	-240x10 ⁶	-1.13x10 ⁶	40.7	-568.7	-247.7	-425.3		
416	λ	28770	26930	24570	21080	21400	19090	1635	2345	812.1	9.666	1.994	14.81	2.326		
	λ_0	2.043	2.074	2.162	1.716	1.932	2.172	1.173	1.158	1.284	1.397	1.824	1.878	3.321		
	1g Load	-1.751x10 ⁶	-1.694x10 ⁶	-1.613x10 ⁶	-1.141x10 ⁶	-1.034x10 ⁶	-899x10 ⁶	-359x10 ⁶	-244x10 ⁶	-1.13x10 ⁶	-4.0	-555.3	-273.2	-413.2		
417	λ	31310	29440	27010	25330	22730	20370	14635	2278	783.7	10.23	1.796	15.79	2.067		
	λ_0	1.947	1.942	2.036	1.648	1.847	2.057	1.239	1.225	1.318	1.448	1.858	1.912	3.321		
	1g Load	-1.578x10 ⁶	-1.560x10 ⁶	-1.487x10 ⁶	-1.071x10 ⁶	-965x10 ⁶	-840x10 ⁶	-345x10 ⁶	-237x10 ⁶	-1.22x10 ⁶	139.2	-627	-203.9	-444.5		
418	λ	28530	27110	24650	21200	21300	18920	1629	2385	824.2	9.647	1.878	14.86	2.128		
	λ_0	2.021	2.046	2.129	1.680	1.917	2.161	1.155	1.136	1.217	1.397	1.858	1.912	3.321		
	1g Load	-1.703x10 ⁶	-1.648x10 ⁶	-1.562x10 ⁶	-1.117x10 ⁶	-1.004x10 ⁶	-874x10 ⁶	-353x10 ⁶	-245x10 ⁶	-1.13x10 ⁶	93.3	-623.6	-232.7	-444.3		
419	λ	28050	21000	19780	18610	17130	16080	1303	1529	538.4	8.543	3.067	11.45	2.884		
	λ_0	2.614	2.702	2.803	2.157	2.324	2.459	1.500	1.571	1.834	1.878	2.336	2.230	3.437		
	1g Load	-1.310x10 ⁶	-1.284x10 ⁶	-1.253x10 ⁶	-802x10 ⁶	-731x10 ⁶	-653x10 ⁶	-244x10 ⁶	-1.70x10 ⁶	-0.959x10 ⁶	-15.61	-764.5	-194.6	-437.6		
420	λ	24770	23500	22160	21030	19270	17960	1536	1749	611.6	9.730	3.339	12.95	3.068		
	λ_0	2.550	2.640	2.749	2.094	2.269	2.418	1.518	1.608	1.870	1.955	2.341	2.195	3.471		
	1g Load	-1.659x10 ⁶	-1.615x10 ⁶	-1.555x10 ⁶	-1.043x10 ⁶	-946x10 ⁶	-786x10 ⁶	-313x10 ⁶	-213x10 ⁶	-1.14x10 ⁶	-89.39	-854.7	-273.0	-479.7		
421	λ	22770	21240	19870	17610	15660	14420	1219	1822	657.6	9.948	3.623	11.76	2.412		
	λ_0	2.700	2.823	2.970	2.214	2.500	2.744	1.512	1.553	1.731	1.858	2.029	2.493	3.244		
	1g Load	-2.059x10 ⁶	-1.996x10 ⁶	-1.909x10 ⁶	-1.319x10 ⁶	-1.237x10 ⁶	-978x10 ⁶	-391x10 ⁶	-266x10 ⁶	-236x10 ⁶	-79.82	-957.0	-359.5	-521.9		
422	λ	22450	20870	19860	17370	15410	14180	1202	1871	653.1	9.868	3.597	11.55	2.355		
	λ_0	2.659	2.774	2.934	2.201	2.496	2.748	1.512	1.514	1.701	1.829	2.029	2.508	3.133		
	1g Load	-2.061x10 ⁶	-1.996x10 ⁶	-1.909x10 ⁶	-1.319x10 ⁶	-1.237x10 ⁶	-978x10 ⁶	-391x10 ⁶	-266x10 ⁶	-236x10 ⁶	-79.82	-957.0	-359.5	-521.9		
423	λ	19110	17970	17310	15710	14210	12810	1099	2403	842.9	7.025	3.135	13.41	3.417		
	λ_0	2.853	2.954	3.082	2.317	2.633	2.939	1.678	2.162	2.413	2.618	3.258	2.145	4.132		
	1g Load	-1.046x10 ⁶	-1.046x10 ⁶	-1.046x10 ⁶	-8.67x10 ⁶	-8.67x10 ⁶	-8.67x10 ⁶	-6.77x10 ⁶	-4.82x10 ⁶	-2.04x10 ⁶	-246.50	-1021.43	-1021.43	-598.31		
424	λ	16330	15580	15710	14480	12920	11730	1099	2403	842.9	7.025	3.135	13.41	3.417		
	λ_0	3.436	3.279	3.268	2.124	2.350	2.540	1.678	2.162	2.413	2.618	3.258	2.145	4.132		
	1g Load	-1.118x10 ⁶	-1.046x10 ⁶	-1.046x10 ⁶	-8.67x10 ⁶	-8.67x10 ⁶	-8.67x10 ⁶	-6.77x10 ⁶	-4.82x10 ⁶	-2.04x10 ⁶	-246.50	-1021.43	-1021.43	-598.31		

TABLE B-2. CONTINUED
(1) WING TORSIONS AND WING SHEAR FLOWS. CASES 425-427

Case	Wing Torsions, K_{θ}										Wing Shear Flows			
	80	81	82	83	84	85	86	87	88	89	90	91	92	
425	W823	W8119	W8167	W8209	W8275	W8346	W8380	W8448	W8516	W8583	W8651	W8719	W8787	
	1.120 1.833 -3.591e6	3.780 1.804 -3.431e6	3.990 1.847 -3.801e6	4.190 1.935 -2.431e6	3.740 1.695 -2.161e6	3.770 1.813 -1.841e6	6.680 1.686 -1.431e6	3.990 1.735 -1.391e6	11.34 1.928 -1.981e6	16.94 1.372 -12.90	4.913 2.827 -108.63	25.40 1.624 -835.0	25.40 1.624 -835.0	
	X No Load											WS 346 Rear Beam	WS 346 Front Beam	
426	W823	W8119	W8167	W8209	W8275	W8346	W8380	W8448	W8516	W8583	W8651	W8719	W8787	
	1.170 2.317 -3.691e6	3.930 2.381 -3.501e6	3.610 2.485 -3.381e6	3.780 1.883 -2.471e6	3.800 2.022 -2.191e6	3.680 2.059 -1.871e6	6.612 1.566 -1.631e6	3.996 1.612 -1.401e6	11.46 1.807 -1.971e6	16.92 1.680 -12.90	4.908 2.820 -1070.02	23.17 2.038 -863.6	23.17 2.038 -863.6	
	X No Load											WS 346 Rear Beam	WS 346 Front Beam	
427	W823	W8119	W8167	W8209	W8275	W8346	W8380	W8448	W8516	W8583	W8651	W8719	W8787	
	1.370 2.347 -3.781e6	1.370 2.632 -3.581e6	1.800 2.718 -3.501e6	1.140 2.860 -1.161e6	1.050 2.404 -2.001e6	1.000 2.498 -2.431e6	1.890 1.102 -1.181e6	8.919 1.164 -1.011e6	313.9 1.409 -1.081e6	3.167 1.868 -868.8	1.895 2.199 -372.83	6.994 2.311 55.13	6.994 2.311 55.13	
	X No Load											WS 346 Rear Beam	WS 346 Front Beam	
428	W823	W8119	W8167	W8209	W8275	W8346	W8380	W8448	W8516	W8583	W8651	W8719	W8787	
	1.980 2.306 -3.781e6	1.970 2.670 -3.641e6	1.870 2.734 -3.581e6	1.140 2.861 -1.161e6	1.060 2.405 -2.301e6	1.010 2.499 -2.411e6	1.845 1.097 -1.181e6	9.04 1.168 -1.121e6	319.1 1.416 -1.071e6	3.197 1.811 -1.811	1.900 2.148 -3.148	6.960 2.897 -2.897	6.960 2.897 -2.897	
	X No Load											WS 346 Rear Beam	WS 346 Front Beam	
429	W823	W8119	W8167	W8209	W8275	W8346	W8380	W8448	W8516	W8583	W8651	W8719	W8787	
	1.460 2.333 -3.781e6	1.460 2.611 -3.641e6	1.860 2.786 -3.581e6	1.150 2.874 -1.161e6	1.060 2.407 -2.301e6	1.010 2.499 -2.411e6	1.845 1.097 -1.181e6	9.04 1.168 -1.121e6	319.1 1.416 -1.071e6	3.197 1.811 -1.811	1.900 2.148 -3.148	6.960 2.897 -2.897	6.960 2.897 -2.897	
	X No Load											WS 346 Rear Beam	WS 346 Front Beam	
430	W823	W8119	W8167	W8209	W8275	W8346	W8380	W8448	W8516	W8583	W8651	W8719	W8787	
	1.700 2.188 -3.781e6	1.700 2.188 -3.781e6	1.460 2.886 -3.581e6	1.730 1.876 -1.876e6	1.490 2.102 -1.391e6	1.110 2.301 -1.861e6	2.973 1.971 -1.281e6	1.861 1.976 -1.161e6	435.9 1.110 -1.071e6	3.988 1.518 -1.518	1.147 5.663 -5.663	8.448 2.040 -2.040	8.448 2.040 -2.040	
	X No Load											WS 346 Rear Beam	WS 346 Front Beam	
431	W823	W8119	W8167	W8209	W8275	W8346	W8380	W8448	W8516	W8583	W8651	W8719	W8787	
	1.660 2.144 -3.781e6	1.660 2.144 -3.781e6	1.460 2.886 -3.581e6	1.730 1.876 -1.876e6	1.490 2.102 -1.391e6	1.110 2.301 -1.861e6	2.973 1.971 -1.281e6	1.861 1.976 -1.161e6	435.9 1.110 -1.071e6	3.988 1.518 -1.518	1.147 5.663 -5.663	8.448 2.040 -2.040	8.448 2.040 -2.040	
	X No Load											WS 346 Rear Beam	WS 346 Front Beam	

TABLE B-2. CONTINUED
(1) FUSELAGE LOADS AND HORIZONTAL TAIL LOAD, CASES 401-412

Case	Fuselage Loads										Horizontal Tail Load	
	33	34	35	36	37	38	39	40	41	42	43	44
	S_z	S_y	S_z	S_y	S_z	S_y	S_z	S_y	S_z	S_y	S_z	S_y
	PL350	PL350	PL350	PL350	PL371	PL371	PL395	PL395	PL405	PL405	PL405	PL405
401	\bar{X} 14.3 2.865 -8085	\bar{Y} 309.30 2.313 -1.582106	\bar{S}_z 219.5 1.968 -11161	\bar{S}_y 57490 2.930 -2.344106	\bar{S}_z 252.9 1.866 -12678	\bar{S}_y 741.60 2.144 -3.763106	\bar{S}_z 73.78 2.190 -18762	\bar{S}_y 46640 2.790 9.097106	\bar{S}_z 98.81 2.113 -18342	\bar{S}_y 31280 2.379 3.283106	\bar{S}_z 199.04 2.783 -16758	\bar{S}_y 31280 2.379 3.283106
402	\bar{X} 179.4 2.485 -8187	\bar{Y} 35760 2.445 -1.536106	\bar{S}_z 246.6 1.131 -11313	\bar{S}_y 66680 2.374 -2.393106	\bar{S}_z 286.3 1.978 -15022	\bar{S}_y 94060 1.442 -3.83106	\bar{S}_z 128.6 2.633 -15017	\bar{S}_y 93210 2.319 7.238106	\bar{S}_z 128.9 2.633 -15017	\bar{S}_y 93210 2.319 7.238106	\bar{S}_z 239.2 2.704 -13148	\bar{S}_y 93210 2.319 7.238106
403	\bar{X} 215.6 2.018 -6881	\bar{Y} 43090 2.041 -1.361106	\bar{S}_z 164.8 1.745 -9453	\bar{S}_y 43920 1.978 -2.537106	\bar{S}_z 195.6 1.611 -10907	\bar{S}_y 56080 1.901 -3.261106	\bar{S}_z 65.21 2.497 -17248	\bar{S}_y 52150 2.888 8.233106	\bar{S}_z 113.8 2.379 -16575	\bar{S}_y 31280 2.379 3.283106	\bar{S}_z 113.8 2.379 3.283106	\bar{S}_y 31280 2.379 3.283106
404	\bar{X} 141.2 2.216 -1007	\bar{Y} 28440 2.211 -1.361106	\bar{S}_z 192.8 1.275 -9642	\bar{S}_y 28750 1.162 -2.581106	\bar{S}_z 224.9 1.812 -11125	\bar{S}_y 73580 1.162 -3.318106	\bar{S}_z 121.3 2.307 -13956	\bar{S}_y 91040 2.307 6.081106	\bar{S}_z 121.3 2.307 -13956	\bar{S}_y 91040 2.307 6.081106	\bar{S}_z 121.3 2.307 -13956	\bar{S}_y 91040 2.307 6.081106
405	\bar{X} 228.9 1.780 -13674	\bar{Y} 34670 1.882 -1.864106	\bar{S}_z 418.1 1.455 -21274	\bar{S}_y 84610 1.708 -4.464106	\bar{S}_z 485.7 1.617 -24321	\bar{S}_y 116600 1.617 -6.083106	\bar{S}_z 88.93 2.899 -16030	\bar{S}_y 62830 2.697 7.382106	\bar{S}_z 138.9 2.449 -14766	\bar{S}_y 35830 2.772 2.609106	\bar{S}_z 138.9 2.449 -14766	\bar{S}_y 35830 2.772 2.609106
406	\bar{X} 229.0 1.953 -13783	\bar{Y} 40780 2.043 -1.881106	\bar{S}_z 468.4 1.637 -21437	\bar{S}_y 97560 1.910 -4.502106	\bar{S}_z 536.9 1.513 -24009	\bar{S}_y 133900 1.513 -6.133106	\bar{S}_z 135.5 2.504 -11991	\bar{S}_y 91260 2.467 5.486106	\bar{S}_z 190.7 2.861 -10798	\bar{S}_y 46200 2.866 1.902106	\bar{S}_z 190.7 2.861 -10798	\bar{S}_y 46200 2.866 1.902106
407	\bar{X} 263.5 1.894 -16991	\bar{Y} 44470 2.054 -2.147106	\bar{S}_z 599.0 1.615 -25305	\bar{S}_y 114000 1.844 -5.349106	\bar{S}_z 644.9 1.784 -28752	\bar{S}_y 156700 1.784 -7.269106	\bar{S}_z 440.1 1.386 -31773	\bar{S}_y 53720 2.632 11.166106	\bar{S}_z 57.32 4.179 -19609	\bar{S}_y 27920 4.179 3.886106	\bar{S}_z 57.32 4.179 -19609	\bar{S}_y 27920 4.179 3.886106
408	\bar{X} 313.4 2.090 -13878	\bar{Y} 43960 2.277 -1.892106	\bar{S}_z 504.5 1.804 -23636	\bar{S}_y 106400 2.076 -3.952106	\bar{S}_z 586.1 1.677 -24860	\bar{S}_y 143100 1.983 -6.052106	\bar{S}_z 451.4 1.771 -31	\bar{S}_y 33940 3.746 9.944106	\bar{S}_z 93.35 4.560 -15678	\bar{S}_y 38600 3.735 2.552106	\bar{S}_z 93.35 4.560 -15678	\bar{S}_y 38600 3.735 2.552106
409	\bar{X} 224.7 1.866 -14332	\bar{Y} 39250 2.033 -1.987106	\bar{S}_z 475.2 1.588 -22755	\bar{S}_y 96340 1.850 -4.689106	\bar{S}_z 522.5 1.468 -25451	\bar{S}_y 132700 1.757 -6.303106	\bar{S}_z 63.93 3.460 -17846	\bar{S}_y 57400 2.860 8.310106	\bar{S}_z 122.0 3.732 -16746	\bar{S}_y 34210 3.515 2.976106	\bar{S}_z 122.0 3.732 -16746	\bar{S}_y 34210 3.515 2.976106
410	\bar{X} 340.9 2.071 -14449	\bar{Y} 46240 2.148 -1.989106	\bar{S}_z 531.5 1.728 -28431	\bar{S}_y 111200 2.015 -4.789106	\bar{S}_z 608.6 1.641 -29654	\bar{S}_y 151700 1.988 -6.437106	\bar{S}_z 111.7 4.086 -13159	\bar{S}_y 86360 3.113 6.142106	\bar{S}_z 178.8 3.113 -12358	\bar{S}_y 46870 3.113 2.192106	\bar{S}_z 178.8 3.113 -12358	\bar{S}_y 46870 3.113 2.192106
411	\bar{X} 285.0 1.725 -14172	\bar{Y} 38230 1.878 -1.942106	\bar{S}_z 459.7 1.479 -25016	\bar{S}_y 91170 1.711 -4.534106	\bar{S}_z 533.9 1.397 -25176	\bar{S}_y 128400 1.688 -6.310106	\bar{S}_z 66.25 4.731 -17257	\bar{S}_y 58530 3.700 8.062106	\bar{S}_z 125.2 3.235 -16193	\bar{S}_y 34470 3.105 2.877106	\bar{S}_z 125.2 3.235 -16193	\bar{S}_y 34470 3.105 2.877106
412	\bar{X} 329.0 1.876 -14889	\bar{Y} 44880 1.947 -1.962106	\bar{S}_z 513.9 1.600 -22198	\bar{S}_y 107400 1.887 -4.674106	\bar{S}_z 588.7 1.499 -25179	\bar{S}_y 146500 1.750 -6.444106	\bar{S}_z 116.3 3.489 -18842	\bar{S}_y 87020 3.046 2.938106	\bar{S}_z 181.0 2.732 -11822	\bar{S}_y 46170 2.732 2.104106	\bar{S}_z 181.0 2.732 -11822	\bar{S}_y 46170 2.732 2.104106

TABLE B-2. CONTINUED
(K) FUSELAGE LOADS AND HORIZONTAL TAIL LOAD, CASES 413-424

Case		Fuselage Loads										Horiz. Tail Load
		33	34	35	36	37	38	39	40	41	42	
		R_z	R_y	R_x	M_z	M_y	M_x	G_z	G_y	G_x	M_y	M_x
		FT350	FT350	FT350	FT350	FT371	FT371	FT371	FT393	FT406	FT406	FT406
413	\bar{X}	278.3	3740	448.5	50960	590.1	125300	70.85	60660	229.5	35060	
	R_z	1.688	1.814	1.474	1.456	1.357	1.576	4.098	2.375	2.959	2.885	
	1g Load	-1.9894	-1.0984106	-21601	-4.5384106	-27699	-6.1834106	-16664	7.104106	-15684	2.774106	
414	\bar{X}	320.8	43740	501.2	104700	974.3	140800	121.9	88580	184.3	46510	
	R_z	1.805	1.873	1.541	1.737	1.684	1.684	3.059	2.807	2.982	2.566	
	1g Load	-1.8149	-1.9402106	-21990	-4.6684106	-82514	-6.3084106	-16006	5.7784106	-11595	2.0384106	
415	\bar{X}	271.1	36680	436.3	88590	506.1	170000	78.34	63690	135.5	35980	
	R_z	1.651	1.795	1.418	1.638	1.341	1.559	3.694	2.098	2.229	2.702	
	1g Load	-1.5741	-1.8754106	-21374	-4.1484106	-84436	-6.1144106	-16865	7.5074106	-15069	2.6664106	
416	\bar{X}	311.7	42490	487.1	101700	558.1	138800	129.3	90880	184.9	47070	
	R_z	1.787	1.856	1.545	1.741	1.450	1.667	2.783	2.680	2.149	2.482	
	1g Load	-1.9851	-1.9035106	-21577	-4.5844106	-84064	-6.1644106	-12547	5.6574106	-11537	2.734106	
417	\bar{X}	267.7	35940	430.5	87480	499.3	120400	84.76	55370	138.8	36480	
	R_z	1.655	1.801	1.419	1.642	1.340	1.563	3.455	2.598	2.633	2.633	
	1g Load	-1.3674	-1.8644106	-21874	-4.1484106	-84381	-6.0834106	-16090	7.3074106	-14766	2.6094106	
418	\bar{X}	307.4	41000	480.4	100320	550.4	136970	133.3	90950	192.4	47400	
	R_z	1.756	1.866	1.530	1.749	1.443	1.675	2.577	2.531	2.898	2.372	
	1g Load	-1.7763	-1.8624106	-21437	-4.5044106	-84509	-6.1334106	-11951	5.4684106	-10798	1.9024106	
419	\bar{X}	284.8	34780	436.3	89110	502.6	128400	36.0	41230	37.04	19030	93.04
	R_z	1.657	1.804	1.465	1.651	1.419	1.594	1.285	2.280	5.288	2.343	1.956
	1g Load	-1.5698	-1.9464106	-23374	-4.9074106	-86386	-6.6794106	-27987	9.0234106	-15084	2.4164106	-10702
420	\bar{X}	323.3	39630	495.4	101400	570.1	139200	384.8	47780	42.93	21390	100.82
	R_z	1.710	1.871	1.540	1.728	1.447	1.679	1.331	2.372	5.762	2.947	2.319
	1g Load	-2.6408	-2.0764106	-84434	-5.1484106	-27739	-7.0044106	-89099	10.0544106	-17191	2.5134106	-12934
421	\bar{X}	348.8	44640	535.6	109400	617.0	150800	412.4	50410	49.27	24670	114.32
	R_z	1.717	1.883	1.546	1.709	1.445	1.645	1.400	2.430	5.894	2.467	2.467
	1g Load	-1.6195	-2.1394106	-23194	-5.3444106	-26884	-7.2364106	-30935	10.9824106	-19794	3.2534106	-15912
422	\bar{X}	321.8	43030	539.8	110300	604.7	151400	405.7	47700	52.45	24670	119.12
	R_z	1.693	1.878	1.503	1.645	1.434	1.681	1.480	2.544	5.742	2.471	2.471
	1g Load	-1.7159	-2.1784106	-23556	-5.4074106	-29093	-7.3474106	-30810	10.9824106	-19317	3.2494106	-15512
423	\bar{X}	213.1	41090	505.9	79400	363.1	103000	108.7	41560	95.65	33080	288.4
	R_z	1.538	1.588	1.513	1.587	1.506	1.519	2.341	4.180	3.489	3.015	2.479
	1g Load	-2.944	-1.8164106	-14086	-3.5844106	-13279	-4.6994106	-27687	14.0994106	-59306	5.2744106	-27996
424	\bar{X}	235.4	47890	538.0	88670	387.7	114400	53.39	70380	133.8	47390	273.0
	R_z	1.544	1.699	1.465	1.493	1.449	1.441	5.768	5.465	2.904	2.793	2.548
	1g Load	-2.965	-1.7024106	-13024	-3.5824106	-15012	-4.3494106	-22608	11.8994106	-24560	4.5334106	-24108

TABLE B-2. CONCLUDED
(1) FUSELAGE LOADS, CASES 425-427

Case		Fuselage Loads									
		33	34	35	36	37	38	39	40	41	42
		B_z	N_y	B_z	N_y	B_z	N_y	B_z	N_y	B_z	N_y
		PSI	PSI	PSI	PSI	PSI	PSI	PSI	PSI	PSI	PSI
425	λ	340.6	660.2	834.3	1638.0	963.1	2335.0	689.8	961.8	82.16	3121.0
	N_o	1.334	1.492	1.262	1.133	1.268	1.314	1.373	1.650	3.418	3.347
	1g Load	-17980	-2.297x10 ⁶	-26786	-3.628x10 ⁶	-30434	-7.722x10 ⁶	-39143	15.782x10 ⁶	-29537	5.150x10 ⁶
426	λ	625.1	780.0	935.8	1960.0	1066	2670.0	512.0	3920.0	111.9	4974.0
	N_o	1.466	1.350	1.370	1.462	1.336	1.459	1.360	1.494	4.521	3.640
	1g Load	-15272	-2.064x10 ⁶	-25721	-4.929x10 ⁶	-26564	-6.692x10 ⁶	-35918	14.722x10 ⁶	-4521	4.472x10 ⁶
427	λ	174.4	2126.0	262.3	2467.0	309.3	7414.0	193.4	1840.0	30.78	1471.0
	N_o	1.268	1.332	1.207	1.269	1.186	1.248	1.501	2.251	2.675	1.638
	1g Load	-15505	-1.912x10 ⁶	-23084	-4.841x10 ⁶	-26193	-6.591x10 ⁶	-23105	6.092x10 ⁶	-6715	1.223x10 ⁶
428	λ	170.6	2076.0	263.7	2352.0	304.6	7366.0	197.8	1940.0	27.10	1377.0
	N_o	1.272	1.340	1.201	1.271	1.175	1.247	1.163	1.095	2.817	1.602
	1g Load	-124.9	1.6870	200.2	4077.0	232.0	5607.0	54.51	3880.0	81.32	2041.0
429	N_o	1.357	1.452	1.508	1.350	1.199	1.259	2.205	1.914	1.727	1.749
	1g Load	-153.6	2057.0	247.7	5017.0	287.6	6014.0	60.06	1421.0	93.90	2362.0
430	N_o	1.365	1.457	1.227	1.359	1.182	1.312	2.276	1.870	1.713	1.695
431	λ	145.7	1945.0	236.4	4761.0	273.1	6574.0	550.8	4124.0	88.19	2228.0
	N_o	1.460	1.568	1.298	1.434	1.245	1.398	2.019	1.697	1.589	1.516
	1g Load	-145.7	1945.0	236.4	4761.0	273.1	6574.0	550.8	4124.0	88.19	2228.0

TABLE B-3. RESULTS OF VERTICAL GUST DYNAMIC ANALYSIS,
MODEL 749 MISSION ANALYSIS SEGMENTS
(a) C. G. ACCELERATIONS AND WING SHEARS, CASES 101-110

Case	C.G. Accel	Wing Shears, g									
		1	2	3	4	5	6	7	8	9	10
		W8103	W8145	W8191	W8263	W8337	W8404	W8480	W8568	W8656	
101	\bar{X} \bar{Y} \bar{Z} 1g Load	194.0 1.091 1.002	140.5 1.784 1.467	194.1 1.467 1.467	166.2 1.601 1.601	194.9 1.776 1.776	127.9 1.076 1.076	87.44 1.200 1.200	39.15 1.161 1.161	11.70 1.931 1.931	
102	\bar{X} \bar{Y} \bar{Z} 1g Load	246.0 1.232 1.000	211.4 1.856 1.856	297.6 1.423 1.423	242.4 1.648 1.648	188.4 1.930 1.930	179.2 1.142 1.142	120.6 1.218 1.218	73.08 1.350 1.350	15.60 1.083 1.083	
103	\bar{X} \bar{Y} \bar{Z} 1g Load	273.8 1.231 1.000	231.1 1.842 1.842	327.5 1.375 1.375	262.7 1.616 1.616	200.0 1.912 1.912	194.7 1.110 1.110	130.3 1.182 1.182	57.18 1.307 1.307	16.82 1.070 1.070	
104	\bar{X} \bar{Y} \bar{Z} 1g Load	238.8 1.267 1.000	210.4 1.863 1.863	292.8 1.439 1.439	243.7 1.688 1.688	192.7 1.929 1.929	181.3 1.129 1.129	122.4 1.257 1.257	74.01 1.389 1.389	15.92 1.141 1.141	
105	\bar{X} \bar{Y} \bar{Z} 1g Load	266.4 1.293 1.000	231.5 1.869 1.869	323.4 1.301 1.301	265.3 1.672 1.672	206.1 1.987 1.987	198.9 1.102 1.102	133.2 1.185 1.185	58.48 1.400 1.400	17.21 1.157 1.157	
106	\bar{X} \bar{Y} \bar{Z} 1g Load	227.3 1.239 1.000	199.6 1.911 1.911	278.7 1.491 1.491	230.8 1.696 1.696	182.2 1.940 1.940	169.7 1.168 1.168	114.5 1.266 1.266	50.52 1.474 1.474	14.82 1.122 1.122	
107	\bar{X} \bar{Y} \bar{Z} 1g Load	269.4 1.296 1.000	238.1 1.856 1.856	322.8 1.335 1.335	259.8 1.635 1.635	199.5 1.947 1.947	191.6 1.135 1.135	128.3 1.211 1.211	56.38 1.341 1.341	16.56 1.090 1.090	
108	\bar{X} \bar{Y} \bar{Z} 1g Load	184.3 1.234 1.000	166.7 1.980 1.980	229.1 1.596 1.596	198.4 1.732 1.732	165.0 1.869 1.869	167.3 1.279 1.279	101.3 1.328 1.328	44.98 1.433 1.433	13.39 1.042 1.042	
109	\bar{X} \bar{Y} \bar{Z} 1g Load	194.5 1.302 1.000	176.4 1.916 1.916	243.2 1.489 1.489	205.8 1.813 1.813	165.3 1.970 1.970	150.6 1.207 1.207	102.4 1.330 1.330	45.45 1.434 1.434	13.32 1.042 1.042	
110	\bar{X} \bar{Y} \bar{Z} 1g Load	265.2 1.263 1.000	227.4 1.872 1.872	318.6 1.416 1.416	257.2 1.653 1.653	198.4 1.961 1.961	188.7 1.160 1.160	126.6 1.240 1.240	55.65 1.376 1.376	16.32 1.112 1.112	
106a	\bar{X} \bar{Y} \bar{Z} 1g Load	244.0 1.265 1.000	215.3 1.807 1.807	294.8 1.514 1.514	242.3 1.700 1.700	189.7 1.935 1.935	179.2 1.197 1.197	121.1 1.304 1.304	53.51 1.494 1.494	15.70 1.157 1.157	
106b	\bar{X} \bar{Y} \bar{Z} 1g Load	207.6 1.263 1.000	186.2 1.916 1.916	246.7 1.478 1.478	207.5 1.692 1.692	165.9 1.869 1.869	154.4 1.207 1.207	101.3 1.328 1.328	44.98 1.433 1.433	13.39 1.042 1.042	
106c	\bar{X} \bar{Y} \bar{Z} 1g Load	244.0 1.265 1.000	215.3 1.807 1.807	294.8 1.514 1.514	242.3 1.700 1.700	189.7 1.935 1.935	179.2 1.197 1.197	121.1 1.304 1.304	53.51 1.494 1.494	15.70 1.157 1.157	
106d	\bar{X} \bar{Y} \bar{Z} 1g Load	207.6 1.263 1.000	186.2 1.916 1.916	246.7 1.478 1.478	207.5 1.692 1.692	165.9 1.869 1.869	154.4 1.207 1.207	101.3 1.328 1.328	44.98 1.433 1.433	13.39 1.042 1.042	
106e	\bar{X} \bar{Y} \bar{Z} 1g Load	244.0 1.265 1.000	215.3 1.807 1.807	294.8 1.514 1.514	242.3 1.700 1.700	189.7 1.935 1.935	179.2 1.197 1.197	121.1 1.304 1.304	53.51 1.494 1.494	15.70 1.157 1.157	
106f	\bar{X} \bar{Y} \bar{Z} 1g Load	207.6 1.263 1.000	186.2 1.916 1.916	246.7 1.478 1.478	207.5 1.692 1.692	165.9 1.869 1.869	154.4 1.207 1.207	101.3 1.328 1.328	44.98 1.433 1.433	13.39 1.042 1.042	

NOTE: Cases 106a, 106b, 106c, 106d, 106e, and 106f rigid re-
flect modified air-
plane configurations
used in comparison
of Lockheed and
Boeing mathematical
models; see region
1b.b.

TABLE B-3. CONTINUED
(b) WING BENDING MOMENTS, CASES 101-110

Case		Wing Bending Moments, M_x									
		11	12	13	14	15	16	17	18	19	
		WB103	WB145	WB191	WB263	WB337	WB404	WB480	WB558	WB668	
101	\bar{X}	62220	56130	48580	39610	29350	16980	8895	2853	222.3	
	M_0	1.308	1.296	1.273	1.268	1.132	1.129	1.145	1.079	.9831	
	1g Load	6.349e106	5.702e106	4.935e106	3.749e106	2.743e106	1.84e106	.982e106	.528e106	.034e106	
102	\bar{X}	90080	80630	69060	49600	35030	19400	12140	3037	296.4	
	M_0	1.377	1.372	1.362	1.331	1.218	1.208	1.253	1.254	1.083	
	1g Load	6.845e106	6.075e106	5.199e106	3.881e106	2.797e106	1.861e106	.978e106	.847e106	.0335e106	
103	\bar{X}	98030	87600	74900	53600	37890	25310	13100	3278	319.6	
	M_0	1.350	1.346	1.338	1.310	1.189	1.173	1.216	1.219	1.070	
	1g Load	6.677e106	6.107e106	5.217e106	3.853e106	2.792e106	1.859e106	.974e106	.845e106	.033e106	
104	\bar{X}	90360	81100	69680	50400	35630	23770	12340	3094	302.4	
	M_0	1.390	1.376	1.357	1.319	1.218	1.225	1.288	1.332	1.141	
	1g Load	7.023e106	6.295e106	5.362e106	4.042e106	2.953e106	1.945e106	1.022e106	.258e106	.034e106	
105	\bar{X}	98780	88520	75930	54750	38770	25870	13390	3349	327.0	
	M_0	1.361	1.345	1.324	1.283	1.176	1.182	1.261	1.314	1.157	
	1g Load	7.079e106	6.595e106	5.602e106	4.091e106	2.919e106	1.939e106	1.017e106	.256e106	.034e106	
106	\bar{X}	89230	78410	65940	47220	33280	22220	11940	2889	281.5	
	M_0	1.417	1.410	1.398	1.363	1.258	1.257	1.307	1.311	1.122	
	1g Load	6.892e106	6.097e106	5.223e106	3.912e106	2.859e106	1.882e106	.989e106	.252e106	.0339e106	
107	\bar{X}	96700	86430	73900	52880	37330	24930	12910	3226	314.7	
	M_0	1.370	1.366	1.358	1.332	1.214	1.201	1.246	1.246	1.090	
	1g Load	6.895e106	6.107e106	5.217e106	3.853e106	2.792e106	1.861e106	.978e106	.847e106	.0335e106	
108	\bar{X}	73320	66060	57060	41740	29090	19480	10160	2894	294.4	
	M_0	1.462	1.453	1.442	1.409	1.350	1.346	1.387	1.432	1.032	
	1g Load	6.592e106	5.883e106	5.072e106	3.842e106	2.807e106	1.862e106	1.022e106	.258e106	.034e106	
109	\bar{X}	75380	67890	58340	42270	29750	19860	10350	2999	293.1	
	M_0	1.460	1.463	1.459	1.436	1.317	1.309	1.342	1.371	1.271	
	1g Load	6.752e106	6.032e106	5.192e106	3.902e106	2.834e106	1.892e106	.997e106	.253e106	.0345e106	
110	\bar{X}	95490	85960	72990	52220	36280	24580	12730	3183	310.1	
	M_0	1.390	1.386	1.379	1.353	1.240	1.230	1.277	1.279	1.112	
	1g Load	6.985e106	6.107e106	5.217e106	3.853e106	2.792e106	1.861e106	.978e106	.847e106	.0335e106	
106x	\bar{X}	89230	80280	68690	49380	35070	23500	12210	3060	296.3	
	M_0	1.403	1.391	1.382	1.352	1.273	1.295	1.362	1.378	1.157	
	1g Load	7.023e106	6.295e106	5.362e106	4.042e106	2.953e106	1.945e106	1.022e106	.258e106	.034e106	
106y	\bar{X}	77410	69580	60070	44130	30890	22360	11990	2986	294.7	
	M_0	1.048	1.034	1.026	1.011	1.003	.996	.997	.972	.968	
	1g Load	6.988e106	6.322e106	5.467e106	3.979e106	2.928e106	1.973e106	1.086e106	.293e106	.283.2	
106y	\bar{X}	61610	55900	48610	35960	27350	18730	9700	2449	246.0	
	M_0	1.880	1.813	1.806	1.791	1.759	1.765	1.773	1.757	1.346	

TABLE B-3. CONTINUED
(c) WING TORSIONS AND WING SHEAR FLOWS, CASES 101-110

Case	Wing Torsions, M_{yA}										Wing Shear Flows			
	20	21	22	23	24	25	26	27	28	29	30	31	32	
	W8103	W8145	W8191	W8263	W8337	W8404	W8480	W8588	W8668	W8103 Front Beam	W8103 Rear Beam	W8337 Front Beam	W8337 Rear Beam	
101	\bar{X} 9409 3.672 -1.791106	\bar{X} 9409 3.453 -1.945106	\bar{X} 8467 3.091 -1.385106	\bar{X} 8373 3.064 -1.521106	\bar{X} 8553 2.934 -1.683106	\bar{X} 657.8 3.574 -1.164106	\bar{X} 508.3 3.461 -1.178106	\bar{X} 393.0 2.217 -1.128106	\bar{X} 153.6 1.487 -1.465106	2.128 3.463 -1.43	2.031 2.828 -1.45	4.106 2.767 -1.45	2.434 2.223 -1.337	
102	\bar{X} 12880 3.846 -1.299106	\bar{X} 12970 3.769 -1.433106	\bar{X} 12890 3.049 -1.735106	\bar{X} 12400 3.049 -1.651106	\bar{X} 12390 2.987 -1.931106	\bar{X} 1074 4.170 -1.312106	\bar{X} 845.6 3.954 -1.295106	\bar{X} 562.7 2.967 -1.199106	\bar{X} 209.5 1.785 -1.077106	3.549 3.270 -1.07	2.788 2.946 -1.35	6.152 2.727 -1.22	3.016 2.743 -1.45	
103	\bar{X} 13440 3.947 -1.428106	\bar{X} 13360 3.810 -1.534106	\bar{X} 13520 2.921 -1.819106	\bar{X} 12880 3.005 -1.928106	\bar{X} 12820 2.959 -1.001106	\bar{X} 1152 4.141 -1.345106	\bar{X} 887.0 3.956 -1.321106	\bar{X} 600.6 2.499 -1.214106	\bar{X} 225.2 1.672 -1.389106	3.895 3.182 -1.25	2.534 2.834 -1.63	6.449 2.698 -1.46	3.091 2.755 -1.468	
104	\bar{X} 12930 3.808 -1.245106	\bar{X} 12860 3.788 -1.393106	\bar{X} 12910 2.946 -1.708106	\bar{X} 12300 3.011 -1.831106	\bar{X} 12200 2.960 -1.913106	\bar{X} 1020.0 3.980 -1.312106	\bar{X} 794.1 3.752 -1.297106	\bar{X} 562.8 2.556 -1.200106	\bar{X} 212.7 1.802 -1.078106	3.567 3.215 -1.01	2.596 3.410 -1.18	6.180 2.079 -1.13	2.943 2.727 -1.448	
105	\bar{X} 13870 3.816 -1.346106	\bar{X} 13820 3.846 -1.507106	\bar{X} 13740 2.893 -1.798106	\bar{X} 12950 2.989 -1.907106	\bar{X} 12780 2.951 -1.963106	\bar{X} 1123 4.059 -1.345106	\bar{X} 871.1 3.866 -1.353106	\bar{X} 609.2 2.585 -1.261106	\bar{X} 230.2 1.824 -1.084106	3.961 3.156 -1.20	2.746 3.434 -1.47	6.329 2.661 -1.32	3.059 2.775 -1.471	
106	\bar{X} 12730 3.827 -1.237106	\bar{X} 12850 3.747 -1.379106	\bar{X} 12760 3.037 -1.693106	\bar{X} 12130 3.079 -1.813106	\bar{X} 12110 3.015 -1.856106	\bar{X} 1069 4.122 -1.296106	\bar{X} 830.8 3.960 -1.283106	\bar{X} 542.4 2.653 -1.192106	\bar{X} 200.0 1.805 -1.0745106	3.396 3.305 -1.09	2.659 3.124 -1.16	6.074 2.745 -1.15	2.963 2.759 -1.435	
107	\bar{X} 13460 3.837 -1.428106	\bar{X} 13400 3.798 -1.544106	\bar{X} 13680 2.940 -1.811106	\bar{X} 13010 3.018 -1.928106	\bar{X} 12940 2.971 -1.001106	\bar{X} 1157 4.165 -1.345106	\bar{X} 892.7 3.971 -1.312106	\bar{X} 596.6 2.544 -1.214106	\bar{X} 222.3 1.714 -1.093106	3.866 3.187 -1.25	2.909 2.896 -1.63	6.493 2.706 -1.16	3.084 2.801 -1.468	
108	\bar{X} 9533 3.599 -1.003106	\bar{X} 9602 3.518 -1.161106	\bar{X} 10130 2.923 -1.342106	\bar{X} 9751 2.946 -1.683106	\bar{X} 9752 2.872 -1.782106	\bar{X} 668.9 3.302 -1.254106	\bar{X} 586.0 2.996 -1.253106	\bar{X} 447.3 2.046 -1.173106	\bar{X} 173.3 1.179 -1.0665106	2.602 3.116 -1.06	1.946 3.182 -1.59	5.116 2.596 -1.92	2.397 2.694 -1.307	
109	\bar{X} 12180 3.815 -1.081106	\bar{X} 12180 3.756 -1.227106	\bar{X} 11940 3.180 -1.589106	\bar{X} 11470 3.166 -1.711106	\bar{X} 11340 3.113 -1.808106	\bar{X} 966.0 3.976 -1.251106	\bar{X} 737.7 3.939 -1.247106	\bar{X} 493.4 2.965 -1.170106	\bar{X} 180.9 2.132 -1.063106	3.072 3.329 -1.30	2.436 3.625 -1.376	5.552 2.760 -1.06	2.756 3.140 -1.403	
110	\bar{X} 13490 3.889 -1.428106	\bar{X} 13440 3.788 -1.544106	\bar{X} 13730 2.958 -1.819106	\bar{X} 13140 3.030 -1.928106	\bar{X} 13070 2.983 -1.001106	\bar{X} 1164 4.190 -1.345106	\bar{X} 899.8 4.007 -1.312106	\bar{X} 597.7 2.611 -1.214106	\bar{X} 219.7 1.759 -1.093106	3.841 3.193 -1.25	2.888 2.941 -1.63	6.539 2.713 -1.16	3.031 2.848 -1.468	
106a	\bar{X} 17780 4.480	\bar{X} 17940 4.800	\bar{X} 13910 3.145	\bar{X} 13980 3.164	\bar{X} 13610 3.086	\bar{X} 1146 4.159	\bar{X} 904.6 3.995	\bar{X} 584.8 2.786	\bar{X} 214.1 1.984	4.317 3.051	3.232 3.407	6.322 2.821	3.322 2.864	
106a B1614	\bar{X} 2951 4.554	\bar{X} 4388 2.627	\bar{X} 2275 2.980	\bar{X} 1480 4.083	\bar{X} 3160 1.879	\bar{X} 437.7 3.922	\bar{X} 203.8 1.840	\bar{X} 143.3 1.013	\bar{X} 182.6 3.564	1.482 2.850	2.187 1.306	1.716 3.002	2.447 1.047	
106b	\bar{X} 19310 3.657	\bar{X} 20660 3.405	\bar{X} 15080 3.359	\bar{X} 14820 3.356	\bar{X} 14780 3.165	\bar{X} 1213 4.513	\bar{X} 1022 4.465	\bar{X} 960.0 3.437	\bar{X} 183.6 2.407	3.357 4.054	4.137 2.758	3.999 3.180	4.126 2.752	
106b B1614	\bar{X} 10840 1.351	\bar{X} 12660 1.333	\bar{X} 3951 1.493	\bar{X} 3966 1.351	\bar{X} 7849 1.314	\bar{X} 447.5 1.054	\bar{X} 130.7 1.709	\bar{X} 339.3 1.830	\bar{X} 137.0 1.189	1.914 1.893	3.330 1.375	1.178 1.460	3.272 1.862	

TABLE B-3. CONCLUDED
(d) FUSELAGE LOADS, CASES 101-110

Case		Fuselage Loads				Horiz. Tail Load
		33	34	35	36	
		\bar{X} \bar{Y} \bar{Z}	\bar{X} \bar{Y} \bar{Z}	\bar{X} \bar{Y} \bar{Z}	\bar{X} \bar{Y} \bar{Z}	
101	\bar{X} \bar{Y} \bar{Z}	137.1 1.540 -1.940	18660 1.784 -1.851	321.9 2.137 -5534	8674 1.832 8351	81.4 1.5 -2568
102	\bar{X} \bar{Y} \bar{Z}	193.4 1.816 -1.916	25450 2.140 -1.779	436.0 2.815 -8500	10720 2.182 1.362	110.90 1.746 -5554
103	\bar{X} \bar{Y} \bar{Z}	211.0 1.818 -1.910	27780 2.136 -1.763	464.5 2.856 -9159	11570 2.220 1.469	116.64 1.689 -6184
104	\bar{X} \bar{Y} \bar{Z}	188.2 1.906 -1.916	24770 2.252 -1.779	434.9 2.851 -8352	11311 2.193 1.337	112.30 1.562 -5406
105	\bar{X} \bar{Y} \bar{Z}	205.8 1.986 -1.910	27120 2.269 -1.764	463.5 2.866 -9021	12050 2.276 1.451	119.88 1.628 -6076
106	\bar{X} \bar{Y} \bar{Z}	180.7 1.899 -1.918	23780 2.197 -1.767	419.9 2.841 -8163	10290 2.179 1.305	104.6 1.539 -5216
107	\bar{X} \bar{Y} \bar{Z}	207.4 1.841 -1.910	27300 2.167 -1.764	467.7 2.890 -9159	11200 2.229 1.469	115.10 1.684 -7184
108	\bar{X} \bar{Y} \bar{Z}	149.7 1.864 -1.960	19500 2.223 -1.809	373.9 2.667 -7066	9869 1.832 1.119	98.46 1.419 -4120
109	\bar{X} \bar{Y} \bar{Z}	158.3 1.928 -1.960	20780 2.277 -1.809	384.5 2.778 -7248	9548 2.240 1.150	95.34 1.471 -4302
110	\bar{X} \bar{Y} \bar{Z}	204.2 1.862 -1.910	26970 2.196 -1.763	457.7 2.918 -9129	11010 2.242 1.469	113.14 1.619 -6184
105a	\bar{X} \bar{Y}	208.5 2.333	28650 2.693	441.9 3.833	7208 2.990	
106a	\bar{X} \bar{Y}	171.3 1.453	22160 1.720	35.47 2.402	6652 2.518	
106b	\bar{X} \bar{Y}	179.4 2.015	25470 2.293	438.1 3.620	8987 2.527	
106c	\bar{X} \bar{Y}	156.8 1.419	21310 1.540	289.1 1.911	9408 2.919	

TABLE B-4. RESULTS OF VERTICAL GUST DYNAMIC ANALYSIS,
MODEL 749 MISSION ANALYSIS SEGMENTS
(a) C.G. ACCELERATIONS AND WING SHEARS, CASES 301-312

Case	C.G. Accel	Wing Shears, S _y									
		1	2	3	4	5	6	7	8	9	10
		WS 103	WS 103	WS 145	WS 191	WS 263	WS 337	WS 404	WS 480	WS 918	WS 668
301	A M ₀ 1g Load	131.0 1.501 1.0	89.31 2.954 1.0	221.3 1.546 1.3888	165.6 1.927 1.0882	119.5 2.568 7650	153.8 1.508 97607	103.8 1.595 6755	46.12 1.706 2895	13.53 1.425 870	13.53 1.425 870
302	A M ₀ 1g Load	130.1 1.389 1.0	81.10 2.977 1.0	211.8 1.430 1.3888	168.7 1.846 1.0882	117.1 2.573 7098	166.4 1.460 9292	112.3 1.438 6448	49.81 1.532 2761	1.481 1.152 831	1.481 1.152 831
303	A M ₀ 1g Load	76.79 1.465 1.0	63.60 3.315 1.0	133.1 1.727 1.2376	111.2 2.003 9524	98.31 2.136 6927	130.4 1.289 1.0629	92.88 1.448 6935	46.56 1.827 3.67	15.74 1.283 3.328	15.74 1.283 3.328
304	A M ₀ 1g Load	75.5 1.154 1.0	61.64 2.727 1.0	147.8 1.462 1.0747	120.4 1.794 8096	105.3 2.065 6069	145.4 1.126 9885	102.3 1.295 6453	50.66 1.431 3359	16.21 1.017 1267	16.21 1.017 1267
305	A M ₀ 1g Load	181.8 1.888 1.0	154.7 1.778 1.0	226.0 1.426 1.7755	193.0 1.610 1.3571	166.2 1.75 9918	172.2 1.23 1.1144	123.9 1.400 8922	59.05 1.660 4289	17.04 1.136 1541	17.04 1.136 1541
306	A M ₀ 1g Load	180.7 1.086 1.0	154.4 1.742 1.0	238.5 1.267 1.6533	197.6 1.509 1.2571	165.8 1.746 9135	181.9 1.124 1.1418	130.4 1.263 8148	61.79 1.418 4094	19.28 1.053 1483	19.28 1.053 1483
307	A M ₀ 1g Load	337.9 1.368 1.0	281.9 1.770 1.0	367.2 1.447 2.0765	295.2 1.690 1.9273	230.6 2.039 1.3707	293.3 1.326 1.4851	129.7 1.401 10111	56.80 1.518 4356	16.31 1.214 1301	16.31 1.214 1301
308	A M ₀ 1g Load	349.6 1.321 1.0	282.1 1.593 1.0	385.8 1.276 2.3156	300.7 1.444 1.8061	225.0 1.961 1.2882	213.7 1.143 1.4115	142.6 1.218 9634	62.63 1.343 4351	19.33 1.021 1240	19.33 1.021 1240
309	A M ₀ 1g Load	353.7 1.574 1.0	268.0 1.863 1.0	349.7 1.480 2.4093	288.1 1.671 1.8717	232.5 1.703 1.415	295.3 1.338 1.4478	134.6 1.652 9379	56.75 1.481 4619	16.50 1.297 1382	16.50 1.297 1382
310	A M ₀ 1g Load	374.5 1.391 1.0	267.7 1.719 1.0	365.5 1.323 2.2348	291.8 1.582 1.7448	227.1 1.892 1.2960	210.7 1.179 1.3709	142.5 1.262 8847	62.66 1.262 4413	18.63 1.089 1322	18.63 1.089 1322
311	A M ₀ 1g Load	318.6 1.317 1.0	260.3 1.789 1.0	337.4 1.396 2.3143	268.3 1.599 1.7756	220.6 1.711 1.2691	186.9 1.291 1.3931	142.6 1.607 8506	62.52 2.015 4436	16.73 1.258 1462	16.73 1.258 1462
312	A M ₀ 1g Load	330.2 1.156 1.0	261.3 1.695 1.0	353.5 1.448 2.1532	270.7 1.495 1.6544	214.9 1.674 1.1847	207.6 1.163 1.3195	145.6 1.509 8029	65.46 1.809 4230	18.92 1.086 1402	18.92 1.086 1402

TABLE B-4. CONTINUED
(b) C.G. ACCELERATIONS AND WING SHEARS, CASES 313-323

Case		1	2	3	4	5	Wing Shears, S_x				9	10			
							C.G. Accel	MC 103	MC 145	MC 192			MC 263	MC 337	MC 404
313	\bar{A}	.01587	288.5	238.4	310.3	257.0	212.4	198.2	144.4	68.39	17.19				
	N_0	1.339	1.611	1.912	1.444	1.549	1.623	1.240	1.529	2.077	1.195				
	1g Load	1.0	23536	19623	22856	17567	12702	10230	8592	4289	1541				
314	\bar{A}	.01705	299.2	239.5	324.2	260.6	208.8	203.4	147.5	69.85	19.40				
	N_0	1.173	1.409	1.758	1.283	1.448	1.585	1.129	1.440	1.888	1.018				
	1g Load	1.0	21775	18111	21454	16467	11889	13564	8148	4094	1483				
315	\bar{A}	.01737	311.5	252.0	345.6	269.3	200.3	196.6	132.2	58.27	17.14				
	N_0	1.080	1.215	1.468	1.211	1.467	1.067	1.131	1.204	1.300	1.053				
	1g Load	1.0	22866	19780	23649	18837	13614	15178	10597	4740	1456				
316	\bar{A}	.02033	363.5	288.4	403.8	309.5	225.2	229.8	153.1	66.94	19.48				
	N_0	1.105	1.230	1.512	1.173	1.429	1.057	1.057	1.127	1.229	1.051				
	1g Load	1.0	22642	19499	23156	18061	12862	14115	9634	4151	1240				
317	\bar{A}	.02104	376.3	286.5	406.3	308.4	221.0	231.5	154.0	67.49	19.98				
	N_0	1.091	1.202	1.522	1.150	1.411	1.084	1.084	1.090	1.186	1.002				
	1g Load	1.0	22642	19499	23156	18061	12862	14115	9634	4151	1240				
318	\bar{A}	.02166	349.6	292.1	395.8	300.7	225.0	213.7	142.6	62.63	18.33				
	N_0	1.175	1.321	1.593	1.276	1.544	1.061	1.143	1.218	1.323	1.021				
	1g Load	1.0	22642	19499	23156	18061	12862	14115	9634	4151	1240				
319	\bar{A}	.03636	204.3	132.6	348.0	219.9	182.9	224.1	145.8	63.69	18.50				
	N_0	1.955	2.506	4.015	1.718	2.207	3.058	2.585	2.585	1.709	1.529				
	1g Load	1.0	12483	13610	14529	14028	12753	11789	9122	4250	1330				
320	\bar{A}	.03661	195.9	115.8	354.1	242.1	168.6	239.1	155.2	67.72	20.10				
	N_0	1.822	2.384	4.290	1.537	2.121	3.155	2.399	2.399	1.316	1.322				
	1g Load	1.0	10049	12341	13181	11109	12214	11207	8771	4103	1288				
321	\bar{A}	.02861	547.9	442.2	603.5	469.9	355.8	307.8	196.7	86.14	24.36				
	N_0	1.599	1.737	2.082	2.580	1.866	1.866	1.553	1.416	1.526	1.409				
	1g Load	1.0	21550	25964	26902	23010	18676	17591	12668	5766	1773				
322	\bar{A}	.03064	553.9	425.2	620.3	462.3	333.7	333.7	215.0	92.98	27.00				
	N_0	1.376	1.540	1.957	1.372	1.707	2.286	1.132	1.132	1.298	1.174				
	1g Load	1.0	25416	24223	25146	21792	17852	16601	12171	5554	1712				
323	\bar{A}	.01490	269.6	228.4	292.8	236.5	183.8	162.5	110.5	48.81	14.45				
	N_0	1.125	1.363	1.600	1.367	1.632	2.002	1.005	1.046	1.102	1.005				
	1g Load	1.0	20487	17409	21876	17086	12163	14033	9760	4366	1841				

TABLE B-4. CONTINUED
(c) WING BENDING MOMENTS, CASES 301-312

Case	Wing Bending Moments, N _x									
	11	12	13	14	15	16	17	18	19	
	WS 103	WS 145	WS 191	WS 263	WS 337	WS 404	WS 480	WS 588	WS 668	
301	A	59070	32210	38270	29130	20160	10490	2635	257.1	
	No 1g Load	1.670 4.075x10 ⁶	1.680 3.541x10 ⁶	1.706 2.664x10 ⁶	1.596 1.961x10 ⁶	1.576 1.333x10 ⁶	1.612 6.93x10 ⁵	1.566 1.732x10 ⁶	1.325 1.723x10 ⁶	
302	A	61790	54810	40340	31300	21830	11360	2859	281.7	
	No 1g Load	1.549 3.839x10 ⁶	1.533 3.332x10 ⁶	1.570 2.519x10 ⁶	1.444 1.865x10 ⁶	1.418 1.262x10 ⁶	1.446 6.68x10 ⁵	1.392 1.659x10 ⁶	1.152 1.083x10 ⁶	
303	A	49550	41440	32840	25980	18340	9975	2690	299.0	
	No 1g Load	1.430 4.059x10 ⁶	1.411 3.551x10 ⁶	1.410 2.732x10 ⁶	1.349 2.132x10 ⁶	1.393 1.498x10 ⁶	1.343 8.14x10 ⁵	1.504 1.037x10 ⁶	1.223 1.035x10 ⁶	
304	A	50030	45510	39660	28660	20270	10980	2984	342.3	
	No 1g Load	1.368 3.983x10 ⁶	1.353 3.220x10 ⁶	1.345 2.553x10 ⁶	1.229 2.001x10 ⁶	1.216 1.403x10 ⁶	1.269 7.65x10 ⁵	1.193 1.225x10 ⁶	1.017 1.034x10 ⁶	
305	A	71200	62820	47640	35020	23910	12790	3229	323.8	
	No 1g Load	1.335 5.439x10 ⁶	1.337 4.673x10 ⁶	1.371 3.563x10 ⁶	1.326 2.668x10 ⁶	1.350 1.826x10 ⁶	1.443 9.85x10 ⁵	1.405 1.043x10 ⁶	1.136 1.043x10 ⁶	
306	A	74170	63260	49590	36920	25430	13530	3479	366.2	
	No 1g Load	1.276 5.684x10 ⁶	1.284 4.375x10 ⁶	1.296 3.356x10 ⁶	1.220 2.530x10 ⁶	1.216 1.738x10 ⁶	1.268 9.39x10 ⁵	1.170 1.170x10 ⁶	1.053 1.039x10 ⁶	
307	A	94610	79820	35920	38100	25090	12970	3226	374.9	
	No 1g Load	1.496 6.889x10 ⁶	1.502 5.812x10 ⁶	1.509 4.249x10 ⁶	1.404 3.007x10 ⁶	1.387 1.987x10 ⁶	1.427 1.339x10 ⁶	1.407 1.039x10 ⁶	1.214 1.039x10 ⁶	
308	A	99480	84230	59390	43600	27720	14340	3579	348.2	
	No 1g Load	1.326 6.466x10 ⁶	1.332 5.459x10 ⁶	1.317 4.232x10 ⁶	1.224 2.697x10 ⁶	1.203 1.693x10 ⁶	1.239 9.90x10 ⁵	1.212 1.049x10 ⁶	1.021 1.021x10 ⁶	
309	A	94070	80020	57030	38860	25440	13090	3233	313.6	
	No 1g Load	1.479 6.736x10 ⁶	1.487 5.686x10 ⁶	1.511 4.176x10 ⁶	1.452 2.960x10 ⁶	1.453 1.958x10 ⁶	1.477 1.053x10 ⁶	1.407 1.076x10 ⁶	1.297 1.076x10 ⁶	
310	A	97600	83170	59410	43400	27410	14190	3596	353.9	
	No 1g Load	1.342 6.315x10 ⁶	1.353 5.484x10 ⁶	1.372 3.945x10 ⁶	1.290 2.807x10 ⁶	1.284 1.863x10 ⁶	1.290 1.004x10 ⁶	1.190 1.049x10 ⁶	1.089 1.049x10 ⁶	
311	A	98770	79700	57610	40140	26670	13980	3383	317.9	
	No 1g Load	1.392 6.407x10 ⁶	1.405 5.395x10 ⁶	1.453 3.964x10 ⁶	1.433 2.809x10 ⁶	1.517 1.844x10 ⁶	1.665 9.93x10 ⁵	1.744 1.049x10 ⁶	1.258 1.049x10 ⁶	
312	A	107200	91220	58830	41570	27750	14550	3635	360.0	
	No 1g Load	1.275 6.004x10 ⁶	1.301 5.072x10 ⁶	1.335 3.738x10 ⁶	1.234 2.660x10 ⁶	1.387 1.749x10 ⁶	1.387 9.44x10 ⁵	1.283 1.049x10 ⁶	1.066 1.066x10 ⁶	

TABLE B-4. CONTINUED
(d) WING BENDING MOMENTS, CASES 313-323

Case	Wing Bending Moments, M_x									
	11	12	13	14	15	16	17	18	19	
	WS 103	WS 145	WS 191	WS 263	WS 337	WS 404	WS 480	WS 588	WS 668	
313	\bar{X} 100800 M_0 1.344 lg Load 7.34x10 ⁶	90120 1.340 6.39x10 ⁶	77810 1.345 5.393x10 ⁶	57610 1.389 3.978x10 ⁶	40810 1.411 2.829x10 ⁶	27440 1.497 1.893x10 ⁶	14651 1.671 .985x10 ⁶	3559 1.783 .280x10 ⁶	326.6 1.195 41323	
314	\bar{X} 103400 M_0 1.246 lg Load 6.903x10 ⁶	92450 1.247 6.027x10 ⁶	79760 1.257 5.094x10 ⁶	58850 1.304 3.769x10 ⁶	42100 1.307 2.691x10 ⁶	28350 1.379 1.765x10 ⁶	15070 1.437 .939x10 ⁶	3747 1.557 .268x10 ⁶	368.7 1.018 .398x10 ⁶	
315	\bar{X} 101900 M_0 1.250 lg Load 7.823x10 ⁶	90150 1.260 6.89x10 ⁶	76490 1.269 5.866x10 ⁶	54250 1.278 4.349x10 ⁶	38340 1.196 3.125x10 ⁶	25670 1.188 2.094x10 ⁶	13320 1.218 1.115x10 ⁶	3136 1.178 .286x10 ⁶	325.7 1.056 39148	
316	\bar{X} 117800 M_0 1.214 lg Load 7.407x10 ⁶	104300 1.219 6.486x10 ⁶	88480 1.224 5.485x10 ⁶	66620 1.229 4.232x10 ⁶	44430 1.129 2.877x10 ⁶	29740 1.114 1.893x10 ⁶	15350 1.149 .990x10 ⁶	3821 1.129 .248x10 ⁶	370.2 1.051 33275	
317	\bar{X} 118100 M_0 1.189 lg Load 7.407x10 ⁶	104400 1.195 6.486x10 ⁶	88580 1.200 5.485x10 ⁶	66650 1.203 4.232x10 ⁶	44660 1.096 2.877x10 ⁶	29970 1.077 1.893x10 ⁶	15430 1.109 .990x10 ⁶	3872 1.090 .248x10 ⁶	370.6 1.042 33275	
318	\bar{X} 114600 M_0 1.318 lg Load 7.401x10 ⁶	99480 1.326 6.486x10 ⁶	84230 1.332 5.485x10 ⁶	59390 1.337 4.232x10 ⁶	41600 1.224 2.877x10 ⁶	27720 1.203 1.893x10 ⁶	14340 1.239 .990x10 ⁶	3579 1.212 .248x10 ⁶	340.2 1.021 33275	
319	\bar{X} 92890 M_0 1.865 lg Load 5.84x10 ⁶	86510 1.831 5.299x10 ⁶	76140 1.814 4.636x10 ⁶	54627 1.618 3.618x10 ⁶	41310 1.612 2.608x10 ⁶	28460 1.571 1.794x10 ⁶	14990 1.618 .985x10 ⁶	3629 1.625 .258x10 ⁶	351.4 1.529 .036x10 ⁶	
320	\bar{X} 92950 M_0 1.725 lg Load 5.472x10 ⁶	87180 1.684 4.991x10 ⁶	77120 1.682 4.389x10 ⁶	55610 1.661 3.451x10 ⁶	43470 1.435 2.496x10 ⁶	30340 1.389 1.724x10 ⁶	15560 1.410 .950x10 ⁶	3685 1.426 .249x10 ⁶	381.8 1.322 .035x10 ⁶	
321	\bar{X} 170000 M_0 1.642 lg Load 9.452x10 ⁶	149600 1.632 8.304x10 ⁶	125800 1.625 7.066x10 ⁶	87140 1.617 5.289x10 ⁶	59210 1.449 3.722x10 ⁶	38750 1.407 2.498x10 ⁶	19780 1.449 1.346x10 ⁶	4871 1.470 .348x10 ⁶	462.8 1.409 .048x10 ⁶	
322	\bar{X} 172800 M_0 1.447 lg Load 8.943x10 ⁶	152600 1.430 1.880x10 ⁶	128800 1.422 6.724x10 ⁶	89640 1.411 5.053x10 ⁶	61110 1.228 3.565x10 ⁶	41990 1.183 2.399x10 ⁶	21420 1.223 1.296x10 ⁶	5302 1.239 .335x10 ⁶	513.7 1.174 .046x10 ⁶	
323	\bar{X} 280800 M_0 1.344 lg Load 7.112x10 ⁶	77720 1.345 6.283x10 ⁶	69820 1.338 5.361x10 ⁶	46670 1.296 3.979x10 ⁶	32280 1.100 2.876x10 ⁶	21420 1.034 1.929x10 ⁶	11150 1.148 1.066x10 ⁶	2807 1.072 .261x10 ⁶	274.6 1.072 .036x10 ⁶	

TABLE B-4. CONTINUED
(e) WING TORSIONS AND WING SHEAR FLOWS, CASES 301-312

Case	Wing Torsions, M_{WT}												Wing Shear Flows			
	20	21	22	23	24	25	26	27	28	33	34	35	36	MS 337	MS 337	MS 337
	MS 103	MS 145	MS 191	MS 263	MS 337	MS 404	MS 480	MS 508	MS 668	MS 103	MS 103	MS 337	MS 337			
301																
\bar{X}	14170	19670	10000	10240	10870	1281	901.0	517.5	183.1	2.810	2.928	4.538	2.935			
\bar{Y}_0	3.926	3.520	3.523	3.390	3.120	4.395	4.586	3.288	2.169	4.451	3.014	3.031	3.224			
1g Load	-1.946x10 ⁶	-2.018x10 ⁶	-1.131x10 ⁶	-1.180x10 ⁶	-1.214x10 ⁶	-0.398x10 ⁶	-0.351x10 ⁶	-0.227x10 ⁶	-0.090x10 ⁶	-0.297.3	-0.470	-279	-465.9			
302																
\bar{X}	15790	17840	10150	10870	11890	1302	917.5	548.2	230.2	2.905	3.400	4.719	3.298			
\bar{Y}_0	3.522	3.093	3.608	3.298	2.947	4.364	4.532	3.089	1.947	4.153	2.715	2.975	2.954			
1g Load	-1.591x10 ⁶	-2.091x10 ⁶	-1.159x10 ⁶	-1.198x10 ⁶	-1.224x10 ⁶	-0.398x10 ⁶	-0.350x10 ⁶	-0.226x10 ⁶	-0.090x10 ⁶	-0.317.6	-0.463	-284.6	-457.8			
303																
\bar{X}	8114	6382	6447	4109	3385	5516	295.6	408.1	104.6	1.860	1.340	2.148	1.300			
\bar{Y}_0	4.486	4.123	2.190	2.880	3.123	2.418	2.365	1.427	1.247	3.718	3.292	2.686	3.251			
1g Load	-1.469x10 ⁶	-1.621x10 ⁶	-0.866x10 ⁶	-1.009x10 ⁶	-1.080x10 ⁶	-0.404x10 ⁶	-0.369x10 ⁶	-0.239x10 ⁶	-0.095x10 ⁶	-0.215.8	-0.364	-280.1	-402.5			
304																
\bar{X}	6439	5955	5034	2991	3534	495.7	388.8	481.5	227.0	1.457	0.967	2.350	1.366			
\bar{Y}_0	4.133	4.188	2.190	3.011	2.340	2.450	1.830	1.134	1.043	4.149	4.263	2.325	2.554			
1g Load	-1.539x10 ⁶	-1.679x10 ⁶	-0.923x10 ⁶	-1.033x10 ⁶	-1.099x10 ⁶	-0.404x10 ⁶	-0.367x10 ⁶	-0.234x10 ⁶	-0.094x10 ⁶	-0.248	-0.354.5	-194.1	-395.3			
305																
\bar{X}	10510	7743	8901	5942	4642	533.4	459.4	497.1	214.7	3.139	1.009	3.682	1.551			
\bar{Y}_0	2.626	3.281	2.173	2.145	2.192	2.424	1.932	1.331	1.200	2.346	3.867	2.054	2.790			
1g Load	-1.242x10 ⁶	-1.427x10 ⁶	-0.764x10 ⁶	-0.915x10 ⁶	-1.013x10 ⁶	-0.404x10 ⁶	-0.376x10 ⁶	-0.246x10 ⁶	-0.097x10 ⁶	-1.10.2	-0.405.2	-134.1	-427.5			
306																
\bar{X}	9210	6040	7257	4640	3874	503.0	490.8	562.6	245.8	2.779	1.040	3.402	1.670			
\bar{Y}_0	3.001	3.962	1.622	2.176	2.461	2.410	1.614	1.123	0.959	2.896	3.664	2.094	2.274			
1g Load	-1.300x10 ⁶	-1.477x10 ⁶	-0.794x10 ⁶	-0.939x10 ⁶	-1.030x10 ⁶	-0.404x10 ⁶	-0.374x10 ⁶	-0.244x10 ⁶	-0.096x10 ⁶	-1.37.4	-0.395.1	-211.8	-420.2			
307																
\bar{X}	16150	15510	17080	16190	15800	1307	1030	634.1	223.5	5.334	3.021	8.178	3.040			
\bar{Y}_0	3.332	3.449	2.762	2.868	2.890	4.390	4.151	2.845	1.929	2.605	2.689	2.582	3.271			
1g Load	-1.488x10 ⁶	-1.627x10 ⁶	-0.884x10 ⁶	-0.998x10 ⁶	-1.072x10 ⁶	-0.404x10 ⁶	-0.374x10 ⁶	-0.242x10 ⁶	-0.094x10 ⁶	-0.4.1	-0.484.4	-143.2	-54.3			
308																
\bar{X}	14840	14030	15500	14820	14740	1320	1044	679.8	249.3	4.795	3.625	7.433	3.389			
\bar{Y}_0	3.700	3.707	2.927	2.992	2.992	4.378	4.111	2.634	1.692	2.746	2.317	2.693	2.951			
1g Load	-1.564x10 ⁶	-1.692x10 ⁶	-0.855x10 ⁶	-1.029x10 ⁶	-1.076x10 ⁶	-0.404x10 ⁶	-0.374x10 ⁶	-0.240x10 ⁶	-0.094x10 ⁶	-1.17.4	-0.538.1	-163.2	-508.8			
309																
\bar{X}	13560	12200	13930	12690	12170	830.0	630.3	563.5	216.0	4.276	2.391	7.124	2.252			
\bar{Y}_0	3.080	3.301	2.378	2.516	2.518	3.339	2.879	2.141	1.698	2.3070	2.804	2.779	2.779			
1g Load	-1.392x10 ⁶	-1.547x10 ⁶	-0.814x10 ⁶	-0.963x10 ⁶	-1.047x10 ⁶	-0.404x10 ⁶	-0.374x10 ⁶	-0.244x10 ⁶	-0.095x10 ⁶	-0.6.4	-0.589.7	-140.1	-508			
310																
\bar{X}	11270	10440	12370	11540	11370	839.5	678.3	618.8	244.3	4.333	2.957	6.520	2.656			
\bar{Y}_0	3.455	3.602	2.536	2.680	2.684	3.477	2.707	1.876	1.427	2.432	2.233	2.399	2.396			
1g Load	-1.481x10 ⁶	-1.623x10 ⁶	-0.883x10 ⁶	-0.999x10 ⁶	-1.076x10 ⁶	-0.404x10 ⁶	-0.374x10 ⁶	-0.242x10 ⁶	-0.094x10 ⁶	-1.103.9	-0.519.4	-160.8	-498.0			
311																
\bar{X}	10180	7922	9779	8159	7325	627.3	470.7	540.5	214.2	4.436	2.997	5.425	1.778			
\bar{Y}_0	2.677	3.182	1.890	2.138	2.240	2.877	1.918	1.735	1.495	1.975	2.793	1.939	2.774			
1g Load	-1.307x10 ⁶	-1.473x10 ⁶	-0.790x10 ⁶	-0.911x10 ⁶	-1.023x10 ⁶	-0.404x10 ⁶	-0.374x10 ⁶	-0.245x10 ⁶	-0.096x10 ⁶	-0.50.2	-0.512.9	-142.7	-444.5			
312																
\bar{X}	7865	5909	8998	6870	6517	620.7	545.1	597.6	244.4	4.038	2.658	4.892	2.130			
\bar{Y}_0	3.113	1.830	1.941	2.296	2.296	2.830	1.696	1.494	1.249	1.975	2.056	2.010	2.055			
1g Load	-1.383x10 ⁶	-1.440x10 ⁶	-0.811x10 ⁶	-0.961x10 ⁶	-1.046x10 ⁶	-0.404x10 ⁶	-0.374x10 ⁶	-0.243x10 ⁶	-0.095x10 ⁶	-0.5.6	-0.502.7	-152.5	-478.9			

TABLE B-4. CONTINUED
(f) WING TORSIONS AND WING SHEAR FLOWS, CASES 313-323

Case	Wing Torsions, M_{in}										Wing Shear Flows					
	20	21	22	23	24	25	26	27	28	29	30	31	32	33	34	35
	WS 103	WS 145	WS 101	WE 263	WS 337	VS 404	WS 480	WS 588	WC 628	WT 103	WS 103	WS 337	WS 337	WS 337	WS 337	WS 337
										Front Beam	Rear Beam	Front Beam	Front Beam	Front Beam	Rear Beam	Rear Beam
313	\bar{K} No Load 1.810 2.995 -1.237x10 ⁶	8201 2.934 -1.417x10 ⁶	9755 2.845 -1.753x10 ⁶	7356 2.194 -1.903x10 ⁶	6067 2.439 -1.003x10 ⁶	660.2 2.752 -1.599x10 ⁶	493.6 2.042 -1.376x10 ⁶	545.5 1.521 -1.246x10 ⁶	218.9 1.343 -94931	4.276 1.918 -42.0	1.631 3.837 -492.8	4.839 1.892 -137.2	4.839 1.892 -137.2	4.839 1.892 -137.2	4.839 1.892 -137.2	4.839 1.892 -137.2
314	\bar{K} No Load 1.810 2.995 -1.237x10 ⁶	6110 3.263 -1.468x10 ⁶	8483 1.784 -1.788x10 ⁶	5996 2.270 -1.928x10 ⁶	5048 2.315 -1.021x10 ⁶	653.3 2.633 -1.599x10 ⁶	558.8 1.776 -1.376x10 ⁶	601.2 1.321 -1.246x10 ⁶	249.2 1.125 -94931	3.954 1.893 -42.0	1.989 2.798 -482.6	4.362 1.893 -137	4.362 1.893 -137	4.362 1.893 -137	4.362 1.893 -137	4.362 1.893 -137
315	\bar{K} No Load 1.810 2.995 -1.237x10 ⁶	13260 3.673 -1.908x10 ⁶	11530 1.091 -1.233x10 ⁶	13240 3.091 -1.407x10 ⁶	13320 3.058 -1.550x10 ⁶	1199 4.345 -1.244x10 ⁶	999.8 4.089 -1.3220	632.3 2.616 -1.3800	233.5 1.653 -12430	3.947 2.907 30.456	3.616 2.798 -380.6	6.467 2.773 -11.355	6.467 2.773 -11.355	6.467 2.773 -11.355	6.467 2.773 -11.355	6.467 2.773 -11.355
316	\bar{K} No Load 1.810 2.995 -1.237x10 ⁶	13920 3.787 -1.564x10 ⁶	14740 2.868 -1.973x10 ⁶	14050 3.065 -1.069x10 ⁶	14060 3.009 -1.096x10 ⁶	1310 4.348 -1.397x10 ⁶	1041 4.069 -1.363x10 ⁶	711.1 2.480 -1.240x10 ⁶	264.0 1.591 -94200	4.284 2.776 -117.4	2.935 2.184 -338.1	6.083 2.705 -163.2	6.083 2.705 -163.2	6.083 2.705 -163.2	6.083 2.705 -163.2	6.083 2.705 -163.2
317	\bar{K} No Load 1.810 2.995 -1.237x10 ⁶	13850 3.827 -1.692x10 ⁶	14660 2.939 -1.923x10 ⁶	13330 3.045 -1.069x10 ⁶	13990 2.990 -1.096x10 ⁶	1282 4.293 -1.397x10 ⁶	1015 4.011 -1.363x10 ⁶	709.9 2.400 -1.240x10 ⁶	269.4 1.518 -94200	4.735 2.739 -117.4	4.095 2.985 -338.1	6.737 2.703 -163.2	6.737 2.703 -163.2	6.737 2.703 -163.2	6.737 2.703 -163.2	6.737 2.703 -163.2
318	\bar{K} No Load 1.810 2.995 -1.237x10 ⁶	14240 3.707 -1.692x10 ⁶	15500 2.927 -1.923x10 ⁶	14520 3.021 -1.069x10 ⁶	14740 2.992 -1.096x10 ⁶	1320 4.378 -1.397x10 ⁶	1044 4.111 -1.363x10 ⁶	679.8 2.634 -1.240x10 ⁶	249.3 1.692 -94200	4.705 2.746 -117.4	3.625 2.917 -338.1	7.433 2.693 -163.2	7.433 2.693 -163.2	7.433 2.693 -163.2	7.433 2.693 -163.2	7.433 2.693 -163.2
319	\bar{K} No Load 1.810 2.995 -1.237x10 ⁶	12450 4.523 -1.847x10 ⁶	12610 3.880 -1.856x10 ⁶	12050 3.933 -1.889x10 ⁶	12390 3.753 -1.951x10 ⁶	1701 4.913 -1.011x10 ⁶	1127 5.055 -1.069x10 ⁶	681.2 3.266 -1.040x10 ⁶	245.6 2.291 -1.011x10 ⁶	3.079 4.828 -283.4	2.522 3.119 -444.3	6.409 3.417 -112.1	6.409 3.417 -112.1	6.409 3.417 -112.1	6.409 3.417 -112.1	6.409 3.417 -112.1
320	\bar{K} No Load 1.810 2.995 -1.237x10 ⁶	15280 4.218 -1.901x10 ⁶	11920 4.039 -1.865x10 ⁶	11770 3.950 -1.904x10 ⁶	13070 3.940 -1.066x10 ⁶	1729 4.857 -1.011x10 ⁶	1137 5.027 -1.068x10 ⁶	714.7 3.091 -1.038x10 ⁶	257.5 1.943 -1.011x10 ⁶	3.190 4.983 -309.7	3.325 2.837 -433.6	6.325 3.327 -155.0	6.325 3.327 -155.0	6.325 3.327 -155.0	6.325 3.327 -155.0	6.325 3.327 -155.0
321	\bar{K} No Load 1.810 2.995 -1.237x10 ⁶	23170 2.307 -1.448x10 ⁶	26650 2.742 -1.534x10 ⁶	23770 2.991 -1.694x10 ⁶	22150 3.118 -1.821x10 ⁶	1793 4.875 -1.011x10 ⁶	1434 4.239 -1.044x10 ⁶	928.0 2.663 -1.094x10 ⁶	388.5 1.293 -1.011x10 ⁶	9.280 1.969 -43.5	2.441 2.751 -537.8	12.38 2.794 -14.7	12.38 2.794 -14.7	12.38 2.794 -14.7	12.38 2.794 -14.7	12.38 2.794 -14.7
322	\bar{K} No Load 1.810 2.995 -1.237x10 ⁶	19500 2.306 -1.495x10 ⁶	23210 2.910 -1.588x10 ⁶	20450 3.235 -1.713x10 ⁶	19790 3.170 -1.834x10 ⁶	1802 4.842 -1.011x10 ⁶	1418 4.249 -1.044x10 ⁶	977.9 2.457 -1.094x10 ⁶	363.2 1.636 -1.011x10 ⁶	8.128 1.941 -75.4	3.406 1.989 -522.3	10.79 2.962 -1.3	10.79 2.962 -1.3	10.79 2.962 -1.3	10.79 2.962 -1.3	10.79 2.962 -1.3
323	\bar{K} No Load 1.810 2.995 -1.237x10 ⁶	10650 3.935 -1.734x10 ⁶	10360 3.250 -1.144x10 ⁶	10190 3.284 -1.102x10 ⁶	10430 3.191 -1.047x10 ⁶	870.4 3.922 -1.066x10 ⁶	719.8 3.642 -1.069x10 ⁶	509.3 2.203 -1.040x10 ⁶	193.8 1.369 -1.011x10 ⁶	3.298 3.154 -46.9	3.024 1.893 -3175	5.323 2.968 -20.4	5.323 2.968 -20.4	5.323 2.968 -20.4	5.323 2.968 -20.4	5.323 2.968 -20.4

TABLE B-4. CONCLUDED
(g) FUSELAGE LOADS, CASE 301-312 (h) FUSELAGE LOADS AND HORIZONTAL TAIL
SHEAR, CASES 313-323

Case	Fuselage Loads				40	41
	S ₁ FS 156	M ₁ FS 156	U ₁ FS 156	M ₂ FS 156		
301	165.8 1.901 -18398	12840 2.126 -2.222x10 ⁶	51.63 2.716 -11215	13790 2.422 1.836x10 ⁶		
302	420.0 1.796 -18398	50860 2.172 -2.222x10 ⁶	-64.52 2.170 -8404	15740 2.001 1.360x10 ⁶		
303	218.5 1.821 -18398	26420 2.132 -2.222x10 ⁶	67.38 1.991 -11067	16110 1.892 1.811x10 ⁶		
304	291.5 1.712 -18398	34070 2.047 -2.222x10 ⁶	96.12 1.942 -6736	20170 1.566 1.077x10 ⁶		
305	217.5 1.655 -18398	24000 1.969 -2.222x10 ⁶	78.72 1.821 -9979	17630 1.768 1.622x10 ⁶		
306	261.9 1.637 -18398	30430 2.019 -2.222x10 ⁶	107.0 1.441 -5932	21670 1.474 1.332x10 ⁶		
307	268.0 1.763 -18398	30110 2.037 -2.222x10 ⁶	69.51 2.129 -11122	15640 2.015 1.822x10 ⁶		
308	323.7 1.819 -18398	39180 2.121 -2.222x10 ⁶	93.36 1.545 -6889	19450 1.531 1.093x10 ⁶		
309	233.2 1.776 -18398	28830 2.070 -2.222x10 ⁶	69.71 2.208 -10813	16940 2.091 1.769x10 ⁶		
310	305.7 1.848 -18398	36630 2.169 -2.222x10 ⁶	98.40 1.394 -6580	20480 1.647 1.040x10 ⁶		
311	234.2 1.729 -18398	26230 2.045 -2.222x10 ⁶	74.79 2.135 -10472	17090 1.981 1.712x10 ⁶		
312	282.2 1.800 -18398	32840 2.147 -2.222x10 ⁶	101.2 1.579 -6911	20940 1.590 1.051x10 ⁶		

Case	Fuselage Loads				40	41
	S ₁ FS 156	M ₁ FS 156	S ₂ FS 156	M ₂ FS 156		
313	222.8 1.765 -18398	24770 2.102 -2.222x10 ⁶	79.32 1.996 -9979	17600 1.862 1.628x10 ⁶		
314	267.0 1.811 -18398	31100 2.176 -2.222x10 ⁶	107.1 1.503 -5932	21590 1.598 1.093x10 ⁶		
315	304.0 1.735 -18398	37050 2.050 -2.222x10 ⁶	101.3 1.469 -5710	20600 1.577 928100		117.50 1.373 -4189
316	334.5 1.750 -18398	43330 2.034 -2.222x10 ⁶	115.4 1.642 -6889	23100 1.701 1.093x10 ⁶		120.7 1.463 -5309
317	368.6 1.725 -18398	44880 2.006 -2.222x10 ⁶	119.2 1.630 -6889	23860 1.698 1.093x10 ⁶		124.7 1.468 -5309
318	323.7 1.819 -18398	39180 2.121 -2.222x10 ⁶	93.36 1.545 -6889	19450 1.531 1.093x10 ⁶		99.84 1.737 -5309
319	367.8 1.746 -18398	49970 2.133 -2.065x10 ⁶	71.09 3.198 -15773	17730 3.131 2.612x10 ⁶		
320	671.5 2.261 -17875	59300 2.460 -2.065x10 ⁶	73.68 3.008 -15773	19760 2.732 2.612x10 ⁶		
321	446.8 1.805 -17875	49010 2.141 -2.365x10 ⁶	88.61 2.747 -14787	20920 2.620 2.449x10 ⁶		
322	518.1 1.784 -17875	62370 2.017 -2.065x10 ⁶	118.4 2.198 -14787	25640 2.081 2.449x10 ⁶		
323	250.0 1.793 -18701	30460 2.030 -2.314x10 ⁶	84.01 1.412 -5932	16990 1.352 1.783x10 ⁶		

TABLE B-5. RESULTS OF LATERAL GUST DYNAMIC ANALYSIS,
MODEL 188 MISSION ANALYSIS SEGMENTS

Case		Fore Body	Fore Body	Aft Body	Aft Body	Aft Body	Fin	Fin	C.G.	Flight Station
		S_y	M_z	S_y	M_z	M_x	P_y	M_x	M_y	M_y
201	\bar{A} M_0	123.4 .6999	44680. .6565	114.4 .5726	.113685 .7315	31550 .6534	228.7 .6534	18070. .6534	.00464 .5799	.00195 2.657
202	\bar{A} M_0	140.4 .7308	51650. .6536	122.7 .6519	.137686 .9856	37330 .7872	269.7 .7872	21310. .7872	.00564 .6170	.00233 3.253
203	\bar{A} M_0	125.6 .6616	46060. .6183	111.8 .5847	.120886 .8023	33310 .7047	240.6 .7047	19010. .7047	.00491 .5544	.00189 3.172
204	\bar{A} M_0	147.9 .7167	53580. .6724	133.1 .6379	.139186 .8711	38070 .7715	275.1 .7715	21740. .7715	.00540 .6053	.00234 3.149
205	\bar{A} M_0	119.1 .6309	42970. .5932	108.5 .5422	.111986 .7125	30560 .6378	220.8 .6378	17440. .6378	.00425 .5304	.00175 2.743
206	\bar{A} M_0	130.9 .7188	48380. .6784	107.4 .6439	.127186 .8506	34700 .7542	250.7 .7542	19810. .7542	.00523 .6214	.00237 2.830
207	\bar{A} M_0	114.6 .6652	42320. .6260	95.21 .5885	.112286 .7795	30650 .6907	221.5 .6907	17490 .6907	.00460 .5719	.00197 2.763
208	\bar{A} M_0	168.7 .7459	61360. .7047	142.2 .6959	.158786 .9576	43080 .8458	311.2 .8458	24590 .8458	.00607 .6466	.00292 3.171
209	\bar{A} M_0	137.5 .6763	50150. .6378	138.4 .5590	.130886 .8375	35570 .7411	256.6 .7411	20270 .7411	.00496 .5815	.00229 2.922

TABLE B-6. RESULTS OF LATERAL GUST DYNAMIC ANALYSIS,
MODEL 188 DESIGN ENVELOPE CASES

Case		Fore Body S_y	Fore Body M_z	Aft Body S_y	Aft Body M_z	Aft Body M_x	Vertical Tail P_y	Vertical Tail M_z	C.G. n_y	Flight Station n_y
601	\bar{A} N_o	189.8 .6711	69050 .6493	125.6 .6213	.127586 .6672	.47900 .7914	346.1 .7914	27340 .7914	.00546 .5017	.00850 3.396
602	\bar{A} N_o	187.9 .6665	68734 .6439	127.1 .6164	.102586 .7008	.47900 .7859	345.7 .7859	27320 .7859	.00486 .6325	.00382 2.214
603	\bar{A} N_o	179.5 .6447	66109 .6222	127.7 .6075	.106686 .6914	.47692 .7735	344.6 .7735	27220 .7735	.00532 .5746	.00224 3.558
604	\bar{A} N_o	152.4 .5575	54890 .5480	106.3 .5390	85491 .6033	39940 .6738	288.6 .6738	22800 .6738	.00444 .5047	.00175 3.337
605	\bar{A} N_o	122.2 .4730	44870 .4566	70.3 .4201	64476 .4936	31610 .5481	228.4 .5481	18043 .5481	.00356 .4174	.00125 3.134
606	\bar{A} N_o	240.4 .7213	88380 .7017	151.1 .6978	128900 .7979	60820 .8936	439.5 .8936	34717 .8936	.00687 .6631	.00315 3.748
607	\bar{A} N_o	235.9 .7183	86631 .6986	202.5 .8061	141500 .8340	61700 .8881	445.8 .8881	35215 .8881	.00686 .6609	.00303 3.781
608	\bar{A} N_o	226.0 .4357	85396 .6946	160.6 .6996	130758 .7953	61418 .8844	443.8 .8844	35058 .8844	.00682 .6602	.00302 3.702
609	\bar{A} N_o	173.7 .6288	63870 .6090	122.8 .6067	99400 .6908	46460 .7704	335.7 .7704	26521 .7704	.00513 .5699	.00206 3.654
610	\bar{A} N_o	135.4 .9064	49994 .4893	96.4 .4801	73980 .5480	36530 .6117	263.9 .6117	20849 .6117	.00402 .4531	.00145 3.293
611	\bar{A} N_o	142.2 .6784	56700 .6621	541.9 1.575	81200 .7448	43860 .8570	316.8 .8570	25030 .8570	.00673 .6466	.00278 3.583
612	\bar{A} N_o	177.2 .7475	70700 .7348	69.0 .7329	99440 .8744	55563 .9806	401.5 .9806	31716 .9806	.00810 .7348	.00331 4.089
613	\bar{A} N_o	235.6 .7061	75780 .7070	95.33 .9224	170050 .7554	40000 .9460	289.1 .9460	22840 .9460	.00824 .7119	.00364 3.552
614	\bar{A} N_o	296.3 .8000	95140 .8020	116.5 .9980	219000 .8246	50045 1.084	367.4 1.080	29022 1.080	.01026 .7968	.00430 4.085
615	\bar{A} N_o	137.4 .6550	53490 .6367	50.85 .6342	71885 .7409	40550 .8393	292.9 .8393	23146 .8393	.00699 .6300	.00249 3.746
616	\bar{A} N_o	151.6 .5587	53772 .5512	99.17 .5398	81850 .6200	39250 .6896	283.6 .6896	22400 .6896	.00437 .5228	.00208 2.784
617	\bar{A} N_o	183.6 .6803	65540 .6991	118.1 .6407	122000 .6937	46700 .8162	337.4 .8162	26650 .8162	.00533 .6300	.00281 2.934
618	\bar{A} N_o	119.7 .4798	43280 .4646	63.78 .4308	60710 .5157	30630 .5676	221.3 .5676	17500 .5676	.00345 .4379	.00153 2.525
619	\bar{A} N_o	172.2 .6292	62380 .6115	114.2 .6146	94950 .7105	45550 .7913	329.1 .7913	26000 .7913	.00503 .5861	.00246 3.077
620	\bar{A} N_o	131.1 .5158	47690 .5000	87.52 .4999	72700 .5745	35000 .6404	252.7 .6404	19951 .6404	.00585 .4757	.00179 2.680
621	\bar{A} N_o	211.0 .4536	81413 .7060	146.7 .7161	122417 .8295	59080 .9214	426.9 .9214	35723 .9214	.00656 .6860	.00355 3.151

TABLE B-7. RESULTS OF LATERAL GUST DYNAMIC ANALYSIS,
MODEL 749 MISSION ANALYSIS SEGMENTS

Case		Fore Body	Fore Body	Aft Body	Aft Body	Aft Body	Vertical Tail	C.G.	Flight Station	Vertical Tail
		S_y	M_z	S_y	M_z	M_x	P_y	H_y	n_y	n_y
101	\bar{A} N_0	28.85 1.182	3220. 1.662	105.4 .5504	11313. .5503	7879 .5501	131.2 .5509	.003545 .5344	.001724 2.190	.008789 .5603
102	\bar{A} N_0	20.74 1.815	2990. 2.539	139.4 .6579	15005. .6542	10347 .6664	171.5 .6762	.00362 .5650	.002574 2.056	.01095 .7786
103	\bar{A} N_0	17.34 2.032	2356. 2.697	148.8 .6640	16054. .6595	11082. .6702	181.4 .6864	.003461 .5641	.002809 1.899	.01052 .8619
104	\bar{A} N_0	20.33 1.756	2479. 2.510	144.8 .6420	15630. .6387	10686. .6496	176.1 .6585	.003557 .5507	.002434 .2053	.01065 .7568
105	\bar{A} N_0	16.72 2.207	2555. 2.614	141.4 .7187	15255. .7141	10449 .7300	172.4 .7428	.003184 .6068	.002949 1.902	.01061 .8856
106	\bar{A} N_0	19.63 1.739	2320. 2.571	140.6 .6172	15158. .6138	10412 .6249	172.1 .6339	.003567 .5289	.002377 2.022	.01071 .7301
107	\bar{A} N_0	18.32 1.953	2432 2.641	150.9 .6644	16292. .6600	11135. .6748	183.4 .6868	.003507 .5659	.002765 1.941	.01111 .8216
108	\bar{A} N_0	17.34 1.668	1994. 2.517	124.7 .5941	13471. .5908	9192. .6017	151.2 .6105	.003062 .5138	.001932 2.075	.009024 .7078
109	\bar{A} N_0	17.91 1.619	2004. 2.515	129.8 .5725	14006. .5696	9599. .5790	158.4 .5867	.003281 .4902	.002094 1.985	.009717 .6107
110	\bar{A} N_0	18.42 2.016	2557. 2.613	151.2 .6769	16308. .6724	11174. .6877	184.4 .6999	.003528 .5772	.002921 1.913	.01134 .8355

TABLE B-8. RESULTS OF LATERAL GUST DYNAMIC ANALYSIS,
MODEL 749 DESIGN ENVELOPE CASES

Case		Fore Body	Fore Body	Aft Body	Aft Body	Aft Body	Vertical Tail	C.G.	Flight Station	Vertical Tail
		S_y	M_z	S_y	M_z	M_x	P_y	H_y	n_y	n_y
501	\bar{A} N_0	29.67 1.625	3309. 2.306	105.6 .645	20190. .643	13450 .651	217.6 .659	.00366 .548	.00242 2.093	.01090 .757
502	\bar{A} N_0	20.86 2.750	2995. 3.299	252.3 .7569	28122. .7383	18142. .7714	291.1 .7880	.00372 .6215	.00381 1.992	.01332 1.031
503	\bar{A} N_0	28.42 1.621	30590. 2.392	183.1 .6282	20800. .6040	13270. .6344	214.6 .6419	.00360 .5249	.00230 2.116	.01074 .7409
504	\bar{A} N_0	36.61 1.521	2725. 3.508	247.6 .7365	27700. .7164	17810. .7516	275.8 .7681	.00364 .5948	.00368 2.043	.01305 1.0164
505	\bar{A} N_0	18.36 2.959	2603. 3.618	246.0 .7282	27558. .7074	17694. .7434	263.9 .7507	.00362 .5844	.00362 2.005	.01217 1.068
506	\bar{A} N_0	27.14 1.632	2814. 2.501	182.3 .610	20705. .584	13139. .6176	212.5 .6255	.00355 .4958	.00220 2.162	.01061 .7290
507	\bar{A} N_0	18.50 2.70	2399. 3.624	229.5 .6894	25030. .6839	16521. .7030	265.4 .7185	.00351 .5439	.00328 1.979	.01226 .9386
508	\bar{A} N_0	25.10 1.530	2529. 2.406	169.4 .5624	19590. .5344	12280. .5682	198.7 .5750	.00335 .4995	.00200 2.045	.00998 .6648
509	\bar{A} N_0	19.13 2.369	2150. 3.550	205.5 .6537	23440. .6284	14900. .6655	239.6 .6791	.00336 .5054	.00282 2.005	.01030 .9402
510	\bar{A} N_0	27.14 1.255	2670. 1.983	159.0 .4902	18840. .4554	11560. .4938	187.6 .4983	.00341 .4090	.00167 2.048	.00972 .5544
511	\bar{A} N_0	33.50 1.036	3591. 1.444	127.4 .4451	15600. .4374	9320. .4858	152.2 .4873	.00337 .4247	.00110 2.783	.00844 .5044
512	\bar{A} N_0	23.53 1.519	2210. 2.591	167.5 .5273	18250. .5246	12160 .5337	196.7 .5413	.00330 .4058	.00187 2.095	.00985 .6375

TABLE B-9. RESULTS OF VERTICAL GUST DYNAMIC ANALYSIS,
MODEL 188 PARAMETER VARIATION
(a) C.G. ACCELERATIONS AND WING SHEARS, CASES 202-202-7

Case	C.G. Accel	Wing Shear, S									
		1	2	3	4	5	6	7	8	9	10
202 (Ref Case)	\bar{X}	WB 83	WB 119	WB 167	WB 209	WB 275	WB 346	WB 380	WB 448	WB 516	
	N_0	253.9	247.8	280.0	274.1	237.8	181.2	162.7	94.74	39.56	
	1g Load	1.886	1.841	2.118	1.993	1.501	1.287	1.237	1.433	1.834	
202 Rigid	\bar{X}	19055	16386	11862	13979	9889	5300	7679	4161	1531	
	N_0	192.5	173.7	129.4	194.5	155.1	97.61	145.5	83.69	31.70	
	1g Load	1.554	1.589	1.575	1.345	1.310	1.328	1.167	1.146	1.125	
202 C.G. Fixed	\bar{X}	280.0	269.0	234.0	296.1	252.6	188.0	152.5	106.3	44.23	
	N_0	1.995	1.758	2.060	1.480	1.513	1.732	1.075	1.255	1.632	
	1g Load	1.764	1.886	2.103	1.595	1.456	1.602	1.272	1.565	2.185	
202-1	\bar{X}	256.5	250.6	283.2	276.9	239.4	182.8	162.9	95.19	40.12	
	N_0	1.764	1.886	2.103	1.595	1.456	1.602	1.272	1.565	2.185	
	1g Load	1.764	1.886	2.103	1.595	1.456	1.602	1.272	1.565	2.185	
202-2	\bar{X}	257.6	251.7	283.7	278.3	241.8	183.8	166.7	97.05	40.48	
	N_0	1.705	1.862	2.139	1.536	1.530	1.702	1.215	1.411	1.813	
	1g Load	1.705	1.862	2.139	1.536	1.530	1.702	1.215	1.411	1.813	
202-3	\bar{X}	267.3	254.8	287.2	281.7	244.5	186.2	167.0	97.92	41.05	
	N_0	1.779	1.902	2.116	1.546	1.538	1.615	1.246	1.553	2.147	
	1g Load	1.779	1.902	2.116	1.546	1.538	1.615	1.246	1.553	2.147	
202-4	\bar{X}	250.3	243.7	215.8	269.8	233.3	177.4	160.0	93.27	39.02	
	N_0	1.757	1.912	2.195	1.647	1.641	1.835	1.282	1.508	1.961	
	1g Load	1.757	1.912	2.195	1.647	1.641	1.835	1.282	1.508	1.961	
202-5	\bar{X}	249.8	242.8	214.0	269.1	232.5	175.9	162.1	94.32	39.31	
	N_0	1.652	1.807	2.093	1.598	1.566	1.759	1.219	1.413	1.811	
	1g Load	1.652	1.807	2.093	1.598	1.566	1.759	1.219	1.413	1.811	
202-6	\bar{X}	250.5	243.2	214.1	270.9	235.3	177.6	166.6	96.37	40.40	
	N_0	1.683	1.849	2.131	1.558	1.579	1.780	1.188	1.383	1.782	
	1g Load	1.683	1.849	2.131	1.558	1.579	1.780	1.188	1.383	1.782	
202-6 Rigid	\bar{X}	194.6	175.2	129.4	199.9	159.1	99.47	151.3	87.09	35.11	
	N_0	1.461	1.438	1.477	1.271	1.240	1.257	1.109	1.088	1.066	
	1g Load	1.461	1.438	1.477	1.271	1.240	1.257	1.109	1.088	1.066	
202-7	\bar{X}	252.3	245.9	218.0	272.5	236.2	179.7	161.6	94.13	39.33	
	N_0	1.669	1.882	2.099	1.598	1.600	1.779	1.251	1.451	1.858	
	1g Load	1.669	1.882	2.099	1.598	1.600	1.779	1.251	1.451	1.858	
202-7 Rigid	\bar{X}	191.5	172.8	128.8	193.1	151.9	96.02	144.2	86.92	33.38	
	N_0	1.509	1.479	1.507	1.288	1.290	1.296	1.174	1.153	1.132	
	1g Load	1.509	1.479	1.507	1.288	1.290	1.296	1.174	1.153	1.132	

TABLE B-9. CONTINUED
(b) C.G. ACCELERATIONS AND WING SHEARS, CASES 202-9-207-1

Case	C.G. Accel	Wing Shears, g									
		1	2	3	4	5	6	7	8	9	10
202-9 Rigid	\bar{X} No 1g Load	.02199 1.160	WS 83 234.7 1.555	WS 119 246.9 1.689	WS 167 216.4 1.944	WS 209 275.6 1.475	WS 275 237.5 1.516	WS 346 178.0 1.711	WS 380 168.1 1.108	WS 448 97.84 1.243	WS 516 40.73 1.544
	\bar{X} No 1g Load	.01943 1.183	196.1 1.433	176.7 1.393	131.4 1.424	199.2 1.202	158.5 1.154	99.34 1.162	149.8 1.030	86.20 1.001	34.12 .970
202-10 Rigid	\bar{X} No 1g Load	.02264 1.243	285.6 1.698 1.0	282.7 1.889 1.0	296.6 2.053 1.1564	303.4 1.576 1.3775	268.7 1.587 9800	210.3 1.742 5289	169.3 1.270 7687	98.69 1.485 4175	41.30 1.980 1539
	\bar{X} No 1g Load	.01965 1.243	205.4 1.575	196.1 1.553	145.1 1.601	200.3 1.367	162.9 1.340	107.0 1.376	153.6 1.176	82.47 1.155	33.22 1.134
202-11 Rigid	\bar{X} No 1g Load	.02601 1.280 1.0	320.9 1.713 1.0	415.3 1.865 1.6238	282.9 2.131 1.0211	303.4 1.550 12401	231.8 1.714 2967	203.9 1.271 5473	118.7 1.440 2646	49.62 1.791 860	1.791 860
	\bar{X} No 1g Load	.02269 1.332	231.5 1.736	209.0 1.706	156.2 1.753	232.1 1.511	185.1 1.469	116.8 1.481	172.7 1.351	99.27 1.298	39.96 1.277
202-12 Rigid	\bar{X} No 1g Load	.01898 1.145	223.5 1.701 1.0	218.1 1.853 1.5376	193.8 2.133 1.1325	201.1 1.618 1.3605	199.1 1.656 1.0146	159.8 1.808 5822	143.2 1.217 8248	83.47 1.418 4601	34.89 1.828 1736
	\bar{X} No 1g Load	.01709 1.135	170.8 1.434	154.2 1.467	114.8 1.513	173.2 1.284	138.2 1.246	86.99 1.260	130.0 1.104	74.82 1.004	30.15 1.064
202-13 Rigid	\bar{X} No 1g Load	.0247 1.067 1.0	344.0 1.409 2.3769	333.3 1.507 2.0708	299.3 1.686 1.5646	339.8 1.488 1.7289	293.1 1.518 1.2495	225.4 1.717 7168	187.3 1.134 9194	110.1 1.270 5054	46.24 1.563 1084
	\bar{X} No 1g Load	.01513 1.106 1.0	175.3 1.772 1.6501	168.3 1.893 1.4358	147.0 2.163 1.0861	191.4 2.063 1.3889	163.6 1.996 1.0637	122.4 2.072 6536	112.1 1.478 6889	65.96 1.726 5181	28.51 1.478 2015

**TABLE B-9. CONTINUED
(c) WING BENDING MOMENTS, CASES 202-202-7**

Case	Wing Bending Moment, M _x									
	12	13	14	15	16	17	18	19		
	WS 83	WS 119	WS 167	WS 209	WS 273	WS 346	WS 380	WS 448	WS 516	
202 (Ref Case)	80620 1.423 3.923x10 ⁶	71710 1.416 3.298x10 ⁶	6076 1.393 2.609x10 ⁶	50610 1.386 2.086x10 ⁶	34030 1.361 1.318x10 ⁶	20050 1.357 1.811x10 ⁶	14650 1.420 1.599x10 ⁶	9006 1.608 1.211x10 ⁶	5006 1.034 1.053x10 ⁶	
202 Rigid	58290 1.333	51700 1.308	44450 1.271	37650 1.245	26240 1.211	17250 1.164	12930 1.150	5137 1.137	1146 1.125	
	Same As Case 202									
202 Stick Fixed	87190 1.312	77450 1.305	65720 1.285	54850 1.274	37070 1.243	22330 1.199	16420 1.245	6615 1.420	1504 1.632	
202-1	81220 1.338	72220 1.322	61160 1.297	50910 1.304	34220 1.336	20140 1.456	14770 1.561	99560 1.852	1364 2.185	
	Same As Case 202									
202-2	82090 1.367	73070 1.358	62000 1.335	51720 1.326	34850 1.315	20550 1.332	15010 1.398	6047 1.587	1376 1.813	
	Same As Case 202									
202-3	82850 1.293	73740 1.275	62520 1.250	52110 1.253	35090 1.301	20650 1.426	15080 1.530	6099 1.817	1396 2.147	
	Same As Case 202									
202-4	79330 1.462 4.274x10 ⁶	70920 1.442 3.638x10 ⁶	59740 1.427 2.900x10 ⁶	49800 1.415 2.307x10 ⁶	33490 1.405 1.500x10 ⁶	19770 1.420 1.950x10 ⁶	14440 1.491 1.659x10 ⁶	5028 1.704 1.257x10 ⁶	1330 1.957 1.069x10 ⁶	
202-5	79230 1.388	70470 1.379	59770 1.356	49840 1.343	33580 1.327	19920 1.335	14580 1.400	5874 1.587	1336 1.811	
	Same As Case 202									
202-6	80070 1.395 3.643x10 ⁶	71290 1.385 3.068x10 ⁶	60610 1.359 2.438x10 ⁶	51640 1.344 1.992x10 ⁶	34270 1.321 1.242x10 ⁶	20420 1.311 1.773x10 ⁶	14990 1.371 1.570x10 ⁶	6040 1.598 1.200x10 ⁶	1374 1.782 1.050x10 ⁶	
202-6 Rigid	59680 1.258	53040 1.235	45740 1.203	38840 1.179	27120 1.147	17920 1.104	13450 1.092	5349 1.078	1194 1.066	
	Same As Case 202-6									
202-7	80120 1.422	71560 1.415	60490 1.395	50300 1.381	33820 1.367	19920 1.373	14550 1.438	5859 1.629	1337 1.858	
	Same As Case 202									
202-7 Rigid	57860 1.359	51310 1.287	44090 1.274	37350 1.235	26020 1.205	17100 1.168	12810 1.157	5089 1.143	1145 1.132	
	Same As Case 202									

TABLE B-9. CONTINUED
(d) WING BENDING MOMENTS, CASES 202-9-207-1

Case	11	12	13	14	15	16	17	18	19
	Wing Bending Moments, M_x								
	WS 8:	WS 119	WS 167	WS 202	WS 275	WS 346	WS 380	WS 448	WS 516
202-9	\bar{K} N_0 lg Load	81270 1.345	72350 1.342	61480 1.325	51340 1.313	34620 1.280	20660 1.211	15120 1.236	6091 1.373
202-9	\bar{K} N_0 lg Load	59280 1.178	52890 1.151	45920 1.116	38990 1.090	26920 1.056	17750 1.017	13310 1.007	5291 1.987
202-10	\bar{K} N_0 lg Load	90150 1.415	80060 1.406	67390 1.387	55880 1.380	37280 1.371	21160 1.356	15260 1.474	6158 1.679
202-10	\bar{K} N_0 lg Load	60890 1.350	51820 1.335	45950 1.296	38610 1.268	26750 1.232	17160 1.175	12760 1.159	5067 1.146
202-11	\bar{K} N_0 lg Load	102700 1.402	91390 1.391	77410 1.369	64660 1.360	43320 1.345	29260 1.323	18360 1.428	7408 1.592
202-11	\bar{K} N_0 lg Load	69640 1.495	61720 1.468	55980 1.439	44840 1.401	31220 1.365	20480 1.317	15140 1.303	6093 1.289
202-12	\bar{K} N_0 lg Load	70870 1.448	63210 1.441	53380 1.418	44450 1.403	29880 1.377	17630 1.351	12900 1.406	5205 1.598
202-12	\bar{K} N_0 lg Load	51910 1.270	46070 1.245	39630 1.208	33990 1.181	23430 1.147	15470 1.101	11560 1.060	4594 1.075
202-13	\bar{K} N_0 lg Load	101900 1.353	89730 1.354	74690 1.336	61410 1.313	40870 1.287	23430 1.214	16990 1.264	6884 1.398
207-1	\bar{K} N_0 lg Load	55020 1.761	49003 1.793	41750 1.810	34820 1.833	23280 1.770	13950 1.687	10210 1.730	4171 1.970

TABLE B-9. CONTINUED
(e) WING TORSIONS AND WING SHEAR FLOWS, CASES 202-202-7

Case	Wing Torsion, V_{TZA}														Wing Shear Flows			
	20	21	22	23	24	25	26	27	28	29	30	31	32					
	US 83	US 119	US 167	US 209	US 275	US 346	US 380	US 448	US 516	US 583	US 63	US 346	US 346					
202 (Ref Case)	18470 2.492 -1.519x10 ⁶	17460 2.962 -1.480x10 ⁶	16410 3.090 -1.429x10 ⁶	15710 2.090 -1.908x10 ⁶	14180 2.261 -1.826x10 ⁶	13080 2.396 -1.732x10 ⁶	3026 1.303 -1.661x10 ⁶	1096 1.328 -1.166x10 ⁶	511.5 1.557 -1.101x10 ⁶	6.109 0.127 61.79	2.152 3.930 -537.51	9.356 2.152 -177.14	9.356 2.152 -177.14	9.356 2.152 -177.14				
202 Rigid	8479 2.547 -1.519x10 ⁶	6586 2.999 -1.480x10 ⁶	4496 3.955 -1.429x10 ⁶	7098 1.851 -1.908x10 ⁶	4479 2.344 -1.826x10 ⁶	2418 3.593 -1.732x10 ⁶	2610 1.153 -1.661x10 ⁶	1792 1.133 -1.133x10 ⁶	484.4 1.112 -1.112x10 ⁶	3.984 1.834	1.418 2.344	2.645 2.135	2.645 2.135	2.645 2.135				
202-1	18580 3.045 -1.519x10 ⁶	17540 3.185 -1.480x10 ⁶	16520 3.323 -1.429x10 ⁶	15660 2.137 -1.908x10 ⁶	14000 2.345 -1.826x10 ⁶	12880 2.496 -1.732x10 ⁶	3388 1.170 -1.170x10 ⁶	1052 1.190 -1.190x10 ⁶	577.4 1.424 -1.424x10 ⁶	6.473 2.211	2.469 3.501	9.272 2.189	9.272 2.189	9.272 2.189				
202-2	18210 2.812 -1.519x10 ⁶	17190 2.931 -1.480x10 ⁶	16120 3.060 -1.429x10 ⁶	15270 2.011 -1.908x10 ⁶	14040 2.175 -1.826x10 ⁶	12940 2.303 -1.732x10 ⁶	3014 1.340 -1.340x10 ⁶	1464 1.428 -1.428x10 ⁶	511.7 1.820 -1.820x10 ⁶	6.095 2.063	2.204 4.371	9.348 2.035	9.348 2.035	9.348 2.035				
202-3	18700 2.719 -1.519x10 ⁶	17680 2.831 -1.480x10 ⁶	16580 2.954 -1.429x10 ⁶	15860 1.974 -1.908x10 ⁶	14280 2.150 -1.826x10 ⁶	13080 2.289 -1.732x10 ⁶	3100 1.302 -1.302x10 ⁶	1505 1.729 -1.729x10 ⁶	5236 1.563 -1.563x10 ⁶	6.203 2.131	2.162 3.767	9.371 2.044	9.371 2.044	9.371 2.044				
202-4	18530 2.674 -1.519x10 ⁶	17500 2.786 -1.480x10 ⁶	16400 2.907 -1.429x10 ⁶	15810 1.894 -1.908x10 ⁶	14220 2.096 -1.826x10 ⁶	13080 2.180 -1.732x10 ⁶	3088 1.330 -1.330x10 ⁶	1499 1.427 -1.427x10 ⁶	5234.6 1.818 -1.818x10 ⁶	6.197 2.071	2.228 4.184	9.422 1.931	9.422 1.931	9.422 1.931				
202-5	18040 2.848 -1.519x10 ⁶	17030 2.975 -1.480x10 ⁶	15980 3.113 -1.429x10 ⁶	15420 2.124 -1.908x10 ⁶	13900 2.299 -1.826x10 ⁶	12840 2.437 -1.732x10 ⁶	3045 1.312 -1.312x10 ⁶	1434 1.337 -1.337x10 ⁶	619 1.567 -1.567x10 ⁶	6.306 2.088	2.021 4.202	9.762 2.166	9.762 2.166	9.762 2.166				
202-6	17580 2.783 -1.519x10 ⁶	16930 2.913 -1.480x10 ⁶	15430 3.056 -1.429x10 ⁶	15070 2.045 -1.908x10 ⁶	13500 2.289 -1.826x10 ⁶	12380 2.377 -1.732x10 ⁶	3021 1.289 -1.289x10 ⁶	1465 1.311 -1.311x10 ⁶	510.1 1.531 -1.531x10 ⁶	5.927 2.057	2.081 3.898	8.923 2.136	8.923 2.136	8.923 2.136				
202-7	17680 2.960 -1.519x10 ⁶	16730 3.084 -1.480x10 ⁶	15780 3.207 -1.429x10 ⁶	15190 2.133 -1.908x10 ⁶	13680 2.317 -1.826x10 ⁶	12640 2.456 -1.732x10 ⁶	3105 1.254 -1.254x10 ⁶	1510 1.277 -1.277x10 ⁶	526.6 1.502 -1.502x10 ⁶	5.881 2.088	2.240 4.202	9.028 2.191	9.028 2.191	9.028 2.191				
202-8	17915 2.667 -1.519x10 ⁶	1686 3.218 -1.480x10 ⁶	1599 4.341 -1.429x10 ⁶	1543 2.045 -1.908x10 ⁶	1399 2.399 -1.826x10 ⁶	1289 2.456 -1.732x10 ⁶	2958 1.101 -1.101x10 ⁶	1441 1.081 -1.081x10 ⁶	501.7 1.099 -1.099x10 ⁶	3.888 1.783	1.530 2.156	2.547 2.146	2.547 2.146	2.547 2.146				
202-9	18340 2.827 -1.519x10 ⁶	17300 2.948 -1.480x10 ⁶	16320 3.080 -1.429x10 ⁶	15330 2.068 -1.908x10 ⁶	13980 2.234 -1.826x10 ⁶	12860 2.367 -1.732x10 ⁶	3004 1.118 -1.118x10 ⁶	1458 1.344 -1.344x10 ⁶	507.9 1.579 -1.579x10 ⁶	6.099 2.086	2.151 3.970	9.221 2.126	9.221 2.126	9.221 2.126				
202-10	1837 2.444 -1.519x10 ⁶	1648 2.865 -1.480x10 ⁶	1590 3.750 -1.429x10 ⁶	15079 1.803 -1.908x10 ⁶	1486 2.270 -1.826x10 ⁶	1343 2.443 -1.732x10 ⁶	2835 1.163 -1.163x10 ⁶	1380 1.143 -1.143x10 ⁶	480.2 1.122 -1.122x10 ⁶	3.976 1.741	1.412 2.427	2.646 2.042	2.646 2.042	2.646 2.042				

TABLE B-9. CONTINUED
(f) WING TORSIONS AND WING SHEAR FLOWS, CASES 202-9-207-1

Case		20	21	22	23	24	25	26	27	28	29	30	31	32
		Wing Torsions, M_{tor}										Wing Shear Flows		
		WS 83	WS 119	WS 167	WS 209	WS 275	WS 346	WS 380	WS 448	WS 516	WS 83 Front Beam	WS 83 Rear Beam	WS 346 Front Beam	WS 346 Rear Beam
202-9	\bar{X} N_0 1g Load	16640 2.822	15530 2.970	14380 3.131	14490 1.970	12820 2.175	11620 2.345	3101 1.132	1906 1.146	522.5 1.325	5.864 2.074	2.096 3.443	8.627 2.098	2.142 3.046
202-9	\bar{X} N_0 1g Load	9247 2.754	6389 3.331	4456 4.462	7012 1.865	4365 2.510	2367 4.386	2935 1.034	1429 1.006	497.1 1.583	3.971 1.766	1.545 2.461	2.591 2.218	1.361 2.330
202-10	\bar{X} N_0 1g Load	22930 2.362	21370 2.464	29980 2.597	19140 1.880	17340 2.033	15900 2.172	3127 1.236	1517 1.254	522.2 1.503	7.431 1.949	1.769 4.640	11.36 2.218	2.330 3.184
202-10	\bar{X} N_0 1g Load	-1.317x10 ⁶	-1.275x10 ⁶	-1.221x10 ⁶	-1.830x10 ⁶	-1.746x10 ⁶	-1.692x10 ⁶	-1.271x10 ⁶	-1.187x10 ⁶	-1.102x10 ⁶	-84	-495	-146	-356
202-11	\bar{X} N_0 1g Load	12960 2.282	11010 2.506	8657 2.923	9270 1.847	6664 2.166	4493 2.763	2341 1.163	1383 1.143	481.5 1.122	4.940 1.833	1.017 3.401	2.814 2.040	.9449 3.449
202-11	\bar{X} N_0 1g Load	22980 2.750	21590 2.874	20010 3.023	19700 2.004	17690 2.185	16100 2.341	3744 1.425	1813 1.442	628.3 1.649	7.773 2.141	2.369 4.112	11.75 2.084	2.712 3.444
202-11	\bar{X} N_0 1g Load	-2.667x10 ⁶	-2.195x10 ⁶	-2.081x10 ⁶	-1.495x10 ⁶	-1.342x10 ⁶	-1.173x10 ⁶	-1.403x10 ⁶	-1.266x10 ⁶	-1.137x10 ⁶	-29	-682	-308	-513
202-12	\bar{X} N_0 1g Load	11220 2.580	9971 2.954	6279 3.748	8835 1.970	5708 2.412	3199 3.502	3397 1.305	1653 1.283	575.0 1.261	4.976 1.976	1.559 2.840	3.320 2.222	4.336 2.340
202-12	\bar{X} N_0 1g Load	16600 2.881	15790 2.937	14970 3.114	14050 2.145	12740 2.300	11030 2.411	2678 1.277	1302 1.308	454.8 1.550	5.395 2.156	2.007 3.858	8.361 2.164	2.291 3.229
202-12	\bar{X} N_0 1g Load	-1.209x10 ⁶	-1.190x10 ⁶	-1.163x10 ⁶	-1.696x10 ⁶	-1.645x10 ⁶	-1.585x10 ⁶	-1.208x10 ⁶	-1.148x10 ⁶	-1.083x10 ⁶	-81	-460	-110	-340
202-13	\bar{X} N_0 1g Load	22790 2.333	21550 2.409	20150 2.512	19120 1.980	17350 2.160	16020 2.320	3385 1.287	1666 1.311	581.9 1.506	8.253 1.680	2.447 3.282	11.62 2.110	2.678 3.072
207-1	\bar{X} N_0 1g Load	19190 3.757	18720 3.819	18250 3.969	12460 2.870	11450 2.984	10770 3.040	2352 1.574	1058 1.707	396.6 2.154	4.772 2.809	2.971 4.049	6.653 2.438	3.198 3.917
207-1	\bar{X} N_0 1g Load	-1.532x10 ⁶	-1.511x10 ⁶	-1.494x10 ⁶	-2.771x10 ⁶	-2.595x10 ⁶	-2.310x10 ⁶	-1.865x10 ⁶	-1.606x10 ⁶	-1.041x10 ⁶				

TABLE B-9. CONTINUED
(g) FUSELAGE LOADS, CASE 202-202-7

Case	Fuselage Loads											
	33	34	35	36	37	38	39	40	41	42		
	σ_z	N_y	σ_z	N_y	σ_z	N_y	σ_z	N_y	σ_z	N_y	σ_z	N_y
202 (Ref Case)	FS 350	FS 350	FS 500	FS 500	FS 571	FS 571	FS 695	FS 695	FS 695	FS 1006	FS 1006	FS 1006
\bar{X}	251.4	384.10	369.9	78890	435.1	107500	296.6	26400	51.00	24690	51.00	24690
N_0	1.336	1.299	1.281	1.339	1.259	1.377	1.443	3.564	3.722	2.577	3.722	2.577
lg Load	-1.0185	-1.601x10 ⁶	-16168	-3.519x10 ⁶	-19242	-4.776x10 ⁶	-21436	7.308x10 ⁶	-12836	1.987x10 ⁶	-12836	1.987x10 ⁶
202 Rigid	\bar{X}	224.9	29360	70490	395.0	95830	254.8	23910	61.86	26170	61.86	26170
N_0	1.962	2.129	1.750	1.966	1.644	1.889	1.310	4.948	4.637	3.518	4.637	3.518
lg Load					Same As Case 202							
202 Stick Fixed	\bar{X}	66.74	432.3	94450	501.8	127600	310.3	26130	31.74	15690	31.74	15690
N_0	1.334	1.367	1.255	1.319	1.224	1.295	1.349	3.139	3.418	1.359	3.418	1.359
lg Load					Same As Case 202							
202-1	\bar{X}	242.0	371.2	79070	436.5	107700	299.1	26930	50.09	24400	50.09	24400
N_0	1.353	1.341	1.309	1.358	1.291	1.339	1.613	3.737	3.689	2.416	3.689	2.416
lg Load					Same As Case 202							
202-2	\bar{X}	253.4	36690	79230	438.9	108300	299.6	25850	47.19	23770	47.19	23770
N_0	1.308	1.296	1.273	1.313	1.259	1.298	1.490	3.257	3.333	2.135	3.333	2.135
lg Load					Same As Case 202							
202-3	\bar{X}	254.2	36840	79790	440.4	108700	302.1	26740	47.17	23680	47.17	23680
N_0	1.348	1.337	1.315	1.353	1.301	1.338	1.611	3.517	3.350	2.051	3.350	2.051
lg Load					Same As Case 202							
202-4	\bar{X}	249.4	37950	78250	430.5	106500	292.3	26910	54.59	25450	54.59	25450
N_0	1.451	1.311	1.357	1.454	1.316	1.417	1.566	3.961	4.060	2.980	4.060	2.980
lg Load	-1.0185	-1.601x10 ⁶	-15168	-3.519x10 ⁶	-19242	-4.776x10 ⁶	-21436	7.308x10 ⁶	-12836	1.987x10 ⁶	-12836	1.987x10 ⁶
202-5	\bar{X}	249.2	38140	78220	431.7	106600	294.3	25740	50.04	24450	50.04	24450
N_0	1.318	1.299	1.299	1.322	1.234	1.298	1.444	3.556	3.670	2.505	3.670	2.505
lg Load					Same As Case 202							
202-6	\bar{X}	274.1	79020	86020	465.0	116600	260.1	18920	73.86	29800	73.86	29800
N_0	1.319	1.218	1.260	1.322	1.234	1.299	1.488	5.205	2.963	2.441	2.963	2.441
lg Load	-1.6248	-203.1x10 ⁶	-26195	-3.095x10 ⁶	-27922	-6.930x10 ⁶	-23606	6.886x10 ⁶	-10681	1.635x10 ⁶	-10681	1.635x10 ⁶
202-6 Rigid	\bar{X}	249.1	35090	78100	419.6	105700	227.9	20750	81.71	30800	81.71	30800
N_0	1.904	1.267	1.708	1.908	1.608	1.838	1.262	6.193	3.841	3.235	3.841	3.235
lg Load					Same As Case 202-6							
202-7	\bar{X}	250.5	36120	78630	433.0	107100	294.5	26920	51.95	24740	51.95	24740
N_0	1.364	1.265	1.290	1.364	1.259	1.336	1.475	3.666	3.943	2.752	3.943	2.752
lg Load					Same As Case 202							
202-7 Rigid	\bar{X}	224.4	33780	70340	384.1	95550	274.9	24940	64.07	26710	64.07	26710
N_0	2.026	1.282	1.777	2.022	1.655	1.935	1.272	4.911	4.778	3.749	4.778	3.749
lg Load					Same As Case 202							

**TABIE B-9. CONCLUDED
(h) FUSELAGE LOADS, CASES 202-9-207-1**

Case	Fuselage Loads											
	33	34	35	36	37	38	39	40	41	42		
	S _x	N _y	S _z	M _y	N _z	N _y	S _z	N _y	S _z	N _y		
202-9	FS 350	FS 350	FS 300	FS 500	FS 571	FS 571	FS 695	FS 695	FS 1006	FS 1006		
X	295.0	38850	375.0	80010	441.0	109000	301.6	29950	46.20	24090		
N ₀	1.367	1.248	1.292	1.369	1.260	1.340	1.366	3.261	3.917	2.580		
1g Load					Same As Case 202							
202-9	FS 350	FS 350	FS 300	FS 500	FS 571	FS 571	FS 695	FS 695	FS 1006	FS 1006		
X	229.8	34580	335.2	72010	393.0	97810	262.8	25920	64.78	27490		
N ₀	1.997	1.308	1.723	1.998	1.589	1.900	1.302	5.356	5.385	4.208		
1g Load					Same As Case 202							
202-10	FS 350	FS 350	FS 300	FS 500	FS 571	FS 571	FS 695	FS 695	FS 1006	FS 1006		
X	270.6	40950	397.6	84970	467.2	115700	319.9	29250	47.67	24770		
N ₀	1.362	1.336	1.313	1.365	1.294	1.345	1.487	3.866	4.036	2.679		
1g Load					-1.965x10 ⁶	-4.946x10 ⁶	-1.9751	4.672x10 ⁶	-5955	-752x10 ⁶		
202-10	FS 350	FS 350	FS 300	FS 500	FS 571	FS 571	FS 695	FS 695	FS 1006	FS 1006		
X	241.7	35010	338.8	72640	397.6	98730	263.8	26280	61.38	26270		
N ₀	1.994	1.347	1.781	1.998	1.675	1.921	1.314	4.726	4.873	3.650		
1g Load					Same As Case 202-10							
202-11	FS 350	FS 350	FS 300	FS 500	FS 571	FS 571	FS 695	FS 695	FS 1006	FS 1006		
X	305.1	47070	450.1	95790	530.1	130600	373.7	33650	49.83	27380		
N ₀	1.394	1.363	1.353	1.398	1.336	1.381	1.508	2.880	3.604	2.268		
1g Load					-1.926x10 ⁶	-6.620x10 ⁶	-1.9391	4.593x10 ⁶	-5858	-747x10 ⁶		
202-11	FS 350	FS 350	FS 300	FS 500	FS 571	FS 571	FS 695	FS 695	FS 1006	FS 1006		
X	264.0	344.5	387.1	82800	454.9	112600	315.0	31070	71.46	30810		
N ₀	2.251	2.457	1.986	2.255	1.896	2.159	1.491	5.427	5.740	4.313		
1g Load					Same As Case 202-11							
202-12	FS 350	FS 350	FS 300	FS 500	FS 571	FS 571	FS 695	FS 695	FS 1006	FS 1006		
X	221.5	34120	325.8	69520	383.3	94660	263.9	25080	53.66	24150		
N ₀	1.493	1.238	1.363	1.495	1.305	1.446	1.449	3.949	3.956	2.954		
1g Load					-1.773x10 ⁶	-6.755x10 ⁶	-1.9844	4.689x10 ⁶	-5977	-753x10 ⁶		
202-12	FS 350	FS 350	FS 300	FS 500	FS 571	FS 571	FS 695	FS 695	FS 1006	FS 1006		
X	197.8	30420	290.1	62000	341.1	84360	230.4	21290	56.96	23940		
N ₀	1.915	1.225	1.699	1.919	1.591	1.841	1.210	4.752	4.286	3.237		
1g Load					Same As Case 202-12							
202-13	FS 350	FS 350	FS 300	FS 500	FS 571	FS 571	FS 695	FS 695	FS 1006	FS 1006		
X	246.5	36560	360.6	77350	422.9	105100	264.8	21580	63.88	26670		
N ₀	1.502	1.147	1.386	1.504	1.321	1.475	1.349	4.628	3.477	2.573		
1g Load												
207-1	FS 350	FS 350	FS 300	FS 500	FS 571	FS 571	FS 695	FS 695	FS 1006	FS 1006		
X	139.2	22220	217.8	48120	259.1	64870	146.0	40000	88.65	32200		
N ₀	2.179	2.376	1.772	2.168	1.981	2.035	1.913	4.271	4.032	3.591		
1g Load												

APPENDIX C

APPLICATION OF THE MATCHING CONDITION TECHNIQUE TO THE MODEL 188 WING

In order to provide a detailed illustration of the application of the principles discussed in Sections 11-1 and 11-2, a set of enveloping design conditions is now generated for the Model 188 wing. These conditions match the loads defined statistically by the mission analysis approach, at an arbitrary frequency of exceedance approximating the limit-strength value. Generation of enveloping conditions to match design envelope, rather than mission analysis, loads would be quite similar. However, as indicated in Section 11.1, matching the mission analysis loads provides a somewhat more severe test of the method, as it brings in problems that do not arise in matching design envelope loads.

The loads generated in this section also provide the basis for extensive stress analysis, which leads to a more exact determination of the value of $N(y)$ corresponding to limit strength of the Model 188 wing. This determination is described in Appendix E, which also makes further use of the results of the stress analysis to indicate an ultimate-strength $N(y)$ value and limit and ultimate strength values of $\sigma_w \eta_d$.

It should be emphasized that the detailed procedure described in the following paragraphs is illustrative only. Wide variations in the specific approach are to be expected, depending upon the degree of conservatism acceptable and the specific airplane being treated. In attempting to follow the details of the work for the Model 188, the reader should not lose sight of the basically simple concepts described in Sections 10, 11.1, and 11.2, which will apply under any circumstances.

C.1 Nomenclature

The following nomenclature is used in this Appendix:

\bar{A}	Ratio of root-mean-square load to root-mean-square gust velocity
C_{La}	Lift curve slope per radian
C_{Ma}	Moment curve slope per radian
E_1	Elementary distribution for static mode
E_2	Elementary distribution for dynamic bending mode

E_3	Elementary distribution for dynamic torsion mode
\bar{E}_1	Ratio of load in static mode elementary distribution to statistically defined load
\bar{E}_2	Ratio of load in dynamic bending mode elementary distribution to statistically defined load
\bar{E}_3	Ratio of load in dynamic torsion mode elementary distribution to statistically defined load
K_{GN}	Unsteady aerodynamic function due to gust on nacelle - i.e., lift at given frequency divided by lift at zero frequency
K_{GW}	Unsteady aerodynamic function due to gust on wing - i.e., lift at given frequency divided by lift at zero frequency
K_{LN}	Unsteady aerodynamic function due to a unit change in angle-of-attack on the nacelle - i.e., lift at given frequency divided by lift at zero frequency
K_{LW}	Unsteady aerodynamic function due to a unit change in angle-of-attack on the wing - i.e., lift at given frequency divided by lift at zero frequency
L	Any load; subscript S denotes statistically defined design-level value; subscript D denotes a design condition value
N_0	Average number of zero crossings with positive slope for rms load quantity
M_x	Wing bending moment (in.-lb.)
M_y	Wing torsion moment (in.-lb.)
S	Aerodynamic reference area (ft. ²)
S_z	Wing shear (lb.)
T	Transfer function
V	Airplane forward velocity (in./sec.)
W	Gust velocity (in./sec.)

X_{nac}	Generalized coordinate of nacelle elastic plunge deflection relative to the wing (chords)
Z_0	Generalized coordinate of fuselage plunge displacement (chords)
Z	Vertical translation of any point on the wing relative to the fuselage (in.)
a_1	Loading coefficient for elementary distribution E_1
a_2	Loading coefficient for elementary distribution E_2
a_3	Loading coefficient for elementary distribution E_3
c	Chord (in.)
\bar{c}	Mean aerodynamic chord (in.)
f	Frequency (cps)
g	Acceleration of gravity (386 in./sec. ²)
i	$\sqrt{-1}$
l_x	Location of mass item relative to wing elastic axis (in.)
n_z	Load factor (g's)
$n_{zc.g.}$	C.G. load factor (g's)
$n_{zbal.}$	Rigid body load factor required to maintain balance in the dynamic elastic modes (g's)
p	Laplace operator
q	Free-stream dynamic pressure in psf, or beam shear flow in pounds per inch
x	Denotes in general a length in the chordwise direction (in.)
y	Denotes in general a length in the spanwise direction (in.)
$\theta_{nac.}$	Generalized coordinate of nacelle elastic pitch rotation relative to wing at nacelle (rad.)

\sum_T	Summation over the wing span from the tip to the root
ϕ_0	Generalized coordinate of fuselage pitch rotation (rad.)
ϕ_y	Output power spectral density for quantity y
Ω	Forcing frequency (rad./chord)
α	Aerodynamic angle-of-attack (rad.)
$\delta_{B_{ij}}$	Wing bending influence coefficient (in./lb.)
$\delta_{T_{ij}}$	Wing torsion influence coefficient (rad./in.-lb.)
ϕ	Wing twist elastic deflection (rad.)

Subscripts:

A	Airload
EA	Wing elastic axis
FB	Wing front beam
I	Inertia load
IA	Arbitrary load axis to which wing loads are referred
RB	Wing rear beam
N or NAC	Nacelle
W	Wing
i	General location of the wing
j	Designation of nacelles

Matrices:

$\begin{bmatrix} & \\ & \end{bmatrix}$	Square matrix
$\begin{bmatrix} & \\ & \end{bmatrix}$	Diagonal matrix

$\left. \begin{array}{c} \{ \\ \} \end{array} \right\}$

Column matrix

*

Matrix multiplication

Dots are used to denote the derivatives of a quantity with respect to time.

A quantity preceded by a Δ denotes that the quantity is the increment for that particular wing panel.

$||$ denotes the modulus of a complex quantity.

C. Preliminary Considerations

The determination of design load conditions divides naturally into two distinct parts. In the first, several "elementary" or "unit" distributions are developed. In the second, these are used as building blocks to generate one or more design load conditions, such as to match or envelope closely the statistically defined loads resulting from the power-spectral analysis.

Before embarking upon the generation of the elementary distributions, it is necessary to decide which mission segment or segments these should be based upon and determine what modes should be used as a basis. Consequently, it is pertinent to look at some results of the power-spectral analysis.

The loads obtained from the Model 188 mission analysis are shear, bending moment, and torsion at wing stations 83, 119, 167, 209, 275, 346, 380, 448, and 516, and front and rear beam shear flows at wing stations 83 and 346. (The nacelle locations are wing stations 188 and 359.) Values of these loads are read from the frequency-of-exceedance curves at a frequency of exceedance of 10^{-5} cycles per hour. The actual frequency of exceedance value to be used for design of a new airplane had yet to be established at this stage of the analysis, but the value selected here is the right order of magnitude and hence will be satisfactory to illustrate the method. Later work, described in Appendix E, indicates this to be quite close to the actual limit strength value for the Electra.

A typical frequency of exceedance curve - for bending moment at wing station 119 - was shown in Figure 9-9(b). It is seen that the bending moment at 10^{-5} cycles per hour is 12.1 million inch-pounds. It is apparent from the figure that mission analysis case 202 is the major contributor to the total bending moment. Similarly, it was established that case 202 is a major contributor to all of the other load quantities,

except for torsions in the outer wing. Outer wing torsions are produced predominantly by mission analysis case 201.

Loads for the total mission, and separately for mission analysis cases 201 and 202, are summarized in Table C-1, at the frequency of exceedance of 10^{-5} cycles per hour. In Table C-1, loads for the total mission are shown in column 3; loads due to mission analysis case 201 alone and 202 alone, at the same frequency of exceedance per hour of total flight, appear as columns 4 and 5 respectively. One-g loads for mission analysis cases 201 and 202 are shown as columns 6 and 7. The resulting "gust incremental" loads are shown in columns 8 through 11. In columns 8 and 10, the gust increment is taken as the difference between the net load based on all mission segments and the one-g load for the segment indicated. In columns 9 and 11, the gust increment is the increment for the given mission segment alone. Columns 12 and 13 show, based on mission segments 201 and 202 respectively, the ratio of gust increment due to the given segment alone to the total gust increment based on all segments.

In column 13, the ratios for shear, bending moment, and beam shear flow are all approximately .90. Ignoring for the present the wing torsions, the following conclusions can be drawn. First, if design conditions were to be generated to match the gust incremental loads for condition 202 alone (column 11), these could then be "ratioed up" by dividing by .90 and would closely reproduce the column 10 incremental loads. Then, if the condition 202 one-g loads were to be added, a match to the net loads of column 3 would result. Thus, to obtain a match to the statistically defined net loads, only the gust increment need be considered, and this can be confined to condition 202.

Now let us examine the torsions. Over the region from the fuselage to the inboard nacelle, the ratio in column 13 is approximately .80; between nacelles it is approximately .85. Since these ratios are not far below the .90 ratio for the other load quantities, use of case 202 on an incremental basis should also give a fair representation of the torsions from the fuselage to the outboard nacelle. For outer wing torsion, case 202 gives a poor representation of the total for the mission; consequently, it is necessary to use mission analysis case 201. Here, however, the cause is primarily the large difference in one-g flight torsion, rather than a difference in gust incremental torsion. Consequently, incremental torsions based on case 202 can be expected to be satisfactory even in the outer wing, if combined with the one-g loads for case 201.

As a result of the foregoing considerations, it is concluded that gust incremental loads for the total mission may be obtained by utilizing elementary distributions derived from a consideration of mission analysis case 202 only. These will then be added to case 201 or case 202 one-g loads as appropriate.

TABLE C-1. MISSION ANALYSIS LOADS AT $N(y) = 10^{-5}$ CYCLES PER HOUR, MODEL 188

①	②	③	④	⑤	⑥	⑦	⑧	⑨	⑩	⑪	⑫	⑬
Load	W.B. In.	Net Loads Mission Analysis	Net Loads Case 201	Net Loads Case 202	One-G Load Case 201	One-G Load Case 202	(Net Miss.) -(1-g 201)	(Net Miss.) -(1-g 202)	(Net Miss.) -(1-g 202)	(Net Miss.) -(1-g 202)	Ratio Case 201 ⑩ / ⑪	Ratio Case 202 ⑩ / ⑬
δ_z												
Wing	83	49200	35400	47400	15773	19055	33427	19687	30145	28345	.587	.940
Shear	119	46700	33000	44300	14841	16386	32499	18759	27914	27914	.578	.921
	167	39800	28500	37200	10979	11862	28821	17521	27938	27938	.608	.907
	209	47600	34300	44600	13663	13979	33937	20637	33621	30621	.608	.911
	273	39500	29000	36700	10998	9889	28902	18462	26811	26811	.637	.905
	346	28700	21000	26100	6787	5300	21913	14213	23400	20800	.649	.885
	380	27700	21500	25400	9257	7679	18443	12243	20021	17721	.664	.885
	448	16300	12700	14800	5384	4161	10815	7315	12039	10639	.676	.884
	516	6450	5200	6100	2087	1531	4353	3113	4919	4569	.713	.929
$10^{-6} M_y$												
Wing	83	13.80	10.20	12.95	4.144	3.923	9.56	6.056	9.877	9.027	.527	.913
Bending	119	12.17	9.05	11.24	3.604	3.298	8.57	5.446	8.872	7.952	.635	.896
Moment	167	10.10	7.55	9.35	2.976	2.669	7.03	4.574	7.491	6.741	.651	.900
About	209	8.30	6.25	7.65	2.458	2.080	5.84	3.792	6.220	5.570	.649	.895
Elastic	273	5.55	4.20	5.05	1.671	1.318	3.88	2.529	4.232	3.732	.652	.882
Axis	346	3.31	2.59	3.04	1.074	.8115	2.24	1.516	2.499	2.229	.577	.842
	380	2.44	1.90	2.20	.791	.5986	1.65	1.109	1.841	1.601	.672	.870
	448	.968	.760	.892	.303	.2114	.757	.457	.7566	.604	.604	.900
	516	.229	.184	.205	.078	.0534	.151	.106	.1756	.1516	.702	.863
$10^{-6} M_x$												
Wing	83	1.130	.980	.570	.498	-1.519	1.628	1.478	2.649	2.089	.908	.789
Torsion	119	1.020	.870	.500	.537	-1.480	1.557	1.407	2.500	1.980	.904	.792
Moment	167	.902	.745	.440	.587	-1.429	1.487	1.332	2.329	1.869	.896	.802
About	209	1.260	1.040	.800	.233	.908	1.433	1.273	2.168	1.808	.853	.834
Elastic	273	1.160	.995	.830	.271	.826	1.411	1.166	1.966	1.656	.826	.842
Axis	346	1.070	.795	.810	.298	.732	1.368	1.093	1.802	1.542	.799	.856
	380	.183	.176	.060	.052	.270	.235	.228	.453	.330	.970	.728
	448	.065	.060	.035	.053	.186	.118	.113	.251	.151	.958	.602
	516	.002	.042	-.044	.037	.101	.039	.035	.103	.057	.997	.953
q												
Beam	83	895	615	745	152	62	663	463	753	683	.698	.907
Shear	119	785	582	775	305	538	480	217	247	237	.452	.960
Flow	167	1080	790	920	20	-177	1060	770	1257	1097	.726	.873
	209	-690	-447	-670	-247	-399	-443	-200	-301	-281	.451	.933

It will be observed that the net load levels obtained from the mission analysis depend primarily on the rms or \bar{A} values, which in turn depend upon the total area under each output power spectral density curve. However, in establishing distributions of loads that might actually occur at particular instants of time, consideration must be given to the shapes of the output power spectral density diagrams.

The output power spectral densities of shear, bending moment, torsion, and front and rear beam shear flow at wing station 83 and 346 were shown in Figure 9-3. It is evident that there are three peaks in the power spectral density plots: the first, at approximately .4 cps, is associated with the short period mode; the second, at 2.1 cps, is due to the first coupled wing bending mode; and the third, at 4.4 cps, is due to the first coupled wing torsion mode. It is also apparent that the relative contributions of the three modes differ from one load quantity to another - for example, as between shear, moment, and torsion at any one wing station, and also, from one wing station to another.

For example, consider first the shear and torsion power spectral density of Figure 9-3(a). The 2.1 cps mode contributes about 1/3 of the total area for shear, but about 3/4 of the total area for torsion. Consider now the shear power-spectral densities of Figures 9-3(a) and (b). In Figure 9-3(a), the 2.1 cps mode contributes about 1/3 of the total area while in Figure 9-3(b) it contributes approximately 2/3 of the total area. The significant conclusions to be reached at this point is that since there are three dominant peaks in the power-spectral densities, it will be necessary to derive three elementary distributions - one corresponding to each of the peaks.

In order to provide a more complete picture of the various power spectral densities, a summary of the relative peak values of the power-spectral densities for all load quantities is shown in Table C-2.

In connection with the power-spectral density information presented in Figure 9-3 and Table C-2, some additional observations are pertinent in anticipation of developing the several elementary distributions. First, it becomes apparent that all loads outboard of the outboard nacelle are predominantly static in nature - i.e., dynamic effects are so small that they are negligible. For the region just inboard of the outboard nacelle shear and torsion are predominantly dynamic and are due to the 2.1 cps mode; bending moment in this region, on the other hand, is predominantly static. Just outboard of the inboard nacelle and between the inboard nacelle and the fuselage, shear and torsion exhibit a somewhat less pronounced dynamic effect, and dynamic effects in the bending moment are no longer small. In general, dynamic effects are more pronounced for torsion than for shear or bending.

TABLE C-2. POWER SPECTRAL DENSITY FUNCTION PEAKS,
MODEL 188 CASE 202

①	②	③	④	⑤
Load	W.S	σ_y f = .4 cps	σ_y f = 2.1 cps	σ_y f = 4.4 cps
$10^{-4} S_z$	83	48.45	33.25	.5066
	119	41.14	38.22	.5987
	167	24.91	39.90	.6707
	209	53.00	41.80	1.661
	275	35.37	37.87	.9835
	346	15.33	28.83	.4423
	380	29.10	3.150	.1271
	448	9.901	1.189	.06636
Wing Shear	516	1.647	.2681	.02866
$10^{-8} M_x$	83	485.9	354.9	8.776
	119	385.6	278.7	7.284
	167	285.6	187.6	5.373
	209	205.2	121.3	3.517
	275	99.98	47.04	1.283
	346	42.09	7.646	.3142
	380	23.48	2.874	.1676
	448	3.773	.5221	.04092
Wing Bending Moment About Elastic Axis	516	.1904	.03099	.003313
$10^{-8} M_y$	83	7.865	27.78	4.103
	119	4.507	27.36	3.958
	167	1.617	26.53	3.779
	209	6.888	25.01	.8719
	275	2.889	23.48	.7431
	346	.7749	21.96	.6236
	380	1.072	.01761	.02532
	448	.2601	.002732	.007162
Wing Torsion Moment About Elastic Axis	516	.03164	.0001018	.001413

C.3 Elementary Distributions

It is now possible to proceed to the generation of the elementary distributions.

Basically, the elementary distributions will consist of one or more static distributions together with one or more distributions associated with dynamic overtravel in each elastic mode.

The static distribution consists of the incremental loads associated with gust encounter on a static aeroelastic basis - i.e., static aeroelastic wing twist is accounted for, but forces due to accelerations and velocities in the elastic modes are not considered. This distribution could be obtained by the usual static loads methods. However, for the Model 188 it was considered more convenient to start from scratch utilizing low frequency results from the dynamic analysis. This approach also ensured combining the right magnitude of inertia forces with the aerodynamic forces, since the inertia forces depend upon how the tail and fuselage forces phase with the wing air loads.

The elastic-mode distributions can be obtained fairly directly when natural modes are used as generalized coordinates in the dynamic analysis. It is required only to obtain the inertia and aerodynamic forces associated with oscillations at the natural frequency of the mode. However, the dynamic analysis of the Model 188 utilized elementary deflection shapes, rather than natural modes, as generalized coordinates. Consequently, for the Model 188, the natural mode shapes are approximated based upon inertia and aerodynamic forces obtained from the dynamic analysis at the respective resonant frequencies.

The solution for the elementary distributions are to a certain extent arbitrary and need be only approximations to the actual distributions of loads in the modes. It is highly desirable, however, that the elementary distributions be fairly good approximations to the actual load distributions in order that the resulting design loads be realistic. It is the intent herein to define a method that is basically simple yet yields realistic loads.

Looking ahead briefly, the procedure for determining the elementary distributions, both static and dynamic, can be summarized as follows:

1. At the appropriate resonant frequency (or, in the case of the static distribution, at any frequency well below the first elastic mode frequency), obtain the wing loads from the dynamic analysis. These are simply values of the appropriate transfer functions. Retain real and imaginary parts.

2. Use these to compute the mode shape. Retain real and imaginary parts.
3. Based on this mode shape, obtain panel aerodynamic and inertia forces. Retain real and imaginary parts.
4. Take either the modulus of these panel loads (with sign that best approximates the actual phasing) or the component in phase with some appropriate single load quantity. Integrate spanwise to obtain shears, bending moments, and torsions. This constitutes the elementary distribution.

In carrying out this procedure, the first step required is to define a reasonable spanwise distribution of unit airloads ($\Delta S_{zA}/a_1$ and $\Delta M_{yA}/a_1$). In addition to this, the spanwise distribution of pertinent unit inertia data (S_z/n_z , M_y/n_z , etc.) and the matrix of wing bending and torsional influence coefficients must also be defined. All other necessary data may be obtained from the transfer functions used in obtaining the output power spectral densities and subsequently the \bar{A} and \bar{N}_0 values.

The static-mode elementary distribution is considered first. For the static mode it will be assumed that velocities and accelerations in the elastic modes are negligible. It is not necessary that the static-mode elementary distribution be defined at the airplane short period frequency; in fact, it is desirable to define the loads at a lower frequency, say about .05 to .10 cps, to ensure that dynamic effects are, in fact, negligible. The determination of the static-mode elementary distribution is as follows:

1. Obtain the complex quantities Z_0 , ϕ_0 , n_{zcg} , and M_{y1} ; these are simply values of the corresponding transfer functions.
2. Define the complex unsteady aerodynamic functions K_{GW} , K_{LW} , K_{GN} , and K_{LN} .
3. Compute the complex root angle-of-attack.

$$\alpha_{\text{Root}} = K_{GW} \frac{W}{U} + K_{LW} (\phi_0 - i\Omega Z_0)$$

4. Verify that α_{Root} , $\theta_{\text{nac.}}$, and M_{y1} are nearly in phase or nearly 180° out of phase relative to n_{zcg} . (This condition normally will be met, at the low frequencies specified.)
5. Convert all quantities to a load per "g" basis by dividing the modulus of the quantity by the modulus of c.g. load factor.

6. Compute the local aerodynamic angle of attack acting at each wing panel:

$$(a/n_z)_i = (a_{\text{Root}}/n_z) + (\Delta a_{\text{Twist}}/n_z)_i$$

where

$$\left\{ (\Delta a_{\text{Twist}}/n_z)_i \right\} = \left[\delta_{T_{ij}} \right] * \left\{ (\Delta T_{M_{y_i}} / |T_{n_{z_{cg}}}|) \right\}$$

(Note that the unsteady aerodynamic effects are neglected in evaluating Δa_{twist} ; this is valid only if $|K_{LW}| = 1.0$.)

7. Compute the local aerodynamic angle of attack for each nacelle:

$$(a/n_z)_j = (a_{\text{Root}}/n_z) + (\Delta a_{\text{Twist}}/n_z)_j + (\theta_{\text{Nac}}/n_z)_j$$

(Note that the unsteady aerodynamic effects are neglected in evaluating θ_{Nac} ; this is valid only if $|K_{LN}| \approx 1.0$.)

8. Plot $(a/n_z)_i$ and $(a/n_z)_j$ versus wing station.
9. Obtain the static-mode elementary distribution

$$S_{z_i} = \sum_T^R \left(\frac{\Delta S_{z_A}}{a} \right)_i * \left(\frac{a}{n_z} \right)_{i,j} + \sum_T^R \left(\frac{\Delta S_z}{n_z} \right)_i * (-1.0)$$

$$M_{x_i} = \sum_T^R S_{z_i} (\Delta y_i)$$

$$M_{y_i} = \sum_T^R \left(\frac{\Delta M_{y_A}}{a} \right)_i * \left(\frac{a}{n_z} \right)_{i,j} + \sum_T^R \left(\frac{\Delta M_{y_I}}{n_a} \right)_i * (-1.0)$$

It should be noted that the wing stations at which loads must be defined for stress analysis purposes are different in

location and number from those at which loads are obtained in the power-spectral analysis. This step is a convenient point at which to go to these more closely spaced stations.

Next, consideration is given to the calculation of the dynamic-mode distributions. In obtaining these distributions, the loads due to gust velocity, body pitch, and rigid body plunge are not considered, since they are included in the static-mode elementary distribution. In other words, the loads to be computed are to be those associated only with the dynamic overtravel in the modes. In obtaining the dynamic mode elementary distributions, it is necessary to utilize values of the transfer functions at the actual peak-response frequency. The determination is as follows:

1. Obtain the complex quantities ΔS_{z_i} , ΔM_{y_i} , $\theta_{nac.}$, and $X_{nac.}$; these are simply values of the corresponding transfer functions.
2. Define the complex unsteady aerodynamic functions K_{IW} and K_{IN} .
3. Compute the complex wing rotation (ϕ_i) and complex wing deflection (Z_i) relative to the fuselage.

$$\{\phi_i\} = [\delta_{T_{ij}}] * \{\Delta M_{y_i}\}$$

$$\{Z_i\} = [\delta_{B_{ij}}] * \{\Delta S_{z_i}\}$$

4. Compute the local complex aerodynamic angle of attack.

Wing

$$\{a_i\} = K_{IW} * \left(\{\phi_i\} - \frac{i\Omega}{c} \{Z_i\} \right)$$

Nacelles

$$\{a_i\} = K_{IN} * \left(\{\phi_i\} + \{\theta_{nac.}\} - \frac{i\Omega}{c} \{Z_i\} - i\Omega \{X_{nac.}\} \right)$$

(Note that the effect of ϕ_i on vertical velocity is neglected, since it is small.)

5. Compute the local complex load factors.

Wing

$$\left\{ n_{z_i} \right\} = - \frac{p^2 v^2}{g \bar{c}^2} \left(\left\{ z_i \right\} + \left[l_{x_{wing}} \right] * \left\{ \phi_i \right\} \right)$$

Nacelles

$$\left\{ n_{z_j} \right\} = - \frac{p^2 v^2}{g \bar{c}^2} \left(\left\{ z_i \right\} + \left[l_{x_{nac}} \right] * \left\{ \phi_i \right\} + \bar{c} \left\{ x_{nac} \right\} \right)$$

6. If mass items are present that have relatively large pitching moments of inertia, compute the local complex pitching

Wing

$$\left\{ \ddot{\phi} \right\} = - \frac{p^2 v^2}{\bar{c}^2} \left\{ \phi_i \right\}$$

Nacelles

$$\left\{ \ddot{\phi} \right\} = - \frac{p^2 v^2}{\bar{c}^2} \left(\left\{ \phi_i \right\} + \left\{ \theta_{nac} \right\} \right)$$

7. Obtain the modulus of $a_{i,j}$, $n_{z_{i,j}}$, $\ddot{\phi}_i$ and $\ddot{\phi}_j$. Check to see that the quantities are relatively in or out of phase, and plot the modulus vs wing station, using the appropriate sign.
8. Solve for the rigid body load factor required to keep the mode in balance - i.e., make the summation of vertical forces equal to zero. (It is assumed that "balancing" the mode does not change the aerodynamic angle-of-attack. It is also assumed that, owing to the extremely large pitching inertia of the fuselage, modal balance in pitch is not required.)

$$n_{z_{balance}} = \frac{- \sum \left(\frac{R}{T} \left(\frac{\Delta S_{Z_A}}{a} \right)_{i,j} * a_{i,j} - \sum \left(\frac{R}{T} \left(\frac{\Delta W}{n_z} \right)_{i,j} * n_{z_{i,j}} \right)}{1/2 \text{ gross weight}}$$

9. Obtain new spanwise load factor distribution.

$$\left\{ n_{z_i} \right\}_{\text{adjusted}} = n_{z_{\text{balance}}} * \left\{ 1.00 \right\} + \left\{ n_{z_i} \right\}$$

10. Obtain the dynamic mode elementary distribution.

$$s_{z_i} = \sum_T^R \left(\frac{\Delta s_{z_A}}{a} \right)_{i,j} * (a_{i,j}) + \sum_T^R \left(\frac{\Delta s_z}{n_z} \right)_{i,j} * (n_{z_{i,j}})_{\text{adjusted}}$$

$$M_{z_i} = \sum_T^R s_{z_i} (\Delta y_i)$$

$$M_{y_i} = \sum_T^R \left(\frac{\Delta M_{y_A}}{a} \right)_{i,j} * (a_{i,j}) + \sum_T^R \left(\frac{\Delta M_{y_I}}{n_z} \right)_{i,j} * (n_{z_{i,j}})_{\text{adjusted}} \\ + \sum_T^R \left(\frac{M_u}{\ddot{\theta}} \right)_{i,j} * (\ddot{\phi} \text{ or } \ddot{\theta}_j)$$

As in the determination of the static-mode elementary distribution, this is a convenient point at which to go to the more closely spaced wing stations at which loads must be defined for use in the stress analysis.

The arbitrary elementary distributions for the Model 188 are now determined, following the procedure outlined in the above discussion. As indicated earlier, mission analysis case 202 is the major contributor to the wing loads and will be used in deriving the elementary distributions.

The required unit airload distributions are presented in Table C-3. In column 2 is shown the spanwise distribution of "additional" airload for the rigid wing, as used in static loads determinations. Column 3 gives the incremental airloads acting at each panel, and column 4 refers airloads to local panel angle of attack. Column 5 gives the nacelle airload shears, and column 6, the combined wing-nacelle airload shears.

TABLE C-3. UNIT AIRLOAD DISTRIBUTIONS MODEL 188 CASE 202

①	②	③	④	⑤	⑥	⑦	⑧	⑨
V.S.	$\frac{s_z}{C_s q \frac{s}{2}}$	$\frac{\Delta s_z}{C_s q \frac{s}{2}}$	$\frac{\Delta s_{zAW}}{\alpha_1}$	$\frac{\Delta s_{zAW}}{\alpha_1}$	$\frac{\Delta s_{zA}}{\alpha_1}$	x_1 (in.)	$\frac{10^{-6} M_{LA MAC}}{\alpha_1}$	$\frac{10^{-6} M_{Y LA}}{\alpha_1}$
	Given	② ₁ - ② ₁₊₁	846550 ③	*	⑥ + ⑤	-.1C ₁ **	Below	10 ⁻⁶ ⑥ ⑦ + ⑧
0	1.000	.138	116820	0	116820	-22.70	0	-2.652
65	.862	.075	63490	0	63490	-21.21	0	-1.347
101	.787	.078	66030	0	66030	-20.39	0	-1.346
137	.709	.067	56720	0	56720	-19.55	0	-1.110
167	.642	0	0	0	0	0	0	0
167	.642	0	0	25110	25110	0	3.700	3.700
167	.642	.022	18620	-14530	4090	-18.88	0	-.077
179	.620	.031	26240	-20480	5760	-18.60	0	-.107
197	.589	.023	19470	-15200	4270	-18.19	0	-.078
209	.566	0	0	0	0	0	0	0
209	.566	0	0	25110	25110	0	3.700	3.700
209	.566	.065	55030	0	55030	-17.91	0	-.985
239	.501	.074	62650	0	62650	-17.23	0	-1.079
275	.427	.037	31320	0	31320	-16.40	0	-.514
293	.390	.075	63490	0	63490	-15.99	0	-1.015
329	.315	.030	25400	0	25400	-15.17	0	-.385
346	.285	0	0	0	0	0	0	0
346	.285	0	0	31300	31300	0	4.339	4.339
346	.285	.033	27940	-50680	-22740	-14.78	0	.336
380	.252	0	0	0	0	0	0	0
380	.252	0	0	19380	19380	0	2.686	2.686
380	.252	.022	18620	0	18620	-14.00	0	-.261
397	.230	.061	51640	0	51640	-13.61	0	-.703
431	.169	.050	42330	0	42330	-12.83	0	-.543
465	.119	.043	36400	0	36400	-12.05	0	-.439
499	.076	.035	29630	0	29630	-11.27	0	-.334
533	.041	.032	27090	0	27090	-10.49	0	-.284
584	.009	.009	7620	0	7620	-9.33	0	-.071

$q = 263.7 \text{ psf}$

$C_{L \alpha_{WH}} = 4.847 / \text{Rad.}$

$q \frac{s}{2} C_{L \alpha_{WH}} = 846,550$

* Macelle Airloads:

** $\alpha_1 = 227 - .229 \text{ (1)}_1$

(At Macelles $x_1 = 0.0$)

	Inboard	Outboard
$q s_{WH} C_{L \alpha_{WH}}$	50222	50679
$q s_{WH} C_{L \alpha_{WH}} \bar{C}_M$	2,430,000	2,454,000
$q s_{WH} C_{L \alpha_{WH}} x_1$	4,972,000	4,571,000

Column 7 lists the wing airload torsion moment arms. Column 8 gives the incremental nacelle airload torsion; and column 9 gives the combined wing-nacelle airload torsions.

The required unit inertia data are shown in Table C-4. Column 2 gives the spanwise distribution of inertia shear, and column 3, the spanwise distribution of inertia torsion. Columns 4 and 5 are the panel increments corresponding to columns 2 and 3 respectively. Column 6 gives the unit inertia pitching moment due to the large mass concentration at the nacelles.

The matrices of wing torsion and of wing bending influence coefficients are shown in Table C-5.

With the necessary preliminary data established, the elementary distributions can now be determined.

The derivation of the static-mode elementary distribution is shown in Table C-6 and Figure C-1.

In Table C-6, the pertinent information taken from the transfer functions is listed first. The computation of unsteady lift growth functions is shown next; this involves taking the Laplace transforms of the familiar Wagner and Kussner functions (as approximated in exponential form) and replacing p with $i\Omega$. Next, the root angle of attack is computed. This is followed, in Table C-6(d) with computation of the increment in angle of attack due to twist and the net angle of attack per "g" as a function of wing station. The resulting spanwise variation of angle of attack per "g" is then plotted in Figure C-1.

The final spanwise variation of loads in the static mode is obtained in Table C-6(e). This table is self-explanatory. The loads defined therein are with respect to the arbitrary load axis that is used in the stress analysis.

In Table C-6(f), the loads of Table C-6(e) are converted to a form such that the design conditions generated using the elementary distributions can be compared directly with the statistically defined loads in Table C-1. The axis with respect to which moments are defined is rotated and shifted to conform to the axis system used in the ten-degree-of-freedom analysis, and the loads are listed at the wing stations where the loads are given in Table C-1. In addition, two rather minor adjustments are made, in order that these distributions be consistent with the less exact way in which the loads were summed in the ten-degree-of-freedom program.

TABLE C-4. UNIT INERTIA LOADS, MODEL 188 CASE 202

① W.S.	② $\frac{S_z}{n_z}$ lb	③ $\frac{10^{-6} M_{yLA}}{n_z}$ In.-lb	④ $\left(\frac{S_z}{n_z}\right)_1$	⑤ $\left(\frac{10^{-6} \Delta M_{yLA}}{n_z}\right)_1$	⑥ $\frac{10^{-6} \Delta M_{yH}}{\theta}$
	Given	Given	② 1 - ② _{i+1}	③ 1 - ③ _{i+1}	Given
0	22798	.1812	740	-.0429	0
65	22058	.224	2948	-.1344	0
101	19110	.3585	1008	-.0874	0
137	18102	.4459	700	-.0381	0
167-	17402	.4840	1179	+.0170	0
167- _H	16223	.4670	1925	+.1915	.01570
167+	14298	.2755	447	-.0093	0
179	13351	.2848	350	-.0074	0
197	13501	.2922	167	-.0035	0
209-	13334	.2957	1108	.0223	0
209- _H	12226	.2834	1925	.1915	.01570
209+	10301	.0919	1157	-.0549	0
239	9144	.1468	1566	-.0700	0
275	7578	.2168	638	-.0276	0
293	6940	.2444	765	-.0327	0
329	6175	.2771	257	-.0108	0
346-	5918	.2879	351	-.0034	0
346- _H	5567	.2913	2378	.2157	.01384
346+	3189	.0756	582	-.0213	0
380-	2607	.0969	218	-.0020	0
380- _H	2389	.0989	1472	+.1335	.00856
380+	917	-.0346	152	-.0070	0
397	765	-.0276	165	-.0073	0
431	600	-.0203	155	-.0063	0
465	445	-.0140	125	-.0043	0
499	320	-.0097	130	-.0041	0
533	190	-.0056	170	-.0050	0
584	20	-.006	20	-.0006	0

TABLE C-5. DEFLECTION INFLUENCE COEFFICIENTS, MODEL 188

Torsional Influence Coefficients $\sim [\delta_{T1j}] \sim (Rad/In.-Lb)$										
WS	65	101	143	188	239	311	359	414	482	550
65	12.2	12.2	12.2	12.2	12.2	12.2	12.2	12.2	12.2	12.2
101	12.2	20.1	20.1	20.1	20.1	20.1	20.1	20.1	20.1	20.1
143	12.2	20.1	30.8	30.8	30.8	30.8	30.8	30.8	30.8	30.8
188	12.2	20.1	30.8	44.6	44.6	44.6	44.6	44.6	44.6	44.6
239	12.2	20.1	30.8	44.6	64.1	64.1	64.1	64.1	64.1	64.1
311	12.2	20.1	30.8	44.6	64.1	103.7	103.7	103.7	103.7	103.7
359	12.2	20.1	30.8	44.6	64.1	103.7	143.9	143.9	143.9	143.9
414	12.2	20.1	30.8	44.6	64.1	103.7	143.9	218.8	218.8	218.8
482	12.2	20.1	30.8	44.6	64.1	103.7	143.9	218.8	369.3	369.3
550	12.2	20.1	30.8	44.6	64.1	103.7	143.9	218.8	369.3	369.3

$10^{10} [\delta_{T1j}] =$

Bending Influence Coefficients $\sim [\delta_{B1j}] \sim (In./Lb)$										
WS	65	101	143	188	239	311	359	414	482	550
65	.9	1.7	2.7	3.6	4.8	6.4	7.4	3.6	10.1	11.6
101	1.1	3.6	5.9	8.3	11.1	15.0	17.7	20.7	24.4	28.1
143	2.7	5.9	10.5	15.6	21.5	29.7	35.1	41.4	49.2	56.9
188	3.6	8.3	15.6	24.8	35.4	50.4	60.5	72.0	86.1	100.4
239	4.8	11.1	21.5	35.4	53.5	79.7	97.2	117.2	142.0	166.7
311	6.4	15.0	29.7	50.4	79.7	128.2	161.7	200.2	247.7	295.2
359	7.4	17.7	35.1	60.5	97.2	161.7	210.2	266.8	336.7	406.7
414	8.6	20.7	41.4	72.0	117.2	200.2	266.8	351.1	457.7	564.3
482	10.1	24.4	49.2	86.1	142.0	247.7	336.7	457.7	630.3	809.4
550	11.6	28.1	56.9	100.4	166.7	295.2	406.7	564.3	809.4	1101.9

$10^5 [\delta_{B1j}] =$

TABLE C-6. CALCULATION OF STATIC MODE ELEMENTARY DISTRIBUTIONS, MC DEL 188 CASE 202

(a) INFORMATION FROM TRANSFER FUNCTIONS AT $f = .1$ CPS

	W.S.	$M_y \sim \text{In.-lb}$	$10^{-6} T_{M_y} $	$10^{-6} \Delta T_{M_y} $
$\Phi_0 = -.59003 + .21672 i$	In.			
$\Phi_0 = .84695 - 26.8331$	67	-115440 + 3,086,000 i	3.0881	1.2093
$z_{cg} = -.12822 + 4.6231 i$	101	-87118 + 1,876,800 i	1.8788	.4974
$ T_{n_x} = 4.6249 \text{ g's}$	143	-75422 + 1,379,300 i	1.3814	.6344
$\theta_{\text{INB'D}} = .000847 + .005487 i$	188	-62884 + 744,310 i	.7470	-1.0695
$ T_{\theta_{\text{INB'D}}} = .005552$	239	-33140 + 1,816,200 i	1.8165	.6768
$\theta_{\text{OUT'B}} = .000918 + .005794 i$	311	-24304 + 1,139,500 i	1.1397	.6089
$ T_{\theta_{\text{OUT'B}}} = .005866$	359	-20531 + 530,370 i	.5308	-.2511
	414	10221 + 781,870 i	.7819	.3932
	482	7935 + 388,650 i	.3887	.2519
	550	3713 + 136,720 i	.1368	.1368

(b) TRANSIENT AERODYNAMIC FUNCTIONS

$$K_{GW} = 1 - \left[\frac{.236 \Omega^2}{.013456 + \Omega^2} + \frac{.513 \Omega^2}{.529984 + \Omega^2} + \frac{.171 \Omega^2}{23.4256 + \Omega^2} \right] - 1 \left[\frac{.027376 \Omega}{.013456 + \Omega^2} + \frac{.373464 \Omega}{.529984 + \Omega^2} + \frac{.82764 \Omega}{23.4256 + \Omega^2} \right] = .99552 - .0498 i; |K_{GW}| = .99603 \approx 1.0$$

$$K_{LM} = 1 - \left[\frac{.165 \Omega^2}{.0081 + \Omega^2} + \frac{.335 \Omega^2}{.36 + \Omega^2} \right] - 1 \left[\frac{.01485 \Omega}{.0081 + \Omega^2} + \frac{.201 \Omega}{.36 + \Omega^2} \right] = .99490 - .03669 i; |K_{LM}| \approx 1.0$$

(c) ROOT ANGLE OF ATTACK

$$\alpha_{\text{Root}} = K_G \frac{W}{V} + K_L (\Phi_0 - 1 \Omega \Phi_0); \text{ Since } W/V = 1$$

$$\alpha_{\text{Root}} = .9952 - .04298 i + (.99490 - .03669 i) [- .59003 + .21672 i - .015699 i (.84695 - 26.8331 i)]$$

$$= -.00315 + .19651 i$$

$$|T_{\alpha_{\text{Root}}}| = .1965$$

TABLE C-6. CONTINUED
(d) SPANWISE VARIATION OF ANGLE OF ATTACK

Solving for α/n_z

$$\frac{\alpha_{\text{ROOT}}}{n_z} = \frac{.1965}{4.6249} = .04249 \text{ RAD}$$

$$\frac{\theta_{\text{INB'D}}}{n_z} = \frac{.005552}{4.6249} = .00120 \text{ RAD}$$

$$\frac{\theta_{\text{OUT'B}}}{n_z} = \frac{.005866}{4.6249} = .00127 \text{ RAD}$$

$$\left[\frac{\Delta \alpha_{\text{TWIST}}}{n_z} \right] = \left[\delta_{T_{1j}} \right] + \left[\frac{\Delta |T_{n_z}|}{|T_{n_z}|} \right] \left[\frac{\alpha_1}{n_z} \right] = \frac{\alpha_{\text{ROOT}}}{n_z} \{1.0\} + \left[\frac{\Delta \alpha_{\text{TWIST}}}{n_z} \right] + \left[\frac{\theta_{\text{MAC}}}{n_z} \right]$$

NOTE: $\left[\delta_{T_{1j}} \right]$ is given in Table C-5

W.S.	$10^{-6} \Delta \left \frac{T_{n_z}}{T_{n_z}} \right $	$\frac{\Delta \alpha_{\text{TWIST}}}{n_z}$	$\frac{\theta_{\text{MAC}}}{n_z}$	$\frac{\alpha_1}{n_z}$
65	+.2615	.00081		.04332
101	+.1075	.00114		.04363
143	+.1372	.00146		.04395
188	-.2313	.00168		.04417
188M	-	.00168	.00120	.04537
239	+.1464	.00244		.04493
311	+.1316	.00342		.04591
359	-.0543	.00388		.04637
359M	-	.00388	.00127	.04764
414	+.0850	.00515		.04764
482	+.0545	.00641		.04890
550	+.0296	.00707		.04956

TABLE C-6. CONTINUED
(e) LOADS AT STRESS ANALYSIS STATIONS

①	②	③	④	⑤	⑥	⑦	⑧	⑨	⑩	⑪	⑫
us	$\frac{A_{sA}}{a_1}$	$\frac{10^{-6} \Delta K_{TA}}{a_1}$	$\frac{a_1}{n}$	s_A	$10^{-6} K_{TA}$	$\frac{s_z}{n_z}$	$\frac{10^{-6} K_{TA}}{n_z}$	$s_{z_{tot}}$	$\frac{\Delta z}{z}$	$10^{-6} K_{z_{tot}}$	$10^{-6} K_{z_{tot}}_{net}$
Reference	Table C-3	Table C-3	Fig C-1	Table C-4	Table C-4	Table C-4	Table C-4	⑤ - ⑦	⑩ - ⑪	*	⑫ - ⑬
0	116820	-2.652	.04249	39406	.0912	22798	.1812	15608	32.5	4.732	-.0900
65	63490	-1.347	.04331	31443	.2038	22028	.2241	11395	18.0	3.853	-.0803
101	66090	-1.346	.04353	30693	.2622	19110	.3585	11583	18.0	3.442	-.0723
137	56720	-1.110	.04393	27812	.3209	18102	.4459	9710	15.0	3.099	-.1250
167	0	0	-	25320	.3697	17402	.4840	7918	-	2.794	-.1143
167	25110	3.700	.04529	25320	.3697	16223	.4670	9097	-	2.794	-.0973
167	4090	-.077	.04409	24183	.2021	14598	.2735	5085	6.0	2.794	-.0734
119	5760	-.107	.04414	24003	.2035	13951	.2848	10152	9.0	2.674	-.0793
197	4270	-.078	.04430	23749	.2102	13501	.2922	10218	6.0	2.490	-.0820
209	0	0	-	23559	.2137	13334	.2957	10225	-	2.367	-.0820
209	25110	3.700	.04568	23559	.2137	12226	.2834	11333	-	2.367	-.0697
209	55030	-.985	.04448	22412	.0446	10301	.0919	12111	15.0	2.367	-.0473
239	62650	-1.079	.04493	19965	.0885	9144	.1468	10821	18.0	2.023	-.0583
275	31320	-.314	.04543	17150	.1369	7578	.2168	9572	9.0	1.656	-.0799
293	63490	-1.015	.04566	15727	.1603	6940	.2444	8787	18.0	1.491	-.0841
309	25400	-.395	.04612	12828	.2066	6175	.2771	6653	8.5	1.213	-.0705
346	0	0	-	11657	.2244	5918	.2879	5739	-	1.108	-.0635
346	31300	4.339	.04755	11657	.2244	5567	.2913	6090	-	1.108	-.067
346	-22740	.336	.04628	10168	.0181	3189	.0756	6979	17.0	1.108	-.0575
380	0	0	-	11221	.0025	2607	.0969	8414	-	.8427	-.0944
380	19380	2.686	.04816	11221	.0025	2389	.0909	8032	-	.8427	-.0954
380	16620	-.261	.04689	10288	-.1268	917	-.0346	9371	8.5	.8427	-.0922
397	51640	-.703	.04726	9415	-.1146	765	-.0276	8650	17.0	.6896	-.0870
431	42330	-.243	.04799	6974	-.0814	600	-.0203	6374	17.0	.4342	-.0611
465	36400	-.459	.04861	4943	-.0553	445	-.0140	4498	17.0	.2494	-.0413
499	29630	-.334	.04911	3173	-.0340	320	-.0097	2853	17.0	.1244	-.0243
533	27090	-.284	.04943	1718	-.0176	190	-.0056	1528	25.5	.0499	-.0120
584	7620	-.071	.04975	379	-.0035	20	-.0006	359	5.0	.0018	-.0029

$$= \frac{1}{2} \left(\frac{12}{n} + \frac{12}{n-1} \right) \frac{1}{n}$$

TABLE C-6. CONCLUDED
(f) LOADS AT DYNAMIC ANALYSIS STATIONS

①	②	③	④	⑤	⑥	⑦	⑧	⑨	⑩	⑪	⑫
Panel	Lump	Wing	S_g	ΔS_g^*	$S_{Z,Adj.}$	$10^{-6} M_x$	$10^{-6} M_{TA}$	$10^{-6} \Delta M_{TA}$	$10^{-6} M_{TA,Adj}$	ΔM_{TA-LA}	$10^{-6} M_{TA}$
Station	Station	Station	Lb	Lb	Lb	In.-Lb	In.-Lb	In.-Lb	In.-Lb	In.-Lb	In.-Lb
Given	Given	Given	Table C-5(e)	Refer to Note 1	④ + ⑤	Refer to Note 2	Table C-6(e)	Refer to Note 1	⑧ + ⑨	67.8 - .0842 ③	Refer to Note 3
2	101	83	11484	-	11484	3.6173	-.0983	-	-.0983	60.81	.3357
3	143	119	10647	-240	10407	3.2233	-.1107	.0049	-.1058	57.78	.2245
4	188	167	7918	+35	7953	2.7826	-.1143	-.0084	-.1167	53.74	.0768
5	239	209	12111	-367	11744	2.3690	-.0473	.0066	-.0407	50.20	.3495
6	311	273	9572	-	9572	1.6721	-.0799	-	-.0799	44.65	.2070
7	359	346	5739	+758	6497	1.1001	-.0635	-.0115	-.0750	38.67	.0839
8	414	380	9371	-334	9037	.8259	-.0922	.0047	-.0875	35.80	.1621
9	482	448	5436	-	5436	.3138	-.0512	-	-.0512	30.08	.0844
10	550	516	2191	-	2191	.0745	-.0182	-	-.0182	24.35	.2089

NOTE 1: In the ten degree-of-freedom analysis, inertia loads are defined at the wing stations listed in Column 3. Airloads, however, were inadvertently defined at wing stations 83, 122, 165.5, 213.5, 273, 335, 386.5, 448, and 516. To provide consistency with the mission analysis loads, the slight correction is applied.

NOTE 2: To provide consistency with the mission analysis results, the bending moment is integrated in a manner consistent with the ten-degree-of-freedom program.

$$M_x = \sqrt{\frac{1}{10}} \left[\frac{1}{10} \left(\frac{1}{10} + 1 - \frac{1}{10} \right) - \frac{1}{10} \left(\frac{1}{10} - \frac{1}{10} \right) \right]$$

NOTE 3: $M_{Y,EA} = .5964 M_{Y,LA} - .0842 M_{X_1} + S_{Z_1} \Delta X_{LA-LA}$

WING SHEAR FORCES

$$q_{73} 83 = .02167 S_g - .26 (10^{-6} M_x) + 164 (10^{-6} M_y) = 209.9 \text{ LB/IN.}$$

$$q_{83} 83 = -.01892 S_g + 18 (10^{-6} M_x) + 163 (10^{-6} M_y) = -97.4 \text{ LB/IN.}$$

$$q_{73+83} = -.03116 S_g - 70 (10^{-6} M_x) + 390 (10^{-6} M_y) = 156.2 \text{ LB/IN.}$$

$$q_{83+86} = -.08636 S_g + 45 (10^{-6} M_x) + 390 (10^{-6} M_y) = 89.0 \text{ LB/IN.}$$

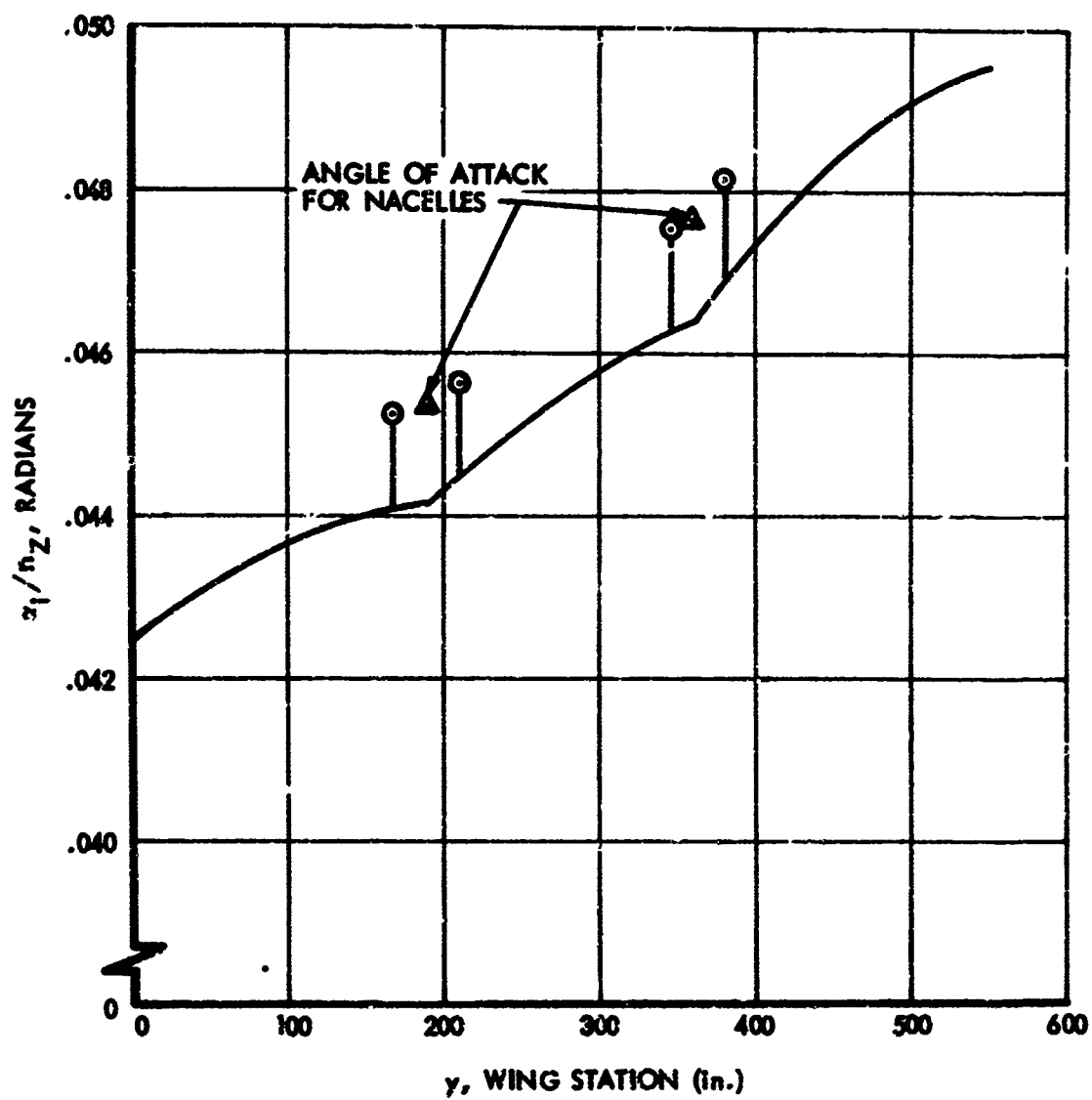


FIGURE C-1. SPANWISE VARIATION OF α_i/n_z IN STATIC MODE, MODEL 188 CASE 202

The derivation of the dynamic bending mode elementary distribution is accomplished next and appears in Table C-7 and Figure C-2.

In Table C-7, the pertinent information taken from the transfer functions is listed first. Next, the computation of the unsteady lift growth functions is shown, followed by the computation of the wing elastic deformations.

The determination of the resulting local angle of attack for the wing and nacelles is next presented, in Table C-7(d). Determination of the local load factors for the wing and nacelles is shown in Table C-7(e) through (h). The spanwise variations of angle of attack and of load factor are then summarized in Table C-7(i). These are shown in complex form in columns 2, 3, and 4. The modulus of each is then obtained in columns 5, 7, and 9; and in columns 6, 8, and 10 the modulus is arbitrarily multiplied by .0400 to reduce the magnitude of the loads to a more convenient level for the ensuing computations. Columns 6 and 8 are plotted in Figure C-2.

Spanwise distributions of the loads in the dynamic bending mode are then obtained in Table C-7(j). In Table C-7(k), the loads are converted to a form such as to permit direct comparison of the design conditions that will be generated with the statistically defined loads. The axis with respect to which moments are defined is rotated and shifted, and the loads are listed at the wing stations where the statistically defined values are available. The same two small adjustments discussed above in connection with Table C-6(f) are also made.

The derivation of the dynamic torsion mode elementary distribution is identical in form to that for the dynamic bending mode distribution. For the sake of brevity, only the final spanwise distribution of loads is presented for the dynamic torsion mode. These are shown as Tables C-8(a) and (b).

The one-g flight loads for mission analysis cases 201 and 202, at the wing stations and in the axis system required for stress analysis, are given in Table C-9. (One-g flight loads consistent with the dynamic analysis appear in columns 6 and 7 of Table C-1.)

In determining the elementary distributions for the Model 188, it was found that, at the resonant frequency, the model displacements and rotations tended to be reasonably well in phase. As a result, the various panel loads also tended to be reasonably well in phase. Consequently, when a set of panel loads was established by taking the modulus of each complex panel load, and these were integrated to give shears and torsions, and the shears in turn were integrated to give bending moments, the shears, torsions and bending moments thus obtained were all in good

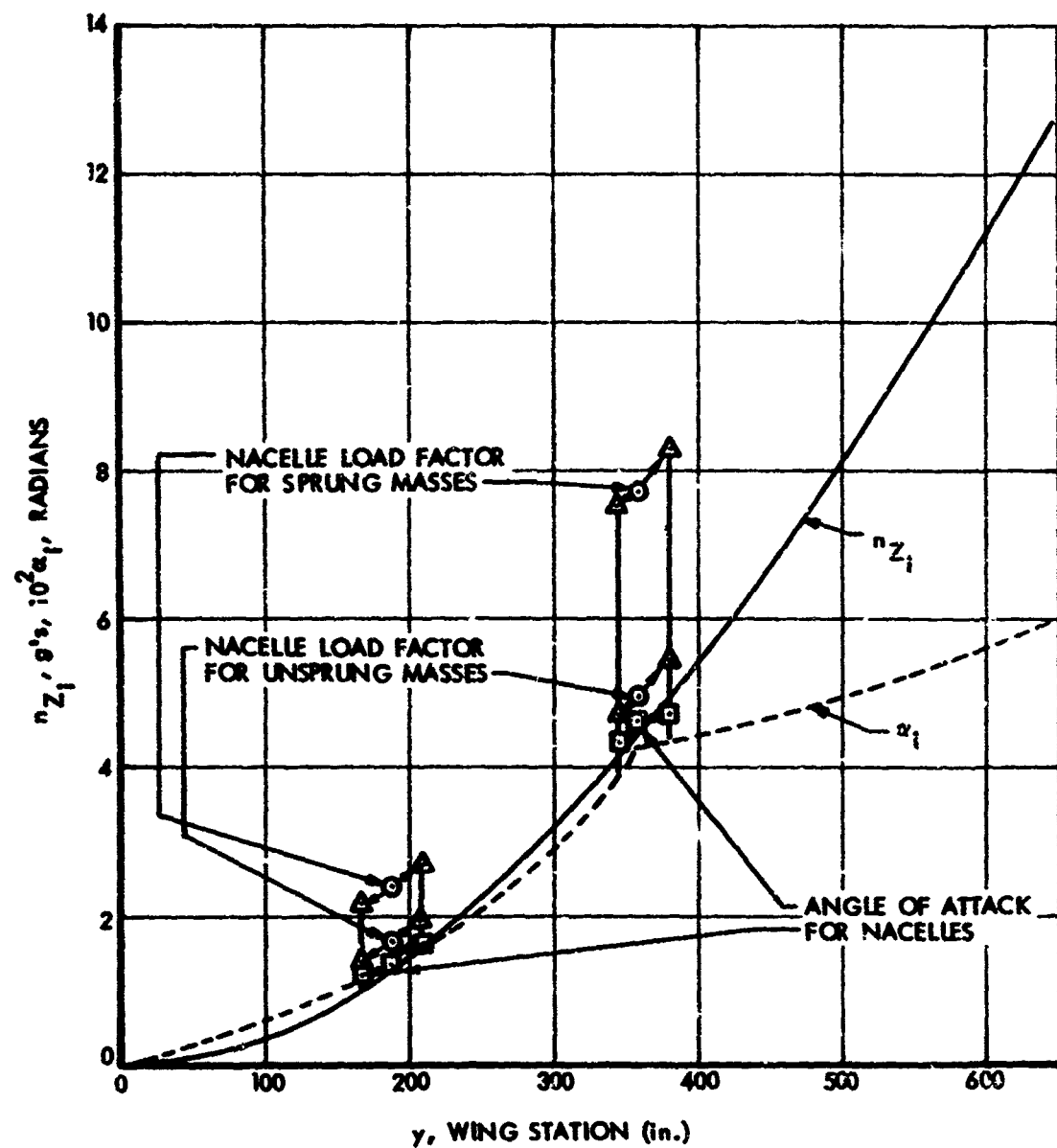


FIGURE C-2. SPANWISE VARIATION OF α AND n_z IN DYNAMIC BENDING MODE, MODEL 188 CASE 202

**TABLE C-7. CALCULATION OF DYNAMIC BENDING MODE
ELEMENTARY DISTRIBUTION, MODEL 188 CASE 202**

(a) INFORMATION FROM TRANSFER FUNCTION AT $f = 2.1$ CPS

W.S. (In.)	$\Delta S_{z1} \sim \text{lb}$ Panel Shear	$10^{-6} \Delta M_{y1} \sim \text{In.-lb}$ Panel Torsion	$\theta_{nac} \sim \text{Rad}$	$X_{nac} \sim \text{Chords}$
65	119453 + 63030 i	5.817 - 1.216 i		
101	36064 + 73300 i	2.292 - .693 i		
143	55049 + 22400 i	2.599 - 1.460 i		
188	-25752 + 26600 i	.812 - 2.641 i	.02259 - .02923 i	.000339 - .003009 i
239	35856 - 55400 i	1.961 - 2.836 i		
311	27708 - 138700 i	1.090 - 2.865 i		
359	-83699 - 620690 i	-7.551 - 78.778 i	.01589 - .10417 i	-.02448 - .07739 i
414	11617 - 119330 i	.179 - 1.414 i		
482	- 1172 - 99819 i	-.063 - .755 i		
550	-11244 - 89261 i	-.109 - .137 i		

(b) TRANSIENT AERODYNAMIC FUNCTION

$$K_{IM} = 1 - \left[\frac{.165 \Omega^2}{.0081 + \Omega^2} + \frac{.335 \Omega^2}{.36 + \Omega^2} \right] - i \left[\frac{.01485 \Omega}{.0081 + \Omega^2} + \frac{.201 \Omega}{.36 + \Omega^2} \right]$$

$$= .76876 - .18331 i$$

$K_{IM} = 1.0 - 0i$ (Macalle airloads tend to develop instantaneously since most of the resulting airload is due to the propeller.)

(c) COMPLEX WING ELASTIC DEFLECTIONS

$$\{ \phi_1 \} = [\delta_{T1,j}] * \{ \Delta M_{y1} \} = \begin{Bmatrix} .0086 - .1132 i \\ .0055 - .1856 i \\ .0084 - .2328 i \\ .0033 - .4062 i \\ -.0055 - .5754 i \\ -.0310 - .9079 i \\ -.0614 - 1.2338 i \\ -.0613 - 1.2511 i \\ -.0639 - 1.2645 i \\ -.0663 - 1.2676 i \end{Bmatrix}, \{ z_1 \} = [\delta_{B1,j}] * \{ \Delta S_{z1} \} = \begin{Bmatrix} -.085 - 8.4791 i \\ -.328 - 20.3721 i \\ -.849 - 40.7741 i \\ -1.84 - 70.81 i \\ -3.44 - 114.85 i \\ -6.77 - 194.02 i \\ -9.60 - 255.87 i \\ -13.2 - 332.9 i \\ -18.2 - 435.2 i \\ -23.7 - 542.4 i \end{Bmatrix}$$

NOTE: $[\delta_{T1,j}]$ and $[\delta_{B1,j}]$ are from Table C-5. ΔM_{y1} and ΔS_{z1} are from the above IM output.

TABLE C-7. CONTINUED
(d) COMPLEX LOCAL AERODYNAMIC ANGLE OF ATTACK

WING

$$\{\alpha_1\} = K_{LW} * \left(\{\phi_1\} - \frac{i\Omega}{c} \{z_1\} \right) = \begin{Bmatrix} -.0269 & -.0854 & 1 \\ -.0572 & -.1366 & 1 \\ -.1064 & -.2030 & 1 \\ -.1776 & -.2848 & 1 \\ -.2810 & -.3951 & 1 \\ -.4793 & -.6126 & 1 \\ -.6544 & -.8312 & 1 \\ -.7719 & -.8115 & 1 \\ -.9282 & -.7772 & 1 \\ -1.0896 & -.7324 & 1 \end{Bmatrix}$$

NACELLES

$$\{\alpha_j\} = K_{LN} * \left(\{\phi_1\} + \{\theta_{MAC}\} - \frac{i\Omega}{c} \{z_1\} \right) - i\Omega \{x_{MAC}\} = \begin{Bmatrix} 0 \\ 0 \\ 0 \\ -.1134 & -.43201 \\ 0 \\ -.6031 & -1.31121 \\ 0 \\ 0 \\ 0 \end{Bmatrix}$$

NOTE: $c = 168.7$ in.

TABLE C-7. CONTINUED
(e) COMPLEX LOCAL LOAD FACTORS

The location of the local masses relative to the wing elastic axis is obtained from the IBM input data. Positive l_x denotes that local mass is forward of the wing elastic axis.

W.S.	l_x wing - in.	l_x nac - in.
65	4.71	-
101	3.51	-
143	1.81	-
188	54.82	151.40
239	1.90	-
311	- 1.11	-
359	14.20	128.21
414	-11.11	-
482	- 8.50	-
550	- 8.40	-

$$p = 1.0 \quad v = 6752 \text{ in./sec.}$$

$$g = 386 \text{ in./sec}^2$$

$$\frac{p^2 v^2}{g c^2} = -.451 \quad \frac{p^2 v^2}{c^2} = -174$$

$$\frac{p^2 v^2}{g c} = -76.08$$

(f) WING TRANSLATIONAL LOAD FACTORS

$$\{n_{z_1}\} = -\frac{p^2 v^2}{g c^2} \left(\{z_1\} + \left[l_{x_{wing}} \right] \{ \phi_1 \} \right) = \begin{Bmatrix} -.020 & -4.0641 \\ -.133 & -9.4821 \\ -.376 & -18.6191 \\ -.750 & -41.9771 \\ -1.56 & -52.291 \\ -3.04 & -87.051 \\ -4.72 & -123.301 \\ -5.64 & -143.881 \\ -7.95 & -191.421 \\ -10.45 & -239.801 \end{Bmatrix}$$

(g) NACELLE TRANSLATION LOAD FACTORS

$$\{n_{z_j}\} = \frac{p^2 v^2}{g c^2} \left(\{z_1\} + \left[l_{x_{wing}} \right] \{ \phi_1 \} \right) - \frac{p^2 v^2}{g c} \{x_{nac}\} = \begin{Bmatrix} 0 \\ 0 \\ 0 \\ -.580 & -59.8991 \\ 0 \\ 0 \\ -9.74 & -192.671 \\ 0 \\ 0 \\ 0 \end{Bmatrix}$$

(h) NACELLE PITCH ACCELERATIONS

$$\{\ddot{\theta}_j\} = \frac{p^2 v^2}{c^2} \left(\{ \phi_1 \} + \{ \theta_{nac} \} \right) = \begin{Bmatrix} 0 \\ 0 \\ 0 \\ 4.50 & -75.761 \\ 0 \\ 0 \\ -13.45 & -232.811 \\ 0 \\ 0 \\ 0 \end{Bmatrix}$$

TABLE C-7. CONTINUED
(1) SUMMARY OF α , n_z , AND θ

(1)	(2)	(3)	(4)	(5)	(6)	(7)	(8)	(9)	(10)
V.S. In.	α_1 - Rad. Table C-7(d)	n_{z1} - g's Table C-7(f)	$\ddot{\theta}_1$ - Rad/Sec ² Table C-7(h)	$ \tau_{\alpha 1} $ Rad Modulus Of (2)	α_1 To Be Plotted .04 (5)	$ \tau_{n_{z1}} $ g's Modulus Of (3)	n_{z1} To Be Plotted .04 (7)	$ \tau_{\ddot{\theta}_1} $ Rad/Sec Modulus Of (4)	θ_1 To Be Plotted .04 (9)
Reference	Table C-7(d)	Table C-7(f)	Table C-7(h)	Modulus Of (2)	.04 (5)	Modulus Of (3)	.04 (7)	Modulus Of (4)	.04 (9)
65	- .0259- .08541	- .020- 4.0641		.0896	.0036	4.06	.16		
101	- .0572- .13661	- .133- 9.4821		.1481	.0059	9.48	.38		
143	- .1064- .20301	- .376- 18.6191		.2293	.0092	18.63	.75		
188	- .1776- .28481	- .750- 41.9771		.3357	.0134	41.20	1.65		
188N	- .1134- .43201	- .580- 59.8991	4.50- 75.761	.4412	.0176	59.92	2.40	77.95	3.04
239	- .2810- .39511	- 1.56- 52.291		.4850	.0194	52.30	2.09		
311	- .4793- .61261	- 3.04- 87.051		.7780	.0311	87.10	3.48		
359	- .6544- .83121	- 4.72- 123.301		1.0575	.0423	123.45	4.94		
359N	- .6031- 1.31121	- 9.74- 192.671	-13.45- 232.811	1.4245	.0570	193.00	7.72	233.0	9.32
414	- .7719- .81151	- 5.64- 143.881		1.1265	.0448	144.00	5.76		
482	- .9282- .77721	- 7.95- 191.421		1.2105	.0484	191.60	7.66		
520	- 1.0896- .73241	- 10.45- 239.801		1.3145	.0526	240.20	9.61		

TABLE C-7. CONTINUED
(J) LOADS AT STRESS ANALYSIS STATIONS

①	②	③	④	⑤	⑥	⑦	⑧	⑨	⑩	⑪	⑫	⑬	⑭	⑮
W	Z_{eq}	$\frac{\Delta s_A}{a_1}$	$\frac{s_1}{\theta \gamma_{eq}}$	$\frac{s_1}{\theta \gamma_{eq}}$	$\left(\frac{s_1}{\theta \gamma_{eq}}\right)_1$	$s_{1,corr}$	\ddot{s}_1	$\frac{10^{-6} \Delta s_A}{\theta}$	$\frac{\Delta s^6 N_A}{s_1}$	$\frac{\Delta s^6 N_A}{s_{eq}}$	s_{eq}	$\frac{\Delta \gamma}{2}$	$10^{-6} N_{s,LA,net}$	$10^{-6} N_{y,LA,net}$
Given	Given	Table C-3	Fig. C-2 ②	Fig. C-2 ②	Table C-4	$s_{1,net} \cdot ③$	Table C-7	Table C-4	Table C-3	Table C-4	$\frac{1}{2} ⑩ \cdot ⑫$	Given	∞	$\frac{1}{2} ⑬ \cdot ⑭$
0	13	116880	.0016	.09	740	-1.96			-2.652	-.0489	43148	32.5	16.762	2.7798
65	83	63490	.0047	.28	2948	-1.77			-1.347	-.1344	44412	18.0	15.916	2.7000
101	119	66030	.0078	.51	1508	-1.54			-1.346	-.0874	49331	18.0	14.229	2.4685
137	152	56780	.0102	.83	700	-1.22			-1.110	-.0381	50368	15.0	12.434	2.344
167	167	0	-	1.40	1179	-.65			0	.0270	50844	-	10.919	2.3092
167	167	23110	.0122	2.13	1595	.08	3.04	.02370	3.700	.1915	51410	-	10.919	2.3803
167	173	4090	.0122	1.10	447	-.95			-.077	-.0093	50950	6.0	10.919	2.8121
179	185	5760	.0132	1.25	350	-.80			-.107	-.0074	51345	9.0	10.305	2.8042
197	203	4270	.0148	1.50	167	-.55			-.078	-.0035	51589	6.0	9.380	2.1997
209	209	0	-	1.96	1108	-.09			0	.0183	51558	-	8.761	2.1989
209	209	23110	.0158	2.71	1985	.66	3.04	.02370	3.700	.1915	51657	-	8.761	2.2000
209	224	55030	.0170	1.82	1157	-.23			-.945	-.0949	49990	15.0	8.761	1.9676
239	257	68650	.0216	2.42	1566	.37			-1.079	-.0700	49381	18.0	7.272	1.9717
275	284	31320	.0260	2.90	638	.85			-.514	-.0276	47588	9.0	5.531	2.0809
293	311	63490	.0311	3.46	765	1.41			-1.015	-.0387	46031	18.0	4.690	2.0517
309	331	29400	.0370	4.00	257	1.95			-.385	-.0108	48978	8.5	3.088	2.1354
346	346	0	-	4.69	351	2.64			0	-.0034	41537	-	2.370	2.1707
346	346	31300	.0433	7.47	2378	5.42	9.32	.02304	4.139	-.2157	40810	-	2.370	2.1797
346	363	22740	.0486	4.54	582	2.49			.336	-.0213	28566	17.0	2.370	.6937
360	360	0	-	5.45	218	3.40			0	-.0080	25086	-	1.4813	.7384
360	360	19580	.0471	8.28	1472	6.23			2.686	.1335	25144	-	1.4813	.7433
360	380	16680	.0435	5.17	152	3.12			-.261	-.0070	19681	8.5	1.4813	-.8577
397	414	51640	.0448	5.80	165	3.75			-.703	-.0073	13777	17.0	1.8361	-.8577
431	448	42330	.0463	6.70	155	4.65			-.943	-.0063	10945	17.0	.8176	-.8068
465	482	36400	.0483	7.63	125	5.58			-.439	-.0043	8164	17.0	.4944	-.1584
499	516	25630	.0502	8.60	130	6.55			-.334	-.0041	5709	17.0	.2956	-.1072
533	558	27030	.0530	9.90	170	7.85			-.284	-.0050	3370	25.5	.1048	-.0656
594	592	7620	.0553	10.96	20	8.91			-.071	-.0006	600	5.0	.0090	-.0093

$$s_{1,net} = \frac{-\sum ③ - \sum ⑤}{\sum \text{Cross Weight}} = \frac{-1974 - 69210}{15750} = -2.05$$

$$s_{eq} = \frac{1}{2} (⑩ + ⑫) = ⑬$$

TABLE C-7. CONCLUDED
(K) LOADS AT DYNAMIC ANALYSIS STATIONS

①	②	③	④	⑤	⑥	⑦	⑧	⑨	⑩	⑪	⑫
Panel	Lump Station	Wing Station	S_z In	ΔS_z In	S_z Adj. In	$10^{-6} M_z$ In.-lb	$10^{-6} M_{yLA}$ In.-lb	$10^{-6} M_y$ In.-lb	$10^{-6} M_{yLA}$ In.-lb	ΔX_{TM-LA} In.	$10^{-6} M_{yLA}$ In.-lb
Given	Given	Given	Table C-7(j)	Refer To Note 1	④ + ⑤	Refer To Note 2	Table C-7(j)	Refer To Note 1	⑧ + ⑨	67.8 - .0842 ⑩	Refer To Note 3
2	101	83	16872	-----	16872	14,995	2,2801	-----	2,2801	60.81	4,1668
3	143	119	19890	- 43	19847	13,2193	2,1023	+ 0009	2,1032	57.78	4,1046
4	186	137	50644	+ 29	50673	10,8077	2,0050	- .0006	2,0044	53.74	4,1145
5	239	209	49990	-140	49850	8,6968	1,7987	+ 0085	1,7612	50.20	3,7340
6	311	275	47308	-----	47308	5,4953	1,8120	-----	1,8120	44.65	3,6675
7	359	346	41537	408	42145	2,3143	1,9618	- .0092	1,9526	38.67	3,5994
8	414	380	19061	310	14751	1,4566	- .8999	+ 0044	- .8945	35.80	.1120
9	482	448	9509	-----	9509	.6319	- .1796	-----	- .1796	30.08	.0538
10	550	516	4510	-----	4510	.1544	- .0854	-----	- .0854	24.35	.0125

Note 1: In the ten degree-of-freedom analysis, inertia loads are defined at the wing stations listed in column ③. Airloads, however, were inadvertently defined at wing stations 83, 122, 165, 5, 213.5, 275, 335, 386.5, 448, and 516. To provide consistency with the mission analysis loads, the slight correction is applied.

Note 2: To provide consistency with the mission analysis results, the bending moment is integrated in a manner consistent with the ten degree-of-freedom program.

$$M_x = \sum_{i=1}^{10} \left[\textcircled{5}_i \textcircled{3}_{1,i} \textcircled{2}_{1,i} + \textcircled{6}_i \textcircled{2}_{1,i} \textcircled{3}_{1,i} \right]$$

$$\text{Note 3: } M_{yLA} = .9954 M_{yLA} - .0842 M_{yLA} + S_z \Delta X_{TM-LA}$$

Beam Shear Flows

$$\begin{aligned} q_{78 \ 83} &= .021678_2 - 26(10^{-6} M_x) + 164(10^{-6} M_y) = 1310.1 \text{ lb/in.} \\ q_{78 \ 85} &= .010928_2 + 18(10^{-6} M_x) + 163(10^{-6} M_y) = 61.6 \text{ lb/in.} \\ q_{78 \ 316} &= .031168_2 - 70(10^{-6} M_x) + 390(10^{-6} M_y) = 2551.1 \text{ lb/in.} \\ q_{78 \ 316} &= .026368_2 + 45(10^{-6} M_x) - 390(10^{-6} M_y) = 393.1 \text{ lb/in.} \end{aligned}$$

TABLE C-8. DYNAMIC TORSION MODE ELEMENTARY
DISTRIBUTION, MODEL 188 CASE 202

(a) LOADS AT STRESS ANALYSIS STATIONS

①	②	③	④	⑤	⑥	⑦	⑧	⑨	⑩	⑪	⑫	⑬	⑭	⑮			
WS	γ_{ag}	$\frac{\Delta S_{HA}}{c_1}$	a_1	n_{H_1}	$\left(\Delta \frac{S_{HA}}{a_1}\right)_{1/2}$	$n_{H_{correct}}$	$\ddot{\theta}_1$	$\frac{10^{-6} \Delta \frac{S_{HA}}{g}}{\ddot{\theta}_1}$	Table C-9	$\frac{10^{-6} W_{HA}}{a_1}$	Table C-3	Table C-4	$\frac{\Delta 10^{-6} W_{HA}}{n_{H_1}}$	$S_{H_{int}}$	$\frac{L}{2}$	$10^{-6} M_{LA_{int}}$	$10^{-6} W_{LA_{int}}$
Given	Given	Table C-3			Table C-4	$n_{Total} + 1$		Table C-9		Table C-3	$\frac{1}{2} \frac{\Delta 10^{-6} W_{HA}}{g}$	$\frac{1}{2} \frac{\Delta 10^{-6} W_{HA}}{g}$	$\frac{\Delta 10^{-6} W_{HA}}{n_{H_1}}$	$S_{H_{int}}$	Given	$10^{-6} M_{LA_{int}}$	$10^{-6} W_{LA_{int}}$
0	33	116820	-.0008	.07	740	-.31				-2.652			-.0429	7935	32.5	4.2998	-2.0706
65	83	63490	-.0022	.23	2948	-.15				-1.347			-.1344	8258	18.0	3.7735	-2.0860
101	119	66030	-.0033	.46	1008	.08				-1.346			-.0874	8843	18.0	3.4657	-2.1091
137	152	56720	-.0045	.74	700	.36				-1.110			-.0381	8777	15.0	3.1450	-2.1066
167	167	0	-	.11	1179	-.27				0			.0170	8981	-	2.8756	-2.0979
167H	167	25110	-.0073	-1.80	1925	-2.18	-9.29	.01570		3.700			.1915	9299	-	2.8756	-2.0933
167*	173	4090	-.0054	.98	447	.60				-.077			-.0093	13679	6.0	2.8756	-1.5186
179	185	5760	-.0059	1.12	350	.74				-.107			-.0074	13433	9.0	2.7230	-1.5134
197	203	4270	-.0065	1.35	167	.97				-.078			-.0035	13808	6.0	2.4732	-1.5086
209	209	0	-	.65	1108	.27	-8.29	.01570		0			.0123	13073	-	2.3155	-1.5057
209H	209	25110	-.0082	-1.27	1925	-1.65				3.700			.1915	12774	-	2.3155	-1.5090
209*	224	55030	-.0071	1.68	1157	1.30				-.985			-.0547	16171	15.0	2.3155	-1.0303
239	257	54650	-.0083	2.29	1566	1.91				-1.079			-.0700	15058	18.0	1.8471	-.9699
275	284	31320	-.0094	2.82	638	2.44				-.514			-.0876	12987	9.0	1.3495	-.8412
293	311	63490	-.0108	3.43	765	3.05				-1.015			-.0327	11325	18.0	1.1343	-.7787
329	337	25400	-.0120	4.17	297	3.79				-.385			-.0108	9677	8.5	.7563	-.6899
346	346	0	-	3.70	351	3.32	-15.99	.01384		0			-.0034	9008	-	.5974	-.6536
346H	346	31300	-.0169	.47	2378	.09				4.339			.2157	7843	-	.5974	-.6410
346*	363	22740	-.0138	4.86	582	4.48				.336			-.0213	8158	17.0	.5974	-.3668
360	380	0	-	4.61	218	4.23	-15.99	.00896		0			-.0020	5236	-	.3697	-.8662
360H	380	19340	-.0183	1.37	1472	.99				2.646			.1335	4315	-	.3697	-.8570
380*	388	18680	-.0145	5.34	152	5.16				-.261			-.0070	3212	8.5	.3697	-.8041
397	414	51640	-.0153	6.26	165	5.88				-.703			-.0073	2897	17.0	.3195	-.1717
431	448	42330	-.0164	7.21	155	6.83				-.543			-.0063	2917	17.0	.2309	-.1396
465	482	36400	-.0176	8.20	125	7.82				-.439			-.0043	2153	17.0	.1515	-.1054
499	516	29630	-.0182	9.19	130	8.81				-.334			-.0041	1816	17.0	.0840	-.0795
533	558	27090	-.0204	10.42	170	10.74				-.284			-.0050	1210	25.5	.0386	-.0495
584	592	7680	-.0217	11.43	20	11.05				-.071			-.0006	56	5.0	.0028	-.0051

$$* n_{H_{tot}} = \frac{-\sum \frac{S_{HA}}{c_1} - \sum \frac{S_{HA}}{c_1}}{\frac{1}{2} \text{ Gross Weight}} = \frac{-7612 - 24211}{53750} = -.34$$

$$n_{H_{tot}} = \frac{1}{n} \left(\frac{S_{HA}}{c_1} + \frac{S_{HA}}{c_1} \right) \frac{1}{n}$$

TABLE C-8. CONCLUDED
(b) LOADS AT DYNAMIC ANALYSIS STATIONS

①	②	③	④	⑤	⑥	⑦	⑧	⑨	⑩	⑪	⑫
Panel	Wing Station	Wing Station	S_z lb	ΔS_z^* lb	S_z Adj. lb	$10^{-6} M_{TA}$ in.-lb	$10^{-6} M_{TA}$ in.-lb	$10^{-6} M_{TA}$ in.-lb	$10^{-6} M_{TA}$ in.-lb	ΔX_{TA-LA} in.	$10^{-6} M_{TA}$
Given	Given	Given	Table C-8(a)	Refer To Note 1	④ + ⑤	Refer To Note 2	Table C-8(a)	Refer To Note 1	⑧ + ⑨	67.8 - .0842 3	Refer To Note 3
2	101	83	8549	----	8549	3.5333	-1.4784	----	-1.4784	60.81	-1.3599
3	143	119	8909	+ 18	8927	3.2187	-1.4897	-.0004	-1.4891	57.78	-1.8582
4	188	167	8981	- 13	8968	2.7892	-1.4787	+ 0.003	-1.4784	53.74	-1.8452
5	239	209	16171	+ 59	16230	2.2601	-.6715	-.0011	-.6786	50.20	-.4045
6	311	275	12567	----	12567	1.3200	-.4824	----	.4824	44.65	-.3886
7	359	346	9008	-197	8811	.5585	-.2948	+ 0.030	-.2918	38.67	-.3559
8	414	380	3212	403	3315	.3744	-.2041	-.0015	-.2096	35.00	-.1177
9	482	448	2335	----	2335	.1823	-.1225	----	-.1225	30.08	-.0672
10	550	516	1513	----	1513	.0514	-.0645	----	-.0645	24.35	-.0318

Note 1: In the ten degree-of-freedom analysis, inertia loads are defined at the wing stations listed in column ③. Airloads, however, were inadvertently defined at wing stations 83, 122, 155, 5, 213, 5, 275, 335, 368, 5, 448, and 516. To provide consistency with the mission analysis loads, the slight correction is applied.

Note 2: To provide consistency with the mission analysis results the bending moment is integrated in a manner consistent with the ten degree-of-freedom program.

$$M_x = \sum_{\text{Tip}}^{\text{Root}} \left[\textcircled{6}_{1,4} (\textcircled{3}_{1,4} - \textcircled{2}_1) + \textcircled{6}_1 (\textcircled{2}_1 - \textcircled{3}_1) \right]$$

Note 3: $M_{TA_1} = .9984 M_{TA_1} - .0842 M_{x_1} + 3 S_{z_1} \Delta X_{TA-LA}$

Beam Shear Flows

$$\begin{aligned}
 q_{TB \ 83} &= .021578_2 - .35(10^{-6} M_{x_1}) + 164(10^{-6} M_{y_1}) = -213.3 \text{ lb/in.} \\
 q_{TB \ 83} &= -.018928_2 + 18(10^{-6} M_{x_1}) + 163(10^{-6} M_{y_1}) = -402.9 \text{ lb/in.} \\
 q_{TB \ 346} &= .031168_2 - 70(10^{-6} M_{x_1}) + 390(10^{-6} M_{y_1}) = 96.7 \text{ lb/in.} \\
 q_{TB \ 346} &= -.026368_2 + 45(10^{-6} M_{x_1}) + 390(10^{-6} M_{y_1}) = -345.9 \text{ lb/in.}
 \end{aligned}$$

TABLE C-9. ONE-g FLIGHT LOADS AT STRESS ANALYSIS STATIONS, MODEL 188

W.S.	Case 201			Case 202		
	S_z lb	$10^{-6}M_x$ In.-lb	$10^{-6}M_y$ In.-lb	S_z lb	$10^{-6}M_x$ In.-lb	$10^{-6}M_y$ In.-lb
65	16373	4.547	-1.1203	20248	4.490	-2.4303
101	15174	3.957	-1.0860	17863	3.781	-2.2450
137	13309	3.455	-1.0182	14910	3.202	-2.0372
167-	10979	3.065	-.9228	11862	2.774	-1.8401
167+	14083	3.065	-.9046	14966	2.774	-1.7771
179	13118	2.885	-.8575	13819	2.585	-1.6965
197	11768	2.701	-.7868	12248	2.390	-1.5799
209-	10630	2.527	-.7395	10946	2.208	-1.5006
209+	13663	2.527	-.7087	13979	2.208	-1.4290
239	11927	2.111	-.6286	11796	1.788	-1.2646
275	10598	1.728	-.6008	9889	1.420	-1.1516
293	9710	1.531	-.5695	8817	1.232	-1.0799
329	7655	1.241	-.5031	6328	.9853	-.9345
346-	6787	1.117	-.4678	5300	.8876	-.8657
346+	9516	1.117	-.4308	8029	.8876	-.7174
380-	7567	.8201	-.3629	5989	.6425	-.5938
380+	9257	.8201	-.3152	7679	.6	-.4929
397	8378	.6749	-.2861	6804	.5263	-.4405
431	6334	.4179	-.2182	4950	.3148	-.3386
465	4437	.2215	-.1589	3373	.1589	-.2461
499	2713	.1109	-.1025	2004	.0794	-.1689
533	1461	.0595	-.0605	1058	.0503	-.0981
584	102	.0045	-.0080	66	.0044	-.0138

agreement with the values given by the modulus of the complex shears, torsions, and bending moments respectively. It is conceivable, however, that in some circumstances the panel loads may be less closely in phase. In such a situation, more than one elementary distribution might be required for each mode. It is believed, however, that such distributions could be obtained without undue difficulty. The procedure would be to retain a_i and n_{zi} in complex form and then obtain panel shears and torsions likewise in complex form. These would then be expressed in the form of modulus and phase angle. Next, the panel loads would be grouped roughly by phase angle. For each group, a representative phase angle would be selected, and the in-phase components of all panel loads determined. Integration spanwise would then give the modal-load distribution. Some experimentation might be required to obtain satisfactory groupings of the panel loads; and checks would be required - either at this stage or later - to assure that in matching the loads in one part of the wing the desired loads at other points were not exceeded.

In order to give added confidence that all necessary ingredients have been included in the determination of the elementary distributions, it is pertinent to compare the loads defined by each elementary distribution with the total loads as taken directly from the transfer functions at the respective frequencies. Exact agreement is not to be expected, of course, since at any one resonant frequency the total load contains some contribution from other modes as well as predominant contribution from the resonant mode. However, as indicated by the plots in Figure 9-3, the contributions of the non-resonant modes should generally be fairly small.

Such a comparison is shown in Table C-10. The loads in column 3 are those comprising the static elementary distribution of table C-6(f). For comparison, column 4 gives the modulus of loads per "g" as obtained from the transfer functions at a forcing frequency of .1 cps. Similarly, column 5 is taken from Table C-7(k), and thus represents the dynamic bending mode elementary distribution. The modulus of the loads obtained from the transfer functions at a forcing frequency of 2.1 cps appears in column 6; the level of loads in column 6, however, is adjusted such that the shear at wing station 346 is the same as that in column 5. Loads for the torsion elementary distribution taken from Table C-8(b) appear in column 7. The corresponding loads from the transfer functions at a forcing frequency of 4.4 cps are shown in column 8. Here the level is adjusted such that shear at wing station 167 is the same as that in column 7. The minus sign on the loads from the transfer functions is used to denote a load modulus that is relatively 180° out of phase.

In comparing column 3 to column 4, and column 5 to column 6, it is seen that the agreement is excellent. The comparison of columns 7 and 8 shows fairly good agreement for spanwise shear and bending and for torsion

TABLE C-10. COMPARISON OF ELEMENTARY DISTRIBUTIONS
WITH LOADS INDICATED BY TRANSFER FUNCTION PEAKS,
MODEL 188

①	②	③	④	⑤	⑥	⑦	⑧
		Static Mode		Dynamic Bending Mode		Dynamic Torsion Mode	
Load	W.S. in.	Elementary Distribution	Transfer Function	Elementary Distribution	Transfer Function	Elementary Distribution	Transfer Function
	Ref.	Table C-6(f)	IBM Output	Table C-7(k)	IBM Output	Table C-8(b)	IBM Output
S _z Wing Shear	83	11484	11133	46872	45260	8549	7794
	119	10407	10236	49807	48526	8327	8473
	167	7953	7984	50673	49583	8968	8968
	209 ⁺	11744	11597	49850	50748	16230	14115
	275	9572	9451	47388	48304	12587	10860
	346	6497	6217	42145	42145	8811	7282
	380 ⁺	9037	8732	14751	13932	3315	3904
	448	5436	5123	9505	8560	2335	2821
	516	2191	2105	4540	4064	1513	1854
10 ⁻⁶ Mx Wing Bending Moment About Elastic Axis	83	3.617	3.532	14.960	14.787	3.533	3.214
	119	3.223	3.147	13.219	13.103	3.219	2.755
	167	2.783	2.710	10.808	10.750	2.789	2.538
	209 ⁺	2.369	2.299	8.697	8.644	2.260	2.054
	275	1.672	1.611	5.495	5.384	1.320	1.241
	346	1.100	1.053	2.314	2.170	.5585	.6138
	380 ⁺	.8259	.7887	1.457	1.332	.3744	.4483
	448	.3338	.3175	.632	.567	.1823	.2215
	516	.0745	.0716	.154	.139	.0514	.0630
10 ⁻⁶ My Wing Torsion Moment About Elastic Axis	83	.3357	.4062	4.1668	4.1374	-1.8699	-2.2180
	119	.2245	.2987	4.1646	4.1060	-1.8582	-2.1785
	167	.0768	.1615	4.1145	4.0432	-1.8452	-2.1287
	209 ⁺	.3495	.3928	3.7340	3.9257	.4045	-1.0225
	275	.2070	.2464	3.6675	3.7923	-.3886	-.9440
	346	.0839	.1148	3.5894	3.6629	-.3559	-.8648
	380 ⁺	.1621	.1691	.1120	.1042	-.1177	-.1742
	448	.0844	.0841	.0543	.0403	-.0672	-.0927
	516	.0289	.0276	.0125	.0062	-.0318	-.0412

inboard of the inboard nacelle. The agreement for torsion outboard of the inboard nacelle, however, is relatively poor. Thus with respect to torsions outboard of the inboard nacelle, it appears that, for the dynamic torsion mode, the loads due to dynamic overtravel in the mode would not be adequately approximated by the total loads developed at the resonant frequency. It is also pertinent to observe, however, that the contribution of this mode to the total mean square value of the torsions outboard of the inboard nacelle is comparatively small, as indicated by Table C-2. Consequently, with respect to these loads, considerable inaccuracy in obtaining the elementary distribution could be tolerated.

C.4 Upending Conditions

With the mission analysis loads of Table C-1, the elementary distributions of Tables C-6, C-7, and C-8, and the one-g flight loads of Table C-9 all available, design loads required for the stress analysis of the wing can now be generated. This is accomplished in Tables C-11 through C-14.

In Table C-11, the statistically defined design load levels which it is desired to envelope appear in column 3. These are taken from column 3 of Table C-1. As pointed out earlier, the incremental and one-g loads can be handled independently. Consequently, the one-g loads for mission analysis cases 201 and 202 are subtracted from the net mission analysis loads of column 3 to define the incremental design level loads to be matched. These statistically defined loads appear in columns 6 and 7 and are designated L_g . Columns 6 and 7 are identical to columns 8 and 10, respectively, in Table C-1.

The elementary distributions obtained in Tables C-6, C-7, and C-8 are shown in columns 8 - 10, respectively. These distributions are designated the E_1 , E_2 , and E_3 distributions. The values of the 31 load quantities for the three distributions are also designated E_1 , E_2 , and E_3 , in order that a single column heading can apply collectively to shears, bending moments, torsions, and front and rear beam shear flows.

The statistically defined loads, L_g , are now to be enveloped by one or more design conditions. Each of these design conditions will be made up of an appropriate combination of the three elementary distributions. The contribution of each elementary distribution will be defined by a value of its respective coefficient, a_1 , a_2 , or a_3 ; the complete set of loads comprising the conditions is then given by the expression,

$$L_D = a_1 E_1 + a_2 E_2 + a_3 E_3$$

For each additional design condition, a new set of values of the coefficients is determined.

In generating the enveloping conditions, it is, of course, desired that as many of the L_S values as possible be matched by the corresponding L_D values defined by a single set of the loading coefficients, a_1 , a_2 , and a_3 . To facilitate determining appropriate values of the loading coefficients, each load for the elementary distributions is divided by its corresponding design level load, L_S . The resulting ratios are designated \bar{E}_1 , \bar{E}_2 , and \bar{E}_3 respectively. The values obtained using the L_S values of column 6 are listed in columns 11, 12, and 13; the values obtained using the L_S values of column 7 are listed in columns 14, 15, and 16.

For the first design condition, torsions in the outer wing will be matched. Outer wing torsion is predominantly a static loading and is produced by mission analysis case 201. As a result, the increment loads to be matched are those of column 6 and can be reproduced by use of the E_1 distribution only, as given by column 8. The required "amount" of this distribution, to be defined by a value of the coefficient a_1 , can be determined by looking at the \bar{E}_1 values in column 11. For torsion at WS 380, 448, and 516, the \bar{E}_1 values are .689, .715, and .734 respectively. The average is approximately .715. The indicated value of a_1 is therefore $1/.715 = 1.40$. Thus the incremental loads for Condition I are simply:

$$1.40 E_1$$

A comparison of the complete Condition I loads thus defined with the statistically defined design level incremental loads is then shown by the ratios,

$$\frac{L_D}{L_S} = \frac{1.40 E_1}{L_S} = 1.40 \bar{E}_1$$

These ratios are shown in column 17. It is seen that the ratios for the outer wing torsions are close to unity, indicating good agreement. For all other loads, the ratio is considerably below unity. In particular, outer wing shear and bending are about 70% of the mission analysis values. This result is consistent with column 12 of Table C-1, which indicates that, whereas the outer wing incremental torsion is produced almost entirely by case 201, the total increments in outer wing shear and bending moment, relative to the case 201 one-g values, are contributed largely by other cases.

TABLE C-11. DETERMINATION OF LOADING COEFFICIENTS FOR
UPBENDING DESIGN CONDITIONS, MODEL 188

(a) COLUMNS 1 - 16

Case		Mission Analysis Loads					Elementary Distributions			Elementary Distribution Ratios					
(1)	(2)	(3)	(4)	(5)	(6)	(7)	(8)	(9)	(10)	Relative to Case 201			Relative to Case 202		
Load		Net Loads	Case-0 Load Case 201	Case-0 Load Case 202	L ₁ Case 201	L ₁ Case 202	E ₁	E ₂	E ₃	E ₁	E ₂	E ₃	E ₁	E ₂	E ₃
	Ref. W.S. (in.)	Table C-1 Col. 3	Table C-1 Col. 4	Table C-1 Col. 5	Table C-1 Col. 6	Table C-1 Col. 7	Table C-6(f)	Table C-7(h)	Table C-8(h)	8/6	9/6	10/6	8/7	9/7	10/7
Wing Shear	83	49200	15773	-3655	33427	30845	11465	46872	8549	.343	1.402	.256	.381	1.555	.284
	119	46700	14241	16386	32435	30315	10407	49887	8927	.321	1.534	.275	.343	1.643	.294
	167	39800	10979	11852	28821	27938	9553	50673	8968	.346	1.758	.311	.285	1.814	.321
	209	47600	13663	13979	33937	33621	11744	43850	16230	.345	1.469	.478	.349	1.483	.483
	275	39500	10998	9089	28902	25611	9572	47388	12587	.331	1.640	.436	.323	1.600	.425
	346	28700	6787	5306	21913	23400	6457	42145	8811	.296	1.923	.402	.278	1.801	.376
	380	27700	9257	7673	18443	20021	9437	14751	3315	.489	.800	.180	.451	.737	.166
	448	16200	5385	4161	10825	12039	4436	9505	2335	.502	.879	.216	.451	.789	.194
Wing Bending Moment About Elastic Axis	516	6450	2087	1531	4363	4919	2191	4544	1513	.502	1.040	.347	.445	.939	.308
	83	13.80	4.144	3.983	9.66	9.877	3.617	14.960	3.533	.374	1.549	.346	.366	1.515	.358
	119	12.17	3.604	3.298	8.57	8.872	3.223	13.219	3.219	.376	1.543	.376	.363	1.490	.363
	167	10.10	2.976	2.609	7.03	7.491	2.783	10.808	2.789	.391	1.517	.381	.371	1.442	.372
	209	8.30	2.498	2.080	5.84	6.220	2.369	8.697	2.260	.405	1.489	.387	.381	1.398	.363
	275	5.95	1.671	1.318	3.88	4.232	1.672	5.495	1.320	.431	1.417	.340	.395	1.298	.312
	346	3.31	1.074	.8115	2.24	2.497	1.100	2.314	.5585	.492	1.035	.249	.440	.546	.283
	380	2.44	.791	.5986	1.65	1.841	.8239	1.457	.3744	.501	.883	.227	.449	.731	.203
Wing Torsion Moment About Elastic Axis	448	.968	.303	.2114	.757	.7566	.3338	.632	.1823	.502	.950	.274	.441	.835	.241
	516	.229	.078	.0534	.151	.1736	.0745	.154	.0514	.493	1.080	.340	.444	.877	.293
	83	1.130	-.498	-1.519	1.628	2.049	.3357	4.167	-1.870	.206	2.599	-1.149	.127	1.573	-.706
	119	1.020	-.537	-1.480	1.957	2.500	.2845	4.165	-1.858	.144	2.675	-1.193	.090	1.666	-.743
	167	.900	-.587	-1.429	1.887	2.389	.0768	4.114	-1.845	.092	2.767	-1.241	.033	1.767	-.792
	209	1.260	-.233	-.908	1.493	2.168	.3495	3.734	-.404	.234	2.501	-.271	.161	1.722	-.187
	275	1.140	-.271	-.826	1.411	1.966	.2070	3.668	-.389	.147	2.600	-.276	.105	1.865	-.198
	346	1.070	-.298	-.732	1.368	1.802	.0839	3.589	-.356	.061	2.623	-.260	.047	1.992	-.197
Mean Shear Flow	380	.153	-.052	-.270	.235	.453	.1621	.112	-.113	.689	.476	-.502	.358	.247	-.260
	448	.065	-.053	-.186	.118	.251	.0844	.0538	-.0672	.715	.456	-.569	.336	.214	-.258
	516	.002	-.037	-.101	.039	.103	.0089	.0125	-.0318	.734	.317	-.607	.281	.121	-.309
	83 FB	815	152	62	663	753	210	1310	-213	.317	1.976	-.311	.279	1.740	-.243
Mean Shear Flow	83 RB	-785	-305	-538	-480	-247	-37	62	-403	.202	-.129	.840	.393	-.251	1.631
	346 FB	1080	20	-177	1066	1257	158	2551	97	.149	2.407	.091	.126	2.089	.077
	346 RB	-690	-247	-382	-443	-301	-89	393	-346	.201	-.887	.781	.256	-1.306	1.150

TABLE C-11. CONCLUDED

(b) COLUMNS 17 - 32

Ratio of Design Net Loads to M.A. Net Loads								Design Net Loads				Ratio of Design Net Loads to M.A. Net Loads			
(17)	(18)	(19)	(20)	(21)	(22)	(23)	(24)	(25)	(26)	(27)	(28)	(29)	(30)	(31)	(32)
Cond. I	First Iter. Cond. II	Second Iter. Cond. II	Cond. II	First Iter. Cond. III	Cond. III	First Iter. Cond. IV	Cond. IV	Net Loads Cond. I	Net Loads Cond. II	Net Loads Cond. III	Net Loads Cond. IV	Ratio Cpn'd. I	Ratio Cond. II	Ratio Cond. III	Ratio Cond. IV
1.40 (11)	1.742 (14) +.180 (15) +.251 (16)	1.80 (14) +.17 (15) +.23 (16)	1.88 (14) +.16 (15) +.20 (16)	.756 (14) +.448 (15) -.042 (16)	.80 (14) +.45 (15)	1.095 (14) +.458 (15) -.187 (16)	.40 (14) +.47 (15) -.25 (16)	6 (17) + (4)	7 (20) + (5)	7 (22) + (5)	7 (24) + (5)	25 (25) + (3)	26 (26) + (3)	27 (27) + (3)	28 (28) + (3)
.480	1.015	1.015	1.022	.973	1.004	1.076	.812	31850	49854	49335	43541	.65	1.01	1.00	.88
.449	.967	.964	.967	.983	1.014	1.073	.836	28811	45706	47125	41726	.62	.98	1.01	.89
.386	.903	.895	.890	1.014	1.044	1.082	.886	22113	36715	41027	36618	.56	.92	1.03	.92
.484	.996	.991	.990	.908	.947	.971	.716	30105	47280	45807	38049	.63	.99	.96	.80
.463	.957	.951	.949	.943	.979	1.007	.775	23999	37984	38871	32843	.61	.96	.98	.83
.414	.903	.893	.885	1.001	1.032	1.058	.863	15883	26020	29463	25829	.55	.91	1.03	.90
.685	.960	.975	1.000	.771	.693	.800	.485	21909	27692	21547	17398	.79	1.00	.78	.63
.703	.976	.990	1.014	.686	.716	.819	.503	12995	16368	12787	10219	.80	1.01	.79	.63
.703	1.019	1.031	1.047	.744	.772	.860	.535	5154	6679	5327	4163	.80	1.04	.83	.65
.524	1.000	.999	1.002	.940	.975	1.028	.769	9.208	13.823	13.549	11.518	.67	1.00	.98	.83
.526	.992	.990	.994	.927	.961	1.012	.755	8.116	12.116	11.825	9.995	.67	1.00	.97	.82
.547	.999	.998	1.004	.912	.946	.998	.734	6.872	10.128	9.699	8.105	.68	1.00	.96	.80
.567	1.006	1.007	1.012	.899	.934	.990	.719	5.775	8.377	7.889	6.550	.70	1.01	.95	.79
.603	1.000	1.003	1.013	.867	.900	.969	.690	4.012	5.605	5.128	4.239	.72	1.01	.92	.76
.689	.990	1.001	1.020	.738	.769	.864	.555	2.614	3.361	2.733	2.199	.79	1.02	.83	.66
.701	.975	.989	1.011	.685	.715	.816	.501	1.947	2.459	1.915	1.520	.80	1.01	.78	.62
.703	.979	.991	1.011	.697	.729	.820	.509	.770	.9765	.7628	.5564	.80	1.01	.79	.62
.690	.970	.980	.997	.701	.734	.811	.509	.1823	.2284	.1823	.1427	.80	1.00	.80	.62
.288	.327	.334	.349	.830	.809	.991	.966	-.0280	-.5952	.625	1.041	-.02	-.53	.55	.92
.202	.270	.274	.287	.845	.821	1.000	1.005	-.2227	-.7632	.574	1.032	-.22	-.75	.56	1.01
.073	.177	.178	.186	.850	.821	.993	1.042	-.4795	-.9952	.484	.997	-.55	-1.11	.54	1.11
.328	.543	.539	.541	.902	.904	1.000	.921	.2563	.2656	1.052	1.088	.20	.21	.83	.86
.206	.469	.460	.456	.924	.924	1.007	.968	.0188	.0722	.990	1.078	.02	.06	.87	.95
.085	.391	.378	.367	.936	.934	1.000	1.004	-.1805	-.0711	.950	1.078	-.17	-.37	.89	1.01
.965	.603	.646	.660	.392	.397	.554	.324	.1749	.0291	-.0899	-.1231	.96	.16	-.49	-.67
1.001	.556	.579	.613	.361	.365	.516	.302	.0652	-.0322	-.0943	-.1102	1.00	-.50	-1.45	-1.70
1.028	.434	.455	.485	.280	.279	.421	.245	.0031	-.0510	-.0723	-.0756	1.55	-25.50	-36.15	-37.80
.444	.728	.733	.746	1.002	1.006	1.155	1.000	446	624	820	815	.55	.77	1.01	1.00
.283	1.049	1.039	1.024	.116	.201	.010	-.369	-441	-791	-588	-447	.56	1.01	.75	.57
.209	.604	.589	.576	1.001	1.014	1.053	.985	241	548	1097	1061	.22	.51	1.02	.98
.281	.569	.575	.577	-.410	-.351	-.489	-.783	-372	-563	-283	-153	.54	.82	.41	.22

For the second design condition, an attempt will be made to match bending moment throughout the span, and shears at least in the outer wing. Loads for this condition are produced predominantly by case 202 and may include contributions from all three elementary distributions. For a first estimate, a_1 , a_2 , and a_3 will be determined such as to provide an exact match of bending moments at wing stations 83, 167, and 275. The following equation must be satisfied for each of these three load quantities:

$$L_s = a_1 E_1 + a_2 E_2 + a_3 E_3 \quad \text{or}$$

$$1 = a_1 \bar{E}_1 + a_2 \bar{E}_2 + a_3 \bar{E}_3$$

Substituting the values of \bar{E}_1 , \bar{E}_2 , and \bar{E}_3 from column 14 - 16 for each of the three load quantities in turn yields three equations in the three unknowns, a_1 , a_2 , and a_3 . Solution of these equations gives:

$$a_1 = 1.742, \quad a_2 = .180, \quad \text{and } a_3 = .25$$

Thus the incremental loads for Condition II as given by this first iteration are:

$$I_D = 1.742 E_1 + .180 E_2 + .25 E_3$$

A comparison of the complete Condition II loads (at this stage) with the statistically defined design level incremental loads is then indicated by the ratios

$$\frac{I_D}{L_s} = \frac{1.742 E_1 + .180 E_2 + .25 E_3}{L_s} = 1.742 \bar{E}_1 + .180 \bar{E}_2 + .25 \bar{E}_3$$

These ratios are listed in column 18. The ratios for shear and bending moment throughout the span are seen to be close to unity, although tending to be several per cent low in the outer wing. However, by referring to columns 14 through 16, it is seen that outer wing shear and bending can be increased relative to inner wing shear and bending by increasing a_1 and reducing a_2 and a_3 . Such a modification is therefore made, with the results shown in column 19.

It is seen that a further adjustment in the same direction would provide a further improvement. This is accomplished in column 20.

The ratio of design load to mission analysis load is now approximately unity for all wing bending moments, outer wing shears, and wing shear at wing stations 83 and 209.

Actually, it is unlikely that such a distribution of load would occur at any single instant in flight through turbulence, since this particular combination of static, dynamic bending, and dynamic torsion distributions is no more likely than any one of numerous others, each of which might produce design level values for only a very few of the 31 loads under examination. However, it is noted that no load quantity at any location in the structure has been exceeded; this condition, in effect, then represents an envelope of many possible conditions.

Reference to columns 17 and 20 shows that an adequate match has not yet been achieved for some of the wing shears, all wing torsions inboard of the outboard nacelle, and front beam shear flows. For Condition III, these wing shears and front beam shear-flows will be matched. Here again the pertinent E's are those in columns 14 through 16. The initial iteration for Condition III is shown in column 21, where a_1 , a_2 , and a_3 are selected such as to provide an exact match for shear at W.S. 346 and front beam shear flows at W.S. 83 and 346. A further adjustment yields the results shown in column 22. This condition represents a predominantly dynamic distribution of load. Load quantities matched are shear at W.S. 83, 167, 275, and 346, and front beam shear flow at W.S. 83 and 346. The wing bending moment ratios vary from about .73 at the tip to .98 at the root. For wing torsion, the ratios are .92 between nacelles and .82 inboard of the inboard nacelle.

Condition IV is included in order to match the wing torsions inboard of the outboard nacelle. The first iteration for condition IV is shown in column 23, based upon an exact match of wing torsion at W.S. 119, 209, and 346. Final condition IV load ratios appear in column 24, where it is seen that front beam shear flows at W.S. 83 and 346 and wing torsions inboard of the outboard nacelle are matched.

A quick review of columns 17, 20, 22, and 24 of Table C-11 indicates that all of the loads listed - except rear beam shear flow at W.S. 346, which will be shown later to be of negligible consequence - have been closely enveloped by one or more of the four design conditions. Closer examination of these numbers, however, is needed to assure that critical phasings have been achieved.

The power-spectral density information contained in Figure 9-3 and Table C-2 as well as the breakdown between mission segments indicated by Figure 9-9(b) and Table C-1, can assist in this examination. However, the most direct information on phasing is provided by the match of internal loads or stresses, either in actual structural elements such as the front and rear beams or in fictitious structural elements as discussed in Section 11.2.

The match of front beam shear flows for Conditions III and IV indicates that, for the wing inboard of the outboard nacelle, Condition III contains an appropriate amount of torsion with its design-level shears, and Condition IV contains an appropriate amount of shear with its design-level torsions.

However, phasing of bending moment and torsion is also important - from the standpoint of strength of the upper and lower surfaces. In order to check the adequacy with which this phasing is represented, as well as to provide a more complete picture of the shear-torsion and shear-bending phasings, use is made of the "equal probability", or phase-plane, ellipses shown in Figure 11-2. Conditions I - IV as generated in Table C-11 are shown spotted in on the ellipses. In spotting in these conditions, it was necessary to ratio down the design condition values to account for the fact that the total increment (relative to the case 202 one-g loads) due to all mission segments is greater than the increment for case 202 alone. To accomplish this, the values plotted were obtained by taking the ratios shown in columns 17, 20, 22, and 24 of Table C-11 and multiplying by the corresponding maximum load values indicated on the ellipses. Thus, in plotting the Condition IV shear-torsion point at W.S. 83 on Figure 11-2(a), for example,

$$S_z = .812 \times 28400 = 23000 \text{ lb.}$$

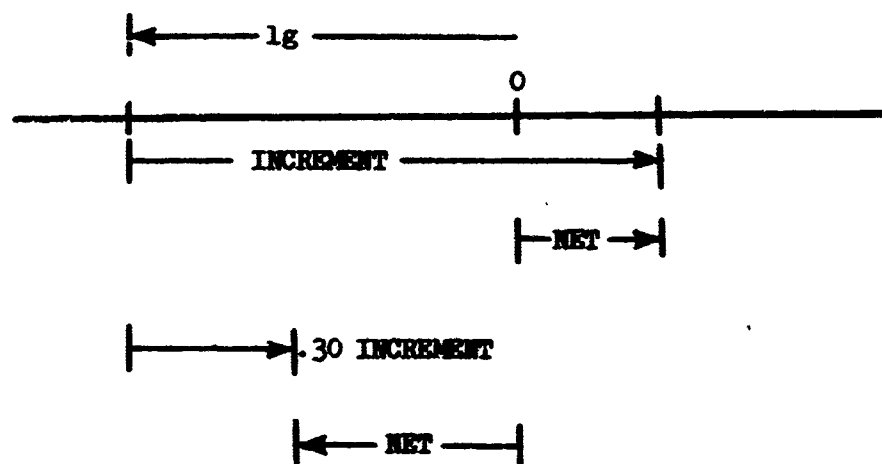
$$M_y = .966 \times 2.10 \times 10^6 = 2.03 \times 10^6 \text{ in.lb.}$$

It is seen that Conditions I through IV excellently represent the equal probability combinations of positive bending moment, shear, and torsion.

To assure that the excellent match indicated on an incremental basis in columns 17, 20, 22, and 24 of Table C-11 is preserved when the one-g loads are added, similar comparisons on a net-load basis are shown in columns 29 - 32. These are based on the net loads for each condition indicated in columns 25 - 28.

For Condition I, the match of outer wing torsions is seen to remain excellent (column 29). The value 1.55 for the ratio at W.8. 516 has no significance, since the net torsions are very small. The difference between the statistically defined and the Condition I net torsion, while 55% of the statistically defined net torsion, is less than 3% of the incremental torsion.

The Condition II shears and bending moments match at least as well on a net load basis as on an incremental basis. The rather drastic change in the torsion ratios is a natural consequence of the one-g and incremental values having opposite sign and is not of concern, as can be seen from the following sketch:



For Condition III, as for Condition II, the match of the pertinent quantities is seen to be at least as good on a net load as on an incremental load basis.

For Condition IV, the match of torsions is slightly less good on a net load basis than on an incremental basis. However, the good match of front beam shear flows is retained.

It is therefore concluded that, on a net load as well as an incremental load basis, the enveloping of the statistically defined loads by the design conditions is satisfactory.

C.5 Downbending Conditions

Design loads for the downbending mission analysis conditions were obtained in a manner similar to that just outlined for the upbending conditions. Mission analysis net loads for the case of downbending are given in column 3 of Table C-12, and the resulting incremental loads are given in column 4. For each design condition the ratio of design incremental load to mission analysis incremental load appears in columns 5 through 8. These are designated as Conditions V, VI, VII, and VIII respectively. The appropriate downbending design condition points are then shown on the phase plane plots of Figure 11-2, with the same adjustment included as described above for the upbending conditions. It is seen that, as for the upbending conditions, Conditions V through VIII excellently represent the equal probability combinations of negative bending moment, shear, and torsion.

A comparison of the downbending design conditions with the statistically defined loads on a net load basis appears in columns 9 - 12 of Table C-12. As in the case of the upbending conditions, the agreement is generally as good on a net as on an incremental load basis. The large values of the ratio for rear beam shear flow are associated with opposite signs for the one-g load and the increment; consequently, they are not of concern. In all cases, the largest value of the ratio, times the statistically defined net load, gives a load that is smaller (arithmetically) than the net load for the upbending conditions shown in Table C-11.

C.6 Loads in Other Quadrants

It will be observed that design conditions have been defined for upbending and downbending conditions. Actually, consideration must be given to four rather than two types of condition - up and down bending, each combined with positive and negative torsion. In other words, in the phase-plane plot of Figure 11-2(f), for example, consideration must be given to possibly critical conditions in all four quadrants. The general shape of the ellipses shown in Figures 11-2(a), (c), (d), and (f), however, suggests that the upper left and lower right quadrants are not likely to be critical; and examination of the design load envelopes based on all the conditions to which the airplane was originally designed confirms this conclusion. Even if the procedure described herein had been employed in the original design of the Model 188, one could probably have established at an early stage that other conditions would be more critical in these quadrants than the power-spectral gust conditions.

TABLE C-12. DOWN BENDING DESIGN CONDITIONS, MODEL 188

Item		Mission Analysis Loads		Ratio of Design Incremental Loads To M.A. Incr. Loads				Ratio of Design Net Loads To M.A. Net Loads			
(1)	(2)	(3)	(4)	(5)	(6)	(7)	(8)	(9)	(10)	(11)	(12)
Load		Net Loads Mission Analysis	L _a Case 202	Cond. V	Cond. VI	Cond. VII	Cond. VII	Cond. V	Cond. VI	Cond. VII	Cond. VIII
	Ref. V.S. (in.)	Frequency of Exceedance Curves	(3) - (5)	$\frac{2.135(8)}{- (4)}$	$\frac{(1.61(8) + .17(9) + .36(10))}{- (4)}$	$\frac{(1.05(8) + .39(9))}{- (4)}$	$\frac{(.65(8) + .43(9) - .10(10))}{- (4)}$	$\frac{(5)(4)}{(3) + (5)}$	$\frac{(6)(4)}{(3) + (5)}$	$\frac{(7)(4)}{(3) + (5)}$	$\frac{(8)(4)}{(3) + (5)}$
Wing Shear	83	-12100	-31155	.787	.948	.974	.859	.46	.87	.93	.64
	119	-14200	-30586	.726	.930	.992	.892	.41	.85	.98	.77
	167	-16000	-27862	.609	.885	1.009	.935	.32	.80	1.01	.89
	209	-19400	-33379	.751	.995	.952	.822	.57	.99	.92	.69
	275	-19800	-29089	.703	.963	.980	.871	.55	.94	.97	.80
	346	-17200	-22500	.617	.924	1.034	.954	.50	.90	1.04	.94
	380	-11400	-19079	1.011	.957	.799	.623	1.02	.93	.67	.37
	448	- 7150	-11311	1.086	.991	.832	.653	1.04	.98	.73	.45
Wing Bending Moment About Elastic Axis	516	- 3250	- 4781	.978	1.013	.852	.675	.97	1.02	.78	.52
	83	-5.55	-9.473	.815	1.017	1.017	.890	.68	1.03	1.03	.81
	119	-5.25	-8.548	.805	1.005	.999	.872	.68	1.01	1.00	.79
	167	-4.70	-7.309	.813	1.002	.976	.845	.71	1.00	.96	.76
	209	-3.95	-6.030	.839	1.013	.975	.838	.75	1.02	.96	.75
	275	-2.70	-4.018	.888	1.021	.970	.826	.83	1.03	.95	.74
	346	-1.57	-2.382	.986	.993	.864	.694	.98	.94	.79	.54
	380	-1.14	-1.739	1.014	.985	.825	.647	1.02	.98	.73	.46
Wing Torsion Moment About Elastic Axis	448	- .500	- .7114	1.002	.999	.839	.661	1.00	1.00	.77	.52
	516	- .110	- .1634	.973	1.007	.846	.670	.96	1.01	.77	.51
	83	-3.70	-2.181	.329	.264	.907	1.007	.60	.57	.94	1.00
	119	-3.56	-2.080	.230	.193	.894	1.020	.55	.53	.94	1.01
	167	-3.40	-1.971	.083	.081	.855	1.017	.47	.46	.91	1.01
	209	-2.81	-1.402	.332	.553	.959	.985	.59	.70	.97	.99
	275	-2.58	-1.754	.252	.466	.939	.998	.49	.64	.96	1.00
	346	-2.36	-1.628	.110	.379	.914	1.003	.39	.57	.94	1.00
Rear Shear Flow	380	- .615	- .345	1.003	.689	.620	.479	1.00	.82	.79	.71
	448	- .360	- .174	1.036	.695	.630	.487	1.02	.85	.82	.75
	516	- .165	- .064	.964	.581	.551	.427	.99	.84	.82	.87
	83 FB	- 666	- 728	.616	.665	1.005	.991	.58	.63	1.01	.99
Rear Shear Flow	83 RB	- 150	+ 388	.534	.749	.200	-.010	2.87	1.65	2.87	3.61
	346 FB	-1350	-1173	.288	.616	.990	1.014	.38	.40	.98	1.01
	346 RB	- 30	+ 359	.529	.560	-.167	-.406	6.64	6.26	14.96	17.82

* Denotes column in Table 11-11

It is because the upper left and lower right quadrants are clearly non-critical that rear beam shear flows could be disregarded in generating the design conditions. In the critical upper right and lower left quadrants, the shear flow due to shear and torsion add in the front beam and subtract in rear beam. Only in the other two quadrants, which have been established as not being critical, do the shear flows due to shear and torsion add in the rear beam.

TABLE C-13. UPBENDING DESIGN CONDITIONS AT STRESS ANALYSIS STATIONS, $N(y) = 10^{-5}$ CYCLES PER HOUR, MODEL 188

Loads are with respect to arbitrary load axis at $F \ 8 \ 571.2$

W.S.	Condition I (Max. Outer Wing Loads)			Condition II (Max. Wing Bending Mom.)			Condition III (Max. Permissible Torsion With Max. Shear-Bending)			Condition IV (Max. Wing Torsion)		
	10^{-3} Lb	$10^{-6} M_x$ In.-lb	$10^{-6} M_y$ In.-lb	$10^{-3} S_x$ Lb	$10^{-6} M_x$ In.-lb	$10^{-6} M_y$ In.-lb	$10^{-3} S_x$ Lb	$10^{-6} M_x$ In.-lb	$10^{-6} M_y$ In.-lb	$10^{-3} S_x$ Lb	$10^{-6} M_x$ In.-lb	$10^{-6} M_y$ In.-lb
65	38.313	9.94	-1.1487	50.409	15.039	-2.4537	49.341	14.736	-1.2315	43.611	12.569	-6.479
101	5.390	8.776	-1.2208	49.300	13.222	-2.4569	49.328	12.938	-1.2112	43.472	10.979	-5.961
137	26.903	7.121	-1.1932	43.019	11.571	-2.3184	45.344	11.245	-1.0822	40.223	9.483	-4.587
167	22.064	6.977	-1.0268	36.647	10.349	-2.1051	40.986	9.923	-0.8924	36.587	8.305	-2.760
167*	27.922	6.977	-1.0074	44.438	10.349	-1.8649	45.802	9.923	-0.8404	39.447	8.305	-3.972
179	27.331	6.689	-	43.803	9.804	-1.7956	45.037	9.361	-0.7681	38.644	7.820	-3.139
197	26.115	6.187	-	42.400	9.067	-1.6838	43.634	8.603	-0.6536	37.261	7.176	-2.017
209*	24.945	5.841	-	41.033	8.523	-1.6041	42.387	8.044	-0.5767	36.000	6.693	-1.235
209*	30.618	5.841	-	47.980	8.523	-1.4092	46.163	8.044	-0.5814	38.276	6.693	-2.656
239	27.076	4.943	-	43.042	7.124	-1.2519	42.647	6.679	-0.4240	35.241	5.553	-1.197
275	23.999	4.046	-	37.984	5.683	-1.1467	38.871	5.234	-0.3061	32.843	4.344	-0.0234
293	22.012	3.618	-	34.967	5.012	-1.0645	36.561	4.535	-0.2212	31.135	3.749	+0.0483
329	16.969	2.939	-	27.648	3.911	-0.8634	30.991	3.345	-0.0400	26.770	2.733	+0.2134
346*	14.822	2.668	-	24.537	3.470	-0.7685	28.583	2.841	+0.0503	24.066	2.896	+0.2929
346*	19.287	2.668	-	27.000	3.470	-0.7879	33.477	2.841	+0.4512	21.173	2.896	-3.227
380*	19.687	2.000	-	27.372	2.537	-0.7074	34.329	1.983	-0.3397	20.292	1.583	-2.207
380*	22.376	2.000	-	28.349	2.537	-0.7349	31.953	1.983	-0.7012	17.703	1.583	-6.192
397	20.488	1.640	-	25.810	2.085	-0.6809	19.924	1.635	-0.6297	16.065	1.304	-0.5573
431	15.258	1.086	-	19.172	1.308	-0.5145	14.929	1.030	-0.4805	11.968	.8150	-4.253
465	10.734	.5707	-	13.566	.7372	-0.3692	10.645	.9809	-0.3477	9.471	.4532	-0.3079
499	6.707	.2651	-	8.644	.3744	-0.2476	6.855	.2953	-0.2366	74	.2297	-0.2091
533	3.600	.1294	-	4.712	.1673	-0.1407	3.797	.1371	-0.1363	2.31	.1111	-0.1204
564	.605	.0070	-	.848	.0083	-0.0212	.623	.0072	-0.0203	.478	.0055	-0.0181

TABLE C-14. DOWN BENDING DESIGN CONDITIONS AT STRESS ANALYSIS STATIONS N(y) = 10-5 CYCLES PER HOUR, MODEL 188

Loads are with respect to arbitrary load axis at 7 & 571.2

	Condition V (Max. Outer Wing Loads)			Condition VI (Max. Wing Bending Mom.)			Condition VII (Max. Permissible Torsion With Max. Shear-Bending)			Condition VIII (Max. Wing Torsion)		
	10 ⁻³ S _x 12	10 ⁻⁶ M _x 12	10 ⁻⁶ M _y 12	10 ⁻³ S _x 12	10 ⁻⁶ M _x 12	10 ⁻⁶ M _y 12	10 ⁻³ S _x 12	10 ⁻⁶ M _x 12	10 ⁻⁶ M _y 12	10 ⁻³ S _x 12	10 ⁻⁶ M _x 12	10 ⁻⁶ M _y 12
4.8	-4.099	-3.740	-2.970	-8.603	-5.781	-2.1037	-9.087	-5.795	-3.1460	-5.144	-4.148	-3.7867
65	-6.867	-3.561	-2.034	-12.354	-3.447	-1.7503	-13.538	-5.382	-3.1066	-9.994	-4.288	-3.1448
101	-5.881	-3.389	-1.7703	-12.517	-4.949	-1.4781	-14.969	-4.899	-2.8203	-12.162	-3.818	-3.1747
137	-5.043	-3.191	-1.5961	-12.783	-4.616	-1.4934	-16.203	-4.418	-2.6807	-11.164	-3.450	-2.9286
167	-6.136	-3.191	-1.6604	-13.125	-4.616	-1.4883	-15.284	-4.418	-2.5647	-12.000	-3.450	-2.8385
197	-7.896	-3.184	-1.5872	-16.037	-4.449	-1.3867	-16.857	-4.448	-2.4789	-13.506	-3.313	-2.7441
209	-9.631	-2.986	-1.4048	-17.766	-4.104	-1.2787	-18.609	-3.883	-2.3517	-15.350	-3.015	-2.6233
209	-10.844	-2.846	-1.3853	-18.987	-3.986	-1.2003	-19.598	-3.694	-2.2701	-16.563	-2.866	-2.5434
239	-11.307	-2.531	-1.3800	-19.840	-3.986	-1.3164	-18.834	-3.694	-2.1467	-13.772	-2.866	-2.3474
273	-10.547	-2.116	-1.1401	-19.431	-3.370	-1.1582	-18.801	-3.178	-1.9773	-14.940	-2.469	-2.1711
293	-9.943	-1.951	-1.003	-17.838	-2.574	-1.0637	-18.643	-2.476	-1.8939	-15.451	-1.900	-2.0288
346	-7.076	-1.604	-0.9003	-15.173	-2.165	-0.936	-17.419	-2.163	-1.7941	-15.335	-1.640	-1.9879
346	-6.953	-1.478	-0.7301	-14.844	-1.514	-0.878	-16.985	-1.800	-1.6456	-15.390	-1.7800	-1.8832
367	-6.871	-1.478	-0.5946	-10.686	-1.514	-0.6107	-9.538	-1.200	-0.9876	-7.009	-1.7800	-1.0150
380	-12.408	-1.137	-0.3983	-14.165	-1.099	-0.4703	-13.151	-0.800	-0.7803	-10.217	-1.502	-0.6740
397	-11.664	-0.960	-0.3448	-10.436	-0.901	-0.2808	-8.034	-0.800	-0.7759	-4.567	-1.502	-0.3849
431	-8.658	-0.612	-0.2088	-8.062	-0.606	-0.1944	-5.978	-0.600	-0.6453	-4.473	-1.421	-0.8669
465	-6.830	-0.3736	-0.1579	-6.032	-0.3812	-0.1158	-4.534	-0.4958	-0.5938	-3.405	-1.299	-0.8239
499	-4.087	-0.1868	-0.1170	-4.214	-0.1931	-0.0889	-3.218	-0.192	-0.5133	-2.846	-1.207	-0.643
513	-2.804	-0.0962	-0.0785	-2.411	-0.0993	-0.0901	-1.861	-0.047	-0.4601	-1.863	-0.837	-0.0579
584	-0.700	-0.006	-0.0076	-0.634	-0.009	-0.0037	-0.543	-0.013	-0.0071	-0.480	-0.080	-0.0084

APPENDIX D

APPLICATION OF THE MATCHING CONDITION TECHNIQUE TO THE MODEL 188 FUSELAGE (VERTICAL GUST LOADS)

The procedure for matching statistically defined fuselage loads with discrete design load conditions is basically identical to the method used for the wing. As applied to the fuselage, however, the procedure is very much simpler, as a result of the absence of torsion and also the absence of aerodynamic and inertia loads resulting from elastic deformations.

The statistically defined loads resulting from the Model 188 mission analysis are used in illustrating the matching technique. The level of the statistically defined loads was established at a frequency of exceedance of 10^{-5} exceedances per hour. This level is the same as used for the wing in Appendix C. The loads are read from frequency of exceedance curves similar to that of Figure 9-9(d) for each of the ten fuselage loads and the horizontal tail load. Table D-1 summarizes the resulting loads in both the upbending and downbending directions. For the purpose of illustrating the technique, however, only the downbending loads will be matched.

D.1 Nomenclature.

The nomenclature used to illustrate the method for obtaining fuselage load distributions is basically the same as given for the wing in Appendix C. The following specific definitions differ from those used in Appendix C:

- E_1 Elementary distribution for unit translational acceleration
- E_2 Elementary distribution for unit pitching acceleration
- E_3 Elementary distribution for tail aerodynamic load
- E_4 Elementary distribution for body aerodynamic load
- \bar{E}_1 Ratio of load in translational acceleration elementary distribution to statistically defined load
- \bar{E}_2 Ratio of load in pitching acceleration elementary distribution to statistically defined load
- \bar{E}_3 Ratio of load in tail aerodynamic load elementary distribution to statistically defined load

TABLE D-1. FUSELAGE MISSION ANALYSIS NET LOADS AT $N(y) = 10^{-5}$
EXCEEDANCES PER HOUR, MODEL 188

①	②	③	④	⑤
Fuselage Station	Downbending Loads		Upbending Loads	
	S_z lb	M_y 10^6 In.-lb	S_z lb	M_y 10^6 In.-lb
350	-31000	-4.87	10900	1.72
500	-49800	-10.75	18200	3.85
571	-60000	-14.60	22000	5.25
695	-43700	9.80	2200	3.47
1000	-20100	5.20	-2350	-1.66
Horiz Tail	-28700	-	13800	-

\bar{E}_4 Ratio of load in body aerodynamic load elementary distribution to statistically defined load

a_4 Loading coefficient for elementary distribution E_4

D.2 Preliminary Considerations.

As in the development of wing loads, the determination of fuselage design load conditions divides naturally into two distinct parts. First, the "elementary" or "unit" distributions are developed. Second, these are used to generate one or more design load conditions, such as to envelope closely the statistically defined loads resulting from the power-spectral analysis.

Before the elementary distribution can be developed, it must be decided which mission segment or segments these should be based upon. From frequency of exceedance curves similar to that of Figure 9-9(d), it is observed that case 202 is the major contributor to the shear and bending moment at the five fuselage stations, with the exception only of shear at FS 1000 and bending at FS 695. At these two stations, Case 208 contributes very slightly more than Case 202 to the load exceedances.

Downbending loads for the total mission and separately for mission analysis case 202 are summarized in Table D-2 at the selected frequency of exceedance of 10^{-5} cycles per hour. In Table D-2 total mission net loads are shown in Column 3. Loads due to mission analysis case 202 alone, at the same frequency of exceedance of total flight, appear in column 4. One-g loads for mission analysis case 202 are shown in column 5. The resulting "gust incremental" loads are shown in columns 6 and 7. In column 6 the gust increment is taken as the difference between net load based upon all mission segments and the one-g load for Case 202. In column 7, the gust increment is the increment for the given mission segment alone. Column 8 shows the ratio of gust increment due to segment 202 alone to the total gust increment based on all segments.

In column 8, the ratios for shear and bending are all approximately .95, with only the shear at FS 1000 being slightly less at .92. It can be concluded that if design conditions were to be generated to match the gust incremental loads for condition 202 alone (column 7), these could be "ratioed up" by dividing by .95 and would closely reproduce the column 6 incremental loads. Then, if the condition 202 one-g loads were to be added, a match of the net loads of column 3 would result. Thus, to obtain a match to the statistically defined net loads, only the gust increment need be considered, and this can be confined to condition 202.

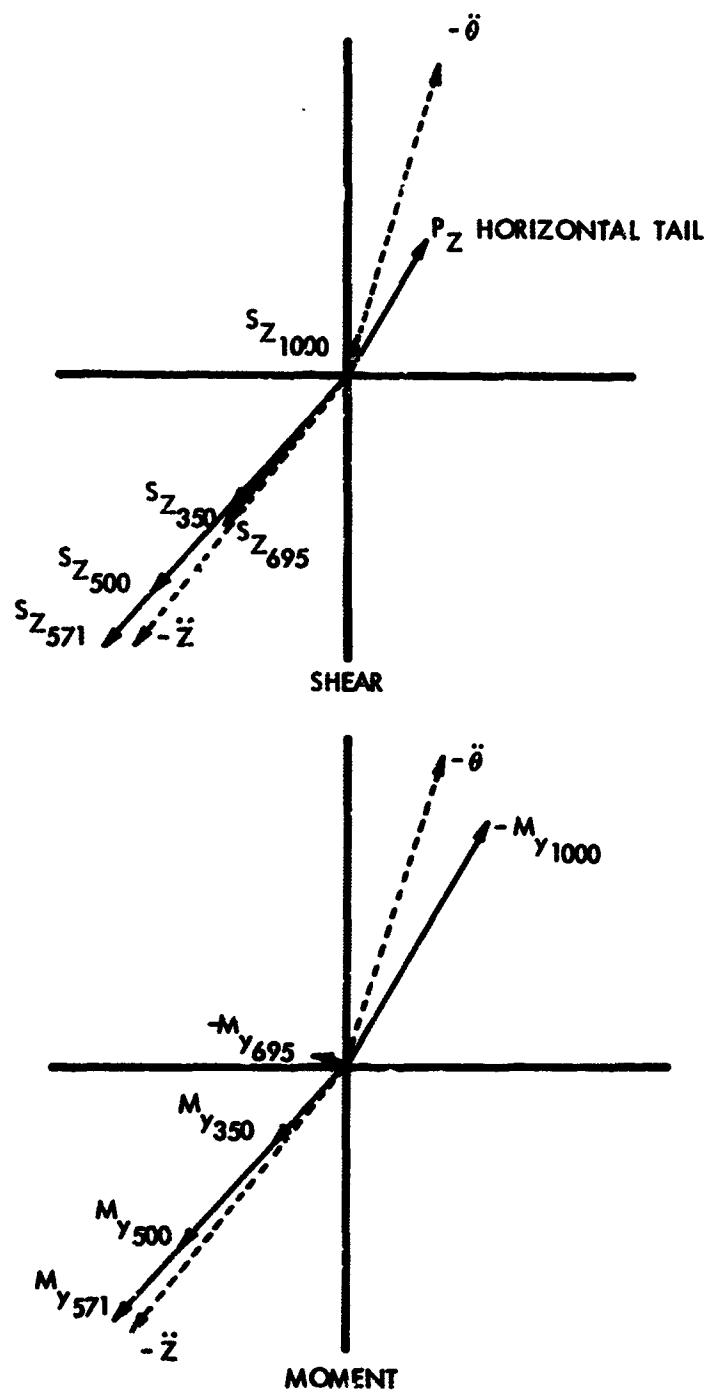
TABLE D-2. MISSION ANALYSIS LOADS AT $N(y) = 10^{-5}$ EXCEEDANCES
PER HOUR, MODEL 188

①	②	③	④	⑤	⑥	⑦	⑧
Load	Fuselage Station	Net Loads Mission Analysis $N(y) \cdot 10^{-5}$ lb	Net Loads Case 202 $N(y) \cdot 10^{-5}$ lb	One G Load Case 202 lb	Net Mission Load-One G lb	Incr 202 lb	Ratio
$N, 10^6$ lb	350	-31000	-30000	-10185	-20815	-19815	.952
	500	-49800	-48100	-16170	-33630	-31930	.949
	571	-60000	-57500	-19240	-40760	-38260	.939
	695	-43700	-42700	-21440	-22260	-21260	.955
	1000	-20100	-19500	-12340	-7260	-6560	.917
$N, 10^6$ In-lb	Horiz Tail	-28700	-27800	-8778	-19922	-19022	.955
	350	-4.87	-4.70	-1.601	-3.27	-3.10	.948
	500	-10.75	-10.40	-3.52	-7.23	-6.88	.952
	571	-14.60	-14.00	-4.78	-9.82	-9.22	.939
	695	9.80	9.66	7.31	2.49	2.35	.944
	1000	5.20	5.06	1.99	3.21	3.07	.956

As a result of the foregoing considerations, it is concluded that gust incremental loads for the total mission may be obtained by utilizing elementary and one-g distributions derived from a consideration of mission analysis case 202 only.

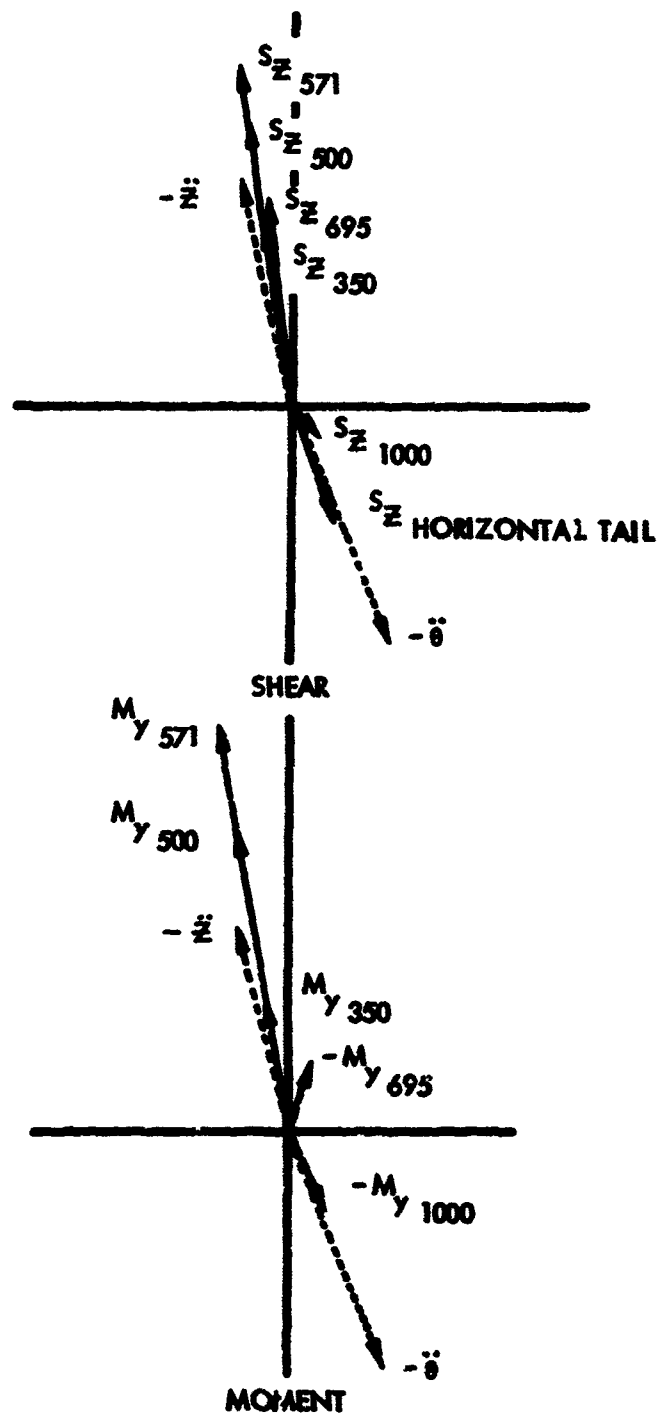
It has been observed that the net load levels obtained from the mission analysis depend primarily on the rms or \bar{A} values, which in turn depend upon the total area under each output power spectral density curve. However, in establishing distributions of loads that might actually occur at particular instants of time, consideration must be given to the shapes of the output power spectral density diagrams.

The power-spectral densities for the fuselage loads for Case 202 are shown in Figure 9-4. For the forebody loads, shown in Figure 9-4(a), it is seen that approximately 90% of the area under the curve is due to the response in the 0.4 cps short period mode. The remaining 10% is due to the first wing bending mode response at 2.1 cps. For the aft body loads, except for bending moment at FS 695, Figure 9-4(b) indicates approximately the same breakdown between the short period and wing bending mode contribution. In addition, small contributions are indicated at the wing torsion frequency (4.2 cps) and the elevator flapping frequency (5.6 cps). Bending moment at FS 695 shows a very small response at the short period frequency, due to the offsetting effects of tail airload and the opposing inertia forces. In fact, the characteristic differences between the forebody and aft body responses are due to the fact that the forebody loads are due almost entirely to inertia forces, whereas the horizontal tail aerodynamic forces contribute substantially to the aftbody loads. The phase relationships of the transfer functions show this effect quite well. Figure D-1(a) is a vector phase plot of various transfer functions at the short period frequency of 0.4 cps. The vectors represent the magnitude and phase relations of the fuselage loads with respect to a steady state sinusoidal gust input. Also shown are fuselage rigid body accelerations. These are plotted as negative accelerations in order to indicate the phasing of the resulting inertia loads. Looking at the shear plot first, it is apparent that all forebody shears and the shear at FS 695 are approximately in phase with each other but approximately 180° out of phase with horizontal tail load and FS 1000 shear. The forebody and FS 695 shears are obviously influenced predominantly by translational inertia whereas shears on the extreme aftbody are influenced predominantly by the tail airload. This conclusion is confirmed by the moment phase plot. The forebody moments like the shears are seen to be in phase with negative acceleration. The aftbody moments including the moment at FS 695, are seen to be strongly influenced by the tail airload. The bending moment of FS 695 is seen to be small compared to that at FS 1000, reflecting the offsetting effect of



(a) FREQUENCY = .4 CPS

FIGURE D-1. PHASE RELATIONSHIPS OF FUSELAGE LOADS



(b) FREQUENCY = 2.1 CPS
FIGURE D-1. CONCLUDED

inertia and airload noted earlier. The phase plots at the wing frequency of 2.1 cps, shown in Figure D-1(b), show similar relations. The principal difference is in the relative magnitudes of translational inertia, pitching inertia, and tail airload. Vector plots for the other frequencies are not shown since these contributions to net load are relatively small.

The conclusions which may be drawn from the phase plots may be summarized as follows:

1. Forebody loads are predominantly due to inertia.
2. Aftbody loads are affected strongly by inertia and tail airloads acting out of phase.
3. Pitching inertia loads are relieving on forebody and additive on aftbody.
4. At least two matching load conditions will be required to match fuselage downbending loads, one for the forebody and one for the aftbody, since the respective loads are seen to be almost exactly 180° out of phase at the predominant frequencies.
5. Bending moment at FS 69, will be difficult to match with the same conditions used to match the other loads because of its unique phase relationship. However, since this load is relatively small, a close matching is not required.

In view of the above, the downbending fuselage loads will be matched by two conditions. In one of these the forebody loads will be matched, in the other, the aftbody loads except at FS 695, will be matched. The shear at FS 695 should be matched by the forebody conditions; bending moment at this location need not be matched, as it is so small as not to contribute significantly to the critical stresses.

D.3 Elementary Distributions.

It is now possible to proceed to the generation of the elementary distributions.

The method of obtaining fuselage load distributions departs slightly from that used for the wing at this point, partly for simplicity and partly to illustrate a variation in the approach. It will be recalled that, for the wing, three elementary distributions were used - one based upon a static response and two based upon dynamic responses. These

elementary distributions included both inertia and aerodynamic loadings. For a comparable method on the fuselage, the dynamic distribution would not be required since the fuselage is assumed rigid. However, two or more static distributions would be required in order to account for the relative phasing of translation acceleration, pitching acceleration, and aerodynamic loads on the body and tail. In order to avoid this complication, the elementary distributions were taken simply as unit airload and inertia distributions. The fuselage loads for any condition, gust or otherwise, can be regarded as produced by four parameters - (1) translation acceleration, (2) pitching acceleration, (3) tail and elevator air load, and (4) body air load. The elementary load distributions are simply the fuselage load produced by unit values of each. These elementary distributions are given in Table D-3(a) and D-3(b) for fuselage shear and moment respectively. These are basic unit loads and require no particular technique to develop. Columns 2 and 3, E_1 and E_2 , depend only on the airplane weight data. Column 4, E_3 , depends only upon the tail load center of pressure (no balancing inertia being included). Column 5, E_4 , depends only upon the original assumption used for distribution of airload along the fuselage (again, no balancing inertia being included). Also shown in Table D-3 are the one-g flight loads for Case 202.

D.4 Fuselage Downbending Conditions.

With the mission analysis loads of Table D-1, the elementary distributions of Table D-3 and the one-g flight loads of Table D-3 all available, discrete distributions of the fuselage may now be generated. This is accomplished in Tables D-4 and D-5. The procedure is identical to that described for the wing in Appendix C, Section C.4 with the exceptions that four elementary distributions are used instead of three, and only one one-g flight load condition need be used.

In Table D-4, the statistically defined load levels which it is desired to match appear in column 3. These are taken from columns 2 and 3 of Table D-1. As pointed out earlier, in Appendix D, Section D.2, only the Case 202 one-g flight loads need be considered. Thus only the incremental statistically defined loads as given by the L_g in column 5 (the difference of columns 4 and 3) need to be matched by combinations of the elementary distributions.

The elementary distributions given in Tables D-3 are shown in columns 6-9. These distributions are designated the E_1 , E_2 , E_3 and E_4 distributions.

TABLE D-3. FUSELAGE ELEMENTARY LOAD DISTRIBUTIONS
CASE 202
(a) SHEAR

①	②	③	④	⑤	⑥
Inboard Fuselage Station	Unit Inertia		Unit Tail Airload	Unit Body Airloads	One G Flight Loads
In.	E_1	E_2	E_3	E_4	S_{z1-g} Lb
	S_z/n_z Lb/G	S_z/δ $\frac{Lb}{Rad/Sec^2}$	S_z/P_{zT} Lb/Lb	S_z/P_{zAFWD} Or S_z/P_{zAFT} Lb/Lb	
FOREBODY					
42	0	0	0	0	0
177	4500	- 5580	0	.255	- 4500
200	5310	- 6417	0	.298	- 5216
300	8677	- 9368	0	.487	- 8524
400	12064	-11456	0	.677	-11852
417	12893	-11842	0	.709	-12670
500	16439	-13034	0	.868	-16169
571	19559	-13459	0	1.000	-19242
AFTBODY					
635	16845	15663	1.000	1.000	-21437
768	14219	14692	1.000	.825	-19306
800	13218	14137	1.000	.750	-18430
900	9731	11832	1.000	.513	-15704
953	7908	10233	1.000	.388	-14236
1000	6118	8420	1.000	.275	-12803
1117	2470	3946	1.000	0	- 9899
1158	1890	3119	1.000	0	- 9319
1186	1500	2528	1.000	0	- 8929
1292	0	0	0	0	0

TABLE D-3. CONCLUDED
(b) MOMENT

①	②	③	④	⑤	⑥
Inboard Fuselage Station	Unit Inertia		Unit Tail Airload	Unit Body Airloads	One G Flight Loads
	E_1	E_2	E_3	E_4	M_y 1-g 10^6 In. -Lb/Lb
	M_y/n_z	$M_y/\ddot{\theta}$	M_y/P_{zT}	M_y/P_{zAFwd} Or M_y/P_{zAft}	
In.	10^6 In. -Lb/g	$\frac{10^6 \text{ In-Lb}}{\text{Rad/Sec}^2}$	In. -Lb/Lb	In. -Lb/Lb	
FOREBODY					
42	0	0	0	0	0
177	.304	.377	0	17.2	- .304
200	.417	- .515	0	23.6	- .409
300	1.116	-1.304	0	62.8	-1.096
400	2.153	-2.345	0	121.0	-2.115
417	2.365	-2.543	0	132.8	-2.323
500	3.582	-3.575	0	198.2	-3.519
571	4.860	-4.516	0	264.7	-4.777
AFTBODY					
695	-4.262	-5.006	-512.8	-210.5	7.317
768	-3.112	-3.883	-439.8	-144.1	5.810
800	-2.675	-3.420	-407.8	-118.9	5.205
900	-1.532	-2.123	-307.8	- 55.7	3.499
953	-1.065	-1.538	-254.8	- 31.6	2.706
1000	- .693	-1.044	-207.8	- 16.1	1.989
1117	- .216	- .358	- 90.8	0	.728
1158	- .127	- .213	- 49.6	0	.335
1186	- .080	- .134	- 21.8	0	.080
1252	0	0	0	0	0

* Center of pressure to be FS 1207.8 (average of tail and elevator)

(a) COLUMNS 1 - 13

D-12

TABLE D-4. CONCLUDED
(b) COLUMNS 14 - 19

Item	Ratio Incremental Loads		Design Net Loads		Ratio - Design to Mission Analysis Loads	
	⑭	⑮	⑯	⑰	⑱	⑲
Fuselage Station	Up Gust	Down Gust	Up Gust	Down Gust	Up Gust	Down Gust
	-2.5634 ⑩	2.5634 ⑩	⑤ ⑭ + ④	⑤ ⑮ + ④	⑯ / ③	⑰ / ③
	-.3292 ⑪	.3292 ⑪				
	+21817.3 ⑫	-24396.7 ⑫				
350 500 571 695 1000 Horus Tail	+4254.4 ⑬	-4782.4 ⑬				
	.993	-.979	-30854	10192	.995	-.481
	1.016	-1.002	-50338	17527	1.011	-.352
	1.017	-1.004	-60672	21683	1.011	-.361
350 500 571 695 1000	1.000	-.861	-43700	2274	1.000	-.052
	-.624	1.000	-8309	-20100	.413	1.000
	-.899	1.028	9132	-29260	-.385	1.019
Bending Moment $M, 10^{-6}$ In.-lb	.981	-.967	-4.808	1.561	.987	-.321
	.990	-.976	-10.678	3.536	.993	-.329
	1.002	-.988	-14.620	4.922	1.001	-.337
	.197	.379	7.80	8.254	.795	.842
350 500 571 695 1000	-.1774	.943	-4.95	5.017	-.095	.965

TABLE D-5. FUSELAGE DESIGN LOADS, MISSION ANALYSIS,
 $N(y) = 10^{-5}$ EXCEEDANCES PER HOUR

Fus Sta	Up Gust		Down Gust	
	S_Z	M_Y	S_Z	M_Y
	Lb	10^6 In.-Lb	Lb	10^6 In.-Lb
	$a_1 = -2.5634$ $a_3 = 21817$	$a_2 = -.3292$ $a_4 = 4254$	$a_1 = 2.5634$ $a_3 = -24397$	$a_2 = .3292$ $a_4 = -4782$
Forebody				
42	0	0	0	0
177	-13114	-.886	3979	.269
200	-15447	-1.208	4858	.378
300	-25611	-3.260	8306	1.035
400	-36125	-6.347	12064	2.053
417	-38805	-6.983	13091	2.267
500	-50325	-10.681	17529	3.538
571	-60695	-14.622	21633	4.929
Aftbody				
695	-43703	7.807	-2279	8.261
768	-35265	4.860	-6363	7.971
800	-31729	3.785	-8107	7.740
900	-20544	1.173	-13714	6.649
953	-14408	.248	-16848	5.830
1000	-8271	-.493	-20060	5.015
1117	4287	-.581	-26665	2.272
1158	6626	-.356	-27844	1.154
1186	9211	-.146	-28649	.363
1292	0	0	0	0
$\begin{Bmatrix} S_Z \\ M_Y \end{Bmatrix} = \begin{Bmatrix} S_Z \text{ 1-g} \\ M_Y \text{ 1-g} \end{Bmatrix} + a_1 E_1 + a_2 E_2 + a_3 E_3 + a_4 E_4$ <p>Values of one-G loads and $E_1 - E_4$ are given on Table D-3.</p>				

The statistically defined loads, L_S , are now to be enveloped by one or more discrete conditions. Each of these conditions will be made up of an appropriate combination of the four elementary distributions. The contribution of each elementary distribution will be defined by a value of its respective coefficient, a_1 , a_2 , a_3 or a_4 ; the complete set of loads comprising the condition is then given by the expression;

$$L_D = a_1 E_1 + a_2 E_2 + a_3 E_3 + a_4 E_4$$

For each additional condition a new set of values of the coefficients is determined.

To facilitate determining appropriate values of the loading coefficients, each load for the elementary distributions is divided by its corresponding design level load, L_S . The resulting ratios are designated \bar{E}_1 , \bar{E}_2 , \bar{E}_3 and \bar{E}_4 and are listed in columns 10 through 13 respectively. Thus a match of the statistically defined load is obtained if

$$L_D/L_S = a_1 \bar{E}_1 + a_2 \bar{E}_2 + a_3 \bar{E}_3 + a_4 \bar{E}_4 = 1.0$$

In generating the conditions it will be remembered that the forebody loads were shown to be closely in phase. Consequently, it should be possible to match these loads very closely. In generating the first condition, the forebody loads will be matched, while a match of the extreme aftbody loads will not be expected. In establishing the coefficients for this condition, the \bar{E}_4 distribution (body airloads) was initially ignored because of its small load contribution; a set of three simultaneous equations was solved to give an L_D/L_S ratio of 1.0 for shear at stations 350 and 695 and for moment at station 571. This gave approximate values of a_1 , a_2 , and a_3 . These were then modified by trial and error to include a value for a_4 roughly consistent with the angle of attack associated with n_z and still give good agreement. The resulting values of coefficients and of the ratio L_D/L_S that they produce are shown in column 14 of Table D-4. This condition is designated "up gust" inasmuch as it is characterized by a down inertia load factor and up tail load as indicated by the coefficients a_1 and a_3 respectively. This condition is seen to match all of the forebody downbending loads very well, since the ratios for these quantities in column 4 are all close to unity. Aftbody loads are not matched, but are in all cases lower than the statistically defined loads, as indicated by ratios arithmetically less than unity in Column 14.

Another set of coefficients is generated similarly to match the shear at FS 1000, horizontal tail load, and moment at FS 1000. These coefficients and load ratios are shown in column 15. This condition is designated "down gust"; it is characterized by an up inertia load factor and down tail load as indicated by the a_1 and a_3 coefficients. It is interesting to note that the moment at 695 is not matched very well, as was predicted, and that the forebody loads have load ratios close to negative unity, indicating an incremental upbending load approximately equal to the downbending load. This seems to be quite reasonable.

To assure that the excellent match indicated on an incremental basis in columns 14 and 15 is preserved when the one-g loads are added, similar comparisons on a net load basis are shown in columns 18 and 19. These are based on the net loads for each condition indicated in columns 16 and 17. It is seen that the agreement is even better than on the incremental load basis.

The final distributed net loads determined for the fuselage are shown in Table D-5 for a fine panel breakdown. These are calculated by applying the appropriate load coefficient to the elementary distributions of Table D-3 and adding the one-g flight loads. These load distributions are plotted in Figure D-2. For comparison, the statistically determined downbending and upbending loads of Table D-1 are spotted in. The downbending loads show excellent agreement; and even the upbending loads show surprisingly good agreement, even though no specific effort was made to match them. This figure gives an excellent indication of the significance of the terms "upbending" and "downbending" and "up gust" and "down gust", particularly on the aftbody.

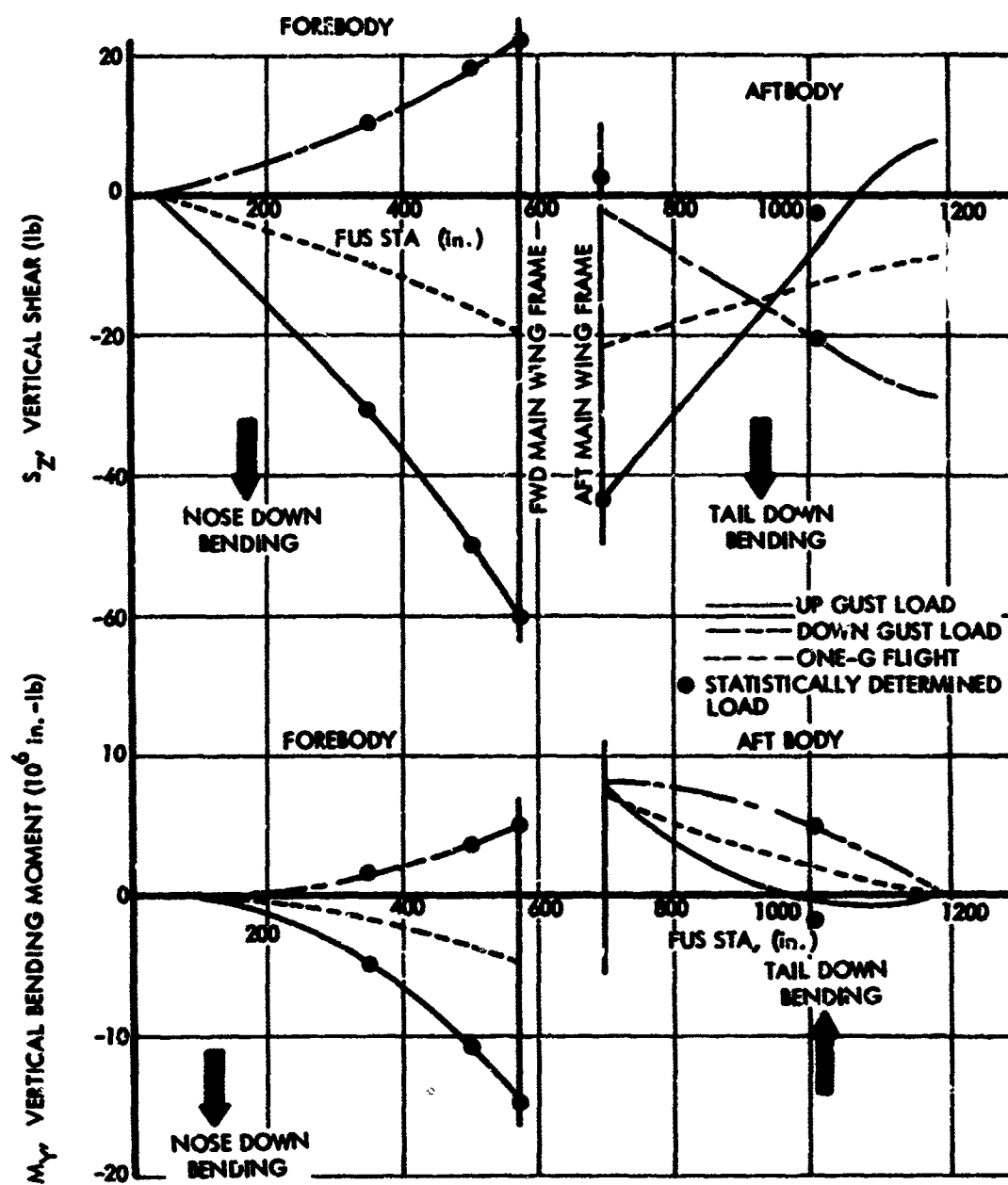


FIGURE D-2. FUSELAGE DESIGN LOAD DISTRIBUTIONS

APPENDIX E

ESTABLISHMENT OF LIMIT-STRENGTH AND ULTIMATE-STRENGTH VALUES OF N(y) AND $\sigma_w \eta_d$, MODELS 188 AND 749

E.1 Model 188 Wing

E.1.1 Mission Analysis, Limit Strength. In Appendix C, a set of eight load conditions was developed for the Model 188 wing such as to envelope closely the statistically defined values of some 31 load quantities. This set of conditions reflected a mission analysis approach and a level of severity defined by a frequency of exceedance of 1.00×10^{-5} cycles per hour.

Stress analysis was then conducted for these eight conditions, with the following negative margins of safety resulting:

Wing Station	Panel	Loading Condition	Margin of Safety
101	4	III	-.05
101	5	II	-.01
101	5	III	-.03
137	6	II	-.05
239	3	II	-.01
239	3	III	-.02
239	5	II	-.02

The negative margins of safety all occurred on the upper surface and resulted from combined compression and shear produced by the upbending conditions. In the table, the panels are numbered from the front beam and are 14" wide; the critical panels are thus seen to be in the deeper part of the box section rather than adjacent to the front or rear beams.

Considering the actual strength of the wing to be reflected by a negative margin of $-.04$, the frequency of exceedance corresponding to zero margin of safety (i.e., limit strength) is determined as follows. Bending moment at W.S. 119 is taken as representative of the loading in the critical region; its frequency of exceedance is shown in Figure 9-9(b). At $N(y) = 1.00 \times 10^{-5}$, where the margin of safety is $-.04$, the bending moment is 12.1×10^6 in.lb. The zero-margin value is then

$$(1 - .04)(12.1 \times 10^6 \text{ in.lb.}) = 11.6 \times 10^6 \text{ in.lb.}$$

The value of $N(y)$ corresponding to limit strength is read from the curve at this value of bending moment as 2.1×10^{-5} cycles per hour.

It should be remarked that the value obtained for $N(y)$ is not sensitive to the particular frequency of exceedance curve selected, as the shape of the curve doesn't change radically from one load quantity to another.

E.1.2 Mission Analysis, Ultimate Strength. Next, $N(y)$ corresponding to ultimate strength was determined. Based upon the stress analysis for the mission analysis limit conditions, together with an examination of the "unphased" loads at the ultimate level, it could be seen that the phasing of loads reflected by Condition III would be critical for ultimate strength. It was also apparent that only the region of the wing inboard of the outboard nacelle would be critical.

It was estimated that for ultimate strength the exceedance level would be approximately $N(y) = 5 \times 10^{-8}$. All wing loads inboard of the outboard nacelle were read from their respective exceedance curves at this level. Phasing ratios were then assumed to be as given by Column 22 of Table C-11 and applied to the unphased loads as read from the exceedance curves.

Stress analysis for the resulting condition led to the following minimum margins of safety:

Wing Station	Panel	Margin of Safety
101	4	+.06
239	3	+.07

These both occurred on the upper surface and reflected combined compression and shear.

Again considering bending moment at W.S. 119 to be a representative load quantity and considering the .06 margin to reflect the strength of the wing, the frequency of exceedance corresponding to zero margin, or ultimate strength, is obtained as follows. At $N(y) = 5 \times 10^{-8}$ cycles per hour, $M_x = 16.1 \times 10^6$ in.-lb. (Figure 9-9(b)). The zero-margin value is then

$$(1 + .06)(16.1 \times 10^6) = 17.0 \times 10^6 \text{ in.-lb.}$$

The value of $N(y)$ corresponding to ultimate strength is read from the curve at this value of bending moment: $N(y) = 1.4 \times 10^{-8}$ cycles per hour.

It may be noted that the ratio of ultimate strength to limit-strength values of $N(y)$ is $(1.4 \times 10^{-8}) / (2.1 \times 10^{-5}) = .7 \times 10^{-3}$.

E.1.3 Design Envelope Criterion. In order to determine the critical design envelope condition for limit strength at V_C , loads for all of cases 401 through 422 were listed for an estimated limit strength level defined by $N(y)/N_0 = 1.25 \times 10^{-6}$ in Figure 5-8. These were, of course, unphased loads, and were obtained by multiplying the \bar{A} values listed in Table B-2 by the appropriate $\sigma_w \eta_d$ values read from Figure 5-8. The $\sigma_w \eta_d$ values were as follows:

Altitude	$\sigma_w \eta_d$
0	57
7000 ft.	62
12000 ft.	60
16000 ft.	59
20000 ft.	57

Loads were also listed for the V_D cases, 423 - 426, at $\sigma_w \eta_d = (25/50)62 = 31$ and for the V_B case, 427, at $\sigma_w \eta_d = (4/3)62 = 83$, where the factor $4/3$ is a rounded-off equivalent of $66/50$. (Cases 428-431 were not included until later, when it became evident that case 427 would not be the critical V_B case.) The multiplying factors included in the $\sigma_w \eta_d$'s for the V_D and V_B cases will be recognized as the ratios of currently specified U_{de} gust velocities at the respective speeds. On the assumption that the same ratios would be retained in a power-spectral criterion, the loads resulting from these $\sigma_w \eta_d$'s are directly comparable as potential critical design conditions.

Spanwise plots of these loads were then made, for comparison with each other and with the loads defined by Conditions I-VIII. These loads were also plotted on shear-torsion, bending-torsion, and shear-bending co-ordinates at wing stations 83, 207, 346 and 397 for comparison with the design load envelopes and with Conditions II, III, and IV.

As a result of these comparisons, it was evident that Case 417, a V_C case, was critical for upbending and Case 425, a V_D case, for downbending. It was also apparent that for Case 417 the critical location would be inboard of the inboard nacelle and for Case 425, either in this region or between the nacelles. It was also observed that c.g. position would have at most about a 1% effect on the allowable $\sigma_w \eta_d$ values; the forward limit was generally the more critical.

In order to properly account for the phasing of shear, bending moment, and torsion, shear flows at W.S. 83 and W.S. 346 were considered.

For Case 417, it was assumed that, at each location, S_z and M_x would be in phase. Conditions such as illustrated by points 2 and 3 in Figure 11-1 were then determined. At W.S. 83, to match the front beam shear flow required 98% of the unphased torsion in combination with 100% of the unphased shear and bending moment (Point 2), or 98% of the unphased shear and bending with 100% of the unphased torsion (Point 3). At W.S. 346, the front beam shear flow was matched with 100% of the unphased values of all three load quantities (Points 2 and 3 coinciding at Point 1).

Because of the close proximity of the Point 2 and Point 3 conditions, a single condition corresponding to Point 2 was defined for stress analysis. This condition, designated 417L, was defined only in the potentially critical region inboard of the inboard nacelle. It was obtained by passing smooth curves through the unphased shears and bending moments at W.S. 83, 119, and 167 and 98% of the unphased torsions at the same locations. The shears thus defined were integrated to assure agreement with the statistically defined bending moments.

Case 425 was treated similarly. At W.S. 83, it was found that the front beam shear flow was matched with 100% of the unphased shear and bending moment in combination with 96% of the unphased torsion; or 100% of the unphased torsion with 97% of the unphased shear and bending moment. In defining a condition for stress analysis, points were plotted representing 100% of the unphased shear and bending moment and 96% of the unphased torsion.

In the region between nacelles, examination of Figure 11-2(e) indicated that shear and bending moment should not be considered in phase. Considering 90% of the unphased bending moment to combine with 100% of the unphased shear, it was found that front beam shear flow was matched with 97% of the unphased torsion. Phasing ratios at the other wing stations in the region between nacelles were then estimated based upon the numbers in column 22 of Table C-11; the following ratios resulted:

W.S.	S_z	M_x	M_y
209	.96	1.00	.97
275	.98	.98	.97
346	1.00	.90	.97

The condition thus defined is designated 425L.

Stress analysis for these conditions resulted in the following minimum margins of safety:

Condition	Wing Station	Location and Description	Margin of Safety
417L	101	Upper Surface, Panel 4, Compression and Shear	-.02
417L	137	Upper Surface, Panel 6 Compression and Shear	0
425L	137-166	Upper Surface, Panel 3, Shear	-.03
425L	209-239	Lower surface to front beam attachments	-.02
425L	275-293	Front beam web, tension and shear	-.02

Limit strength values of $\sigma_w \eta_d$ corresponding to these two conditions were obtained as follows:

For condition 417L, the value of M_x at W.S. 83 is 13.61×10^6 in.lb. The zero margin value is then

$$(1 - .02)(13.61 \times 10^6 \text{ in.lb.}) = 13.34 \times 10^6 \text{ in.lb.}$$

Subtracting the 1-g value and dividing by \bar{A} (Table B-2) gives

$$\sigma_w \eta_d = \frac{13.34 \times 10^6 - 5.00 \times 10^6}{138800} = 60 \text{ fps (at } h = 12000 \text{ ft.)}$$

Similarly, for Condition 425L, the zero margin value of M_x at W.S. 167 is

$$(1 - .03)(-5.13 \times 10^6 \text{ in.lb.}) = -4.98 \times 10^6 \text{ in.lb.}$$

and the limit strength value of $\sigma_w \eta_d$ is

$$\sigma_w \eta_d = \frac{-4.98 \times 10^{-6} - 2.04 \times 10^{-6}}{166700} = 31.1 \text{ fps (at } h = 7000 \text{ ft.)}$$

To establish the $\sigma_w \eta_d$ value corresponding to ultimate strength at V_C , a condition 417U was defined at an estimated $\sigma_w \eta_d$ level of 95 fps. This condition was identical to 417L except that the incremental loads were increased in the ratio 95/62.

The minimum margin of safety for this condition was found to be + .05, in upper surface panel 4 at W.S. 101, due to combined compression and shear.

The zero margin value of M_x at W.S. 83 is then

$$(1 + .05)(18.20 \times 10^6 \text{ in.lb.}) = 19.10 \times 10^6 \text{ in.lb.}$$

and the ultimate strength value of $\sigma_w \eta_d$ is

$$\sigma_w \eta_d = \frac{19.10 \times 10^6 - 5.00 \times 10^6}{138800} = 101 \text{ fps (at } h = 12000 \text{ ft.)}$$

As a result of the work to this point, it appeared that - for the assumed relative turbulence intensities at V_B , V_C , and V_D - conditions not yet specifically investigated were not likely to be critical. At this stage, however, it was considered desirable to make an over-all survey by determining approximate allowable $\sigma_w \eta_d$ values at both limit and ultimate levels, for all available cases, considering both upbending and downbending individually. Such a survey would provide a basis for possible reassessment of the relative turbulence intensities to be specified for design at V_B , V_C , and V_D . In providing an overall picture it would also constitute a check to assure that critical conditions had not been overlooked.

It was found that a rather reliable survey could readily be made. For the cases so far investigated, critical stresses were seen to result predominantly from combined bending moment and torsion. The most critical regions were found to be near the root and just outboard of the inboard nacelle, and in both regions the appropriate phasing ratios were found to be close to unity. Accordingly, unphased loads were plotted on bending-torsion coordinates at W.S. 83 (upbending and downbending) and at W.S. 209 (downbending only).

Limit and ultimate design load envelopes were then drawn based on the various available airplane design conditions. Inasmuch as the various conditions for which stress analysis was performed in this study (after adjustment to zero-margin levels) fell very close to the design load envelopes, these envelopes were used directly as limit and ultimate strength envelopes. (In the region of more-positive torsion characterized by Cases 427-431, an actual-strength line was used; this was defined by stress analysis for Case 430 at $\sigma_w \eta_d = 94$, which gave a margin of safety of +.05.) To obtain limit and ultimate $\sigma_w \eta_d$ values for each condition, a ray was drawn from the one-g point to the net load point and extended to intersect the limit and ultimate strength envelopes. Relative distances along this ray, in conjunction with the known $\sigma_w \eta_d$ value for which the condition was defined, then determined the limit and ultimate strength values of $\sigma_w \eta_d$.

The results of this survey are shown in Table E-1 and Figures E-1 and E-2.

In both the table and the figures, the $\sigma_w \eta_d$ values have been adjusted to an altitude of 12,000 ft. by moving along one of the family of lines in Figure 5-8. In effect, the allowable $\sigma_w \eta_d$ at the actual altitude for the condition defines a line of the family shown in Figure 5-8; this line is then designated not by its $N(y)/N_0$ value but by the $\sigma_w \eta_d$ value where it intersects the 12,000 ft. altitude.

For the V_B and V_D conditions, the adjustment could be either along lines of constant $N(y)/N_0$ as for the V_C conditions, or along lines such as to maintain a constant ratio of V_B to V_C $\sigma_w \eta_d$ and V_D to V_C $\sigma_w \eta_d$. The latter basis was used.

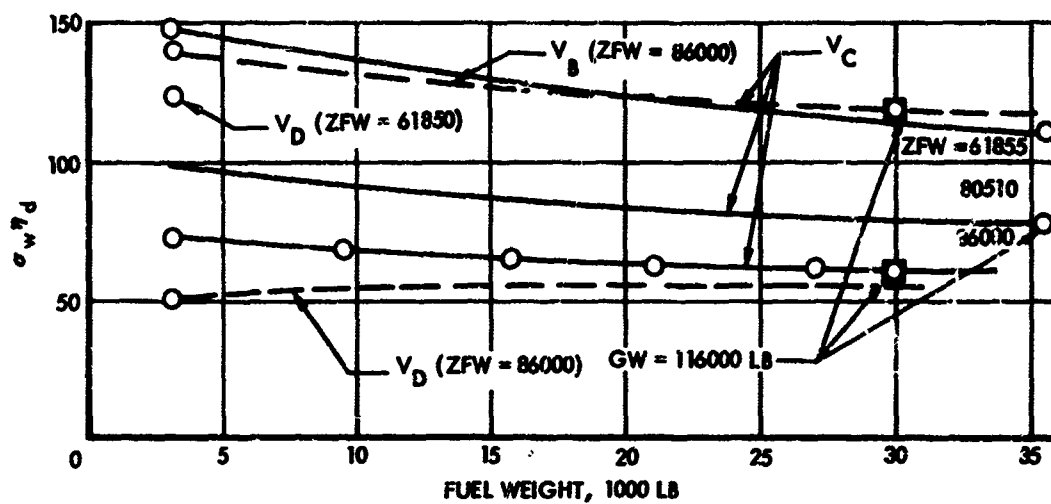
In the figures, calculated points from Table E-1 are indicated by circles. Where only one calculated point is available for a curve, the estimated trend is indicated by a dash line. The large squares denote the critical conditions for the three speeds respectively.

As a result of the trend with fuel weight shown for the V_C cases (Figure E-1 (a)), it was obvious that case 427 did not reflect the critical fuel weight at V_B . It was at this point that cases 428 through 431 were added. These were selected not only to cover the effect of increased fuel weight, but also to confirm that the critical altitude had been included and to provide a basis for review of the V_B speed selected somewhat arbitrarily in Section 7.

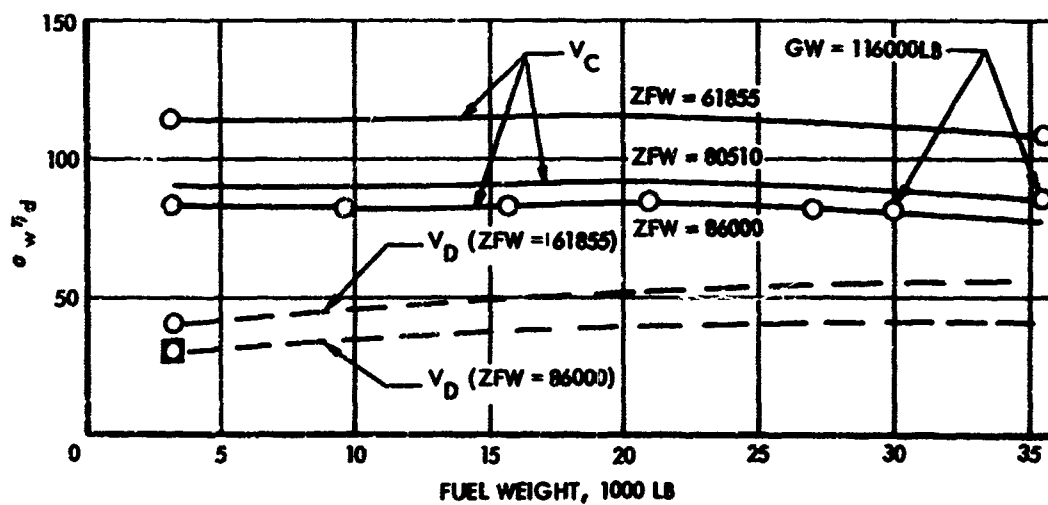
On a limit basis, it is seen that the allowable $\sigma_w \eta_d$ for V_D is just 25/50 of that for V_C . The allowable $\sigma_w \eta_d$ for V_B is clearly well in excess of 66/50 of the V_C value.

TABLE E-1. SUMMARY OF LIMIT STRENGTH AND ULTIMATE STRENGTH
 $\sigma_w \eta_d$ VALUES (ADJUSTED TO $h = 12000$ FT), MODEL 188 WING

Case No	Cond	Gross Weight Lb	Fuel Weight Lb	Zero Fuel Weight Lb	C.G. % MAC	Altitude Ft	Equivalent Airspeed V_e , Kts	Limit		Ultimate	
								Up Gust	Down Gust	Up Gust	Down Gust
								$\sigma_w \eta_d$	$\sigma_w \eta_d$	$\sigma_w \eta_d$	$\sigma_w \eta_d$
401	V_c	65000	3145	61855	12.0	12000	324	110	114	240	167
403	V_c	97345	35490	61855	16.2	12000	324	110	108	152	157
405	V_c	116000	35490	80510	20.2	12000	324	77	85	120	119
407	V_c	89145	3145	86000	14.5	12000	324	73	83	125	113
409	V_c	95620	9620	86000	15.8	12000	324	68	81	116	110
411	V_c	101860	15860	86000	17.2	12000	324	65	83	114	112
413	V_c	107000	21000	86000	18.3	12000	324	62	84	106	113
415	V_c	113100	27000	86000	19.6	12000	324	61	82	103	111
417	V_c	116000	30000	86000	20.2	12000	324	60	81	100	110
419	V_c	89145	3145	86000	14.5	20000	275	87	115	144	154
420	V_c	89145	3145	86000	14.5	16000	299	80	101	135	134
421	V_c	89145	3145	86000	14.5	7000	324	80	92	144	130
422	V_c	89145	3145	86000	14.5	0	324	90	105	164	149
423	V_D	65000	3145	61855	12.0	7000	405	124	40	193	83
425	V_D	89145	3145	86000	14.5	7000	405	51	30	88	51
427	V_B	89145	3145	86000	14.5	7000	180	140	231	256	279
428	V_B	89145	3145	86000	14.5	12000	180	140	224	243	266
429	V_B	116000	30000	86000	20.2	12000	180	119	220	220	267
430		116000	30000	86000	20.2	12000	220	99	176	180	233
431		116000	30000	86000	20.2	27000	220	105	165	171	216

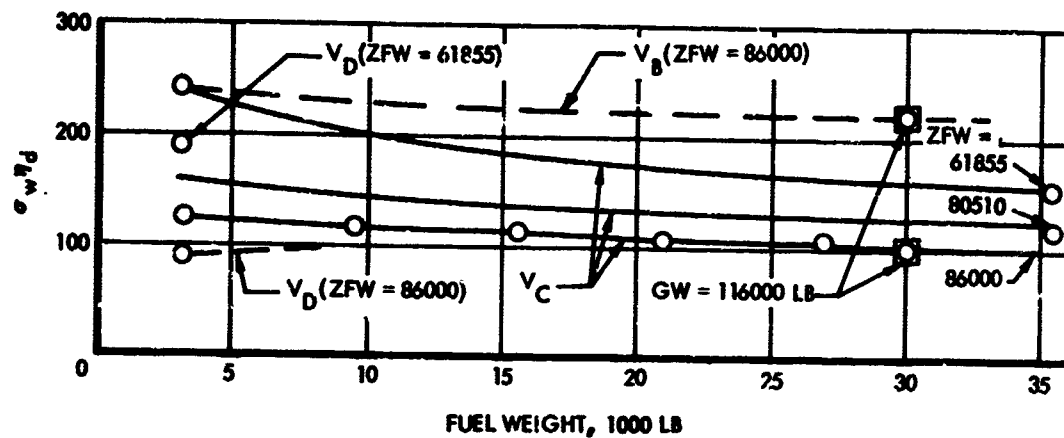


(a) UPBENDING

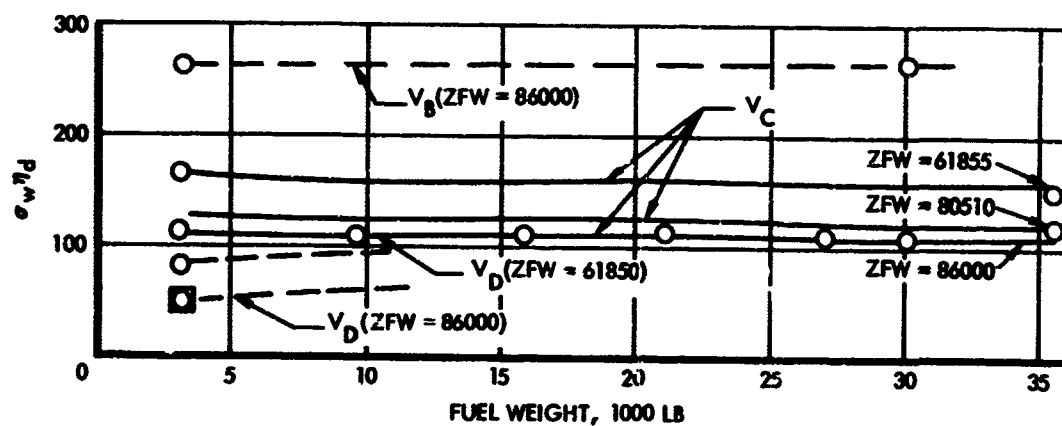


(b) DOWN BENDING

FIGURE E-1. LIMIT STRENGTH VALUES OF σ_w/d (ADJUSTED TO $h = 12000$ FT), MODEL 188 WING



(a) UPBENDING



(b) DOWN BENDING

FIGURE E-2. ULTIMATE STRENGTH VALUES OF $\sigma_w t_d$ (ADJUSTED TO $h = 12000 \text{ FT}$), MODEL 188 WING

On an ultimate basis, the allowable $\sigma_w \eta_d$ for V_D again is just 25/50 of the V_C value, and the allowable for V_B is again well in excess of 60/50 of the V_C value.

At V_C , the ultimate strength value of $\sigma_w \eta_d$ is 1.67 times the limit strength value. The ratio of ultimate-strength to limit-strength $N(y)/N_0$ values is $(2 \times 10^{-8})/(1.3 \times 10^{-6}) = 1.5 \times 10^{-2}$.

In order to confirm that the V_B speed selected in Section 7 is realistic, as well as to indicate how a V_B speed might rationally be selected in a power-spectral context, limit-strength, ultimate-strength, and stall values of $\sigma_w \eta_d$ (or y/A) for the Model 188 are plotted vs speed in Figure E-3.

The limit-strength and ultimate-strength values were taken directly from Table E-1 (Cases 417, 429, and 430).

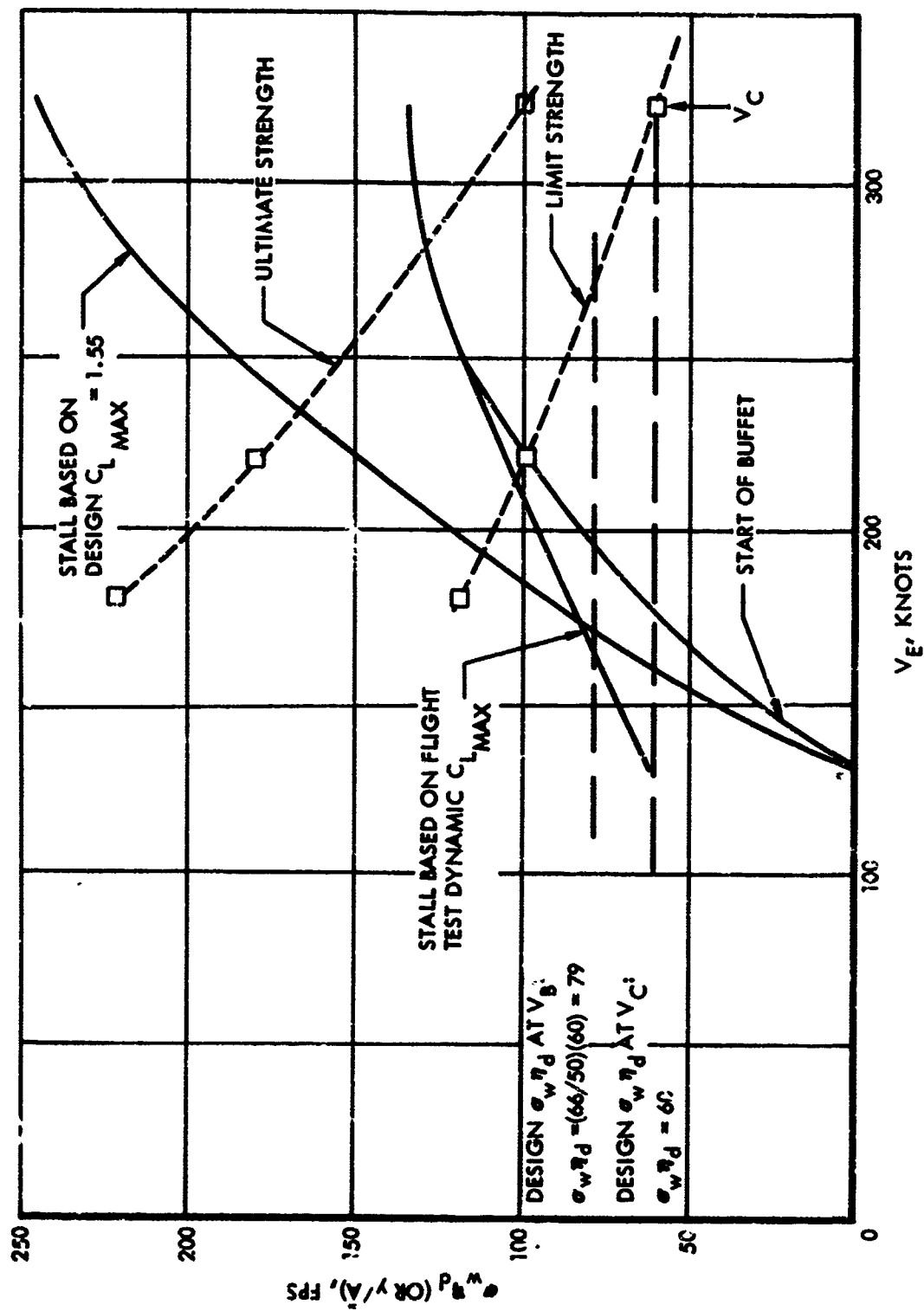
The stall values were obtained as follows:

$$n_{\text{stall}} = \frac{q C_{L_{\text{max}}}}{\left(\frac{W}{S}\right)}$$

$$(\sigma_w \eta_d)_{\text{stall}} = \frac{n_{\text{stall}}^{-1}}{\bar{A}_{\Delta n}}$$

The $\bar{A}_{\Delta n}$ value is a static-elastic value, inasmuch as the elastic-mode overtravel increment does not reflect airload on the airplane and therefore does not influence stall. In this instance, $\bar{A}_{\Delta n}$ was obtained by dividing the elastic-airplane values listed in Table B-2(a) - (c) by an estimated dynamic factor of 1.10. Results are shown separately for three different bases for $C_{L_{\text{max}}}$. The $C_{L_{\text{max}}}$ value of 1.55 was the best-estimate value used in the initial design of the airplane. The "dynamic $C_{L_{\text{max}}}$ " and "start of buffet" C_L values were based upon later flight tests of a similar airplane and vary with Mach number.

As indicated in Section 15.2.2, an appropriate definition of the V_B speed would be the speed at which stall would just occur at a load level given by the V_B design value of $\sigma_w \eta_d$. On this basis, Figure E-3 indicates a V_B speed for the Model 188 (at 116,000 lbs. gross weight) of either 165 or 170 knots depending upon the $C_{L_{\text{max}}}$ value selected. If start of buffet, rather than full stall, were utilized as the criterion, the V_B speed would increase to about 200 knots. It is concluded that the V_B speed of 180 knots selected in Section 7 is satisfactory for the purpose of the present analysis.

FIGURE E-3. V_B SPEED DETERMINATION, MODEL 188 AT 116,000 LB

It is interesting to observe from Figure E-3 that, in order to maintain the greatest margin against both buffet and exceedance of limit strength, a recommended rough air penetration speed for this airplane would be 220 knots. (This is higher than the V_B speed because of the excess strength at the V_B speed, for this airplane.) If a recommended rough air speed were to be based upon ultimate rather than limit strength, the speed would be much greater still.

E.2 Model 749 Wing

E.2.1 Design Envelope Criterion. In determining limit and ultimate strength values of $N(y)$ and of $\sigma_w \eta_d$ for the Model 749 wing, it was considered desirable to first generate a set of enveloping conditions for the critical V_C design envelope case, using generally the technique illustrated for the Model 188 wing in Appendix C. Stress analysis for these conditions would then indicate the most critical regions of the wing, as well as leading to an estimate of the V_C limit-strength value of $\sigma_w \eta_d$. It was felt that a set of conditions enveloping a design envelope case would be as useful for this purpose as one enveloping mission analysis loads, and it would be appreciably easier to generate.

Inasmuch as Case 308 appeared to be the critical V_C case, it was selected as the case to be enveloped. Three upbending conditions were generated, designated I, II, and III. These were roughly comparable to the Model 188 conditions I, II, and IV listed in Table C-11; some indication as to their nature is evident from their locations on the equal probability ellipsoids of Figures 11-3(e) and (f). They were generated at a $\sigma_w \eta_d$ level of 92, corresponding to an $N(y)/N_0$ value of 4×10^{-8} , which was estimated to be approximately the limit strength level. Downbending loads were also considered; however, as a result of the excess strength in downbending of the Model 749 wing, it became obvious with only limited investigation that downbending gust loads would not be critical.

As in the corresponding Model 188 work, conditions were defined only for phasings of torsion with shear and bending in the upper right and lower left quadrants of the phase plane plot (Figure 11-3(c), for example). This phasing tends to match the statistically defined shear flow in the front beam. Closer scrutiny, however, of the "equal probability ellipses" for the Model 749, shown in Figures 11-3(c) and (f), made it clear that maximum rear beam shear flow conditions might be more critical, and the results of the stress analysis confirmed this conclusion.

Minimum margins of safety obtained for these conditions were:

Station	Condition	Location and Description	Margin of Safety
97	I	Lower surface skin, tension and shear	-.01
145	I	Rear beam web splice, attachments	-.03
145	II	Rear beam web splice, attachments	-.03
145	II	Lower surface cut-out, chordwise compr.	-.02
191	II	Front beam web splice, attachments	-.01
191	II	Front beam web, tension and shear	-.04

Inasmuch as the critical conditions for the rear beam had not been included, additional work was necessary in order to define a limit strength value of $\sigma_w \eta_d$.

Before proceeding further, however, it appeared desirable to make a systematic survey of all of the design envelope cases in order to establish with greater certainty which ones might be critical. Accordingly, loads for all of cases 301 through 318 were listed for an estimated limit strength level of $\sigma_w \eta_d = 93$. Loads were also listed for the V_D cases, 319 - 322, at $\sigma_w \eta_d = (25/50)(93) = 46.5$ and for the V_B case, 423, at $\sigma_w \eta_d = (4/3)(93) = 124$, where the factor $4/3$ is a rounded-off equivalent of $66/50$. These were unphased loads and were obtained simply by multiplying the \bar{A} values listed in Table 9-3 by the given $\sigma_w \eta_d$ values. Spanwise plots of these loads were then made, for comparison with each other and with the loads defined as Conditions I - III.

On the basis of these plots, it became clear that only Cases 307, 308, and 317 at V_G , and Case 323 at V_B , were likely to be critical; also, that the region of the wing outboard of the outboard nacelle would not be critical for any of the cases.

In order to determine actual limit-strength values of $\sigma_w \eta_d$ for these four cases, it was necessary to account for the phasing of the shear, bending moment, and torsion. Phasing factors to be applied to the unphased loads were determined separately for the regions of the wing between nacelles and inboard of the inboard nacelle. Appropriate phasing of the bending moment and shear was estimated with the assistance of the

"equal probability ellipses" in Figures 11-3(b) and (e). Phasing of the torsions relative to the shears and bending moments was then obtained such as to match the shear flows in, alternately, the front and rear beams. The resulting phasing factors are listed in Table E-2. In the "A" and "B" conditions, front beam shear flow was matched; these conditions correspond to points 2 and 3, respectively, in Figure 11-1. In the "C" conditions, rear beam shear flow was matched, with maximum shear and bending moment and reduced torsion. It is seen that 12 separate conditions were defined. No check was made to assure that the shears thus defined were integrated to give the bending moments, since at this stage these conditions were not to be used in actual stress analysis.

The 12 load conditions thus defined were then plotted on bending-torsion, shear-torsion, and shear-bending coordinates at each of wing stations 63, 145, 191, 263, and 337. Both the one-g and the net upbending loads were shown, along with the upbending and downbending loads from Conditions I, II, III.

Although 12 realistic conditions were now defined, they were defined only at a limited number of wing stations and were not necessarily exactly consistent from one wing station to another. It was quite desirable to avoid having to generate conditions that would be consistent over the entire wing, and also to minimize the number of conditions and the regions of the wing for which stress analysis would be required.

Accordingly, four new conditions for stress analysis were now defined, by arbitrarily spotting in four points on each shear-torsion diagram such as to envelope the conditions plotted. Conditions IV, V, and VI were upbending conditions. Shear (and hence bending moment) were comparable for all of these; the torsions, however, varied over a wide range, with Condition IV having the highest positive torsion and Condition VI the highest negative torsion. Condition VII was a conservatively defined downbending condition. In defining these four conditions, consistency of shears and torsions from one wing station to the next was maintained only qualitatively. To determine bending moments, the shears defined on the five shear-torsion plots were plotted vs wing station and integrated to give bending moments. Points representing the four enveloping conditions were then added to the bending-torsion and shear-bending plots to assure that the 12 conditions were adequately enveloped with respect to bending moment as well as shear and torsion. Spanwise plots of all three load quantities were made for use in the stress analysis.

Stress analysis for Conditions IV through VII led to the following minimum margins of safety:

TABLE E-2. PHASING FACTORS, MODEL 749 DESIGN ENVELOPE CONDITIONS

Condition	Where Shear Flow Was Matched	Phasing Factors		
		S_z	M_x	M_y
307A	Front Beam, WS103	1.000	1.000	.824
	Front Beam, WS337	1.000	.950	.935
307B	Front Beam, WS103	.801	.801	1.000
	Front Beam, WS337	.821	.534	1.000
307C	Rear Beam, WS103	1.000	1.000	.200
	Rear Beam, WS337	.800	1.000	-.095
308A	Front Beam, WS103	1.000	1.000	.690
	Front Beam, WS337	1.000	.950	.890
308B	Front Beam, WS103	.702	.702	1.000
	Front Beam, WS337	.755	.491	1.000
308C	Rear Beam, WS103	1.000	1.000	.042
	Rear Beam, WS337	.800	1.000	-.228
317A	Front Beam, WS103	1.000	1.000	.618
	Front Beam, WS337	1.000	.950	.841
317B	Front Beam, WS103	.674	.674	1.000
	Front Beam, WS337	.694	.451	1.000
317C	Rear Beam, WS103	1.000	1.000	0
	Rear Beam, WS337	.800	1.000	-.324
323A	Front Beam, WS103	1.000	1.000	.571
	Front Beam, WS337	1.000	.950	.839
323B	Front Beam, WS103	.619	.619	1.000
	Front Beam, WS337	.729	.474	1.000
323C	Rear Beam, WS103	1.000	1.000	-.089
	Rear Beam, WS337	.800	1.000	-.231

Loading Condition	Wing Station	Location and Description	Margin of Safety
IV	115	Lower surface door, attachments	-.06
	145	Front beam web splice, attachments	-.01
	145	Lower surface cut-out, chordwise compr.	-.04
	191	Front beam web splice, attachments	-.07
	191	Front beam web, tension and shear	-.11
	289	Front beam web, tension and shear	-.09
V	97	Lower surface skin, tension and shear	-.03
	145	Rear beam web splice, attachments	-.01
	168	Lower surface cut-out, spanwise tension	-.03
	191	Front beam web splice, attachments	-.04
	191	Front beam web, tension and shear	-.07
VI	97	Lower surface skin, tension and shear	-.03
	145	Rear beam web splice, attachments	-.04

No negative margins were found for Condition VII, confirming that down-bending would not be critical.

Based on these margins, Conditions IV, V, and VI were adjusted in level, independently over various regions of the wing, such that zero margins of safety would result. Strength envelopes on bending-torsion and shear-torsion coordinates were thus defined at wing stations 103, 145, 191, 263, and 337.

It was now possible to go back to the 12 conditions, 307 A - C, 308 A - C, 317 A - C, and 323 A - C and obtain for each case a good approximation to the limit strength value of $\sigma_w \eta_d$ and the critical location in the structure. This limit-strength value of $\sigma_w \eta_d$ was determined separately at each wing station and separately based on the bending-torsion and shear-torsion envelopes. For each $\sigma_w \eta_d$ determination, a ray was drawn from the one-g point to the net load point and extended if necessary to intersect the strength envelope. Relative distances along this ray, in conjunction with the known $\sigma_w \eta_d$ value for which the condition was defined, then determined the limit strength value of $\sigma_w \eta_d$.

The resulting limit strength values of $\sigma_w \eta_d$ are shown in Table E-3(a). Each number is the minimum for the three subconditions A, B, and C. The lowest value in each column is the critical value and is underlined.

Approximate ultimate strength values of $\sigma_w \eta_d$ were obtained similarly and are shown in Table E-3(b).

TABLE E-3. PRELIMINARY LIMIT STRENGTH AND ULTIMATE STRENGTH VALUES OF $\sigma_w \eta_d$, MODEL 749 DESIGN ENVELOPE CONDITIONS

(a) LIMIT

WS	Case 307 (h = 16000 ft)		Case 308 (h = 16000 ft)		Case 317 (h = 7000 ft)		Case 323 (h = 7000 ft)	
	S_Z-M_Y	M_X-M_Y	S_Z-M_Y	S_Z-M_Y	S_Z-M_Y	M_X-M_Y	S_Z-M_Y	M_X-M_Y
103	93.0 (A,C)	92.2 (C)	95.5 (C)	92.3 (A,C)	88.7 (C)	88.2 (A,C)	97.0 (A,C)	91.6 (A,C)
145	<u>77.8 (C)</u>	88.3 (C)	<u>80.5 (C)</u>	87.0 (C)	<u>78.6 (C)</u>	<u>82.5 (C)</u>	92.0 (C)	89.3 (C)
191	81.5 (A)	<u>85.3 (A)</u>	83.6 (A)	<u>86.2 (A)</u>	80.2 (A)	83.6 (A)	<u>80.5 (A)</u>	<u>80.3 (A)</u>
263	87.8 (A)	93.0 (A)	93.0 (A)	93.0 (A)	93.0 (A)	93.0 (A,C)	83.7 (A)	84.0 (A)
337	(A)	(A)	(A)	(A,C)	(A)	(A)	85.3 (A)	87.0 (A)

NOTE: $\sigma_w \eta_d$ values for Case 323 have been multiplied by .75 for comparison. Letters A, B, and C denote critical condition. Values for critical WS in each column are underlined.

(b) ULTIMATE

Case WS	307		308		317		323	
	S_Z-M_Y	M_X-M_Y	S_Z-M_Y	M_X-M_Y	S_Z-M_Y	M_X-M_Y	S_Z-M_Y	M_X-M_Y
103	168.5 (A,C)	173.2 (A,C)	172.8 (A,C)	172.0 (A,C)	162.0 (A,C)	153.0 (A,C)	170.3 (A,C)	166.3 (A,C)
145	1.660 (C)	173.9 (C)	165.6 (C)	165.5 (C)	161.8 (C)	158.5 (C)	169.1 (C)	165.6 (C)
191	<u>146.0 (A)</u>	<u>156.2 (A)</u>	<u>147.1 (A)</u>	<u>156.1 (A)</u>	<u>143.2 (A)</u>	<u>151.0 (A)</u>	<u>144.5 (A)</u>	<u>148.2 (A)</u>
263	149.5 (A)	160.0 (A)	156.7 (A)	159.6 (A)	157.0 (A)	159.6 (A)	146.0 (A)	150.0 (A)
337	152.1 (A)	169.6 (A)	160.8 (A)	166.1 (A)	168.0 (A)	159.8 (A)	149.0 (A)	153.8 (A)

NOTE: $\sigma_w \eta_d$ values for Case 323 have been multiplied by .75 for comparison. Letters A, B, and C denote critical phasing. Values for critical WS in each column are underlined.

It was now possible to select critical conditions and locations for stress analysis of specific conditions. Stress analysis for Conditions IV, V, and VI had indicated that the critical stress generally resulted from combinations of bending and torsion moments; consequently, more weight was given to the results in the M_x - M_y column than in the S_z - M_y column in Table E-3.

It was not entirely certain from Table E-3(a) which of the 4 cases would be critical. It was clear, however, that the actual limit strength values of $\sigma_w \eta_d$ corresponding to each case could be determined by examining only cases 307C, 308C, and 317C at WS 145, and Cases 307A, 308A, 317A, and 323A at WS 191. Further, it was clear from the above listing of margins of safety that the critical element for the "C" conditions at WS 145 was the rear beam web splice, and for the "A" conditions at WS 191, the front beam web.

Similarly, in Table E-3(a), it was clear that the ultimate strength values of $\sigma_w \eta_d$ could be determined by examining only the front beam web at WS 191 for each of the "A" conditions.

As a result, only very limited stress analysis would suffice to finally determine the limit and ultimate strength values of $\sigma_w \eta_d$.

Before performing this stress analysis for the potentially critical conditions, two refinements were made in the definition of the loads. First, since one of the critical regions was found to be between the ribs supporting the inboard nacelle, the nacelle loads, which previously had been brought into the wing arbitrarily at the nacelle centerline, were redistributed to the two ribs. Second, it had become apparent from the stress analysis that axial stress, far more than shear flow, was governing the wing strength. Consequently, in selecting the relative phasing of shear and bending moment for the "A" conditions in Table E-2, it appeared that S_z , rather than M_x , should have been assigned the .950 phasing factor. Further, examination of the complete spanwise distributions available for Conditions I, II, and III indicated that for both the "A" and "C" conditions, S_z and M_x should be more nearly in phase at WS 191 than at WS 337. Consequently, revised phasing factors were defined, as shown in Table E-4. The phasing factors for M_y were not re-computed, as they were expected not to change significantly. In addition, in the stress analysis, the basis for the web shear-tension margin of safety was changed from the maximum tension maximum shear criterion used in the original design analysis to a circular interaction criterion now generally considered more realistic.

Consideration of the probable effects of these changes on the $\sigma_w \eta_d$ values given in Table E-3 indicated that the critical locations would not change.

TABLE E-4. REVISED PHASING FACTORS, MODEL 749
DESIGN ENVELOPE AND MISSION ANALYSIS CONDITIONS

		"A" Conditions			"C" Conditions		
		WS103, 145	WS191	WS337	WS103, 145	WS191	WS337
S _Z		1.000	1.000	1.000	1.000	.900*	.800
M _X		1.000	1.000*	.950	1.000	1.000	1.000
M _X	Case 307	.824	.935	.935	.200	-.095	-.095
	Case 308	.690	.890	.890	.042	-.228	-.228
	Case 317	.618	.844	.844	0	-.324	-.324
	Case 323	.571	.839	.839	-.089	-.231	-.231
	Mission Anal. Limit	.697	.854	.854	-.257	-.295	-.295
	Mission Anal. Ult	.712	.872	.875	-.198	-.281	-.281

* The corresponding values in Table E-2 were .80 and .95 for S_z and M_x respectively.

Accordingly, the pertinent conditions were redefined, at the necessary wing stations, at revised $\sigma_w \eta_d$ levels as follows:

Limit conditions:	Cases 307, 308, and 317	$\sigma_w \eta_d = 83$
	Case 323	$\sigma_w \eta_d = \frac{66}{50} 83 = 109.6$
Ultimate conditions:	Cases 307 and 308	$\sigma_w \eta_d = 155$
	Case 317	$\sigma_w \eta_d = 146$
	Case 323x	$\sigma_w \eta_d = \frac{66}{50} 155 = 205$

The ultimate $\sigma_w \eta_d$ values of 155 and 146 reflected a constant value of $N(y)/N_0$ in Figure 5-8 as the altitude varies. Case 323x is identical to Case 323 except for an increase in altitude from 7000 to 16000 ft. The 16000 ft. altitude became more critical for the V_F speed at the ultimate load level because of the opposite slope of the family of lines in Figure 5-8 at the ultimate as contrasted to the limit level. Loads were obtained for Case 323x from those of Case 323 by retaining the 1-g loads and decreasing the \bar{A} values 5%, in accordance with the relations indicated by comparison of the corresponding V_C cases, 308 vs 317.

The resulting margins of safety are shown in Table E-5. The limit-strength or ultimate strength values of $\sigma_w \eta_d$ were then computed as

$$\frac{(1 + MS)(\text{Net shear at given } \sigma_w \eta_d) - (\text{One-g shear})}{\bar{A}_{\text{Shear}}}$$

and are also shown in the table. Values underlined are at the altitude listed for the case. The other value for each case is an adjusted value obtained by moving along one of the family of lines in Figure 5-8. For the V_B conditions, the adjustment was along lines such as to maintain a constant ratio of V_B to V_C $\sigma_w \eta_d$. In other words, the underlined $\sigma_w \eta_d$ was divided by 66/50, the adjustment made to the new altitude, and the resulting value multiplied by 66/50.

TABLE E-5. FINAL LIMIT STRENGTH AND ULTIMATE STRENGTH
VALUES OF $\sigma_w \eta_d$, MODEL 749 WING

Condition And Location	Assumed $\sigma_w \eta_d$	Margin Of Safety	Altitude, Ft	Limit Strength $\sigma_w \eta_d$	
				h = 7000 Ft	h = 16000 Ft
307C, WS145	83	.06			
307A, WS191	83	.04	16000	90.0	<u>89.2</u>
308C, WS145	83	.06	16000	92.2	<u>92.0</u>
308A, WS191	83	.06			
317C, WS145	83	.03	7000	<u>87.5</u>	86.1
317A, WS191	83	.05			
323A, WS191	109.6	0	7000	<u>109.6</u>	106.9
				Ultimate Strength $\sigma_w \eta_d$	
				h = 7000 Ft	h = 16000 Ft
307A, WS191	155	0	16000	145.5	<u>155.0</u>
308A, WS191	155	.01	16000	146.2	<u>157.2</u>
317A, WS191	146	.05	7000	<u>156.2</u>	164.4
323A, WS191	205	.01	16000	194.8	<u>207.9</u>

It is seen that, for limit strength, Case 317, at $h = 7000$ ft., is slightly more critical than the 16,000 ft. cases. The effect of c.g. location is indicated by a comparison of Cases 307 and 308. The effect of c.g. location on $\sigma_w \eta_d$ is slightly greater than indicated in Table E-3, but still only about 3%. The forward c.g. case (307) is the more critical, contrary to earlier indications that led to omitting the forward c.g. cases at $h = 7000$ ft. A forward c.g. case at 7000 ft. would presumably be slightly more critical than Case 317. The difference is so small, however, that further refinement of the limit strength $\sigma_w \eta_d$ is not considered justified.

For ultimate strength, the 16000 ft. cases are critical, and the effect of c.g. location is less than 2%.

As a result of the work to this point, it became apparent that, for the assumed relative turbulence intensities at V_B , V_C , and V_D , cases other than the four specifically investigated were not likely to be critical. As in the Model 188 investigation, however, it was considered desirable at this stage to make an overall survey by determining, at least roughly, allowable $\sigma_w \eta_d$ values at both limit and ultimate levels, for all cases, considering upbending and downbending individually.

For this purpose, wing bending moment at WS 191 was used as the measure of strength. For all the cases investigated, WS 191 either was the critical location, or missed being critical by only a few percent. And at the critical location in the structure, the net stress was produced predominantly by the bending moment. Values of the WS 191 bending moment corresponding to limit and ultimate strength were taken as follows, based on the margins of safety shown in Table E-5:

	<u>Limit</u>	<u>Ultimate</u>
V_B , upbending	12.6×10^6 in.lb.	18.4×10^6 in.lb.
V_C and V_D , upbending	13.2×10^6 in.lb.	19.1×10^6 in.lb.
V_B , V_C , and V_D , downbending	7.90×10^6 in.lb.	11.85×10^6 in.lb.

The downbending limit value is taken as 60% of the higher of the two upbending values, and the downbending ultimate value as 1.5 times the limit.

The results of this survey are shown in Table E-6 and Figures E-4 and E-5.

TABLE E-6. SUMMARY OF LIMIT STRENGTH AND ULTIMATE STRENGTH
 $\sigma_v \eta_d$ VALUES (ADJUSTED TO $h = 16000$ FT), MODEL 749 WING

Case No	Cond	Gross Weight Lb	Fuel Weight Lb	Zero Fuel Weight Lb	C.G. % MAC	Altitude ft	Equivalent Airspeed V_e , Kts	Limit		Ultimate	
								Up Gust	Down Gust	Up Gust	Down Gust
								$\sigma_v \eta_d$	$\sigma_v \eta_d$	$\sigma_v \eta_d$	$\sigma_v \eta_d$
302	V_C	58480	2500	55980	32.0	16000	235	180	205	288	280
304	V_C	90900	34920	55980	32.0	16000	235	219	244	349	331
306	V_C	107000	34920	72080	32.0	16000	235	135	188	225	249
308	V_C	88964	2500	86464	32.0	16000	235	92	159	157	206
310	V_C	95000	8536	86464	32.0	16000	235	94	159	165	207
312	V_C	101000	14536	86464	32.0	16000	235	100	160	173	208
314	V_C	107000	20536	86464	32.0	16000	235	102	163	176	212
315	V_C	88964	2500	86464	32.0	20000	218	96	174	168	222
316	V_C	88964	2500	86464	32.0	12000	235	86	157	158	204
317	V_C	88964	2500	86464	32.0	7000	235	86	167	167	214
320	V_D	58480	2500	55980	32.0	7000	313	126	179	209	241
322	V_L	88964	2500	86464	32.0	7000	313	51	125	105	161
323	V_B	88964	2500	86464	32.0	7000	175	107	214	211	286
323X	V_B	88964	2500	86464	32.0	7000	175	116	208	208	275

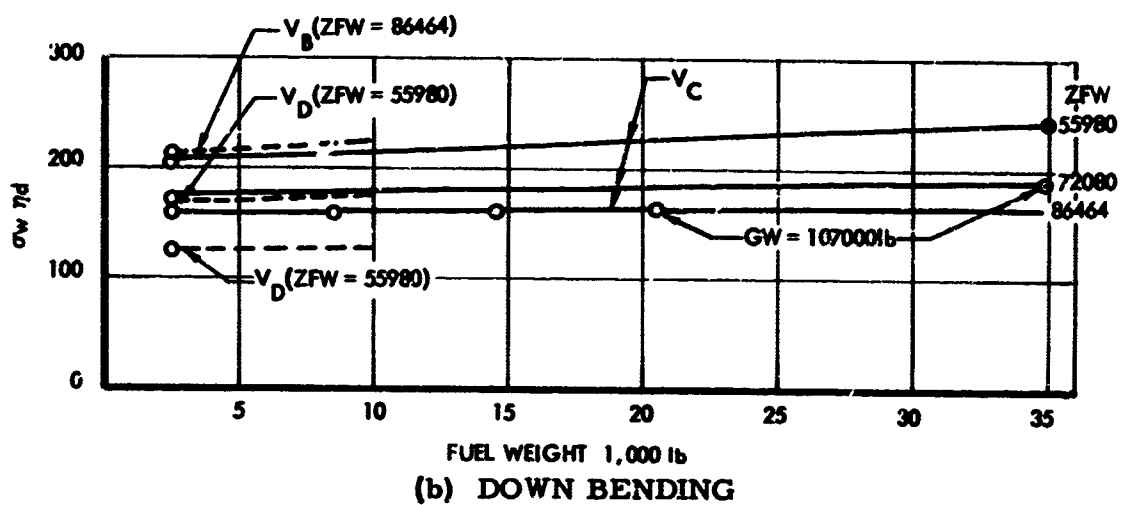
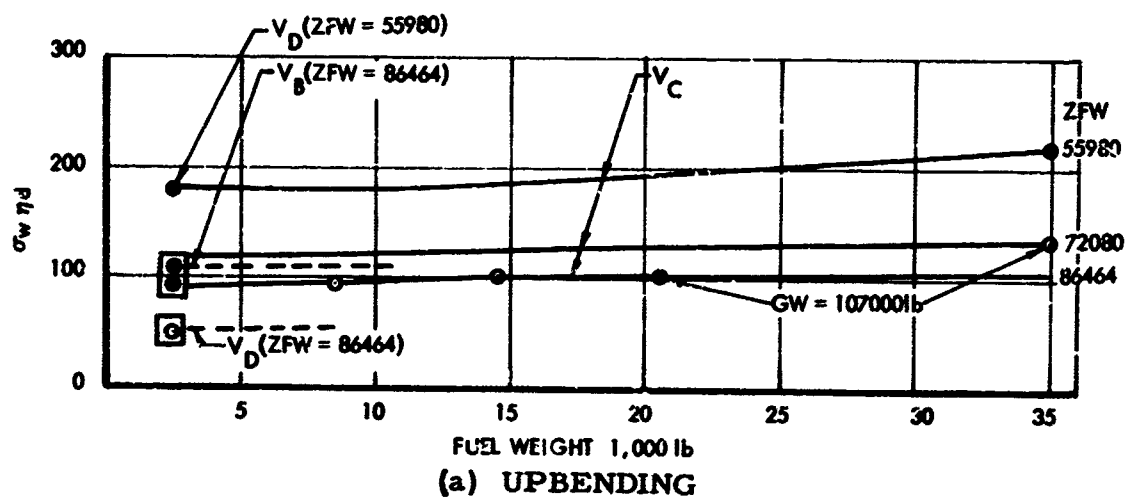
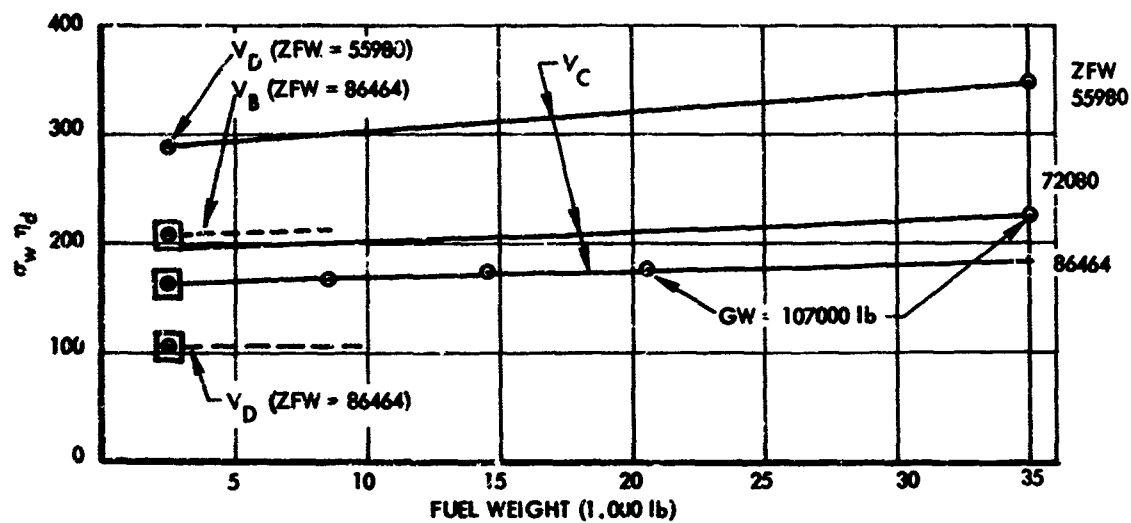
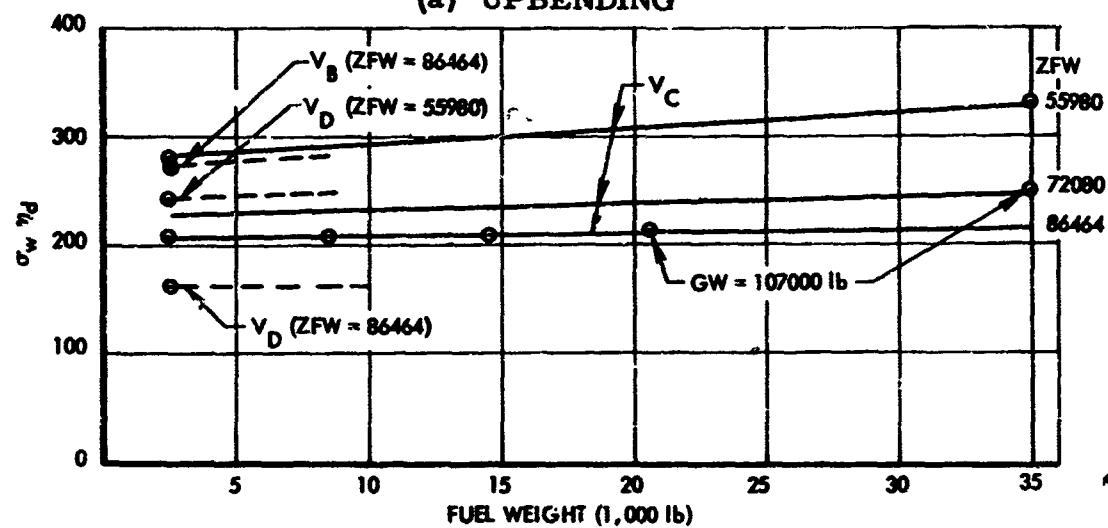


FIGURE E-4 LIMIT STRENGTH VALUES OF $\sigma_w \eta_d$ (ADJUSTED TO $h = 16000$ FT), MODEL 749 WING



(a) UPBENDING



(b) DOWN BENDING

FIGURE E-5 ULTIMATE STRENGTH VALUES OF σ_{wtd} (ADJUSTED TO $h = 16000$ FT), MODEL 749 WING

Where values obtained by the approximate method differ from those shown in Table E-5, the latter are substituted. In no case, however, did the difference amount to over 3%, and for the limit conditions it was less than 1%.

In both the table and the figures, the $\sigma_w \eta_d$ values were adjusted to an altitude of 16,000 ft. by moving along one of the family of lines in Figure 5-8. For the V_B and V_D conditions, the adjustment was along lines such as to maintain a constant ratio of the V_B or V_D $\sigma_w \eta_d$ value to the V_C value.

The figures are directly comparable to those for the Model 188, Figures E-1 and E-2. Calculated points are indicated by circles. Where only one calculated point is available for a curve, the estimated trend is indicated by a dash line. The large squares denote the critical conditions for the three speeds respectively.

On a limit basis, it is seen that the allowable $\sigma_w \eta_d$ for V_D is somewhat greater than 25/50 of that for V_C . The allowable $\sigma_w \eta_d$ for V_B is somewhat greater than that at V_C , but not by the full 66/50 ratio. The down-bending conditions are clearly much less critical than the upbending conditions.

On an ultimate basis, the allowable $\sigma_w \eta_d$ for V_D is well in excess of 25/50 of that for V_C . The allowable $\sigma_w \eta_d$ for V_B is just 66/50 of that for V_C .

At V_C , the ultimate-strength value of $\sigma_w \eta_d$ is 1.82 times the limit strength value. The ratio of ultimate-strength to limit strength $N(y)/N_0$ values is $1.0 \times 10^{-10}/8 \times 10^{-8} = 1.2 \times 10^{-3}$.

E.2.2 Mission Analysis Criterion. By entering the mission analysis exceedance curves with limit-strength and ultimate-strength values of bending moment at WS 191 obtained from the work described above, it was possible to make good preliminary estimates of limit and ultimate frequencies of exceedance. The following values were thus selected at which to define load conditions for stress analysis.

Limit: $N(y) = 1.0 \times 10^{-5}$ exceedances per hour

Ultimate: $N(y) = 3.0 \times 10^{-9}$ exceedances per hour

A set of loads at each of these two levels was read from the exceedance curves. Inasmuch as Case 106 was generally among the predominant

contributors to the exceedances, its one-g loads were considered representative. These were subtracted from the net loads to give a set of incremental loads to which phasing factors could be applied.

At each of two levels, limit and ultimate, two conditions were defined. These corresponded to the "A" and "C" conditions defined for the design envelope cases, and were similarly designated. Phasing factors were obtained in the same way as for the design envelope conditions. The resulting values have been included in Table E-4. The corresponding loads are listed in Table E-7.

Critical locations were known from the design envelope analyses. As a result, stress analysis was performed only for the front beam at WS 191 ("A" conditions) and the rear beam at WS 145 ("C" conditions). The following margins were obtained:

Limit Condition A (front beam, WS 191)	-.02
Limit Condition C (rear beam, WS 145)	+.01
Ultimate Condition A (front beam, WS 191)	+.02
Ultimate Condition C (rear beam, WS 145)	+.10

The corresponding limit and ultimate frequencies of exceedance were obtained from the exceedance curve for bending moment at WS 191. The curves were entered with allowable bending moments equal to $(1 - .02)$ and $(1 + .02)$ times the values at 1.0×10^{-5} and 3.0×10^{-9} respectively; the corresponding frequencies of exceedance were found to be:

Limit:	$N(y) = 1.8 \times 10^{-5}$ cycles per hour
Ultimate:	$N(y) = 4.2 \times 10^{-9}$ cycles per hour

The ratio of ultimate to limit frequencies of exceedance is 2.3×10^{-4} , or $10^{-3.4}$.

E.3 Model 188 Fuselage and Tail, Vertical Gust

E.3.1 Mission Analysis, Limit Strength. In Appendix D, load conditions were developed for the Model 188 fuselage such that statistically defined loads were matched. This set of conditions reflected a mission analysis approach and a level of severity defined by a frequency of exceedance of 1.00×10^{-5} cycles per hour. Preliminary comparison of these loads with Model 188 limit design fuselage loads indicated that at no point in the fuselage were the limit design loads exceeded. At this

TABLE E-7. MISSION ANALYSIS LOAD CONDITIONS, MODEL 749 WING

Load Quantity	Wing Station	Limit, $N(y) = 1.0 \times 10^{-5}$					Ultimate, $N(y) = 3.0 \times 10^{-9}$				
		Unphased Net Loads	One-g Loads (case 106)	Increment	Phased Net Loads		Unphased Net Loads	One-g Loads (case 106)	Increment	Phased Net Loads	
					Cond A	Cond C				Cond D	Cond F
$10^3 N_z$	103	48.1	18.721	29.379	48.100	48.100	67.5	18.721	48.779	67.5	67.5
	145	42.0	16.350	25.650	42.000	42.000	58.3	16.350	41.950	58.3	58.3
	191	55.7	20.542	35.158	55.700	52.184	78.7	20.542	58.158	78.7	72.884
	337	35.1	12.180	22.920	-	-	49.6	12.180	37.420	-	-
$10^6 M_x$	103	17.40	6.850	10.550	17.400	17.400	24.35	6.850	17.500	24.35	24.35
	145	15.50	6.041	9.509	15.550	15.550	21.75	6.041	15.709	21.75	21.75
	191	13.30	5.223	8.107	13.330	13.330	18.65	5.223	13.427	18.65	18.65
	337	6.90	2.825	4.075	-	-	9.58	2.825	6.755	-	-
$10^{-6} M_y$	103	.41	-1.237	1.647	-.089	-1.660	1.45	-1.237	2.687	.676	-1.769
	145	.27	-1.379	1.649	-.230	-1.830	1.31	-1.379	2.689	.536	-1.911
	191	.91	-.693	1.603	+.676	-1.166	1.93	-.693	2.623	1.594	-1.430
	337	.64	-.896	1.536	-	-	1.62	-.896	2.516	-	-
a	103 FB	339	-99	438	-	-	630	-99	729	-	-
	103 RF	-786	-416	-370	-	-	-998	-416	-582	-	-
	337 FB	640	-115	755	-	-	1130	-115	1245	-	-
	337 RF	-820	-435	-385	-	-	-1050	-435	-615	-	-

Note: Torsions are with respect to elastic axis (FS 561.2).

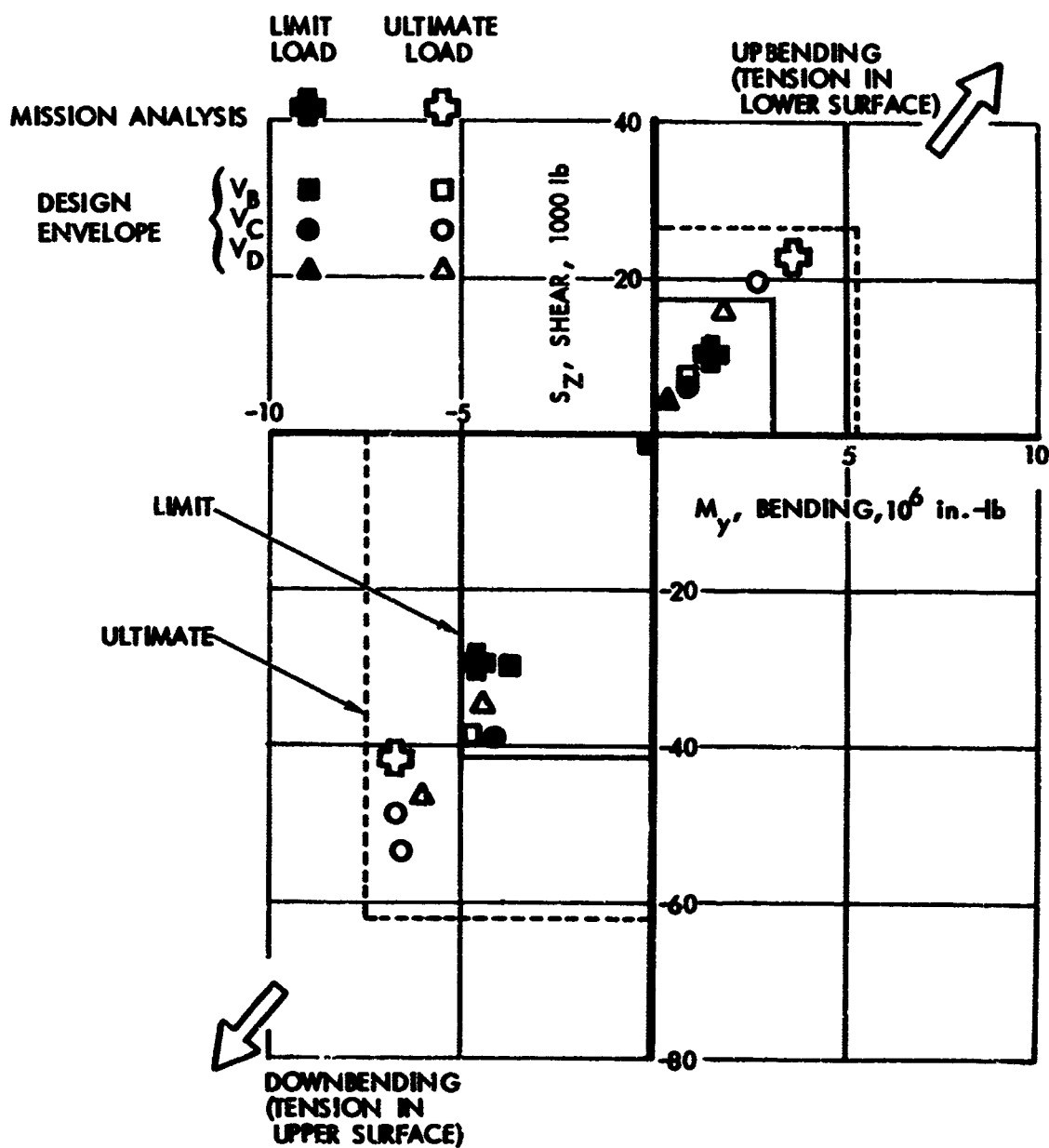
frequency of exceedance the Model 188 wing, on the other hand, actually showed slight negative margins of safety. Hence it was clear that the fuselage would be less critical than the wing and therefore would not influence the vertical gust design level.

However, in order to obtain a clearer picture of the critical regions of the fuselage, as well as a direct measure of how much less critical the fuselage is than the wing, this comparison was now made on a more formal basis.

In Figures E-6(a) through (f), design load envelopes are shown for the Model 188 fuselage at the various locations where load outputs were obtained from the ten-degree-of-freedom analysis. These locations, it will be recalled, were potentially critical locations as indicated by the design stress analysis. In all cases, the envelopes are shown as rectangles. These are defined by design conditions at or very close to the upbending and downbending corners. The rectangular shape is believed to approximate closely the shape of the actual strength envelopes, since the stress analysis indicated relatively little interaction between shear and bending moment. For the design downbending conditions, design margins of safety were rather low and the design load envelopes are believed to be fairly good approximations to actual strength envelopes. For the upbending conditions, considerably greater strength was available than indicated by the envelopes.

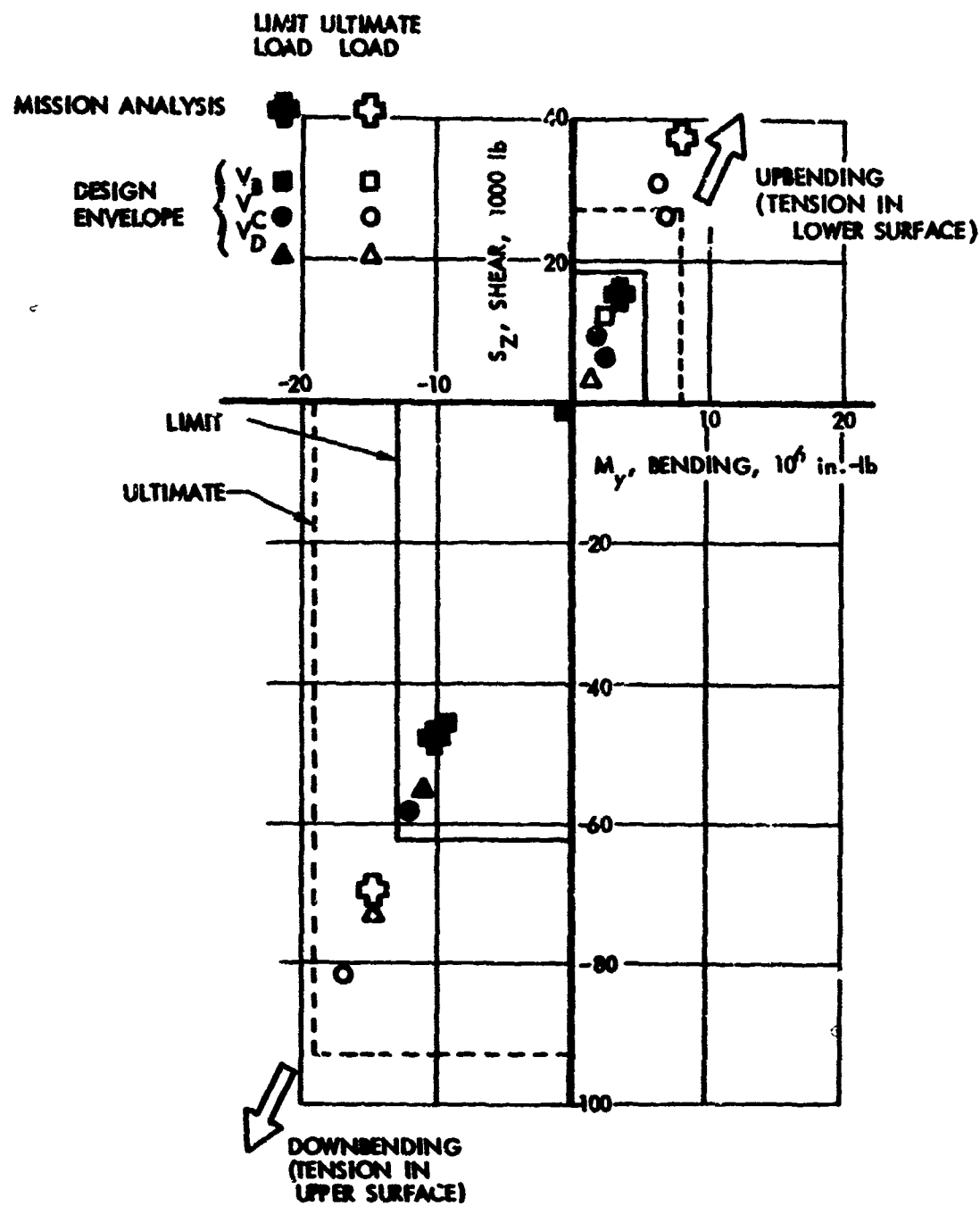
The mission analysis limit points shown on the figures were read from load exceedance curves, such as given in Figures 9-8 and 9-9, at a frequency of exceedance of 2.4×10^{-5} cycles per hour. This level corresponds approximately to the limit strength of the Model 188 wing, as established in Appendix E. The plotted points reflect unphased values of shear and bending moment in all cases. As can be inferred from the results given in Appendix D, actual phasing factors are generally close to unity. Also, because of the absence of significant interaction between shear and bending moment, the validity of the comparison does not depend upon the shear and bending moment being exactly in phase.

It is seen that at all locations the mission analysis limit load is well below the design limit load given by the solid line in the figures. Based on downbending strength - upbending being found less critical when account is taken of the higher margins of safety for the upbending design conditions - the critical location is F.S. 350; and the limit strength value of $N(y)$ at this location, as read from the exceedance curve for bending moment at the limit design load level of -5.0×10^6 in.lb., is 6×10^{-5} exceedances per hour. This is considerably lower than the value of 2.1 exceedances per hour for the wing.



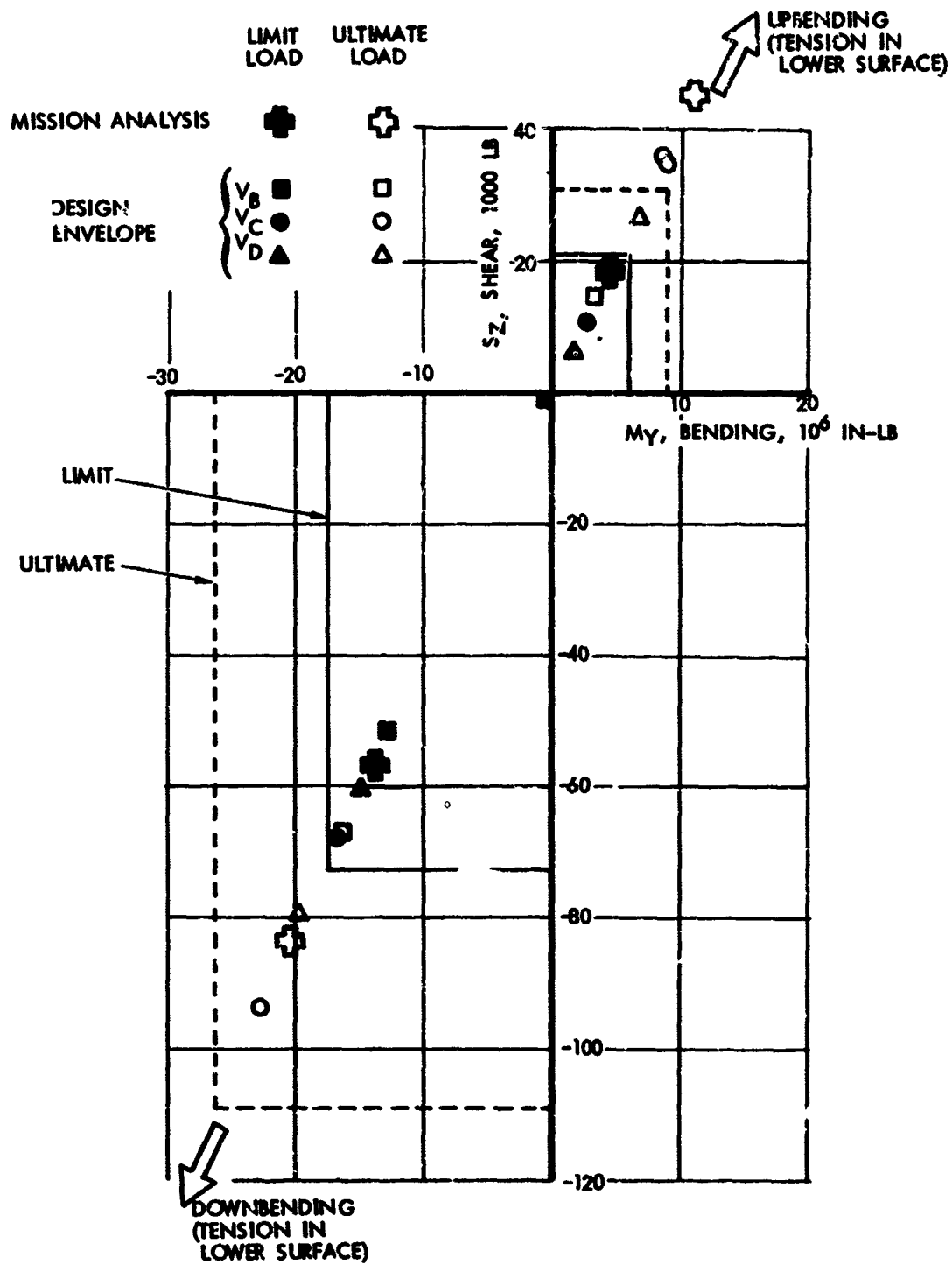
(a) FS 350

FIGURE E-6 COMPARISON OF APPLIED FUSELAGE LOADS WITH DESIGN STRENGTH - MISSION ANALYSIS AND DESIGN ENVELOPE CRITERIA - MODEL 188



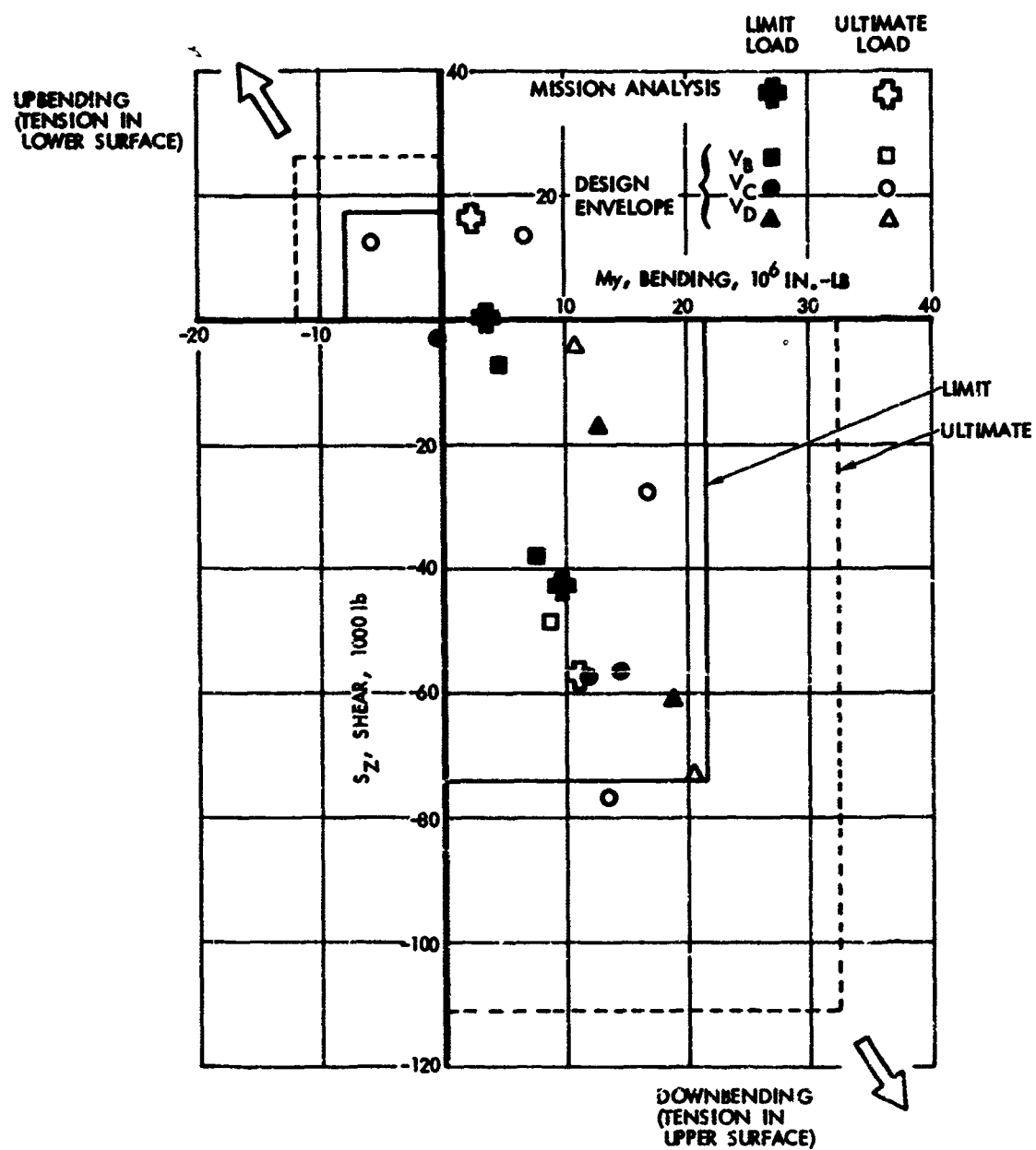
(b) FS 500

FIGURE E-6 CONTINUED

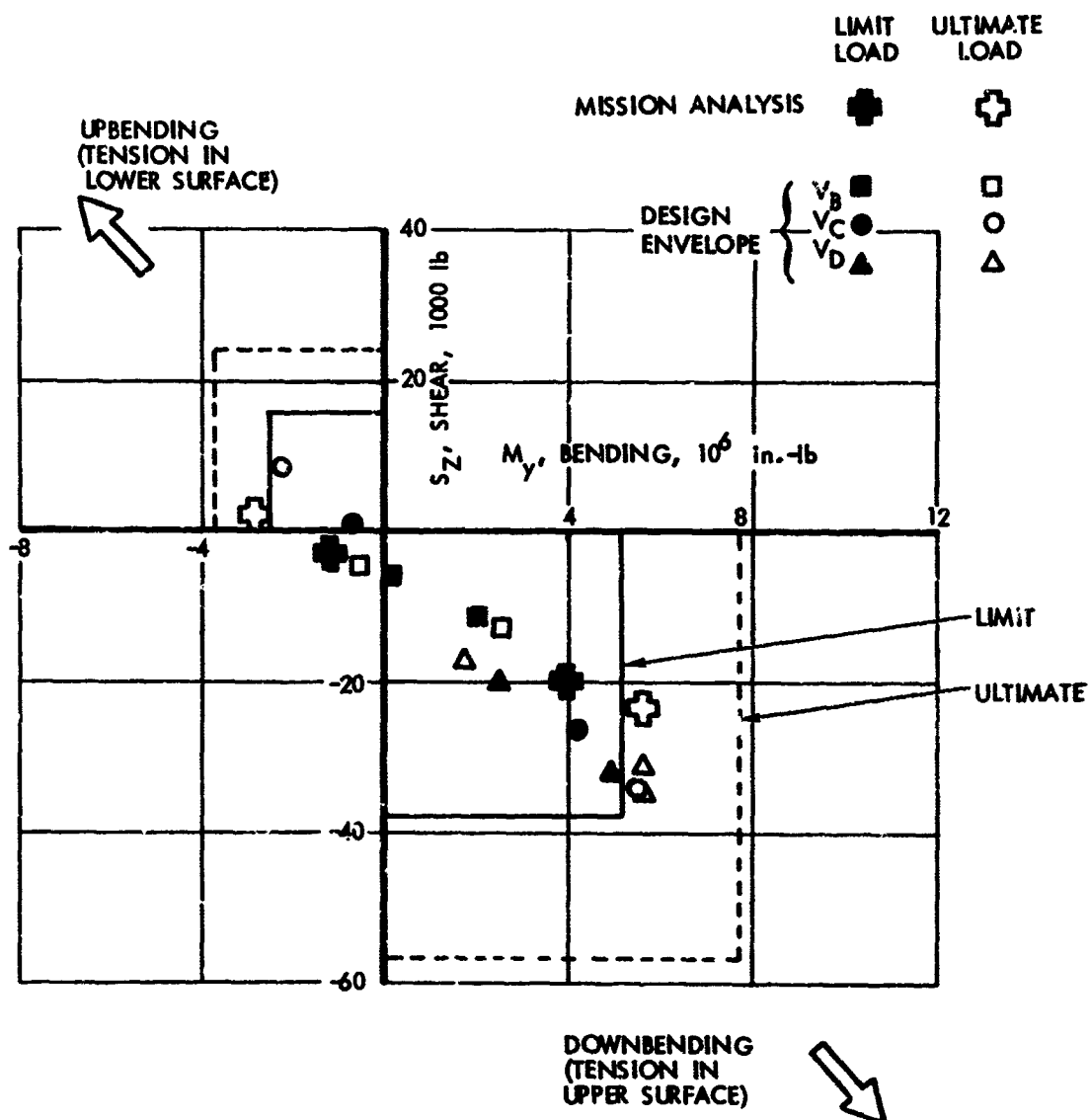


(c) FS 571

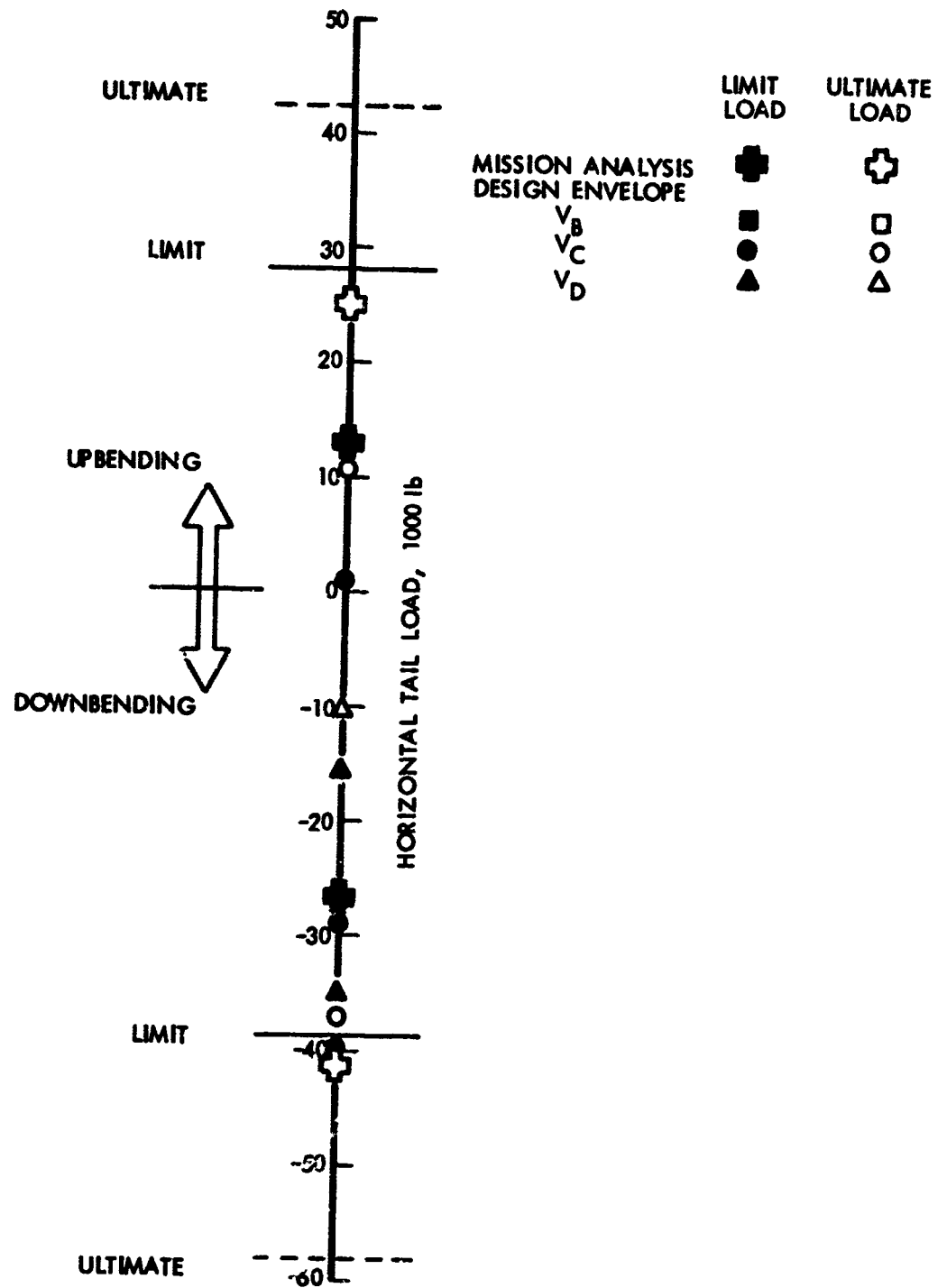
FIGURE E-6 CONTINUED



(d) FS 695
FIGURE E-6 CONTINUED



(e) FS 1000
FIGURE E-6 CONTINUED



(f) HORIZONTAL TAIL
FIGURE E-6 CONCLUDED

E.3.2 Mission Analysis, Ultimate Strength. As in the above investigation of the limit strength level, statistically defined loads were also obtained for the Model 188 fuselage and horizontal tail at an appropriate ultimate strength frequency of exceedance; these were then added to Figures E-6(a) through (f). The frequency of exceedance was taken as that corresponding to ultimate strength of the Model 188 wing, or 1.4×10^{-8} cycles per hour.

The statistically defined loads are larger than the design ultimate loads only for upbending at FS 500 and FS 571. However, as noted above, the design loads for upbending have large positive margins of safety due to the inherent strength resulting from the high downbending loads. The allowable shear is essentially the same in upbending as in downbending. An indication of the allowable bending moment in upbending is given by the minimum margin of safety for the design upbending conditions at FS 500 and FS 571. This was + .37 (at FS 571), due to buckling of an upper longeron due to bending moment alone. As a result, it became clear that the ultimate strength value of $N(y)$, like the limit-strength value, is governed by downbending, and that again the fuselage is less critical than the wing. The critical fuselage location is FS 350, and the ultimate strength value of $N(y)$ is approximately 1×10^{-9} .

E.3.3 Design Envelope Criterion. Statistically defined loads based on design envelope cases are also shown on Figures E-6(a) through (f). In obtaining these loads, the limit and ultimate strength values of $\sigma_w \eta_d$ were taken as defined by Model 188 wing strength, at 60 and 100 fps respectively. The loads are then given by

$$\text{Load} = (\text{one-g value}) \pm (\bar{A}) (\sigma_w \eta_d)$$

Factors of 66/50 and 25/50 were applied to $\sigma_w \eta_d$ for the V_B and V_D conditions respectively. As noted in Appendix E, these factors are the ratios of currently specified U_{de} gust velocities at the respective speeds. On the assumption that the same ratios would be retained in a power-spectral criterion, the loads resulting from these $\sigma_w \eta_d$'s are directly comparable as potential critical design conditions.

Each plotted point represents the most critical of the various cases. A variety of cases were critical, as indicated by Table E-8.

Again bearing in mind the conservatism of the upbending design load envelopes, it is seen that in all cases, both limit and ultimate, the statistically defined loads are well within the fuselage strength. Therefore it is concluded that the fuselage is not critical and will not influence the selection of design $\sigma_w \eta_d$ levels.

Approximate limit-strength and ultimate-strength values of $\sigma_w n_d$, adjusted to an altitude of 12,000 ft. (in the same manner described in Appendix E) are as follows:

	Case	Altitude	Location	Limit	Ultimate
V_B	427	7000 ft.	FS 350 downbending	141 fps	270 fps
V_C	407	12000 ft.	FS 571 downbending	67 fps	120 fps
V_D	426	7000 ft.	FS 350 downbending	38 fps	73 fps

The critical cases and locations noted above are also indicated by underlining in Table E-8. It is seen that the V_B values are far greater than 66/50 of the corresponding V_C values, and that the V_D values are greater than 25/50 of the V_C values. Consequently, the V_B and V_D conditions are less critical than the V_C conditions.

E.4 Model 749 Fuselage and Tail, Vertical Gust

A comparison of statistically defined loads for the Model 749 fuselage and tail with the corresponding design loads (as approximate measures of limit and ultimate strength) is given in Figures E-7(a) through (c).

As in the corresponding Model 188 comparison presented in Appendix E, Section E.3 the design load envelopes are shown as rectangles. The maximum shear and maximum bending moment conditions defining the envelopes were the same, in all cases.

The statistically defined loads also are obtained in the same way as in the Model 188 comparison.

The mission analysis points are plotted at frequency of exceedance levels, for the limit and ultimate conditions respectively, of 2.4×10^{-5} and 1.4×10^{-8} cycles per hour. These are the same values used in the Model 188 comparison in Appendix E, Section E.3.

The design envelope points are plotted at limit and ultimate $\sigma_w n_d$ values of 60 and 100 fps, as in the Model 188 analysis. Factors of 66/50 and 25/50 were again applied to $\sigma_w n_d$ for the V_B and V_D conditions respectively.

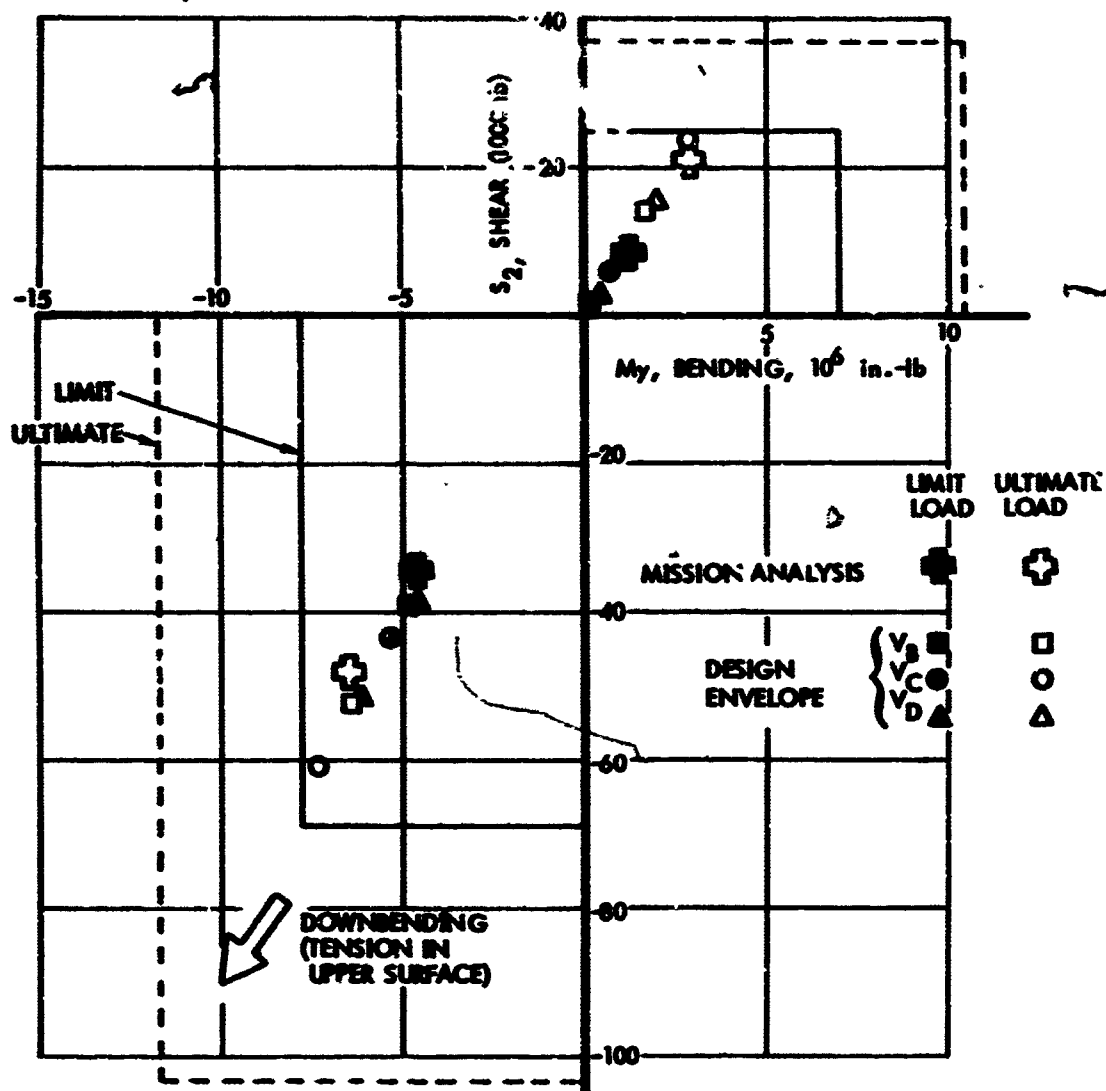
In all cases, the statistically defined loads are far below the design loads. As a result, the Model 749 fuselage and tail strength will not influence the selection of design levels of $H(y)$ or of $\sigma_w n_d$.

TABLE E-8. CRITICAL FUSELAGE CASES, MODEL 188
(a) DOWN BENDING

Location	Critical Case					
	Limit			Ultimate		
	V _B	V _C	V _D	V _B	V _C	V _D
FE 350	427	407	<u>426</u>	427	410	<u>426</u>
500	<u>427</u>	407	426	<u>427</u>	407	426
571	427	<u>407</u>	425	427	<u>407</u>	426
695	427	408	425	427	408	425
1000	427	402	425	427	402	423
Horiz. Tail	-	401	423	-	402	423

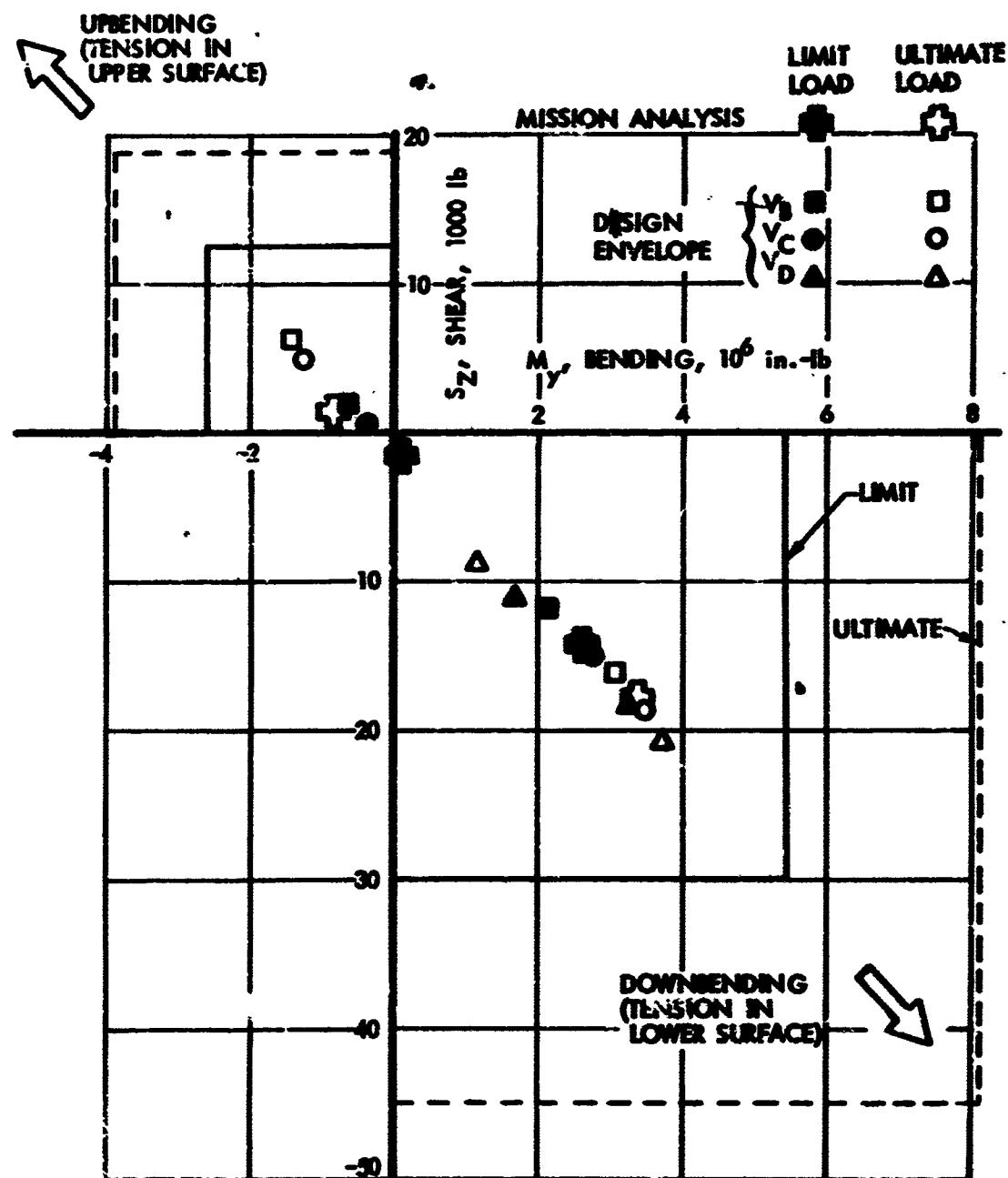
(b) UPBENDING

Location	Critical Case					
	Limit			Ultimate		
	V _B	V _C	V _D	V _B	V _C	V _D
FS 350	427	410	426	427	410	426
500	427	408	426	426	408	426
571	427	410	426	427	407	426
695	427	418	425	427	407	425
1000	427	418	424	427	418	424
Horiz. Tail	402	424	190	-	402	424

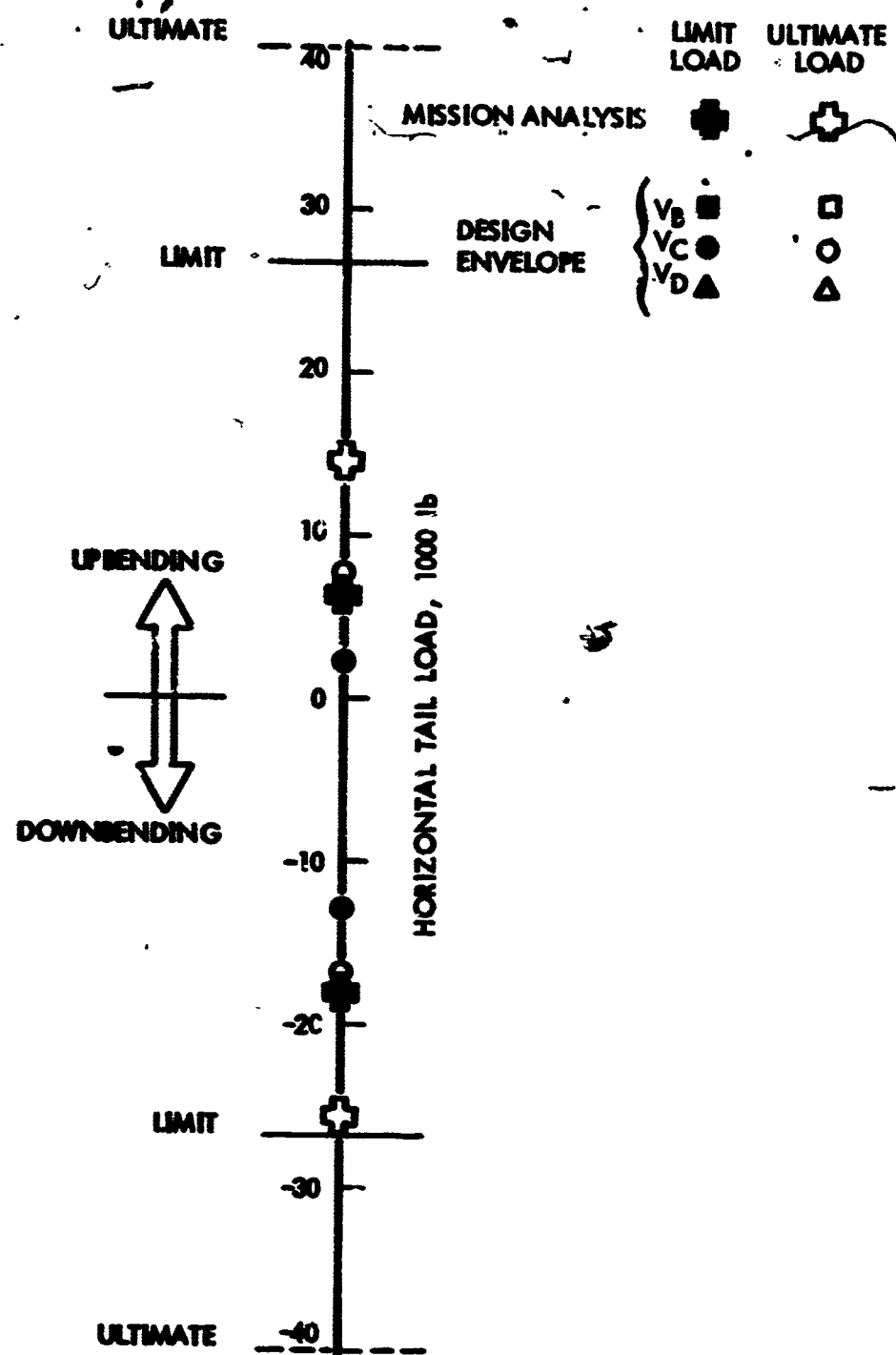


(a) FS 476

FIGURE E-7 COMPARISON OF APPLIED FUSELAGE LOADS WITH DESIGN STRENGTH - MISSION ANALYSIS AND DESIGN ENVELOPE CRITERIA - MODEL 749



(b) FS 976
FIGURE E-7 CONTINUED



(c) HORIZONTAL TAIL
FIGURE E-7. CONCLUDED

Approximate limit and ultimate strength values of $N(y)$, based on the design load envelopes shown are:

Limit: $N(y) = 4.5 \times 10^{-9}$ exceedances per hour

Ultimate: $N(y) = 1.7 \times 10^{-14}$ exceedances per hour

The critical location in both cases is the horizontal tail in downbending.

Approximate limit and ultimate strength values of $\sigma_w \eta_d$, adjusted to an altitude of 16,000 feet as described in Appendix E, are:

	Case	Altitude	Limit	Ultimate
V_B	323	7000	185 fps	310 fps
V_C	302	16000	110 fps	186 fps
V_D	320	7000	71 fps	120 fps

The critical location in both cases is the forebody in downbending.

It should be remarked that the $\sigma_w \eta_d$ values shown would have been materially higher if realistic payload running loads had been assumed, in accordance with present-day practice. The values used were taken from the original design loads determination of the airplane and were roughly 50% higher than would be used today.

E.5 Model 188 Fuselage and Tail, Lateral Gust

In establishing the limit and ultimate strength values of $N(y)$ and $\sigma_w \eta_d$ for lateral gust for the Model 188, major attention was given to the fin. The fin loading is measured by a single quantity, namely fin side load, and its limit and ultimate strength, in terms of allowable side load, can readily be determined. For the fuselage, on the other hand, many locations throughout the aftbody are potentially critical. At any given location, the stresses arise from airloads on the vertical tail and the fuselage, relieving inertia forces due to the lateral and yawing accelerations, balancing airloads on the horizontal tail, and the one-g level flight gravity forces. Variations in gross weight, c.g. position, and payload never affect all of these loads sources in the same way. As a result, it is virtually impossible to eliminate potential design conditions by inspection. To find the critical fuselage conditions would require generating design conditions and performing stress analysis for a multitude of combination . . . g. position (forward and aft limit),

gross weight, and payload-fuel quantities. The original design analysis, however, encompassed such lateral loading conditions as discrete lateral gust, yaw maneuver, and engine failure. For these conditions, the fuselage was not significantly more limiting than the fin. Also, there was some indication that if the fuselage were to be found critical, it would be in the far aft region, close to the tail, where the amount of aftbody payload would have a negligible effect.

Consequently, it was decided that a thorough investigation of all potentially critical aftbody conditions was not justified. It did appear desirable, however, to make at least a cursory fuselage stress analysis. For this purpose, three conditions were defined.

Inasmuch as the original limit design side load on the vertical tail had been 24000 lb., all three conditions were defined at this level. Each condition, however, was at a different speed, since equivalent airspeed has a large effect on the balancing tail load and hence on the one-g flight loads upon which the lateral gust increment superimposes. The three conditions selected were:

Mission analysis Case 202,	282 knots EAS at 11000 ft.
V_C	324 knots EAS at 12000 ft.
V_D	405 knots EAS at 8000 ft.

Aftbody payload was rather arbitrarily assumed to be zero, inasmuch as this condition appeared to be critical in the original design analysis. Balancing tail loads were arbitrarily based on a gross weight of 113,000 lb. for the V_D condition and 77500 lb. for the V_C condition. Fuselage torsions due to unsymmetrical horizontal tail load in one-g flight were based on flight load measurements instead of the arbitrary percentages specified in FAR 25. Lateral accelerations and body airloads consistent with the 24000 lb. side load on the vertical tail were approximated by use of the appropriate transfer functions; values of β , n_y , and $\dot{\psi}$ in phase with the side load on the vertical tail, at the Dutch roll natural frequency, were used for this purpose. The side loads were calculated for the mission analysis case only, and the same ratios to the tail side load were assumed to apply for the V_C and V_D cases. Fuselage torsions due to the dissymmetry of horizontal tail load produced by induction effects from the vertical tail were obtained theoretically.

For each of the three conditions, the minimum aftbody margin of safety was determined by stress analysis. Also determined was the amount that the vertical tail side load would have to be reduced to give a zero margin of safety. The resulting margins of safety and allowable side loads were as follows:

Case	Speed, Knots EAS	Margin of Safety	Allowable Tail Side Load, P_y	
			Factor	Load
I	282	-.02	.94	22500
II	324	-.08	.81	19400
III	405	-.25	.57	13700

The critical location in the structure in each case was found to be the upper forward corner of the aft passenger door, at FS 800. Inasmuch as this was relatively far forward, the actual payload present could have a substantial effect on the margins of safety.

For the fin itself and the frames that transmit its load into the fuselage shell, the minimum margin of safety was + .05. Accordingly, the limit allowable fin load is $(1.05)(24000 \text{ lb.}) = 25200 \text{ lb.}$

In view of the probably sizeable effect of payload on the fuselage margins of safety in the vicinity of FS 800, any results based on the margins of safety tabulated would have to be considered as only very roughly indicative. Within this limitation, approximate limit and ultimate values of $N(y)$ and of σ_{w1} were computed.

The variation in allowable side load, P_y , for the three conditions was due almost exclusively to variation of the balancing load on the horizontal tail, P_z . Consequently, it was possible to plot allowable P_y vs balancing tail load, P_z , and read from the curve the allowable value of P_y corresponding to intermediate values of P_z . For ultimate conditions, P_z was divided by 1.5, the corresponding value of P_y was read, and this was multiplied by 1.5 to reconvert to an ultimate basis. For aft c.g. conditions, the down balancing tail load was reduced appropriately.

Before proceeding further, the effect of cabin pressure on the margins of safety was examined. It was found that at the critical location the cabin pressure contributed significantly to the stresses. The maximum differential pressure was used in the analysis; at the pertinent altitudes, on the other hand, even if full sea level cabin pressure were maintained, the differential pressure would have been much lower. Elimination of this conservatism appeared to permit a sizeable increase in the tail side load. However, other locations would then become critical. One such location, where the cabin pressure did not contribute to the stress, showed a + .03 margin with the reduced P_y indicated. It was estimated that the P_y values tabulated above could probably be increased by about 5% before zero margins would be developed at these locations. Accordingly, the allowable P_y values tabulated above were all multiplied by 1.05 before plotting vs P_z .

The various cases of interest are listed in Table E-9. The allowable P_y values shown were read from the curve. The limit and ultimate strength values of $\sigma_w \eta_d$ were then computed as shown. The \bar{A} values used were taken from the critical cases for tail side load and are not necessarily consistent with the gross weights and payloads used in the fuselage loads determination. The limit and ultimate strength values of $N(y)$ were read from Figure 9-13.

For the fin itself and the frames that transmit its loads into the fuselage shell, the limit allowable side load was indicated above to be 25200 lb. This value provides a cut-off for those conditions for which consideration of fuselage strength alone would result in a high allowable side load.

As noted in Section 7, preliminary analysis, based on tail load alone, had indicated the V_B loads to be appreciably lower than the V_C loads, on the basis of a ratio of V_B to V_C $\sigma_w \eta_d$'s of 66/50. It is clear from Table E-9 that consideration of fuselage strength would not reverse this conclusion.

As noted above, detailed analysis of a sufficient number of design envelope conditions to establish a firm set of limit and ultimate strength $\sigma_w \eta_d$ values for the Model 188 aftbody did not appear justified. It did appear, however, that a realistic set of aftbody loads could be derived readily for the mission analysis segment giving the highest fin side load, and that these loads would be quite representative of loads for the mission analysis as a whole. As a result, a more refined set of mission analysis loads was now defined. Actual aftbody payload was included. A more realistic cabin differential pressure, of 3.9 psi, was used, corresponding to a 2000 ft. cabin altitude at an airplane altitude of 11000 ft. Stresses due to cabin pressure, as before, were neglected where they acted to relieve the stresses due to the flight loads. This condition was defined with lateral loads corresponding to a fin side load of 24000 lb. The minimum margin of safety was found to be +.14. It was clear, therefore, that the full limit-strength fin side load of 25200 lb could be carried without exceeding limit strength anywhere in the aftbody. As a result, the limit and ultimate strength $N(y)$ values for lateral gust, for the Model 188, became:

Limit: $N(y) = 6 \times 10^{-5}$ cycles per hour

Ultimate: $N(y) = 5 \times 10^{-7}$ cycles per hour

TABLE E-9. CALCULATION OF LIMIT AND ULTIMATE
STRENGTH VALUES OF $N(y)$ AND $\sigma_w \eta_d$, LATERAL GUST,
MODEL 188

①	②	③	④	⑤	⑥	⑦	⑧
	Case	P_s (Limit)	P_y Limit	P_y Ultimate	$\bar{\lambda}$	$\sigma_w \eta_d$ P_{ps} $\frac{P_{ps}}{P_{br}}$	Altitude P_t
V_D LIM FWD CG	621	-28900	14400		426.9	33.7	7000
AFT CG	608	-24600	16200		443.8	36.5	7000
V_D ULT FWD CG	621	-19800	18600	27300	426.9	65.4	7000
AFT CG	608	-16400	19800	29700	443.8	66.9	7000
V_C LIM FWD CG	617	-15100	20400		337.4	60.2	7000
AFT CG	602	-10900	22200		345.7	64.2	7000
V_C ULT FWD CG	617	-10100	22500	33900	337.4	101	7000
AFT CG	602	-7300	23700	35600	345.7	103	7000
V_B LIM FWD CG	-	-2600	25800*				
AFT CG	-	1600	25800*				
V_B ULT FWD CG	-	-1700	26200*	39300			
AFT CG	-	1100	26200*				
MA LIM		-7400	23700			$N(y) = 1.0 \times 10^{-4}$	
MA ULT		-4900	24900	37400		$N(y) = 5.5 \times 10^{-7}$	

*Use 25200 lb as limited by tail.

E.6 Model 749 Fuselage and Tail, Lateral Gust

Based on the original stress analysis of the Model 749 outboard fins, the limit strength value of the side load on one fin is 6270 lb. The actual distribution of load amongst the three fins was later determined by loads measurements in flight. It was found that .45 of the total load was developed on the leading outboard fin. The resulting limit strength value of total side load for the three fins is therefore $(6270 \text{ lb.})/.45 = 14000 \text{ lb.}$ The corresponding ultimate strength is 21,000 lb.

Based on these strength values, the limit and ultimate strength $N(y)$ values are read from Figure 9-15:

Limit: $N(y) = 2.4 \times 10^{-4}$ exceedances per hour

Ultimate: $N(y) = 5 \times 10^{-6}$ exceedances per hour

Limit and ultimate strength values of $\sigma_w \eta_d$ were obtained utilizing the \bar{A} values from Table B-8:

Speed	Case	Altitude	Limit or Ultimate	Allowable P_y	\bar{A}	$\sigma_w \eta_d = P_y / \bar{A}$
V_C	501, 503	7000 ft.	Limit	14000 lb.	218 lb/fps	64.6
V_D	502, 504	7000 ft.	Limit	14000 lb.	291 lb/fps	48.3
V_C	501, 503	7000 ft.	Ultimate	21000 lb.	218 lb/fps	96.8
V_D	502, 504	7000 ft.	Ultimate	21000 lb.	291 lb/fps	72.4

It is seen that the V_D values are in both cases well in excess of 25/50 of the corresponding V_C values. As indicated in Section 7, V_B cases were not included, as it appeared that the resulting allowable $\sigma_w \eta_d$ values would be greater than 66/50 of the corresponding V_C values.

Lateral gust conditions based on power-spectral analysis were not defined for the Model 749 fuselage. It appeared, however, that the fuselage would probably be found to be less critical than the tail. The original design analysis showed the fuselage to be no more critical than the outboard fin; and with the more adverse distribution of load amongst the three fins used in the present analysis, the fuselage should become

relatively less critical. It is believed, moreover, that the relative severity of loading on the fuselage and tail should be about the same for a power-spectral gust condition as for the discrete gust and yaw maneuver conditions to which the airplane was originally designed. As a result, the substantial effort that would be required for present personnel to perform meaningful stress analysis of the Model 749 fuselage (bearing in mind that the original stress analysis is now nearly 20 years old) did not appear justified.

E-49